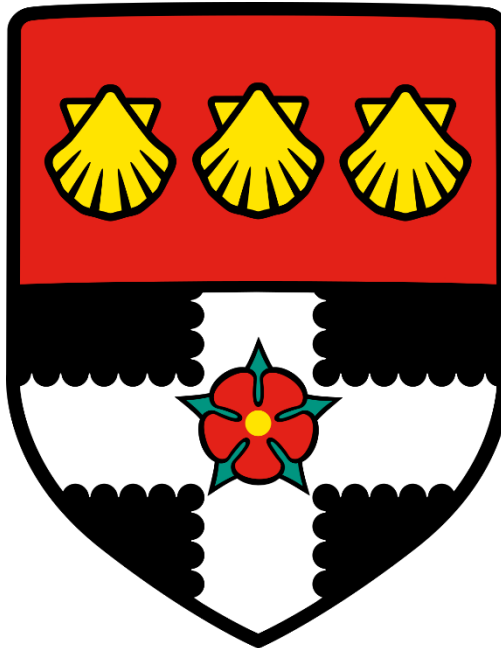


University of Reading



**Investigating the reprogramming of the hypertrophic
Myostatin null muscle with Estrogen-related receptor
gamma; implications for muscle structure and
function**

Saleh Omairi

Thesis submitted for the degree of Doctor of Philosophy

School of Biological Sciences

May 2018

Declaration

I confirm that this is my own work and the use of all material from other sources has been properly and fully acknowledged.

I would like to dedicate this work

To

My parents

My brothers and sisters

My wife

My children

My country

IRAQ

Acknowledgement

First, praises and thanks to the God for the blessings and given me the ability to complete this work. Foremost, I would like to express my deep and sincere gratitude to my supervisor Professor Ketan Patel for giving me this opportunity to do research and providing invaluable guidance throughout this project. His motivation, dynamism and encouragement have deeply inspired me. His guidance helped me in all the time of research and writing of this thesis. It was a great privilege and honour to work and study under his supervision. I am extremely grateful for what he has offered me. I express my thanks to the Higher Committee for Education Development in Iraq (HCED) for their generous funding for this project. I would also like to send special thanks to Dr. Antonios Matsakas who helped me a lot and showed me the stunning techniques. I'm also grateful for my colleagues Dr. Henry Collins-Hooper and Dr. Robert Mitchell, Ben Mellows and Danielle Vaughan for the willing to help me with anything. I'm very appreciative of the support that was provided by the team that Professor Ketan Patel had around during my PhD. A massive thank you to the following people, Dr. Roberta Sartori (University of Padua, Italy), Dr. Oliver Kretz (University of Freiburg, Germany), Dr. Jo C Bruusgaard (University of Oslo, Norway), Dr. Natasa Giallourou (University of Reading), Dr. Federica Montanaro and Dr. Silvia Torelli (UCL, UK) for their collaboration to complete this research work.

I am extremely grateful to my parents for their love, prayers, and sacrifices for educating me. I would also like to say a huge thank you to my brothers and sisters for their constant support and encouragement. I am very much thankful to my wife, my daughter, and my son for their love, patience, care and continuing support during my PhD. My Special thanks goes to my friends Moafaq Samir and Khalid Alyodawi for their constant support and encouragement.

Abstract

Skeletal muscle is a highly compliant organ system that is composed of muscle fibres, nerves, sensory cells, blood vessels and connective tissue. A central concept of skeletal muscle biology is the existence of an inverse relationship between muscle fibre size and its oxidative capacity which has been used to explain why small fibres are oxidative and large fibres glycolytic. However, sturdiness of this relationship is unknown. In order to investigate the rigour of this relationship we made use of a genetic model that enhances oxidative metabolism, mediated by estrogen-related receptor gamma (*Errγ*) (a constitutively active orphan nuclear receptor belongs to the ERR subfamily), and the hypertrophic background of *Myostatin* (a member of the Transforming Growth Factor beta (TGF-β) superfamily that is negatively regulating skeletal muscle mass development) null (*Mtn^{-/-}*) mice. We show that superimposition of *Errγ* on the *Mtn^{-/-}* background results in hypertrophic muscle that displays a high oxidative capacity (*Mtn^{-/-}/Errγ^{Tg/+}*), thus violating the inverse relationship between muscle fibre cross-sectional area and its oxidative capacity. Thereafter, we examined the canonical view that there is a high number of satellite cells (skeletal muscle resident stem cells) in oxidative muscles. Surprisingly, I found that hypertrophic oxidative muscle fibres from *Mtn^{-/-}/Errγ^{Tg/+}* mice showed a deficit in the number of satellite cells. Unexpectedly, the lower population of satellite cells in the hypertrophic oxidative model is not associated with a lower regenerative capacity. We also examined the relationship between muscle fibre phenotype (size and metabolism) and components of its force transducer apparatus that consists of both extracellular matrix (ECM) and dystrophin-glycoprotein complex (DGC). Interestingly, I showed that levels of ECM and DGC entities can be influenced by muscle fibre phenotype.

Observations of this work firstly, challenge the notion of a constraint between skeletal muscle fiber size and oxidative capacity, secondly, indicate the important role of the microcirculation in the regenerative capacity of a muscle even with low population of satellite cells, and thirdly, show that the metabolic properties of a muscle fibre are a critical factor to regulate the levels of ECM and DGC proteins.

List of abbreviations

4E-BP1	4E-binding protein 1
AAV	Adeno-associated virus
AAV8ProMyo	Adeno-associated virus Myostatin propeptide
Acadl	Acyl-Coenzyme A dehydrogenase, long chain
Acadm	Acyl-Coenzyme A dehydrogenase, medium-chain
Ach	Acetylcholine
AChE	Acetylcholinesterase enzyme
ActRIIB	Activin receptor type IIB
ADP	Adenosine diphosphate
AF	Activation function
AIDS	Acquired immune deficiency syndrome
AKT	Serine/threonine kinase
ALK4 and ALK5	Activin receptor-like kinase 4 and 5
AMPK	AMP-activated protein kinase
ATP	Adenosine triphosphate
ATPase	Adenosine triphosphatase enzyme
BB	Biceps brachii
BMD	Becker muscular dystrophy
BMP1	Bone morphogenetic protein 1
BNIP3	BCL2/adenovirus E1B interacting protein 3
CAS	Cross-sectional area
CD36	Cluster of differentiation 36
Cdk	Cyclin dependent kinase
CDK2	Cyclin dependent kinases2
CHO	Chinese hamster ovary
Ckmt2	Mitochondrial creatine kinase
CLFS	Chronic low-frequency stimulation
CTX	Cardiotoxin
Cyts	Cytochrome c, somatic
DAG	Diacylglycerol
DBD	DNA-binding domain
DG	Dystroglycan
DGC	Dystrophin-glycoprotein complex
DHE	Dihydroethidium
DMD	Duchene muscular dystrophy
EC	Excitation-Contraction
ECM	Extracellular matrix

ECRL	Extensor carpi radialis longus
EDL	Extensor digitorum longus
eMHC	Embryonic myosin heavy chain
eIF4E	Eukaryotic translation initiation factor 4E
ERRE	Estrogen-related responds element
Errα	Estrogen-related receptor alpha
Errβ	Estrogen-related receptor beta
Errγ	Estrogen-related receptor gamma
ETC	Electron transport chain
Fabp3	Fatty acid-binding protein 3
FAO	Fatty Acid Oxidation
Fatp1	Fatty acid transport protein 1
FGF	Fibroblast growth factor
FoxO	Fork head box O
Glut 1	Glucose transporter type 1
Glut 4	Glucose transporter type 4
GRIP 1	Glucocorticoid receptor-interacting protein-1
GSK-3β	Glycogen synthase kinase-3 beta
H₂O₂	Hydrogen peroxide
Had	Haloacid dehalogenase
HIF	Hypoxia-inducible factor
HPRT	Hypoxanthine Phosphoribosyltransferase
HAS	Human α -skeletal actin
hSMN	human Survival of Motor Neuron
IGF1	Insulin like growth factor 1
IL6	Interlukin 6
IMs	Inflammatory myopathies
IP	Intraperitoneal
IRS	Insulin receptor substrate
I-Smads	Inhibitory Smads
LBD	Ligand-binding domain
LGMD	Limb-girdle muscular dystrophy
LN₂	Liquid nitrogen
Lpl	Lipoprotein lipase
MCK	Muscle Creatine Kinase
MDs	Muscular dystrophies
MHC	Myosin heavy chain
MLC	Myosin light chain
MPCs	Muscle progenitor cells
Mrf4	Myogenic regulatory factor 4

MRFs	Myogenic regulatory factors
mtNOS	Mitochondrial nitric oxide synthase
mTOR	Mammalian Target of Rapamycin
MuRF1	Muscle ring finger 1
Myf5	Myogenic determination factors
MyoD	Myogenic differentiation antigen
MyoPPT	Myostatin propeptide
NFAT	Nuclear factor of activated T cells
NMJ	Neuromuscular junction
NMR	Nuclear magnetic resonance
NO	Nitric oxide
NRF	Nuclear respiratory factor
NRs	Nuclear receptors
OCT	Optimal Cutting Temperature compound
OXPHOS	Oxidative phosphorylation
P13K	Phosphoinositide 3-kinase
Pax3	Paired box3
Pax7	Paired box7
PCA	Principal Components Analysis
PCR	Polymerase chain reaction
PDC	Pyruvate dehydrogenase complex
PDK4	Pyruvate dehydrogenase kinase 4
Perm1	PPARGC1 and ESRR-induced regulator in muscle 1
PGC-1α	PPARgamma-coactivator 1 α
PPAR	Peroxisomal proliferator-activated receptor
Ppard	Peroxisome proliferator-activated receptor delta
Ppargc 1b	Peroxisome proliferator-activated receptor gamma coactivator 1-beta
PPM	Parts per million
Rb	Retinoblastoma
RBP- Jk	Recombining binding protein-Jk
RIP140	Receptor-interacted protein 140
ROS	Reactive oxygen species
RyR1	Ryanodine receptor 1
S6K	Ribosomal protein S6 kinase
sActrIIB	Soluble activin receptor IIB
SDH	Succinate dehydrogenase
SERCA	Sarco (endo) plasmic reticulum Ca ⁺² ATPase pump
SG	Sarcoglycan
Slc25a20	Solute carrier family 25 member 20

SMA	Spinal muscular atrophy
Smarcd3	SWI/SNF-related matrix-associated actin-dependent regulator of chromatin subfamily D member 3
Sox6	Sex determining region Y-box 6
sPo	Specific force
SR	Sarcoplasmic reticulum
SRC	Steroid receptor co-activator
STAT	Signal transducer and activator of transcription
TA	Tibialis anterior
TCA	Tricarboxylic acid cycle
TEM	Transmission electron microscopy
TGF-β	Transforming Growth Factor-beta
Tn-C	Troponin C polypeptide
Tn-I	Troponin I polypeptide
Tn-T	Troponin T polypeptide
T-tubule	Transvers tubule
UCP1	Uncoupling protein 1
Vegf	Vascular endothelial growth factor
WT	Wild type

Contents

Declaration	2
Acknowledgement	4
Abstract	5
List of abbreviations	6
Contents	10
Figures and Tables	17
Chapter 1; General Introduction	21
1.1. Muscle tissue	22
1.2. Skeletal muscle	25
1.2.1. Structure of skeletal muscle	25
1.2.1.1. Macroscopic anatomy of skeletal muscle.....	25
1.2.1.2. Microscopic appearance of skeletal muscle	26
1.2.1.2.1. Transverse tubule system and sarcoplasmic reticulum.....	27
1.2.2. Skeletal muscle physiology	29
1.2.2.1. Mechanism of contraction.....	29
1.2.2.2. Contraction cycle	30
1.2.3. Skeletal muscle metabolism and energy production	33
1.2.4. Skeletal muscle plasticity.....	34
1.2.4.1. Muscle fibre types and distribution.....	34
1.2.4.2. Muscle fibres transition	37
1.2.5. Skeletal muscle supporting tissues.....	38
1.2.5.1. Skeletal muscle capillarization.....	38
1.2.5.2. Skeletal muscle connective tissue	39
1.2.5.3. Skeletal muscle innervation.....	42
1.2.6. Skeletal muscle development.....	43
1.2.6.1. Embryonic origin of skeletal muscles	43
1.2.6.2. Satellite cells and muscle regeneration.....	45
1.7. Myostatin.....	49
1.7.1. Effects of Myostatin on muscle cells proliferation and differentiation.....	51
1.7.2. Structure and proteolytic processing of Myostatin.....	52
1.7.3. Myostatin signalling pathway	52
1.7.4. Post-developmental blocking of Myostatin.....	54

1.8. Mechanisms regulate skeletal muscle mass.....	56
1.9. Estrogen-related receptor gamma (Errγ)	58
1.9.1. Errγ is orphan nuclear receptor	58
1.9.2. Errγ is an inducible transcriptional factor.....	60
1.9.3. Roles of Errγ and transgenic approach	64
Hypothesis, aims and objectives	68
Chapter 2; Methods	74
2. Genetic In vivo experimentation	75
2.1. Animal maintenance.....	75
2.2. Genotyping	76
2.3. Assessment of mice fatigue resistance.....	78
2.4. Assessment of forelimb muscle strength using grip strength meter	78
2.5. Behavioral and Locomotor measurements using Open Field Animal Activity Monitoring system	78
2.6. Mice euthanasia.....	79
2.7. Muscle tension measurements	79
2.8. Skeletal muscles dissection.....	80
2.8.1. Hind limb muscles dissection.....	80
2.8.1.1. Tibialis Anterior (TA) muscle dissection.....	80
2.8.1.2. Extensor Digitorum Longus (EDL) muscle dissection.....	81
2.8.1.3. Gastrocnemius and Soleus muscles dissection	81
2.8.2. Forelimb muscles dissection	82
2.8.2.1. Biceps brachii (BB) muscle dissection.....	82
2.8.2.2. Extensor Carpi Radialis Longus (ECRL) muscle dissection	83
2.9. Ex vivo skeletal myofibre experimentation	83
2.9.1. Isolation of intact single myofibres of EDL muscle	83
2.9.2. Single myofibre fixation and culture.....	84
2.9.3. Immunocytochemistry staining	84
2.9.4. Myonuclear organization.....	85
2.10. Tissue freezing and preparing for cryosectioning.....	85
2.11. Haematoxylin and Eosin staining protocol (H&E).....	86
2.12. Immunohistochemical staining.....	86
2.13. Antigen Retrieval Immunostaining protocol	87
2.14. Macrophage immunocytochemistry	88

2.15. Succinate Dehydrogenase Stain (SDH)	88
2.16. Periodic Acid-Schiff (PAS) Stains	89
2.17. Dihydroethidium (DHE) stain.....	89
2.18. Acid Phosphatase essay	89
2.19. Transmission electron microscopy (TEM).....	90
2.20. ¹ H NMR spectroscopy-based metabonomic analysis	90
2.21. Western blotting.....	91
2.22. RT-qPCR	91
2.23. In vivo assessment of regeneration capacity following Cardiotoxin injection	92
2.23.1. Anesthetising mice.....	92
2.23.2. Intramuscular (IM) injection of Cardiotoxin into TA muscle	92
2.24. In vivo Post-natal blocking of Myostatin	93
2.24.1. Intraperitoneal injection of soluble activin receptor IIB (sActrIIB-Fc)	93
2.25. Semi-quantitative measurement of Collagens and dystrophin-glycoprotein complex (DGC) proteins expression by immunofluorescence	93
2.26. Sarcolemma thickness measurement.....	94
2.27. Imaging and analysis.....	94
2.28. Statistical analysis	94
Chapter 3 Results; Morphometric, Physiological and Histological analysis of hyper-oxidative hypertrophic muscle	95
3.1. Introduction	96
3.2. Muscle-specific expression of Erry into Mtn ^{-/-} background mice using human α -skeletal actin promoter.....	101
3.3. Body weight and skeletal muscle mass following Myostatin deletion and Erry overexpression on Myostatin null background mice	103
3.4. Erry overexpression into Myostatin null background mice induces fatigue resistance	107
3.5. Increased muscle force generation capacity following muscle-specific manner Erry overexpression into the Myostatin null background mice	109
3.6. Erry overexpression induces forelimb muscles grip strength that was compromised due to Myostatin deletion	111
3.7. Locomotor activity of Myostatin null and Erry overexpression into Mtn ^{-/-} background mice	113
3.8. Erry overexpression sustains myofibres hyperplasia exhibited by Myostatin null muscles.....	115
3.9. Muscle fibres hypertrophy following Myostatin deletion was not affected by Erry overexpression into Mtn ^{-/-} mice.....	118

3.10. Mechanisms underpinning muscle enlargement following Myostatin deletion and Erry overexpression	125
3.11. MHC profiling in hind limb muscles of Mtn ^{-/-} mice reforms by Erry overexpression	127
3.12. Erry introducing into Myostatin null muscles alters MHC profiling at transcriptional level	134
3.13. Erry overexpression normalizes ultra-structural abnormalities of Mtn ^{-/-} muscles.....	136
3.14. Discussion	139
Chapter 4 Results; Introducing of Erry into Mtn^{-/-} mice normalizes metabolic and molecular, but not cellular features of Myostatin null muscles	150
4.1. Introduction	151
4.2. Erry introducing into Mtn ^{-/-} mice induces robust increase of mitochondrion-associated enzyme succinate dehydrogenase (SDH) activity	156
4.3. Remodelling muscle glycolytic status following Erry overexpression into Myostatin null mice.	160
4.4. Muscle-specific expression of Erry is efficacious to promote angiogenesis program in a muscle lacking Myostatin.....	163
4.5. Erry overexpression is required for synchronizing of myofibre size and capillary density	165
4.6. Remodelling of muscle NMR profile of Mtn ^{-/-} mice following Erry modification	167
4.7. Erry is required for regulating of muscle energy metabolism	169
4.8. The effects of Myostatin deletion and Erry overexpression on biomarker genes that regulate glucose metabolism.....	171
4.9. Erry overexpression promotes expression level of genes regulates fatty acid metabolism	173
4.10. Hyper-oxidative hypertrophic muscle fibres show high oxygen diffusion rate.....	175
4.11. Erry overexpression into Mtn ^{-/-} mice induces biomarker genes that regulate fatty acid transport, uptake and oxidation.....	177
4.12. Hyper-oxidative hypertrophic muscle fibres show low ROS emission rate.....	180
4.13. Erry overexpression into Mtn ^{-/-} mice does not rescue the reduction of satellite cells number in hyper-oxidative hypertrophic myofibres.....	182
4.14. Proliferation and differentiation rate of hyper-oxidative hypertrophic myofibres	186
4.15. Muscle-specific expression of Erry into Mtn ^{-/-} promotes myonuclei number.....	190
4.16. Myonuclei distribution do not normalizes by introducing of Erry into Mtn ^{-/-} mice	192
4.17. Discussion	194
Chapter 5 Results; Superimposition of Erry onto Myostatin null background muscles accelerates regeneration capacity	205
5.1. Introduction	206
5.2. Assessment of skeletal muscles degeneration after 3 days of cardiotoxin injection.....	210

5.3. Muscle-specific overexpression of Erry in the Mtn ^{-/-} background attenuates necrosis induced by cardiotoxin treatment at day 3 post-injury	214
5.4. Lower levels of cell death in injured TA muscles of Mtn ^{-/-} /Erry ^{Tg/+} mice after three days of cardiotoxin treatment	216
5.5. Overexpression of Erry promotes macrophages accumulation in damaged muscle	218
5.6. High number of committed muscle cells in the damaged TA muscles from Mtn ^{-/-} /Erry ^{Tg/+} mice at day 3 post-injury	220
5.7. Less severity of TA muscle damage at day 6 compared to day 3 post-injury.....	222
5.8. Advanced removal of necrotic and dying cells in Mtn ^{-/-} /Erry ^{Tg/+} muscle at day 6 post-injury.....	224
5.9. High macrophages activity in Mtn ^{-/-} /Erry ^{Tg/+} muscles at day 6 post-injury.....	227
5.10. Erry overexpression increases the number of committed cells at day 6 post-injury	229
5.11. Greater degree of regeneration in Mtn ^{-/-} /Erry ^{Tg/+} muscles at day 6 post-injury	231
5.12. Day 14 post-injury show high regeneration capacity of Mtn ^{-/-} /Erry ^{Tg/+} muscles	234
5.13. Discussion	237
Chapter 6 Results; Impact of post-natal antagonism of Myostatin signalling on the skeletal muscles of the Erry mice	244
6.1. Introduction	245
6.2. Erry expression following post-natal inhibition of Myostatin using sActRIIB.....	249
6.3. Treatment with Activin ligand trap increases body and muscle mass in WT and Erry ^{Tg/+} mice ..	250
6.4. Skeletal muscle enlargement induced by sActRIIB treatment is not associated with muscle fibre hyperplasia.....	253
6.5. Increase in muscle mass following sActRIIB administration is caused by myofibre hypertrophy	255
6.6. Myosin heavy chain profile does not alter by sActRIIB treatment.....	259
6.7. Treatment with sActRIIB attenuates oxidative capacity of muscles from WT, but not Erry ^{Tg/+} mice	263
6.8. Post-natal inhibition of Myostatin caused an increase in CSA of both SDH ⁺ and SDH ⁻ muscle fibres	267
6.9. sActRIIB treatment increases blood vessels density of Erry ^{Tg/+} muscles	270
6.10. Inhibition of Myostatin causes elevation in level of superoxide in WT but not in Erry ^{Tg/+} muscles	272
6.11. Muscle-specific expression of Erry prevents the decrease in connective tissue level that induced by sActRIIB treatment in WT muscles.....	274
6.12. Discussion	284
Chapter 7 Results; Regulation of extracellular matrix and dystrophin-associated glycoprotein complex compositions by the metabolic properties of muscle fibres	294

7.1. Introduction	295
7.2. Muscle-specific expression of Erry restores the reduction in basal lamina and interstitial components of ECM resulted from Myostatin absence.....	298
7.3. Overexpression of Erry redresses the decrease of dystrophin level in Mtn ^{-/-} muscles	302
7.4. Myostatin mutation has disparate impacts on expression levels of transmembrane proteins of DGC	304
7.5. Superimposition of an oxidative metabolic programme increases expression levels of extracellular components of DGC.....	310
7.6. Muscle fibre properties influence DGC molecules at transcriptional level and total protein expression.....	313
7.7. Discussion	315
Chapter 8; General discussion and conclusion.....	320
General discussion	321
Conclusion	341
Future direction priorities.....	343
Appendices	347
Appendix 1 - Antibodies used	348
Antibodies used for Immunostaining	348
Antibodies used for western blotting.....	349
Appendix 2 - Materials.....	351
Reagents:	351
Solutions:	352
Taq 2X Master Mix.....	352
TAE buffer	352
Krebs solution	352
1 x Phosphate Buffer Saline (PBS).....	352
4% Paraformaldehyde (PFA).....	353
Permeabilisation buffer	353
Wash buffer	353
Preparation of type 1 collagenase	353
Single Fibre Culture Medium (SFCM).....	353
Chick embryo extract.....	353
Antigen retrieval solution	354
Nitro blue tetrazolium (NBT) stock.....	354

Sodium succinate stock	354
Formal calcium.....	354
Acid phosphatase incubation medium	354
Preparation of fixative solution for TEM samples	354
Appendix 3 – RT-PCR Primer sequences.....	355
References	357
Publications	389

Figures and Tables

Figure 1.1.	Structure of three muscle types, Cardiac, Smooth and Skeletal muscles	24
Figure 1.2.	Skeletal muscle arrangement	26
Figure 1.3.	Sarcomere structure	28
Figure 1.4.	Steps involved in skeletal muscle excitation, contraction and relaxation	32
Table 1.1.	Muscle fibre isoforms and their physiological performance	36
Figure 1.5.	The dystrophin-glycoprotein complex (DGC) in skeletal muscle	40
Figure 1.6.	Satellite cells self-renewal	49
Figure 1.7.	Myostatin signalling pathway	54
Figure 1.8.	Muscle mass balance	57
Figure 1.9.	Erry as conductor of angiogenic and metabolic program	62
Figure 3.1.	Erry expression induced by using human α -skeletal actin promoter	102
Figure 3.2.	Myostatin deletion and Erry introducing into Myostatin null background mice doesn't affect body weight	103
Figure 3.3.	Hind limb muscle mass of WT, Mtn and Mtn:Er mice	104
Table 3.1.	Weight of hind limb muscles from WT, Mtn and Mtn:Er mice	105
Figure 3.4.	Muscle-specific expression of Erry maintains hypertrophy features of Myostatin null background muscles	106
Figure 3.5.	Exercise tolerance test for WT, Mtn and Mtn:Er animals, using mouse treadmill protocol	108
Figure 3.6.	Erry overexpression into Mtn mice is required to improve muscle force generation capacity	110
Figure 3.7.	Muscle-specific manner overexpression of Erry attenuate Mtn muscle strength decreasing	112
Figure 3.8.	Erry over expression promotes behavioral and locomotor features of Myostatin null mice	114
Table 3.2.	Myofibre number of Soleus and EDL muscles from WT, Mtn and Mtn:Er mice. All data are show as mean \pm SEM	116
Figure 3.9.	Myostatin deletion increased muscle fibres number and Erry overexpression maintained this increase	117
Figure 3.10.	Myofibres size following Myostatin deletion and Erry introducing into Mtn ^{-/-} mice	121
Table 3.3.	Cross sectional area for type I, IIA, IIX and IIB myofibres of (Soleus, EDL and TA) muscles from WT, Mtn and Mtn:Er mice. Size in (μ m ²) with SEM of 5 muscle sections	121
Figure 3.11.	Myofibres of hind limb muscles from Mtn and Mtn:Er mice show larger CSA than their counterpart myofibres from WT mice	124
Figure 3.12.	Muscle-specific expression of Erry maintains the hypertrophy in the Myostatin null background muscles	126
Figure 3.13.	Myosin heavy chain profiling of hind limb muscles affects by Myostatin ablation and Erry overexpression into Mtn ^{-/-} mice	130
Figure 3.14.	Muscle-specific expression of Erry into Myostatin null mice normalizes myosin type II phenotype	133

Figure 3.15.	Gene expression levels of MHCs in hind limb muscles from WT, Mtn and Mtn:Er mice	135
Figure 3.16.	Transmission Electron Microscopy (TEM) investigation of mitochondrial numbers, size and distribution in muscles from Mtn and Mtn:Er mice	138
Figure 4.1.	Er overexpression into Mtn ^{-/-} background muscle restores oxidative capacity to WT condition	159
Figure 4.2.	Er overexpression into Myostatin null muscles reduces number of glycolytic myofibres	162
Figure 4.3.	Molecular reprogramming of Myostatin null muscle by Er overexpression	164
Figure 4.4.	Revascularization of Myostatin null muscles following Er overexpression	166
Figure 4.5.	Muscle-specific expression of Er normalizes the metabolic of Myostatin null mice (Mtn)	168
Figure 4.6.	Molecular reprogramming of Myostatin null muscle by Er overexpression and its ability to regulate expression of transcriptional regulators	170
Figure 4.7.	Molecular reprogramming of Myostatin null muscle by Er overexpression and its ability to regulate glucose metabolism genes	172
Figure 4.8.	Molecular reprogramming of Myostatin null muscle by Er overexpression and its ability to restore the expression of fat metabolism genes	174
Figure 4.9.	Molecular reprogramming of Myostatin null muscle by Er overexpression and its ability to induce antioxidant genes	176
Figure 4.10.	Molecular reprogramming of Myostatin null muscle by Er overexpression and its ability to regulate the expression of fatty acid transport, uptake and oxidation genes	179
Figure 4.11.	Er overexpression required for preventing excessive superoxide production	181
Figure 4.12.	Fewer number of Satellite cells in EDL myofibre of Mtn:Er than other genotypic groups	184
Figure 4.13.	Muscle-specific expression of Er does not influence the satellite cell number	185
Figure 4.14.	Proliferation rate in myofibres of EDL muscles from three genotypic groups	187
Figure 4.15.	Pax7 and MyoD expressions in EDL myofibres from WT, Mtn and Mtn:Er mice	189
Figure 4.16.	Hyper-oxidative hypertrophy myofibres show more myonuclei	191
Figure 4.17.	Myonuclei distribution in myofibres from EDL muscles of WT, Mtn and Mtn:Er mice	193
Figure 5.1.	Schematic model of muscle degeneration/regeneration cycle	209
Figure 5.2.	Intramuscular administration of cardiotoxin induces different levels of injury in TA muscles from WT, Mtn and Mtn:Er mice	212
Figure 5.3.	Intramuscular administration of cardiotoxin induces different	

	levels of degeneration in TA muscles from WT, Mtn and Mtn:Ey mice	213
Figure 5.4.	Skeletal muscle regeneration is accelerated by the expression of Errγ in Myostatin null mice through enhanced clearing of necrotic fibres in response to cardiotoxin injury	215
Figure 5.5.	Skeletal muscle regeneration is accelerated by the expression of Errγ in myostatin null mice through reduce amount of cell death	217
Figure 5.6.	Skeletal muscle regeneration is accelerated by the expression of Errγ in myostatin null mice through promoted macrophages activity in response to cardiotoxin injury	219
Figure 5.7.	Skeletal muscle regeneration is accelerated by the expression of Errγ in myostatin null mice through enhanced myoblast response to cardiotoxin injection	221
Figure 5.8.	Intramuscular administration of cardiotoxin induces different levels of degeneration in TA muscles from WT, Mtn and Mtn:Ey mice at day 6	223
Figure 5.9.	Skeletal muscle regeneration is accelerated by the expression of Errγ in myostatin null mice through enhanced clearing of necrotic fibres in response to cardiotoxin injury at day 6 post-injury	225
Figure 5.10.	Skeletal muscle regeneration is accelerated by the expression of Errγ in myostatin null mice through reduce cell death	226
Figure 5.11.	Skeletal muscle regeneration is accelerated by the expression of Errγ in myostatin null mice through promoted macrophages activity in response to cardiotoxin injury	228
Figure 5.12.	Skeletal muscle regeneration is accelerated by the expression of Errγ in myostatin null mice through enhanced myoblast population in response to cardiotoxin injection	230
Figure 5.13.	Skeletal muscle regeneration is accelerated by the expression of Errγ in myostatin null mice at day 6	233
Figure 5.14.	Skeletal muscle regeneration is accelerated by the expression of Errγ in myostatin null mice through decrease density of the eMHC fibres, and generates new fibres with normal size	236
Figure 6.1.	Post-natal inhibition of Myostatin in the WT and muscle-specific Ey mice doesn't affect Ey expression	249
Figure 6.2.	Post-natal inhibition of Myostatin in the WT and muscle-specific Ey mice induces body weight	251
Figure 6.3.	Post-natal inhibition of Myostatin in the WT and muscle-specific Ey mice increases muscle mass	252
Figure 6.4.	Myostatin blocking doesn't change fibre number of WT and muscle-specific Ey mice	254
Figure 6.5.	Treatment of WT and Ey mice with sActRIIB increases muscle fibres cross-sectional area	258
Figure 6.6.	Post-natal inhibition of Myostatin do not impact Myosin Heavy Chain profile of EDL and soleus muscles of WT and Ey mice	262
Figure 6.7.	sActRIIB treatment induces glycolytic transformation of WT but not Ey muscles	266

Figure 6.8.	sActRIIB induces enlargement of both SDH+ and SDH- myofibres	269
Figure 6.9.	Post-natal inhibition of Myostatin induces blood vessels number in muscle-specific Ey mice	271
Figure 6.10.	Ey overexpression is necessary to mitigate ROS emission	273
Figure 6.11.	Expression of Dystrophin in the entire EDL and soleus muscle sections	277
Figure 6.12.	sActRIIB treatment caused a reduction in Collagen IV intensity and thickness in muscles from WT but not Ey	279
Figure 6.13.	sActRIIB treatment caused a reduction in Dystrophin intensity and thickness in muscles from WT but not Ey	281
Figure 6.14.	sActRIIB treatment caused a reduction in Laminin intensity and thickness in muscles from WT but not Ey	283
Figure 7.1.	Collagen IV profiles in WT, Mtn and Mtn:Ey mouse muscle	300
Figure 7.2.	Collagen I profiles in WT, Mtn and Mtn:Ey mouse muscle	301
Figure 7.3.	Dystrophin profiles in WT, Mtn and Mtn:Ey mouse muscle	303
Figure 7.4.	β -Dystroglycan profiles in WT, Mtn and Mtn:Ey mouse muscle	305
Figure 7.5.	α -Sarcoglycan profiles in WT, Mtn and Mtn:Ey mouse muscle	306
Figure 7.6.	γ -Sarcoglycan profiles in WT, Mtn and Mtn:Ey mouse muscle	307
Figure 7.7.	β -Sarcoglycan profiles in WT, Mtn and Mtn:Ey mouse muscle	308
Figure 7.8.	δ -Sarcoglycan profiles in WT, Mtn and Mtn:Ey mouse muscle	309
Figure 7.9.	α -Dystroglycan profiles in WT, Mtn and Mtn:Ey mouse muscle	311
Figure 7.10.	Laminin profiles in WT, Mtn and Mtn:Ey mouse muscle	312
Figure 7.11.	Molecular and Western blot profiling of Soleus ECM associated molecules	314

Chapter 1

General Introduction

1.1. Muscle tissue

Muscle tissue is one of the four primary types of body tissues, together with epithelial, connective and nervous tissues. Muscle cells are highly specialized for contraction; it produces movement within certain organs and the body as a whole. There are three types of muscle tissues can be uniquely identified by functional characteristics and the basis morphological features. The structure of each type is adapted to its physiological role. These muscle types are, cardiac muscle, smooth muscle and skeletal muscle (Mesher, 2010).

Cardiac muscle cells develop from splanchnic mesoderm surrounding the endocardial heart tube, and myoblast cells adhere one to another by a special attachment that later develops into an intercalated disc (Sadler, 2012). The cells are relatively small, although a few cardiac cells may have two or more nuclei; a typical cardiac muscle cell has a single centrally located nucleus. The cardiac muscle is striated not voluntary that found specifically in the heart to provide the force required for circulating blood around the body. It contracts at a steady rate set by the heart's pacemaker (Marieb, 2008). The intercalated discs are responsible to stabilize the relative positions of adjacent cells and maintain the three-dimensional structure of the tissue (Figure 1.1). Furthermore, the more longitudinal portions of each disc have multiple gap junctions, which provide ionic continuity between adjacent cells. Building on this, tightly knit bundles of cardiac cells and its interwoven organisation provides for a characteristic wave of contraction that leads to wringing out of heart ventricles (Martini, 2006).

Smooth muscles are constituents of internal organs and blood vessels. Smooth muscles for dorsal aorta and large arteries are derived from lateral plate mesoderm and neural crest cells, in the coronary arteries, smooth muscles originated from proepicardial cells and neural crest cells. Moreover, smooth muscles in the wall of the gut and gut derivatives are derived from a splanchnic layer of lateral plate mesoderm. Only sphincter and dilator muscles of the eye pupil and muscle tissue in the mammary and sweat glands are derived from ectoderm (Sadler, 2012). Smooth muscle cells are relatively long and slender with a single centrally located nucleus. They are nonstriated and involuntary cells, and their contraction mechanism is performed by calcium interacting with calmodulin, a calcium-binding protein (Mesher, 2010). Both intermediate and thin filaments of smooth muscles

insert into dense bodies, this attachment is essential to transmit contractile force to adjacent cells. Smooth muscle cells control the distribution of blood and regulate the blood pressure. Extensive layers of smooth muscle cells in the walls of digestive tract play an essential role in moving materials along the tract. Furthermore, contraction and relaxation of smooth muscle in respiratory system can alter the diameter of respiratory passageways. In addition, layers of smooth muscles in the walls of urinary and reproductive systems' organs, enable these organs to move their contents from one part to other (Martini, 2006).

Skeletal muscle is the most abundant tissue in the human body constituting 40-50% of the total body mass. It is essential for voluntary movement through its attachment points to the skeleton. In addition, skeletal muscle is involved in a number of involuntary actions such as breathing and swallowing (Bannister, 1995). Skeletal muscles vary in their size, shape, attachments and relative myosin isoform proportion. They range from extremely tiny strands like the stapedius muscle in the middle ear, to the gluteus maximus being the largest muscle is an example of the range of different sized muscles in the body. They are capable of producing various motions, such as the extra ocular muscle of the eye which performs fine contracting motion, as well as gross movement in large muscles like quadriceps muscle of the thigh (Williams, 1999). There is also a huge disparity in skeletal muscles shape, the Obicularia oculi are circular, whereas the sartorius that stretches along the thigh length is very long. As a result of these variations exhibited by skeletal muscle, it has been documented to have many important functions within the body: (1) Maintain posture and body position, skeletal muscles responsible for balancing the body above the feet during walk as a result of skeletal muscles tension. (2) Support soft tissues, the floor of the pelvic cavity and an abdominal wall formed from layers of skeletal muscle. (3) Produce skeletal movement, contractions of skeletal muscle moves the bones of the skeleton by pulling the tendons. (4) Guard entrances and exits of the mammalian orifices. (5) Maintain body temperature via heat production (Martini, 2006). Muscle fibres have a dynamic structure capable of changing their phenotypes in term of size and composition in response to environmental and physiological challenges such as mechanical loading or unloading, hormonal alteration and ageing (Pette and Staron, 2001).

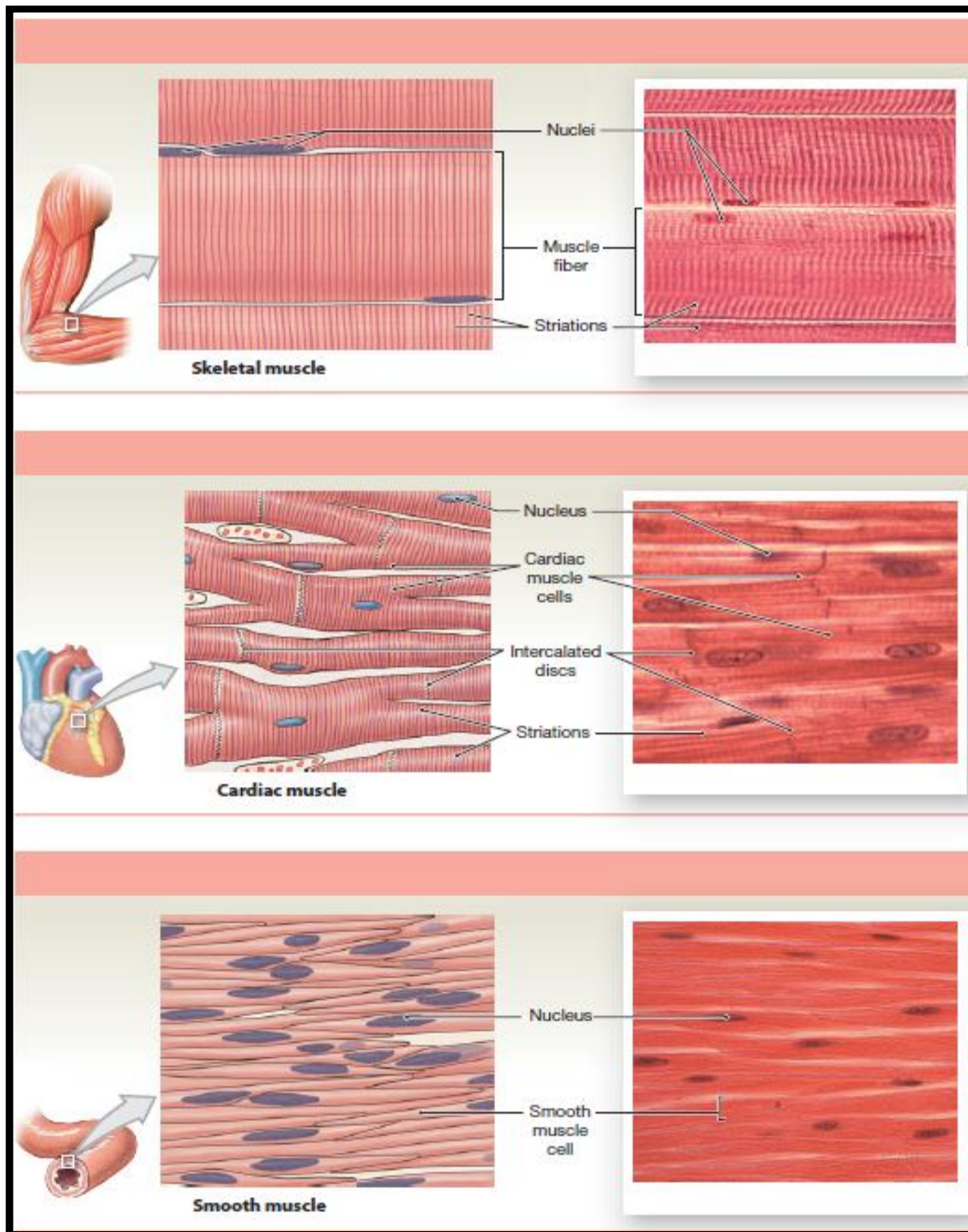


Figure 1.1. Structure of three muscle types, Cardiac, Smooth and Skeletal muscles (Martini, 2006)

1.2. Skeletal muscle

1.2.1. Structure of skeletal muscle

1.2.1.1. Macroscopic anatomy of skeletal muscle

Skeletal muscle is made up of parallel bundles of long, cylindrical, and multinucleated cells that show cross-striations, each cell contains hundreds of oval nuclei just internal to the basement membrane (Figure 1.1). Multinucleation of skeletal muscle results from the fusion of multiple myoblast cells during myogenesis. The peripheral location of nuclei in skeletal muscle cells is an important feature to distinguish these cells from cardiac and smooth muscles, both of which have central location nucleus. Moreover, contractile proteins within the individual muscle fibre allow for powerful contractions and also give the striated appearance of the muscle. The contraction in skeletal muscle is voluntary and controlled by somatic motor innervation (Williams, 1999).

Skeletal muscle is comprised of different tissues such as blood vessels, nerve fibres and a substantial amount of connective tissue. Each muscle is served by one artery, one or more vein and one nerve, usually all of these components enter and exit near to the central part and branch profusely through its connective tissue sheath (Marieb, 2008, Gumerson and Michele, 2011). The whole mass of each muscle that formed from regular bundles surrounded by a dense layer of collagen called the epimysium. The epimysium separates the muscle from surrounding tissues and organs and is connected to the deep fascia. From the epimysium, there are thin septa of connective tissue extended and surrounding the bundles of fibres within a muscle, this connective tissue around each bundle or fascicle called perimysium. Within fascicles there is a delicate connective tissue layer termed the endomysium, surrounds the individual muscle fibre and interconnect adjacent muscle fibres (Figure 1.2). The epimysium, perimysium and endomysium come together at both ends of muscle to form a bundle known as a tendon or a broad sheet called an aponeurosis. Tendons usually attach skeletal muscle fibres to the bone. Force generated by skeletal muscle contraction transmitted via tendon to cause bone movement. The blood vessels and the nerve supply generally enter the muscle together and follow the same branching pattern through the perimysium as well as endomysium (Martini, 2006).

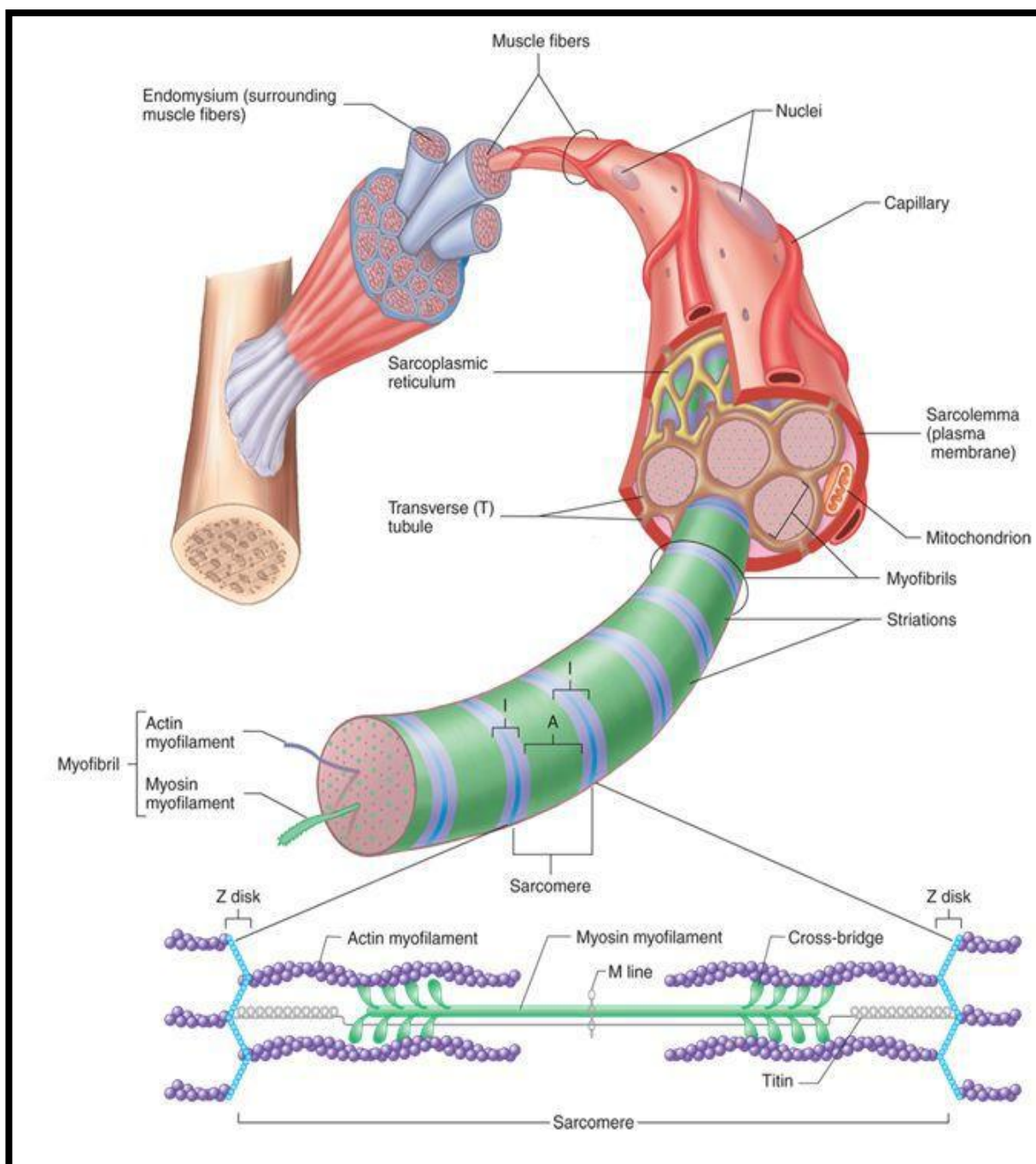


Figure 1.2. Skeletal muscle arrangement (Mescher, 2010)

1.2.1.2. Microscopic appearance of skeletal muscle

Skeletal muscle fibre is a highly specialised structure filled with predominantly filament proteins that comprise myofibrils, the contractile apparatus of the tissue. The myofibrils align longitudinally and form series of contractile units called sarcomeres (Aidley, 1998).

Each sarcomere consists of (1) thick filaments, (2) thin filaments, (3) proteins that stabilize the positions of thick and thin filaments, and (4) proteins that regulate the interaction between thick and thin filaments (Martini, 2006). The interaction between thick and thin filaments of sarcomere is responsible for muscle contraction. It has been shown that the sarcomeres within the myofibrils are demarcated by a dense line called Z- line. The region between the Z- line can be divided into light area consisting of the thin actin protein filaments which called (I-band), and the dark area which mainly comprises the thick myosin protein filaments (A-band) which has a central lighter area called H-Zone. This central area is bisected vertically by a dark line called M-line (Figure 1.3). In addition, there are cross bridges projected from myosin filaments to establish the contraction with the actin filaments. During muscle contraction, the filaments slide over each other pulling the Z- discs together and shortening the length of the muscle (Sciote and Morris, 2000). Each myosin molecule consisted of two rod-like tails woven around each other and terminates into two globular heads. These heads contain ATPase enzyme that hydrolyses ATP molecules to generate energy require for contraction, as well as contain actin binding sites to link together and forming cross bridges. On the other hand, thin filaments are formed by two twisted strands of actin polymer, as well as regulatory proteins such as tropomyosin and troponin. Troponin composed of three polypeptides, Tn-I which act as myosin binding inhibitory, Tn-T which helps the binding of tropomyosin to actin, and Tn-C which bind to calcium ions (Marieb, 2008).

1.2.1.2.1. Transverse tubule system and sarcoplasmic reticulum

In large muscle cells, the signal causes a contraction of peripheral myofibrils before those more centrally positioned. In order to get a simultaneous contraction of all muscle cell regions, the signal has to be distributed rapidly throughout the cell interior. The sarcolemma has a transverse tubule (T-tubule) system that through invaginations penetrates throughout the myofibre to form a complex network of narrow tubes extending to the sarcoplasm, and encircles every myofibril near the sarcomere (Mescher, 2010). As the T-tubule have same properties of muscle sarcolemma, so electrical impulses conducted by the sarcolemma travel along the T-tubules into the cell interior, which in turn provide a uniform muscle

contraction. In the same line of thought, the T-tubules are short and broad in a cardiac muscle, while smooth muscle has no T-tubules.

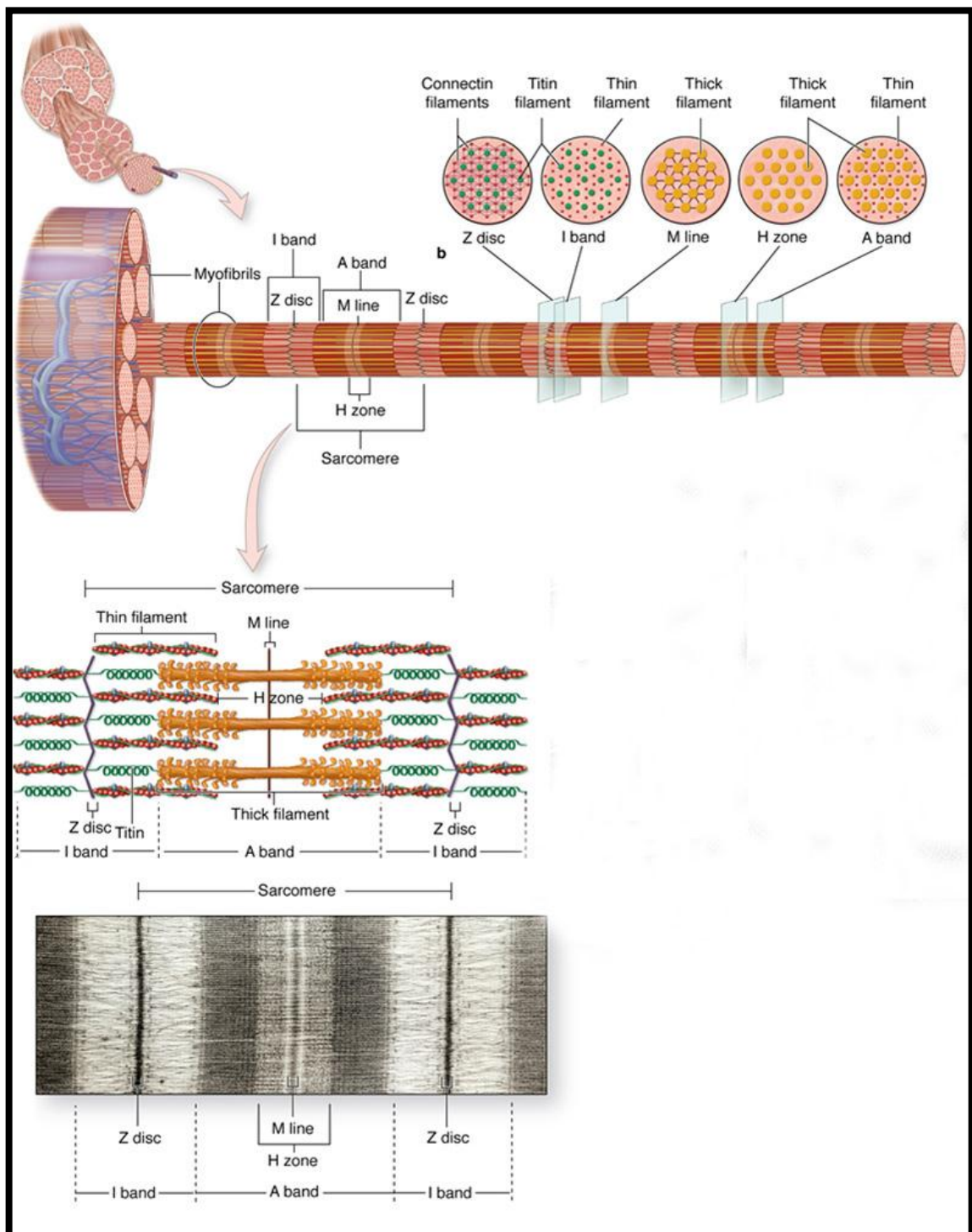


Figure 1.3. Sarcomere structure (Mescher, 2010)

Wherever transverse tubules encircle myofibrils, the tubules are linked to the membrane of sarcoplasmic reticulum (SR), which is a specialised endoplasmic reticulum of skeletal muscles that consist of a network of membrane passages. Adjacent to opposite sides of each T-tubule, there are expanded terminal cisternae of sarcoplasmic reticulum, a pair of small cisternae of sarcoplasmic reticulum plus T-tubule is known as a triad. In spite of a tight binding of the two cisternae, their fluid contents are completely separate and distinct. In the cardiac muscle cell, the sarcoplasmic reticulum lacks terminal cisternae, whereas it forms a loose network throughout the sarcoplasm of smooth muscle cells (Martini, 2006).

1.2.2. Skeletal muscle physiology

1.2.2.1. Mechanism of contraction

Resting sarcomeres show partial overlap of thick and thin filaments. Increase in amount of overlap between the filaments triggered by sliding of thin and thick filaments on each other, which lead to muscle contraction. Muscle contraction occurs following the discharge of a motor neuron at the neuromuscular junction (Mescher, 2010).

A neuron stimulates a muscle fibre through orderly steps:

1- Arrival of an action potential. When the neuronal signal arrives to nerve presynaptic terminal at the neuromuscular junction, an action potential propagates leading to calcium ion flow in the extracellular fluid which in turn causes release of acetylcholine (ACh) into the synaptic cleft as a result of permeability of the synaptic terminal membrane that induced by the action potential (Marieb, 2008).

2- ACh binds at the motor end plate. The released ACh molecules bind to their sarcolemma nicotinic receptors. This binding induces the permeability of motor end plate to sodium ions that present in a high concentration in the extracellular fluid, whereas its concentration is very low inside the cell. The Na^+ ions influx into the sarcoplasm lasts until acetylcholinesterase (AChE) enzyme eliminates ACh from its receptors (Martini, 2006).

3- Development of the action potential in the sarcolemma. Inrushing of Na^+ ions depolarize the sarcolemma. The action potential then spreads throughout the myofibrils via depolarization of sarcolemma T-tubules system which pass transversely into the muscle cells and surround each myofibril forming a membranous network with the sarcoplasmic

reticulum and end at flattened terminal cisternae which released the Ca^{2+} at the junction between the A and I bands of each sarcomere (Burkitt, 1993) (Figure 1.4).

1.2.2.2. Contraction cycle

In the resting sarcomere, myosin head charged with energy that is going to be used to power contraction. At the beginning of the contraction cycle, myosin head split ATP molecule and store the energy released in the process. ADP and phosphate which are products of ATP molecules breakdown, remain bound to the myosin head. During muscle contraction, membrane depolarization activates voltage-sensing Ca^{2+} channels in the T-tubules that in turn activates ryanodine receptor 1 (RyR1) on SR membrane to release Ca^{2+} . Subsequently, rise level of Ca^{2+} in muscle cytoplasm which is essential for contraction process (Andersson and Marks, 2010). The Ca^{2+} ions then bind to troponin-C. This binding weakens interrelate of troponin, tropomyosin and actin complex, that causes tropomyosin to be displaced, so exposing of myosin binding sites on the actin filaments. This permits the formation of cross-linkages between actin and myosin through sliding of thin on thick filaments producing contraction. Following contraction, Ca^{2+} ions are releasing from troponin and actively pumped back into the sarcoplasmic reticulum. Then the active sites of actin are re-covered by tropomyosin, resulting in the release of myosin-actin binding hence causing muscular relaxation (Ganong, 2005) (Figure 1.4).

It has established that Ca^{2+} storage, release and re-uptake require feedback control through the sarcoplasmic reticulum (SR). In fact, there are three Ca^{2+} proteins regulate these tasks. Firstly, luminal calcium-binding protein that is required for calcium storage. Secondly, sarco (endo) plasmic reticulum calcium release channels for calcium release. Finally, sarco (endo) plasmic reticulum Ca^{2+} ATPase pump (SERCA) for calcium re-uptake. The proper calcium storage, release and re-uptake are important for efficient skeletal muscle contraction and relaxation (Rossi and Dirksen, 2006). A single stimulus-contraction-relaxation sequence in a muscle is called Twitch. Twitch varies in its duration depending on the muscle type, location, internal and external environmental conditions. A single twitch can be divided into three phases: (1) The latent period. During this period, the action potential sweeps across the sarcolemma and the sarcoplasmic reticulum release Ca^{2+} ions. (2) The contraction phase. As the tension rise, calcium ions are binding to troponin, active sites on thin filaments are being

exposed, and cross-bridge interactions are occurring. (3) The relaxation phase. During this phase, calcium levels fall, active sites are covered by tropomyosin, and the number of active cross-bridges is decreased. Thereby tension falls to resting levels (Martini, 2006). When stimuli are delivered slowly enough, the tension in the muscle will relax between successive twitches. On the contrary, the high frequency delivered stimuli, the sarcoplasmic reticulum does not have time to reclaim the Ca^{2+} ions, which eliminates the relaxation phase and resulting in tetanic contraction due to twitches overlap. Such case, the contracting tension in the muscle remains constant in a steady state, and this is the maximal possible contraction (Martini, 2006).

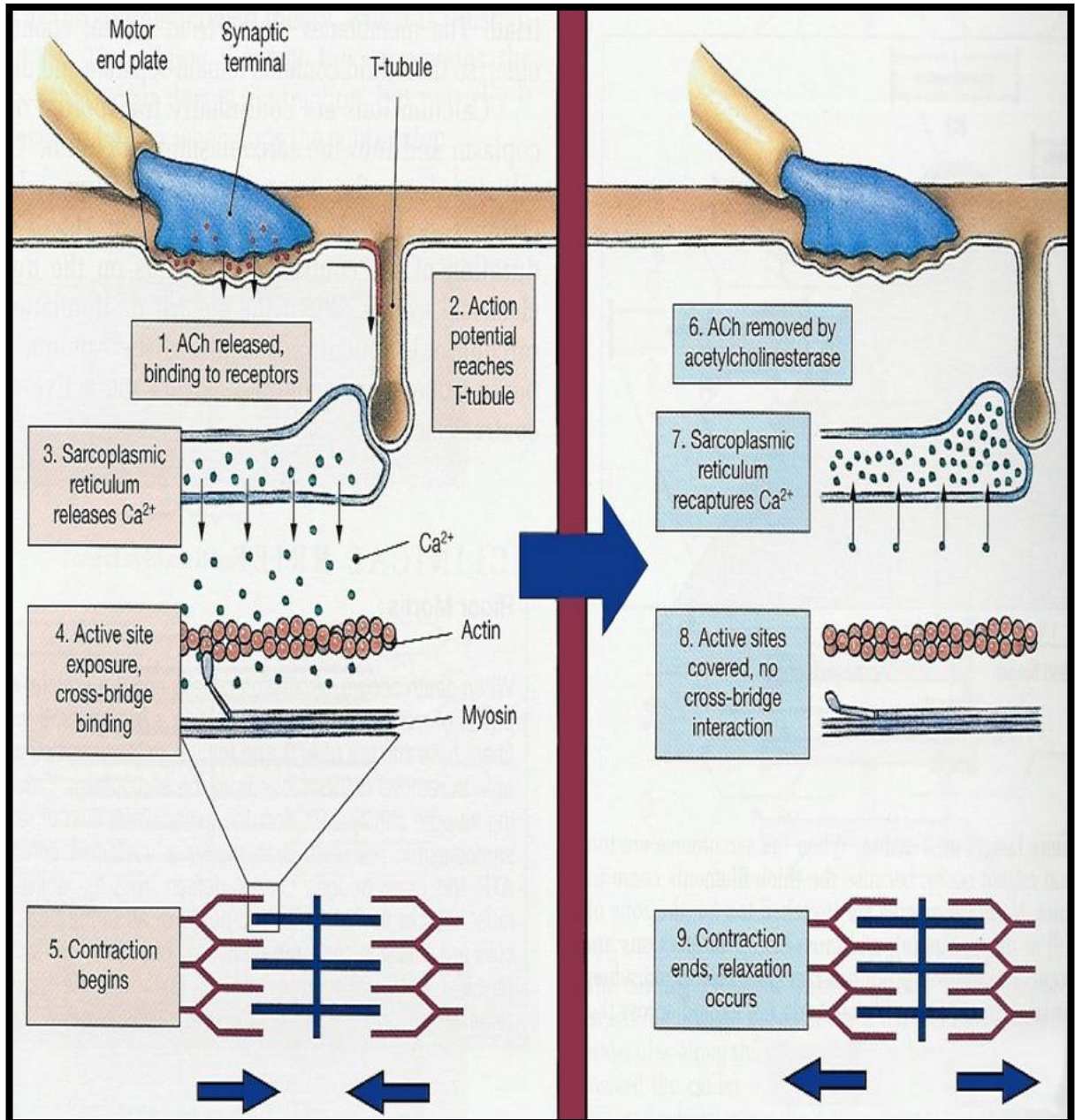


Figure 1.4. Steps involved in skeletal muscle excitation, contraction and relaxation (Martini, 2006)

1.2.3. Skeletal muscle metabolism and energy production

Skeletal muscle is a large contributor to total body mass, thus offers an important role in maintaining whole body metabolism and energy homeostasis at normal levels. It recognises as one of the key regulators of metabolism and energy by way of metabolic crosstalk between body organs (Meyer et al., 2002). Glucose and Fatty acid metabolism largely regulated by skeletal muscle. At both muscle fibres and body organs, glucose regulation is the centre of energy balance. Interestingly, skeletal muscle is able to store glucose in the form of glycogen that imparts rapid energy production for muscle contraction when glucose is not available from diet. Skeletal muscle stores amino acid in order to support energy production when other sources are depleted in elsewhere in the body (Wolfe, 2006). In support of this view, proteolysis in skeletal muscle is a critical process that can provide amino acid substrates like glutamine and alanine to augment glycogen synthesis by regulating gluconeogenesis (Perriello et al., 1997).

Skeletal muscle fibres exhibit remarkable diversity in energy metabolism initiation. Oxidative muscles using lipids as a main source for energy production, with glycolytic phenotypes depending on glucose (Demontis et al., 2013). Energy turnover in skeletal muscle increase in response to exercise and contraction. Production of ATP molecules by skeletal muscle to provide sufficient level of energy that maintain muscle contraction is dependent on the contents and activities of organelles required for a particular process (Richter et al., 2001, Kiens, 2006). Indeed, muscle cells generate ATP molecules through (1) Aerobic metabolism in mitochondria and (2) Anaerobic metabolism in the cytoplasm. During aerobic metabolism, mitochondria absorb oxygen, ADP, phosphate ions, and organic substrates such as pyruvic acid from the surrounding cytoplasm, and through Tricarboxylic Acid cycle, an enzymatic pathway that breaks down these molecules and then generates a large amount of energy which is used to make ATP. This metabolism process relies on the glucose and fatty acid which is absorbed from the circulation, as well as oxygen necessary for aerobic metabolism acquired from blood stream and so it is known as oxidative metabolism. On the other hand, when the muscle start to contract, the mitochondria begin breaking down molecules of pyruvic acid, which is providing by the enzymatic pathway of glycolysis, which breaks down glucose in the cytoplasm.

This shift from fatty acid metabolism (aerobic oxidative metabolism) to glucose metabolism enables the muscle fibres to contract for an extended period with limited availability of oxygen (Martini, 2006).

It has been documented that production and utilization of energy lead to constant metabolic rate and effective functional performance at a broad range of environmental conditions. Conversely, extend disturbance in energy homeostasis might contribute to the aetiology of many diseases. Complex pathways have evolved to adequately respond to constantly changing metabolic needs in particular for long-term adaptation that requires transcriptional regulation of metabolic genes. Moreover, nuclear receptors have been implicated in the regulation of a network of genes that involved in metabolic processes such as thermogenesis, lipogenesis and fatty acid oxidation (Desvergne et al., 2006).

1.2.4. Skeletal muscle plasticity

1.2.4.1. Muscle fibre types and distribution

In mammalian skeletal muscle, there are different types of muscle fibres that contribute to a variety of functional capabilities. The fibre types differ according to their metabolic, structural, contractile and molecular properties. During the last decades, the classification of muscle fibres based on the isoforms of myosin heavy chain (MHC), become most prevalent (Schiaffino and Reggiani, 1996, Pette and Staron, 1990, Pette and Staron, 2001). MHC encoded by a multigene family and it is the major component of the contractile apparatus combining with actin to form the actomyosin complex, which is responsible for muscle elastic and contractile properties (Kammoun et al., 2014). Classification of muscle fibres as slow or fast has traditionally been related to the type of myosin expressed which is a structural and functional protein in the muscle sarcomere, and specifically myosin heavy chain, an integral component of native myosin (Smerdu et al., 1994). Based on the myosin heavy chain content, the mammalian skeletal muscle fibres can be classified into I β , α , extra-ocular, neonatal, embryonic, IIA, IIX, IIB and IIM (masticatory) which are expressed from a large genes family (Weiss and Leinwand, 1996). The major fast isoforms present in limb muscles of small mammals are MHC IIB, MHC IID/X and MHC IIA. Other fast MHC isoforms exist, but limited distribution to specific muscles, e.g. extra ocular and masticatory

muscles. The abundant MHC isoform in slow-twitch muscle is the slow MHC I β (Pette and Staron, 2000).

Immunohistochemistry analysis of muscle tissue has revealed the existence of pure and hybrid fibre types. Pure fibre types with single MHC isoform, whereas hybrid fibres contain two or more MHC isoforms. Pair of major MHC isoforms coexists in hybrid fibres, which are classified according to their predominant isoform. Thus, the following hybrid fibres can be distinguished, type I/IIA, also termed IC, type IIA/I, also termed IIC, type IIAD, type IIDA, type IIDB and type IIBD. Collectively, the pure and hybrid fibres form a continuum from slow to fast (Pette et al., 1999). Unlike to myofibrillar proteins, C-protein, myosin-binding protein at the A-bands of the myofibril that stabilizing thick filaments of striated muscles during sarcomere assembly (Winegrad, 1999), does not show a strict correlation with the fibre type distribution in adult skeletal muscle. For instance, type II muscle fibres contain both slow and fast isoforms of the C-protein (Dhoot et al., 1985).

There are also differences in fibre types between mammalian skeletal muscles. A number of investigators have reported that the fibre type profile in rodents is different to that in human muscles. Although the presence of corresponding gene in the human genome, the type MHCIIIB protein is not detectable (Smerdu et al., 1994, Schiaffino and Mammucari, 2011).

Quantitative differences in metabolic enzyme levels in particularly of aerobic and anaerobic pathways of energy metabolism, have been also exploited to delineate muscle fibres. Aerobic (oxidative) fibres have small fibres cross-sectional area (CSA), high content of myoglobin and mitochondria. In contrast, anaerobic (glycolytic) muscle fibres display large cross-sectional area, less myoglobin, few mitochondria and rich in glycogen (Burkitt, 1993) (Table 1.1). Although classification based on MHC content does not necessarily correlate with oxidative capacity of muscle fibres, type I and IIA fibres tend to be oxidative, with type IIX and IIB muscle fibres being more glycolytic (Smerdu et al., 1994, Ciciliot et al., 2013).

As myofibre types robustly correlate to functional demands placed on the muscles. A number of studies have investigated pathways and mechanisms underpinning muscle fibre development. It was well established that the development of the slow muscle fibre phenotype is largely controlled by Protein Kinase C, Calcineurin/nuclear factor of activated T

cell (Calcineurin/NFAT), AMP Activated Protein kinase (AMPK), peroxisome proliferator-activated receptor gamma co-activator 1-alpha (PGC-1a) and Sex determining region Y-box 6 (Sox6) (Gundersen, 2011, von Hofsten et al., 2008).

Table 1.1. Muscle fibre isoforms and their physiological performance

Fiber type	Type I	Type IIA	Type IIX	Type IIB
Contraction time	Slow	Fast	Fast	Very fast
Fatigue resistance	High	Fairly high	Intermediate	Low
Activity	Aerobic	Moderate	Anaerobic	Anaerobic
Force	Low	Medium	High	Very high
Mitochondrial density	High	High	Medium	Low
Oxidative capacity	Oxidative	Oxidative	Medium	Glycolytic
Cross-sectional area	Small	intermediate	intermediate	Large
Myoglobin content	High	Low	Low	Low
Satellite cells	High	High	low	low
Connective tissue	Thick	Thick	Thin	Thin

Fast glycolytic muscle development on the other hand seems to involve the activation of the Akt signalling pathway through the transcriptional regulation by molecules including Baf60c (also called Smarcd3) and T-box 15 (Tbx15) (Meng et al., 2014, Lee et al., 2015).

The majority of studies in relation to muscle fibres distribution have unveiled that myofibres arranged in a way that slow-twitch and oxidative fast-twitch fibres increase toward the deep regions in muscles, with fast-twitch glycolytic myofibres accumulating at the superficial areas (Pullen, 1977, Gunn, 1978). Consistently, a number of investigators have reported that the deepest extensor muscles from rats, cats and pigs have a high proportion of muscle fibre type I, with less percentage of type IIB fibres. In contrast, the superficial muscles contain few number of type I fibres, and the majority is type IIB muscle fibres (Armstrong and Phelps, 1984).

1.2.4.2. Muscle fibres transition

Muscle fibres are dynamic structures with remarkable adaptive potential. Their phenotypic profiles are influenced by innervation, altered neuromuscular activity, exercise training, mechanical loading/unloading, hormonal profile and ageing. The changes in MHC isoforms tend to follow a general scheme of sequential transition from fast to slow and from slow to fast: MHCII β \leftrightarrow MHCIIA \leftrightarrow MHCIIID \leftrightarrow MHCIIIB (Pette and Staron, 2001). Remodelling of muscle fibres takes place by means of signal transduction where an extracellular stimulus interacts with cell receptors that result in activation of signalling pathways, which in turn remodel the fibres by eliciting changes in gene expression (Pette and Staron, 2001). In order to inspect genetic alteration and transition of muscle fibres in response to functional demands, numerous studies have been performed using exercise, electrical stimulation, transgenic animal models, and disease status (Bassel-Duby and Olson, 2006).

The impact of innervation on the establishment of specific muscle fibre phenotypes during development stages and the subsequent maintenance of their phenotypic properties has been demonstrated in numerous studies (Buller et al., 1960). Fast muscles turn slow when reinnervated by slow nerve, and slow muscles turn fast when reinnervated by fast nerve, most probably due to specific neural impulse patterns delivered to the muscle fibres. Similar to cross-reinnervation, chronic electrical stimulation with slow or fast motoneuron-specific impulse patterns provokes profound changes in muscle phenotype (Pette and Staron, 2001).

MHC composition of skeletal muscle is readily altered by physical exercise. It has been demonstrated that endurance exercise causes an increase in MHCIIA concomitant with a reduction in MHCIIB/X in human muscles (Scott et al., 2001). Moreover, exercise training induces muscle adaptation in order to improve the physical performance which characterized by an increase of mitochondrial biogenesis, angiogenesis and fibre type transformation (Yan et al., 2011). In the line of thought, it was revealed that the metabolic enzymes activity are largely unchanged following resistance exercise in human (Tesch et al., 1990), but a reduction in the citrate synthase activity and glycolytic capacity has been reported (Baldwin et al., 1976). Recently, it has been shown that the estrogen-related receptor gamma (*Errγ*) is robustly expressed in slow muscle and can promote the formation of oxidative fibres (Narkar et al., 2011). In addition, previous work has shown that lifting the inhibition of Akt signalling mediated by Myostatin is also a potent means of inducing the formation of glycolytic muscle fibres (Trendelenburg et al., 2009).

1.2.5. Skeletal muscle supporting tissues

1.2.5.1. Skeletal muscle capillarization

A number of physiological processes in skeletal muscle are regulated by muscle capillarization, as the density of blood vessels that serve muscle fibres can be a limiting factor to the delivery of oxygen, substrates, and hormones (Gudbjornsdottir et al., 2003). Consequently, a lower level of muscle fibre blood supply may be an important determinant of a wide range of muscle or whole-body functions.

Arteries that originated from large conduit arteries are positioned to control the total blood entering the muscle where they branching into networks of arterioles (Segal, 2005). The terminal arterioles of these networks control perfusion through blood distribution along the full length and depth of the muscle. Ultimately, the capillaries organized into microvascular units that represent the smallest volume of muscle to which blood flows and, therefore, oxygen, glucose and fatty acids delivery can be controlled (Lund et al., 1987).

The microvasculature of skeletal muscles is subject to a large number of mechanisms that responsible for blood flow regulation. Such point of view might ensure that blood supply matches the metabolic demands of the muscle fibres under resting conditions and during exercise (Mortensen and Saltin, 2014). In line with this thought, previous studies have

demonstrated that oxidative myofibres are densely vascularized due to their high expression levels of angiogenic factors, which is not the case in glycolytic phenotypes (Annex et al., 1998, Hudlicka et al., 1992, Cherwek et al., 2000).

In fact, numerous factors affect skeletal muscle capillarization. Regular exercise that boosts oxidative myofibre phenotypes can profoundly influence muscle blood supply. Such positive impact of exercise on muscle capillary density might be linked to the ability of oxidative fibres to induce a high angiogenic response (Yang et al., 2008, Cherwek et al., 2000). Recent studies have revealed a number of transcriptional regulators of oxidative myofibres can stimulate neoangiogenesis. For instance, nuclear receptor PPARgamma-coactivator-1 α (PGC-1 α) an important regulator of oxidative fibre type (Arany et al., 2008a), and peroxisomal proliferator activator receptor (PPAR δ) are known to be able to promote angiogenic genes expression in skeletal muscle (Narkar et al., 2008, Gaudel et al., 2008). Further study that investigated treating ischaemic disease in skeletal muscle has reported ameliorative effect of *Erry* on ischaemia, which might link to this nuclear receptor ability to remodel fibres types, thereby inducing angiogenic factors expression, as well as basal blood flow in the transgenic skeletal muscles (Matsakas et al., 2012b).

1.2.5.2. Skeletal muscle connective tissue

Skeletal muscle is an organ system composed not only of myofibres but also of nerves, sensory cells, blood vessels and connective tissue (Gumerson and Michele, 2011, Gillies and Lieber, 2011). Almost all connective tissue components are produced by fibroblast cells, primary cells in muscles and tendons that majorly responsible of connective tissue maintain and repair (Kuhl et al., 1984, Gatchalian et al., 1989). Although skeletal muscle myoblast cells have also been shown to contribute to collagen production, presence of fibroblast is indispensable for proper assembly of collagens into the functional extracellular matrix (ECM) (Lipton, 1977). The ECM in skeletal muscle is formed of a dynamic network of collagens and non-collagenous components like glycoproteins, proteoglycans and elastin. Fibrillar collagens (collagen I and collagen III) of ECM bear great stress within muscle and provide ECM capacity to transmit muscle contraction force to the bone via the tendons, thereby produce the movement. Non-fibrillar collagen (collagen IV) is concentrated in the basement membrane (Kjaer, 2004). Collagen IV with other components such as laminin are unique

molecules that bind to skeletal muscle complex named dystrophin-glycoprotein complex (DGC). DGC is a multicomponent complex that linking muscle fibre cytoskeleton, the sarcolemma, and the ECM into a functional unit that maintains muscle integrity (Ohlendieck et al., 1991). It is composed of three sub-complexes: (1) the sarcoglycans (α , β , γ , and δ); (2) syntrophin, nNOS, and dystrobrevin; and (3) α and β dystroglycan (Matsumura et al., 1993) (Figure 1.5). In addition to the mechanical properties of ECM compositions, they have a critical role in regulating skeletal muscle stem cells (satellite cells) activity and self-renewal, thereby muscle regeneration process (Calve et al., 2010). Moreover, there is a body of evidence that ECM components profoundly contribute and play a dynamic role in different cell signalling, facilitating cell proliferation and migration (Gillies and Lieber, 2011).

The skeletal muscle connective tissue is functionally organised into three distinct layers (Gillies and Lieber, 2011). Individual muscle fibres are surrounded by the innermost layer of

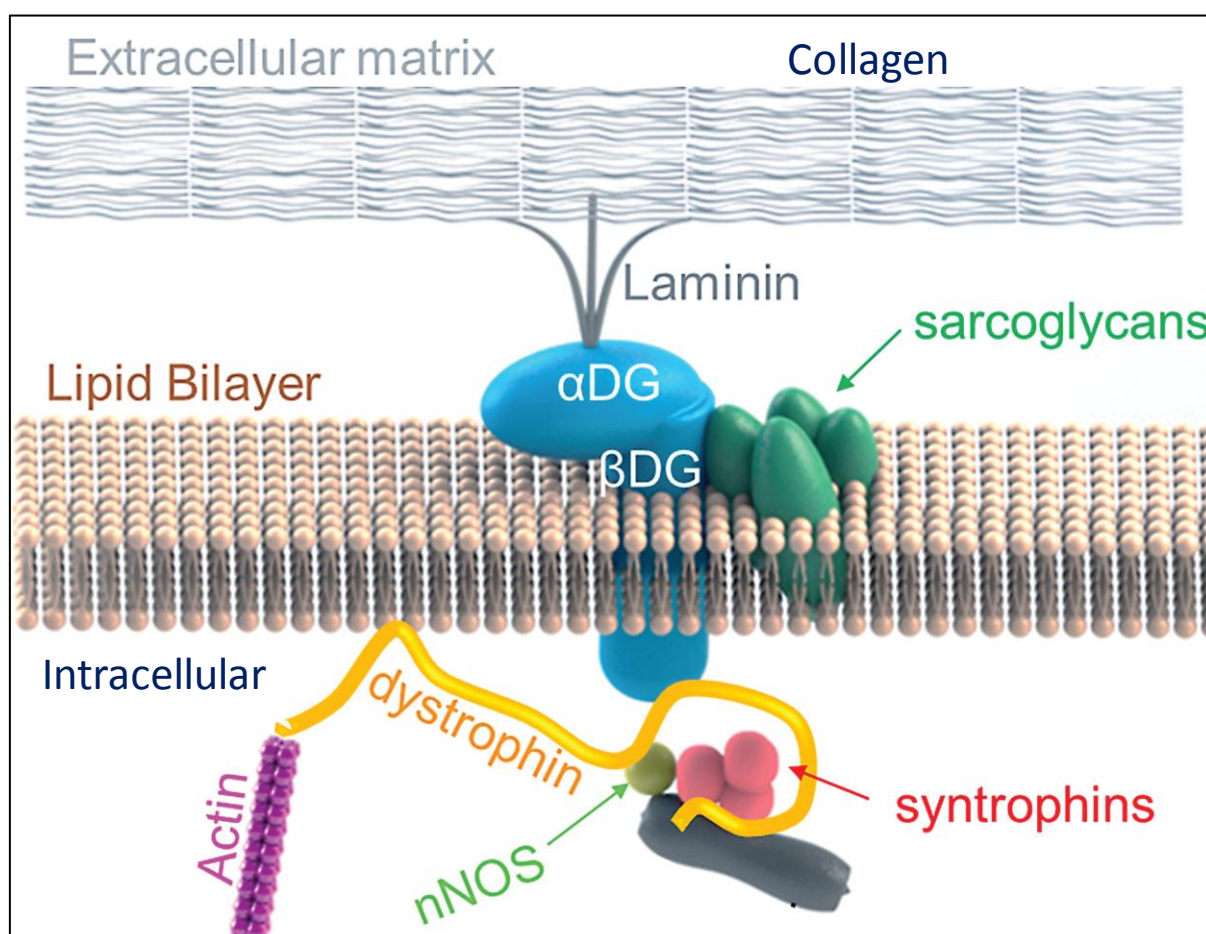


Figure 1.5. The dystrophin-glycoprotein complex (DGC) in skeletal muscle (Rodrigues et al., 2016)

connective tissue, the endomysium. The endomysial ECM is a highly ordered layer of collagen I and collagen III. It functions to transfer tension between overlapping muscle fibres and a load bearing structure upon myofibre contraction. The endomysium connecting to the sarcolemma via basement membrane that formed from two layers, internal basal lamina directly connect to the sarcolemma, and the external reticular lamina (Sanes, 2003, Campbell and Stull, 2003, Trotter and Purslow, 1992).

A number of muscle fibres are bundled together in what is termed a fascicle. Each fascicle enclosed by the second type of skeletal muscle connective tissue, the perimysium. The perimysium layer is composed of mainly collagen I and the proteoglycan decorin, and it is continuous with the tendon, so it is responsible to transmit force from muscle to bone to create movement. Blood vessels and nerves are contained within the perimysium tissue (Passerieux et al., 2007, Gillies and Lieber, 2011).

The third and outermost layer of skeletal muscle connective tissue that surrounds the entire muscle is epimysium (Gillies et al., 2014). The components of the epimysium layer are more similar to the endomysium than the perimysium, however, the collagen structure has a particular 'crimp' patterning more similar to the perimysium and tendon than the 'mesh' patterning in the endomysium (Gillies and Lieber, 2011).

A number of studies have illustrated that the amount of ECM is not constant in all muscle types. The concentration of ECM components is much lower in fast muscles compared to the slow ones (Kovanen et al., 1980). The correlation extends to the level of individual muscle fibres. The endomysium and perimysium connective tissue are greater between slow type I than the fast type II myofibres, indicating that the differences in function would be reflected on the muscle connective tissue components (Kovanen et al., 1984a).

Nevertheless, connective tissue is a part of a muscular organ, a number of studies have reported diverse impacts of molecules that regulate muscle development on muscle fibres and connective tissue compositions. Study by McPherron et al. has shown that muscle connective tissue entities fail to develop to their normal levels in mice and cattle that had mutation in their *Myostatin* gene (McPherron et al., 1997).

1.2.5.3. Skeletal muscle innervation

Proper motor control of nervous system where muscle performance can be adapted in a short term is a critical factor that enables accurate muscle functionality. Such interaction might indicate an essential role of the neural system in regulating muscle properties and determination of muscle phenotype (Buller et al., 1960). Nevertheless, skeletal muscles are often under voluntary control, a number of skeletal muscles may also be controlled at a subconscious level, such as skeletal muscles involved in breathing, like diaphragm usually works outside conscious awareness (Martini, 2006). Like that in skeletal muscle connective tissue arrangement, each nerve consists of groups of nerve axons surrounded by three connective tissue layers. The epineurium is a sheath of longitudinal collagen fibres that enclosed the entire nerve. The perineurium which is formed of connective tissue layer of concentrically laminated structure wrapped a group of nerve axons. Third layer is the endoneurium, a longitudinal collagen fibres layer condensed around each individual nerve axon (Thomas, 1963). Myelinated motor nerve gives rise to several terminal twigs within perimysium connective tissue layer. The axon loses its myelinated sheath at the site of innervation where it forms a dilated termination situated within a trough on the muscle cell surface, a structure called motor end-plate or the neuromuscular junction. There are numerous mitochondria and synaptic vesicles within the axon terminal, and other containing neurotransmitter acetylcholine (ACh). The space between axon and muscle is called synaptic cleft (Mesher, 2010).

The motor unit, consisting of a motor neuron and the myofibres it innervates. A coordination between groups of motor units is required for a single muscle contraction (Gutmann and Hanzlikova, 1966). Study on human muscles has reported positive correlation between muscle size and the number of motor units. Large muscles of the limb contain a greater number of motor units compared to small ones. For instance, Extensor digitorum brevis muscle has about 200 motor units, whereas the intrinsic muscle of the hand contains 100 motor units (McComas, 1991).

A number of studies have demonstrated that muscle fibres are regulated by the innervation pattern. Expression of myosin heavy chain (MHC) type I (slow fibre) depends on activity of slow nerve fibre. In contrast, fast MHCs (IIA, IIX and IIB) are regulated by fast innervation

pattern (Ohira et al., 2006, Patterson et al., 2006). In this line of thought, previous work has demonstrated that loss of neuronal influence may cause a slow-to-fast shift in fibre type and MHC isoform profile (Herbison et al., 1979). Moreover, muscle fibre conversion from slow-to-fast phenotypes due to denervation usually but not always accompanied by muscle atrophy that is characterized by a decrease in muscle fibre cross-sectional area (CSA) and protein content (Herbison et al., 1979). Same muscle fibre may respond differently to the denervation according to muscle type. Muscle fibres type I and type IIA from rat's soleus muscles undergo dramatic atrophy following denervation, whereas same fibre types from the extensor digitorum longus (EDL) muscles of same animal maintain essentially same size (Aravamudan et al., 2006). In addition, an increase of neuromuscular activity through endurance exercise and chronic electrical stimulation causes an increase of fast-to-slow fibre type transition evidenced by an increase in MHC type I and MHC type IIA (Pette and Vrbova, 1992). Conversely, reduction of neuromuscular activity through complete spinal cord transection appeared to induce slow-to-fast muscle fibre type conversion in soleus muscle of the cat (Roy et al., 1992). According to Buller's group (Buller et al., 1960), cross-reinnervation pattern was able to induce muscle fibre transition according to the new motor connection.

1.2.6. Skeletal muscle development

1.2.6.1. Embryonic origin of skeletal muscles

Skeletal myogenesis is an important field for studying the restriction of cell fate during embryonic, fetal and post-natal development. Skeletal muscle develops in sequential but overlapping stages (Ordhal, 2000). Muscles of the body arise from somites, segmented structures that form from paraxial mesoderm in an anterior to posterior manner. Somites receive signals from the neighbouring tissues that induce primordial muscle precursor cells to be committed in a myogenic fate (Borycki and Emerson, 2000). The somite then divides into ventromedial and dorsolateral portions. The ventromedial portion disperses into mesenchymal sclerotome where it forms the cartilages of the vertebrae and ribs. The dorsolateral portion of the somite that facing the surface ectoderm called dermomyotome epithelial that gives rise to muscle progenitor cells. The dermomyotome also gives rise to cells of the endothelial, vascular smooth muscles, dermal and brown fat lineages.

Diaphragm and tongue muscles also originated from dermomyotome via long-range migration of muscle progenitor cells (MPCs) (Tajbakhsh and Buckingham, 2000, Biressi et al., 2007). Moreover, unsegmented head mesoderm and prechordal mesoderm give rise to ocular, mandibular and superficial facial muscles (Brand-Saberi and Christ, 2000). The dermomyotome is further subdivided into two cell populations, medial and lateral that giving rise to the epaxial and hypaxial muscles (Ordhal, 2000).

In response to signals from adjacent tissues, the dermomyotomal progenitor cells become committed to the skeletal muscle lineage and form the myotome, a population of differentiated muscle cells (Tajbakhsh and Buckingham, 2000). The differentiated cells (committed muscle cell precursors) align and fuse to form the mature multinucleated myotubes. Whereas a population of undifferentiated cells remain quiescent, but are activated upon injury or degeneration of mature fibres, these are termed satellite cells and defining as stem cells (Seale and Rudnicki, 2000). Cells differentiation is accompanied by the transcriptional activation of muscle-specific genes encoding for metabolic enzymes, ion channels, neurotransmitter receptors and contractile proteins (Hastings and Emerson, 1982).

Delamination of cells from lips dermomyotome gives the start step of myogenesis process. The delaminating cells that already expressed myogenic determination factors Myf5 and Mrf4, move below the dermomyotome and rapidly differentiate into the skeletal muscle cells. In the absence of the determination factors, the early myotome does not form and instead the delaminated cells are dislocated (Bajanca et al., 2006). Study by Manceau et al. on chick and mouse embryos has shown that the epithelial cells in the central part of mature dermomyotome express Paired box3 (Pax3) and its paralogue Paired box7 (Pax7) during disintegration (Manceau et al., 2005). These cells proliferate and do not express myogenic regulatory factors or muscle proteins, however, they can give rise to skeletal muscle cells, as a result of activation of myogenic determination factor (Myf5) and myogenic differentiation (MyoD) leading to subsequent skeletal muscle differentiation. Mutation of Pax3 and Pax7 genes lacked fetal muscle development, Pax3 is transcribed in satellite cells in many, but not all skeletal muscles (Zammit et al., 2006). In fact, the majority of body muscles are derived from a highly proliferative Pax3⁺/Pax7⁺ cells that derived from the

central dermomyotome (Relaix et al., 2005, Gros et al., 2005, Kassar-Duchossoy et al., 2005). The emergence time of this cell population is mainly regulated by myotome-derived Fibroblast Growth Factor (FGF8) that stimulates expression of transcriptional factor *Snail1* in dermomyotomal cells, which in turn induce epithelial-to-mesenchymal transition (Delfini et al., 2009). Importantly, the Pax3⁺/ Pax7⁺ progenitor cells are able of both proliferation/self-renewal and differentiation along the skeletal muscle lineage (Kang and Krauss, 2010).

1.2.6.2. Satellite cells and muscle regeneration

Stem cells of skeletal muscles named satellite cells (SCs) that located beneath basal lamina were first discovered by electron microscopic study of skeletal muscle fibres (MAURO, 1961). Reznik was the first who showed that satellite cells function as myoblast and he labelled them as stem cells (Reznik, 1969). These cells were firstly identified in the muscle of the frog, but then immediately confirmed to reside in rat muscle and later found to occupy a common anatomical position in a majority of vertebrates (Grounds and Yablonka-Reuveni, 1993). In normal muscle cell (non-injured), satellite cells are quiescent and it has few organelles with high nuclear-to-cytoplasm ratio, and small size nuclear compared to the adjacent nucleus of myotubes. However, it appears as swelling on the myofibres with cytoplasmic processes after activation (Schultz and McCormick, 1994).

Almost all quiescent satellite cells are expressing CD34 and Myf5, thus it was believed that these markers playing a role in maintenance satellite cells quiescence (Beauchamp et al., 2000). However, Bjornson et al. demonstrated that Notch signalling is crucial for maintenance satellite cells quiescence. Same study reported that deletion of satellite cell specific recombining binding protein- κ (RBP- κ) led to spontaneous activation of the cells, which terminated by cell differentiation and fusing with muscle fibre. Thus, depletion of satellite cells pool, hence the skeletal muscle lost the capacity of regeneration following injury (Bjornson et al., 2012).

It was well established that satellite cells on isolated muscle fibre were stimulated to activate and divide by a mitogen originated from crushed skeletal muscle, indicating an external factor act upon the quiescent satellite cells (Bischoff, 1986). Consistently, Allen and Boxhorn have shown that the inhibitory effect of Transforming Growth Factor beta (TGF- β)

on satellite cells differentiation is probably mediating by the mitogen lineage (Allen and Boxhorn, 1987). The mitogenic response of satellite cells in contact with cultured myofibres is reduced compared to the isolated cells, indicating a vital role of myofibre to initiate satellite cells activation response, which provides evidence of the critical role of niche environment in regulating satellite cells behaviour (Bischoff, 1990).

For a better understanding of satellite cells functions, describing of molecular mechanisms that control their behaviour is required. A number of studies have demonstrated that Pax3 and Pax7 are members of Paired Box family of transcriptional factors play a vital role during muscle myogenesis (Bopp et al., 1986, Goulding et al., 1991). Although their structural homology, Pax3 and Pax7 have different functions during embryological development. Pax3 is expressed in the developing presomitic mesoderm, however, it becomes localized into the dermomyotome following somite differentiation (Goulding et al., 1991). It is necessary for myoblast migration, thus its absence results in the loss muscle precursor migration from the hypaxial dermomyotome into the limbs and tongue (Goulding et al., 1994, Epstein et al., 1996). Moreover, it was well established that Pax3 is involving in regulating precursor cells entry to the myogenic lineage through acting upstream of the myogenic regulating factor MyoD in mouse embryo (Tajbakhsh et al., 1997). Further investigation has revealed a high affinity of Pax3 to Myf5 promoter enables it to bind 145-base pair elements, which is essential for Myf5 transcription (Bajard et al., 2006). Pax7 is expressed in the developing dermomyotome, indicating its role during muscle myogenesis (Jostes et al., 1990). Previous studies have demonstrated that Pax7 is essential for satellite cells lineage specification, as well as renewal and propagation of satellite cells population throughout embryogenesis and adulthood (Seale et al., 2000, Oustanina et al., 2004). Furthermore, Pax7 has been shown to have a critical role as a cell survival signal for satellite cells mediating by the prevention of the expression of the myogenic regulating factors MyoD and myogenin (Olguin and Olwin, 2004). In support of this view, myogenin has been shown to downregulate Pax7 expression in order to allow muscle cells differentiation to proceed (Olguin et al., 2007). Additionally, *Pax7*-null mice, progressive loss of satellite cells during adulthood with or without expressing of Pax3, indicating that Pax3 cannot compensate Pax7 anti-apoptotic role (Relaix et al., 2005).

Using Pax3 and Pax7 as satellite cell markers has provided evidence that these cells remain as progenitors throughout late foetal development, then developed beneath basal lamina where they take up the position of quiescent satellite cells (Gros et al., 2005, Relaix et al., 2005). Indeed, embryonic and foetal muscle develops through two stages, primary and secondary myogenesis, and these processes are carried out by primary and secondary myoblasts, respectively (Feldman and Stockdale, 1992). Nevertheless, it was thought that satellite cells are a final population of myoblasts during late foetal development, Gros and Relaix have demonstrated that satellite cells emerge from an undifferentiated population of stem cells that originated from embryonic dermomyotome (Gros et al., 2005, Relaix et al., 2005).

Satellite cell numbers per single myofibres vary in different muscles depending on the muscle fibre composition (i.e. slow oxidative, fast oxidative or fast glycolytic fibres). It has been illustrated that soleus muscle, which is mainly made up of slow oxidative fibres, contains a higher number of satellite cells compared to the Extensor digitorum longus (EDL) muscle that shows fast glycolytic fibres predominant. Moreover, despite the reduction in satellite cell populations in both soleus and EDL muscle with age advance, it has been shown that soleus muscle shows an increase in satellite cell numbers between 1-12 months of mice age, which is not the case in EDL muscle (Gibson and Schultz, 1983).

Muscle development and regeneration share common features because the molecular mechanisms underpinning the development are reactivated for tissue reconstruction after injury (Charge and Rudnicki, 2004, Hawke and Garry, 2001). Satellite cells characterised by its ability to regenerate damaged skeletal muscle fibres (Moss and Leblond, 1971). Further work has reported that the satellite cells pool not only responsible for replenishing of damaged muscles, but also repopulate its own cell pool that is essential for tissue repairing following further injuries (Collins et al., 2005). It seems that the satellite cells carry out dual functions: it provides differentiating progeny that will fuse with both new and damaged myofibre, meanwhile repopulate the stem cells pool through a self-renewal mechanism. Two possible mechanisms by which satellite cells maintain their pool. A subpopulation of satellite cells stop progression down the myogenic lineage and revert to the quiescent state, alternatively, a subpopulation of satellite cells must divide into differentiating and stem cell

progeny (Zammit et al., 2004, Kuang et al., 2008). Following muscle injury, satellite cells activate, then the majority of the activated cells switch on the expression of the myogenic regulating factor MyoD, and thereafter differentiate (Cornelison and Wold, 1997, Zammit et al., 2004). Zammit then showed that a subset of the activated satellite cells (MyoD⁺) switch off this marker, simultaneously retaining Pax7 expression, thereby these cells retain to a quiescent state and replenish the satellite cell pool (Zammit et al., 2004) (Figure 1.6). Others demonstrated that satellite cells have also been shown to divide asymmetrically giving differential daughter (Shinin et al., 2006, Kuang et al., 2007).

It was well documented that satellite cell in contact with basal lamina of the muscle fibre retains its stem cell state, whereas cell that loses its contact initiates Myf5 expression and subsequently differentiate. Such scenarios indicate the crucial role of the niche environment in controlling satellite cells proliferation and differentiation (Bischoff, 1990).

Previous work has reported that canonical Wnt plays a role in regulating satellite cells proliferation in response to muscle damage (Otto et al., 2008). Moreover, canonical Wnt regulates MyoD during muscle development and regeneration (Munsterberg et al., 1995). In addition, study by Wei and Paterson (Wei and Paterson, 2001) has demonstrated that cyclin D1 (a Wnt β -catenin target gene) induces expression of cyclin dependent kinase (Cdk) Cdk4. The later directly bind to MyoD and inactivate it, allowing cell cycle progression until mitogenic signal is depleted. Following mitogen depletion, cyclin D1 level drops, and thereby Cdk4 repression of MyoD activity is disappear, ultimately allowed MyoD to induce myogenic gene transcription and myoblast proliferation and differentiation.

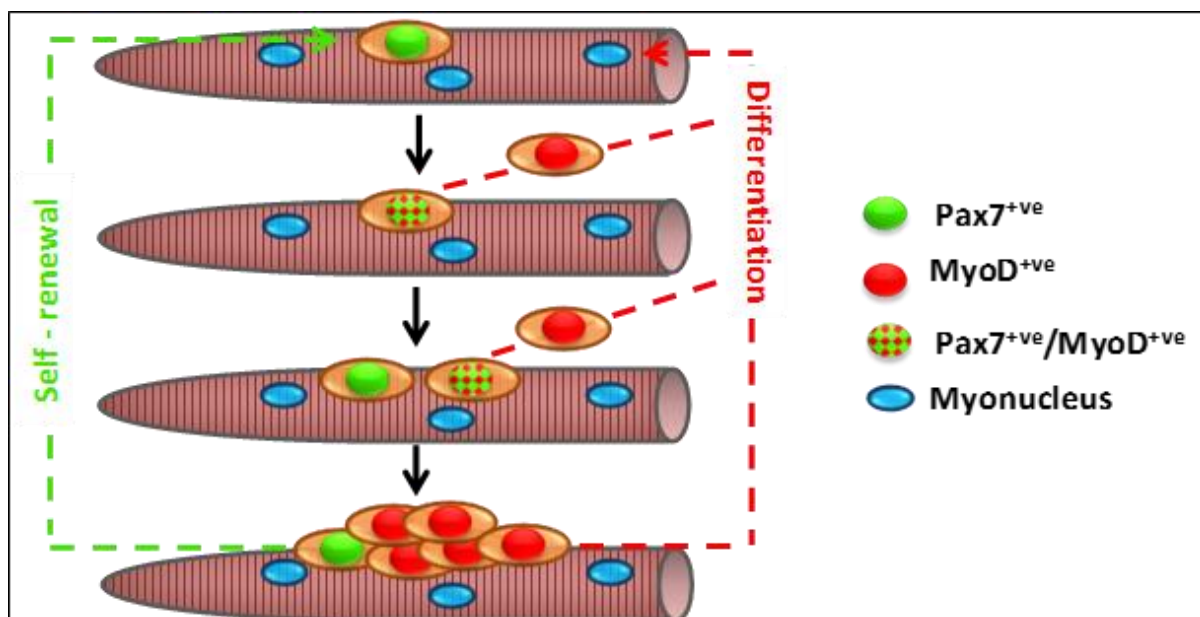


Figure 1.6. Satellite cells self-renewal

Quiescent satellite cells (green) activate, co-express Pax7 and MyoD (green and red tartan), and then most proliferate, down-regulate Pax7, maintain MyoD (red), and differentiate (red pathway) to produce myonuclei. A subpopulation of activated (green and red tartan) satellite cells down-regulate MyoD expression and cycle while maintaining only Pax7 (green). Thus renewing the satellite cell pool (green pathway), adapted from (Musaro, 2014).

1.7. Myostatin

Myostatin is a member of the Transforming Growth Factor- β (TGF- β) superfamily, is predominantly secreted by skeletal muscle to negatively regulate its growth and development. It is an autocrine/paracrine inhibitor of muscle growth that expressed in cells of the skeletal muscle lineage from embryonic myotome to striated muscle in adult (McPherron et al., 1997). Consistent with this view, localized ectopic expression of *Myostatin* was attained by vector modulate gene electro transfer to tibialis anterior (TA) muscle of adult rat results in a decrease in muscle fibre cross-sectional area (CSA) and subsequently muscle mass diminish. Moreover, noticeable reduction in the expression of muscle structural genes (MHC IIB, troponin I and desmin), as well as expression of myogenic

transcription factors MyoD and myogenin, was also reported (Durieux et al., 2007). Genetic evidence demonstrates that *Myostatin* has a pivotal role in regulating skeletal muscle mass and function, since deletion of the gene produces mice with a phenotypes exhibiting a dramatic increase in skeletal muscle mass due to hyperplasia, an increase in absolute number of muscle fibres, and hypertrophy, an increase in the cross-sectional area of individual muscle fibre (McPherron et al., 1997, Mendias et al., 2006). Beside mouse model, the double-muscling phenotype due to *Myostatin* mutation has been observed in cattle, sheep, dogs and human (McPherron and Lee, 1997, Kambadur et al., 1997, Clop et al., 2006). A sequence designated *Myostatin* was obtained by using oligonucleotide corresponding to highly conserved regions among the TGF- β superfamily members as primers for polymerase chain reaction (PCR) on mouse genomic DNA. The obtained Myostatin protein sequence had all the features of TGF- β superfamily members, including secretion single sequence, a proteolytic processing site and a carboxylic terminal region containing the conserved pattern of nine cysteine residues (McPherron et al., 1997).

In fact, the biological function of *Myostatin* is not only restricted to suppress skeletal muscle growth. It regulates muscle stem cells proliferation and differentiation, as well as fibre type switch (McCroskery et al., 2003, Thomas et al., 2000). *In vitro* study by Taylor et al. has revealed an inhibitory effect of *Myostatin* on protein synthesis in both myoblast and myotubes (Taylor et al., 2001). Although it is expressed in lower level in adipose tissue compared to muscle tissue, it has been demonstrated that *Myostatin* is profoundly involved in adipogenesis (Feldman et al., 2006). Moreover, previous work has reported that *Myostatin* induces proliferation of muscle fibroblast therefore it increases the deposition of ECM components (Li et al., 2008).

Despite the enormous muscle develops in the absence of *Myostatin*, loss of this gene expression in young mice is associated with specific metabolism features in skeletal muscles. Early studies provided evidence that absence of *Myostatin* leads, despite the enlarged muscle mass, to loss of oxidative properties, with impaired in oxidative enzymes activity, and a reduction in muscle capillary density (Amthor et al., 2007, Lipina et al., 2010, Savage and McPherron, 2010). Further evidence regarding a metabolic deregulation due to *Myostatin* deficient was shown by Ploquin et al. reported perturbations in the inter-

myofibrillar mitochondrial respiration of young *Myostatin* knockout (*Mtn*^{-/-}) glycolytic muscles, that was associated with an increase in muscle fatigability during contractility tests (Ploquin et al., 2012). Furthermore, there was a decline in muscle force generation, as well as specific tetanic tension in *Mtn*^{-/-} muscles, suggesting that muscle mass increase in *Myostatin* mutant animals confers no strength advantage more than the control animals (Amthor et al., 2007). Other findings by Amthor et al. illustrated predominantly of muscle fibre type IIB, with a marked reduction in type IIA and IIX fibres in the extensor digitorum longus (EDL) muscle from *Myostatin* null mice, as well as in tibialis anterior (TA) and gastrocnemius muscles of the same genotype (Amthor et al., 2007). These data were supported by findings of Girgenrath's work (Girgenrath et al., 2005). In addition, a reduction of oxidative enzymes activity in *Mtn*^{-/-} muscle was associated with high proportion of fast glycolytic myofibres that contains fewer mitochondria compared to oxidative phenotypes. Consistently, Mitochondrial density, and the mtDNA copies number per myonucleus in muscle with *Myostatin* mutation was lower than that seen even in glycolytic fibres of wild type muscle (Amthor et al., 2007, Girgenrath et al., 2005).

1.7.1. Effects of *Myostatin* on muscle cells proliferation and differentiation

Myostatin is a negative regulator of skeletal muscle growth, an effect attributed to inhibition of both myoblast proliferation and differentiation. It arrests myoblast cell cycle at the G1-phase. Several studies have demonstrated that *Myostatin* induces satellite cells quiescence is associated with the up-regulation of the cyclin-dependent kinase (Cdk) inhibitor p21, the decrease in Cdk2 activity, and decrease phosphorylation of retinoblastoma (Rb) protein (Thomas et al., 2000, Joulia et al., 2003). Moreover, it has been shown that *Myostatin* increases cyclin D1 protein degradation that in turn causes G1 cell cycle arrest through PI3K/Akt/ (Glycogen synthase kinase-3 beta) GSK-3 β signalling pathway (Yang et al., 2007). Importantly, *Myostatin* inhibits myoblast differentiation by downregulating the expression of myogenic regulating factors, MyoD, myogenin and Myf5, as well as the activity of their downstream target creatine kinase (Huang et al., 2007, Joulia et al., 2003, Langley et al., 2002).

Satellite cell promotes post-natal muscle growth and repair. McCroskery reported that *Myostatin* has also been able to maintain satellite cells quiescence at this stage (McCroskery

et al., 2003). Analysis of cell cycle has confirmed *Myostatin* potential to up-regulate p21, simultaneously reduces Cdk2 level and activity, indicating *Myostatin* potential to prevent transition from G1 to S-phase of the cell cycle, thereby maintains satellite cells at quiescent status (McCroskery et al., 2003).

1.7.2. Structure and proteolytic processing of Myostatin

Similar to other members of TGF- β superfamily, Myostatin is synthesized as a precursor protein composed of a signal sequence, an N-terminal propeptide domain, and a C-terminal considered as the active molecule. *Myostatin* is expressed in mouse muscles at about 9.5 days post-coitum, and it can be detected in the developing skeletal muscle throughout the myogenic embryogenesis (Lee, 2004, McPherron and Lee, 1997). The full length Myostatin protein is proteolytically processed to form an amino terminal propeptide and a disulfide-linked dimer of carboxy-terminal fragments. The Myostatin protein can be detected in skeletal muscle and in circulation in an inactive latent complex (Myostatin propeptide bound to the mature region) (Lee, 2004, Patel and Amthor, 2005, Walsh and Celeste, 2005). Indeed, two proteolytic cleavages are required to liberate the mature region and allow Myostatin signalling. The first cleavage by furin family enzymes that removes the 24 amino acid signal peptide, and the second cleavage by Bone morphogenetic protein 1 BMP1/Tolloid matrix metalloproteinase (Lee, 2004). Mature Myostatin dimer can be found bound to a number of proteins that are able to moderate its secretion, activation, or receptor binding (Lee and McPherron, 2001).

1.7.3. Myostatin signalling pathway

Mechanism of Myostatin signal is similar to that of TGF- β . It initiates an intracellular signalling cascade by firstly binding to the activin type II receptor (ActRIIB), which leads to the recruitment and activation of the activin receptor-like kinase 4 and 5 (ALK4 and ALK5) to form a heterotetrameric receptor complex (Shi and Massague, 2003). Two intracellular signalling cascades have been described that are activated through phosphorylation mediated by the receptor complex. Phosphorylation of Smad2 and Smad3 enabling an interaction and form a complex with Smad4 that translocates into the nucleus, where it is involved in regulating the transcription of target genes (Shi and Massague, 2003, Feldman et

al., 2006). Myostatin initiates another signalling pathway without the involvement of Smad2 and Smad3 phosphorylation, by preventing phosphorylation and thereby inhibition of Akt, which in turn results in activation of FoxO that leads to protein degradation, and hence muscle atrophy through either proteasome or autophagy mechanisms (Trendelenburg et al., 2009) (Figure 1.7).

It has been shown that there is another group of Smads, Inhibitory Smads (I-Smads) that are responsible to terminate TGF- β signalling (Shi and Massague, 2003), include Smad6 and Smad7 (Attisano and Wrana, 2000). There is evidence that Smad7 provides a negative feedback loop mechanism to inhibit Myostatin signal pathway (Zhu et al., 2004).

Another molecule can interact and influence Myostatin signalling pathway is FoxO1. FoxO1 is a member of the Fork head box O (Fox O) transcription factor family (Murray et al., 2013). It is known to be expressed in skeletal muscle and to be involved in regulating of genes expression during muscle atrophy, particularly in the activation of ubiquitin ligase expression, which leads to protein degradation. FoxO1 has recently been associated with Myostatin pathway. Several FoxO boxes have been characterized in the mouse *Myostatin* promoter, and activity of this promoter can be profoundly induced by FoxO1. This suggests that FoxO1 could enhance muscle atrophy through two paths, inducing protein degradation, as well as through inhibition of myogenesis and protein synthesis mediating by promoting *Myostatin* expression (Allen and Unterman, 2007).

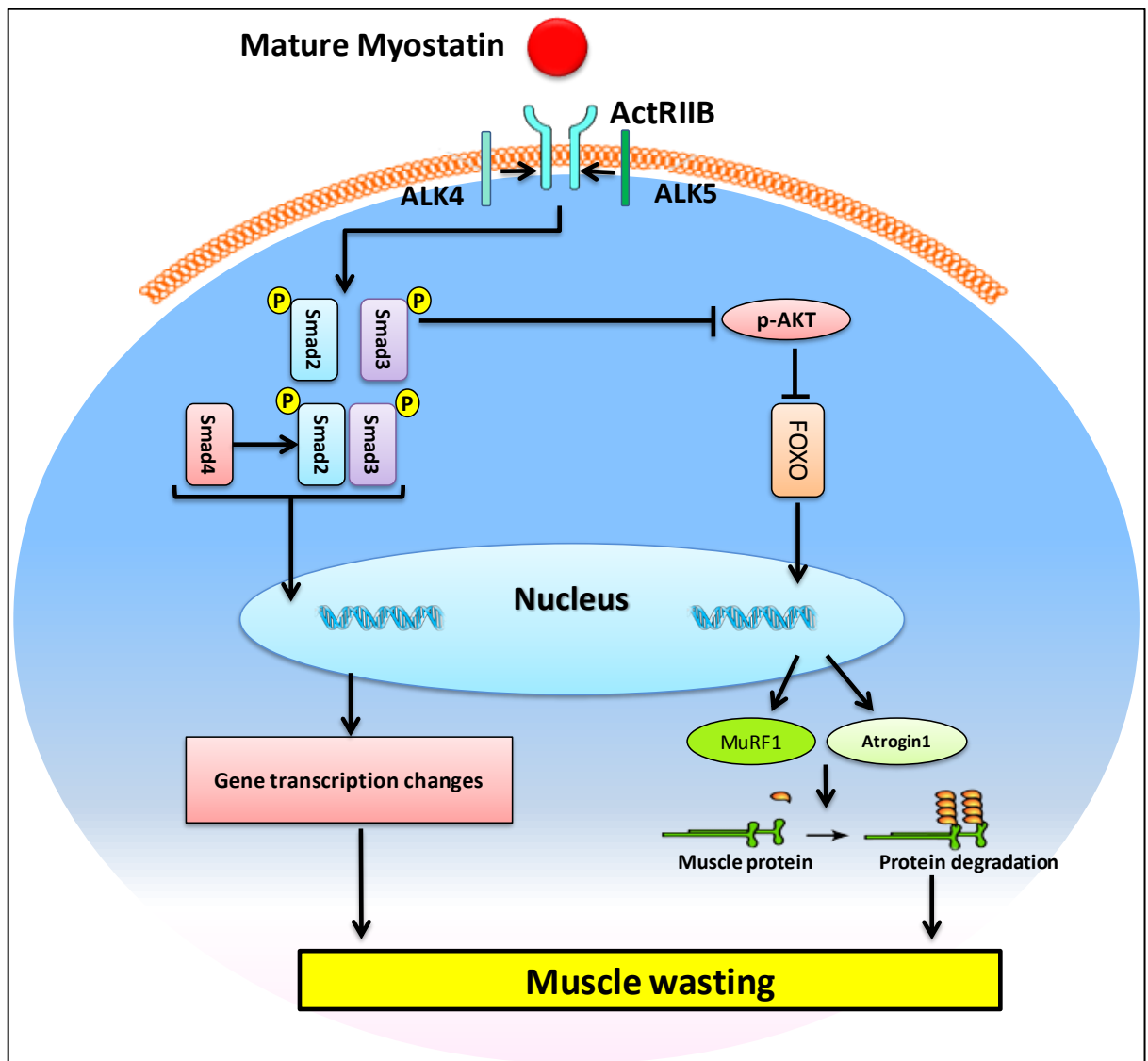


Figure 1.7. Myostatin signalling pathway

1.7.4. Post-developmental blocking of Myostatin

Skeletal muscle wasting occurs in a variety of pathological settings. A majority of studies into the relationship between *Myostatin* and muscle mass have revealed an increase in *Myostatin* expression in disease states causing muscle wasting. Previous studies have found an increase in *Myostatin* level in ageing subjects (Yarasheski et al., 2002), as well as due to immobilization or prolonged bed rest (Reardon et al., 2001, Zachwieja et al., 1999). Consistently, it has been shown that patients with acquired immune deficiency syndrome AIDS, renal failure and heart failure show a high level of *Myostatin* (Gonzalez-Cadavid et al.,

1998, Sun et al., 2006, Breitbart et al., 2011). Following *Myostatin* discovery (McPherron et al., 1997), extensive studies have unveiled a remarkable increase in muscle mass of a range of species due to *Myostatin* ablation (McPherron and Lee, 1997, Schuelke et al., 2004, Mosher et al., 2007). Therefore, a number of strategies to inhibit Myostatin signalling have been proposed, given the therapeutic potential of stimulating muscle growth or preventing muscle loss in settings of diseases that induce muscle wasting. A modified Myostatin propeptide which blocks Myostatin signalling has been applied to enhance muscle growth in normal mice, as well as to ameliorate the dystrophic characteristics of the *mdx* mice, a model of Duchenne muscular dystrophy (DMD) (Matsakas et al., 2009, Bogdanovich et al., 2005). Similarly, administration of follistatin, a secreted glycoprotein that can bind Myostatin and inhibit its interaction with ActRIIB, has been reported to induce muscle mass (Haidet et al., 2008, Nakatani et al., 2008). Moreover, neutralizing Myostatin antibody was described as a potential method to block Myostatin pathway in adult mice, hence motivate muscle growth (Krivickas et al., 2009, Wagner et al., 2008). Furthermore, administration of soluble ActRIIB causes an increase in muscle mass of wild type and *Myostatin* null mice, indicating that in addition to Myostatin, there are other ligands contribute to limit muscle development (Lee et al., 2005). Indeed, these investigations indicate that the regulatory role of Myostatin is not limited to muscle developmental stage.

Unlike *Myostatin* genetic deletion, hypertrophy without hyperplasia was found in mice with Myostatin inhibition at post-natal stage (Girgenrath et al., 2005, Lee et al., 2005, Whitemore et al., 2003, Zhu et al., 2000). The changes in muscle fibre number and distribution seen in *Myostatin* null mice, do not occur following Myostatin inhibition in adult animals (Girgenrath et al., 2005, Matsakas et al., 2009, Welle et al., 2007). In this line of thought, it has been shown that treatment with anti-Myostatin antibody did not rescue the decrease in force output in *mdx* mice, however, administration of Myostatin propeptide results in an increase of specific force output of these animals, implies different implications of Myostatin blocking strategies (Lee, 2004, Bogdanovich et al., 2002, Bogdanovich et al., 2005).

1.8. Mechanisms regulate skeletal muscle mass

Skeletal muscle mass increases during post-natal development through hypertrophy process. In adult muscle, a similar process can be induced in response to contractile activity such as strength exercise and specific hormones (Bottinelli et al., 1991). Muscle mass is tightly regulated by a dynamic control of the processes of protein synthesis and degradation (Conlon and Raff, 1999). In fact, multiple processes operate according to highly interconnected signalling networks that coordinate quality control mechanisms to maintain protein homeostasis (Morimoto and Cuervo, 2014). Insulin-like growth factor-1 (IGF-1) has long been implicated in controlling skeletal muscle growth. It is able to increase protein synthesis within cells (Russell-Jones et al., 1994). Previous work has demonstrated that transgenic mice overexpression of *IGF-1* show muscle hypertrophy (Coleman et al., 1995), whereas *IGF-1* null mice are smaller than wild type (Miyake et al., 2007). Insulin-like growth factor 1- phosphoinositide- 3-kinase - Akt/protein kinase B - mammalian target of rapamycin (IGF1-PI3K-Akt/PKB-mTOR) pathway has been positively implicated in muscle growth (Glass, 2010, Sandri, 2008). IGF-1 signalling acts through IGF-1 receptor at the cell membrane, binding of IGF-1 to its receptor leads to generate docking sites for insulin receptor substrate (IRS), which is also phosphorylated by the IGF1 receptor. Phosphorylated IRS then acts as docking site to recruit and activate phosphatidylinositol-3-kinase (PI3K) which phosphorylates membrane phospholipids, generating phosphoinositide-3,4,5-trisphosphate (PIP3) from phosphoinositide-4,5-bisphosphate (PIP2). Then PIP3 acts as a docking site for two kinases, phosphoinositide dependent kinase 1 (PDK1) and Akt. PDK1 in turn phosphorylates and activates Akt. The phosphorylated Akt stimulates protein synthesis via the mammalian target of rapamycin (mTOR) and glycogen synthase kinase 3 β (GSK3 β), meanwhile, inhibits protein degradation by phosphorylating and thus repressing the transcription factors of the FoxO family (Manning and Cantley, 2007). Akt activates mTOR in an indirect way; it inhibits the tuberous sclerosis complex (TSC) proteins 1 and 2 in order to activate mTOR signalling. mTOR forms two complexes, mTORC1 when bound to Raptor, and mTORC2 when bound to Rictor that is required for Akt phosphorylation and activation (Zoncu et al., 2011). mTORC1 stimulates protein synthesis by phosphorylating S6 kinase (S6K) to activate ribosomal protein S6 and other factors involved in translation initiation and elongation. Simultaneously, mTORC1 phosphorylates the inhibitory eIF4E binding proteins

(4EBPs) in order to activate eukaryotic translation initiation factor 4E (eIF4E) (Guertin et al., 2006). S6K can negatively affect this pathway by phosphorylating and inhibiting IRS, thus inducing its degradation and alters cell localization (Harrington et al., 2004). On the other hand, FoxO factors that were phosphorylated and inactivated by Akt, are required for the transcriptional regulation of the ubiquitin ligases Atrogin-1, and muscle ring finger 1 (MuRF1), leading to the ubiquitylation and degradation of myosin and other muscle proteins via the proteasome. FoxO factors are also required for the transcriptional regulation of the microtubule-associated protein 1 light chain 3 (LC3), which together with BCL2/adenovirus E1B interacting protein 3 (BNIP3) are essential for the autophagy-lysosome pathway activation (Sandri et al., 2004, Stitt et al., 2004, Li et al., 2007a). In feed-forward mechanism, Atrogin-1, which is activated by FoxO can act as a coactivator of FoxO (Li et al., 2007a) (Figure 1.8).

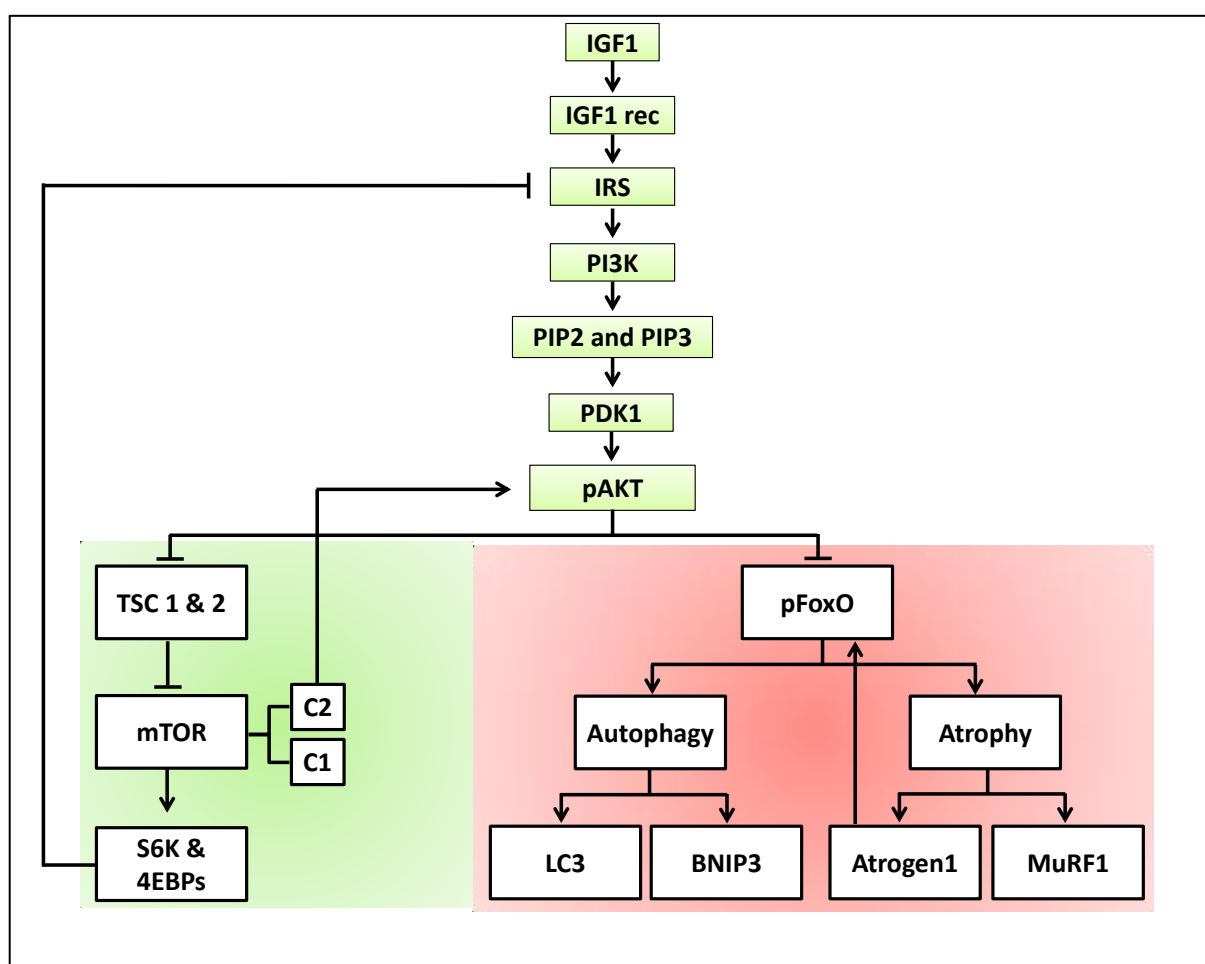


Figure 1.8. Muscle mass balance, adapted from (Schiaffino and Mammucari, 2011)

Alternatively, it has been mentioned that Myostatin acts via its receptor (ActRIIB) on Smad2 and Smad3, inhibitors of Akt, thereby downregulating IGF1-PI3K-Akt/PKB-mTOR hypertrophy pathway (Trendelenburg et al., 2009, Sartori et al., 2009). Myostatin also increases the level of the active form of FoxO, enabling increased expression of atrophy and autophagy-related genes, ultimately induces protein degradation (Greer et al., 2007). A number of studies have provided evidence that Myostatin acts as a negative regulator of Akt/mTOR signalling pathway consistent with its inhibitory effects on protein synthesis (Lipina et al., 2010, Sartori et al., 2009, Trendelenburg et al., 2009). By contrast, *Myostatin* deletion or post-natal inhibition that causes inhibition of Smad3 activity, is critical for activation of Akt/mTOR signalling, which drives muscle growth by stimulating protein synthesis. Therefore, a direct interaction between Smad3 and Akt, may be involved in cross-talk between the Myostatin and IGF1 pathway in skeletal muscle (Conery et al., 2004).

Autophagy, a dynamically regulated process that is responsible for degradation of long lived proteins and other organelles (Eisenberg-Lerner et al., 2009, Klionsky, 2010), begins with the formation of double-membrane autophagosomes that is initiated by PI3 kinase (PI3K) type III-Atg6/Beclin-1 cascade (Xie and Klionsky, 2007). In the same line of thought, previous work has reported that PI3K /Akt/mTOR pathway is a negative regulator for the formation of autophagosomes, thereby prevents autophagy process (Geng and Klionsky, 2008). On the other hand, a number of investigators have demonstrated that AMPK induces autophagy. It phosphorylates and activates TSC1, which in turn results in inhibiting of mTORC1, and hence suppresses protein synthesis (Meley et al., 2006, Inoki et al., 2003). These studies suggest that the interaction between the mentioned anabolic and catabolic pathways is crucial for proper skeletal muscle growth.

1.9. Estrogen-related receptor gamma (*Errγ*)

1.9.1. *Errγ* is orphan nuclear receptor

Nuclear receptors (NRs) are members of a large family of transcription factors that coordinate and regulate gene expression in cellular processes. The NRs comprised of two groups, ligand-regulated receptors, or receptors for which no endogenous ligands have been yet identified, thus they are defined as orphan nuclear receptors (Mangelsdorf et al., 1995, Gronemeyer and Laudet, 1995, Giguere, 2008). Mitochondria perform functions

related to several biochemical processes. A number of nuclear receptors have implicated in controlling a network of genes that regulate mitochondrial function. Peroxisome proliferator-activated receptors (PPARs) α , δ and γ have been associated with control of expression of genes related to fatty acid oxidation (FAO) and oxidative phosphorylation (OXPHOS) pathways, but not expression of genes that make up the respiratory chain (Gulick et al., 1994, Alaynick, 2008). The nuclear receptors known nuclear respiratory factor 1 and 2 (NRF-1 and NRF-2) have also been associated with regulation of a number of nuclear-encoded mitochondrial proteins (Scarpulla, 2008).

A large body of recent work has established that the estrogen-related receptors (Errs), a specific class of orphan nuclear receptors, act as comprehensive regulators of nuclear mitochondrial gene expression (Giguere, 2008). Although the name reflects their molecular origin, the ERRs do not bind natural estrogens and they do not have roles in classic estrogen signalling pathway. Previous work has reported that there is a marked preference for the recognition of the sequence TCAAGGTAA for the ERRs that named estrogen-related response element (ERRE). The important functional characteristic of ERRs is their ability to bind close to the promoters, which provides profound advantages to these receptors in term of identification and characterization of their target genes (Deblois et al., 2009). Notably, the ERRs are expressed in lipid metabolism and highly energy demands tissues, and their transcriptional activity is largely associated with presence of co-regulators that implicated in controlling complex metabolic programs. Along the same lines, ERRs control the expression of a wide range of genes, in particular those genes involved in mitochondrial biogenesis and functions (Giguere, 2008).

ERRs subfamily consisting of three members, estrogen-related receptor alpha (*Err α*), estrogen-related receptor beta (*Err β*) and estrogen-related receptor gamma (*Err γ*). *Err α* and *Err β* were identified as the first orphan nuclear receptors, whereas *Err γ* has been recognized ten years later as the third member of ERRs subfamily (Eudy et al., 1998, Heard et al., 2000). Like other nuclear receptors, *Err γ* comprises of N-terminal activation function (AF)-1 domain that is involved in the transcriptional regulation of the receptor, centrally located DNA-binding domain (DBD), a ligand-binding domain (LBD), and C-terminal (AF)-2 domain that interacts with coactivators and co-repressors (Huss et al., 2015). Eudy et al. first identified

Erry through its connection with a critical region of Usher syndrome type IIa (Eudy et al., 1998), then it was described by Hong et al. as a protein that interacts with nuclear receptor co-activator glucocorticoid receptor-interacting protein (GRIP)-1 (Hong et al., 1999). Despite excessive functional overlap between *Erry* and other members of ERRs due to the high similarity in their DBDs (Alaynick et al., 2007, Wang et al., 2015), it controls a various metabolic processes that do not involve both *Errα* and *Errβ* (Kim et al., 2011, Zhang et al., 2015). The ligand-independent orphan nuclear receptor *Erry* is highly expressed in metabolically active and densely vascularised fetal and adult tissues, including the placenta, brain, skeletal muscle, kidney, heart, and liver (Giguere, 2008). These findings might indicate a crucial role of *Erry* in differentiation and maintenance of these tissues. Subsequently, *Erry* null mice die shortly after birth due to a reduction in mitochondrial activity, abnormal heart and spinal cord functions. There is also evidence that phenotypic characterized of *Erry* knockout mice displayed a clear reduction in expression and activity of enzymes that regulate tricarboxylic acid cycle (TCA) and electron transport chain (ETC) (Alaynick et al., 2007).

1.9.2. *Erry* is an inducible transcriptional factor

Several studies have demonstrated that a number of orphan receptors are directly implicated in the control of specific cell mechanisms and metabolic pathways, even with the absence of natural ligands that could link these receptors to their functions (Desvergne et al., 2006, Rangwala et al., 2010). Indeed, the transcriptional activity of nuclear receptors is dependent on the presence of co-regulatory proteins. Approximately 200 nuclear receptor co-activator and co-repressor proteins have been identified to date, with a specificity of each protein to interact with the members of nuclear receptor superfamily (Lonard and O'Malley B, 2007). Importantly, the co-regulator proteins are able to impart specific transcriptional properties to the nuclear receptors that they interacting with, thereby inducing the biological functions of these receptors (Feige and Auwerx, 2007).

Like other orphan nuclear receptors, the transcriptional activity of *Erry* depends on tissue-specific co-regulators that can be stimulated by different cell signalling. In particular, *Erry* transcriptional activity has extensively linked to the members of peroxisome proliferator-activated receptor gamma co-activator 1 (PGC-1) family that integrate nutrient and

energetic signals in diverse metabolic pathways (Giguere, 2008, Huss et al., 2015). More specifically, it has been shown that PGC-1 α , a member of PGC-1 family, binds to the AF-2 domain of the *Erry*, resulting in a profound modulating of the later transcriptional complex (Devarakonda et al., 2011). Interestingly, study by Wang et al. has provided evidence of *Erry* potential to transactivate the PGC-1 α promoter (Wang et al., 2005), indicating the presence of a feed-forward loop in which *Erry* activates PGC-1 α , and the later then co-activates *Erry*. Furthermore, previous studies have established that signalling factors such as Transforming Growth Factor- β 1 (TGF β 1), Platelet-Derived Growth Factor, Fibroblast Growth Factor (FGF) 1 and 2, and Vascular Endothelial Growth Factor (VEGF) are known to stimulate angiogenesis. One possible explanation for these factors orchestration potential is by co-activator PGC-1 α that is induced by exercise and during hypoxia (Arany et al., 2007). Several other studies, however, reported that genetic deletion of PGC-1 α has no impact on muscle vasculature, as PGC-1 α knockout mice are viable, show normal capillary density with oxidative muscles (Arany et al., 2007, Li et al., 2004). *Erry* is abundantly expressed in muscle fibre type I, and its forced expression in fast-twitch anaerobic type II muscles triggers aerobic transformation, mitochondrial biogenesis, and robust myofibrillar vascularization in the absence of exercise (Narkar et al., 2011). Although the co-regulator PGC-1 α along with nuclear receptors controls diverse aspect of aerobic respiration (Wang et al., 2004, Arany et al., 2007), there is a considerable controversy on this role with *Erry*. Previous work has reported that the intrinsic effects of *Erry* are not dependent on PGC-1 α , but rather are linked to activation of aerobic master regulator named AMP-activated protein kinase (AMPK) (Narkar et al., 2008). Further study has illustrated that AMPK is naturally activated during exercise (Fujii et al., 2000), and it is a remarkable contributor in muscle metabolic and vascular adaptation (Fujii et al., 2007). Consistently, oxidative muscles from wild type mice show a high level of AMPK than the predominantly glycolytic fast muscle phenotypes (Narkar et al., 2011). Same study surprisingly found that AMPK was constitutively activated in *Erry* transgenic mice, which suggests a convergence between *Erry* and AMPK pathways to direct intrinsic vascularization and oxidative metabolism in type I muscle fibres (Narkar et al., 2011) (Figure 1.9).

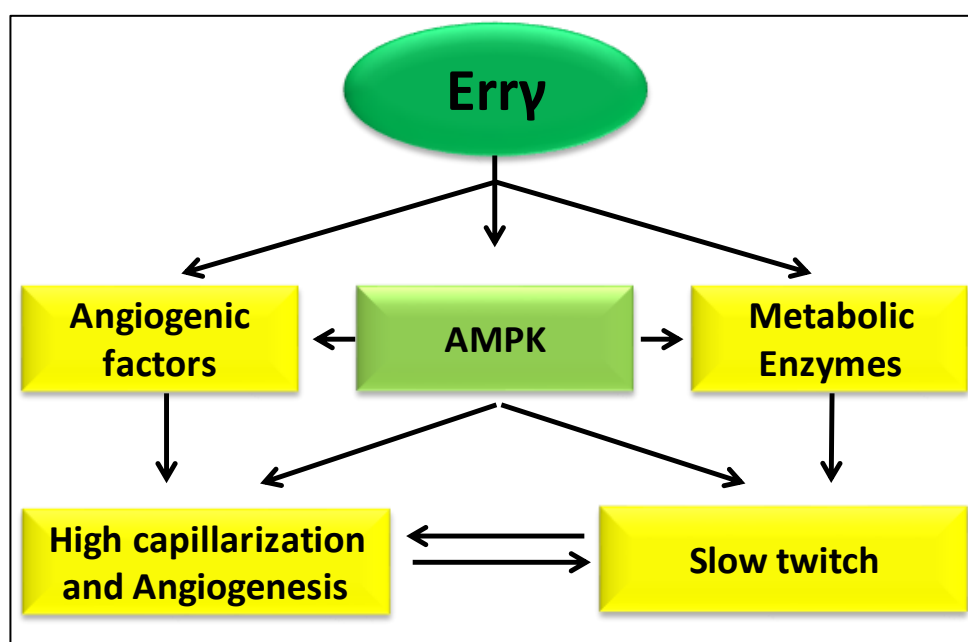


Figure 1.9. *Erry* as conductor of angiogenic and metabolic program (Gadeau and Arnal, 2012)

A number of genetic studies in mice have shown that steroid receptor co-activator (SRC)-1, -2, and -3 play a crucial role in regulating of hepatic metabolism, fat storage, and energy balance (Jeong et al., 2006, Louet et al., 2006). Importantly, these co-regulator proteins directly interact with the members of ERRs. The three classes interact with ERRs in mammalian cells (Xie et al., 1999), whereas SRC-2 has been shown to be specifically interacted with LBD of *Erry* and stimulate its transcriptional activity (Hong et al., 1999).

The activity of *Erry* is also modulated by receptor-interacted protein 140 (RIP140). RIP 140 has been known as ERRs co-repressor that critically implicated in the regulation of important metabolic pathways such as OXPHOS (Augereau et al., 2006, Castet et al., 2006, Seth et al., 2007). Interestingly, RIP140 can function as both a co-repressor and co-activator of *Erry*, its dual effects on *Erry* transcriptional activity can be determined depending on the target gene. For instance, RIP140 inhibits *Erry* activity on estrogen response element (ERE) constructs, whereas it activates *Erry* activity on several promoters containing Sp1 response elements (Castet et al., 2006). It is worth noting that the co-repressors inhibit *Erry*

transactivation by directly competing with the binding of the coactivators to the AF-2 domain of *Erry* (Misra et al., 2017).

Growing evidence also suggests that *Erry* gene expression is tightly controlled by membrane receptors. In response to glucose concentration decrease during fasting, both glucagon and insulin receptors can modulate *Erry* activity. Glucagon induces hepatic *Erry* expression, whereas insulin suppresses *Erry* activity in response to fasting (Kim et al., 2012a, Misra et al., 2016). Moreover, expression of *Erry* can also be induced by cytokine interleukin (IL)-6 receptor during bacterial infection. Binding of the cytokine to its receptor promotes the binding of signal transducer and activator of transcription (STAT)-3 to *Erry* promoter, which in turn upregulates *Erry* expression (Kim et al., 2014).

In the line of thought, it was well established that activity of *Erry* can be influenced in response to various stresses. Hypoxia regulates the transcriptional activity of *Erry* in a tissue-specific manner. Hypoxia-inducible factor (HIF)-1 α positively regulates *Erry* expression in hepatocyte (Lee et al., 2012a). Additionally, intrinsic metabolic requests can induce *Erry* expression. Kida et al. has revealed a high level of *Erry* during somatic cell programming in order to match the metabolic demands through enhanced mitochondrial aerobic OXPHOS (Kida et al., 2015). There is ample evidence of interaction between *Erry* and miRNAs. Although *Erry* induces expression of miR-208b and miR-499 that are known to contribute in muscle fibre types formation (Gan et al., 2013), *Erry* itself is regulated by miRNA. Previous work has documented that miR-378 robustly inhibits *Erry* expression in breast cancer, which leads to a metabolic shift from oxidative to a glycolytic pathway that was associated with an increase in cells proliferation (WARBURG, 1956, Eichner et al., 2010).

Structural studies have provided evidence that the LBD of *Erry* contains a flexible small ligand-binding pocket (Greschik et al., 2002), however it is able to be re-arranged in order to accommodate large volume synthesized molecules (Wang et al., 2006). Although *Erry* shows constitutive transcriptional activity, previous investigators have demonstrated that structurally related phenolic acyl hydrazone compound, GSK4716, and Bisphenol A, a ubiquitous environmental endocrine disruptor, both able to bind it and positively regulate its transcriptional activity (Yu and Forman, 2005, Tohme et al., 2014). By contrast, GSK5182, a derivative of 4-hydroxytamoxifen, has been identified as an inverse agonist selectivity for

Erry (Chao et al., 2006). These studies indicate that the transcriptional activity of *Erry* can be upregulated or inhibited by pharmacological agents.

1.9.3. Roles of *Erry* and transgenic approach

Like other members of ERRs superfamily, estrogen-related receptor gamma (*Erry*), is constitutively active orphan nuclear receptor that is selectively expressed in metabolically active and highly vascularized tissues such as heart, kidney, brain and skeletal muscle (Giguere, 2008, Heard et al., 2000, Hong et al., 1999). The *Erry* activity might attribute to the active conformation of its ligand binding domain (LBD) even in the absence of a ligand (Greschik et al., 2002).

Recent findings have established that *Erry* is directly or indirectly regulates the expression of numerous target genes related to different metabolic pathways in various tissues. One of the most important and well-described role of *Erry* is its actively contribution in mitochondrial bioenergetics pathways, TCA cycle, fatty acid oxidation, OXPHOS, and electron transport chain (ETC). Furthermore, it has a pivotal role in regulating multiple genes that linked to mitochondrial biogenesis and fatty acid oxidation in cardiac muscles (Alaynick et al., 2007, Dufour et al., 2007). In addition to its critical role to activate FAO in neonatal heart (Kubo et al., 2009), *Erry* upregulates expression of a network of genes that are crucial for normal heart function including fatty acid oxidation, such as fatty acid-binding protein 3 (*Fabp3*), mitochondrial creatine kinase (*Ckmt2*) and ATP/ADP translocator genes (Alaynick et al., 2007). *Erry* is also involved in lipid metabolism in the liver. It induces the formation of diacylglycerol (DAG), which are the precursors of triglycerides and phospholipids (Kim et al., 2011). Moreover, *Erry* contributes to maintain body temperature. It has been shown that increased expression of *Erry* leads to induce oxidative metabolism and heat generation (Dixen et al., 2013). *Erry* has emerged as a promising target in the treatment of certain metabolic disorders and cancers. It is a negative regulator of anaerobic glycolysis in breast cancer cells, thus its inhibition results in an increase in lactase production and a decrease in aerobic respiration (Kumar and Mendelson, 2011). Furthermore, it has been shown by a number of investigators that *Erry* plays a critical role in gluconeogenesis regulation that can be drug target in order to reverse hyperglycaemia and hepatic fat accumulation in the milieu of insulin resistance (Heard et al., 2000, Kim et al., 2011).

In skeletal muscles, gene array analysis has found that *Erry* regulates a total of 1123 genes, the up-regulated genes were mainly belonge mitochondrial biology (90) or oxidative metabolism (43) that encoding numerous components of fatty acid oxidation pathway as well as the oxidative respiratory chain reflective of aerobic adaptation. (Narkar et al., 2011). Consistently, *Erry* has been known as a transcriptional factor that is highly expressed in slow muscles and other tissues with high oxidative metabolism levels where it promotes mitochondrial biogenesis and activity. Moreover, a gene set analysis identified an increase in the expression of the contractile genes, particularly the ones that associated with slow muscle due to *Erry* overexpression. Additionally, introducing of *Erry* into WT muscles causes a subsequent coordinate increase in mitochondria function via increased in TCA cycle activity, induced mitochondrial size, and enhanced muscle oxidative capacity (Narkar et al., 2011, Rangwala et al., 2010). In fact, *Erry* is not only contributing to controlling of mitochondrial programs such as FAO, TCA cycle and OXPHOS pathways, it also implicated in regulation of a wide range of genes that involved in ATP transport across the membrane, uptake and modifying energy substrates, Ca^{2+} handling, as well as intracellular fuel sensing (Dufour et al., 2007, Alaynick et al., 2007). Study by Luo et al. (Luo et al., 2013) has revealed critical roles of *ERRy* during human pregnancy, it is necessary to promote hormone secretion and angiogenesis, as well as it required for the transcription of several voltage-gated K^+ channels. Consistent with these observations, *Erry* transgenic mice displayed an activated angiogenic response that consisted of the secretion of pro-angiogenic factors and robust fibre vascularization (Narkar et al., 2008). Interestingly, the increased oxidative capacity and mitochondrial size in transgenic *Erry* mice were associated with an increase in exercise capacity, suggesting that *Erry* may control the metabolic response of the muscle during exercise (Narkar et al., 2011, Rangwala et al., 2010, Badin et al., 2016). Conversely, *Erry* heterozygous mice (*Erry*^{+/-}) show a reduction in expression of genes that related to fatty acid uptake and fatty acid oxidation, indicating that the utilization of fatty acids as fuels is compromised (Rangwala et al., 2010). *Erry* is an indispensable part of mitochondrial oxidative phosphorylation, which is essential for normal muscle differentiation and growth. In muscle-specific *Erry*-null mice, there was a reduction in mitochondrial content and alteration in their distribution, an increase of medium chain FAO, and a decrease of glucose oxidation. Thus, myotubes maturation in these animals (*Erry*^{-/-}) is hampered mainly due to

an increase in Reactive Oxygen Species (ROS) generation that induces muscle atrophy by upregulating components of the ubiquitin proteasome system during differentiation (Murray and Huss, 2011, Li et al., 2003b).

These studies indicate that *Erry* acts as a central transcriptional factor that controls mitochondrial functions and metabolism together with angiogenesis that anatomically synchronizes vascular arborisation to oxidative metabolism. Several recent reports suggested that transcriptional regulators that induce muscle oxidative metabolic properties, can promote angiogenic gene expression in skeletal muscle (Gaudel et al., 2008, Narkar et al., 2008). Such combination of factors is profoundly required for better physiological performance and normal pace of regeneration and repair processes. Given these considerations, muscle-specific overexpression of *Erry* using specific promoter has been widely performed (Narkar et al., 2011, Rangwala et al., 2010). Two skeletal muscle promoters have been extensively utilised. Muscle creatine kinase (MCK) promoter that is expressed at high levels in skeletal and cardiac muscle tissues was applied. Jaynes et al. has reported that several regions of the mouse MCK are responsible for tissue-specific expression in transgenic mice (Jaynes et al., 1988). Thus, MCK has been exploited as a specific promoter in order to overexpress *Erry* on a C57Bl/6 background mice, and the transgenic construct consists of the 4.8kb fragment from the mouse genome to drive hemagglutinin-tagged *Erry* gene construct (Rangwala et al., 2010). Alternatively, a number of studies have demonstrated that human α -skeletal actin (HSA) gene promoter is complex and spanning at least 1,300 bp, and that three segments of this region when adjacent to simian virus 40 (SV40) promoter act as regulatory domains which respond to muscle-specific factors to regulate transcription. Muscat and Kedes have dissected the promoter and found that the proximal domain (positions -153 to -87) of the HSA gene promoter is crucial for muscle-specific expression in two different myogenic cell lines (L8 and C2C12). They also established that the distal domain (positions -1300 to -626) of the promoter is only positively modulating transcription in C2C12 but not in L8 cells. It seems that the tissue-specific transcription of the HSA gene promoter resulted from the interaction of the upstream regions with trans-acting positive regulatory factors in muscle cells (Muscat and Kedes, 1987). Consequently, a number of investigators have used a large portion of the promoter (2.2kb) to express *Erry* in a mouse skeletal muscle (Matsakas et al., 2012b, Narkar

et al., 2011). Importantly, we have used the same 2.2kb human actin skeletal muscle promoter for all experiments in our study.

Hypothesis, aims and objectives

First hypothesis

The main hypothesis of this study is that muscle-specific manner overexpression of *Erry* into *Mtn*^{-/-} background muscles using specific promoter (HSA) would overcome the deficits in hypertrophic muscle fibres developed in the absence of *Myostatin* at different levels.

Aims and objectives 1

1- To determine whether the constraint between muscle fibre size and its oxidative capacity can be broken, thereby produce large oxidative myofibre

A fundamental concept of skeletal muscle biology is the existence of the inverse relationship between the oxidative capacity of a fibre and its cross-sectional area (CSA) (van Wessel et al., 2010, Degens, 2012). Previous studies have reported that genetic deletion of *Myostatin* results in hypermuscular phenotypes called (Muscle Doubling) due to both hyperplasia and hypertrophy (McPherron et al., 1997, McPherron and Lee, 1997). *Erry* is a master regulator of oxidative phenotypes that is highly expressed in tissues with high oxidative metabolic demands where it has been demonstrated to trigger mitochondrial biogenesis (Giguere, 2008, Narkar et al., 2011).

Therefore, we postulated three possible outcomes of the introducing of *Erry* into *Mtn*^{-/-} muscles:

- a- *Mtn*^{-/-} phenotype is fixed, so it maintains hypertrophic and glycolytic state.
- b- Oxidative features imparted by *Erry* programme would follow the inverse relationship and results in small mitochondrial-rich fibres.
- c- The constraint is broken in this strain and results in the development of hypertrophic yet oxidative fibres.

I aim to utilise a panel of *in vitro* assays to investigate muscle mass, muscle fibre size, muscle fibre number and oxidative properties, these experiments will indicate which possibility is the truth.

2- To determine if overexpression of *Erry* can influence specific muscle force generation capacity and physical performance of the animals

Although *Mtn*^{-/-} enlarged muscles appear normal at histological level, their ability to generate force is impaired in particular for long time of work (Amthor et al., 2007, Mendias et al., 2006). Amthor also suggests that the high fatigability of *Mtn*^{-/-} mice might attribute to the low content of mitochondria that results from *Myostatin* ablation (Amthor et al., 2007). On the other hand, *Erry* forced expression in fast-twitch anaerobic muscles causes aerobic transformation, mitochondrial biogenesis, and induces muscle fibres capillarization in the absence of exercise (Narkar et al., 2011). To accomplish this aim, mice will be subjected to a series of tests in order to detect the physiological activities. Thereafter, a number of histological protocols and metabolic assays will be performed to identify skeletal muscle fibre profiling, mitochondrial quality and quantity, and metabolic status.

3- To determine the identity of the metabolic programme that is imparted by introducing of *Erry* into *Mtn*^{-/-} muscles at molecular level

Following the investigations into the previous aims, further investigation will be performed to identify whether the differences in oxidative metabolism in muscles from the three genotypes of this study (WT, *Mtn*^{-/-} and *Mtn*^{-/-}/*Erry*^{Tg/+}) would be mirrored at transcriptional level. Using quantitative polymer chain reaction (qPCR) technique, the expression levels of key genes that associated with transcriptional regulators, different metabolic aspects and angiogenesis programme will be examined.

4- To determine if overexpression of *Erry* can influence skeletal muscle stem cells (satellite cells) population and behaviour

There was a controversy regarding the effect of *Myostatin* deletion on satellite cells population. Although McCroskery referred to an increase in satellite cell number following *Myostatin* ablation (McCroskery et al., 2003), his findings were robustly contradicted by others who demonstrated that muscle hypertrophy resulted from genetic alteration of *Myostatin* was not due to increase in satellite cells number and activity (Amthor et al., 2009, Matsakas et al., 2009). It was well established that muscle metabolic properties can

influence satellite cells population; satellite cells number increases as a muscle become progressively oxidative (Peuker et al., 1999, Christov et al., 2007).

To accomplish this aim, isolated and cultured single myofibres from EDL muscles of the three animal cohorts will be processed for immunocytochemistry against satellite cells and activated/proliferated myoblast cells markers including Pax7 and MyoD. This will enable detailed investigation of effects of the metabolic programme on satellite cells number and activity.

5- To determine whether muscle metabolic properties affect not only muscle fibres but other tissues

I sought to establish whether supporting tissues such as entities of extracellular matrix (ECM) and dystrophin-glycoprotein complex (DGC) would be changed in response to metabolic reprogramming. ECM and DGC of skeletal muscle are essential structures for myofibres force transmission and protection against injury (Gumerson and Michele, 2011, Alameddine, 2012). *Myostatin* induces fibroblast proliferation, hence connective tissue depositions (Li et al., 2008). Subsequently, genetic deletion of this gene results in a remarkable reduction of ECM components compared to counterpart wild type mice (Elashry et al., 2012).

Therefore, investigation of ECM and DGC compositions at transcriptional and protein levels would give insights into the relationship between muscle fibre phenotype (size and metabolism) and its force transduction apparatus.

Second hypothesis

The microenvironment plays a crucial role in regulation and function of skeletal muscle stem cells (satellite cells), helping to maintain tissue homeostasis and regeneration capacity (Carlson and Faulkner, 1989). Muscle regeneration rate could be severely hindered due to a fall in satellite cells population (Schuster-Gossler et al., 2007, Vasyutina et al., 2007). Additionally, published studies unveiled a positive correlation between muscle oxidative metabolism and regeneration capacity (Lowrie et al., 1982, Matsakas et al., 2013).

Consistently, muscle blood supply and ECM components are critical contributors in skeletal muscle regeneration (Bencze et al., 2012, Calve et al., 2010).

Erry transgenic mice displayed an increase in oxidative capacity and activated angiogenic program that consisted of the secretion of pro-angiogenic factors and robust fibre vascularization (Narkar et al., 2011, Badin et al., 2016).

The second hypothesis emanated from the findings of the primary investigations.

I hypothesise that the oxidative environment imparted by overexpressing of *Erry* into *Mtn*^{-/-} muscle would enhance the process of muscle regeneration in response to acute muscle injury.

Aims and objectives 2

1- To determine if high levels of muscle oxidative capacity and capillarization are sufficient to influence muscle regeneration even with lower population of satellite cells

I aimed to find whether muscle-specific expression of *Erry* into *Mtn*^{-/-} muscles can drive normal regeneration process in response to skeletal muscle injury through the use of an established skeletal muscle injury model – cardiotoxin (CTX) injection. The number of necrotic fibres, density of macrophages, amount of cell death in damaged areas were followed through immunohistochemistry using endogenous immunoglobulin, F4.80 and cleaved-caspase-3 antibodies respectively, along with satellite cell marker (Pax7) and proliferative myoblast marker (MyoD). Antibody against formed embryonic myosin heavy chain (eMHC) will also be applied to quantify regenerated fibres. Similar experiment carried out to advanced stage of regeneration (14 days) after injury in order to identify whether prematurely regeneration can affect size of newly formed muscle fibres.

Third hypothesis

Post-natal inhibition of *Myostatin* signalling has been extensively applied as promising therapeutic against muscle wasting (Collins-Hooper et al., 2014, Matsakas et al., 2009). Unlike genetic alteration of *Myostatin* gene, hypertrophic phenotypes result from *Myostatin* blocking is due to muscle fibre hypertrophy, but not hyperplasia (Whittemore et al., 2003, Lee et al., 2005). Beside fibre hypertrophy resulted from *Myostatin* inhibition, there is a

remarkable decrease in expression of genes related to muscle mitochondrial functions and oxidative phosphorylation pathways (Rahimov et al., 2011). Moreover, *mdx* mice injected with sActRIIB that antagonizes Myostatin signalling, show low levels of muscle capillarization, force generation capacity and high fatigability (Relizani et al., 2014).

The third hypothesis of my study stems from attractive observations of previous investigations.

I hypothesize that inhibition of Myostatin signalling at post-natal stages in *Erry*^{Tg/+} mice that display high oxidative capacity, would enable the generation of hyper-trophic / hyper-oxidative phenotypes.

Aims and objectives 3

1- To determine if oxidative metabolic programme established by overexpressing of *Erry* would be appropriate to complement the increased muscle mass

There is uncertainty over whether induction robust oxidative metabolic programme would be enough to provide a protective effect against the decrease in oxidative capacity and physical activity following post developmental blocking of Myostatin. The investigations into the muscle morphological, histological and metabolic properties that have been utilised in our laboratory may help to answer this question. The adequate level of skeletal muscle function and size is paramount importance for health. Thus, this work will present possible therapeutic targets when looking to improve muscle function and size, ultimately improve life quality of human.

2- To investigate whether it is possible to induce muscle fibre size while maintaining high oxidative metabolic level

Previous studies have reported that ActRIIB signalling is a key regulator of oxidative metabolism (Relizani et al., 2014), thus treatment with a soluble form of ActRIIB leads to downregulation of genes involved in oxidative phosphorylation and mitochondrial functions (Rahimov et al., 2011). There is ample of evidence regarding *Erry* potential to induce muscle oxidative capacity in parallel to promote a network of genes that involved in muscle energy production, metabolism and vasculature pathways (Narkar et al., 2011, Alaynick et al.,

2007). Thus, I set out a series of investigations in adult WT and *Erry*^{Tg/+} mice treated with sActRIIB to determine how post-natal blocking of Myostatin using this ligand trap might affect oxidative metabolism features imparted by *Erry* overexpression.

3- To determine whether overexpression of *Erry* would attenuate complications of post-natal blocking of Myostatin on muscle fibre only, or exceed to the supporting tissues

Although widespread beneficial effects have been observed with post-natal inhibition of Myostatin, there is evidence of muscle blood supply and physiological activities compromise (Relizani et al., 2014). I aimed to utilize immunohistochemistry technique using a panel of specific antibodies to discover whether the metabolic reprogramming can affect muscle fibre supporting tissues such as the amount of ECM members and capillary density.

Chapter 2

Methods

2. Genetic *In vivo* experimentation

2.1. Animal maintenance

Three lines of mice were used in this study:

- Wild type (strain-C57BL/6JOla/Hsd), from Harlan laboratories, UK.
- *Myostatin* null mice ($Mtn^{-/-}$), were a gift of Se-Jin Lee (John's Hopkins USA) (McPherron and Lee, 1997).
- *Erry* transgenic mice were a gift of Ronald Evans (Salk Institute for Biological

Studies, La Jolla, USA).

Erry was overexpressed on *Myostatin* null background mice ($Mtn^{-/-}/Erry^{Tg/+}$).

Mouse *Erry* cDNA was placed downstream on the human α -skeletal actin promoter and upstream of the simian virus 40 (SV 40) intron/poly (A) sequence. The purified transgene was injected into C57BL/6J x CBA F1 zygotes. Two transgenic founders (TG 425 and 421) were obtained that were backcrossed with C57BL/6J (Narkar *et al.*, 2011).

The *Erry* transgenic mice were bred to *Myostatin* null ($Mtn^{-/-}$) mice, which resulted in 50% *Myostatin* heterozygous with WT *Erry* alleles ($Mtn^{-/+}/Erry^{+/+}$), and 50% *Myostatin* heterozygous with *Erry* transgenic ($Mtn^{-/+}/Erry^{Tg/+}$). Males $Mtn^{-/+}/Erry^{Tg/+}$ were then backcrossed with females *Myostatin* null ($Mtn^{-/-}$) mice which produced ($Mtn^{-/-}/Erry^{+/+}$) and ($Mtn^{-/-}/Erry^{Tg/+}$), males offspring were genotyped and categorized into $Mtn^{-/-}$ and $Mtn^{-/-}/Erry^{Tg/+}$.

Mice were bred and maintained in accordance to the Animals (Scientific Procedures) Act 1986 (UK) and approved by the University of Reading in the Biological Resource Unit of Reading University. They were housed under standard environmental conditions (20–22°C, 12h–12h light–dark cycle) and provided food and water ad libitum.

Three months old mice were used for the study, and each experimental group consisted of 5-9 mice.

2.2. Genotyping

Genotyping was performed to determine differences in the genetic make-up (genotype) of the individual mouse line.

DNA Isolation

Samples (ear clips) were collected in Biological Resource Unit and placed in Eppendorf tubes, then were transferred to the laboratory on ice. Samples were submerged in 100 μ l of 50 mM NaOH, left in rocking machine (PLATFORM SHAKER STR6) for 1 hr at 95°C. 10 μ l Neutralizing solution (Tris 1.5 M pH: 7.4) was then added and samples were left at room temperature for 10 minutes. This method produces solubilised DNA which was used for genotyping by PCR.

Primers Concentrations Calculation and Master Mix preparation

For *Erry* PCR genotyping reaction, primers using are:

mErrG-F 5'-TTGGTGGTTATCATTGGATGGG-3' (Eurofins Genomics)

mErrG-R 5'-TAGAAGTGCTGGACTGCCTTGG-3' (Eurofins Genomics)

Primers were dissolved in water to produce concentrated stocks (0.1 mM). A (0.1 mM) concentration stock was diluted 1:10 in water to make the working solution which is (10 μ M) concentration. The final concentration of primer in the PCR genotyping reaction is (250 nM). Master Mix for each reaction was prepared in sterile Eppendorf tube by mixing 20 μ l Taq 2x Master Mix, 1 μ l of each primer (Forward and Reverse), and volume was then made to 35 μ l with nucleic acid free water. Finally, 5 μ l of DNA was added to make the final volume reaction 40 μ l.

PCR Cycling

Small PCR tubes of total volume reaction (40 μ l) were centrifuged quickly, and moved into the T100TM Thermal Cycler machine (BIORAD).

The cycler was set up with following conditions for *Erry* PCR reaction:

- | | | |
|---------|--------------|-------|
| 1- 94°C | 1min | |
| 2- 94°C | 20secs | } x35 |
| 3- 52°C | 30secs | |
| 4- 72°C | 1min 30secs | |
| 5- 72°C | 3min | |
| 6- 4°C | Indefinitely | |

Erry+ band runs at 482 bp.

For *Myostatin* PCR genotyping reaction, primers using are:

mMyo 13 5'-AGAAGTCAAGGTGACAGACACAC-3' (Eurofins Genomics)

mMyo 168 5'-GGTGACACAAGATGAGTATGCGG-3' (Eurofins Genomics)

mMyo 169 5'-GGATCGGCCATTGAACAAGATG-3' (Eurofins Genomics)

mMyo 170 5'-GAGCAAGGTGAGATGACAGGAG-3' (Eurofins Genomics)

Same conditions of *Erry* PCR reaction have been used, with different annealing temperature (57°C), a heterozygous sample produces a 350 bp Knockout specific band and a 225 bp WT band, 35 cycles.

Agarose gel electrophoresis preparation

To prepare 1.5% gel, 0.75 g agarose was dissolved in 50 ml 1 x Tris acetate EDTA (TAE) buffer (pH 7.8) by boiling, then allowed to cool to RT and SYBER Safe DNA gel stain was added (0.5 µl /10 ml TAE buffer). The gel was cast and allowed to set before being submerged in the (TAE) buffer with SYBER Safe DNA gel stain (0.5 µl /10 ml TAE buffer) (to increase the visualisation) in the gel tanking. A 100 bp DNA Ladder (Promega) was loaded as a molecular weight marker, then 15 µl of PCR reaction were loaded in the gel wells after mixing with 1 µl orange G stain. The gel was run at 70 V, and DNA bands were visualized using UV light illuminator (Syngene/ U:Genius).

2.3. Assessment of mice fatigue resistance

Mice were acclimatised to run on a treadmill in three sessions ($10 \text{ m}\cdot\text{min}^{-1}$ for 15 minutes followed by a $1 \text{ m}\cdot\text{min}^{-1}$ increase per minute to a maximum of $12 \text{ m}\cdot\text{min}^{-1}$) (Columbus Instruments Model Exer 3/6 Treadmill, Serial S/N 120416). Exhaustion was determined by exercising the mice at $12 \text{ m}\cdot\text{min}^{-1}$ for 5 minutes, followed by $1 \text{ m}\cdot\text{min}^{-1}$ increases to a maximum of $20 \text{ m}\cdot\text{min}^{-1}$ until the mouse was unable to stay at front of the treadmill and repeatedly falling back to the treadmill brushes ~ 5 times over 30 seconds.

2.4. Assessment of forelimb muscle strength using grip strength meter

For all tests, mice were moved to the experimental room 5-20 minutes before testing to ensure they are properly awake. The grip strength meter (Chatillon DFM-2) was tested before the experiment to ensure it was functioning. The grip strength meter was fixed on the bench and positioned horizontally, and it was set to zero or reset before each measurement was made, to allow proper values to be detected. Maximal force was measured in grams. The mouse was held by the tail base and lowered towards the bar (the front paws were at the same height as the bar) and moved until the bar was within reach. The mouse was allowed to grab triangular pull bar and was then pulled backwards in the horizontal plane. The force applied to the bar just before it loses grip was recorded as the peak tension. Measurements were discarded if the animal used only one paw or if it used its hind paws, turned backwards during the pull, or leaves the bar without resistance. The test was repeated for two days with three measurements per day to achieve the best performance. To avoid habit formation and to allow recovery, one minute time was between trails, then the single best recorded value was used for analyzing.

The mice were weighed just before measuring grip strength, so the maximal force values were normalized to animals' body weights.

2.5. Behavioral and Locomotor measurements using Open Field Animal Activity Monitoring system

Open field activity monitoring was used to offer a comprehensive assessment of behavioral and locomotor activities of mice, without require to special training. These assessments are

done with multiple photocell receptors and emitters. Animal activity is measured via a grid of invisible infrared light beams.

Mice were acclimatised to the test chamber environment for two days. This was attained by placing each mouse alone in one chamber, then mice were left uninterrupted for 60 minutes every day to reduce variation in data.

All data collection performed in an undisturbed environment, in the mornings at the same time for 3 days to reduce variability in the behavioral measurements.

The primary data collection duration (Bine time 10 minutes, n Bine 9 for total duration of 1hr and a half) was set in advance. The buttons that designate the individual cages should turn green, indicating that there is no block between the sensors. When all cages are ready, note the ID of the mouse insert into the test chamber, making sure that the mouse ID matches the one entered into the software. A 5 minutes extra time was set to allow the mice to acclimatize into the test chamber before starting data collection. While the animals are in the test chamber, external noise was minimized. When the experiment time elapsed, the data were saved and exported to Excel sheet. Mice were replaced in their cages, and all chambers were cleaned.

2.6. Mice euthanasia

Animals of all experiments were humanely sacrificed via Schedule 1 killing by carbon dioxide asphyxiation followed by cervical dislocation.

2.7. Muscle tension measurements

Dissection of the hind limb muscles was carried out under oxygenated Krebs solution (95% O₂ and 5% CO₂). Under circulating oxygenated Krebs solution one end of a silk suture was attached to the distal tendon of Extensor Digitorum Longus (EDL) muscle and the other to a Grass Telefactor force transducer (FT03). The proximal tendon of EDL tied to a fixed immovable hook using a silk suture.

The leg was pinned to a Sylgard-coated experimental chamber. Two silver electrodes were positioned longitudinally on either side of the EDL. A constant voltage stimulator (S48, Grass Telefactor) was used to directly stimulate the EDL which was stretched to attain the optimal

muscle length to produce maximum twitch tension (P_t). Tetanic contractions were provoked by stimulus trains of 500 ms duration at 10, 20, 50, 100 and 200 Hz. The maximum tetanic tension (P_o) was determined from the plateau of the frequency-tension curve. Specific force was estimated by normalising tetanic force to EDL muscle mass (g).

2.8. Skeletal muscles dissection

2.8.1. Hind limb muscles dissection

Tibialis anterior (TA), *Extensor Digitorum Longus* (EDL) and *Soleus* muscles were chosen to identify the morphological and cellular features of hind limb muscles, due to their ideal anatomical location permitting ready isolation without damages muscle's mid-belly region, and because they show the major types of contractile properties.

Gastrocnemius muscle was used for the molecular work, as its anatomical shape makes it impossible to obtain the same mid-belly sections for histological analysis, and its large size imparts us with sufficient amount of RNA to use for genes expression assessment.

Once death had been ascertained the animals were weighed. The hind limbs of the mice were sprayed with 70% ethanol in order to make the fur damp to avoid hair contamination. Circular incision was made through the skin around the proximal end of thigh using a sterile surgical scalpel blade (ensuring no damage to the muscles). The isolated skin of the limb was then pulled distally to a point beneath the ankle joint, so exposing the (TA) which lies over the EDL muscle. Skin covering foot and ankle joint was removed by carefully slicing down the footplate and pulling the skin distally free by hand. The muscles were dissected within 10 minutes post mortem.

2.8.1.1. *Tibialis Anterior* (TA) muscle dissection

Tibialis anterior muscle lies on the anterior-medial surface of the leg region of the hind limb. The fascia layer (connective tissue) surrounding the TA muscle was removed by inserting grad 4 forceps (Dumostar, A. Dumont & Fils, Switzerland) between distal tendons of the TA and EDL and pulling the fascia toward the knee joint. Using curved Vanna's microscissors (Agar Scientific T5220), the distal tendon was cut from the insertion point at the dorsal surface of the tarsal and metatarsal bones (about 1 cm below the TA muscle). The muscle

was pulled from the insertion tendon until the proximal attachment to the tibial tuberosity using the tendon. The TA muscle was carefully disassembled by cutting it at its origin. Free TA muscle was transferred immediately into Phosphate buffer saline (1 x PBS).

2.8.1.2. Extensor Digitorum Longus (EDL) muscle dissection

Extensor digitorum longus muscle (EDL) lies on the lateral part of the anterior of the hind leg. The EDL has two tendons at its origin, which have attachment points to lateral condyle of the tibia and the head and anterior surface of the fibula. Both tendons of EDL muscle appear as one white structure lateral to the knee joint. The EDL muscle runs distally from the knee joint, lateral and beneath the TA muscle to the ankle joint. The distal tendon splits into four tendons, which then run under the retinaculum, cross the dorsal footplate and inserting separately on the dorsal surface of the middle and end phalanges of the four outer digits.

The fascia layer covering the TA and EDL muscles was removed, and to locate the proximal tendon of EDL, the fascia and muscles covering this tendon were removed using Grade 4 forceps. The distal tendon of TA muscle was cut using curved Vanna's microscissors, and the muscle was pulled proximally to the knee using the tendon. The four distal EDL tendons were raised from the footplate and all cut using microscissors, (ensuring all tendons were cut to avoid muscle tearing). Tendons were then pulled free of the cartilage around the ankle by pulling the tendon from just below the muscle. The EDL muscle was pulled proximally to the knee using the tendons and while the muscle was kept taut, the two proximal tendons of the EDL were cut as far from the muscle as possible using microscissors. The free EDL muscle was then pulled away from the limb and placed immediately either in the prepared 2% type 1 collagenase solution or Phosphate buffer saline (1 x PBS), depending on requirements.

2.8.1.3. Gastrocnemius and Soleus muscles dissection

The gastrocnemius and the soleus muscles are situated at the posterior of the hind leg. The lateral head of gastrocnemius muscle originates from the lateral condyle of the femur, and its medial head originates from the medial condyle of the femur. Soleus muscle arises at the head of the fibula and the medial border of tibial shaft.

Both muscles run distally along the leg and inserts via the calcaneal tendon into the tuber calcanei.

The skin was removed around the thigh to avoid muscle damage. The fascia layer covering gastrocnemius muscle was removed using Grade 4 forceps thus expose it, and then Biceps femoris muscle which covers a part of the gastrocnemius muscle was cut using microscissors. The mouse was turned on the belly and the foot pinned to cork board. The calcaneal tendon (s) was cut at the calcaneus and the gastrocnemius and the soleus were pulled proximally to the knee. The posterior muscles were pulled with forceps while cutting gently with scissors on both sides. The distal tendon of the soleus muscle was then cut and muscle free from the leg. The gastrocnemius muscle was a way from the thigh by cutting as close as possible to the femur.

Both muscles were weighed prior to move soleus muscle into pre-cooled iso-pentane for snap freezing, and gastrocnemius muscle into liquid nitrogen, then storage on dry ice.

2.8.2. Forelimb muscles dissection

Biceps brachii (BB) and *Extensor carpi radialis longus* (ECRL) muscles were chose for investigating ultra-structures of skeletal muscle using transmission electron microscopy (TEM) technique.

Forelimbs were completely separated from animal body and transferred immediately into 1 x PBS, the facial layers covering BB and ECRL muscles were removed, and both muscles were fixed in-situ prior to their dissection.

The muscles were dissected within 10 minutes post mortem.

2.8.2.1. *Biceps brachii* (BB) muscle dissection

The whole forelimb was fixed by pins on a cork board. Biceps brachii muscle lies in front of the arm. The fascia layer covering Pectoral and Biceps Brachii muscles was removed, and in order to locate tendon of origin, part of the pectoral muscle was removed. The tendon was severed from the supraglenoid tuberosity of the scapula, then the whole muscle pulled away to the radial tuberosity of the radial bone where the muscle been inserted. The Biceps

Brachii muscle was carefully freed by cutting its insertion tendon, and free muscle was transferred immediately into fixative solution (2.5% Glut in 0.1 M Na-Cacodylate pH 7.4).

2.8.2.2. Extensor Carpi Radialis Longus (ECRL) muscle dissection

Extensor Carpi Radialis Longus muscle lies on the ulnar (medial) side of the forearm. After BB muscle disabusing, the fascia layer covering ECRL muscle was removed gently. Whole muscle was detached from all surrounding muscles; and origin tendon severed from the lateral condyle of the humerus. ECRL muscle was then pulled away using its tendon toward the insertion site in the lateral dorsal surface of the base of the third metacarpal bone where the muscle was removed completely, and transferred immediately into the fixative solution.

2.9. Ex vivo skeletal myofibre experimentation

2.9.1. Isolation of intact single myofibres of EDL muscle

The EDL muscle was placed in 1ml of 2% type 1 collagenase (2mg/ml) after dissection. 1ml collagenase was sufficient to digest both EDL muscles from one mouse. The bijous that contain the EDL muscles were incubated at 37°C, 5%CO₂. The tubes of EDL muscles were agitated gently every 15 minutes to augment the digest speed. After approximately 30 minutes, individual myofibres began to peel away from the muscle. By 1.5 - 2 hours, the bulk of the myofibres had separated from the muscle mass. Prior to transfer the myofibres into a sterile washing dish, the dish was coated with horse serum to prevent myofibres attach on plastic.

A stereomicroscope (Nikon SMZ1500) with under stage light source was used to visualise the myofibres. Bundles of myofibres were gently aspirated using the sterile glass pipette until single isolated myofibres were seen. To remove residual collagenase, the myofibres were washed twice in Dulbecco's Modified Eagle Medium (DMEM), and twice with Single Fibre Culture Medium (SFCM). Care was taken during the washing to ensure that not all media was removed which can lead to myofibres contracting and so rendering the tissue useless for analysis. At this point, myofibres were either fixed at time-zero (T₀) or cultured for desire time point (maximum 72 hours). Fixed myofibres were stored in 1.5 ml clear microtubes (Axygen MCT-175-C-S) at 4°C.

2.9.2. Single myofibre fixation and culture

Cells (single myofibres) were fixed using 4% PFA/PBS at a volume ratio of 1:1 (final concentration 2% PFA/PBS) in 1.5 ml clear microtubes. To remove the fixative solution after 15 minutes of incubation at room temperature, 1 x PBS was used for three washes each wash lasting 5 minutes before being stored at 4°C.

For culturing, single myofibres were transferred carefully using a sterile glass pipette into 12-well plate (approximately 20 fibres per well), then 1 ml of SFCM was subsequently added to each well. All wells were checked to contain intact myofibres and any myofibre bundles liberated. Plates were transferred to a humid incubator at 37°C, 5% CO₂ and incubated for the required time period. Once myofibres had been cultured for the desired time period they were fixed as above, and stored in 1.5 ml clear microtubes at 4°C for immunocytochemistry.

2.9.3. Immunocytochemistry staining

After samples (EDL muscle fibres) fixation in 2% PFA, they were washed three times in 1 x PBS, with each wash lasting 5 minutes using Pasteur pipet. The myofibres then treated with permeabilisation buffer at room temperature for 15 minutes. Another two five minutes washes in 1 x PBS were performed prior to pre-blocked the myofibres in wash buffer for 30 minutes at room temperature. Primary antibodies (Pax7 and MyoD) (Appendix I) were pre-blocked in wash buffer for 30 minutes prior to incubate with the myofibres overnight at 4°C. In order to remove primary antibodies, samples were washed in fresh wash buffer three times 10 minutes each. Secondary antibodies were used to identify the primary antibodies, they pre-blocked in wash buffer for 30 minutes before incubating with myofibres for 1hr in the dark at room temperature. Samples were then washed three times in fresh wash buffer with each wash lasting 10 minutes. Myofibres were then transferred onto poly L-lysine slides. Once the myofibres were evenly distributed around the slides they were mounted with fluorescent mounting media (Dako S3023) which had been supplemented with 7.5 µl of 4, 6-diamidino-2-phenylindole (DAPI) (2.5µg/ml) for nuclear visualization.

2.9.4. Myonuclear organization

This work has been done by Jo C Bruusgaard, University of Oslo, Norway.

For visualizing myonuclei, fibres were mounted with ProLong Diamons Antifade Mountant with DAPI (Molecular Probes, P36962), and a confocal microscope (Olympus FluoView 1000, BX61W1, Olym-pus, Japan) was used to observe single muscle fibres. Pictures were taken in confocal planes, separated by z-axis steps varying between 0.4 and 2 μm according to the optical thickness and the desired Nyquist sampling frequency. Confocal microscope images used for mapping of Euclidean positions of myonuclei were processed and analysed using Imaris (Bitplane) and ImageJ (NIH, Bethesda, MD, USA). For each muscle fibre, an idealized circular cylinder segment with constant radius was constructed, and the distance from each nucleus to its nearest neighbour was calculated. In order to measure how ordered the nuclei distribution for a particular fibre is, the mean nearest neighbour distance was calculated for the experimental data, as well as for the random and optimal distribution using parameters from the experiment. We denote the experimental, random and optimal means by M_E , M_R and M_O . An 'orderness-score', $g(M_E)$, was then calculated as:

$$g(M_E, M_R, M_O) = \frac{M_E - M_R}{M_O - M_R}$$

2.10. Tissue freezing and preparing for cryosectioning

Following dissection, the muscles were immediately washed in 1 x PBS, dabbed onto tissue, weighed and placed on a strip of foil to snap freeze on the isopentane was frozen solid by liquid nitrogen (LN_2). Once the muscles were completely frozen, they were removed from the foil and placed in labelled Eppendorf tubes that had been precooled in dry ice, and placed in dry ice for short term before transferring to -80°C .

Prior to transfer the tissue from -80°C , a metal block was placed onto dry ice, and a dry ice alcohol bath was set up, both allowed to cool down for 15 minutes. The frozen tissue was placed on the cooled metal surface and drop by drop coated in cryo-embedding medium (Optimal Cutting Temperature compound (OCT) (TAAB O023)) until completely enclosed. The coated tissue was placed quickly into aluminium foil holder and filled with (OCT), before being froze in the dry ice alcohol path. Therefore a moderately quick freezing technique was

used in order to obtain fast freezing (within 10-15 seconds). The frozen muscle blocks were stored at -80°C prior to cryo-sectioning.

The frozen blocks were transferred into the cryostat chamber (-20°C) (Bright 5040 Cryostat), and OCT medium was used to mount the tissue onto the chuck. The temperature of the tissue was allowed to equilibrate with the cryostat. 10 µm transvers mid-belly cryo-sections for each muscle were obtained and transferred to poly-L-Lysine coated slides. The sections were dried at room temperature for 1 hr, and either directly processed or stored at -80°C for further immunohistochemistry or histological staining.

2.11. Haematoxylin and Eosin staining protocol (H&E)

Sectioned slides were dried for 20 minutes and then washed in 1 x PBS for 2 minutes followed by a 18 minutes incubation in the haematoxylin stain to stain the nucleic materials. The haematoxylin stain was removed by a 2 minutes wash in distilled water followed by two immersions in acidic alcohol in 0.1%HCl in order to control the staining intensity. The slides were submerged in running water for 5 minutes before being placed in the Eosin stain for 2 minutes to stain the protein materials. The sections were then washed in ascending gradient of ethanol concentrations (70% for 1 minute, 90% for 2 minutes, 100% three times for 2 minutes) to remove unbound eosin stain before a final 2 washes in xylene for 3 minutes each.

2.12. Immunohistochemical staining

Prior to stain, slides were left 20 minutes at room temperature for drying. Muscle sections were then washed three times in 1 x PBS with each wash lasting 5 minutes to remove the embedding media. Following PBS washing, muscle sections were incubated in permeabilisation buffer solution for 15 minutes at room temperature. To remove excess permeabilisation buffer, another three five minutes washes in 1 x PBS were performed before being pre-blocked in wash buffer for 30 minutes at room temperature. Primary antibodies (Appendix I) were pre-blocked in wash buffer 30 minutes prior to their addition onto the muscle sections and incubate overnight at 4°C. In order to remove the primary antibodies, muscle sections were washed three times in wash buffer with each wash lasting 10 minutes. Primary antibodies were identified using Alexa Fluor 488, 594 and 633

secondary antibodies (Appendix I). Pre-blocked in wash buffer was performed for all secondary antibodies (in dark) for minimum of 30 minutes prior to their addition onto the slides. Sections were then incubated for 1 hr in the dark at room temperature. Following the secondary antibodies incubation, the sections were then washed for a further three times in wash buffer with each wash lasting 10 minutes. Finally, slides were mounted in fluorescent mounting medium, and myonuclei were visualised using (2.5µg/ml) 4, 6-diamidino-2-phenylindole (DAPI).

2.13. Antigen Retrieval Immunostaining protocol

In order to improve the presentation of our target antigens and enhance immunoreactivity by breaking down the protein cross-links formed, pre-treatment with the antigen retrieval reagents was performed. Briefly, Sectioned slides were dried for 20 minutes at RT and then washed three times in 1 x PBS with each wash lasting 5 minutes before being fixed in 4% PFA for 20 minutes at RT. Following fixation, slides were again washed 3 times in 1 x PBS, before being incubated in 100% methanol for 5 minutes. The antigen retrieval solution (Appendix 2) was prepared and heated to 90-95°C by placing the staining jar filled with retrieval solution into a water bath. The sectioned slides were then washed in 1 x PBS three times with 5 minutes each before being immersed into the preheated retrieval solution for 2-10 minutes. After the incubation is finished, the staining jar with retrieval solution and slides were removed from the water bath and left to cool to room temperature. To remove excess retrieval solution from the slides, further three five minutes washes in 1 x PBS were performed before sections being pre-blocked in wash buffer for 30 minutes at room temperature. Primary antibodies (Appendix I) were pre-blocked in wash buffer for 30 minutes prior to their addition onto the muscle sections and incubated overnight at 4°C. Primary antibodies were identified using Alexa flour 488, 594 and 633 secondary antibodies (Appendix I). Steps of day 2 of immunostaining protocol were followed before slides being mounted in fluorescent mounting medium and coverslip was placed over the top. Details of reagents are given in (Appendix 2).

2.14. Macrophage immunocytochemistry

For macrophages identification, the Vector Laboratories ImmPRESS™ Excel Staining kit Peroxidase was used and the protocol with the kit being followed.

Muscle sections were transferred from -80 freezer to room temperature and left for 20 minutes for drying. Prior to fix with acetone, the sections were washed in 1 x PBS three times with each wash lasting 5 minutes. For quenching of endogenous peroxidase activity, the sections were incubated with BLOXALL blocking solution for 10 minutes. Another two three minutes washes in 1 x PBS were performed before the slides being incubated with 2.5% of Horse Serum for 20 minutes. Primary antibody F4.80 (rat anti-mouse, BioRad MCA497R) was diluted in washing buffer prior to incubate on the muscle sections overnight. The slides washed twice in 1 x PBS each wash lasting three minutes before being incubated with Amplifier antibody for 15 minutes, washed a further twice in 1 x PBS three minutes each, and incubated for 30 minutes with ImmPRES Excel reagent. The sections were again washed twice with 1 x PBS for 5 minutes each prior to incubate with ImmPACT DAP *EqV* for 2-10 minutes and keep monitoring the stain develop till get the desire intensity. Another two washes in 1 x PBS each wash lasting 5 minutes were performed before slides being rinsed in tab water for 2 minutes. The sections were dehydrated in series concentrations of ethanol (70%, 90%, 100% and 100%) 30 seconds each before two washes in xylene for 30 seconds each. The slides were then mounted using DPX mounting media and covered with cover slip.

2.15. Succinate Dehydrogenase Stain (SDH)

Slides were left for 20 minutes at room temperature for drying purpose. Nitro blue tetrazolium (NBT) and Sodium Succinate stocks were prepared and stored as aliquots of 2 ml in -20°C freezer, the stocks were thawed on ice before mixing. Incubation medium (SDH stain) (NBT Stock 2 ml, Succinate stock 0.2 ml and Phenazine methosulphate 0.7 mg) was prepared shortly just before using and stored in dark. Muscle sections were incubated in the incubation medium (SDH stain) for about 2-5 minutes (2-3 minutes for soleus muscle, and 3-4 minutes for TA and EDL muscles). Care was taken during the staining to determine the optimal time of incubation for each muscle. Slides were washed in distilled water for 1 minute to stop enzymatic reaction. Then samples were fixed in 10% formal-calcium for 15

minutes. Finally, slides were mounted in aqueous mounting media (Hydro mounting media) and coverslip was placed over the top. Details of reagents are given in (Appendix 2).

2.16. Periodic Acid-Schiff (PAS) Stains

Slides were moved from -80°C freezer and left 20 minutes at room temperature for drying. Muscle sections were hydrated in distilled water. The slides were then incubated with Periodic Acid Solution for 5 minutes at room temperature. Sections were rinsed well in tap water, prior to incubate in Schiff Reagent for 15 minutes to achieve desired contrast. Samples were washed in tap water for 10 minutes to produce a bright magenta colour. The muscle sections were stained with Haematoxylin stain for 1 minute to achieve desired contrast, followed by 30 seconds washing in tap water. The slides were placed in Bluing Reagent for 1 minute; then rinsed in deionized water for 30 seconds. The sections were dehydrated in two changes of anhydrous alcohol for 1 minute each, then cleared in three changes of clearing reagent for 1 minute each. Finally, slides were mounted in DPX media and coverslip was placed over the top. Details of reagents are given in (Appendix 2).

2.17. Dihydroethidium (DHE) stain

Muscle sections were transferred from -80 freezer to room temperature and left for 20 minutes. The sections were rehydrated in 1 x PBS for 5 minutes before being incubated with 10 µM of DHE stain for 30 minutes at 37°C. The slides were then washed in 1 x PBS three times with each wash lasting 5 minutes. Finally, slides were mounted in fluorescent mounting medium, and myonuclei were visualised using (2.5µg/ml) 4, 6-diamidino-2-phenylindole (DAPI). Details of reagents are given in (Appendix 2).

2.18. Acid Phosphatase assay

Prior to incubate muscle sections with acid phosphatase incubating solution at 37°C for 1:30 hr, slides were left for 20 minutes at room temperature. Stain progression was monitored every 30 minutes at low magnification of a light microscope. When incubation time finished, the slides were washed with ddH₂O three times with each wash lasting 30 seconds to remove residues of the incubation solution. The sections were counterstained using Harris Haematoxylin was diluted 1:30 for 1 minute. The slides were then rinsed with tap water

before being washed in running tap water for 5 minutes and then rinsed twice in ddH₂O. The slides were mounted in aqueous mounting media (Hydro mounting media) and coverslip was placed over the top. Details of reagents are given in (Appendix 2).

2.19. Transmission electron microscopy (TEM)

This work has been done by Oliver Kretz, University of Freiburg, Germany.

To identify size and distribution of the mitochondria in the muscle fibres, Biceps Brachii and Extensor Carpi Radialis Longus muscles were removed and cut in pieces of 1 mm³. Small slices of muscles were immersed in fixative solution (2.5% glutaraldehyde in 0.1 M Na-cacodylate buffer pH 7.4), samples were then stored at 4°C. Tissue blocks were contrasted using 0.5% OsO₄ for 1.:30 hr in RT, and 1% uranyl acetate in 70% ethanol for 1 hr in RT. After dehydration tissue blocks were embedded in epoxy resin and ultrathin sections of 40 nm thickness were cut using a Leica UC6 ultramicrotome (Leica, Wetzlar, Germany). Sections were imaged using a Zeiss 906 TEM (Zeiss, Oberkochen, Germany) and analysed using ITEM software (Olympus, Germany).

2.20. ¹H NMR spectroscopy-based metabonomic analysis

This work has been done by Natasa Giallourou, University of Reading, Uk.

Gastrocnemius muscles were pulverised, 40–50 mg of muscle tissue was snap frozen in liquid nitrogen and finely ground in 300 µL of chloroform : methanol (2:1) using a tissue lyzer. The homogenate was combined with 300 µL of water, vortexed and spun (13,000 g for 10 min) to separate the aqueous (upper) and organic (lower) phases. A vacuum concentrator (SpeedVac) was used to remove the water and methanol from the aqueous phase before reconstitution in 550 µL of phosphate buffer (pH 7.4) in 100% D₂O containing 1 mM of the internal standard, 3-(trimethylsilyl)-(2,2,3,3-²H₄)-propionic acid (TSP). For each sample, a standard one-dimensional NMR spectrum was acquired with water peak suppression using a standard pulse sequence (recycle delay (RD)-90°-t1-90°-tm-90°-acquire free induction decay (FID)). RD was set as 2 s, the 90° pulse length was 16.98 ms, and the mixing time (tm) was 10 ms. For each spectrum, 8 dummy scans were followed by 128 scans with an acquisition time per scan of 3.8 s and collected in 64 K data points with a spectral

width of 12.001ppm. ^1H nuclear magnetic resonance (NMR) spectra were manually corrected for phase and baseline distortions and referenced to the TSP singlet at δ 0.0. Spectra were digitized using an in-house MATLAB (version R2009b, The Mathworks, Inc.; Natick, MA) script. To minimize baseline distortions arising from imperfect water saturation, the region containing the water resonance was excised from the spectra. Principal components analysis (PCA) was performed with Pareto scaling in MATLAB using scripts provided by Korrigan Sciences Ltd, UK. Details of reagents are given in (Appendix 2).

2.21. Western blotting

Frozen muscles were pulverized in order to obtain fine powder from the muscles. Muscles' powder was then homogenized in lysis solution (4M Urea, 125mM Tris pH6.8, 4% (w/v) SDS, protease inhibitors). Protein amounts were quantified with the Bradford Protein assay. Proteins (20 μg /lane) were separated on 4–12% gradient SDS-PAGE mini-gels (Invitrogen), transferred to nitrocellulose membranes (Whatman), and blocked with 5% skim milk in 0.1% (w/v) Tween-20/Tris buffered saline. Membranes were cut at appropriate molecular weights in order to allow for simultaneous probing of the exact same samples for dystrophin and multiple DGC proteins, as well as alpha-actinin that was used as an internal control for protein loading. Membrane strips were incubated with appropriate primary antibodies overnight at 4°C, followed by a 1 hour incubation at room temperature with the appropriate horseradish peroxidase-conjugated secondary antibodies (Jackson ImmunoResearch). Protein bands were visualized using enhanced chemiluminescence reagents (BioRad). Signal was detected on a ChemiDoc MP Imaging System (BioRad) at an automated range of exposures ranging from 1 second to 1 minute. For densitometric analysis, protein band intensities were quantified using ImageJ (NIH). Values in the linear range of pixel intensities were selected for quantifications. Signal intensities were normalized to alpha-actinin. Details of primary and secondary antibodies are given in (Appendix I).

2.22. RT-qPCR

Gastrocnemius muscles were dissected, weighed and placed on a strip of foil to snap freeze in liquid nitrogen (LN_2). Once the muscles were completely frozen, they were placed in dry ice for short term before being transferred to -80°C .

Frozen Gastrocnemius muscles were chopped into three thirds, and (40 – 50 mg) pieces of each muscle were pulverised and solubilised in TRIzol® (Fisher) using a tissue homogenizer (QIAGEN). Total RNA was isolated and purified using a sequence of chloroform and isopropanol, following the protocol included in the RNesay Mini Kit from Qiagen (74104). RNA concentrations were measured using the Nanodrop 2000 (Thermo Scientific).

5 µg of total RNA was revers-transcribed to cDNA with SuperScript II Reverse Transcriptase and analyse by quantitative real-time RT-PCR on a StepOnePlus™ Real-Time PCR system, using the applied Biosystems SYBRGreen PCR Master Mix and StepOne software v.2.1. Primers were designed using the software Primer Express 3.0 (Applied Biosystems). Relative expression was calculated using the $\Delta\Delta C_t$ method with normalization to the housekeeping genes cyclophilin-B and Hypoxanthine-guanine Phosphoribosyltransferase (hppt). Details of reagents are given in (Appendix 2), and specific primer sequences are given in (Appendix 3).

2.23. *In vivo* assessment of regeneration capacity following Cardiotoxin injection

2.23.1. Anesthetising mice

Induction of anesthesia was carried out with 3.5% isoflurane in oxygen before being maintained at a lower than 2% isoflurane concentration during the procedure using face mask.

2.23.2. Intramuscular (IM) injection of Cardiotoxin into TA muscle

Prior to anesthetising, the solution to be injected was prepared in 30G, 8 mm long 1 mL insulin needles (Insumed 3079264). Animals were anesthetised and the fur at anterior side of the hind leg, around the TA was shaved to allow more accurate orientation. The first injection was carried out with an insertion point parallel to the muscle, at the distal end of the anterior part of the TA. The needle was inserted approximately 7 mm into the muscle and 10 µL of solution was injected. The following two injections were carried out with insertion points vertical to the leg, lateral to the left and right of the proximal end of the TA, with 10 µL solution injected in both sites. In total, 30 µL of 50 µM Cardiotoxin from *Naja mossambica mossambica* was injected into the right TA, and 30 µL of sterile 1 x PBS was injected into the left TA muscles of all mice. Following injection, the animals were returned to their cages and allowed to recover from the anesthesia. The mice were closely monitored

for at least 30 minutes to ensure full recovery. The animals were allowed to convalesce before being culled at three time points (day 3, 6 and 14), then TA muscles were dissected and snap frozen for analysis. Details of reagents are given in (Appendix 2).

2.24. *In vivo* Post-natal blocking of Myostatin

2.24.1. Intraperitoneal injection of soluble activin receptor IIB (sActRIIB-Fc)

One month-old males WT (C57BL/6J01a/Hsd) and *Erry*^{Tg/+} mice were injected intraperitoneally twice weekly with 10 mg/kg of the soluble activin receptor IIB (sActRIIB-Fc) for a total period of two months before culling. Prior to inject the animals, they were weighed, and doses of (sActRIIB-Fc) to be injected were calculated for all animals considering their weights. Animals were held by the tail base, then grabbed at the scruff over the shoulder, turned upside down, and the soluble activin receptor IIB was administrated intraperitoneally using 30G, 8 mm long 1 mL insulin needles (Insumed 3079264). Following each injection, the animals were returned to their cages, and they were monitoring for at least 20 minutes at the day of injection, and day after to ensure they are fine and no bleeding followed the injection.

2.25. Semi-quantitative measurement of Collagens and dystrophin-glycoprotein complex (DGC) proteins expression by immunofluorescence

Membrane signal intensities of approximately 30 muscle fibres of MHC phenotype (IIB⁻/IIB⁻ and IIB⁺/IIB⁺) in muscle sections (EDL, Soleus and TA) from WT, *Mtn*^{-/-} and *Mtn*^{-/-}/*Erry*^{Tg/+} mice, and approximately 50 muscle fibres of MHC phenotype (IIB⁻/IIB⁻, IIB⁺/IIB⁺ and I⁺/I⁺) in EDL and Soleus muscle sections from WT.PBS, *Erry*^{Tg/+}.PBS, WT.sActRIIB and *Erry*^{Tg/+}.sActRIIB were measured. 10 random fibres of a specific phenotype from a central region of each muscle section were counted from three mice of each cohort. Fiji software was used to measure signal intensity from an area of interest after images have been corrected for background to avoid regions of signal saturation. As well as internal controls, all images were taken at the same exposure time based on a non-saturation level in WT tissue. To calculate relative signal intensity levels, individual measurements from fibres of all cohorts were taken as a percentage of mean of MHC IIB⁻ and MHC I of WT muscles.

2.26. Sarcolemma thickness measurement

Connective tissue thickness between 30 -50 chosen fibres of MHC phenotypes (IIB⁻/IIB⁻, IIB⁺/IIB⁺ and I⁺/I⁺) of (EDL, Soleus and TA) muscle sections was measured using Fiji software. 10 random fibres of a specific phenotype from a central region of each muscle section were counted from three mice of each cohort. One measurement on the constant connective tissue thickness, with multi measurements on the fluctuating connective tissue thickness areas between each two myofibres that expressed same MHC isoform were taken on all muscle sections of WT, *Mtn*^{-/-} and *Mtn*^{-/-}/*Errγ*^{Tg/+} as well as muscle sections of WT.PBS, *Errγ*^{Tg/+}.PBS, WT.sActRIIB and *Errγ*^{Tg/+}.sActRIIB mice. Importantly, all analysed images were taken at the same light intensity (exposure time).

2.27. Imaging and analysis

Haematoxylin and Eosin (H&E), Succinate Dehydrogenase (SDH) and Periodic Acid-Schiff (PAS) stained sections were examined using Zeiss Axioskope2 microscope, and images were captured using an Axiocam digital camera with Zeiss Axiovision computer software version 4.8. Fluorescence microscope (Zeiss AxioImegar A1) was used to examine immunofluorescent stained sections, and images were captured using an Axiocam digital camera with Zeiss Axiovision computer software version 4.8. To examine entire muscle, the images at mid-belly were reconstructed using Adobe Photoshop CS3. ImageJ software was used for counting analysis. For the detection of differences in myofibres cross-sectional area (CSA), Zeiss Axiovision software version 4.8 was used.

2.28. Statistical analysis

Data were presented as mean ± SE. Significant differences between two groups were performed by Student's t-test for independent variables. Differences among groups were analysed by one-way analysis of variance (ANOVA) followed by Bonferroni's multiple comparison tests as appropriate, and Twa-way ANOVA followed by Bonferroni post-tests to compare replicate means by row. Statistical analysis was performed on GraphPad Prism software. Differences were considered statistically significant at p < 0.05 (one asterisk), p < 0.01 (two asterisks) or p < 0.001 (three asterisks).

Chapter 3; Results

Morphometric, Physiological and Histological analysis of hyper-oxidative hypertrophic muscle

3.1. Introduction

The maintenance of muscle mass and function has important health implications and loss of muscle mass in particular is associated with increased morbidity and mortality and a reduced quality of life (Huss et al., 2002, Wang and McPherron, 2012).

Skeletal muscle plasticity concept was applied by John Eccles and colleagues to describe the effect of cross-innervation on the size and fibre characteristics of skeletal muscle of cats (Buller et al., 1960). It was well established that skeletal muscle is a highly compliant tissue that undergoes both qualitative and quantitative changes as a part of its adaptation to physiological and environmental stimuli. Most skeletal muscles are composed of a heterogeneous population of muscle fibres that differ in their metabolic and molecular properties as well as contractile speeds, a feature imparted by the expression of the type of myosin heavy chain (MHC) being expressed. Moreover, muscle fibres are affected by different factors, for instance innervation, genetic background, neuromuscular activity, exercise training, mechanical loading/unloading, and ageing (Pette and Staron, 2001). Further studies have described skeletal muscle as a dynamic tissue that displays varied responses to internal and external stimuli by changing its phenotypic profile in terms of size as well as its composition through changing genes expression and metabolic properties (Matsakas and Patel, 2009b).

One of the main factors that induce muscles mass and imparts high quality of life is mechanical loading. Conversely, loss of skeletal muscle mass as a result of genetic disorders, ageing and energy shortage has a major effect on public health (Thomas, 2007, Matsakas and Patel, 2009b). Modification in muscle mass following mechanical loading or resistance exercise requires a high level of oxygen consumption that is realized by an increase in capillary density to maintain maximal mass specific blood flow (Armstrong et al., 1986).

Skeletal muscle mass depends chiefly on the fibre number (hyperplasia) and fibre size (hypertrophy). However genetic background and animal breed are major factors that determine muscle mass (Martyn et al., 2004). The skeletal muscles constitute ~ 40% of the animal body mass, therefore whole body weight can be affected as a result of muscle fibre number and size changes. The number of myofibres is fixed at the prenatal stage. At the post-natal stage, muscle growth is accompanied by fusion of myogenic precursor cells to the

existing myofibres (Sandri, 2008). Nader (Nader, 2005) has shown that muscle mass maintenance or loss is fundamentally the consequences of a balance between two important processes, skeletal muscle protein synthesis and protein degradation. This balance is regulated by two important pathways, AKT/mammalian target of rapamycin (mTOR) that control protein synthesis, and AKT/fork head box O (FOXO) pathway that controls protein breakdown (Glass, 2005). Further work has described *Myostatin* as a key regulator of muscle mass, since its absence leads to muscle hypertrophy, whereas its overexpression causes muscle atrophy (Elliott et al., 2012).

Numerous studies have demonstrated that skeletal muscle fibres are generally classified as slow or fast fibres, where slow fibres express the myosin heavy chain (MHC) isoform I, whereas fast fibres express MHC IIA, IIX and/or IIB. They display noticeable differences in term of their metabolism, contractile properties and susceptibility to fatigue. Slow fibres generally show a small cross-sectional area (CSA), contain more mitochondria which sustain a high oxidative capacity, and a denser microvascular network than fast fibres that rely predominantly on glycolysis for ATP production, with low mitochondrial content and oxidative enzymes, and they are fatigue susceptible. Muscle fibres can change their phenotype, such as the expression of MHC, mitochondrial content and capillary supply in response to external stimuli (Pette and Staron, 1997, Pette and Staron, 2001, Olson and Williams, 2000).

Previous works have established that during the development of skeletal muscle fibres in response to endurance exercise, there is also increase in the proportion of type IIA and type IIX fibres at the expense of IIB fibres (Hather et al., 1991, Erskine et al., 2010). Other studies have reported that exercise training induces fast to slow transition in fibre type and myosin isoforms within the fast fibres population shift from type IIB toward type IIA (Andersen and Henriksson, 1977, Jansson and Kaijser, 1977). There is also evidence of myofibres adaptation in order to improve the physical performance which characterized by an increase of mitochondrial biogenesis, angiogenesis and fibre type transformation, in response to endurance exercise (Yan et al., 2011). In the line with these investigations, findings by (Amthor et al., 2007, Girgenrath et al., 2005) have revealed a shift of myofibres toward type IIB, with a noticeable reduction in type IIA and IIX myofibre types of the extensor digitorum

longus (EDL) and tibialis anterior (TA) muscles from *Myostatin* null mice. Conversely, increase in the proportion of slow myofibres, with simultaneously decrease of fast-twitch myofibres has been reported following *Erry* overexpression (Matsakas et al., 2012b).

Until recently it has been shown that mitochondria need a high level of oxygen that diffuses from capillaries to generate ATP for muscle contractile and aerobic metabolism. Therefore, there might be a trade-off between muscle fibre size and aerobic metabolism determined by diffusion limitation (van Wessel et al., 2010). In fact, an inverse relationship between muscle fibre size and maximal oxygen uptake has been reported (Van der Laarse WJ, 1998). This relationship, in theory, ultimately imparts a constraint on the size that mitochondria-rich and therefore high O₂-dependent oxidative fibres can attain before they become anoxic or adapt to a glycolytic phenotype less reliant on O₂ (Desplanches et al., 1996, Deveci et al., 2001).

Here we investigated whether inverse relationship between muscle fibre size and aerobic metabolism mediated by mitochondrial density can be broken, and sought to develop large fibres without compromising function, such as fatigue resistance and exercise capacity.

Previous studies have shown that *Myostatin* is a potent inhibitor of skeletal muscle growth and its deletion results in a hypermuscular phenotype called "Muscle Doubling" as a result of generalized hyperplasia and hypertrophy which seen in mice, cattle and even in humans (McPherron et al., 1997, McPherron and Lee, 1997, Schuelke et al., 2004). Although such enlarged muscles appear essentially normal at the histological level, their ability to generate tension is impaired, particularly during prolonged periods of work (Amthor et al., 2007, Mendias et al., 2006, Relizani et al., 2014). In this section we determined whether altering the metabolic profile of skeletal muscles through *Erry* overexpression would influence these features of *Myostatin* null muscles. To that end, we developed a novel mouse line by introducing an *Erry* overexpression allele driven by a skeletal muscle fibre promoter (Human α -Skeletal Muscle Actin) (Muscat and Kedes, 1987) that enhances the oxidative capacity (Narkar et al., 2011) into a hypertrophic *Mtn*^{-/-} background. Based on the concept of a constraint between the CSA and aerobic metabolism of a fibre, there are three possible consequences of the cross: Firstly, absence of *Myostatin* resulted in de-represses and prevails of Akt pathway that leads to hypertrophic, but glycolytic fibres. Secondly, oxidative

features would be imparted by the *Erry* programme that would follow the inverse size relationship and lead to mitochondria-rich fibres which would be smaller than wild type (Rangwala et al., 2010). And finally, the constraint is broken resulting in the development of hypertrophic hyper-oxidative fibres.

Three genotypes of male mice (WT, *Mtn*^{-/-} and *Mtn*^{-/-}/*Erry*^{Tg/+}) (n=5) were bred, housed under standard environmental conditions and provided food and water ad libitum in the Biological Resource Unit, University of Reading, to an adult age (3 months).

Animals' physiological properties like fatigue test, muscle strength and locomotor activities were examined using exhaustion running protocol on treadmill, grip strength meter, and open field activity monitoring respectively.

The hind limb muscles (Soleus, Extensor digitorum longus (EDL), Tibialis Anterior (TA) and Gastrocnemius) were isolated and weighed. These muscles have been selected because they represent a sufficient variety of myofibre composition. One side EDL muscles were used to measure force generating capacity. Then muscles were frozen, cryosectioned and immunostained using antibodies for myosin heavy chains (MHC) (types I, IIA and IIB) to determine total muscle fibre number, types and size (CSA), and CD31 antibody to identify capillary density per muscle fibre. Gastrocnemius muscles were pulverised, divided into three thirds, one third was homogenized and RNA samples were extracted to determine expressions of *Erry* and MHC genes using qPCR technique. Another third was powdered and lysed, then protein samples were extracted and used to determine the expression of molecules responsible for protein synthesis and degradation. Biceps brachii (BB) and Extensor carpi radialis longus (RECL) muscles were isolated, fixed and used for transmission electron microscopy (TEM) work.

The main observations of this chapter are, firstly, muscles from *Mtn*^{-/-}/*Erry*^{Tg/+} mice maintain the same muscle fibre number and size exhibited by *Myostatin* null mice. Secondly, *Mtn*^{-/-}/*Erry*^{Tg/+} mice show fatigue resistance characteristics not only more than *Mtn*^{-/-} mice, but even outperform wild type mice during an incremental exercise test. Thirdly, we show that *Erry* overexpression into *Mtn*^{-/-} background drives a partial reversal transition of MHCs profiling toward WT muscle condition. Finally, forelimb muscles from *Mtn*^{-/-}/*Erry*^{Tg/+} mice show absence of ultrastructure abnormalities seen in *Mtn*^{-/-} muscles, with a remarkable

increase of mitochondrial numbers in particular at the sub sarcolemma location, that exceed mitochondrial density not only in muscles from *Mtn*^{-/-}, but also that of WT mice.

3.2. Muscle-specific expression of *Erry* into *Mtn*^{-/-} background mice using human α -skeletal actin promoter

Previous studies have demonstrated that estrogen-related receptor- γ (*Erry*) is exclusively expressed in metabolically active and densely vascularised tissues like skeletal muscles (Giguere, 2008, Hong et al., 1999). Further investigations have reported that *Erry* has a potential role to regulate not only mitochondrial programs involved in Fatty Acid Oxidation (FAO), Tricarboxylic Acid Cycle (TCA), and Oxidative phosphorylation (OXPHOS), but also the expression of genes network that controls angiogenesis programme, and calcium handling pathways in skeletal muscle that are required for longer term adaptation to exercise (Stein and McDonnell, 2006, Alaynick et al., 2007). Moreover, evidence has been provided that *Erry* overexpression in skeletal muscle is sufficient to enable anaerobic muscles to attain enhanced oxidative capacity, and increase treadmill endurance (Rangwala et al., 2010).

Therefore, transgenic overexpression of *Erry* in skeletal muscles using specific promoters have been broadly applied to enhance muscle mitochondrial functions, induce expression of fuel uptake genes, and restoration of blood perfusion in different cases of muscle disorders (Rangwala et al., 2010, Narkar et al., 2011).

Outcomes of previous transfection studies have shown that sequences upstream of the transcription start site of the rat and chicken skeletal actin gene were sufficient for both stage- and tissue-specific expression (Melloul et al., 1984, Grichnik et al., 1986, Bergsma et al., 1986). Further study has demonstrated that the human α -skeletal actin (HSA) gene promoter is complex and large, spanning 1,300 bp. Three segments of this region when adjacent to simian virus 40 (SV40) promoter act as regulatory domains that respond to specific factors produced by muscle itself to regulate positive modulation of transcription (Muscat and Kedes, 1987). The proximal domain (positions -153 to -87) of the HSA gene promoter is crucial for muscle-specific expression in two different myogenic cell lines (L8 and C2C12), and the distal domain (positions -1300 to -626) of the promoter is only necessary in C2C12 cells for tissue-specific expression (Wang et al., 2004). Moreover, it has been reported that the tissue-specific transcription of the human α -skeletal actin gene promoter resulted from the interaction of the upstream regions with trans-acting positive regulatory factors in muscle cells (Muscat and Kedes, 1987).

In the present study, we found that introduction of *Erry* in a skeletal muscle-specific manner into the *Mtn*^{-/-} background to generate double transgenic *Mtn*^{-/-}/*Erry*^{Tg/+} resulted in viable, fertile offspring that were born at the normal Mendelian ratios.

Next we examined the expression of *Erry* gene in gastrocnemius muscle (n=5) from all three cohorts (WT, *Mtn*^{-/-} and *Mtn*^{-/-}/*Erry*^{Tg/+}) mice. Our results showed that using HSA promoter induced robust overexpression of *Erry* in the *Mtn*^{-/-} background mice, indicating by a significant increase of *Erry* gene expression (~ 250 folds) in muscle samples of *Mtn*^{-/-}/*Erry*^{Tg/+} mice compared to other genotypic groups (Figure 3.1).

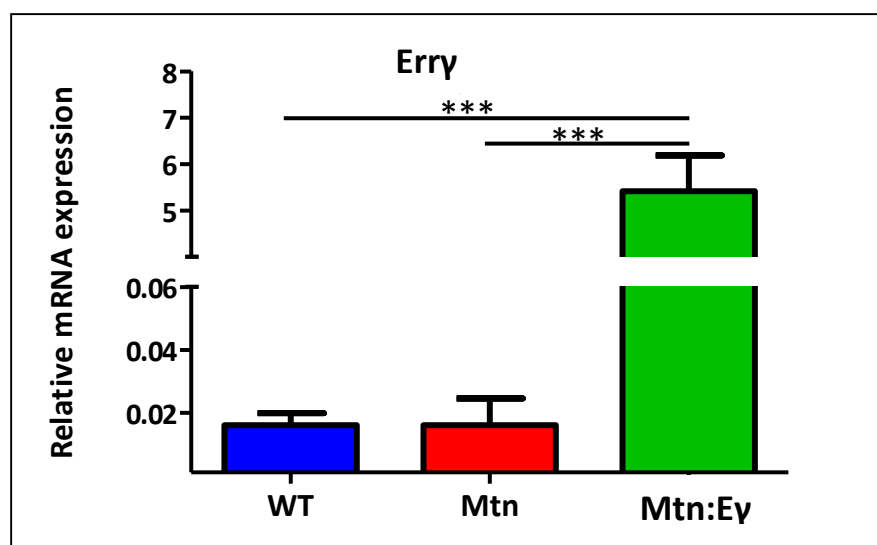


Figure 3.1. *Erry* expression induced by using human α -skeletal actin promoter

Displaying *Erry* mRNA level in Gastrocnemius muscles of wild type (WT), *Myostatin* null (*Mtn*) and *Erry* transgenic mice on the *Myostatin* null background (*Mtn:Ey*) mice.

(n = 5) male twelve-week old mice per group; One-way ANOVA followed by Bonferroni's multiple comparison tests, ***=p<0.001.

3.3. Body weight and skeletal muscle mass following *Myostatin* deletion and *Erry* overexpression on *Myostatin* null background mice

Myostatin has been known as a member of the Transforming Growth Factor beta (TGF- β) superfamily that its gene is highly conserved among vertebrate species, and functions as a negative regulator of skeletal muscle mass development (McPherron et al., 1997, McPherron and Lee, 1997). Thereafter, number of studies have shown that lack of *Myostatin* results in a dramatic and widespread increase in skeletal muscle mass, demonstrating the existence of a powerful mechanism to control muscle growth (Amthor et al., 2007, McPherron and Lee, 1997).

Once death had been ascertained, we first examined the consequences of *Erry* overexpression in a muscle-specific manner on whole body weight of mice lacking *Myostatin* ($n=5$). Our results showed that body mass of WT, *Mtn*^{-/-} and *Mtn*^{-/-}/*Erry*^{Tg/+} animals were similar at 12 weeks of age (Figure 3.2).

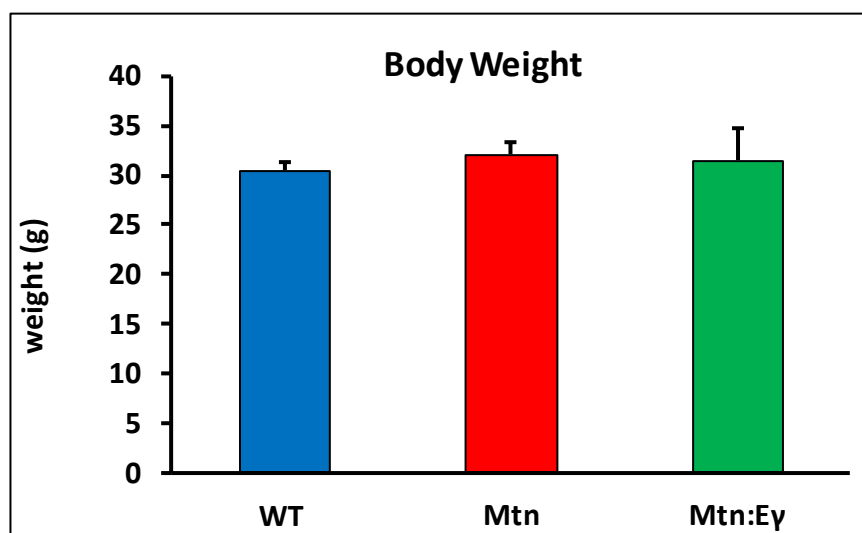


Figure 3.2. *Myostatin* deletion and *Erry* introducing into *Myostatin* null background mice doesn't affect body weight

Body weights of wild type (WT), *Myostatin* null (*Mtn*) and *Erry* transgenic mice on the *Myostatin* null background (*Mtn:Er*) mice.

($n = 5$) male twelve-week old mice per group; One-way ANOVA followed by Bonferroni's multiple comparison tests.

Then we examined the weight of hind limb muscles (EDL, Gastrocnemius, Soleus and TA,) of the three genotypic groups.

In agreement with previous study by McPherron and Lee (McPherron and Lee, 1997), we found that all the examined hind limb muscles (n=10) of *Myostatin* null animals were heavier than the wild type. The EDL, gastrocnemius, soleus and TA muscles were in both *Mtn*^{-/-} and *Mtn*^{-/-}/*Erry*^{Tg/+} approximately 43%, 44%, 47% and 70% larger than their WT counterpart respectively (Figure 3.3 and Table 3.1).

Importantly, the increase in muscle weight in *Myostatin* knockout mice was maintained following *Erry* overexpression. Of particular note there was no significant difference in mass for any of the muscles from *Mtn*^{-/-} and *Mtn*^{-/-}/*Erry*^{Tg/+} mice. These data show that in the absence of *Myostatin*, the skeletal muscles become bigger, and *Erry* transgenic mice preserved the increase of muscle mass exhibited by *Myostatin* null mice (Figure 3.4).



Figure 3.3. Hind limb muscle mass of WT, *Mtn* and *Mtn:Er* mice

Displaying clear disparate of hind limb muscles size of (WT), *Myostatin* null (*Mtn*) and *Erry* transgenic mice on the *Myostatin* null background (*Mtn:Er*) mice.

Male twelve-week old mice.

Table 3.1. Weight of hind limb muscles from WT, *Mtn* and *Mtn:Ey* mice.

Muscle / Weight (mg)	WT	<i>Mtn</i>	<i>Mtn:Ey</i>
Extensor Digitorum Longus	14.9±1	21.4±0.8	21.2±0.9
Gastrocnemius	195.3±5.5	284.5±15.8	276±10
Soleus	12.6±1	18.5±1	17.2±0.5
Tibialis Anterior	54±0.5	92.8±5.6	90.4±3.2

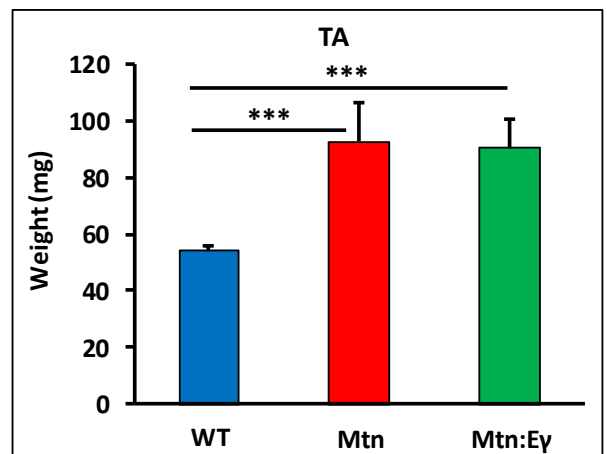
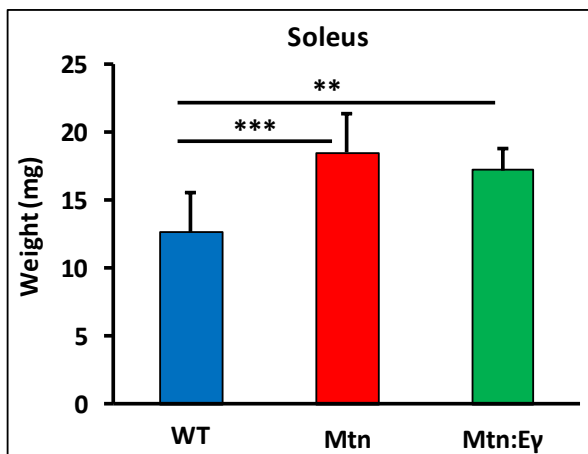
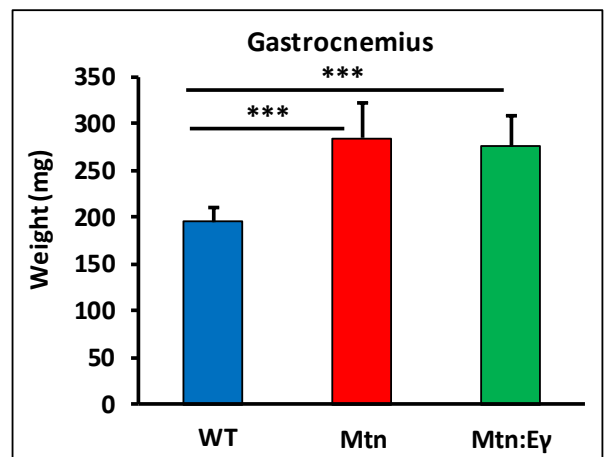
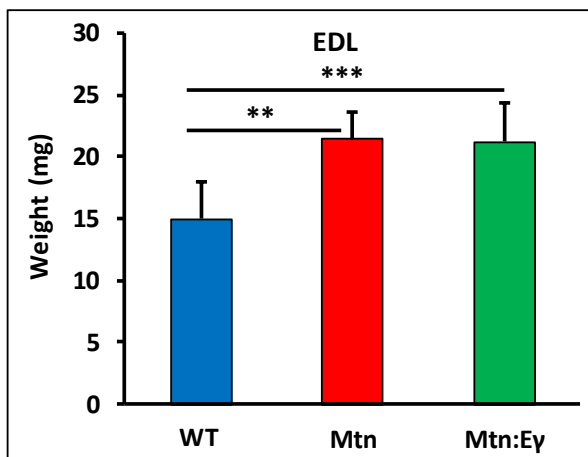


Figure 3.4. Muscle-specific expression of *Errγ* maintains hypertrophy features of *Myostatin* null background muscles

Quantification of skeletal muscle (EDL, gastrocnemius, soleus and TA) mass of wild type (WT), *Myostatin* null (*Mtn*) and *Errγ* transgenic mice on the *Myostatin* null background (*Mtn:Er*).

(*n* = 10) male twelve-week old mice per group; One-way ANOVA followed by Bonferroni's multiple comparison tests, ** = $P < 0.01$ and *** = $P < 0.001$.

3.4. *Erry* overexpression into *Myostatin* null background mice induces fatigue resistance

We showed that *Myostatin* deletion resulted in a dramatic increase in muscle mass compared to wild type without change of whole body weights. Previous study by Savage's group has shown that the exercise intolerance is not related to body weight, as they demonstrated a reduction of exercise capacity in young *Myostatin* knockout compared to wild type mice while body weights were similar (Savage and McPherron, 2010). Other studies have illustrated that cattle with muscular hypertrophy as a result of *Myostatin* gene mutation, are prone to muscle damage after mild exercise (Holmes et al., 1973, Marchitelli et al., 2003).

On the other hand, Rangwala and his team provided evidence that induce *Erry* expression is sufficient to increase treadmill endurance and exercise tolerance (Rangwala et al., 2010). Therefore, to determine whether the increase of *Erry* expression into hypertrophic *Myostatin* null mice would enhance the exercise capacity of these animals, we subjected mice (n=5) of three cohorts WT, *Mtn*^{-/-} and *Mtn*^{-/-}/*Erry*^{Tg/+} to the exhaustion treadmill running protocol. In accord with previous observations, we found that *Mtn*^{-/-} mice reached exhaustion significantly earlier than WT control and had shorter total running time. However, the *Mtn*^{-/-}/*Erry*^{Tg/+} mice ran for approximately 80% longer than the *Mtn*^{-/-} and 25% longer than the WT mice.

These results show that *Erry* overexpression in a muscle lacking *Myostatin* improved the exercise capacity to not only out run *Mtn*^{-/-} but also WT mice (Figure 3.5).

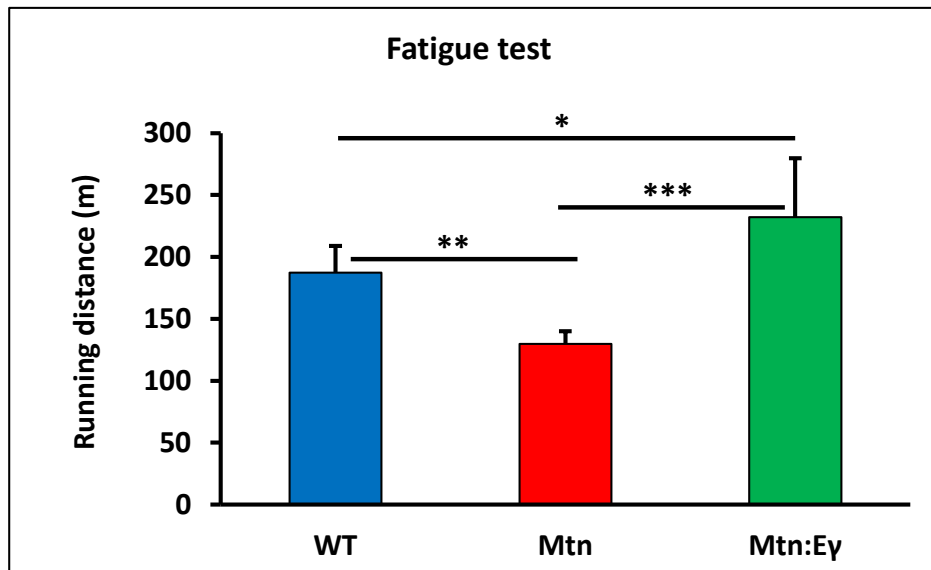


Figure 3.5. Exercise tolerance test for WT, *Mtn* and *Mtn:Ey* animals, using mouse treadmill protocol

Quantification of running distance of WT, *Mtn* and *Mtn:Ey* mice on treadmill showing a remarkable exercise capacity for the *Mtn:Ey* mice, with worse performed of *Mtn* mice ($n = 5$) male twelve-week old mice per group; One-way ANOVA followed by Bonferroni's multiple comparison tests, $*=P<0.05$, $** = P<0.01$ and $***= P<0.001$.

3.5. Increased muscle force generation capacity following muscle-specific manner *Erry* overexpression into the *Myostatin* null background mice

We demonstrated above that overexpression of *Erry* using specific promoter is efficacious to induce exercise capacity and attenuate muscle fatigability of *Myostatin* null mice. Thereafter, we performed a series of tests for muscle force generation aptitude.

In this regard, conflicting results have been reported. Previously it was well established that treatment of *mdx* mice with stabilized Myostatin propeptide resulted in an increase of muscle-specific force output (Wagner et al., 2002, Bogdanovich et al., 2002). Several other studies have reported, despite a remarkable increase of skeletal muscle mass following *Myostatin* deletion (McPherron and Lee, 1997, McPherron et al., 1997), this increase was not accompanied by propionate increase of muscle force generation (Amthor et al., 2007). Here we examined the potential of a muscle-specific manner *Erry* overexpression to promote force generation in the muscles lacking *Myostatin*.

We found that the maximal isometric tetanic force generated by the EDL muscles of 12 weeks age *Mtn*^{-/-} mice was not significantly different to that of age-matched WT mice, despite the larger muscle mass (Figure 3.6A). The tetanic force generated by *Mtn*^{-/-}/*Erry*^{Tg/+} EDL muscles was, however, greater than that of the EDL from both WT and *Mtn*^{-/-} mice (n=5) (Figure 3.6A). We next calculated the Specific Force (sPo), the tetanic force per muscle mass. The (sPo) of the EDL of *Mtn*^{-/-} mice was lower than that of the other groups, with that of the *Mtn*^{-/-}/*Erry*^{Tg/+} mice being significantly greater than *Mtn*^{-/-} mice, but not normalized to WT levels (Figure 3.6B).

We also examined the force generating capacity of the soleus muscles from all three cohorts. The tetanic force of *Mtn*^{-/-} soleus muscle was significantly lower than those of WT. There was no difference in this parameter between the soleus muscles of WT and *Mtn*^{-/-}/*Erry*^{Tg/+} (Figure 3.6C). The specific force of the soleus muscles showed the same overall profile as that of the EDL but did not reach statistical significance, possibly due to low sample size (Figure 3.6D).

Altogether, these data show that lack of *Myostatin* compromises muscle force production even with a marked increase of muscle mass. However the muscle-specific expression of

Erry in *Mtn*^{-/-} mice not only induces muscles maximum tetanic force generation, but also improves specific force production.

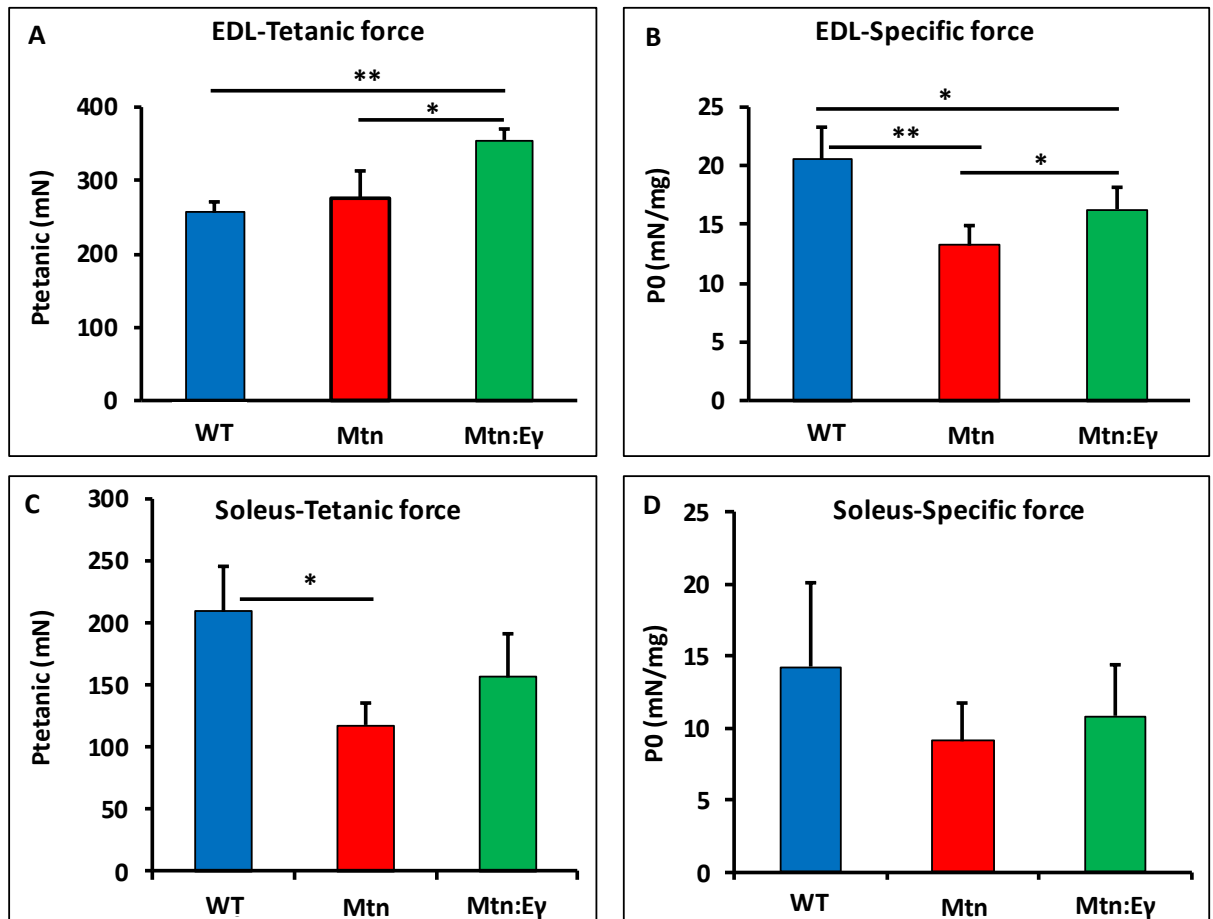


Figure 3.6. *Erry* overexpression into *Mtn* mice is required to improve muscle force generation capacity

Contractile properties of EDL and Soleus muscles from WT, Mtn and Mtn:Erry mice. Specific force denotes tetanic force normalized to wet muscle mass

(A) Quantification of maximal isometric tetanic force generated by EDL muscles

(B) Quantification of specific force generated by EDL muscles

(C) Quantification of maximal isometric tetanic force generated by soleus muscles

(D) Quantification of specific force generated by soleus muscles

(*n* = 5) male twelve-week old mice per group; One-way ANOVA followed by Bonferroni's multiple comparison tests. *=*P*<0.05 and ** = *P*<0.01.

3.6. *Erry* overexpression induces forelimb muscles grip strength that was compromised due to *Myostatin* deletion

We demonstrated that the increase in muscle mass following *Myostatin* deletion was not accompanied by a proportionate increase of exercise capacity and muscle force generation. However, muscle-specific manner overexpression of *Erry* was sufficient to improve these features. Previous work has shown that normalised gripping strength of forelimb muscles to body weights of *Mtn*^{-/-} and WT mice, was not significantly different (Guo et al., 2016). Here we examined whether 12 weeks old of age *Myostatin* knockout mice show a difference of muscle grip strength compared to matched age WT mice (n=5), and to what extent that *Erry* overexpression in a muscle lacking *Myostatin* would affected this parameter.

Using a grip meter to assess muscle strength, our observations showed that *Myostatin* null mice had reduced strength compared to controls. However, muscle strength was significantly improved following *Erry* overexpression into *Myostatin* null background muscles (Figure 3.7). These data suggest that introduction of *Erry* into a muscle lacking *Myostatin* can attenuate the decline of muscle strength following *Myostatin* ablation.

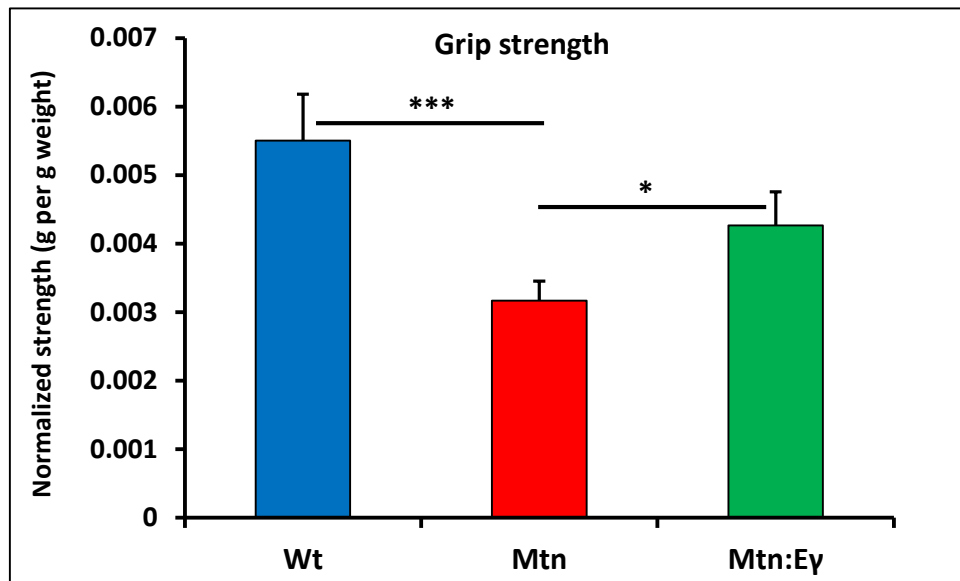


Figure 3.7. Muscle-specific manner overexpression of *Er* attenuate *Mtn* muscle strength decreasing

Forelimb muscles contraction measurement through assessment of grip strength for WT, *Mtn* and *Mtn:Er* mice, using grip strength meter. Grip strength was normalised to the weight of the mice.

($n = 5$) male twelve-week old mice per group; One-way ANOVA followed by Bonferroni's multiple comparison tests, $*=P<0.05$ and $***= P<0.001$.

3.7. Locomotor activity of *Myostatin* null and *Erry* overexpression into *Mtn*^{-/-} background mice

To further solidify of our results at a functional level, behavioural and locomotor activity of mice from our three cohorts (WT, *Mtn*^{-/-} and *Mtn*^{-/-}/*Erry*^{Tg/+}) (n=5) were measured using open field activity monitoring. Previous work has illustrated a reduction of muscle physiological function following *Myostatin* deletion (Matsakas et al., 2012a). Conversely, Study by Rangwala's group has reported a significant increase of travelled distance and work performed of *Erry* transgenic into WT background mice compared to controls (Rangwala et al., 2010). Therefore, in this section we determined whether *Erry* overexpression into *Myostatin* null background mice would induce locomotor activity of these animals.

We found that *Myostatin* null mice were the least active indicated by spending longer periods of immobility compared to other genotypic groups (Figure 3.8A, B and C). However, *Mtn*^{-/-}/*Erry*^{Tg/+} mice showed higher activity than both *Myostatin* null and control mice with less static time (Figure 3.8A, B and C). Moreover, muscle-specific expression of *Erry* into *Myostatin* null mice enables these animals to travel longer distances than WT and *Mtn*^{-/-} mice without arriving at significant differences (Figure 3.8D).

Taking together, these data suggest that introducing of *Erry* into a muscle lacking *Myostatin* is efficacious in enhancing behavioural and locomotor characteristics.

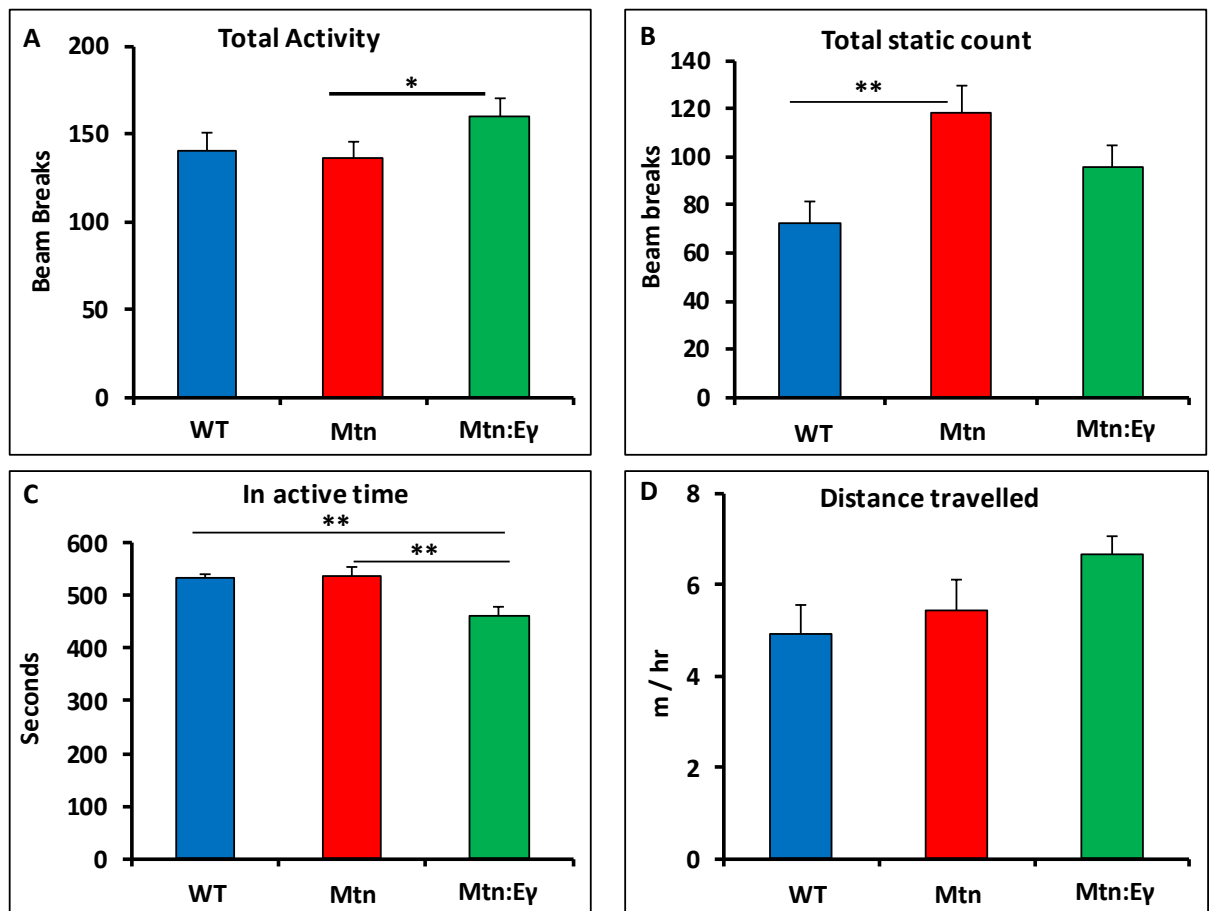


Figure 3.8. *Ery* over expression promotes behavioral and locomotor features of *Myostatin* null mice

Organismal activity measurements through activity cages for WT, *Mtn* and *Mtn:Eye* mice.

(A) Quantification of total activity of each animal from the three genotypes

(B) Static time of each animal from the three cohorts

(C) Quantification of the inactivity time

(D) Quantification of the distances were travelled by each mouse

($n = 5$) male twelve-week old mice per group; One-way ANOVA followed by Bonferroni's multiple comparison tests, *= $P < 0.05$, and **= $P < 0.01$.

3.8. *Erry* overexpression sustains myofibres hyperplasia exhibited by *Myostatin* null muscles

We showed that *Myostatin* null mice exhibit a dramatic increase in muscle mass compared to controls. However this increase was concomitant with reduction of exercise capacity, and was not accompanied with a proportionate increase of muscle force generation. Strikingly, *Erry* overexpression into *Mtn*^{-/-} mice maintained the increase of muscle mass, improved muscle force generation, and not only normalised muscle function-fatigability but also exceeds the WT values.

Pervious work has reported that a large part of the increase of muscle mass of growth-differentiation factor 8 (*GDF-8*) mutant mice resulted from muscle cell hyperplasia (McPherron et al., 1997). Other studies have illustrated that the increase in muscle mass following germline deletion of *Myostatin* gene is due to an increase in muscle fibres size and number (Elashry et al., 2009, McPherron et al., 2009).

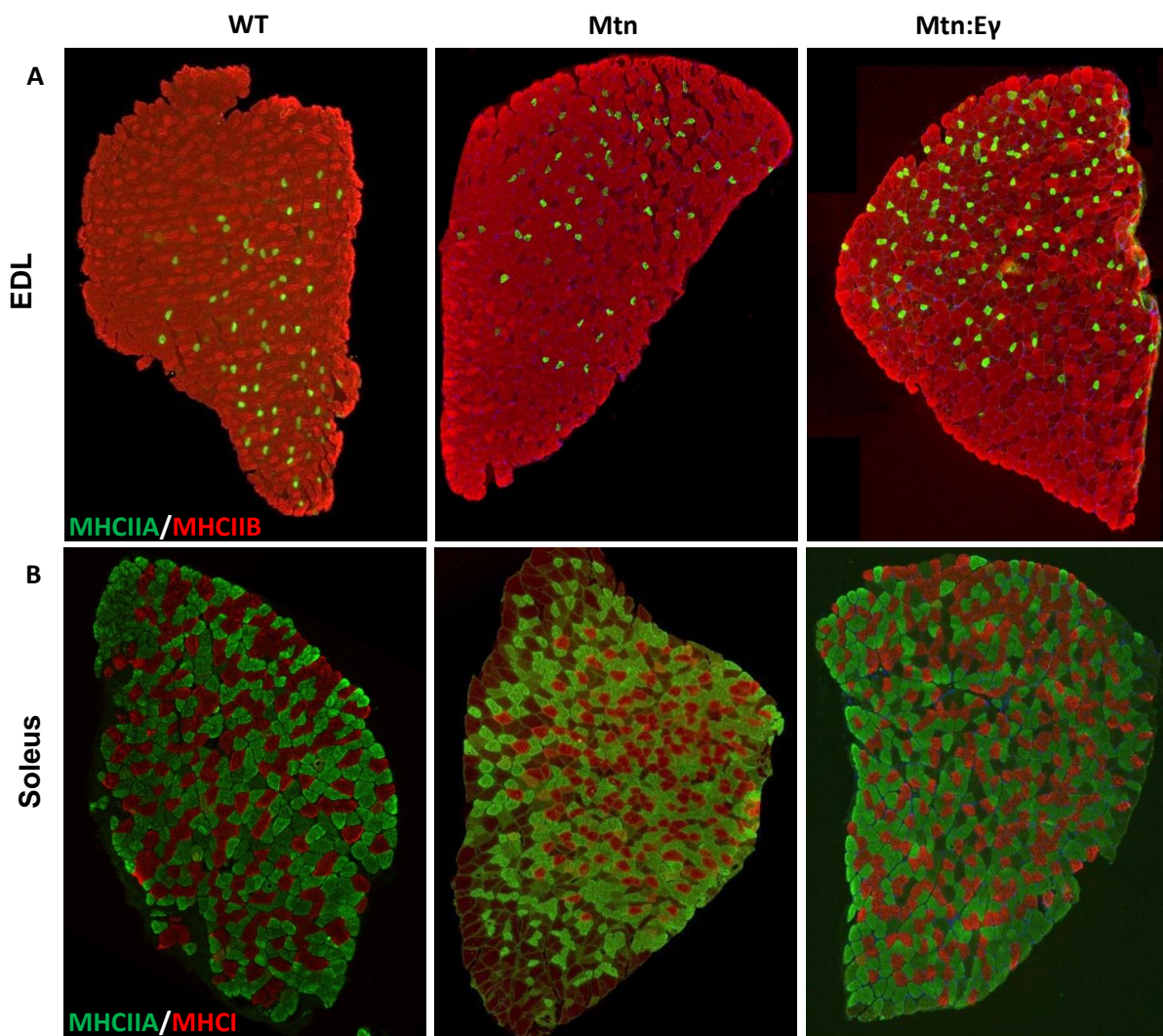
In present study, we determined whether the increase in muscle mass of *Mtn*^{-/-} and *Mtn*^{-/-}/*Erry*^{Tg/+} mice resulted from an increase in muscle fibre numbers or sizes, or both of them. Therefore, Immunohistochemistry protocol using antibodies against myosin heavy chain (MHC) isoforms (type I, IIA and IIB) was performed to determine total fibre number in both EDL and soleus muscles (n=5) of each genotype (WT, *Mtn*^{-/-} and *Mtn*^{-/-}/*Erry*^{Tg/+}) (Figure 3.9A and B). Total fibre number of TA muscles was not included in this analysis, as its anatomical shape makes it impossible to obtain the same mid-belly section.

Here we examined the effect of a muscle-specific manner *Erry* expression into hypertrophic *Myostatin* null EDL and soleus muscles fibre numbers.

Our data showed a significant increase in total fibres number of EDL and soleus muscles from both *Mtn*^{-/-} and *Mtn*^{-/-}/*Erry*^{Tg/+} compared to their counterpart muscles of wild type mice (Table 3.2, and Figure 3.9 C and D). Interestingly, we found that the introduction of *Erry* into *Mtn*^{-/-} muscles did not significantly changed the number of fibres seen in *Mtn*^{-/-} EDL (Figure 3.9 A and C) or soleus muscles (Figure 3.9 B and D). These data reveal that loss of *Myostatin* induces an increase muscles hyperplasia. Most importantly, overexpression of *Erry* into *Mtn*^{-/-} mice conserved the increase of total fibres number of these muscles.

Table 3.2. Myofibre number of Soleus and EDL muscles from WT, *Mtn* and *Mtn:Ey* mice.All data are show as mean \pm SEM.

Muscle	Genotype	Average total fibre number
Extensor digitorum longus (EDL)	WT	882 \pm 32
	<i>Mtn</i>	1127 \pm 29
	<i>Mtn:Ey</i>	1010 \pm 36
Soleus	WT	721 \pm 46
	<i>Mtn</i>	890 \pm 28
	<i>Mtn:Ey</i>	896 \pm 47



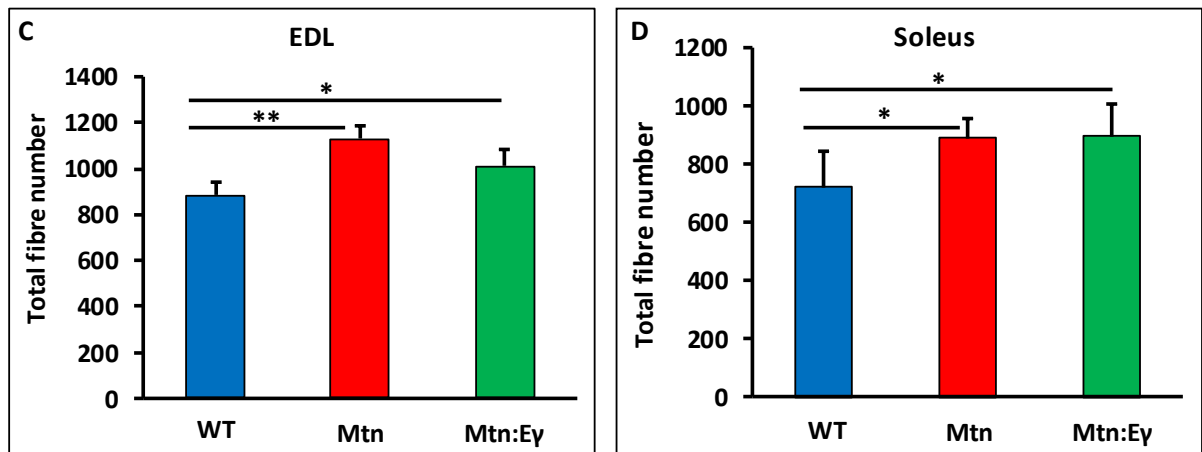


Figure 3.9. *Myostatin* deletion increased muscle fibres number and *Erry* overexpression maintained this increase.

Muscle-specific expression of *Erry* didn't affect the hyperplasia of *Myostatin* null background muscles

(A) Immunohistochemical images of EDL muscles from WT, *Mtn* and *Mtn:Ey* mice. Green fibres signify the expression of MHCIIA with MHCIIIB appearing as red.

(B) Immunohistochemical images of soleus muscles from WT, *Mtn* and *Mtn:Ey* mice. Green fibres signify the expression of MHCIIA with MHCI appearing as red.

(C) Quantification of total fibres number in EDL muscles.

(D) Quantification of total fibres number in soleus muscles.

($n = 5$) male twelve-week old mice per group; One-way ANOVA followed by Bonferroni's multiple comparison tests, $*=P<0.05$, and $**=P<0.01$.

3.9. Muscle fibres hypertrophy following *Myostatin* deletion was not affected by *Erry* overexpression into *Mtn*^{-/-} mice

We demonstrated that overexpression of *Erry* conserved myofibres hyperplasia induced by germline deletion of *Myostatin*. Previous work has shown that hind limb muscles of *Mtn*^{-/-} mice undergo large and show remarked levels of size increase (McPherron and Lee, 1997). Further study has reported that the large size of muscles lacking *Myostatin* is attributed mainly to individual muscle fibre hypertrophy (Amthor et al., 2007). Moreover, it has been established that *Myostatin* plays a fundamental role in regulating of muscle mass and size, since its inactivation induces a marked increase of muscle fibre cross-sectional areas (Rodriguez et al., 2014). Here we investigated whether metabolic reprogramming imparted by *Erry* introducing into *Mtn*^{-/-} mice affected the increase of myofibres size promoted by *Myostatin* ablation. Therefore, muscle sections were immunostained using antibodies against MHC isoforms (type I, IIA and IIB). Then measurement of cross-sectional area (CSA) for myofibres (type I, IIA, IIX and IIB) of hind limb muscles (EDL, soleus and TA) from three cohorts of mice (WT, *Mtn*^{-/-} and *Mtn*^{-/-}/*Erry*^{Tg/+}) was performed. A minimum of 150-200 measurements per myofibre type were taken in each muscle section (n=5) (Figure 3.10A-C).

We found that the fibre sizes were equivalent in the EDL muscles of *Mtn*^{-/-} and *Mtn*^{-/-}/*Erry*^{Tg/+} mice (Table 3.3). Of particular note was that the MHCIIA in EDL muscles of *Mtn*^{-/-} mice displayed a significant increase in fibre size compared to controls. MHCIIA of the EDL muscles of *Mtn*^{-/-}/*Erry*^{Tg/+} mice were smaller than *Mtn*^{-/-}, but they were still larger than those in the WT mice. Consistently, CSA of MHCIIIX and MHCIIIB of EDL muscles from both *Mtn*^{-/-} and *Mtn*^{-/-}/*Erry*^{Tg/+} mice were significantly larger than the corresponding fibres in the EDL muscles of WT mice. Interestingly, there was no significant difference in the fibre sizes of MHCIIIX and MHCIIIB in the EDL muscles from *Mtn*^{-/-} and *Mtn*^{-/-}/*Erry*^{Tg/+} mice (Figure 3.11 A).

Next we examined myofibre sizes in the soleus muscles. We found that there was no significant difference in CSA of myofibres type I (which were measured only in soleus muscle sections as there was insufficient numbers in other muscles (EDL and TA)) in the soleus muscles from the three genotypes (WT, *Mtn*^{-/-} and *Mtn*^{-/-}/*Erry*^{Tg/+}) mice.

Further, fibre size of MHCIIX in the soleus muscles from *Mtn*^{-/-} and *Mtn*^{-/-}/*Erry*^{Tg/+} mice was greater than those fibres in the soleus muscles from wild type animals. Of particular observations, fibre size of MHCIIB from *Mtn*^{-/-}/*Erry*^{Tg/+} mice was significantly smaller than this isoform of fibres in the soleus muscles of *Mtn*^{-/-} mice (Table 3.3 and Figure 3.11 B)

Finally, myofibres sizes in the TA muscles (deep and superficial regions) from WT, *Mtn*^{-/-} and *Mtn*^{-/-}/*Erry*^{Tg/+} mice were measured. We found that the size of MHCIIA in the deep region of TA muscles from *Mtn*^{-/-} and *Mtn*^{-/-}/*Erry*^{Tg/+} mice was significantly larger than those of WT mice. Importantly, the fibre sizes of MHCIIA in this region of TA muscles from *Mtn*^{-/-} and *Mtn*^{-/-}/*Erry*^{Tg/+} showed no significant difference. On the other hand, MHCIIA were completely absent in superficial regions of TA muscles from WT and *Mtn*^{-/-} mice. Along the same lines, we found that the CSA of MHCIIX in the deep region of TA muscles from *Mtn*^{-/-} were slightly larger than these myofibres in the same region of TA muscles from WT mice, with a significant increase in CSA of MHCIIX in the deep region of TA muscles from *Mtn*^{-/-}/*Erry*^{Tg/+} compared to other two cohorts. Superficial area of TA muscle sections from *Myostatin* null mice displayed a significant increase in CSA of myofibres type IIX. Remarkably, this increase of MHCIIX size was preserved in the same region of TA muscles from *Mtn*^{-/-}/*Erry*^{Tg/+} mice. Moreover, our data highlighted that glycolytic type IIB myofibres in both deep and superficial regions of TA muscles are most prone to undergo hypertrophy following *Myostatin* deletion. Most importantly, fibre sizes of MHCIIB in the deep and superficial regions of TA muscles from both *Mtn*^{-/-} and *Mtn*^{-/-}/*Erry*^{Tg/+} were significantly larger than the size of MHCIIB in both regions of TA muscles from WT mice (Table 3.3 and Figure 3.11 C-D).

Altogether, these data show that germline deletion of *Myostatin* induces muscle fibres hypertrophy. Importantly muscle-specific overexpression of *Erry* into *Mtn*^{-/-} mice had no effect on their myofibre size.

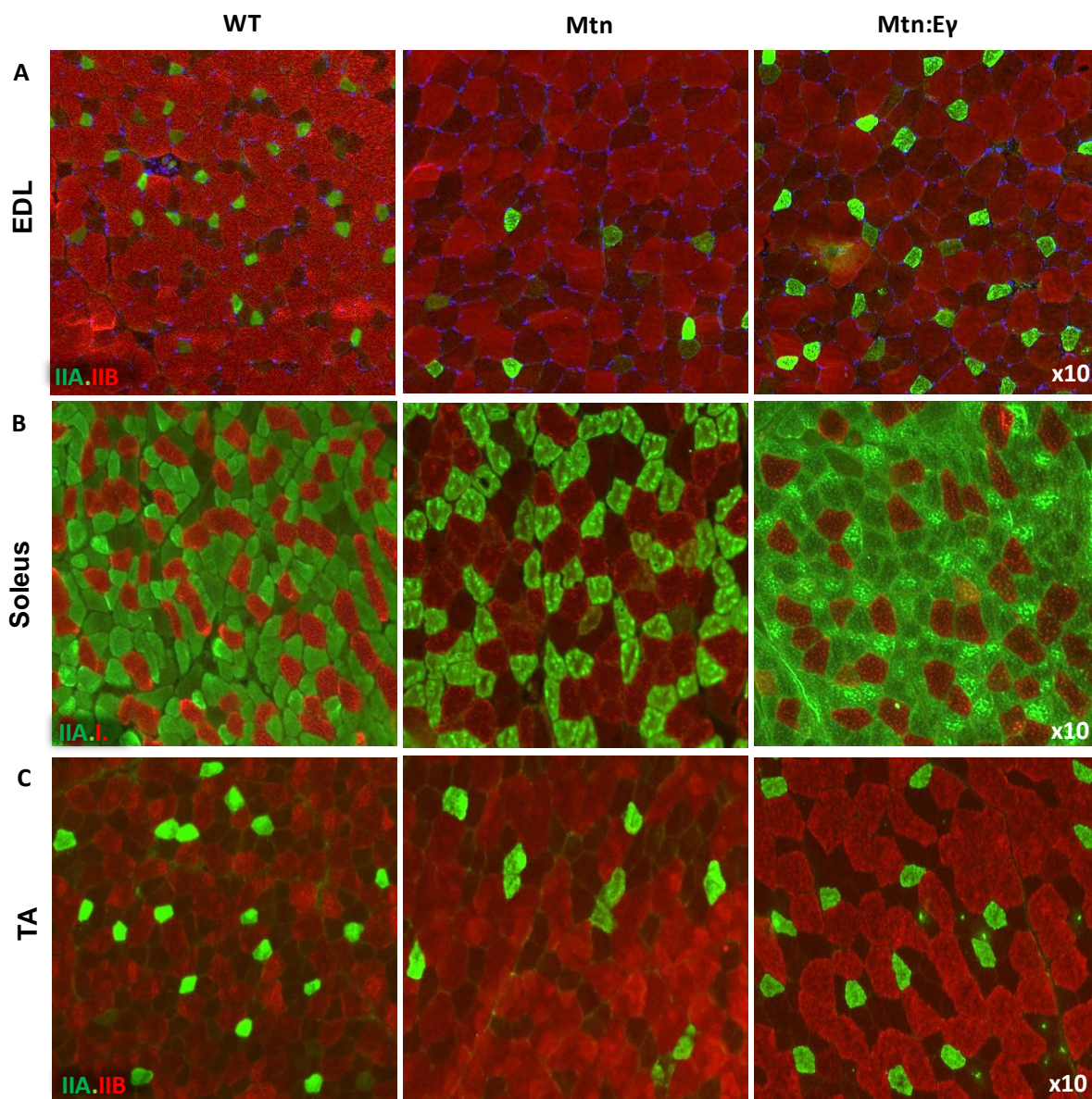


Figure 3.10. Myofibres size following *Myostatin* deletion and *Erry* introducing into *Mtn*^{-/-} mice

Muscle-specific expression of *Erry* maintains muscle fibres hypertrophy exhibited by *Myostatin* null muscles.

(A) Immunohistochemical images of EDL muscles from WT, *Mtn* and *Mtn:Erry* mice. Green fibres signify the expression of MHCIIA with MHCII B appearing as red. Non green and red fibres represent MHCII X.

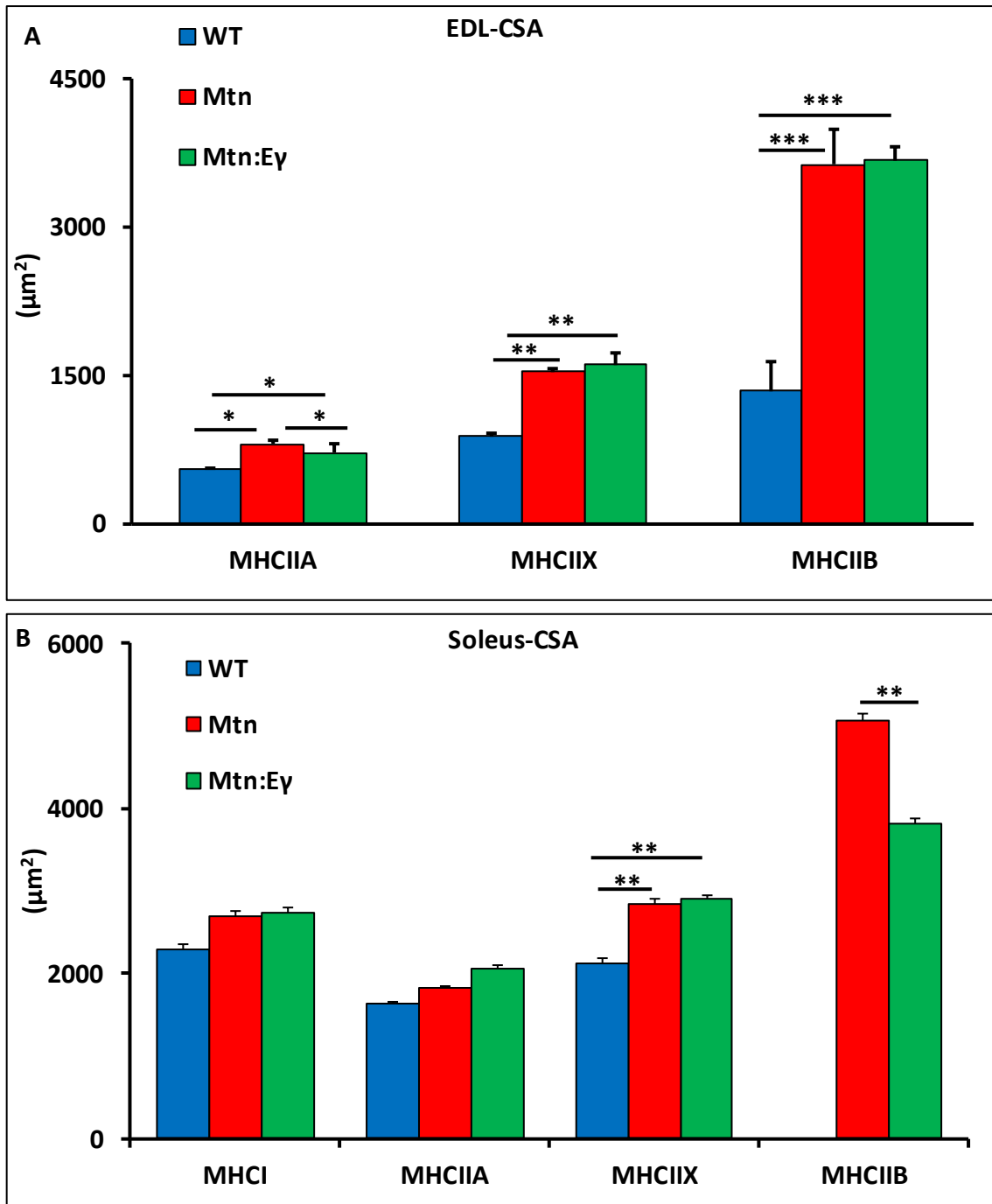
(B) Immunohistochemical images of soleus muscles from WT, *Mtn* and *Mtn:Erry* mice. Green fibres signify the expression of MHCII A with MHC I appearing as red.

(C) Immunohistochemical images of TA muscles from WT, *Mtn* and *Mtn:Erry* mice. Green fibres signify the expression of MHCII A with MHCII B appearing as red. Non green and red fibres represent MHCII X.

(*n* = 5) male twelve-week old mice per group.

Table 3.3. Cross sectional area for type I, IIA, IIX and IIB myofibres of (EDL, soleus, and TA) muscles from WT, *Mtn* and *Mtn:Erry* mice. Size in (μm^2) with SEM of 5 muscle sections

Genotype	WT				<i>Mtn</i>				<i>Mtn:Erry</i>			
	I	IIA	IIX	IIB	I	IIA	IIX	IIB	I	IIA	IIX	IIB
EDL	n/a	553.7±2	883.8±21	1345±208	n/a	802.3±25	1535±19	3634±249	n/a	714.5±71	1611±87	3678±91
Soleus	2300±46	1640±24	2127±69	n/a	2694±56	1820±27	2842±58	5073±73	2738±56	2069±24	2909±48	3816±70
Deep TA	n/a	1087±20	1202±16	3050±42	n/a	1334±75	1274±23	3622±47	n/a	1246±29	1516±31	3774±57
Sup. TA	n/a	n/a	1184±26	2834±40	n/a	n/a	1511±51	3681±37	n/a	1115±73	1509±52	4006±61



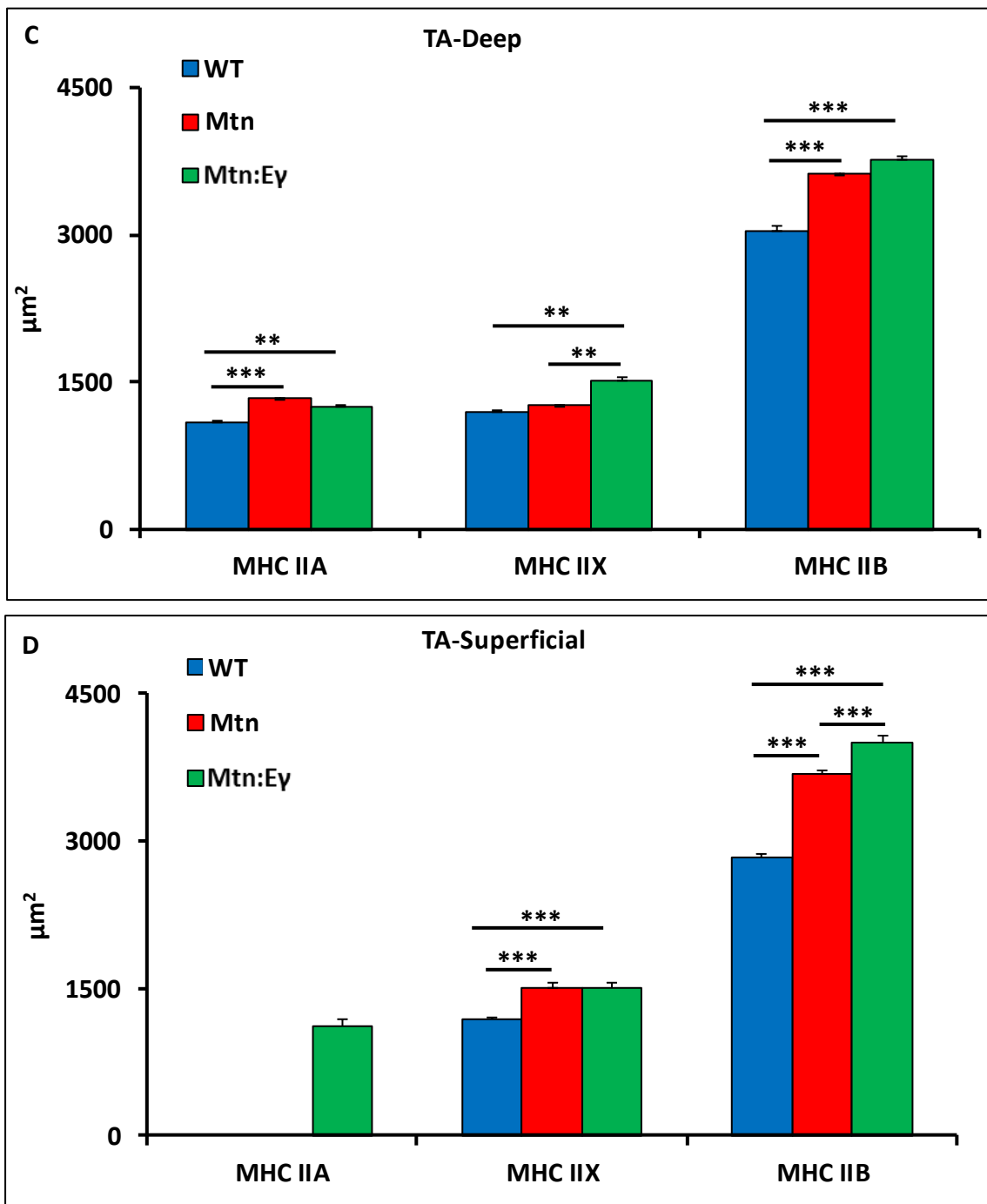


Figure 3.11. Myofibres of hind limb muscles from *Mtn* and *Mtn:Er* mice show larger CSA than their counterpart myofibres from WT mice

Myostatin deletion induces muscle fibre size, and *Er* overexpression preserved the increase.

(A) Graph showing measurements of the cross sectional area (CSA, μm^2) of MHCIIA, IIX and IIB in EDL muscles from WT, *Mtn* and *Mtn:Er* mice.

(B) Graph showing measurements of the cross sectional area (CSA, μm^2) of MHCI, IIA and IIX in soleus muscles from WT, *Mtn* and *Mtn:Er* mice.

(C-D) Graphs showing measurements of the cross sectional area (CSA, μm^2) of MHCIIA, IIX and IIB in Deep and Superficial regions for TA muscles WT, *Mtn* and *Mtn:Er* mice.

($n = 5$) male twelve-week old mice per group; One-way ANOVA followed by Bonferroni's multiple comparison tests, $*=P<0.05$, $**=P<0.01$ and $***= P<0.001$.

3.10. Mechanisms underpinning muscle enlargement following *Myostatin* deletion and *Erry* overexpression

In addition to induce exercise capacity and muscle force generation, we showed that *Erry* introducing into *Mtn*^{-/-} mice maintained the increase in muscle fibre numbers and sizes exhibited by *Myostatin* deletion. We believe it is necessary to develop the understanding of mechanisms underpinning muscle fibres enlargement. Previous work has established that skeletal muscle mass is the result of a dynamic balance between two crucial processes, protein synthesis, that regulated by AKT/mTOR pathway, and protein degradation, that controlled by AKT/FoxO pathway (Sandri, 2008, Glass, 2005). Further investigation has revealed a central role of *Myostatin* in regulating of muscle protein synthesis and degradation, indicating by a cross talk between *Myostatin* and AKT/mTOR signalling pathway (Elliott et al., 2012). Here we examined the consequences of *Myostatin* deletion on the key molecules that control protein synthesis and degradation processes. Then, we determined whether a muscle-specific manner overexpression of *Erry* into *Mtn*^{-/-} muscles would affect expression of these molecules. We found that levels of phosphorylated AKT that induce muscle anabolism was significantly higher in muscles from *Mtn*^{-/-} and *Mtn*^{-/-}/*Erry*^{Tg/+} mice compared to WT. Interestingly, there was no significant difference in pAKT level between muscles from *Mtn*^{-/-} and *Mtn*^{-/-}/*Erry*^{Tg/+} mice (Figure 3.12).

Next we examined the level of pAKT downstream target (4EBP1) in all cohorts. The same relationship of pAKT was discovered in muscle samples of the three genotypic groups. AKT not only promotes protein synthesis but also suppresses catabolism partly by phosphorylating and thereby inactivating FoxO3. Thus, we next examined expression of FoxO, we found that that deletion of *Myostatin* resulted in an increased ratio of the inactive:active (phosphorylated:non-phosphorylated) form of FoxO3. However, in muscles of *Mtn*^{-/-}/*Erry*^{Tg/+} mice the levels of inactive FoxO3 was significantly lower than in that of the *Mtn*^{-/-} mice, with no difference in FoxO3 level in muscles from *Mtn*^{-/-}/*Erry*^{Tg/+} and WT mice (Figure 3.12). Collectively, these observations suggest that *Myostatin* could be a key regulator molecule that control muscle protein metabolism (synthesis and breaking down) that support myofibre enlargement in absence of *Myostatin*. Importantly, overexpression of *Erry* into *Mtn*^{-/-} muscle has not affected this feature.

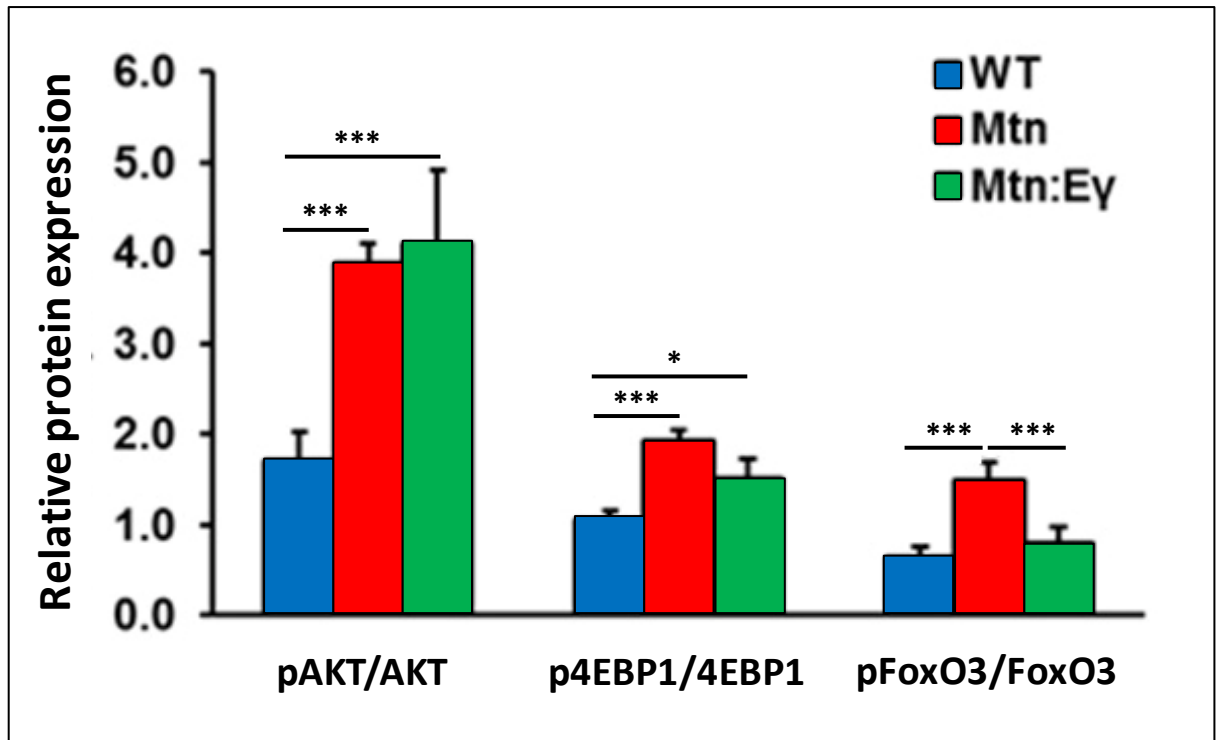


Figure 3.12. Muscle-specific expression of *Ery* maintains the hypertrophy in the *Myostatin* null background muscles

Protein expression of key regulators that control anabolism (pAKT, p4EBP1) and catabolism (pFoxO3) in the gastrocnemius muscle.

($n = 5$) male twelve-week old mice per group; One-way ANOVA followed by Bonferroni's multiple comparison tests, $*=P<0.05$ and $***= P<0.001$.

This work has been done by Roberta Sartori, University of Padua, Italy.

3.11. MHC profiling in hind limb muscles of *Mtn*^{-/-} mice reforms by *Erry* overexpression

We showed that overexpression of *Erry* into a muscle lacking *Myostatin* is efficacious to improve muscle force generation and general physiological functions, while maintained the increase of muscle fibre number and size induced by *Myostatin* ablation. We speculate that it is necessary to identify whether the metabolic re-programming driven by *Erry* overexpression into *Mtn*^{-/-} mice would impact muscle fibres profiling. Previous work has established the striking feature of skeletal muscle fibres plasticity and ability to undergo conversion between different fibre types in response to intrinsic and extrinsic factors. Moreover, the transitions between muscle fibre types have primarily limited within the fast myosin isoforms (shift from MHCIIA to MHCIIB and from MHCIIB to MHCIIA), as a response to environmental and physiological stimuli (Pette and Staron, 2001). Further work using animal models has concluded that *Myostatin* deletion induced fibre types conversion from the slow (type I and IIA) into fast (type IIX and IIB) phenotypes (Girgenrath et al., 2005). On the other hand, Matsakas and his group have referred to an increase in the proportions of myosin heavy chain type IIA and IIX, and a decrease of glycolytic myofibre type IIB following *Erry* overexpression into WT background mice (Matsakas et al., 2012a). However, the potential of muscle-specific overexpression of *Erry* into *Mtn*^{-/-} mice for myofibres re-patterning remain to be elucidated. Here we examined MHC profiling of hind limb muscles (EDL, soleus and TA) (n=5) from three cohorts of mice (WT, *Mtn*^{-/-} and *Mtn*^{-/-}/*Erry*^{Tg/+}), that were immunostained using antibodies against MHC isoforms (type I, IIA and IIB) (Figure 3.13).

Our observations revealed that each muscle displayed varied levels of transition between myofibre types following *Myostatin* deletion and *Erry* introducing into *Mtn*^{-/-} mice. Muscles isolated from *Mtn*^{-/-} mice exhibited an increase expression of fast fibres and a concomitant decrease of slow fibres. In contrast, muscles of *Erry* overexpression mice showed an increase of slow fibres in expense of fast phenotypes within the MHCII subtypes, but did not extend to normalize the proportion of MHCI fibres in the soleus muscles.

Of particular note, we found that EDL muscles from *Mtn*^{-/-} mice showed a high percentage of MHCIIB (70.8%) compared to counterpart muscle from WT mice (64.2%). *Erry* introducing into *Mtn*^{-/-} resulted in a significant decrease of fast (IIB) myofibres percentage (61.6%)

compared to *Mtn*^{-/-} muscles with no significant difference compared to WT mice (Figures 3.13A and 3.14A).

Next we examined MHC proportions in soleus muscles that made up mainly of MHCI (31.4%) and MHCIIA (63.3%) and devoid of MHCIIIB myofibres in wild type animals. Contrary, in *Mtn*^{-/-} muscles, we found that MHCIIIB was (17%), and type MHCIIIX myofibres increased significantly (18.7%) compared to soleus muscles of wild type mice (5.2%). The proportion of MHCIIIB fibres of soleus muscles from *Mtn*^{-/-}/*Erry*^{Tg/+} was lower than that in *Mtn*^{-/-}, while that of MHCIIA fibre was higher. Nevertheless, both *Mtn*^{-/-} and *Mtn*^{-/-}/*Erry*^{Tg/+} displayed a lower proportion of MHCI fibres in the soleus muscle than WT (Figures 3.12B and 3.13B).

Then we determined the MHC profiling of TA muscles (n=5) from the three genotypic groups. We showed that TA muscles from *Mtn*^{-/-} mice displayed high percentages of MHCIIIB (62.9% and 91.7%) compared to WT (36.2% and 72.1) in deep and superficial regions respectively. Interestingly, *Erry* overexpression into *Myostatin* null muscles resulted in a significant decrease of MHCIIIB compared to *Mtn*^{-/-} mice (38.1% and 77.3%) in deep and superficial regions respectively (Figures 3.13C-D and 3.14C-D).

Together these data show that *Myostatin* deletion resulted in a significant increase of fast muscle fibres compared to WT. However, introduction of *Erry* into *Mtn*^{-/-} mice was efficacious to drive a partial reversal of MHC profile of *Mtn*^{-/-} towards the WT condition in all muscles examined, without rescue deficit of type I myofibre. Such data with above observations, raise possibility to challenge the trade-off that is thought to exist between aerobic metabolism and fibre size (van Wessel et al., 2010).

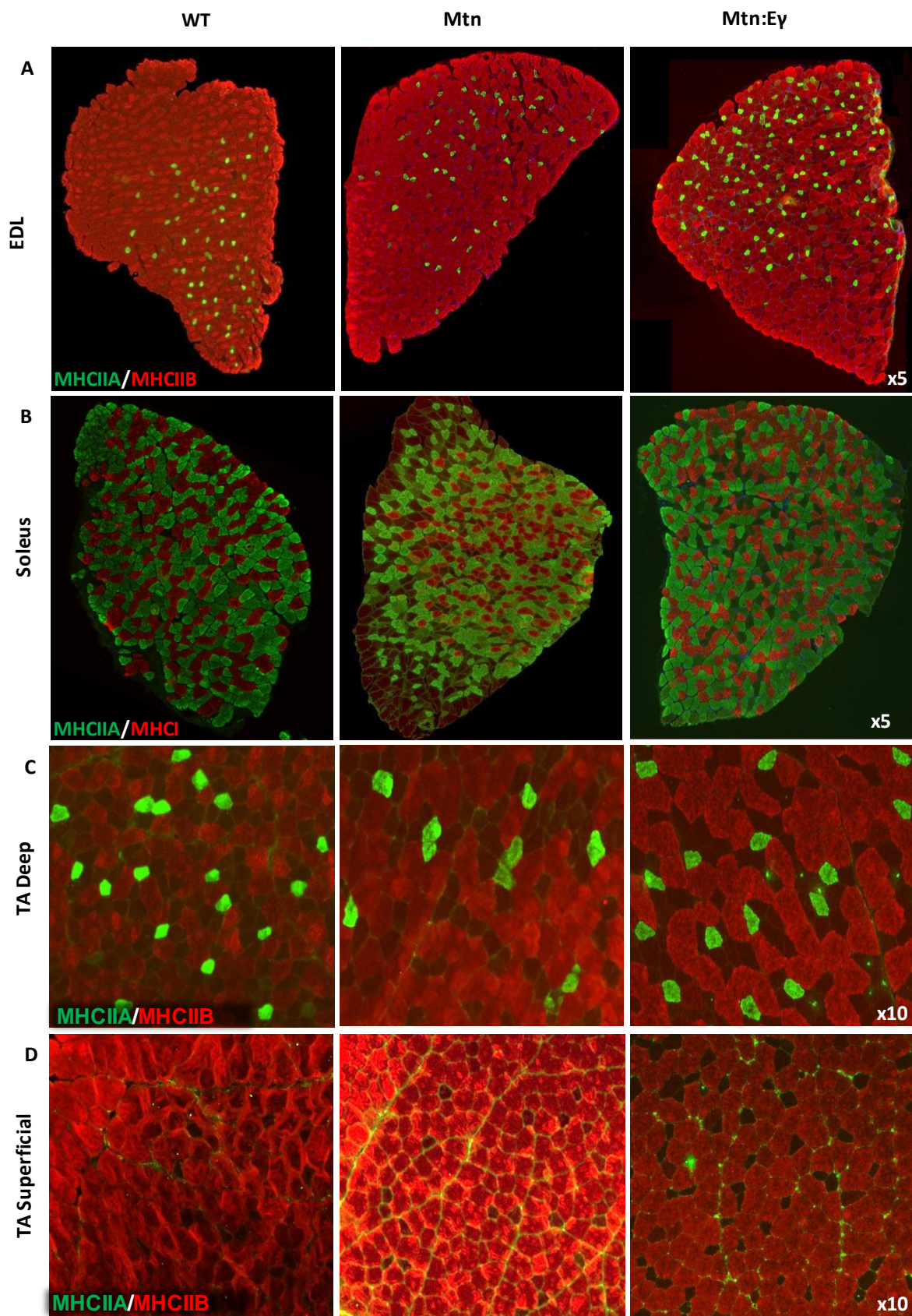


Figure 3.13. Myosin heavy chain profiling of hind limb muscles affects by *Myostatin* ablation and *Erry* overexpression into *Mtn*^{-/-} mice.

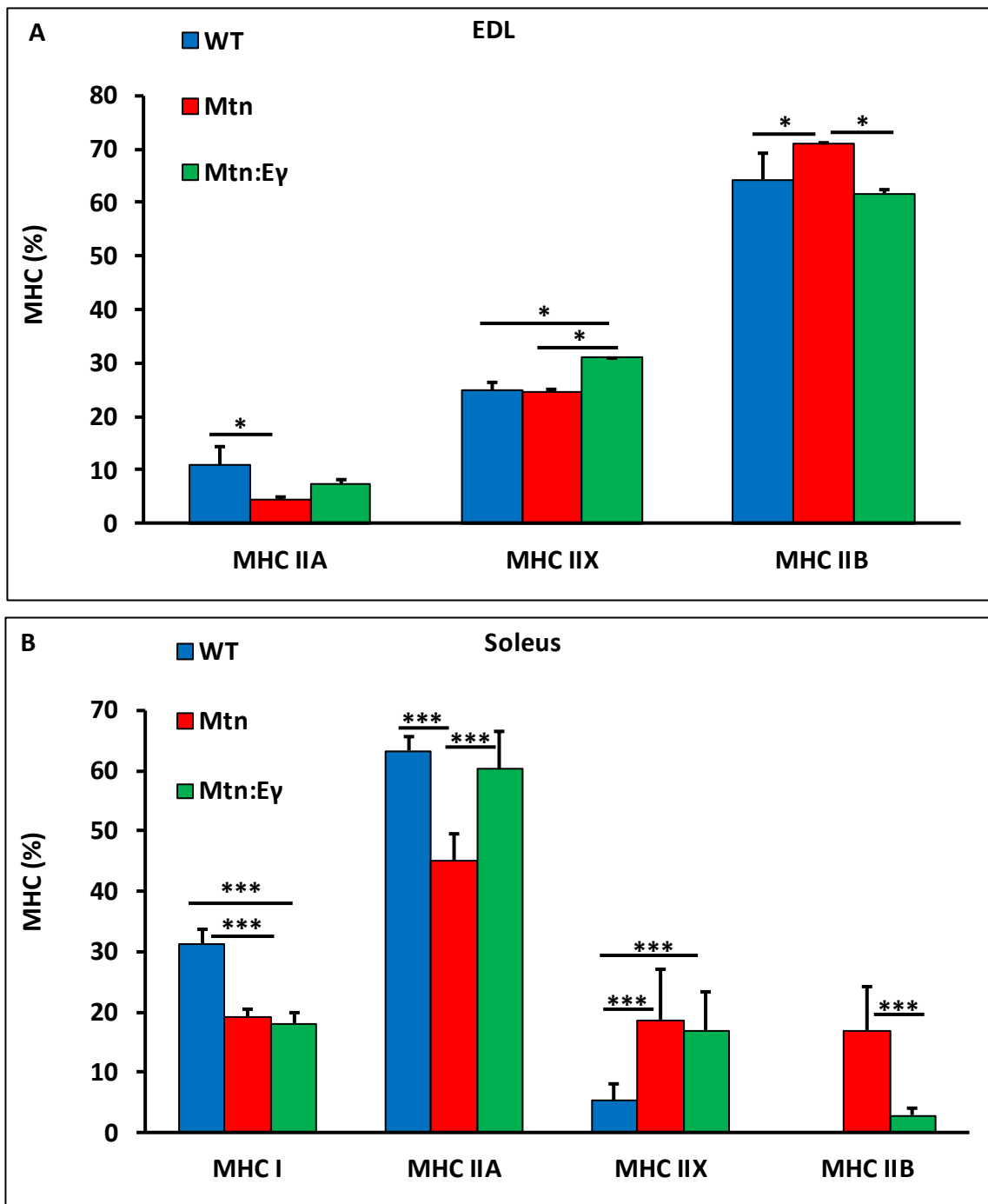
Muscle-specific expression of *Erry* in *Myostatin* null mice induced muscle fibres conversion toward WT conditions.

(A) Immunohistochemical images of EDL muscles from WT, *Mtn* and *Mtn:Er* mice. Green fibres signify the expression of MHCIIA with MHCIB appearing as red. Non green and red fibres represent MHCIX.

(B) Immunohistochemical images of soleus muscles from WT, *Mtn* and *Mtn:Er* mice. Green fibres signify the expression of MHCIIA with MHC I appearing as red. Non green and red fibres represent MHCIX.

(C-D) Immunohistochemical images of (deep and superficial regions) of TA muscles from WT, *Mtn* and *Mtn:Er* mice. Green fibres match MHCIIA with MHCIB appearing as red. None green and red fibres represent MHCIX.

(*n* = 5) male twelve-week old mice per group.



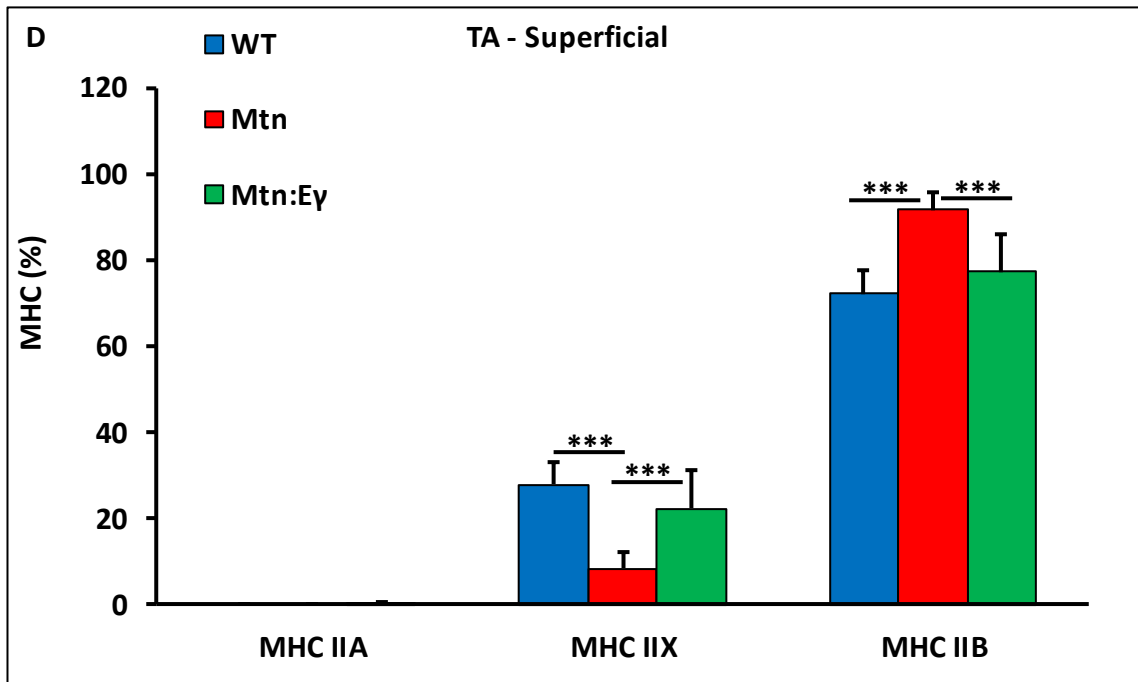
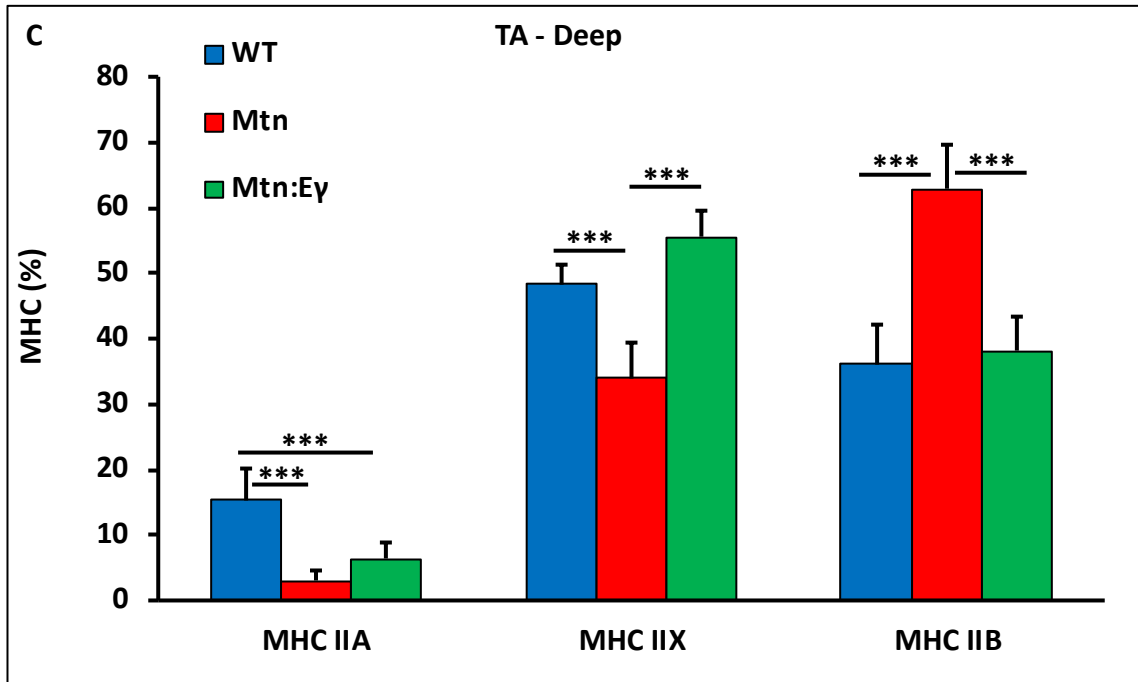


Figure 3.14. Muscle-specific expression of *Erry* into *Myostatin* null mice normalizes myosin type II phenotype

Erry overexpression is sufficient to derive a partial reversal transition of MHC profiling in a muscle lacking *Myostatin*.

(A) Graph showing fibre type composition in EDL muscles from WT, *Mtn* and *Mtn:Er* mice

(B) Graph showing MHC profiling in soleus muscles from the same animals above.

(C-D) Graphs showing fibre composition in deep and superficial regions of TA muscles from same three genotypes.

($n = 5$) male twelve-week old mice per group; One-way ANOVA followed by Bonferroni's multiple comparison tests, $*=P<0.05$ and $***= P<0.001$.

3.12. *Erry* introducing into *Myostatin* null muscles alters MHC profiling at transcriptional level

To further solidify of our results, we examined the expression of MHCs at transcriptional level. Gastrocnemius muscles (n=5) from WT, *Mtn*^{-/-} and *Mtn*^{-/-}/*Erry*^{Tg/+} mice were homogenised and total RNA was reverse-transcribed to cDNA and analyzed using quantitative real-time RT-PCR. We found that the expression of *MHCIIA* in *Mtn*^{-/-} muscles was lower than the other two genotypic groups, with that of *Mtn*^{-/-}/*Erry*^{Tg/+} higher than that of *Mtn*^{-/-}, but not normalized to WT level (Figure 3.15A). The expression level of *MHCIIX* was the lowest in muscles from *Mtn*^{-/-} mice compared to other two cohorts, however, in muscles from *Mtn*^{-/-}/*Erry*^{Tg/+} mice the level of *MHCIIX* was not only higher than in *Mtn*^{-/-} but also more than the WT condition (Figure 3.15B). Finally, we found that the expression level of *MHCIIB* was the lowest in muscles from *Mtn*^{-/-}/*Erry*^{Tg/+} mice, with no difference of this MHC isoform level in muscles from *Mtn*^{-/-} and WT mice (Figure 3.15C).

These data adds to grow body of evidences that muscle-specific manner overexpression of *Erry* into *Mtn*^{-/-} muscles is sufficient to induce a reverse transition of muscle fibres from fast to slow phenotypes within MHCII subsets.

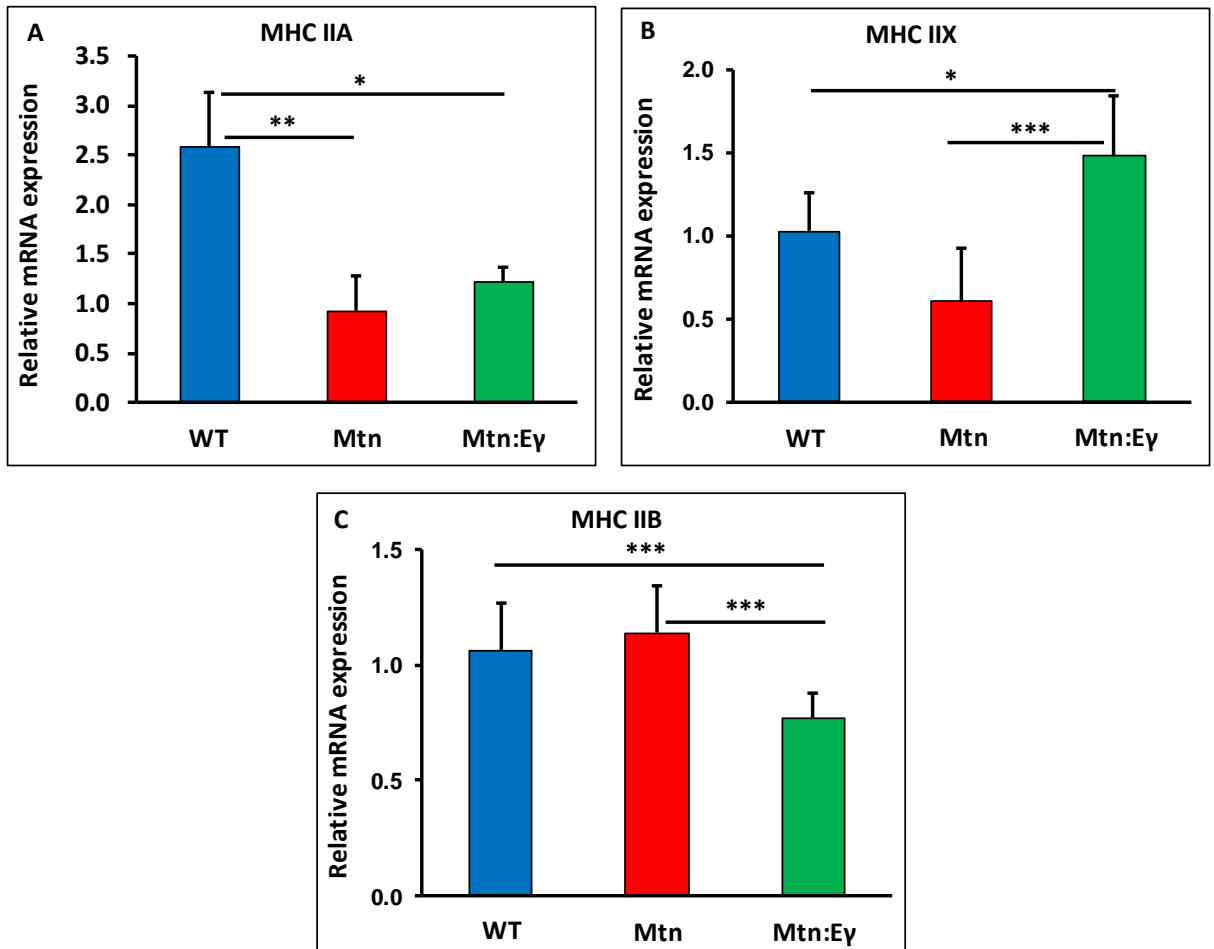


Figure 3.15. Gene expression levels of MHCs in hind limb muscles from WT, *Mtn* and *Mtn:Ey* mice

Erry overexpression in a muscle lacking *Myostatin* promotes fibre types transition toward normal condition indicating by gene expression levels of MHCs.

(A) Expression level of *MHCIIA* gene in gastrocnemius muscles from WT, *Mtn* and *Mtn:Ey* mice.

(B) Robust expression of *MHCIIIX* gene in muscles from *Mtn:Ey* mice.

(C) Lower expression level of *MHCIIIB* gene in muscles from *Mtn:Ey* mice.

($n = 5$) male twelve-week old mice per group; One-way ANOVA followed by Bonferroni's multiple comparison tests, $*=P<0.05$, $**=P<0.01$ and $***= P<0.001$.

3.13. *Erry* overexpression normalizes ultra-structural abnormalities of *Mtn*^{-/-} muscles

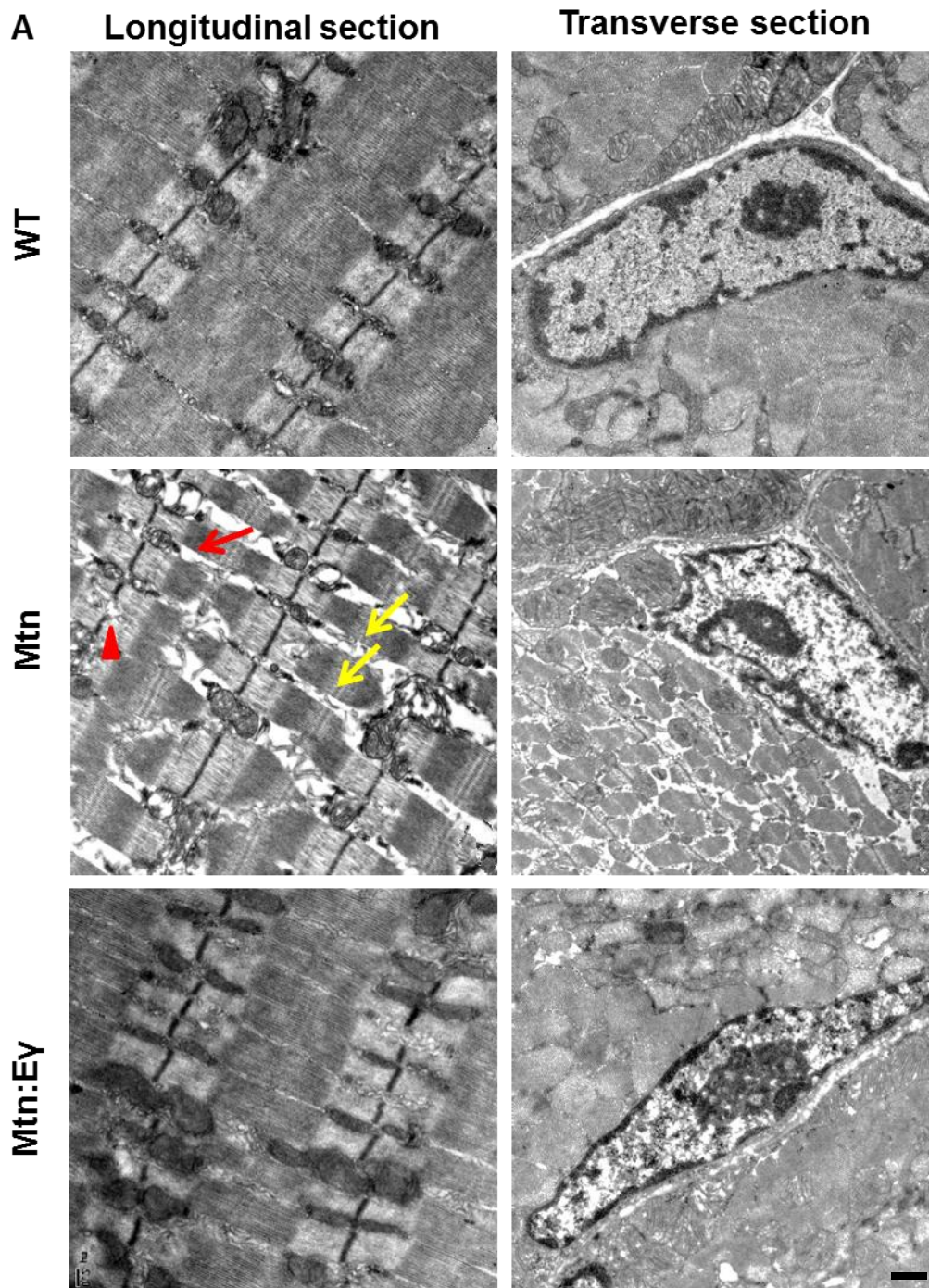
We showed that absence of *Myostatin* resulted in suppressing of FoxO3 expression, however, *Erry* introducing in *Mtn*^{-/-} normalised its level to control condition. It was well established that the maintenance of muscle structure is largely mediated by mechanisms that remove unwanted proteins and organelles through either the proteasome or autophagic pathways (Sandri, 2013). Previous study has reported a marked reduction of mitochondrial numbers in myofibres from a muscle lacking *Myostatin* (Amthor et al., 2007). In contrast, electron microscopy study by Rangwala's group (Rangwala et al., 2010) has revealed an increase in mitochondrial numbers in muscle fibres of *Erry* transgenic on wild type background mice compared to the controls. However, to what extent that muscle-specific manner overexpression of *Erry* into *Mtn*^{-/-} mice would mitigate the reduction of mitochondrial density and ultrastructural abnormalities following *Myostatin* absence, was not been explored. Therefore, the ultra-structure of forelimb muscles in the three cohorts were examined. Using transmission electron microscopy, we found a number of abnormalities in the structure of muscle from *Mtn*^{-/-} mice, heterogeneously sized sarcomeres, misaligned and disrupted Z-Lines, large inter-sarcomeric spaces and altered mitochondrial distribution and size. Contrary, the muscle from *Mtn*^{-/-}/*Erry*^{Tg/+} largely lacked these abnormalities (Figure 3.16A).

Thereafter, we examined the numbers of mitochondria in sub-membrane and intrafusal regions in muscles from all genotypic groups. We found that the density of mitochondria in both sub-membrane and intrafusal locations was decreased significantly following the deletion of *Myostatin*. Interestingly, the expression of *Erry* significantly increased the mitochondrial density at both locations compared to *Mtn*^{-/-} and at the major site, the sub-membrane region, increased it even compared to WT (Figure 3.16B-C).

Mitochondrial hypertrophy has been postulated to compensate for decreased mitochondrial number or function. Hypertrophy is thought to either protect against apoptosis or for functional mitochondria to fuse with aberrant ones resulting in the maintenance of cell function (Frank et al., 2001, Ono et al., 2001).

Mitochondrial hypertrophy was evident in both compartments in muscle from *Mtn*^{-/-} (Figure 3.16D–E) and was normalized by *Erry* in the sub-membrane region (Figure 3.16D).

Taken together, these results show that the deletion of *Myostatin* leads to numerous ultra-structural abnormalities. Over-expression of *Erry* in the *Mtn*^{-/-} prevented almost all the ultra-structural abnormalities.



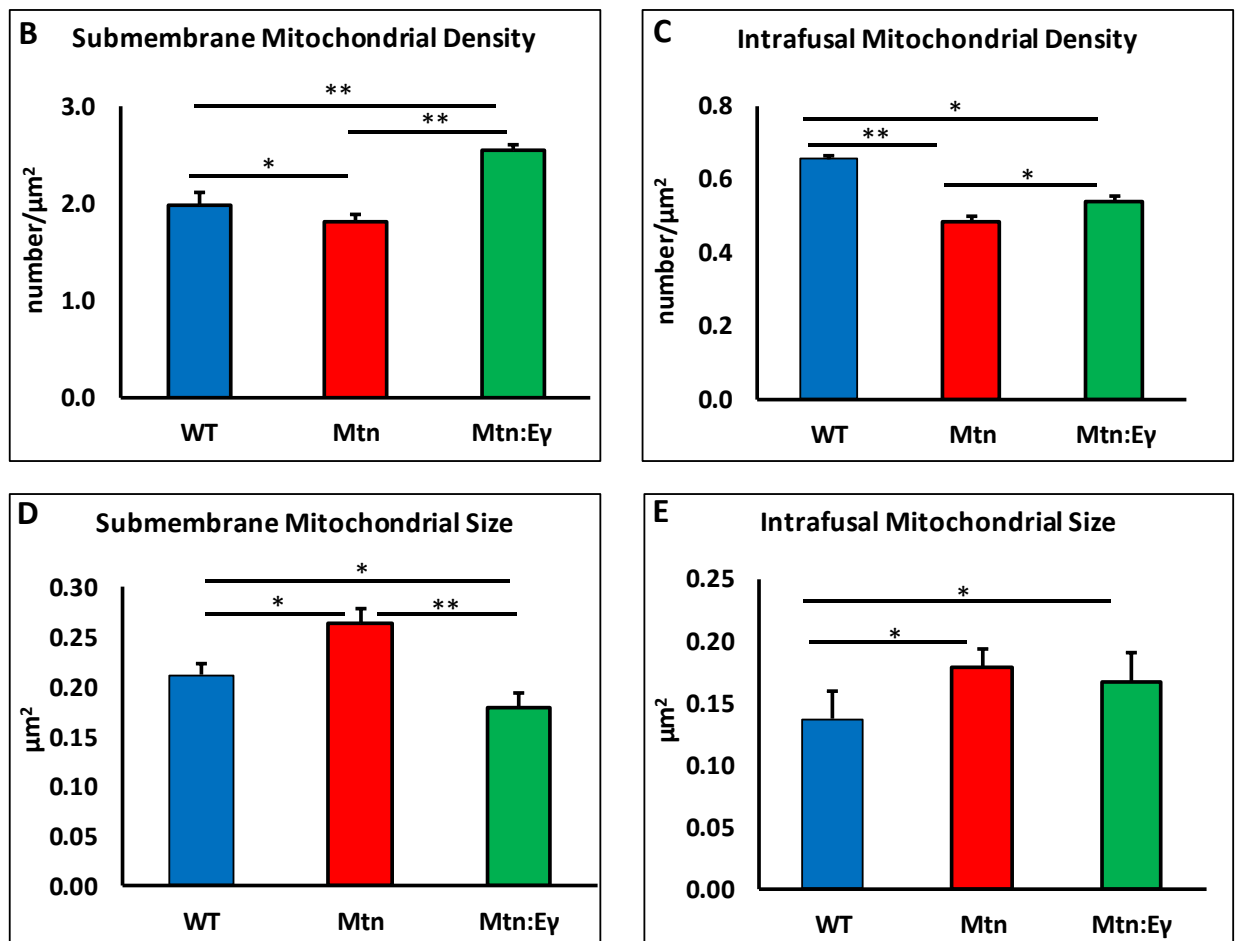


Figure 3.16. Transmission Electron Microscopy (TEM) investigation of mitochondrial numbers, size and distribution in muscles from *Mtn* and *Mtn:Er* mice

Muscle-specific expression of *Erry* normalizes ultra-structural abnormalities of *Myostatin* null mice.

(A) Transmission electron microscopy images in longitudinal and transverse sections of WT, *Mtn* and *Mtn:Er* muscle, scale 0.5 μm . Note the large spaces (red arrow) disrupted Z-lines (red arrowhead) and non-uniform sarcomere width (yellow arrows).

(B) Quantification of sub-membrane mitochondrial density.

(C) Quantification of Intrafusal mitochondrial density.

(D) Quantification of sub-membrane mitochondrial size.

(E) Quantification of intrafusal mitochondrial size.

($n = 3$) male twelve-week old mice per group; One-way ANOVA followed by Bonferroni's multiple comparison tests, *= $p < 0.05$ and **= $P < 0.01$.

This work has been done by Oliver Kretz, University of Freiburg, Germany.

3.14. Discussion

Classical training experiment has established that skeletal muscles have limited capacity to get a commensurate improvement of their mass (hypertrophy) and fatigue resistance (Hickson, 1980). Further study has illustrated that skeletal muscle is a highly compliant tissue that undergoes both quantitative as well as qualitative changes in response to intrinsic and extrinsic stimuli (Matsakas and Patel, 2009b). In consistence, previous work has referred to the plasticity nature of skeletal muscle that capable to alter almost all its features at metabolic, ultrastructure and molecular levels in response to environmental stimuli or gene mutation (Pette and Staron, 2001). A profound example is the phenotype of *Myostatin* mutation in mice. Myostatin is a member of the TGF- β family of secreted protein that been defined as a potent inhibitor of muscle development oxidative metabolism, and mutation of its gene leads to hypertrophic fast contracting fibres (McPherron and Lee, 1997, Amthor et al., 2007). Despite the enlarged muscle mass following *Myostatin* absence, their ability to generate tension is impaired, particularly during long periods of work (Mendias et al., 2006). The higher than normal fatigability of the muscle could be attributable to the lower number of mitochondria consequent to deletion of *Myostatin* in the germline (Amthor et al., 2007). Alternative efficacious molecule that induces oxidative slow-twitch muscle fibre in parallel to promote a network of genes linked to muscle energy, metabolism and vasculature pathways is estrogen-related receptor gamma (*Err γ*) (Narkar et al., 2011, Alaynick et al., 2007). Structural studies have established that *Err γ* is constitutive active in the absence of added ligand (Greschik et al., 2002). Since *Err γ* might potentially contribute in regulation of mitochondrial biogenesis and genes encoding pathways for contractile proteins for slow muscles (Dufour et al., 2007, Rangwala et al., 2010) we asked whether selective induction of *Err γ* into *Mtn*^{-/-} muscles via transgenic approach using specific promoter (HSA), would affect morphological, physiological and histological features of *Myostatin* null muscles.

The investigations of *Err γ* expression, body and muscle mass, physiological features and force generation capacity, muscle fibre number and size, mechanism underpinning muscle fibres enlargement, myosin heavy chain (MHC) profiling, and mitochondrial content and distribution undertaken in the work unveil a number of interesting features regarding

genetic deletion of *Myostatin* and muscle-specific expression of *Erry* into a muscle lacking *Myostatin*.

Firstly, we showed that the human α -skeletal actin promoter (HSA) used in this experiment induced a robust over-expression of *Erry* in the *Mtn*^{-/-} background muscles. Secondly, we demonstrated that the body mass of all genotypic groups was similar. However, all muscles examined from both *Mtn*^{-/-} and *Mtn*^{-/-}/*Erry*^{Tg/+} were markedly larger than their WT counterpart. Importantly, there was no significant difference in mass for any of the muscles from *Mtn*^{-/-} and *Mtn*^{-/-}/*Erry*^{Tg/+} mice. Examining muscle physiological features of animals of this study highlighted that the exercise capacity was reduced significantly in *Mtn*^{-/-} compared to WT mice, however, *Mtn*^{-/-}/*Erry*^{Tg/+} mice were running longer than the *Mtn*^{-/-} and even longer than WT mice. Furthermore, the tetanic force generated by *Mtn*^{-/-}/*Erry*^{Tg/+} EDL muscles was greater than the other two genotypic groups. Subsequently, specific force (sP₀) of EDL muscles from *Mtn*^{-/-} was lower than the other cohorts, with that of *Mtn*^{-/-}/*Erry*^{Tg/+} mice being greater than *Mtn*^{-/-}, but not normalised to WT level. Moreover, we showed that muscle-specific expression of *Erry* into *Mtn*^{-/-} was sufficient to attenuate the reduction in muscle strength of *Mtn*^{-/-} mice. Additionally, we found that the *Mtn*^{-/-}/*Erry*^{Tg/+} displayed better behavioural and locomotor characteristics than *Mtn*^{-/-} mice.

We also provided evidence that the increase of muscle mass followed *Mtn*^{-/-} resulted from both hyperplasia and hypertrophy. Interestingly, the introduction of *Erry* into *Mtn*^{-/-} muscles did not significantly change the number and the size of *Mtn*^{-/-} myofibres. Our work examining level of protein molecules offered interesting insights regarding mechanism underpinning muscle fibres hypertrophy. We showed that both *Mtn*^{-/-} and *Mtn*^{-/-}/*Erry*^{Tg/+} muscles expressed high level of protein synthesis that induce muscle mass, importantly muscle-specific expression of *Erry* in the *Mtn*^{-/-} normalised the level of molecules that induce muscle catabolic and maintain the tissue homeostasis. An important finding in present study was that the introduction of *Erry* into *Mtn*^{-/-} caused a partial reversal transition of MHC profile of *Mtn*^{-/-} toward WT condition within MHCII subtypes, without induce the transition to MHC type I isoform. Finally, an interesting features highlighted by examining muscle ultra-structure using TEM in this section was that muscles from *Mtn*^{-/-} mice displayed

number of abnormalities in sarcomeres and mitochondria. In contrast, the muscles from *Mtn*^{-/-}/*Erry*^{Tg/+} mice largely lacked almost all these abnormalities.

We commenced the study by examining the efficiency of HSA promoter to drive *Erry* overexpression. We found that muscle-specific expression of *Erry* using HSA onto *Mtn*^{-/-} background muscles induced *Erry* expression significantly. A number of investigators have revealed a critical role of *Erry* in regulating a network of genes linked to fatty acid oxidation and mitochondrial biogenesis (Alaynick et al., 2007, Dufour et al., 2007). Further study has described *Erry* as a key regulator of nuclear-encoded mitochondrial genes that maintain the oxidative metabolic genes (Dufour et al., 2007). On the same line of thought, it has been demonstrated that muscle fibre type I maintain high oxidative and vasculature capacity in the absence of exercise (Cherwek et al., 2000). Subsequently, it has been shown that *Erry* is exclusively and abundantly expressed in oxidative type I myofibre of skeletal muscles (Narkar et al., 2011), which might indicate the *Erry* potential role in regulating the intrinsic angiogenic pathway in oxidative slow-twitch muscles. Based on aforementioned reports, transgenic overexpression of *Erry* in skeletal muscles using specific promoters has been widely applied to enhance muscle mitochondrial biogenesis and functions, oxidative capacity and restoration of blood perfusion in muscular tissue disorders (Rangwala et al., 2010, Narkar et al., 2011). Notably, numerous studies have revealed that the transgenic *Erry* overexpression onto WT background induces aerobic transformation, mitochondrial biogenesis and robust myofibrillar vascularization, all in the absence of exercise (Matsakas et al., 2012b, Narkar et al., 2011). On the other hand, it has been established that the sarcomeric α -skeletal actin is synthesized in large amount during differentiation process of muscle tissue, and expressed in adult human skeletal muscle (Bains et al., 1984, Nir et al., 1986). Further, it was firmly demonstrated that the ability of the HSA regulatory domains to positively modulate expression in different cell lines is variable. This mutability suggest that the particular combination of domains used is dependent on the availability of trans-acting transcription-modulating factors present in each cell type (Miwa and Kedes, 1987). It seems that the tissue-specific transcription of the HSA gene promoter construct resulted from the interaction between the promoter domains and trans-acting positive-regulatory factors in skeletal muscle cells, or with negative regulatory factors in nonmuscle cells (Muscat and Kedes, 1987).

Despite such combination of *Erry* potential roles to enhance muscle oxidative and vasculature capacity, and tissue-specific expression criteria of the HSA promoter, it remains important to be determined to what extent this mechanism is operative in animal models with metabolic disorders.

In addition, it is not known whether this approach can provide a therapeutic benefit for the patients with muscle wasting, a question that we are going to address at different muscle aspects.

In this study, we showed that body mass of all genotypic groups (WT, *Mtn*^{-/-} and *Mtn*^{-/-}/*Erry*^{Tg/+}) was similar. Previous work has revealed a critical role of *Myostatin* to enhance muscle fibroblast proliferation, thus induces connective tissue deposition in extracellular matrix (Li et al., 2008). In support of this view, it has been reported that *Myostatin* deletion resulted in a significant reduction of muscle connective tissue content compared to control (Elashry et al., 2012). In the same line of investigation, it has been established that one of the intriguing aspects of the *Mtn*^{-/-} phenotype is the concurrence of a large muscle mass, decreased fat deposition and increased resistance to obesity (Lebrasseur, 2012).

Indeed, number of investigators have illustrated that *Myostatin* involved in adipogenesis by inhibiting brown adipocytes differentiation through the activin receptors IIB (ActRIIB)-Smad3 pathway (Feldman et al., 2006, Kim et al., 2012b). Further study has shown that *Myostatin* inhibition promotes brown adipose phenotype in mice (Zhang et al., 2012). Consistently, it was well established that *Myostatin* deletion leads to an elevation in expression levels of brown adipose tissue BAT signature markers (*Ucp1* (Uncoupling protein 1) and *PGC-1α* (PPARGgamma-coactivator 1α) (Kim et al., 2012b). In addition, the newly identified myokine Irisin that encode by the gene *Fndc5* (Fibronectin type III domain-containing protein 5), that regulated by *PGC-1α*, secreted from muscles into blood and activates thermogenic in adipose tissue (Bostrom et al., 2012). Notably, it has been demonstrated that *Mtn*^{-/-} increased the expression of Irisin and AMP-activated protein kinase in skeletal muscles (Shan et al., 2013). On the same line of thought, AMPK which is essential for exercise-mediated to aerobic myofibres, it is activated by *Erry* in skeletal muscle (Jensen et al., 2007). By a way of explanation, mutation of *Myostatin* drives browning of white adipose tissue WAT in an indirect way by activating (AMPK-PGC1α-Fndc5)

pathway in muscles, leads to increase production of a myokine Irisin hence enhances adipose tissue thermogenic and reduces fat mass.

Although the three cohorts of mice in present study showed similar body weights, muscle mass of all examined muscles were remarkably larger in *Mtn*^{-/-} and *Mtn*^{-/-}/*Erry*^{Tg/+} than their counterparts from WT mice, with no significant difference in mass for any of the muscles from *Mtn*^{-/-} and *Mtn*^{-/-}/*Erry*^{Tg/+} mice. A number of studies have shown that deletion of *Myostatin* leads to the development of large muscle mass as a result of both hyperplasia and hypertrophy, however the increased muscle mass was not accompanied with proportional increase of muscle force generation and specific tetanic tension, particularly during prolonged periods of work (Amthor et al., 2007, Mendias et al., 2006, Relizani et al., 2014). To investigate this further, we examined mitochondria density, size and distribution in muscles from the three genotypic groups of this study. Our findings with aforementioned reports on correlation between muscle mass and force generation capacity strengthen the notion that the higher than normal fatigability of *Mtn*^{-/-} (Figure 3.5) could be attributable to the lower number of mitochondria as a result of germline deletion of *Myostatin* (Amthor et al., 2007) (Figure 3.16, the TEM work has been done by Oliver Kretz, University of Freiburg, Germany).

To alleviate this mitochondrial deficit in muscle from *Mtn*^{-/-} mice, we introduced the expression of *Erry* into skeletal muscle. Numerous studies have reported that this gene is highly expressed in tissues with a high oxidative capacity, such as the heart, kidneys, brain and slow oxidative skeletal muscle where it has been demonstrated to trigger mitochondrial biogenesis (Hong et al., 1996, Heard et al., 2000, Giguere, 2008, Narkar et al., 2011). We hypothesised that muscle-specific overexpression of *Erry* that would promote mitochondrial density, thereby increase muscle oxidative capacity on a *Mtn*^{-/-} background that is associated with hypertrophy would challenge the exist trade-off between aerobic metabolism and muscle fibre size (Van der Laarse WJ, 1998, Degens, 2012).

One of the main features of *Myostatin* deletion or loss of its function is the dramatic increase of muscle mass in phenomenon called muscle doubling (Kambadur et al., 1997, McPherron and Lee, 1997, Hulmi et al., 2013a). In agreement with aforementioned reports, we showed that the increase in muscle mass resulted from an increase in muscle fibre

number and size (Elashry et al., 2009, McPherron et al., 2009, McPherron et al., 1997, Amthor et al., 2007). Therefore a better understanding of mechanisms that drive skeletal muscle overgrowth upon *Myostatin* absence is required.

Myostatin signalling modulates the expression of target genes that involved in the control of myoblast proliferation and terminal differentiation (Thomas et al., 2000, Taylor et al., 2001). Further, in vitro study has shown that the proliferation and differentiation rates of satellite cells from *Mtn*^{-/-} mice much faster than those of WT (Magee et al., 2006). Previously it has been documented that *Myostatin* anti-proliferative action is associated by up-regulating of p21 (Cyclin-dependent kinase inhibitor) and a Cdk inhibitor, decreases the cyclin-dependent kinases (CDK2 and CDK4) and phosphorylation of retinoblastoma protein (RB), thereby satellite cells quiescence and interfere with the cell cycle progression from G1 to S-phase (Taylor et al., 2001, McCroskery et al., 2003). Consistently, number of investigators have reported that *Myostatin* regulates myoblast differentiation through inhibition of myogenic regulating factors (Rios et al., 2002, Amthor et al., 2002). In the line with these investigations, previous work has demonstrated that the embryonic program of the primary and secondary myogenesis was accelerated by *Myostatin* ablation, which offers developmental origin of the hyper-muscular phenotype (Matsakas et al., 2010). Moreover, it was well established that post-natal *Myostatin* inhibition caused an increase in muscle fibres size but no enhance myofibre numbers (Matsakas et al., 2009).

We suggest that the hyperplasia following genetic deletion of *Myostatin* imply excess proliferation of muscle progenitors during early stage of muscle development. In support of this view, previous work has reported that *Myostatin* limits proliferation rate of myogenesis cell through prioritizing their entry into terminal differentiation (Manceau et al., 2008). In the same line of thought, it has been illustrated that *Erry* implicated in regulating of myogenesis process reflects by highly up-regulation of its expression during muscle differentiation (Murray et al., 2013). By a way of explanation, *Myostatin* knockout enhances the proliferation pace of the muscle precursors, and *Erry* overexpression was sufficient to regulate differentiation process. Therefore, the muscles of *Mtn*^{-/-} and *Mtn*^{-/-}/*Erry*^{Tg/+} animals reach the peak and maturation comparatively faster than the wild type muscles.

Despite a notable part of muscle mass increase resulted from muscle fibres hyperplasia, myofibres cross-sectional area also appeared to contribute significantly to the overall increase of muscle mass (McPherron et al., 1997, Amthor et al., 2007). It was well documented that the balance between muscle protein synthesis and degradation processes is a critical factor in regulating of muscle mass (Sandri, 2008, Rugg and Glass, 2011). Several signalling pathways are known for their role in regulating of muscle fibre size through control the rate of muscle protein turnover. A number of studies have defined the role of specific signalling pathway, the insulin like growth factor 1- Phosphoinositide 3-kinase-Akt (IGF1/PI3K/Akt) pathway in muscle mass regulation (Glass, 2005, Sandri, 2008).

In contrast, FoxO transcriptional factor has been described as a key mediator of muscle atrophy that coordinate the activation of two most important cellular proteolytic mechanisms, the autophagy-lysosome and ubiquitin proteasome systems (Sandri et al., 2004, Stitt et al., 2004). Moreover, *Myostatin* has merged as a key regulator of skeletal muscle mass, since its deletion or inhibition induces muscle overgrowth, whereas its overexpression causes muscle atrophy (McPherron et al., 1997, Rodriguez et al., 2014).

Previous studies have established that muscle protein synthesis and muscle mass are promoted by (IGF1/PI3K/Akt/mTOR) pathway, as the expression of constitutively active Akt robustly enhances muscle hypertrophy (Rommel et al., 2001, Bodine et al., 2001). Further studies have shown that Akt mainly acts via mTOR activation, that promote muscle protein synthesis by phosphorylating and inhibiting of 4E-binding protein 1 (4E-BP1) and activation of the ribosomal protein S6 kinase (S6K) (Wullschleger et al., 2006, Tee and Blenis, 2005). Another important role of Akt is compromising the negative regulation of protein degradation via inhibiting FoxO3 mediating proteasome activity (Stitt et al., 2004). Others have shown that the suppressing of FoxO3 by Akt leads to prevent the expression of two critical atrophy-related ubiquitin ligases, *MAFbx/Atrogin-1* and *MuRF-1* (Sandri et al., 2004, Stitt et al., 2004).

In present study, as the proteasome and autophagy pathways are involved in muscle atrophy, it seems intuitive that they should be tuned down in order to support muscle growth, as we showed that muscle fibres from *Mtn^{-/-}* and *Mtn^{-/-}/Errγ^{Tg/+}* displayed a significant increase in their size compared to the control. Indeed, we found that the activity

of a key regulator of these processes, FoxO3 is suppressed in the absence of *Mtn*. However, we showed that *Erry* expression in muscle leads to a substantial restoration of its level to normal condition (Figure 3.12, this work has been done by Roberta Sartori, University of Padua, Italy). Giving our explanation, several studies have referred to a cross-talk between *Myostatin* and Akt/mTOR pathway, since *Myostatin* absence leads to upregulation of PI3K/Akt/mTOR pathway in mouse and cattle (Chelh et al., 2011). Consistently, other studies have reported a clear elevation in activity of Akt/mTOR signalling components in skeletal muscle from *Mtn*^{-/-} mice (Morissette et al., 2009, Lipina et al., 2010). We suggest that *Myostatin* deletion leads to activate PI3K/Akt/mTOR pathway that support protein synthesis, while FoxO3 was blocked, leading to decrease the expression levels of *Atrogin-1* and *MuRF* genes, increase protein synthesis, decrease protein degradation rates, increase myofibres size hence promote muscle mass. On the same line of thought, it was revealed an important role of *Erry* in supporting protein synthesis; thereby prevent muscle atrophy. Previous work has referred to a marked elevation in the expression level of *Atrogin-1* in muscle cells from *Erry*^{-/-} mice (Brunet et al., 1999). It seems that the increase in muscle fibre cross-sectional area exhibited by *Mtn*^{-/-} was maintained by introducing of *Erry*, since the latter regulate protein synthesis and prevent muscle atrophy.

The increase in fibre number and size thereby muscle mass of *Mtn*^{-/-} mice was associated with a larger proportion of type MHCIIB fibres than seen in muscles from WT mice. We also showed that even though the muscle mass and fibre size did not differ between *Mtn*^{-/-} and *Mtn*^{-/-}/*Erry*^{Tg/+} mice, the latter caused partial normalisation of the MHC fibre profile; a decrease in the proportion of IIB fibres in all muscles examined. What was conspicuous, however, was the absence of normalization of the proportion of MHC I fibres. Our data were in agreement with previous findings that revealed the increase of hind limb muscle mass following *Myostatin* deletion was accompanied by fibre type conversion, predominantly of MHCIIB with a marked reduction in proportions of MHC types IIA and IIX (Girgenrath et al., 2005, Amthor et al., 2007). On the contrary, study by Matsakas' group (Matsakas et al., 2012b) has demonstrated that muscle-specific transgenic overexpression of *Erry* into WT background muscles robustly induces proportions of IIA and IIX myofibres, simultaneously leads to reduce the number of MHCIIB. We also provided evidence of the absence normalization of the proportion of MHC I fibres. Such finding was supported by

previous work that revealed complete fibre type shift from MHCIIA to MHC I in muscles from *Erry* transgenic mice did not occur (Matsakas et al., 2012b). We believe that this is significant and reveals a key feature of the influence of a metabolic programme on muscle physiology. We suggest that the oxidative programme, here driven by *Erry*, readily converts IIB to IIA fibres but that it is unable to induce the transition to type I MHC isoforms. The reversal transition between MHCII subsets following *Erry* overexpression without formation of type I fibres, adds to a growing body of evidence that the type II programme is plastic and adaptable, whereas the type I fibres are more resistant to change (Sutherland et al., 1998), and may not be part of the IIB ↔ IIX ↔ IIA continuum. Indeed a number of studies have questioned whether the "final step" (conversion of type IIA to I) is even possible. Development of type I fibres has been described in a number of conditions, for example following chronic low-frequency stimulation (CLFS) (Peucker et al., 1999, Kwong and Vrbova, 1981). However, these studies never examined whether type I were formed as a consequence of the remodelling of type II fibres or through the formation of new fibres, a process that would require satellite cells. Indeed the development of type I fibres following extended CLFS can only be induced to significant levels when accompanied by robust myofibre regeneration (Pette and Staron, 2001, Maier et al., 1988).

Taken together, these studies imply that *Myostatin* signalling acts at an embryonic/foetal stage of muscle development to pattern a subpopulation of satellite cells/muscle precursors in a muscle-specific manner to form type I fibres. The protocol of overexpressing *Erry* used in this study is unable to influence this process.

In this study, we investigated the functional characteristics of enlarged skeletal muscle from *Mtn*^{-/-} and *Mtn*^{-/-}/*Erry*^{Tg/+} mice. In accord with previous reports, our findings showed that the increased muscle mass following germline deletion of *Myostatin* (McPherron et al., 1997, Whittemore et al., 2003) was not accompanied by a proportional increase in force output (Amthor et al., 2007). We also provided evidence that the muscle hypertrophy which develops following *Myostatin* deletion has many ultrastructural abnormalities including splitting of sarcomeres, misaligned Z-lines and alteration in mitochondrial density, distribution and morphology. A number of studies have reported that the relationship between muscle fibre cross-sectional area and mitochondrial density implies that the

myofibres can hypertrophy in expense of its endurance capacity (Hickson, 1980, Des Tombe et al., 2002). However, the decline in maximum steady state power can be prevented by reducing the diffusion distance for oxygen to mitochondria by relocating the mitochondria to the sarcolemma (Devecei et al., 2001), and by increasing myoglobin and capillary density per muscle fibre (van Beek-Harmsen et al., 2004). Moreover, the maintenance of muscle structure is largely mediated by mechanisms that remove unwanted proteins and organelles through either the proteasome or autophagy pathways (Sandri, 2013, Bonaldo and Sandri, 2013). Further investigators have demonstrated that deregulated proteasome activity or autophagy leads to muscle wasting in a number of disease conditions (Sandri et al., 2004). We have mentioned previously that the expression level of the key regulators (FoxO3) of both autophagy and proteasome pathways was suppressed in muscles from *Mtn*^{-/-} mice to support the high level of protein synthesis required for initial muscle hypertrophy and maintenance of the large muscle mass. However, we showed that muscle-specific expression of *Erry* into the *Mtn*^{-/-} muscle leads to elevate FoxO3 level, a substantial normalization of almost all the abnormalities in the ultrastructures of *Mtn*^{-/-} muscles, as well as improvement in the exercise capacity, specific force generation, grip strength and animal activities. Most importantly, we showed that a physiological measure of muscle function-fatigability is not only normalized but exceeds the value of WT mice (Figures 3.5). We suggest that the molecular and organelle clearance programmes being mediated by FoxO3 are generally not anabolic but are rather there to maintain cellular homeostasis. However, when its activity is attenuated in muscles from *Mtn*^{-/-} mice, it leads to an accumulation of structural abnormalities that compromises muscle function.

In summary, we can conclude that the complex physiological properties such as fatigue and running capacity can be genetically manipulated. Such alterations might be attained by supporting protein synthesis rate thereby maintaining the increase of muscle mass followed germline deletion of *Myostatin*, and relocating the mitochondria particularly to the sarcolemma region. Interestingly, these adaptations were not associated with the loss of muscle force generating capacity and in fact even resulted in improved exercise capacity. Furthermore, findings of mitochondrial re-localization that might enhance muscle oxidative capacity, indeed raise the possibility of challenging the trade-off between muscle fibre size and aerobic metabolism (Van der Laarse WJ, 1998). Determine of *Erry* potential to activate

pathways that would promote muscle oxidative capacity in hypertrophic muscle fibres is required to be investigated.

Chapter 4; Results

Introducing of *Erry* into *Mtn*^{-/-} mice normalizes metabolic and molecular, but not cellular features of *Myostatin* null muscles

4.1. Introduction

A central notion of skeletal muscle biology is the existence of an inverse relationship between the oxidative capacity of a fibre and its size, which might interpret why small fibres are oxidative and large fibres glycolytic (van Wessel et al., 2010, Degens, 2012). Small oxidative fibres are characterised by high mitochondrial content, high level of blood supply that supports a steady and prolonged supply of oxygen and nutrients, and hence are fatigue resistance (Annex et al., 1998, Cherwek et al., 2000). Conversely, large glycolytic fibres show low mitochondrial content, a reduced capillary density, and are fatigue sensitive (Annex et al., 1998, Narkar et al., 2011). Several studies have defined a relationship between muscle fibre size, force generation capacity and metabolism. Wherein fibre that relies on oxidative phosphorylation (OXPHOS) for ATP generation, tend to have a small size and high capillary density in order to facilitate O₂ diffusion. These fibres have high fatigue threshold, however their small CSA means the individual muscle fibre generate low force level. On the contrary, fibres that rely on glycolysis show increased CSA and high force generation capacity, but their low fatigue resistance might attribute to the metabolic pathways that produce energy rapidly but lead to build up of lactate (Bottinelli et al., 1991, Jones et al., 2008, Krivickas et al., 2011). Skeletal muscle fibre ability to transform and remodel in response to various physiological and environmental demands has been established as a striking feature of this tissue (Matsakas and Patel, 2009b). In some cases the response of muscle fibre takes place when signal stimulates extracellular milieu then interact with cell surface receptors and lead to activate signalling pathways that ultimately remodel the fibres by eliciting changes in gene expression (Pette and Staron, 2001). Moreover, it has been reported that skeletal muscles remodelling can be induced by aerobic exercise which results in an increase in muscle fibres oxidative capacity and new blood vessels formation per myofibres. Such changes are essential for the physiological adaptation to exercise (Bloor, 2005, Egginton et al., 1998, Gavin et al., 2007). Consistent with these investigations, previous work has reported that skeletal muscle remodels the fibre composition to sustain muscle performance by activating distinct pathways that reprogram gene expression (Bassel-Duby and Olson, 2006, Olson and Williams, 2000).

A number of studies have revealed a tight positive correlation between muscle fibre oxidative capacity and vascular supply, which is especially evident in skeletal muscles as

each enriched in either oxidative slow-twitch or glycolytic fast-twitch (Pette and Staron, 2000, Fluck and Hoppeler, 2003). Moreover, it has been firmly established that formation of new blood vessels is required to reduce the average and maximum diffusion distance from the capillaries to the mitochondria in the hypertrophic muscle fibres (Egginton et al., 1998, Degens et al., 1992). Further work has reported that oxygen diffusion problem in large fibre can be attenuated by facilitating this process. Despite myoglobin molecule has defined to facilitate oxygen diffusion from capillaries to mitochondria, it remains uncertain whether myoglobin concentration increase in muscle hypertrophy (de Koning et al., 1981).

Muscle fibre is large single post-mitotic cells that form from the fusion of differentiated myoblast (MAURO, 1961). Indeed multinuclear feature of muscle fibres provides more transcriptional capacity, as the myonucleus provides a template for the production of all the RNA in the cell (Bruusgaard et al., 2003, van der Meer et al., 2011). Further work has defined cytoplasm volume that supplied by myonuclei as the myonuclei domain, which is size limited by half-life of RNA as well as the diffusion rate of RNA (van der Meer et al., 2011). Although the positive correlation between muscle fibre size and number of myonuclei has been firmly established (Allen et al., 1999, Bruusgaard et al., 2003), there is a considerable debate whether fibre hypertrophy has to accompanied by addition of myonuclei, or marked increase in muscle fibre size possible without the addition of myonuclei (McCarthy et al., 2011, van der Meer et al., 2011). The nuclei are distributed evenly and orderly throughout cytosol indicates the challenge of transport distance in these cells (Bruusgaard et al., 2003). In addition, myonuclei distribution was observed in both IIA and IIB muscle fibre, but the degree of order was much higher in IIB than IIA isoforms (Bruusgaard et al., 2006). Skeletal muscle repair and regeneration is mediated by a pool of stem cells referred to as satellite cells which are located beneath the basal lamina (MAURO, 1961, Zammit et al., 2006). In normal muscle cell (non-injured), satellite cells are quiescent and have few organelles with the high nuclear-to-cytoplasm ratio, and small size nuclear compared to the adjacent nucleus of myotubes. However, it appears to swell on the myofibres after activation (Schultz and McCormick, 1994). Myoblasts are satellite cells after division and proliferation, which then undergo terminal differentiation and incorporate into mature muscle fibre as post-mitotic myonuclei (Bischoff and Heintz, 1994). Moreover, numerous correlative studies have revealed the number of satellite cell increases as a muscle becomes progressively oxidative

(Putman et al., 1999, Christov et al., 2007). Another investigation reported that the soleus muscle which is mainly made up of slow oxidative fibres, has a higher number of satellite cells than the Extensor digitorum longus (EDL) muscle, which predominantly contains fast glycolytic fibres (Gibson and Schultz, 1983).

We can infer from this, the metabolic properties of muscle are believed not only to control fibre size but also the number of satellite cells.

Previous investigation of skeletal muscle features has shown that *Erry* expressed exclusively in metabolically demanding and highly vascularized aerobic muscles (Narkar et al., 2011). Further studies have reported that transgenic overexpression of *Erry* into WT background muscles is efficacious to enable anaerobic muscles to attain dense capillary density and enhanced oxidative capacity (Narkar et al., 2011, Rangwala et al., 2010). Moreover, muscle remodelling driven by *Erry* overexpression in WT mice functions by regulating a network of genes that control oxidative phosphorylation and fatty acid oxidation pathways parallel with induction of angiogenic markers that regulate muscle vasculature (Matsakas et al., 2012b, Arany et al., 2008b). Additionally, Harper's study (Harper et al., 2004) revealed that increase of intracellular ROS level, which is mainly produced through mitochondrial ETC pathway of myocyte, induces a level of oxidative stress capable to inhibit myogenesis. Since *Erry* regulates the expression of genes that control mitochondrial pathways including ETC and TCA cycle, it protects muscle cells and myogenic processes by precluding excessive ROS emission (Eichner and Giguere, 2011).

On the other hand, functional studies of *Myostatin* knockout animal models have illustrated a reduction in oxidative fibres number and a concomitant increase in the fast glycolytic phenotypes (Girgenrath et al., 2005, Amthor et al., 2007). Moreover, previous work provided evidence of a decrease in muscle capillary density following *Myostatin* deletion (Lipina et al., 2010, Rehfeldt et al., 2005). In addition, muscle hypertrophy generated by *Myostatin* ablation involved no increase in a number of myonuclei as well as a marked reduction of satellite cells population on each muscle fibre (Amthor et al., 2007). Here we investigated whether muscle-specific expression of *Erry* in *Mtn*^{-/-} muscle that maintained the increase of muscle fibre size exhibited by *Myostatin* deletion, while driving a partial transition of muscle fibre from fast to slow phenotypes, as we showed previously, would

enhance muscle oxidative capacity, capillary density and molecular features of *Mtn*^{-/-} muscles, thereby break down the constraint between muscle fibre size and oxidative capacity.

We also sought to examine the canonical view that oxidative muscle phenotype positively correlates with resident stem cell number.

In order to investigate the robustness of the inverse relationship between fibre size and oxidative capacity, as well as between myofibre phenotype and satellite cells number, we made use of a genetic model that enhances oxidative metabolism, mediated by estrogen-related receptor gamma (*Erry*), into the hypertrophic background of *Myostatin* null (*Mtn*^{-/-}) mice.

Three genotypes of male mice (WT, *Mtn*^{-/-} and *Mtn*^{-/-}/*Erry*^{Tg/+}) (n=5) were bred, housed under standard environmental conditions and provided food and water ad libitum in the Biological Resource Unit, University of Reading, to an adult age (3 months).

The hind limb muscles (Soleus, Extensor digitorum longus (EDL), Tibialis anterior (TA) and Gastrocnemius) were isolated and weighed. The sectioned slides were stained for the mitochondrion-associate enzyme succinate dehydrogenase (SDH), Periodic acid–Schiff (PAS) and Dihydroethidium (DHE) stains to identify oxidative, glycolytic status, and Reactive Oxygen Species (ROS) level respectively in muscles from the three genotypic groups. Immunostaining for CD31 antibody was performed to identify capillary density per muscle fibre. Gastrocnemius muscles were pulverised, divided into three thirds, one third was homogenized and RNA samples were extracted to determine the expression level of genes that are involved in regulating of angiogenesis, energy metabolism, oxygen handling and antioxidants, glucose and fatty acid oxidation, transport and metabolism pathways. Another third was powdered, homogenised and used to determine the muscle metabolic profile by ¹H NMR. Finally, single muscle fibres from EDL muscles were cultured and fixed in different time points, time zero (T0) and 48 hours culture (T48), thereafter immunostained with two myogenic markers (Pax7 and MyoD).

We show in this section, firstly, muscles of *Mtn*^{-/-}/*Erry*^{Tg/+} mice that resulted from superimposition of *Erry* on the *Mtn*^{-/-} background have a high oxidative capacity, evidenced

by the supernormal activity of succinate dehydrogenase (SDH) thus violating the inverse relationship between fibre size and oxidative capacity. Interestingly, the increase of muscle oxidative capacity was paralleled with hyper-capillarization of muscle. Secondly, *Erry* overexpression into *Mtn*^{-/-} resulted in a remodelling of phenotype to a state that differentiates it not only from *Mtn*^{-/-} but also WT muscles NMR profiles. Thirdly, introducing of *Erry* reprogramed *Myostatin* null muscles at molecular level, show the normalization of the expression levels of biomarker genes that regulate energy metabolism, glucose metabolism, and oxygen handling pathways. In addition, *Erry* overexpression increases the transcriptional level of antioxidant, fatty acid transport, uptake and oxidation, and angiogenesis program genes to that level above even the control. Finally, our observations demonstrated that hyper-oxidative hypertrophic muscles from *Mtn*^{-/-}/*Erry*^{Tg/+} mice do not follow the dogma regarding metabolism and satellite cells number.

4.2. *Erry* introducing into *Mtn*^{-/-} mice induces robust increase of mitochondrion-associated enzyme succinate dehydrogenase (SDH) activity

We demonstrated that muscle-specific expression of *Erry* into a muscle lacking *Myostatin* not only significantly improved exercise and muscle force generation capacity of *Mtn*^{-/-} mice, but also maintained the increase of muscle fibre number and size that followed *Myostatin* deletion, and caused a partial reversal in the MHC profiling of *Mtn*^{-/-} muscles toward normal condition.

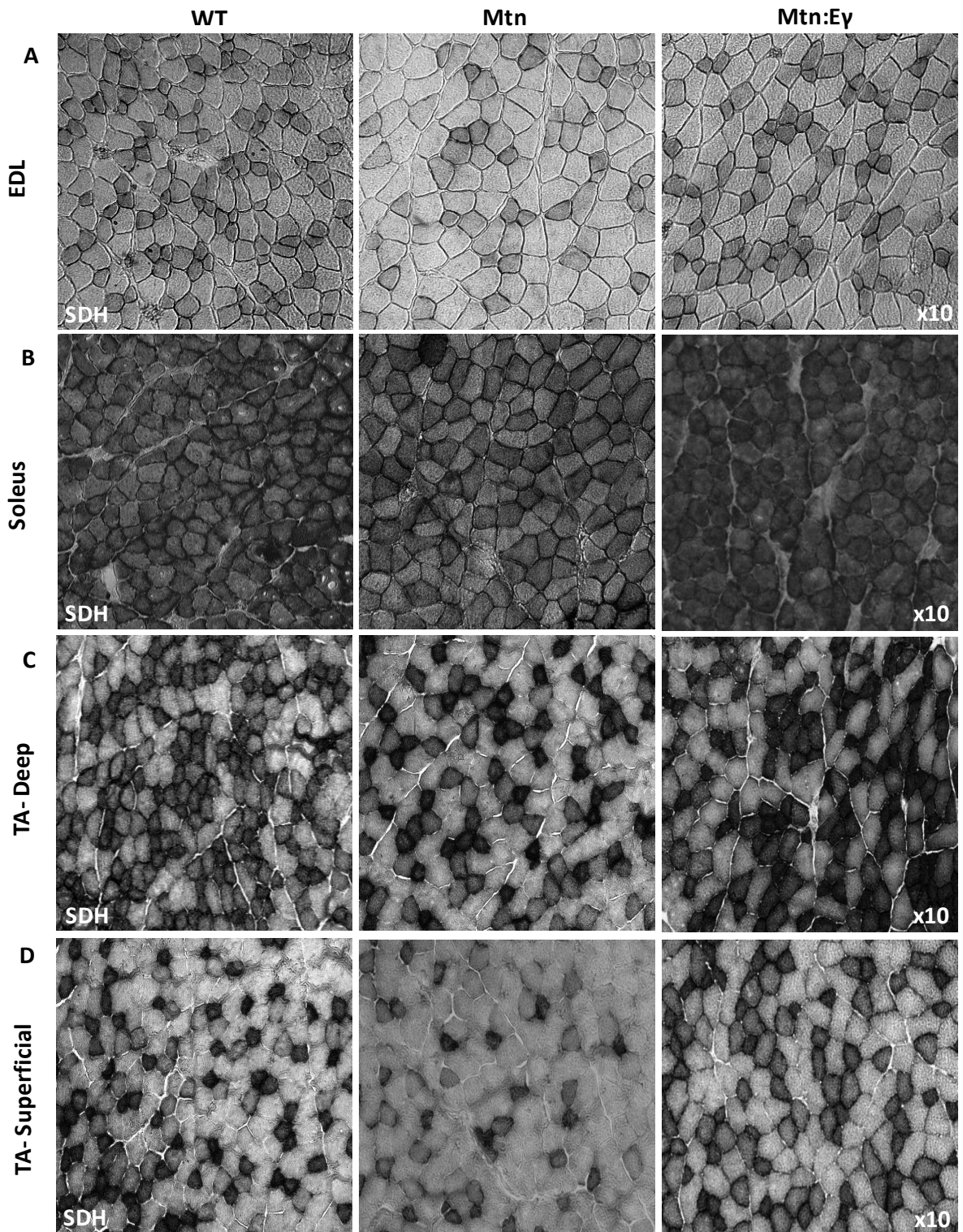
In agreement with previous study (Girgenrath et al., 2005), our findings showed a shifting of hind limb muscle fibres toward fast phenotypes following *Myostatin* deletion. However, introducing of *Erry* into *Mtn*^{-/-} mice resulted in restoration of myofibres profiling to WT state. We speculate that muscle fibre-types bias toward fast phenotypes as a result of *Myostatin* knockout, and toward slow-twitch phenotypes following *Erry* overexpression, might attribute to alter of mitochondrial enzymes activity.

Previously has been reported that lack of *Myostatin* resulted in a reduction of oxidative myofibres with concurrently increase of glycolytic myofibres, indicating by fewer number of succinate dehydrogenase (SDH) positive fibres from muscles lacking *Myostatin* compared to WT (Amthor et al., 2007). Further investigation which referred to succinate dehydrogenase that is located at the inner membrane of mitochondria as a component of electron transport chain (ETC) as well as the tricarboxylic acid cycle (TCA), has reported a robust increase of the SDH positive area as well as intensity in muscle sections from *Erry* transgenic mice compared to the control (Rangwala et al., 2010).

Therefore, we performed staining for the mitochondrion-associate enzyme succinate dehydrogenase (SDH) to investigate whether *Erry* overexpression would promote the oxidative capacity in hypertrophic-glycolytic myofibres from *Myostatin* null mice (Figure 4.1A-D). A minimum of 200-300 myofibres were counted per each muscle section (EDL, soleus and TA) (n=5) from WT, *Mtn*^{-/-} and *Mtn*^{-/-}/*Erry*^{Tg/+} mice. In all muscles examined, we found markedly few strongly stained fibres (high SDH activity) (measure oxidative capacity), and an increase in proportion of very pale fibres (low SDH activity) in *Mtn*^{-/-} muscles compared to wild type. However, upon over-expression of *Erry*, the intensity of SDH staining in fibres of *Mtn*^{-/-} muscle was restored to that of WT level. Indeed, the number of SDH

positive fibres was higher than that seen even in the WT muscles albeit not significantly (Figure 4.1E-H). Of particular note, soleus muscles from *Mtn*^{-/-} mice showed lower percentage of SDH positive fibres (38%) compared to WT animals (67.6%), counterpart muscles from *Erry* transgenic mice displayed a significant increase in the proportion of oxidative myofibres (76.3%) (Figure 4.1B and F). Same scenario has been seen in all muscle examined (Figure 4.1E-H).

Taken together, these results imply that muscle-specific expression of *Erry* into *Mtn*^{-/-} mice is sufficient to break down the suggested constraint between muscle fibres size and oxidative capacity (Degens, 2012), indicated by high SDH activity of hypertrophic muscle fibres.



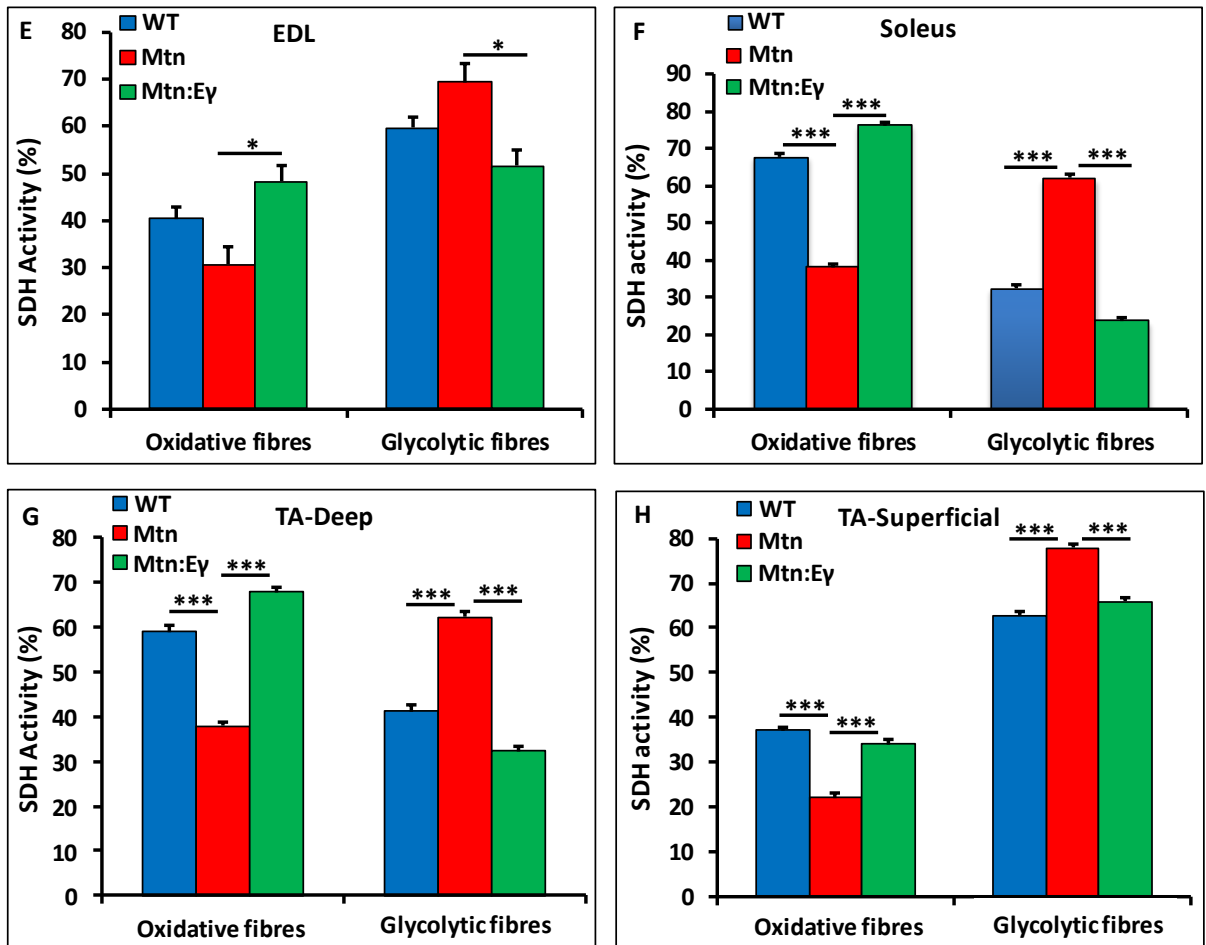


Figure 4.1. *Erry* overexpression into *Mtn*^{-/-} background muscle restores oxidative capacity to WT condition

Muscle-specific expression of *Erry* normalizes the metabolic profile of *Myostatin* null mice (*Mtn*).

(A – D) Succinate dehydrogenase (SDH) staining Images of (EDL, soleus and TA-deep and superficial) muscles from WT, *Mtn* and *Mtn:Er* mice. Black fibres signify the SDH positive fibres (Oxidative fibres), and pale (white) fibres signify the SDH negative fibres (Glycolytic fibres).

(E – H) Quantification of SDH activity in EDL, soleus, TA-Deep and TA-Superficial muscles respectively.

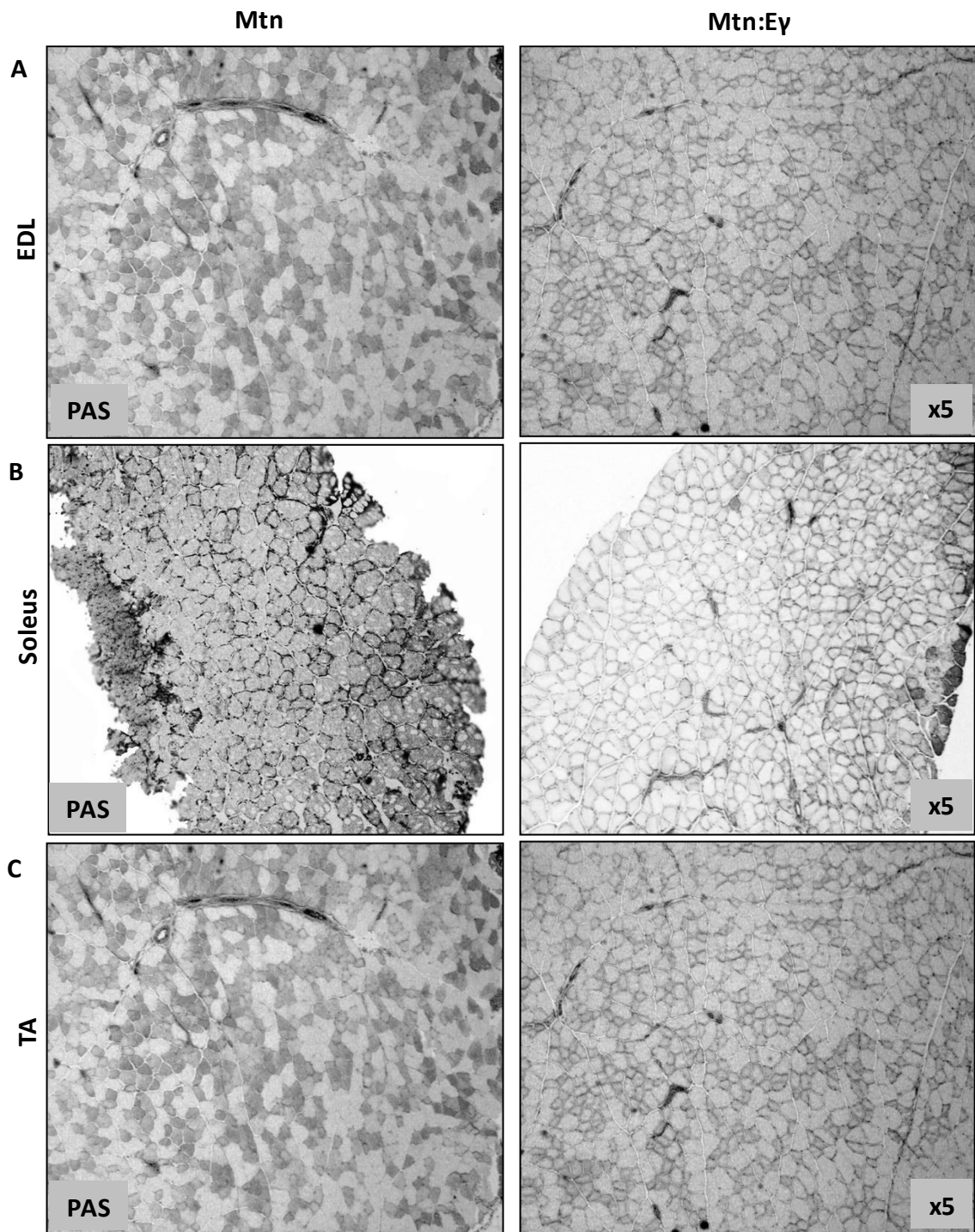
(*n* = 5) male twelve-week old mice per group; One-way ANOVA followed by Bonferroni's multiple comparison tests, *=*P*<0.05 and ***=*P*<0.001.

4.3. Remodelling muscle glycolytic status following *Erry* overexpression into *Myostatin* null mice

In presented study, we showed a partial reverse in transition of myofibres toward the slow phenotypes driven by muscle-specific overexpression of *Erry* into *Myostatin* null mice which was accompanied by a remarkable increase of SDH activity that indicated a high oxidative status of these muscles. At the same time we maintained the increase in muscle fibre size exhibited by *Mtn*^{-/-} muscles. Such combination of a high oxidative capacity and large fibre size is clear evidence for the violating of the trade-off between the oxidative capacity of muscle fibre and its size.

Previous work has illustrated predominantly of glycolytic type IIB fibres in hind limb muscles from *Myostatin* knockout mice, with obvious reduction of type IIA and IIX phenotypes (Girgenrath et al., 2005). On the other hand, *Erry* has been described as a key regulator of fatty acid oxidation, mitochondrial biogenesis and oxidative metabolism pathways (Dufour et al., 2007). To further explore of *Erry* potential to promote remodelling of muscle metabolism status, we applied a specific protocol Periodic acid–Schiff (PAS) stain to identify glycolytic status in muscles (EDL, soleus and TA) (n=5) from *Mtn*^{-/-} and *Mtn*^{-/-}/*Erry*^{Tg/+} mice (Figure 4.2A-C).

Our findings showed higher numbers of positive glycolytic fibres (dark colour) with concomitant reduction of the negative (pale-white colour) fibres in all muscles examined from *Mtn*^{-/-} mice. In contrast, muscles from *Mtn*^{-/-}/*Erry*^{Tg/+} mice displayed a considerable decrease of dark stain fibres (high PAS activity) and increase in non-glycolytic (low PAS activity) fibres (4.2D-F). Of particular note, we found a high percentage (29.1%) of positive fibres (Glycolytic fibres) in EDL muscles from *Mtn*^{-/-} mice, compared to counterpart muscles from *Mtn*^{-/-}/*Erry*^{Tg/+} (8.9%). However, *Erry* overexpression increased the proportion of PAS negative fibres (76.3%) compared to (49.1%) in EDL muscles from *Mtn*^{-/-} mice (4.2A and D). The intermediate fibres from both cohorts showed no significant differences in all muscles examined (Figure 4.2D-F). Both soleus and TA muscles from *Mtn*^{-/-} and *Mtn*^{-/-}/*Erry*^{Tg/+} displayed approximately same myofibres distribution (Figure 4.2E-F). These data highlight the potential role of *Erry* introducing into *Mtn*^{-/-} mice to normalize muscle glycolytic status.



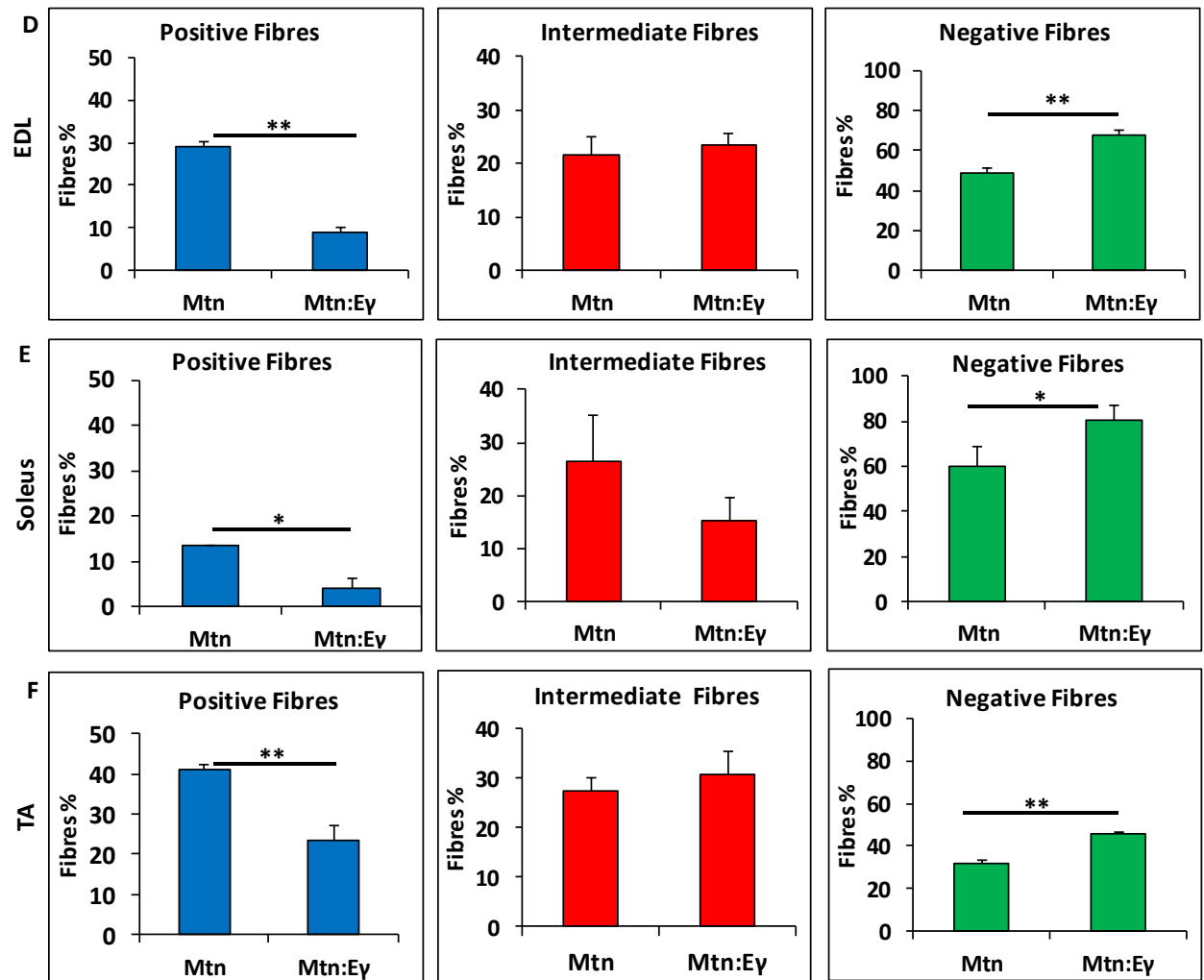


Figure 4.2. *Erry* overexpression into *Myostatin* null muscles reduces number of glycolytic myofibres

Muscle-specific expression of *Erry* normalizes the number of PAS positive fibres of *Myostatin* null mice (*Mtn*).

(A – C) Periodic acid–Schiff (PAS) staining Images of (EDL, soleus and TA) muscles from *Mtn* and *Mtn:Er* mice. Black fibres signify the PAS positive fibres (Glycolytic fibres), and pale (whit) fibres signify the PAS negative fibres (Oxidative fibres).

(D – F) Quantification of PAS activity in (EDL, soleus and TA) muscles respectively.

($n = 5$) male twelve-week old mice per group; statistical analysis between each two groups performed by two-tailed Student's t-test for independent variables, *= $P < 0.05$ and **= $P < 0.01$.

4.4. Muscle-specific expression of *Erry* is efficacious to promote angiogenesis program in a muscle lacking *Myostatin*

In agreement with aforementioned studies, we demonstrated a predominantly of fast-twitch glycolytic fibres profile following genetic ablation of *Myostatin* (McPherron and Lee, 1997). In addition, our findings which conform with previous reports, showed that the glycolytic muscle phenotypes of *Myostatin* null mice are associated with marked reduction of mitochondrial number, mitochondrial enzymes expression and capillary density (Amthor et al., 2007, Lipina et al., 2010). However, introducing of *Erry* into *Mtn*^{-/-} mice restored almost all these features in *Mtn*^{-/-} muscles indicated by high mitochondrial density and a high number of SDH positive fibres (oxidative fibres), thereby driven a partial reverse conversion of myofibres toward slow-twitch phenotype. A number of studies have established that the capillary density per muscle fibres is related to myofibre size, therefore an increase in the capillary number that follows a similar time course as the hypertrophy, is required (Degens et al., 1992, Plyley et al., 1998). Several other studies have recognised *Erry* as a key transcriptional regulator that regulates the intrinsic vascular features and oxidative metabolism in the skeletal muscle (Rangwala et al., 2010, Narkar et al., 2011). Here we sought to determine whether the restoration of muscle oxidative capacity followed *Erry* introducing into *Mtn*^{-/-} mice would be accompanied by increasing of factors related to the microvascular supply of the muscle that known to regulate angiogenesis program.

We found that the expression of endothelial mitogenic factors (*Vegf-α165* (Vascular endothelial growth factor α 165), *Vegf-α189* (Vascular endothelial growth factor α 189) and *Fgf1* (Fibroblast growth factor 1) was lower in the muscles of *Mtn*^{-/-} than WT mice, but similar in *Mtn*^{-/-}/*Erry*^{Tg/+} and WT mice (Figure 4.3A-B). Of particular note, *Fgf1* expression was similar in muscles from WT and *Mtn*^{-/-} mice (Figure 4.3C), however, its level induces significantly by *Erry* overexpression not only more than *Mtn*^{-/-} but also WT. The expression levels of *Vegf-α165* and *Vegf-α189* were significantly lower in *Mtn*^{-/-} than in WT, and *Erry* overexpression normalized them to the control condition (Figure 4.3A-B) and induced *Fgf1* to be even higher than in WT (Figure 4.3C). These observations suggest that features induced by germline deletion of *Myostatin* are not genetically looked down, but can be modified and thereby normalized by muscle-specific expression of *Erry*. Therefore, the

angiogenesis program imparted by *Erry* overexpression was responsive to myofibres size and metabolic features changes.

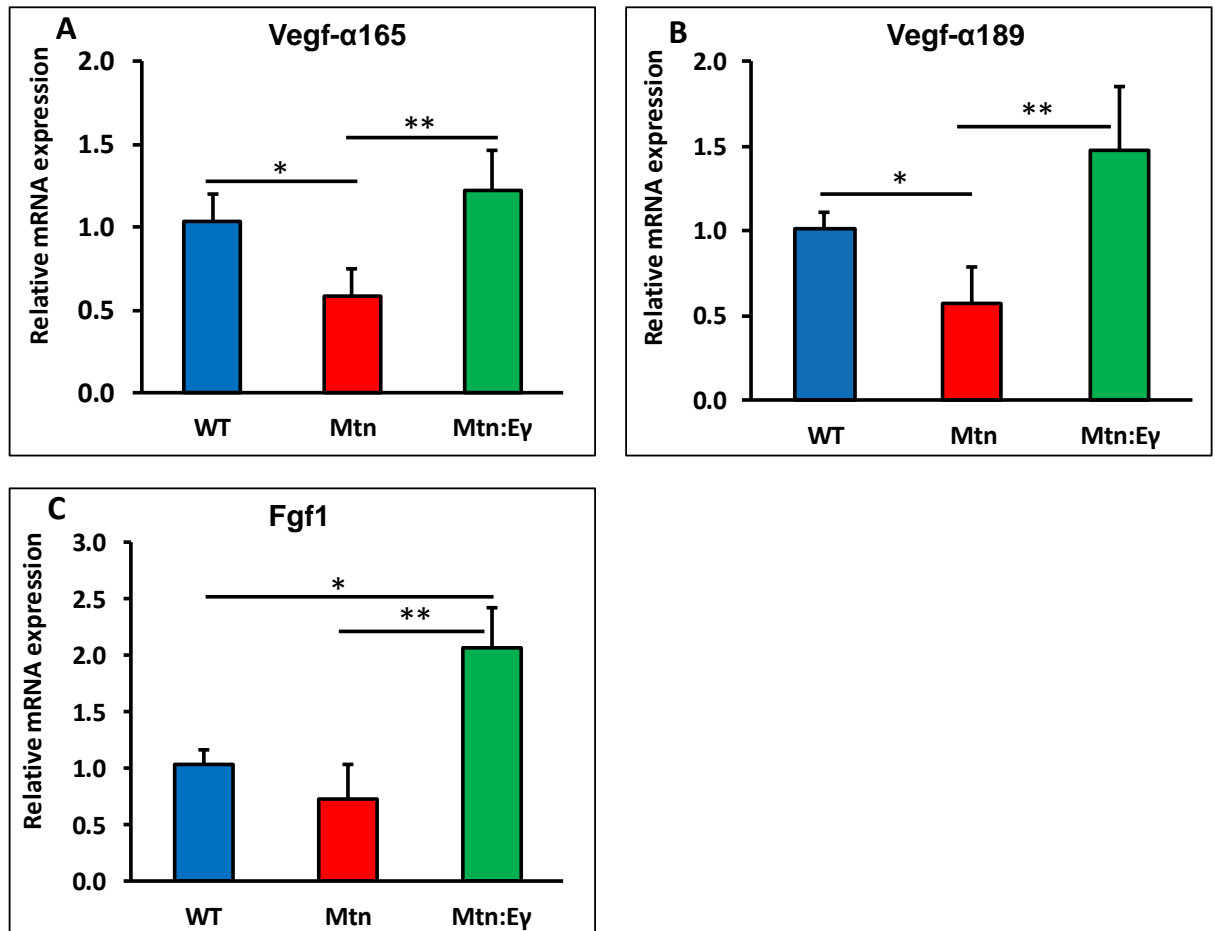


Figure 4.3. Molecular reprogramming of *Myostatin* null muscle by *Erry* overexpression.

Erry introducing into *Mtn* mice significantly increases expression levels of biomarker genes that regulate angiogenesis program

(A) Quantification of *Vegf-α 165* gene expression.

(B) Quantification of *Vegf-α 189* gene expression.

(C) Quantification of *Fgf1* gene expression.

(n = 5) male twelve-week old mice per group; One-way ANOVA followed by Bonferroni's multiple comparison tests, * = P<0.05 and ** = P<0.01.

4.5. *Erry* overexpression is required for synchronizing of myofibre size and capillary density

We established that introducing of *Erry* into a muscle lacking *Myostatin* preserves the increase of muscle fibre cross-sectional area (CSA) induced by *Myostatin* ablation, while simultaneously promoting muscle oxidative capacity. Several studies have indicated a marked decrease of mitochondrial enzymes expression and capillary density in *Myostatin*-deficient muscles (Rehfeldt et al., 2005, Amthor et al., 2007, McPherron and Lee, 1997, McPherron et al., 1997). Recently, *Erry* has been described as an orphan nuclear receptor that drives a network of transcriptional programmes would encode highly oxidative myofibres (Narkar et al., 2011). We wondered whether muscle-specific *Erry* overexpression into *Mtn*^{-/-} mice in addition to its potential to hold the increase of muscle fibre size and promote the oxidative capacity, could induce blood vessels formation to match the increased size and oxidative demands of the muscles. To test this, we examined TA muscle sections (n=5) from WT, *Mtn*^{-/-} and *Mtn*^{-/-}/*Erry*^{Tg/+} mice for (CD31) expression, an endothelial cell marker that is routinely used to identify blood vessels (Figure 4.4A).

We found that capillary to fibre ratio (C:F) was the lowest in TA muscle sections from *Mtn*^{-/-} mice, and the highest in those of *Mtn*^{-/-}/*Erry*^{Tg/+} mice. More specifically, muscles lacking *Myostatin* showed a significant decrease in a number of blood capillary per muscle fibre (1.3 blood vessels per myofibre) compared to control muscles (1.8 blood vessels per myofibre). However, *Erry* overexpression in a muscle-specific manner markedly increased the number of blood vessels per each muscle fibre (2.6 blood vessels per myofibre). Interestingly, muscles from *Mtn*^{-/-}/*Erry*^{Tg/+} mice showed higher (C:F) ratio not only than those from *Myostatin* null, but also exceeded those of WT mice (Figure 4.4B).

These data with aforementioned observations on muscle fibres size, physiological functions and oxidative capacity, strengthen the hypothesis that muscle-specific expression of *Erry* into *Mtn*^{-/-} mice would challenge the dogma of the existence of an inverse relationship between muscle fibre CSA and oxidative capacity.

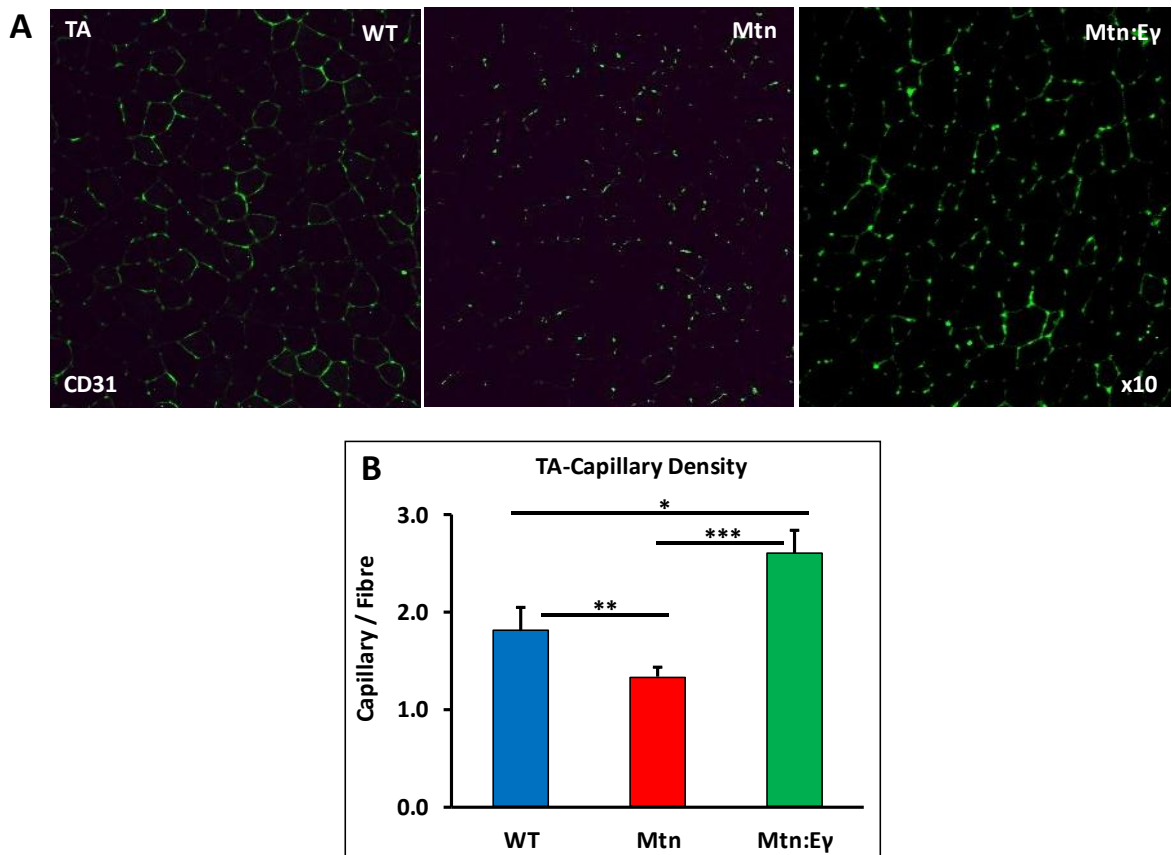


Figure 4.4. Revascularization of *Myostatin* null muscles following *Erry* overexpression

Muscle-specific expression of *Erry* normalizes capillary profile of *Myostatin* null mice (*Mtn*).

(A) Muscle capillary density determined by CD31 staining on TA muscle sections of WT, *Mtn* and *Mtn:Er* mice.

(B) Quantification of blood vessels per muscle myofibre in TA muscle sections.

($n = 5$) male twelve-week old mice per group; One-way ANOVA followed by Bonferroni's multiple comparison tests, $*=P<0.05$, $**=P<0.05$ and $***= P<0.001$.

4.6. Remodelling of muscle NMR profile of *Mtn*^{-/-} mice following *Erry* modification

We demonstrated that *Erry* overexpression into *Mtn*^{-/-} background mice even maintain muscles hyperplasia and hypertrophy statues, also attenuated muscle fatigability and drives a partial reversal of muscle fibre types toward normal condition, induce oxidative capacity, and promotes muscle vasculature. It was well established that skeletal muscle function is linked to its structure and metabolic processes that maintain this tissue (Jones et al., 2008, Krivickas et al., 2011). We speculated whether the modifications in muscle metabolic status that resulted from *Erry* overexpression would be followed by increasing/decreasing of particular metabolic enzymes and amino acids that match the oxidative metabolic phenotype demands. To examine this line of thought, gastrocnemius muscles (n=5) from WT, *Mtn*^{-/-} and *Mtn*^{-/-}/*Erry*^{Tg/+} mice were homogenized and the metabolite profile was characterized by 1H NMR spectroscopy.

To identify any metabolic variation driven by the genotypic differences, principal components analysis (PCA) was applied to these profiles. We found a clear clustering observed in the scores plot comparing all three genotypic groups demonstrating that they had distinctive metabolite profiles (Figure 4.5). Comparing the metabolic signature of the *Mtn*^{-/-} muscle to the *Mtn*^{-/-}/*Erry*^{Tg/+} showed clear differences between the two groups characterised by significantly greater levels of muscle lactate in *Mtn*^{-/-} muscle compared to that of the *Mtn*^{-/-}/*Erry*^{Tg/+} consistent with a greater glycolytic phenotype. Furthermore, the levels of creatine/phosphocreatine were also more pronounced in the muscle from *Mtn*^{-/-} compared to *Mtn*^{-/-}/*Erry*^{Tg/+}. Additionally, *Erry* modification leads to higher taurine and anserine content in the muscle of these animals (Figure 4.5).

We infer from the histochemical and NMR muscle profiles of the three genotypic groups that *Erry* modification of *Mtn*^{-/-} results in a remodelling of phenotype to a state that differentiates it not only from *Mtn*^{-/-} but also WT muscles.

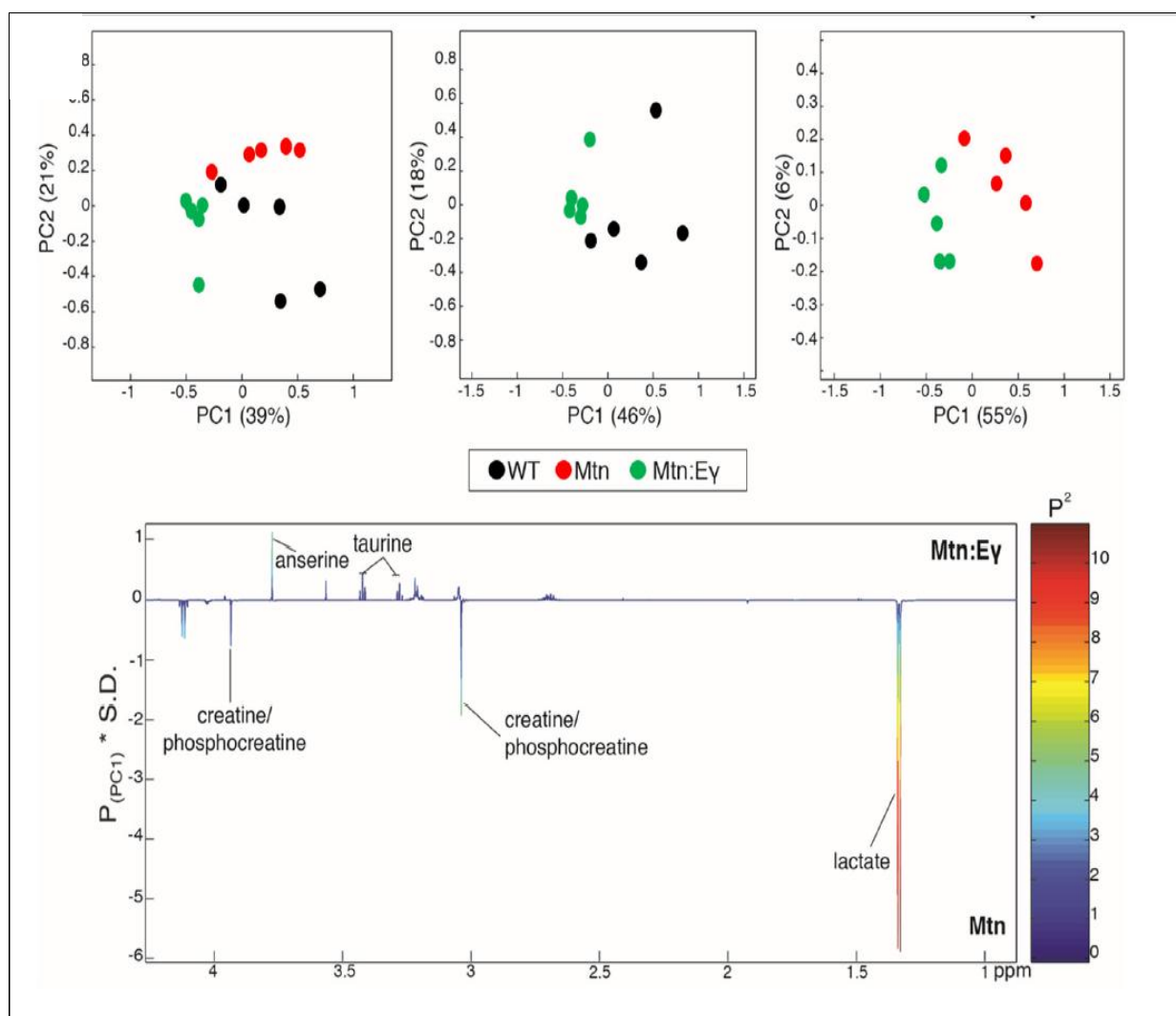


Figure 4.5. Muscle-specific expression of *Eryr* normalizes the metabolic of *Myostatin* null mice (*Mtn*)

Pair-wise comparisons of the metabolic profiles obtained from the gastrocnemius muscle from WT, *Mtn* and *Mtn:Ey* mice. Principal components analysis (PCA) score plots comparing WT, *Mtn* and *Mtn:Ey*; WT and *Mtn:Ey*; as well as *Mtn* and *Mtn:Ey*; (% variance in the parenthesis). Colour loadings plots shown for PC1 of the model comparing *Mtn* and *Mtn:Ey*. Product of PC loadings with standard deviation of the entire data set coloured by the square of the PC loading.

($n = 5$) male twelve-week old mice per group; One-way ANOVA followed by Bonferroni's multiple comparison tests.

This work has been done by Natasa Giallourou, University of Reading, UK.

4.7. *Erry* is required for regulating of muscle energy metabolism

The potential loss of exercise, oxidative and vascular capacity that we showed in muscles from *Myostatin* null mice, encouraged us to identify whether the expression of genes that encode for instance metabolic and oxygen handling features would be altered following germline deletion of *Myostatin*. And we asked whether muscle-specific expression of *Erry* into *Mtn*^{-/-} mice would be capable of restoring gene expressions to their normal levels, or modify them in a way that can meet the aerobic metabolic demands that were imparted by *Erry* reprogramming.

Previously it has been reported that *Myostatin* deletion or its inhibition results in high level of *PGC1α* expression (Shan et al., 2013). Several other studies have established that the nuclear receptors in coordinate with number of co-regulators such as *PGC1α* control a wide range of aerobic respiration signalling pathways including mitochondrial biogenesis, fatty acid oxidation and oxidative phosphorylation in skeletal muscles (Arany et al., 2007, Huss et al., 2002, Wang et al., 2004, Narkar et al., 2011). Further investigations have revealed *Erry* potential to enhance key transcriptional regulators of skeletal muscle oxidative metabolism including Peroxisome proliferator-activated receptor delta (*Ppard*) and Peroxisome proliferator-activated receptor gamma coactivator 1-beta (*Ppargc 1b*) (Lin et al., 2002, Wang et al., 2004). In this section of present study, we examined the expression level of key transcriptional regulators and nuclear receptors that involved in regulating of muscle energy metabolism. Thus, gastrocnemius muscles (n=5) from WT, *Mtn*^{-/-} and *Mtn*^{-/-}/*Erry*^{Tg/+} mice were homogenised and total RNA was reverse-transcribed to cDNA and analysed using quantitative real-time RT-PCR. We found that the expression of *PGC1α* was increased significantly in muscles from *Mtn*^{-/-} mice. However, upon overexpression of *Erry*, *PGC1α* expression was normalized to that level of WT muscles (Figure 4.6A). The expression level of *Perm1* (PPARGC1 and ESRR-induced Regulator in Muscle 1) was increased significantly following *Erry* overexpression not only above its level in muscles from *Mtn*^{-/-} but also exceeded that of WT muscles (Figure 4.6B). However, we found that the transcriptional levels of another two genes *Ppard* (Peroxisome proliferator-activated receptor delta) and *Rev-erb-a* that are associated with muscle oxidative metabolism were not significantly affected by neither *Myostatin* ablation, nor *Erry* introducing into *Mtn*^{-/-} muscle (Figure 4.6C-D). These data show that *Erry* acts as a critical upstream genetic switch that might govern

skeletal muscle metabolism by controlling the expression of multiple but not all aerobic transcriptional regulators.

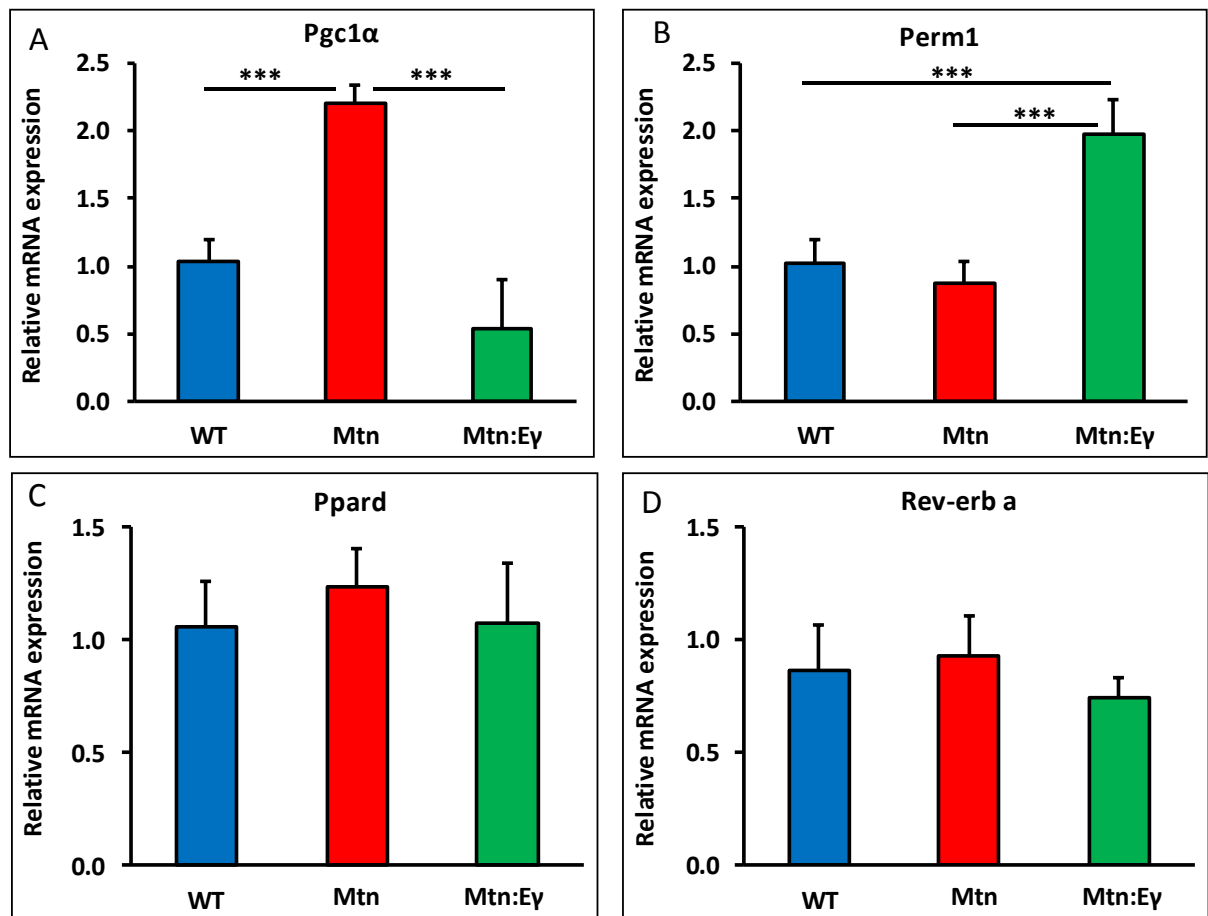


Figure 4.6. Molecular reprogramming of *Myostatin* null muscle by *Erry* overexpression and its ability to regulate expression of transcriptional regulators

Gene expression levels of key transcriptional regulators of metabolism in muscles from WT, *Mtn* and *Mtn:Er* mice.

(A) Quantification of *PGC1α* gene expression, *Erry* overexpression normalised this gene level.

(B) Quantification of *Perm 1* gene expression. *Erry* overexpression significantly increased this gene level.

(C-D) Quantification of (*Ppard* and *Rev-erb a*) genes expression, show no changes of these genes level in muscles from the three genotypic groups.

(*n* = 5) male twelve-week old mice per. One-way ANOVA followed by Bonferroni's multiple comparison tests, ***= *P*<0.001.

4.8. The effects of *Myostatin* deletion and *Erry* overexpression on biomarker genes that regulate glucose metabolism

We showed that introducing of *Erry* into *Mtn*^{-/-} mice was sufficient to modify the expression level of genes that regulate muscle energy metabolism in a way that matched the improvement of muscle oxidative capacity and force generation. Previous work has reported that cellular glucose utilization is tightly regulated by the pyruvate dehydrogenase complex (PDC) that mediating pyruvate entry into the TCA. The study also revealed PDC can be phosphorylated and thereby inactivated by members of pyruvate dehydrogenase kinase (PDK 1-4) family (Giguere, 2008). Further investigations have reported that PGC1 α could influence glucose oxidation via transcriptional control of PDK4 expression (Wende et al., 2005).

On the other hand, several studies have indicated that in addition to the notable improvement of insulin sensitivity, loss of functional *Myostatin* resulting in a marked increase of glucose utilization (Guo et al., 2009, Wilkes et al., 2009). Therefore, to further confirm of these findings, and to determine the potential role of *Erry* to promote glucose metabolism and oxidation, we compared the expression levels of selective biomarkers genes that regulating glucose metabolism, transport and uptake. We found that the expression level of *Glut1* (Glucose transporter type 1) gene was not significantly changed neither by *Myostatin* absence, nor by *Erry* overexpression (Figure 4.7A). Moreover, both *Glut4* (Glucose transporter type 4) and *PDK4* genes showed the highest expression levels in muscles from *Mtn*^{-/-} mice, however *Erry* introducing normalizes their levels to WT condition (Figure 4.7B-C). Of particular note, there was no significant difference between the expression level of *Glut4* gene in muscles from WT and *Mtn*^{-/-} mice, while *PDK4* was increased significantly in *Mtn*^{-/-} compared to WT muscles. Interestingly, all gene levels were similar in muscles from WT and *Mtn*^{-/-}/*Erry*^{Tg/+} mice (Figure 4.7B-C). These data show that muscle-specific expression of *Erry* into *Mtn*^{-/-} mice was sufficient to normalize the expression level of biomarker genes that control glucose metabolism to WT condition.

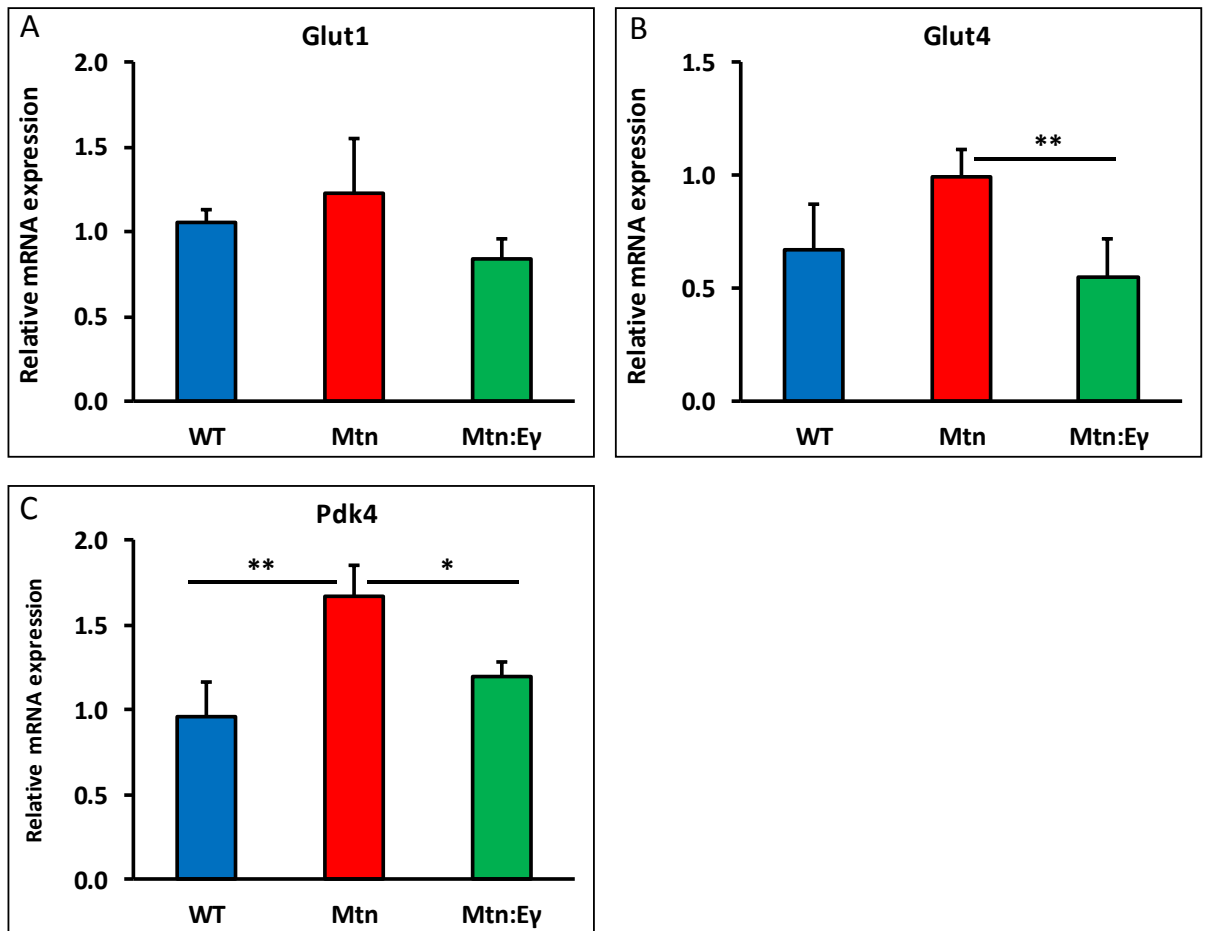


Figure 4.7. Molecular reprogramming of *Myostatin* null muscle by *Erry* overexpression and its ability to regulate glucose metabolism genes

Gene expression levels of selective biomarker genes that regulating glucose metabolism in muscles from WT, *Mtn* and *Mtn:Er* mice.

(A) Quantification of *Glut1* gene expression.

(B-C) Quantification of (*Glut4* and *PDK4*) genes expression, *Erry* overexpression significantly normalizes these genes level.

($n = 5$) male twelve-week old mice per group; One-way ANOVA followed by Bonferroni's multiple comparison tests, * = $P < 0.05$ and ** = $P < 0.01$.

4.9. *Erry* overexpression promotes expression level of genes regulates fatty acid metabolism

Present study demonstrated that introducing of *Erry* into a muscle lacking *Myostatin* normalized expression level of biomarker genes that responsible for regulating skeletal muscle vasculature, energy and glucose metabolism. In agreement with previous study (Narkar et al., 2011), we reported that *Erry* overexpression tightly regulated oxidative metabolism and vasculature in the skeletal muscles. Furthermore, transgenic induction of *Erry* into skeletal muscle from *mdx* mice resulting in restoration of fat metabolism genes like (*Had* and *Cygs*) (Matsakas et al., 2013). Despite the essential role of *Erry* in activating of genes that regulates muscle metabolism has been firmly established (Huss et al., 2002, Zhang et al., 2006), little is known about its role that direct fat metabolism biomarker genes in a muscle lacking *Myostatin*. Therefore, we examined the expression level of key regulators molecules of fatty acid metabolism (*Had* (haloacid dehalogenase), *Lpl* (Lipoprotein lipase) and *Cygs* (Cytochrome c, somatic)) in muscles (n=5) from WT, *Mtn*^{-/-} and *Mtn*^{-/-}/*Erry*^{Tg/+} mice. Our findings illustrated that the expression of fatty acid metabolism markers were higher in muscles from *Mtn*^{-/-}/*Erry*^{Tg/+} mice than the other genotypic groups. Of particular note, the expression levels of (*Had* and *Lpl*) were the lowest in muscle samples from *Mtn*^{-/-}, and the highest in *Mtn*^{-/-}/*Erry*^{Tg/+} mice (Figure 4.8A-B). Most importantly, both biomarker genes were not only higher in *Mtn*^{-/-}/*Erry*^{Tg/+} than in *Mtn*^{-/-}, but also more than in the WT (Figure 4.8A-B). The same pattern of expression level of (*Cygs*) gene was identified, without reaching significance difference between the three cohorts (Figures 4.8C). These data provide evidence that muscle-specific expression of *Erry* into *Mtn*^{-/-} mice, changes fat metabolism levels to even greater than of WT.

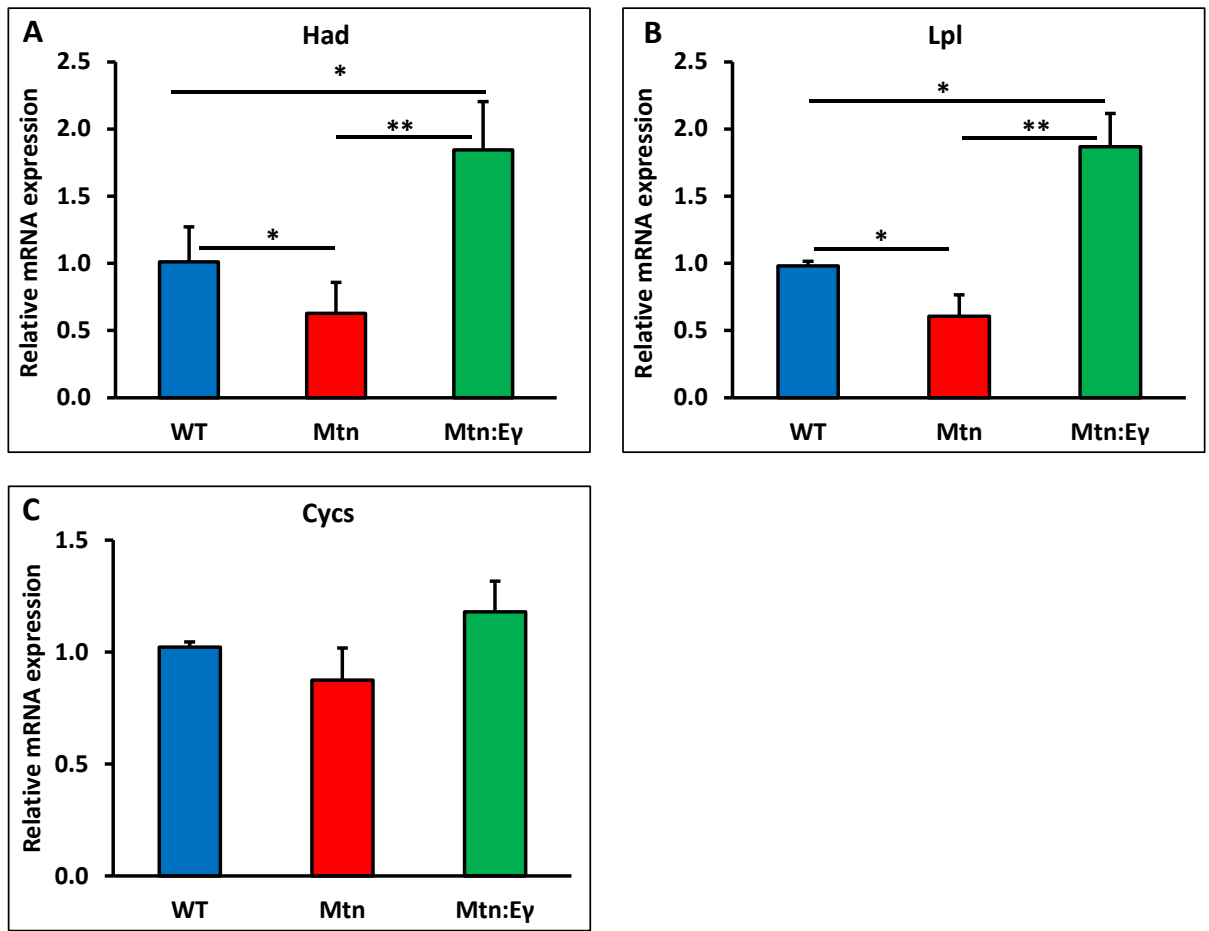


Figure 4.8. Molecular reprogramming of *Myostatin* null muscle by *Eryr* overexpression and its ability to restore the expression of fat metabolism genes

Expression levels of biomarker genes that regulating fat metabolism in muscles from WT, *Mtn* and *Mtn:Ey* mice.

(A-B) Quantification of (*Had* and *Lpl*) genes expression, *Eryr* overexpression significantly induces these genes level compared to *Mtn*^{-/-} and WT mice.

(C) Quantification of (*Cyps*) genes expression, no significant difference between any of the three genotypic groups.

(*n* = 5) male twelve-week old mice per group; One-way ANOVA followed by Bonferroni's multiple comparison tests, * = *P* < 0.05 and ** = *P* < 0.01.

4.10. Hyper-oxidative hypertrophic muscle fibres show high oxygen diffusion rate

We showed that the reverse transition driven by *Erry* introducing into *Mtn*^{-/-} muscle was not limited to the myosin heavy chain profile as a fast to slow fibres within MHCII subtypes, but also occurred at metabolic level (glycolytic to oxidative) indicating by SDH activity. These modifications were synchronized with a marked increase of muscle fibres size, capillary density, and re-localized of mitochondria in particular at sub-membrane areas, thereby breaking down the suggested constraint between muscle fibres size and oxidative capacity. To sustain the large oxidative myofibres developed as a consequence of muscle-specific overexpression of *Erry* into *Mtn*^{-/-}, high oxygen diffusion is required.

It was well established that high myoglobin concentration is essential to facilitate oxygen diffusion from capillaries to mitochondria of hypertrophied myofibres (de Koning et al., 1981, Masuda et al., 1997). Further work has revealed a remarkable increase of *myoglobin* expression in muscles from *Erry* transgenic mice compared to WT (Narkar et al., 2011). On the other hand, study by Matsakas's group (Matsakas et al., 2012a) has detected a reduction of *myoglobin* expression level in muscle from *Mtn*^{-/-} mice. Here we determined whether the increase of muscle fibres oxidative capacity and size that induced by *Myostatin* deletion and introducing of *Erry* into *Mtn*^{-/-} muscle was accompanied by any changes in expression of marker genes for oxidative phenotypes, and that able to reduce the effects of destructive radicals would generate by oxidative metabolism. Therefore, we examined the expression level of *myoglobin* which facilitates oxygen diffusion, and *catalase* as anti-oxidant enzyme in homogenised gastrocnemius muscles (n=5) from WT, *Mtn*^{-/-} and *Mtn*^{-/-}/*Erry*^{Tg/+} mice.

We found that the expression of *myoglobin* was the lowest in muscles from *Mtn*^{-/-} mice. *Erry* overexpression induced a significant increase of *myoglobin* transcriptional level. Interestingly, there was no significant difference in *myoglobin* level in muscle samples from WT and *Mtn*^{-/-}/*Erry*^{Tg/+} mice (Figure 4.9A). As number of destructive radicals might produce in the oxidative environment, thus, we examined *catalase* expression, we found that this anti-oxidant marker was not only higher in muscles from *Mtn*^{-/-}/*Erry*^{Tg/+} than *Mtn*^{-/-} mice, but also exceeded its level in the WT muscles (Figure 4.9B). These data show that muscle-specific expression of *Erry* into *Mtn*^{-/-} mice induces the expression levels of biomarkers that are essential for oxygen diffusion and oxidative radical scavenging.

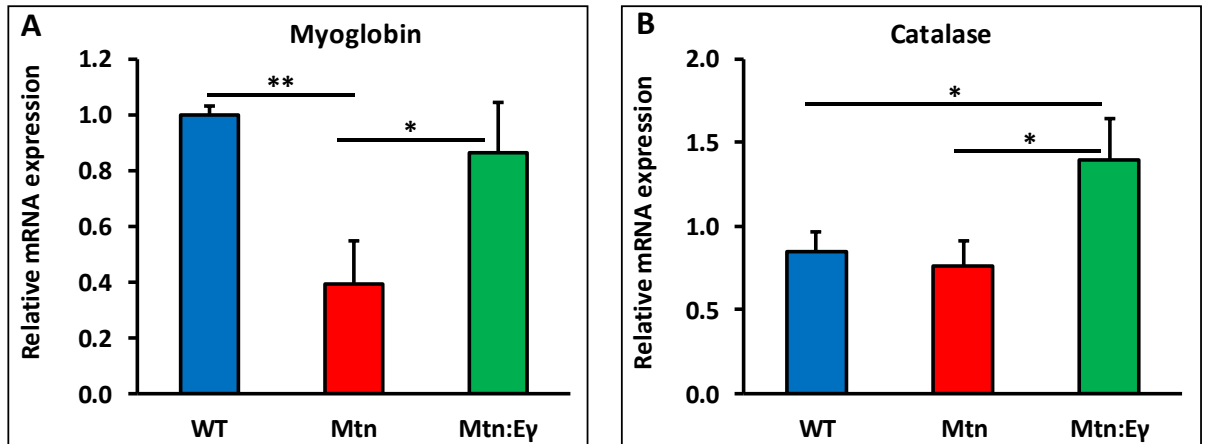


Figure 4.9. Molecular reprogramming of *Myostatin* null muscle by *Erry* overexpression and its ability to induce antioxidant genes

Expression levels of oxygen handling and antioxidant genes induced significantly by *Erry* introducing into Mtn mice.

(A) Quantification of *Myoglobin* gene expression.

(B) Quantification of *Catalase* gene expression.

($n = 5$) male twelve-week old mice per group; One-way ANOVA followed by Bonferroni's multiple comparison tests, * = $P < 0.05$ and ** = $P < 0.01$.

4.11. *Erry* overexpression into *Mtn*^{-/-} mice induces biomarker genes that regulate fatty acid transport, uptake and oxidation

We demonstrated that muscle-specific expression of *Erry* potentially contributes to the regulation of biomarker genes that responsible for regulating muscle angiogenesis, energy and metabolism profiles. Previously has been reported that inhibition of *Myostatin* signalling specifically in skeletal muscles resulting in a marked reduction of fat mass (Guo et al., 2009). On the other hand, several studies have illustrated that *Erry* is a key regulator of a network of genes that linked to fatty acid oxidation and mitochondrial biogenesis (Dufour et al., 2007, Alaynick et al., 2007). Furthermore, genome-wide expression analysis revealed *Erry* coordinately inducing a number of genes that promoting oxidative of fat (Wang et al., 2004).

Therefore, we speculate that induction of *Erry* would promote fat transport, uptake and oxidation in a muscle lacking *Myostatin*. To do so, we examined the expression of genes controlling fat metabolism (fatty acid transport and uptake molecules: *Cd36*, *Slc25a20* (solute carrier family 25 member 20), *Fatp1* (Fatty acid transport protein 1), *Fabp3* (fatty acid binding protein 3), and regulators of fatty acid oxidation (*Acadl* (Acyl-CoA dehydrogenase (long chain)), *Acadm* (Acyl-Coenzyme A dehydrogenase medium-chain,)) in muscles (n=5) from WT, *Mtn*^{-/-} and *Mtn*^{-/-}/*Erry*^{Tg/+} mice. We found that all six genes were expressed to a higher degree in muscles from *Mtn*^{-/-}/*Erry*^{Tg/+} than *Mtn*^{-/-} and WT mice (Figure 4.10). Of particular note, all genes showed same expression level in muscles from WT and *Mtn*^{-/-} mice, except *Fabp3* gene showed a significant reduction in *Mtn*^{-/-} compared to WT (Figure 4.10D).

These data show that *Erry* introducing into a muscle lacking *Myostatin* is sufficient to promote the expression levels of biomarker genes that regulate fatty acid transport, uptake and oxidation in skeletal muscle.

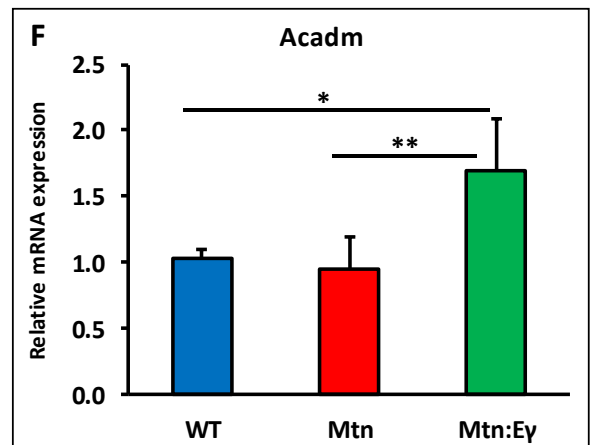
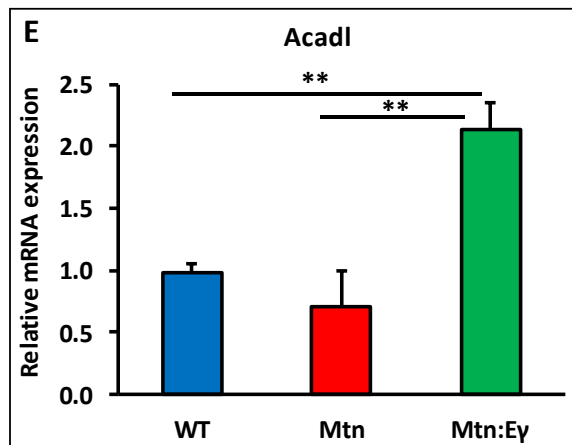
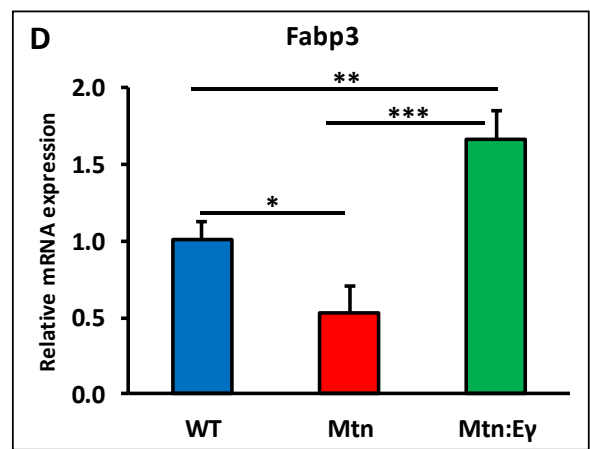
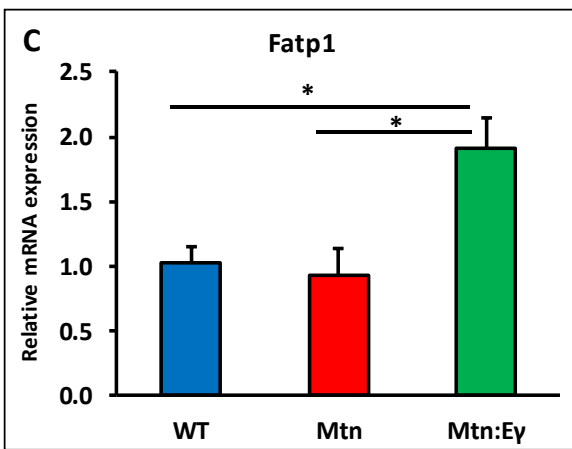
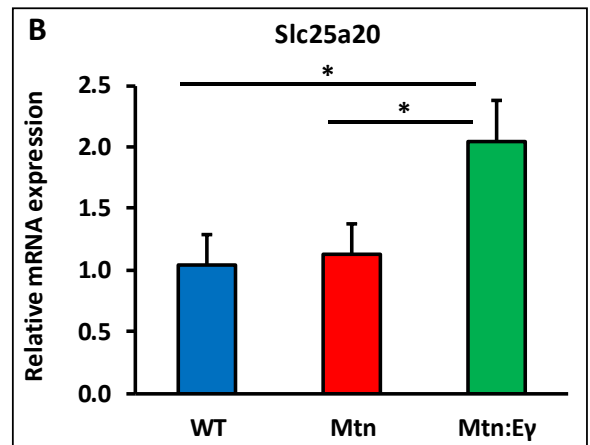
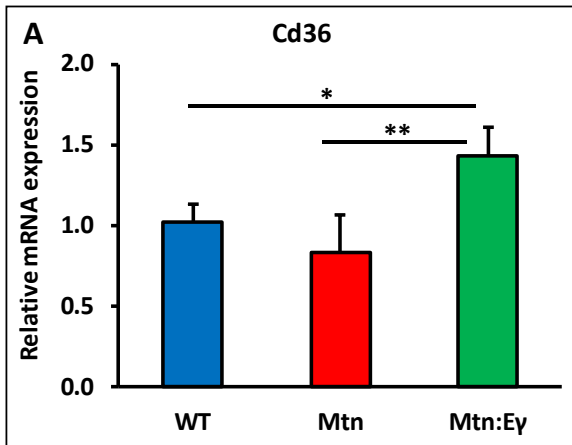


Figure 4.10. Molecular reprogramming of *Myostatin* null muscle by *Erry* overexpression and its ability to regulate the expression of fatty acid transport, uptake and oxidation genes

Erry introducing into *Mtn* mice promote expression levels of genes regulate fatty acid transport, uptake and oxidation.

(A) Quantification of *CD36* gene expression.

(B) Quantification of *Slc25a20* gene expression.

(C) Quantification of *Fatp1* gene expression.

(D) Quantification of *Fabp3* gene expression.

(E) Quantification of *Acadl* gene expression.

(F) Quantification of *Acadm* gene expression.

(*n* = 5) male twelve-week old mice per group; One-way ANOVA followed by Bonferroni's multiple comparison tests, *= P<0.05, **= P<0.01 and ***= P<0.001.

4.12. Hyper-oxidative hypertrophic muscle fibres show low ROS emission rate

Using transmission electron microscopy, we showed that germline deletion of *Myostatin* resulted in alteration of mitochondrial number, size and distribution. However, introducing of *Erry* into *Mtn*^{-/-} muscles largely normalized almost all these abnormalities, in particular re-localization of mitochondria at the sub-membrane area. In addition, we showed that *Erry* overexpression induced a transcriptional level of anti-oxidant (*Catalase*) to scavenge destructive radicals that might produce during oxidative metabolism. Previous work has reported that mitochondrial electron transport chain (ETC) pathway is the main source of Reactive Oxygen Species (ROS) (Harper et al., 2004). Further, chronic production of ROS as a result of mitochondrial dysfunction can lead to protein, DNA and lipids damage (Jackson, 2011). Numerous studies have established a central role of *Erry* in regulating of mitochondrial biogenesis, activity and fatty acid oxidation in skeletal muscles (Narkar et al., 2011, Rangwala et al., 2010). Further investigation has demonstrated a marked reduction of expression level and activity of TCA and ETC enzymes, and severely impairment of mitochondrial formation thereby increase emission rate of ROS in *Erry* knockout phenotype (Alaynick et al., 2007, Murray et al., 2013). Here we determined whether muscle-specific expression of *Erry* into *Mtn*^{-/-} mice would reduce ROS production that might follow the disruption in mitochondrial size and distribution we described previously in *Mtn*^{-/-} muscles. Therefore we gauged the level of superoxide using Dihydroethidium (DHE) dye (Bindokas et al., 1996, Li et al., 2003a) in TA muscle sections (n=5) from WT, *Mtn*^{-/-} and *Mtn*^{-/-}*Erry*^{Tg/+} mice (Figure 4.11A). We found elevated levels of superoxide indicating by high DHE intensity in both small (slow oxidative) and large (fast glycolytic) myofibres in TA muscles from *Mtn*^{-/-} mice compared to counterpart muscles from WT (Figure 4.11B). However, *Erry* overexpression significantly lowered the level of ROS of *Mtn*^{-/-} muscles indicated by low DHE intensity in both myofibre cohorts were examined (Figure 4.11B). Importantly, the ROS in large myofibres from *Mtn*^{-/-}/*Erry*^{Tg/+} muscles was even lower than those of WT (Figure 4.11B). These data indicate an essential role of *Erry* in preventing disproportionate increase of ROS, thereby maintaining mitochondrial function.

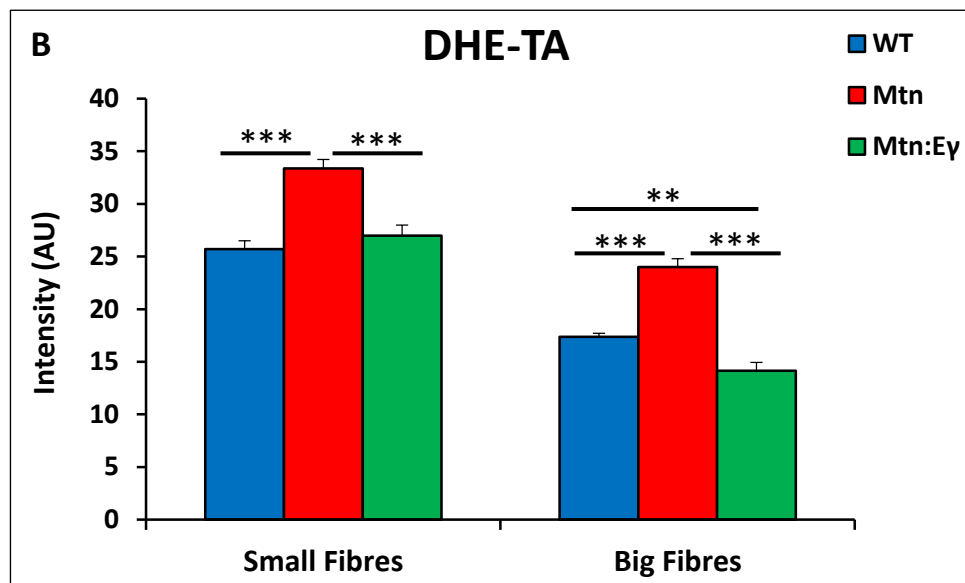
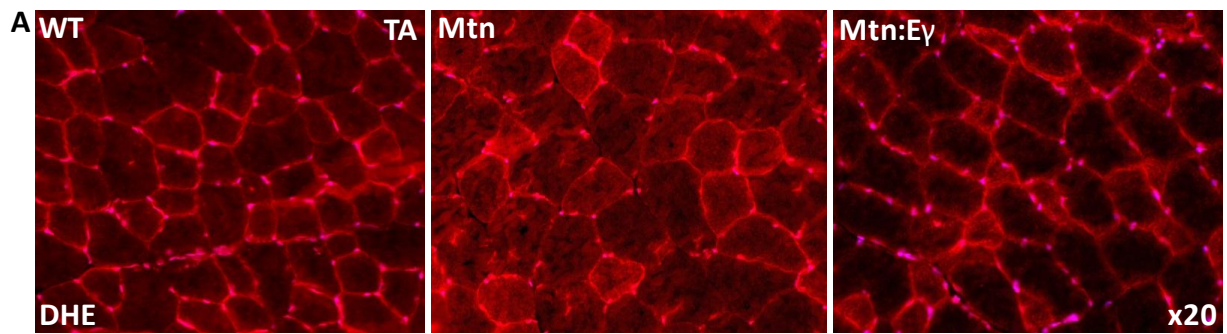


Figure 4.11. *Er* overexpression required for preventing excessive superoxide production
Muscle-specific expression of *Er* normalizes level of Reactive Oxygen Species (ROS) of *Myostatin* null mice (*Mtn*).

(A) DHE fluorescence in the body of TA muscle fibres from WT, *Mtn* and *Mtn:Er* mice.

(B) Quantification of DHE intensity in small and large myofibres in TA muscles.

($n = 5$) male twelve-week old mice per group; One-way ANOVA followed by Bonferroni's multiple comparison tests, **= $P < 0.01$ and ***= $P < 0.001$.

4.13. *Erry* overexpression into *Mtn*^{-/-} mice does not rescue the reduction of satellite cells number in hyper-oxidative hypertrophic myofibres

We demonstrated that muscle-specific expression of *Erry* into *Mtn*^{-/-} mice was efficacious in challenging the dogma of an inverse relationship between muscle fibres size and oxidative capacity. The deviation from this relationship may be realized by an increase of muscle oxidative capacity indicated by high SDH activity, increase capillary density that was confirmed with a marked elevation of genes that regulate angiogenesis program at the transcriptional level, increase myoglobin content, and re-localization of mitochondria to subsarcolemmal location. Importantly all these modifications were synchronised with maintaining muscle fibre size increase due to *Myostatin* absence.

Next we examined the consequences of *Myostatin* absence and *Erry* introducing into *Mtn*^{-/-} on individual muscle fibres.

It has been established that a myofibre is a cellular unit of adult skeletal muscle that is sustained by high numbers of post-mitotic myonuclei, and competently repaired and regenerated by a pool of satellite cells that located beneath the basal lamina (MAURO, 1961, Zammit and Beauchamp, 2001). In order to adapt to growing demand, early post-natal satellite cells provide the muscle with new myonuclei. However, in the adult's satellite cells become the source of myonuclei required for muscle repair and regeneration (Moss and Leblond, 1971, Zammit et al., 2006). Further studies have reported that satellite cells (SC) retain the ability to proliferate and differentiate in response to the routine need of myofibre hypertrophy or myonuclei turnover (Schmalbruch and Lewis, 2000, Snow, 1977).

Previously it was demonstrated that muscle hypertrophy arising from *Myostatin* deletion is not associated with an increase in a number of satellite cells, a significant reduction of satellite cell numbers per myofibres from EDL muscle of *Mtn*^{-/-} compared to WT mice was reported (Amthor et al., 2009). On the other hand, Murray's review (Murray et al., 2013) has referred to a marked up-regulation of *Erry* expression during muscle cells differentiation which supports a potential role of the *Erry* in regulating myogenesis, a field of *Erry* function that has not been completely explored. In addition, number of studies have shown an increase in satellite cells population in muscle fibres becoming oxidative (Putman et al., 1999, Christov et al., 2007).

Our findings showed that *Erry* overexpression into *Myostatin* knockout mice implicates in a partial shift of myofibres toward an oxidative phenotype. Therefore, we sought to determine satellite cells number and recruitment following germline deletion of *Myostatin*, and whether *Erry* overexpression in the *Mtn*^{-/-} muscles would influence the quantity of the resident satellite cells, and their proliferation and differentiation programs. To do so, satellite cells on single muscle fibre from EDL muscles (n=4) from WT, *Mtn*^{-/-} and *Mtn*^{-/-}/*Erry*^{Tg/+} mice were cultured and fixed in different time points, time zero (T0) and 48 hours culture (T48), thereafter immunostained with two myogenic markers (Pax7 and MyoD). Pax7 as a marker of satellite cells, and MyoD expressed as a marker of activated satellite cells and a key transcription factor for myogenic differentiation (Christov et al., 2007) (Figures 4.12A and 4.13A).

We found that deletion of *Myostatin* resulted in fewer satellite cells per myofibre (2.8 ± 0.3 and 10.9 ± 1) compared to WT (3.6 ± 0.3 and 12.7 ± 0.9) at T0 and T48 time points respectively. At both time points, the number of satellite cells was even lower in the muscles of the *Mtn*^{-/-}/*Erry*^{Tg/+} mice (1.7 ± 0.1 and 4.1 ± 0.5) compared to the other genotypic groups (Figures 4.12A and B, and 4.13A and B). These results show that muscle-specific expression of *Erry* in the *Mtn*^{-/-} does not attenuate the deficit of satellite cell numbers that follows *Myostatin* ablation.

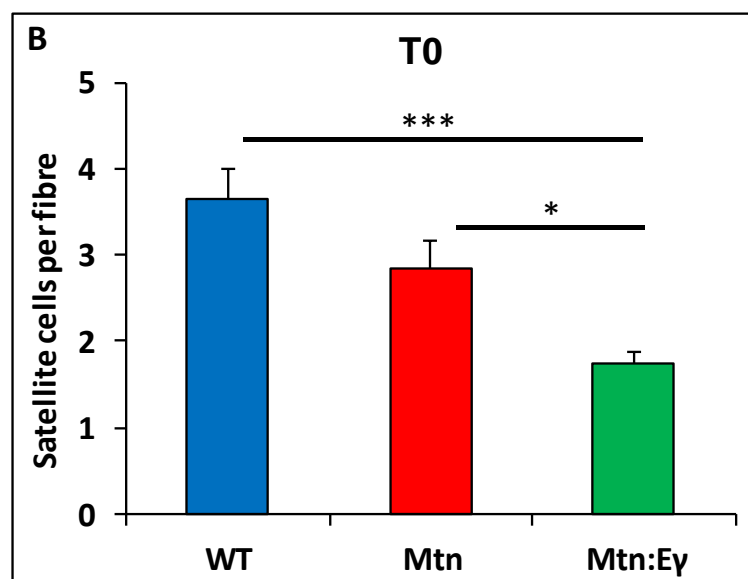
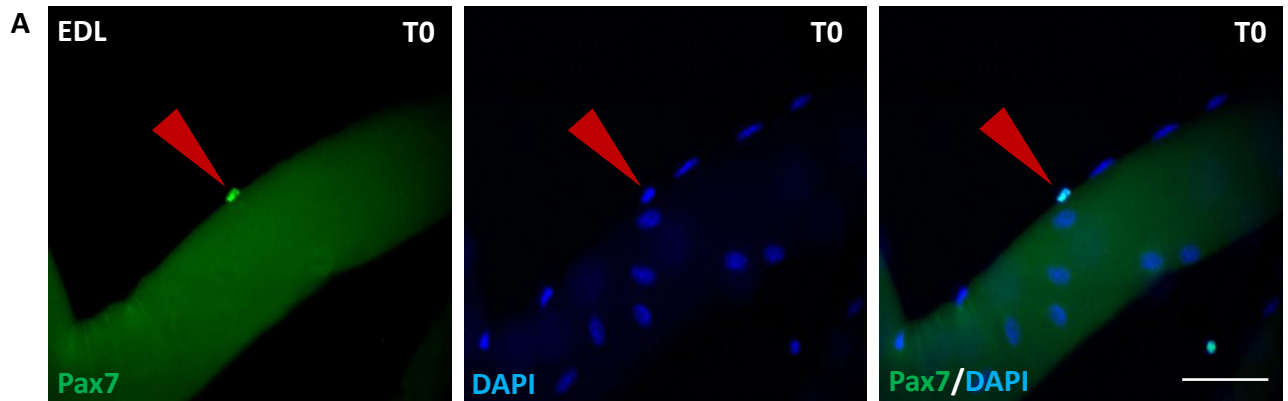


Figure 4.12. Fewer number of Satellite cells in EDL myofibre of *Mtn:Er* than other genotypic groups

Hypertrophied oxidative muscle developed through introduction of *Erty* on the muscle of *Myostatin* null mice (*Mtn*) shows depletion of satellite cells.

(A) Quiescent satellite cells stained for DAPI and Pax7 on freshly isolated (T = 0 hr) muscle fibres from the EDL muscles (arrowhead), scale 50 μ m.

(B) Quantification of satellite cell number on freshly isolated EDL muscle fibres of WT, *Mtn* and *Mtn:Er* mice.

Fibres were from 4 male twelve-week old mice per group; One-way ANOVA followed by Bonferroni's multiple comparison tests, *= P<0.05 and ***= P<0.001.

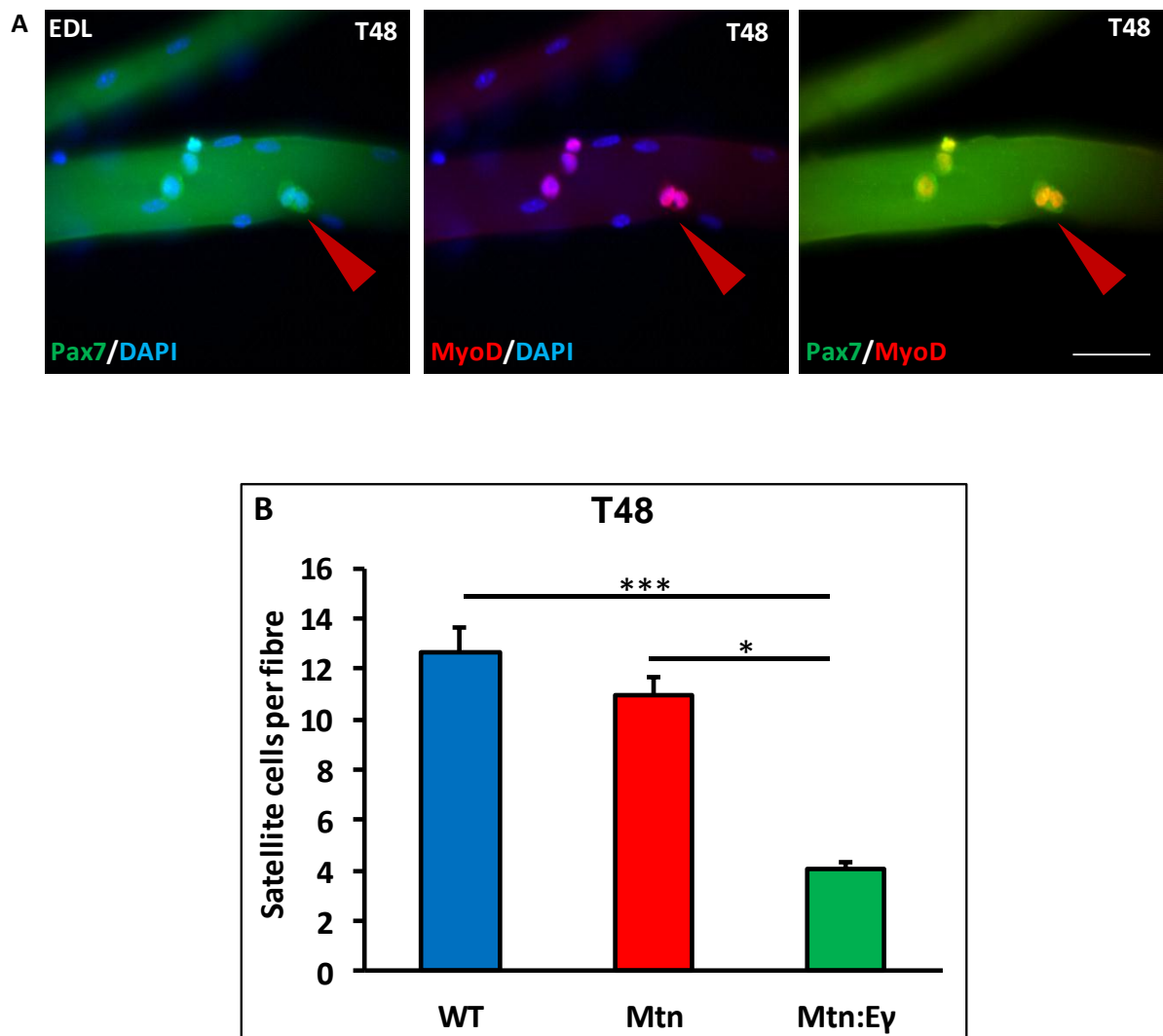


Figure 4.13. Muscle-specific expression of *Erry* does not influence the satellite cell number

Hypertrophied oxidative muscle developed through introduction of *Erry* on the muscle of *Myostatin* null mice shows depletion of satellite cells.

(A) Single muscle fibres from the EDL muscles after 48 hr in cell culture stained for DAPI, Pax7 and MyoD (arrowhead), scale 50 μ m.

(B) Quantification of satellite cell number on EDL muscle fibres at 48 hr.

Fibres were from 4 male twelve-week old mice per group; One-way ANOVA followed by Bonferroni's multiple comparison tests, *= P<0.05 and ***= P<0.001.

4.14. Proliferation and differentiation rate of hyper-oxidative hypertrophic myofibres

We showed that introducing of *Erry* into a muscle lacking *Mtn*^{-/-} did not rescue satellite cells depletion that following *Myostatin* absence.

The activation of satellite cells from a quiescent state and their subsequent progression along the myogenic lineage is controlled by the myogenic regulatory factors (MRFs) (Zammit and Beauchamp, 2001, Rudnicki et al., 1993, Hasty et al., 1993). Previous studies have illustrated that *Myostatin* administration to C2C12 muscle cell line results in a reduction of myoblast proliferation due to its interaction with the factors that control the progression of the cell cycle from G1 to S-phase through up-regulation of p21 inhibitor and its ability to downregulate Cdk2 (Thomas et al., 2000). Further work has demonstrated fewer number of myoblast that accumulated in clusters around the isolated myofibres from EDL muscles of *Mtn*^{-/-} compared to age-matched WT mice (Amthor et al., 2009). In this section we sought to determine proliferation and differentiation characteristics of satellite cells in EDL muscles from the three cohorts (WT, *Mtn*^{-/-} and *Mtn*^{-/-}/*Erry*^{Tg/+}). Therefore, in order to examine whether *Erry* overexpression into *Myostatin* null mice would influence satellite cells activation and proliferation, we monitored the number of these cells' clusters around isolated myofibres of EDL muscles of the three genotypic groups. Our findings showed that during the 48 hr period of culture, satellite cells not only divide but also form clusters (Figure 4.14A). We also found that the number of clusters was similar in isolated myofibres from WT and *Mtn*^{-/-} muscles, but fewer myoblast had accumulated in clusters in the *Mtn*^{-/-}/*Erry*^{Tg/+} derived cultures compared to *Mtn*^{-/-} and WT mice (Figure 4.14B).

Next, we counted the number of satellite cells per cluster along the isolated myofibres. We found that the number of cells per cluster was highest in WT and lowest in the *Mtn*^{-/-} with that of the *Mtn*^{-/-}/*Erry*^{Tg/+} in between albeit do not show significant differences (Figure 4.14C).

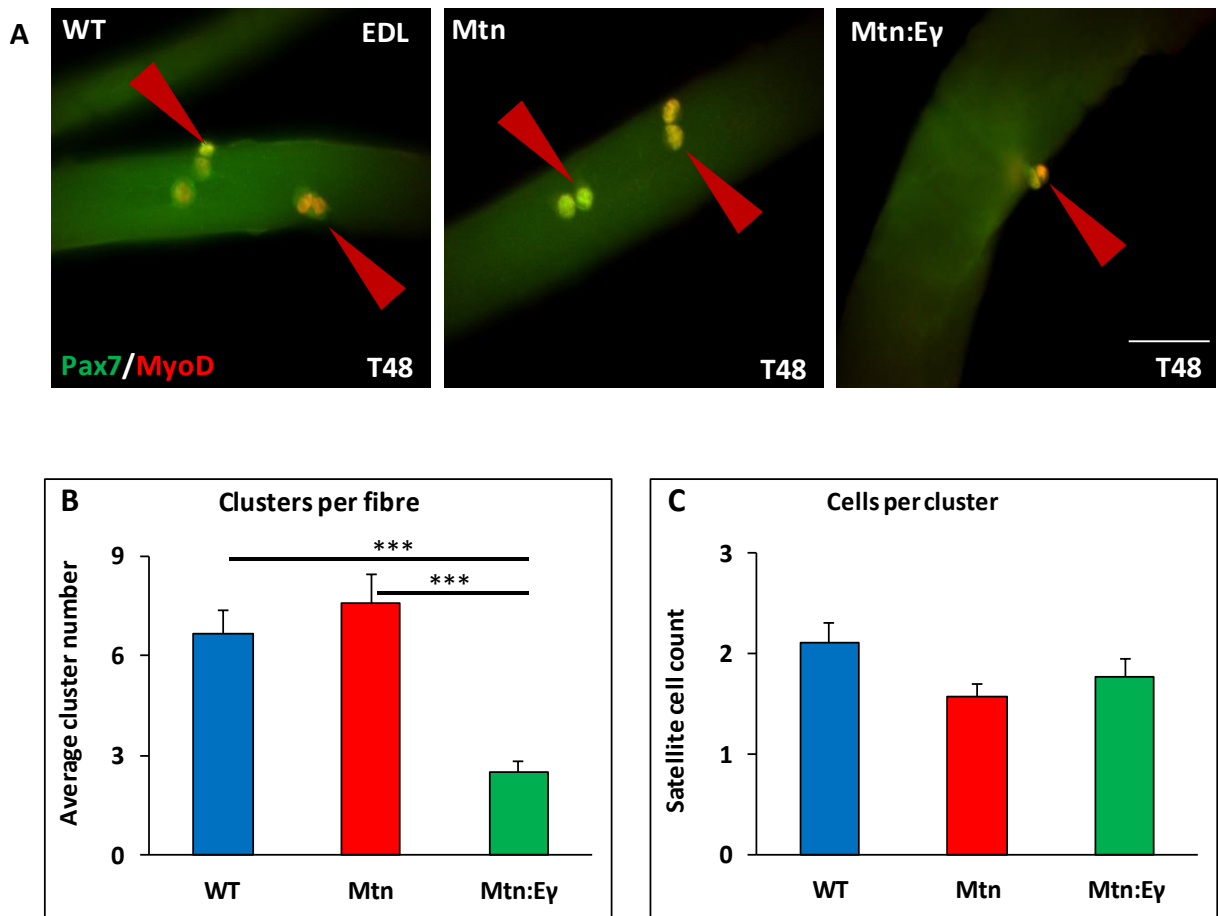


Figure 4.14. Proliferation rate in myofibres of EDL muscles from three genotypic groups

Hypertrophied oxidative muscle developed through introduction of *Erry* on the muscle of *Myostatin* null mice shows reduction of clusters of satellite cells

(A) Single EDL muscle fibres from WT, *Mtn* and *Mtn:Er* mice after 48 hr in cell culture stained for Pax7 and MyoD (arrowhead), scale 50µm.

(B) Quantification of satellite cell clusters at 48 hr.

(C) Cluster size at 48 hr on muscle fibres.

Fibres were from 4 male twelve-week old mice per group; One-way ANOVA followed by Bonferroni's multiple comparison tests, ***= P<0.001.

Previously has been reported that most activated satellite cells then proliferate, and Pax7 progressively become transcriptionally inactive as the progeny satellite cells committed to differentiation. In contrast, other proliferating cells conserve Pax7 expression but lose MyoD and withdraw from both cell cycle and instead myogenic differentiation, returning to a state resembling quiescence (Zammit et al., 2004). We determined satellite cells progression by examining the expression of Pax7 and MyoD markers on isolated myofibres from EDL muscles of WT, *Mtn*^{-/-} and *Mtn*^{-/-}/*Erry*^{Tg/+}. Satellite cells were categorised according to the expression of myogenic markers into satellite cells (Pax7⁺), differentiating muscle cells (MyoD⁺), and myoblast (Pax7⁺ and MyoD⁺) (Figure 4.15).

Our results showed no significant differences in numbers of satellite cells specifically express any of these markers (Figure 4.15). These observations, and in agreement with previous findings (Amthor et al., 2009), confirmed that the myofibres hypertrophy resulted from blocked or absence of *Myostatin* is independent satellite cells number or recruitment. In addition, it has been revealed that presence of Pax7 is compatible with myogenic differentiation and downregulation of this protein is not prerequisite for this process (Zammit et al., 2006). Therefore, high expression of Pax7 that we showed in our findings, might not contradict with normal differentiation process of satellite cells following *Erry* overexpression on a muscle lacking *Myostatin*.

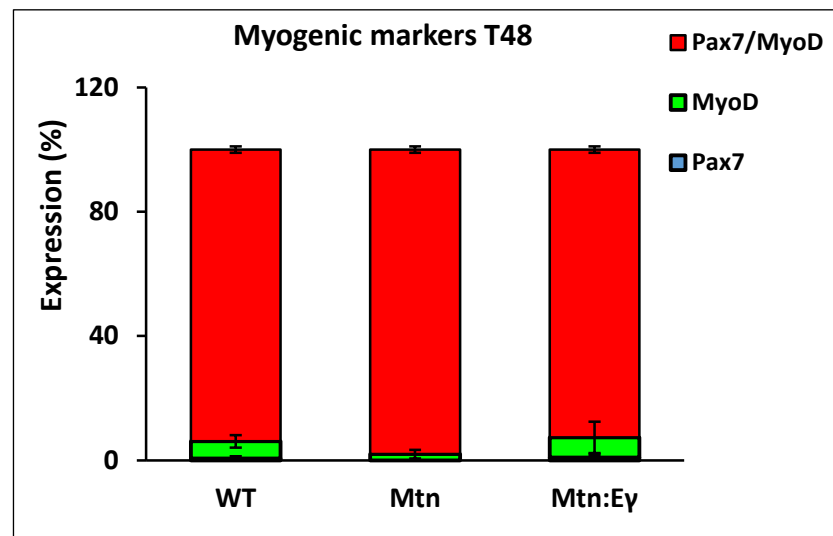


Figure 4.15. Pax7 and MyoD expressions in EDL myofibres from WT, *Mtn* and *Mtn:Ey* mice

Muscle-specific expression of *Erry* does not affect muscle differentiation process.

Profiling of satellite cells differentiation at 48 hr in cell culture.

Fibres were from 4 male twelve-week old mice per group; One-way ANOVA followed by Bonferroni's multiple comparison tests.

4.15. Muscle-specific expression of *Erry* into *Mtn*^{-/-} promotes myonuclei number

We showed that the increase of myofibres size in muscles from *Mtn*^{-/-} and *Mtn*^{-/-}/*Erry*^{Tg/+} was not accompanied by increasing in satellite cells number, however, this depletion in satellite cells number following *Myostatin* deletion and *Erry* overexpression did not affect proliferation and differentiation processes. Previous work has demonstrated that during muscle fibres growth, the number of myonuclei per muscle fibres reflects the accumulative history of muscle precursor recruitment and activity (Amthor et al., 2009). Moreover, a number of studies have referred to linear correlation between myonuclei number and size of individual muscle fibre (Bruusgaard et al., 2006, Allen et al., 1995, Roy et al., 1992). Until recently, data reported a slight reduction but not significantly in the average of total myonuclei number per individual myofibres from *Mtn*^{-/-} compared to WT mice (Wang and McPherron, 2012). Here we determined whether introducing of *Erry* into a muscle lacking *Myostatin* can impact myonuclei content.

Therefore, we quantified myonuclei numbers at (T0) time point on isolated myofibre of EDL muscles from WT, *Mtn*^{-/-} and *Mtn*^{-/-}/*Erry*^{Tg/+} mice (Figure 4.16A). Our studies showed that the numbers of myonuclei were similar in myofibres of EDL muscles from WT and *Mtn*^{-/-} mice, as well as between EDL myofibres from *Mtn*^{-/-} and *Mtn*^{-/-}/*Erry*^{Tg/+}. However, the number of myonuclei was significantly higher in the fibres of *Mtn*^{-/-}/*Erry*^{Tg/+} compared to WT (Figure 4.16B). These data suggest that introducing of *Erry* into *Mtn*^{-/-} was sufficient to influence myonuclei number per individual muscle fibre.

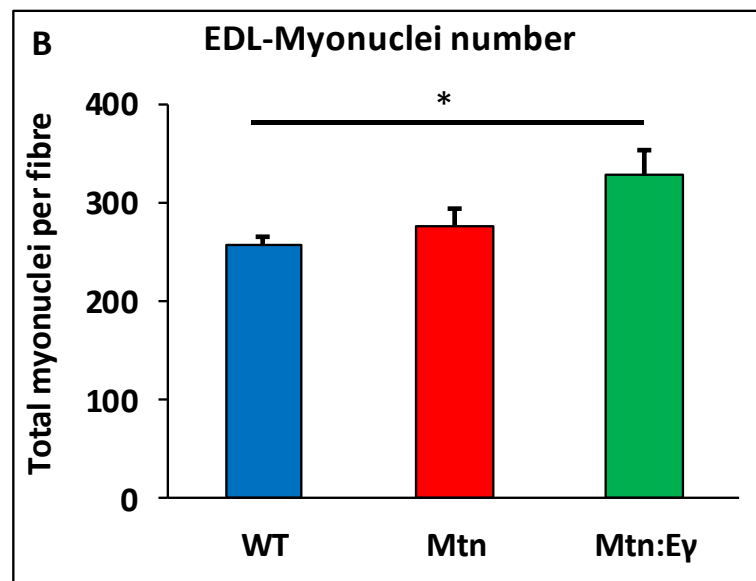
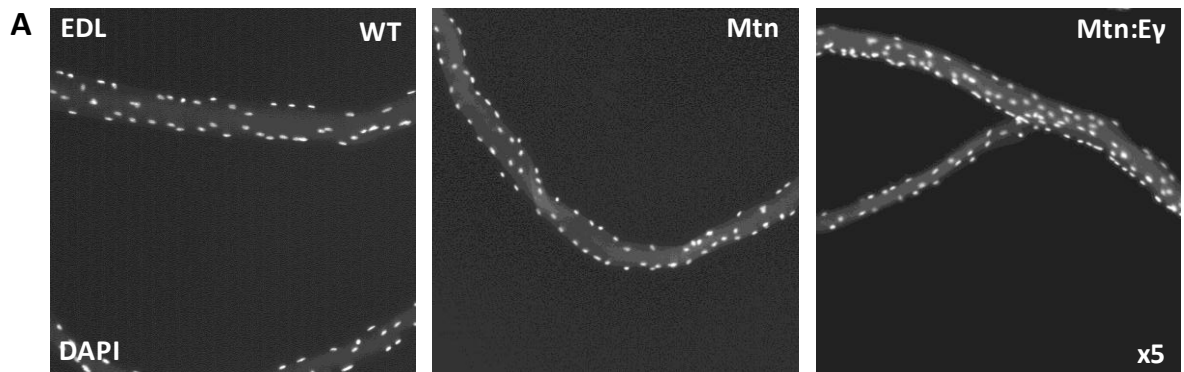


Figure 4.16. Hyper-oxidative hypertrophy myofibres show more myonuclei

Hypertrophied oxidative muscle developed through introduction of *Erry* on the muscle of *Myostatin* null mice shows increase of myonuclei content.

(A) Single EDL muscle fibres from WT, *Mtn* and *Mtn:Ey* mice stained with DAPI to visualize myonuclei.

(B) Quantification of myonuclear number in EDL fibres.

Fibres were from 4 male twelve-week old mice per group; One-way ANOVA followed by Bonferroni's multiple comparison tests, * = $P < 0.05$.

4.16. Myonuclei distribution do not normalize by introducing of *Erry* into *Mtn*^{-/-} mice

We demonstrated a significant elevation in numbers of myonuclei per myofibres of EDL muscles from *Mtn*^{-/-}/*Erry*^{Tg/+} compared to WT, with no differences in between either WT and *Mtn*^{-/-} or between *Mtn*^{-/-} and *Mtn*^{-/-}/*Erry*^{Tg/+} muscles.

Published study has illustrated that myonuclei distribution with individual myofibres is a regulated process, since myonuclei position is important to minimize issues related to macromolecule movement in larger cells. Therefore the degree of regulation is inversely proportional to random positioning of the nuclei (Bruusgaard et al., 2003). In order to quantify this, we calculated the distance to the nearest neighbour for the nuclei located at the periphery of single fibres of EDL muscles (n=4) from WT, *Mtn*^{-/-} and *Mtn*^{-/-}/*Erry*^{Tg/+} mice. Confocal stacks of single fibres labelled with DAPI (Figure 4.17A) were used to generate the 3D coordinates of each nucleus in fibre (Figure 4.17B) using Imaris software.

Using custom made software, a simulation of randomly and optimally distributed nuclei was compared to the actual distribution (see methods). The WT fibres displayed an improvement from a random distribution of 20%. However, *Mtn*^{-/-} and *Mtn*^{-/-}/*Erry*^{Tg/+} fibres had distributions that were more random, with significantly lower improvements of 10% and 4%, respectively (Figure 4.17C).

Together, these results show that muscle-specific expression of *Erry* in the *Mtn*^{-/-} does not normalize key features related to the myonuclei distribution and positioning.

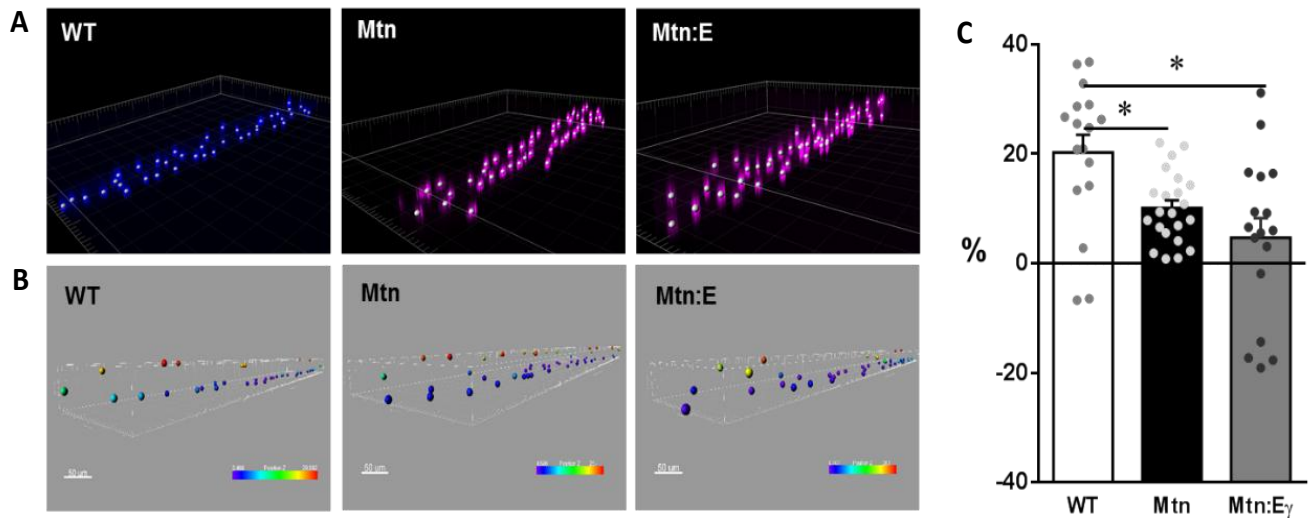


Figure 4.17. Myonuclei distribution in myofibres from EDL muscles of WT, *Mtn* and *Mtn:E_γ* mice

Muscle-specific expression of *Eryr* does not normalize myonuclei positioning

(A) Confocal stacks of single fibres labelled with DAPI to study myonuclear organization.

(B) Virtual reconstruction of single muscle fibres, colour encodes distance in the z-plane.

(C) Improvement in myonuclear organization, where 0% denote a random distribution.

Fibres were from 4 male twelve-week old mice per group; One-way ANOVA followed by Bonferroni's multiple comparison tests, *= P<0.05.

This work has been done by Jo C Bruusgaard, University of Oslo, Norway.

4.17. Discussion

Skeletal muscle is a plastic tissue composed of a heterogeneous population of muscle fibres that differ in their metabolic, molecular and contractile properties. It continuously adapts in response to a variety of stimuli (Rodriguez et al., 2014). *Myostatin* has been described as a negative regulator of muscle development, since its deletion leads to an increase in muscle mass that accompanied by predominantly of glycolytic fibres and reduction of oxidative phenotype (McPherron and Lee, 1997, Matsakas et al., 2012a). The glycolytic muscle phenotype that develops due to genetic deletion of *Myostatin* is associated with a marked reduction of mitochondrial enzyme activity and blood supply (McPherron et al., 1997, Amthor et al., 2007, Lipina et al., 2010). Furthermore, it has been reported that germline deletion of *Myostatin* results in a notable reduction of satellite cells population per myofibre (Amthor et al., 2009). On the other hand, several studies have described estrogen-related receptor gamma (*Errγ*) as a key molecular mediator in the mitochondrial function, angiogenesis and the development of oxidative phenotype in skeletal muscle (Giguere, 2008, Alaynick et al., 2007). Moreover, the potential role of *Errγ* in regulating the skeletal muscle intrinsic angiogenic program and oxidative metabolism pathways has been firmly established (Rangwala et al., 2010, Narkar et al., 2011). Currently, it was not known to what extent that *Errγ* introducing into a muscle lacking *Myostatin* using specific promoter (HSA) would rescue the metabolic, molecular and cellular deficits resulted from *Myostatin* absence.

The detailed analysis of muscle metabolic status, blood supply efficiency, molecular profile of key marker genes that regulate angiogenesis, energy metabolism, oxygen handling and antioxidant, glucose and fatty acid oxidation and metabolism programs, as well as cellular features undertaken in this study highlight some key aspects of the skeletal muscle response to *Myostatin* deletion and specific expression of *Errγ* into *Mtn^{-/-}* mice. Firstly, we show that myofibres of all muscles examined from *Mtn^{-/-}* mice display a marked reduction of oxidative capacity indicated by low SDH activity, and high PAS activity (indicative high glycolytic status). However, muscle-specific expression of *Errγ* in the *Mtn^{-/-}* restored the oxidative capacity to a normal level, as muscles from *Mtn^{-/-}/Errγ^{Tg/+}* mice show higher SDH activity than other genotypic groups. Secondly, we demonstrated that the reduced oxidative capacity in *Mtn^{-/-}* muscles was accompanied by a significant decrease in blood supply. In contrast, muscles from *Mtn^{-/-}/Errγ^{Tg/+}* mice display the highest ratio of capillary per myofibre

(C:F), that exceeded even the vasculature level of WT mice. We also provided evidence that muscles from *Mtn*^{-/-} and *Mtn*^{-/-}/*Erry*^{Tg/+} mice had a distinctive metabolite profile characterised by significantly high levels of lactate and creatine/phosphocreatine in *Mtn*^{-/-} compared to that of the *Mtn*^{-/-}/*Erry*^{Tg/+} muscles which is consistent with a greater glycolytic phenotype. On the other hand, muscles from *Mtn*^{-/-}/*Erry*^{Tg/+} mice displayed greater content of taurine and anserine. Our work examining gene expression levels offers interesting insight into the molecular program that would explain the metabolic profile of *Mtn*^{-/-}/*Erry*^{Tg/+} muscles. We showed that *Erry* introducing into *Mtn*^{-/-} mice was efficacious for inducing of endothelial mitogenic factors expression that regulate angiogenesis program, normalizing expression level of the key regulators of energy metabolism, promoting the expression of glucose metabolism and fatty acid metabolism markers, upregulating gene levels of oxygen handling and antioxidant enzymes, and enhancing the level of genes that regulate fat metabolism. Furthermore, this data showed that the normalization of mitochondrial size and distribution that followed overexpression of *Erry* into *Mtn*^{-/-} muscles, concomitant with a significant reduction of ROS levels compared to muscles from *Mtn*^{-/-} mice that displayed the highest intensity of DHE. Additionally, our results challenged the notion that slow oxidative muscle fibres contain a high number of muscle resident stem cells (satellite cells), as hyper-oxidative hypertrophic myofibres from *Mtn*^{-/-}/*Erry*^{Tg/+} muscles showed the lowest number of satellite cells per myofibre compared to the other genotypic groups. Finally, an interesting feature highlighted by our work in this section was the high number of myonuclei per myofibres of *Mtn*^{-/-}/*Erry*^{Tg/+} muscles compared to WT and *Mtn*^{-/-} muscles.

In agreement with aforementioned findings (Girgenrath et al., 2005, Amthor et al., 2007), our study demonstrates that the key feature of *Mtn*^{-/-} is the lower SDH activity, indicative of a low muscle oxidative capacity. We showed previously that germline deletion of *Myostatin* led to dramatic increase in muscle fibres size, which is also associated with the large proportion of myosin heavy chain (MHC) type IIB fibres. This combination of a low oxidative capacity and a large fibre size fits nicely with the concept of the trade-off between fibre size and oxidative capacity (Van der Laarse WJ, 1998). On the contrary, even our previous observations demonstrated no difference in fibre CSA between muscles from *Mtn*^{-/-} and *Mtn*^{-/-}/*Erry*^{Tg/+} mice, the latter had significantly high SDH activity. The higher SDH activity in

Mtn^{-/-}/*Erry*^{Tg/+} than *Mtn*^{-/-} muscles was associated with a partial normalisation of the MHC fibre profile, a decrease in the proportion of IIB fibres in all muscles examined.

It is uncertain which program causes a conversion of myofibres toward glycolytic phenotypes following *Myostatin* ablation. Previously has been shown that post-natal blocking of Myostatin does not induce significant glycolytic muscle fibres transition (Matsakas et al., 2009), indicating that the glycolytic myofibres resulted from genetic deletion of *Myostatin* may be pre-natally programmed (Girgenrath et al., 2005). We showed earlier that mitochondrial number was reduced significantly in *Mtn*^{-/-} muscles compared to WT, such observations that have been reported by Amthor's group (Amthor et al., 2007), indicating a reduction of oxidative capacity. We also demonstrated an abnormality of mitochondrial distribution and size in muscles from *Mtn*^{-/-} mice. This would infer that the mitochondrial depletion might be a causative reason for the observed myofibre type shifting toward glycolytic phenotype in muscles from *Mtn*^{-/-} mice. To avoid fibre shifting toward the glycolytic phenotypes, we need to increase mitochondrial density. Numerous studies have demonstrated that *Erry* is constitutively active orphan nuclear receptor that is highly expressed in metabolically active with high oxidative capacity tissues, such as the heart, kidneys, brain and oxidative skeletal muscles (Hong et al., 1999, Giguere, 2008, Narkar et al., 2011). Moreover, *Erry* has been described as a key regulator of a gene network linked to fatty acid oxidation and mitochondrial biogenesis (Dufour et al., 2007). Therefore, to alleviate mitochondrial deficit in *Mtn*^{-/-} mice, we introduced the expression of *Erry* into skeletal muscle using specific promoter (human α -skeletal actin promoter (HSA)). *Erry* overexpression that would induce oxidative properties on a *Mtn*^{-/-} background that is associated with hypertrophy as we showed earlier, would challenge the trade-off that is thought to be existent between muscle fibre oxidative capacity and its size (Van der Laarse WJ, 1998, Degens, 2012). Thus, we explored the potential role of *Erry* to restore the oxidative capacity in muscles from *Mtn*^{-/-} to that level of WT, robustly mediated by attenuating the mitochondrial deficits that following *Myostatin* ablation.

A number of studies have suggested that fibres that rely on oxidative phosphorylation limit their size in order that oxygen from the capillaries diffuses efficiently into the cells and to the mitochondria for ATP production (Kinsey et al., 2007, Van der Laarse WJ, 1998, van Wessel et

al., 2010). The large fibres with a low oxidative capacity in *Mtn*^{-/-} mice as we showed above conform to this concept and have a low capillary supply per fibre.

During compensatory hypertrophy the time course of angiogenesis and fibre hypertrophy are similar (Egginton et al., 1998, Plyley et al., 1998), and the capillary supply to a fibre is related to fibre size (Ahmed et al., 1997, Degens et al., 1992). In our study, we illustrate that a coupling between the fibre size and capillary supply seems to be altered in the *Mtn*^{-/-} muscles in such a way that they have fewer capillaries than expected for the size of the fibre. However, overexpression of *Erry* in *Mtn*^{-/-} drives a robust angiogenic gene programme, increases the number of capillaries per fibre and ultimately increased muscle blood flow as we showed previously (See Figures 4.3A-B, and 4.4A and B). These observations are consistent with previous reports providing evidence of potential transgenic expression of *Erry* in fast-twitch fibres trigger aerobic transformation, mitochondrial biogenesis and robust myofibrillar vascularization, thus it promotes and coordinates vascular supply and metabolic demand in oxidative slow-twitch myofibres (Narkar et al., 2011, Matsakas et al., 2012b). We suggest that as *Erry* is highly expressed in highly vascularised organs such as skeletal muscle, thus its targeting to potentiate and orchestrate a reparative angiogenesis programme of a muscle lacking *Myostatin* would be very powerful. An important finding here is that the angiogenesis programme promoted by muscle expression of *Erry* is responsive to change in fibre size so that when a fibre grows, it stimulates the formation of blood vessels presumably to ensure optimal perfusion.

Next, we determined the mechanisms that deliver the changes in the oxidative capacity of *Mtn*^{-/-} muscles following *Erry* introduction by examining the expression of a molecule that regulate oxygen diffusion from capillary to mitochondria in the hyper-oxidative hypertrophied fibres. It has been reported that presence of molecule that facilitate diffusion of oxygen may be essential to overcome the problem of oxygen diffusion in large muscle fibres (Hoofd and Egginton, 1997). Further studies have shown that myoglobin, which facilitates oxygen diffusion in mammalian muscle fibres, concentration unaltered in hypertrophied muscles (de Koning et al., 1981, Masuda et al., 1997).

In present study, we showed that hyper-oxidative hypertrophic muscles displayed a high mitochondrial density in particular at the sarcolemma. Moreover, an additional modification takes place, an increase of *myoglobin* transcription that would facilitate oxygen diffusion

from capillary to mitochondria, thereby sustaining large oxidative fibres developed as a consequence of *Erry* introducing into *Mtn*^{-/-} muscles. These outcomes have been postulated to prevent a decline in maximum steady state power as an oxidative fibre increases size (Hickson, 1980, Heard et al., 2000).

Basis on our data, we challenge the notion of inverse relationship between muscle fibre size and oxidative capacity taking advantage of the ability of oxidative muscle fibres that imparted by muscle-specific *Erry* overexpression to secrete cocktail of angiogenic factors. Thus, it allows recruitment of new blood supply, thereby improved muscle exercise capacity as demonstrated in advance.

Skeletal muscle function mainly related to its structure and metabolic processes that conserve the tissue (Krivickas et al., 2011). Myostatin signalling suppresses muscle fibres enlargement and the reliance on glycolytic metabolism, thus co-ordinate muscle metabolism and structure (Matsakas et al., 2012a). The outcomes of present study, however, shows that muscle-specific expression of *Erry* can modulate the phenotype of muscle from animals that lack *Myostatin*. Therefore, the oxidative phenotype not only promoted by *Myostatin* signalling, but also by *Erry* overexpression. Here we show that *Erry* introducing alters the metabolic profile of *Mtn*^{-/-} muscles by increasing, hence normalizing the oxidative phenotype.

Energy status (ATP/ADP or phosphocreatine) has been implicated as a determinant of muscle fibre type with high levels inducing ever more fast forms in keeping with their myofibrillar ATPase activity (Conjard et al., 1998, Bottinelli et al., 1994b). We show here from our NMR profiling that indeed the muscle of *Mtn*^{-/-} has high levels of phosphocreatine, which would be in keeping with the high ATPase activity of type IIB fibres found in its muscle, however, *Erry* introducing in *Mtn*^{-/-} muscles partially normalizes this feature.

In agreement with previous studies, we confirmed that *Erry* is a key molecule in the development of the oxidative phenotype in skeletal muscles (Narkar et al., 2011, Rangwala et al., 2010). Consistent with the oxidative metabolic phenotype of the *Mtn*^{-/-}/*Erry*^{Tg/+} mice there are higher levels of taurine and anserine observed in the NMR metabonomic analysis, (This work has been done by Natasa Giallourou, University of Reading, Uk), since taurine is positively correlated with the oxidative capacity of muscle tissues (Dunnett et al., 1997). Anserine is β -alanine and histidine related dipeptide with antioxidant properties commonly

found in skeletal muscle of many animals (Kohen et al., 1988). Furthermore, we show that the expression level of *catalase* an anti-oxidant enzyme was increased significantly in *Mtn*^{-/-}/*Erry*^{Tg/+} muscles. One possible explanation of the simultaneous robust increase of anserine and *catalase* levels in these muscles, is that both of them may act as scavenging agent of the byproducts arising from elevated oxidative activity in the muscle of *Mtn*^{-/-}/*Erry*^{Tg/+} mice.

The gene-profiling analysis gives an insight into the mechanisms that regulate the oxidative phenotype induced by muscle-specific overexpression of *Erry* into *Mtn*^{-/-} muscles. Our analysis at transcriptional level revealed that *Erry* acts by co-ordinately normalising genes that regulate muscle energy metabolism, glucose transport and metabolism, and fat transport, uptake and metabolism. Apart of (*Perm 1*), we show that *Erry* overexpression into *Mtn*^{-/-} muscles normalised the expression of all key transcriptional inducers of oxidative metabolism including (*PGC1 α* , *Ppard* and *Rev-erb a*), and biomarker genes that regulate glucose metabolism and transport such as (*Glut1*, *Glut4* and *PDK4*). The observed increase of *Perm 1* expression level following *Erry* overexpression might indicate its role in regulating of glucose and lipid metabolism, mitochondrial biogenesis and energy transfer (Heesch et al., 2016). Important finding of our study was the normalization of *PGC1 α* , an inducible of aerobic muscle, to normal condition following *Erry* overexpression. It has been reported that de-acetylation of *PGC1 α* is critical for its activation in the skeletal muscles (Canto et al., 2010, Gerhart-Hines et al., 2007, Lagouge et al., 2006). We suggest that the genetic deletion of *Myostatin* resulted in a significant increase of *PGC1 α* level mediated by de-acetylation of this gene. However, *Erry* introducing in *Mtn*^{-/-} muscles was efficacious in restoring *PGC1 α* to normal expression level, probably by bringing it back to acetylated status. Moreover, it has been shown that *PGC1 α* is not essential for fibre type specification in skeletal muscle (Zechner et al., 2010). We infer from this, *Erry* is sufficient to induce both metabolic and vascular pathways to drive aerobic remodelling of *Mtn*^{-/-} muscles independent of *PGC1 α* .

Previous work has been reported that *PDK4* is a key molecule that initiate a switch from glucose oxidation to fatty acid oxidation (FAO) through inhibiting of pyruvate dehydrogenase complex (PDC) that regulates pyruvate entry into the TCA cycle (Giguere, 2008). Moreover, it has been illustrated that there is a possibility of *PGC1 α* to induce glucose oxidation via transcriptional control of *PDK4* (Wende et al., 2005). Accordingly we believe that the reduction of *PGC1 α* following *Erry* overexpression results in downregulation

of *PK4* expression level. Another possible explanation is that the oxidative program promoted by *Erry* introducing in *Mtn*^{-/-} muscles was sufficient to downregulate *PK4* expression to drive a shifting from glucose to fatty acid oxidation.

Previous work has reported that high fat diet can have detrimental effects on skeletal muscle structure and functions, and impaired regeneration in response to injury (Nguyen et al., 2011). The expression gene analysis that we performed identified *Erry* as a key regulator of multiple genes linked to both fatty acid oxidation and metabolism (Alaynick et al., 2007). Furthermore, it was illustrated that *Erry* transgenic mice gained 35% less weight than wild type mice during a course of a high-fat diet (Narkar et al., 2011). An interesting outcome here is muscle-specific expression of *Erry* into *Mtn*^{-/-} muscle robustly promotes expression level of all examined genes that linked to fat metabolism (fatty acid transport and uptake molecules: *Cd36*, *Slc25a20*, *Fatp1*, *Fabp3* and regulators of fatty acid oxidation: *Acadl*, *Acadm*). For instance, acyl-coenzyme A dehydrogenase Medium-chain (*Acadm*) is an enzyme that mediates the first step in the mitochondrial β -oxidation of fatty acids (Schulz, 1991). Subsequently, it has been firmly established that tissues utilize fatty acids as energy substrate such as heart and skeletal muscles express high level of *Acadm* gene (Nagao et al., 1993). We have shown overexpression of *Erry* in *Mtn*^{-/-} muscles increased oxidative capacity reflecting by robust SDH activity, high capillary density and better oxygen diffusion. By way of explanation, we suggest that muscle-specific introducing of *Erry* in *Mtn*^{-/-} muscles significantly promoted the expression level of genes that regulate fat metabolism and fatty acid oxidation to maintain these parameter at high level that match the increased metabolic and oxidative capacity demands.

The muscle of *Mtn*^{-/-} mice not only showed notable shifting toward glycolytic fast phenotype fibre, and low capillary density, but also those displayed lower exercise capacity indicated by shorter running time compared to the other genotypic groups which might attribute to perturb of muscle cells organelles. In the present study using transmission electron microscopy (TEM), we showed a number of ultrastructural abnormalities in the organisation of the contractile apparatus and the cellular organelles. More specifically was the finding that genetic deletion of *Myostatin* led to a disruption in the quantity and quality of mitochondria in these muscles. However, *Erry* introducing into *Mtn*^{-/-} muscles largely normalised these abnormalities. It was well established that high mitochondrial number and

oxidative capacity are essential for integral skeletal muscle performance (Hamai et al., 1997, Rochard et al., 2000). *Erry* has been described as a master regulator of skeletal muscle mitochondrial biogenesis and activity mediated by regulating a network of genes involved in the TCA cycle, fatty acid oxidation (FAO) and oxidative phosphorylation pathways (Dufour et al., 2007, Alaynick et al., 2007). Furthermore, previous investigation of phenotypic characterization of *Erry* knockout mice showed a reduction in the expression and activity of TCA and electron transport chain (ETC) complex 1 enzyme (Alaynick et al., 2007). In the line of this investigation, several studies have shown that mitochondrial ETC complexes I and III are the major sources of ROS in muscle cells (Harper et al., 2004), that resulted in protein and DNA damage thereby inhibit muscle activities such as contraction time and myocyte differentiation (Jackson, 2011, Langen et al., 2002).

Conversely, treatment with antioxidants that can scavenge ROS leads to attenuate the effects of H₂O₂ and stimulate myocyte differentiation (Hansen et al., 2007). Our study show elevated levels of ROS through the profiling of DHF activity (Diaz et al., 2003) in muscles from *Mtn*^{-/-} mice, whereas muscle-specific expression of *Erry* normalized ROS level. We therefore suggest the *Myostatin* deletion leads to ultimately compromised mitochondria function, resulting in increased ROS production which may compromise the function of the contractile apparatus (Powers et al., 2012). In contrast, *Erry* overexpression into *Mtn*^{-/-} muscle was sufficient to promote mitochondrial density and re-localization in particular at sub-membrane areas. Furthermore, it increases the expression level of anti-oxidant, thereby reduces ROS emission in skeletal muscle cells of *Mtn*^{-/-}/*Erry*^{Tg/+} mice.

Present study gives new perspective on the relationship between metabolism and satellite cells number per muscle fibres. Our data has challenged comprehensively the generally accepted mechanism of *Myostatin* action on satellite cells in skeletal muscle. Strikingly, the observations of the study contradict the dogma that slow muscles contain more satellite cells than the fast phenotypes (Putman et al., 1999, Christov et al., 2007). We show that at least in the EDL as the fibres transitioned from type IIB to type IIA in muscles from *Mtn*^{-/-}/*Erry*^{Tg/+} mice, the number of associated satellite cells was significantly reduced, with a concurrent increase of myonuclei number. Numerous studies have revealed *Myostatin* as a negative regulator of muscle growth (McPherron and Lee, 1997, Taylor et al., 2001). However, there is uncertainty about how this activity is mediated. Thomas (Thomas et al.,

2000) has demonstrated that *Myostatin* acts to suppress the activity of skeletal muscle stem cells. On the contrary, others have reported that *Myostatin* inhibits muscle growth and regeneration mediated by controlling protein synthesis and breakdown in myofibres through a mechanism mostly if not completely independent of satellite cells (Amthor et al., 2009, Lee et al., 2012b). In support of this view, previous work has shown that Myostatin propeptide-mediated inhibition of this molecule resulted in muscle fibre hypertrophy liberated of satellite cell activity (Matsakas et al., 2009).

In agreement with our findings, previous work has reported that muscles from *Mtn*^{-/-} mice had reduced number of satellite cells without altering their rate of proliferation (Amthor et al., 2009). Same study has shown a constant number of clusters and satellite cells per cluster along isolated myofibres from *Mtn*^{-/-} mice compared to the wild type (Amthor et al., 2009). Consistently, Welle (Welle et al., 2011) has referred that post-developmental inactivation of Myostatin leads to muscle fibres hypertrophy without myonuclear accretion. These findings were contradict by McCroskery et al. who reported that *Myostatin* deletion results in an increase in number of satellite cells (McCroskery et al., 2003). We suggest that myofibres hypertrophy following *Myostatin* deletion is independent satellite cells number. It implicates instead mechanism whereby *Myostatin* absence up-regulates PI3K/AKT/mTOR pathway that influences protein synthesis in hypertrophic myofibres (Chelh et al., 2009). We showed that muscle-specific expression of *Erry* into *Mtn*^{-/-} caused transition of glycolytic fibres toward oxidative phenotypes. As hypertrophic fibres from *Mtn*^{-/-} mice showed a reduction in satellite cell number, imperative question is whether myofibres shifting toward oxidative phenotypes following *Erry* overexpression would increase satellite cells number. Further, does the alteration in myofibre type can affect myonuclei number and distribution? We found fewer satellite cells and clusters per fibre, no change in the number of cells per cluster, and increase in myonuclei number per muscle fibre from *Mtn*^{-/-}/*Erry*^{Tg/+} mice compared to other genotypic groups. One possible explanation for this finding is by taking into account the concomitant increase in the number of nuclei in the myofibre. Here, the relationship is opposite to satellite cell fibre number. We postulate that the absence of *Myostatin* promotes myoblast fusion at the expense of satellite cell. Furthermore, that overexpression of *Erry* exacerbates this relationship. We provide evidence that the reduction in satellite cells number in myofibres of *Mtn*^{-/-}/*Erry*^{Tg/+} mice does not affect these

cells proliferation and differentiation. By way of an explanation, *Erry* overexpression might reduce satellite cells migration on the fibre, consequently reduces the number of clusters per myofibre. However, when these cells migrate to their destination, they divide into a similar number of daughter cells.

The number of myonuclei per myofibres can indicate satellite cells recruitment and activity (Amthor et al., 2009). A number of studies have established that there is a good correlation between number of nuclei and muscle fibre size (Allen et al., 1999, Bruusgaard et al., 2003, Roy et al., 1999). In the line with this investigation, it has been demonstrated that muscle fibre hypertrophy is a concomitant with an increase in the number of myonuclei and a stable myonuclear domain (Hall and Ralston, 1989, Edgerton and Roy, 1991, Allen et al., 1999). Additionally, accretion of myonuclei is a prerequisite for maintaining specific force during hypertrophy and mitochondrial protein systems have been suggested to play a role in defining myonuclear domain size in rodents (Liu et al., 2009). It was well established that fibre nuclei are not positioned randomly, but are more or less regularly spaced out in myofibres (Bruusgaard et al., 2003). Furthermore, proper nuclear positioning is probably required for normal muscle function, possibly due to irregular size and spacing of myonuclear domains (Metzger et al., 2012), and myonuclear disorganization is observed both in ageing skeletal muscle and in models of muscular dystrophies (Bruusgaard et al., 2006, Meinke et al., 2014). Myonuclei in *Mtn*^{-/-} and *Mtn*^{-/-}/*Erry*^{Tg/+} muscles were more disorganized than those in WT fibres (Figure 4.16, myonuclei distribution work has been done by Jo C Bruusgaard, University of Oslo, Norway). We suggest that the increased number of myonuclei and increased synthesis of mitochondria in the *Mtn*^{-/-}/*Erry*^{Tg/+} mice might compensate for the observed disorganized myonuclei, restoring specific force and ultrastructure, and maintain an appropriate level of transcriptional for protein synthesis to accommodate the increased cytoplasmic volume.

In summary, our work challenges the dogma of an inverse relationship between muscle fibre size and oxidative capacity. This achieved by maintaining the increase in muscle fibre size exhibited my *Myostatin* deletion as we showed previously, increased oxidative capacity, promote muscle vasculature, and normalised energy, metabolic and oxidative profiles at transcriptional levels. Moreover, our observations contradict the notion that slow oxidative myofibres have to have a high number of muscle resident stem cells (Satellite cells). It

remains to be determined whether the depletion in satellite cells would affect skeletal muscle regeneration capacity.

Chapter 5; Results

**Superimposition of *Erry* onto *Myostatin* null
background muscles accelerates regeneration
capacity**

5.1. Introduction

Skeletal muscles possess a high regenerative potential underpinned by the resident quiescent muscle progenitors cells known as satellite cells (SCs) (MAURO, 1961, Scharner and Zammit, 2011). The satellite cells reside between the basal lamina and sarcolemma of muscle fibre as a dormant myoblast, but they are activated in response to physiological stimuli for instance exercise, and pathological conditions such as injury and degenerative diseases (Gayraud-Morel et al., 2009). Subsequently, SCs enter the cell cycle and generate a committed population of muscle precursors that proliferate, differentiate and then either fuse with existing myofibres, repairing damaged muscle fibres, or fuse with each other to form new myofibres (Charge and Rudnicki, 2004, Gayraud-Morel et al., 2009). In parallel, a subset of SCs does not differentiate, but instead re-enter quiescence, thereby replenishing the stem cell pool (Zammit et al., 2004, Collins et al., 2005).

Muscle regeneration recapitulates many aspects of prenatal development, and it is an important homeostatic process of adult skeletal muscle. A number of chemicals have been utilised in order to investigate skeletal muscle degeneration/regeneration (Tajbakhsh and Cossu, 1997, Charge and Rudnicki, 2004). One of the most frequently used and reproducible method to induce muscle regeneration is based on cardiotoxin (CTX) injection (d'Albis et al., 1988). CTX has been described as a peptide that is able to interact with membrane's proteins, acts as protein kinase C-specific inhibitor, and increases cytosolic calcium, thereby causes cell damages (Charge and Rudnicki, 2004, Pelosi et al., 2007, Wang et al., 1997, Raynor et al., 1991). Moreover, it has been documented that this cytotoxic drug is a snake venom fraction that induces muscle injury in a way similar to those observed in disease cases such as inflammatory myopathies (IMs) and muscular dystrophies (MDs) (Ramadasan-Nair et al., 2014). Furthermore, previous work has shown that CTX induces degeneration in the muscle fibres, but do not affect blood vessels, muscle innervation, ECM content and muscle resident stem cells (SCs) (Shi and Garry, 2006). Alternatively, skeletal muscle degeneration/regeneration can be investigate utilising other techniques, such as muscle crushing (Jager et al., 2014, Chatterjee et al., 2015), or the administration of different chemicals, such as barium chloride (Cornelison et al., 2004).

Skeletal muscle degeneration/regeneration following CTX injection occurs in five interrelated and time-dependent phases. Firstly, trauma to the muscle cause degeneration

of the myofibres, loss of sarcolemma, contractile materials, and cellular organelles dissolution (Prisk and Huard, 2003). Necrotic fibres appear enlarged with altered internal architectures and presence of internal nuclei (Matsuda et al., 1995). Releasing of free radical species and proteases from ruptured myofibres and damaged blood vessels leads to the necrosis in the surrounding tissues thereby accelerate inflammatory response as the second phase of muscle regeneration (Mann et al., 2011, Grounds, 1987). The inflammatory response is a critical step that controls homeostasis and regeneration of the injured skeletal muscle (Teixeira et al., 2003). During the first 24 hours following muscle injury, neutrophil invades the site of muscle damage, and secretes chemicals that stimulate other cell populations, namely, monocytes which rapidly differentiate into a pro-inflammatory macrophage (M1) when arrive at the damaged area (Tidball, 2005). Macrophages promptly increase in number within 24 hours after injury, and act to remove the tissue debris (St Pierre and Tidball, 1994). Previous work has reported that macrophages sequentially change their phenotypes as a response to the alterations in the surrounding microenvironment (Stout et al., 2005). Thus, as the degeneration process ongoing due to the effects of pro-inflammatory cytokines, prostanoids and collagenases are secreted from M1, break up the surrounding tissue and stimulate it to produce cytokines, hence switch M1 to the anti-inflammatory macrophages (M2) (Villalta et al., 2011). Macrophages change their phenotypes within 1-3 days after injury, and this phenotype switch from inflammatory to anti-inflammatory macrophages occurs after phagocytosis of both apoptotic and necrotic myofibres (Serhan and Savill, 2005). The M2 population is subdivided into three cohorts, M2a that associated with chronic inflammation in particular during parasitic infection, M2b which with M2a exerts immunoregulatory functions, and thirdly M2c that related to the suppression of immune responses and stimulate tissue repair (Stout and Suttles, 2004, Mantovani et al., 2004).

The anti-inflammatory macrophages and satellite cells population begin to dominant after day 3 of muscle injury to start the third stage. Indeed, satellite cells are initially activated about 24 hours following injury, once activated they either maintain *MyoD* expression and downregulate *Pax7*, thus commit to proliferation and differentiation. Alternatively, SCs they downregulate *MyoD* and sustain *Pax7* positive quiescent satellite cells pool (Relaix and Zammit, 2012).

The fourth stage of degeneration/regeneration cycle is characterised by remodelling connective tissue and angiogenesis. TGF- β is a key factor to induce fibrosis formation after skeletal muscle injury, a process that seems initially beneficial as it provides strength and protects the injured area. However, overproduction of collagens within the injured area leads to lose muscle function due to scar formation (Li et al., 2004).

Finally, the rescuing of myofibre functional performance and contractile apparatus, complete the reparative process (Pelosi et al., 2007). Moreover, previous work has illustrated that the regenerated muscles become effectively innervated within two weeks, as newly formed neuromuscular junctions (NMJs) between the surviving axons and the regenerated myofibres can be identified (Mozdziak et al., 2001) (Figure 5.1).

Work carried out in the previous chapters demonstrated that muscle-specific overexpression of *Erry* onto *Myostatin* null background led to a decrease in satellite cell number. We infer from this, that all the changes in muscle resulting from the introducing of *Erry* in the *Mtn*^{-/-} muscles were beneficial except for a lower number of satellite cells. Thus, in this section we want to determine the consequences of the reduction in SCs number on the ability of skeletal muscle to regenerate.

A number of studies have demonstrated that the genetic manipulations which induce muscle oxidative properties accelerate muscle regeneration capacity (Li et al., 2007b). We hypothesised that the increased oxidative capacity and microvascular network following superimposition of *Erry* in the *Mtn*^{-/-} background muscles might enhance the regeneration capacity of these muscles. To test this hypothesis, we induced injury of the TA muscles from male (WT, *Mtn*^{-/-} and *Mtn*^{-/-}/*Erry*^{Tg/+}) mice at 12 weeks old age using cardiotoxin (CTX) (*Naja mossambica mossambica*) and assessed the progression of regeneration at three crucial time points; day three (D3) as the process of debris clearance is on-going and regeneration of fibres begins, day six (D6) when a robust fibre regeneration can be quantified, and day fourteen (D14) when debris clearance has been completed.

Observations of this chapter show advance clearance process of necrotic fibres in TA muscles from *Mtn*^{-/-}/*Erry*^{Tg/+} mice than WT and *Mtn*^{-/-} counterpart muscles at day 3 and day 6 after CTX treatment. Secondly, at both day 3 and day 6, macrophages density was the highest in the *Mtn*^{-/-}/*Erry*^{Tg/+} compared to either *Mtn*^{-/-} or WT muscles. Thirdly, TA muscles from *Mtn*^{-/-}/*Erry*^{Tg/+} mice show a high number of committed cells than the other two

genotypic groups at both time points (day 3 and day 6). Furthermore, there was a greater degree of regeneration (number and size of newly formed eMHC⁺ fibres) in *Mtn*^{-/-}/*Erry*^{Tg/+} compared to either *Mtn*^{-/-} or WT mice after six days of CXT injection. In addition, we show a lower amount of cell death in the regenerating areas of *Mtn*^{-/-}/*Erry*^{Tg/+} muscles than the other two cohorts. Finally, we provided evidence that there was a reduction in the density of fibres expressing eMHC at day 14. Moreover, newly regenerated fibre in the *Mtn*^{-/-}/*Erry*^{Tg/+} muscles showed no deficient in their size after 14 days of CTX injection.

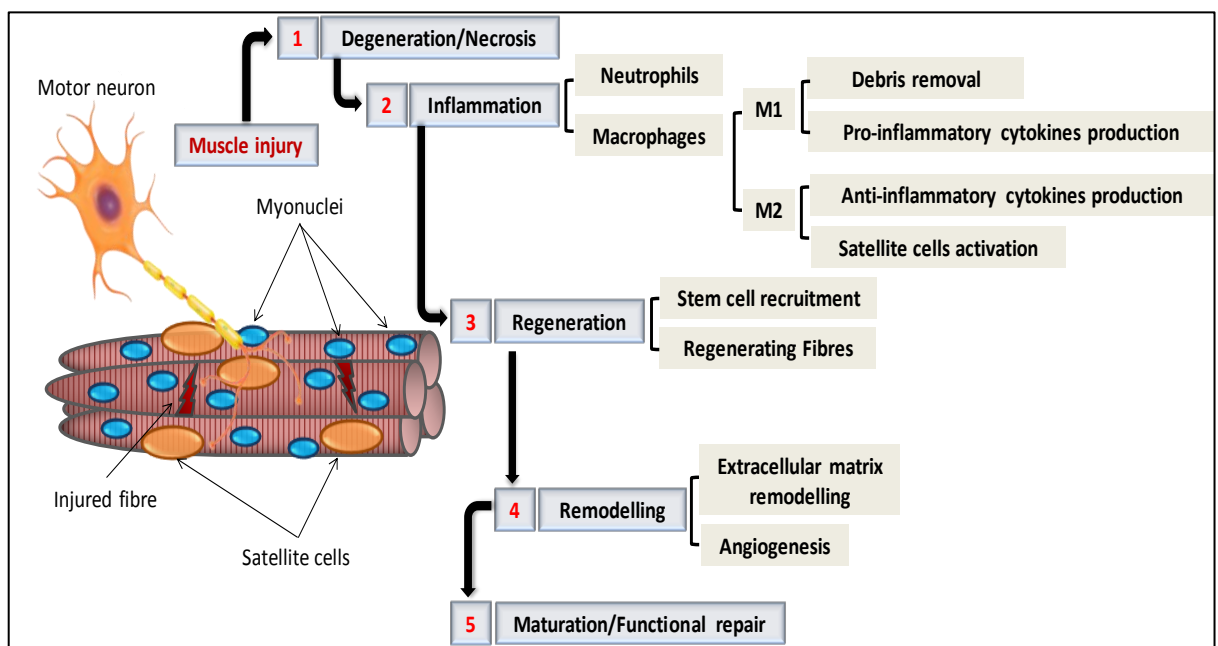


Figure 5.1. Schematic model of muscle degeneration/regeneration cycle

Five phases of muscle degeneration/regeneration cycle after injury. Muscle fibre necrosis activates muscle inflammation to remove necrotic cellular debris. Inflammation is followed by a regeneration phase that driving by satellite cells to replace damaged fibres. Fourth phase characterized by the remodeling of ECM and angiogenesis. The cycle completed by the reinnervation of newly formed fibres, adapted from (Musaro, 2014).

5.2. Assessment of skeletal muscles degeneration after 3 days of cardiotoxin injection

The injury model of this study was obtained by injecting 30 μ l of 50 μ M of cardiotoxin (CTX) in the tibialis anterior (TA) muscles from WT, *Mtn*^{-/-} and *Mtn*^{-/-}/*Erry*^{Tg/+} mice. The injected animals were allowed to convalesce for at least three days after CTX treatment, and the injured muscles were collected at day 3, day 6 and day 14 following the injection.

To determine skeletal muscle injury level, Hematoxylin and Eosin stain (H and E) was performed on 10 μ m thickness sections from the mid-belly of collected TA muscles (n=5) of the three mentioned genotypic groups (Figure 5.2A-C). We found that all muscles have an adequate damaged level that enables an appropriate assessment of degeneration/regeneration process.

Next we examined whether overexpression of *Erry* in the *Mtn*^{-/-} background muscles would affect the severity of CTX damage after three days of injury. Thus, we analysed acid phosphatase (a marker for lysosomal activity) stained TA muscle sections (n=5) from the same three animal cohorts.

In order to measure muscle damage levels, a value of 0 - 3 was set to damaged TA muscle sections for overall intensity of acid phosphatase staining.

Following this scheme of score, we found that the intensity of acid phosphatase was the highest in TA muscle sections from *Mtn*^{-/-} mice (2.7 ± 0.14), and the lowest in *Mtn*^{-/-}/*Erry*^{Tg/+} muscles (2 ± 0.57), with WT in between (2.2 ± 0.11) (Figure 3.3 A and B).

These data show that overexpression of *Erry* in the *Mtn*^{-/-} background reduced damage severity in the TA muscles that had received CTX injection.

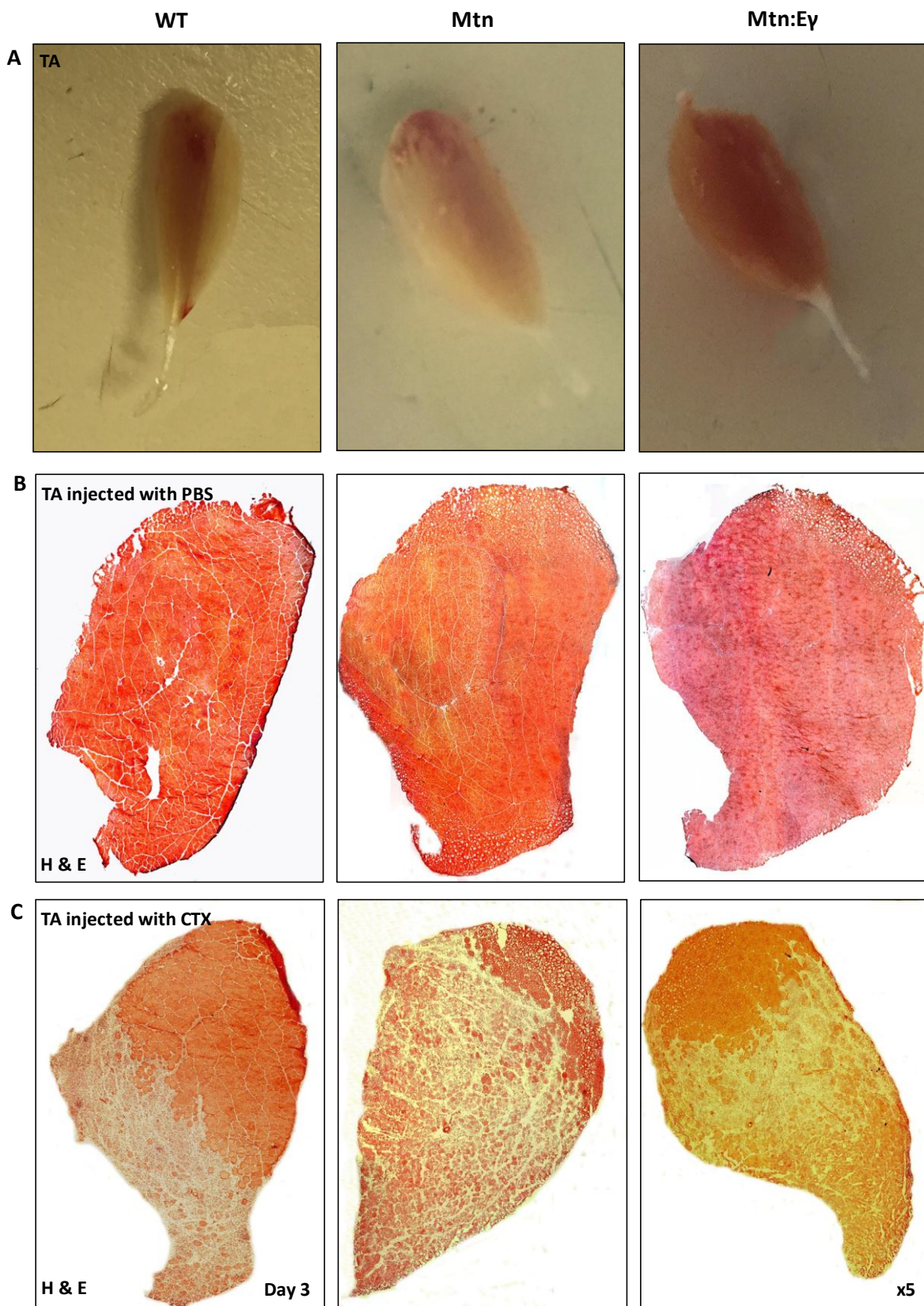


Figure 5.2. Intramuscular administration of cardiotoxin induces different levels of injury in TA muscles from WT, *Mtn* and *Mtn:Ey* mice

(A) Harvested TA muscles after 3 days of CTX administration.

(B) Representative images for Hematoxylin and Eosin staining on the TA muscles were injected with 30 μ l of PBS.

(C) Representative images for Hematoxylin and Eosin staining on the TA muscles were injected with 30 μ l of CTX, after 3 days.

($n = 5$) male twelve-week old mice per group.

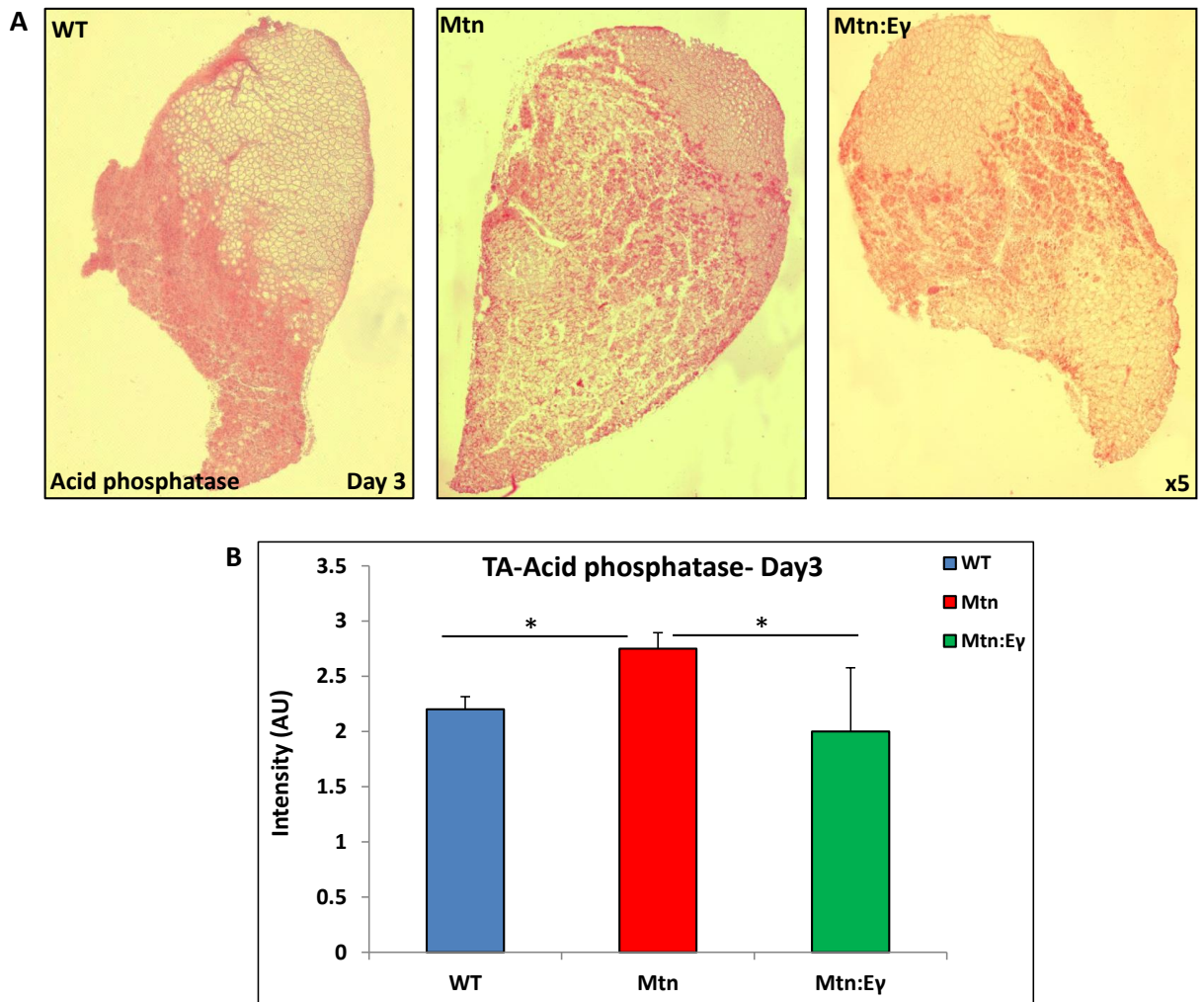


Figure 5.3. Intramuscular administration of cardiotoxin induces different levels of degeneration in TA muscles from WT, *Mtn* and *Mtn:Ey* mice

(A) Representative images for acid phosphatase staining in the damaged TA muscles from WT, *Mtn* and *Mtn:Ey* mice after 3 days of receiving IM 30 μ L of cardiotoxin .

(B) Quantification of acid phosphatase intensity in the injured areas of TA muscles at day 3 post-injury.

($n = 5$) male twelve-week old mice per group; One-way ANOVA followed by Bonferroni's multiple comparison tests, $*=p<0.05$.

5.3. Muscle-specific overexpression of *Erry* in the *Mtn*^{-/-} background attenuates necrosis induced by cardiotoxin treatment at day 3 post-injury

Previous work has shown that CTX injection induces skeletal muscle necrosis that is mainly triggered by an overload of calcium in the cytoplasm (Langone et al., 2014). At day 3 post-injection, the damaged muscle fibres became infiltrated with circulating IgG molecules, fibres that identified as necrotic fibres, which characterized by the present of internal nuclei, and altered architectures (Matsuda et al., 1995). As removing of necrotic myofibres is required to carry out the regeneration process, so counting the number and measuring the size of these fibres were performed to assess the progression of muscle degeneration/regeneration cycle.

We investigated this by staining damaged TA muscle sections (n=5) from WT, *Mtn*^{-/-} and *Mtn*^{-/-}/*Erry*^{Tg/+} mice for (IgG) expression in order to identify the necrotic fibres.

Counting the number of necrotic myofibres at day 3 of CTX injection showed that TA muscles from *Mtn*^{-/-} mice contain the highest number of necrotic myofibres (217.5 ± 11.2) compared to other genotypic groups (146.5 ± 25.1 and 194 ± 5.1) for WT and *Mtn*^{-/-}/*Erry*^{Tg/+} respectively (Figure 5.4 A and B).

Measurement of necrotic myofibres area found that the CSA of these fibres was the largest in *Mtn*^{-/-} muscles, and the smallest in TA muscles from WT mice, with CSA of necrotic fibres of *Mtn*^{-/-}/*Erry*^{Tg/+} muscles in between (Figure 5.4 A and C).

Together, these data suggest that the clearance process of necrotic fibres was the slowest in muscles from *Mtn*^{-/-} mice after 3 days of CTX treatment. However, muscle-specific expression of *Erry* in the *Mtn*^{-/-} background enhanced the necrotic fibres removal that evidenced by fewer number of these fibres with significantly smaller size.

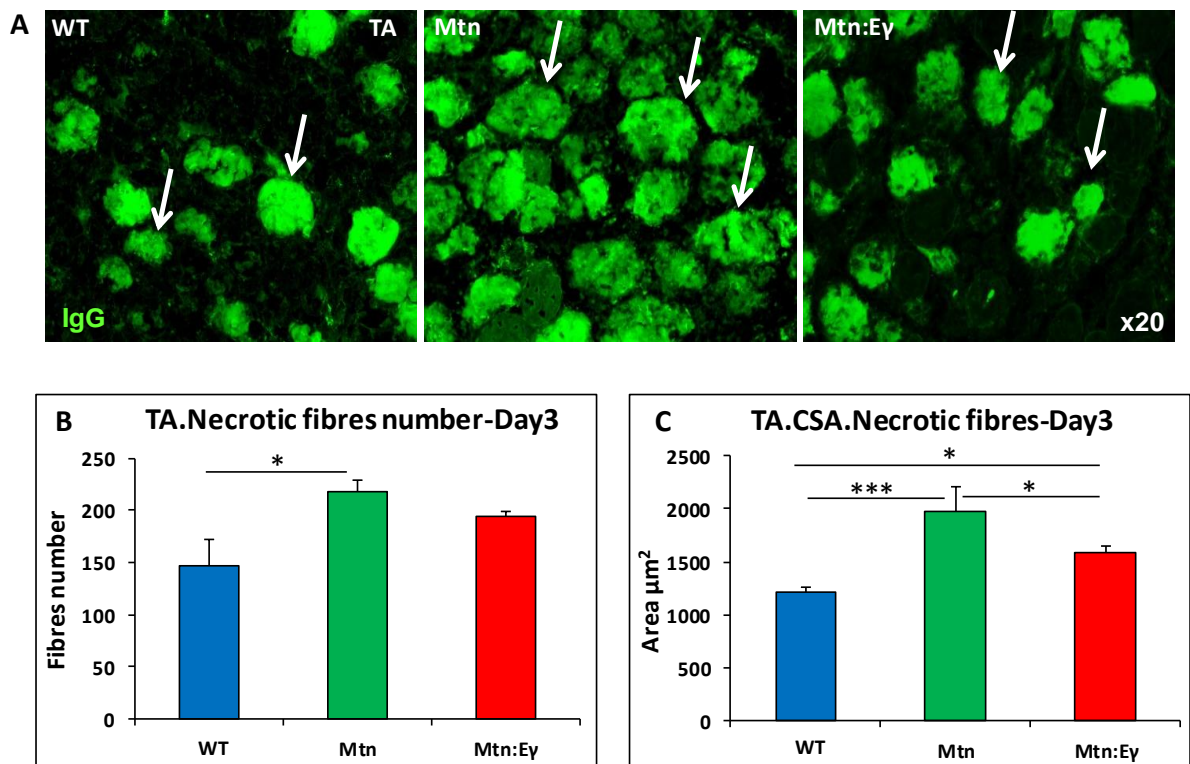


Figure 5.4. Skeletal muscle regeneration is accelerated by the expression of *Erry* in *Myostatin* null mice through enhanced clearing of necrotic fibres in response to cardiotoxin injury

(A) Muscle necrotic fibres (white arrows) visualized by IgG staining on damaged TA muscles of WT, *Mtn* and *Mtn:Ey* mice at day 3 after CTX injection.

(B) Quantification of dying fibre number after 3 days of CTX injection.

(C) Measurement of dying fibre size after 3 days of CTX injection.

($n = 5$) male twelve-week old mice per group; One-way ANOVA followed by Bonferroni's multiple comparison tests, $*=p<0.05$ and $***= p<0.001$.

5.4. Lower levels of cell death in injured TA muscles of *Mtn*^{-/-}/*Errγ*^{Tg/+} mice after three days of cardiotoxin treatment

Previous work has reported that cell death is one of the main factors that negatively impact satellite cells cycle, thereby delay formation of new myofibres during muscle regeneration (Castets et al., 2011). Moreover, it has been shown that phagocytosis of both apoptotic and necrotic myofibres is essential for macrophage to switch from inflammatory to anti-inflammatory phenotype (Serhan and Savill, 2005).

Since CTX treatment is well known to induce skeletal muscle cells death (Ramadasan-Nair et al., 2014). Thus, to further characterize the potential of *Errγ* overexpression in the *Mtn*^{-/-} background muscles in clearing process of debris in damaged areas following CTX treatment, we expanded our investigation to determine its effect on the amount of cell death.

To assess this, immunostaining of Cleaved caspase-3 (marker of apoptotic cells) was carried out on damaged TA muscle sections (n=5) from WT, *Mtn*^{-/-} and *Mtn*^{-/-}/*Errγ*^{Tg/+} mice at day 3 post CTX injection.

Counting the number of apoptotic cells per damaged areas of TA muscles showed no significant difference in these cells number between muscles of the three genotypic groups (Figure 5.5A and B).

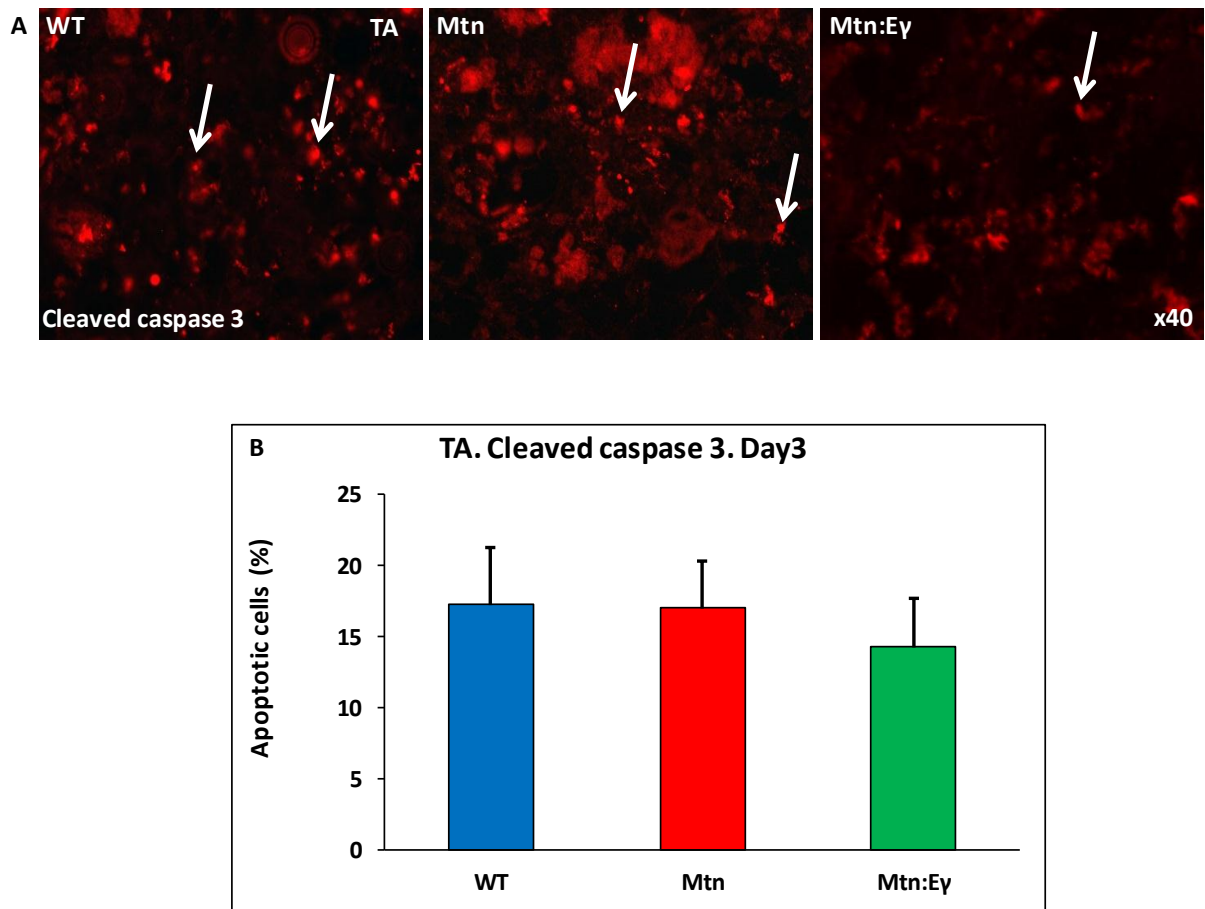


Figure 5.5. Skeletal muscle regeneration is accelerated by the expression of *Eryr* in *Myostatin* null mice through reduced amount of cell death

(A) Representative images of damaged TA muscle sections of WT, *Mtn* and *Mtn:Ey* mice immunostained for Cleaved caspase 3 at day 3 post-injury as a marker of apoptosis (white arrows).

(B) Quantification of apoptotic fibres density after three days of CTX injection.

($n = 5$) male twelve-week old mice per group; One-way ANOVA followed by Bonferroni's multiple comparison tests.

5.5. Overexpression of *Erry* promotes macrophages accumulation in damaged muscle

Macrophages role in skeletal muscle regeneration has been known (McLennan, 1996, St Pierre and Tidball, 1994), and several studies have shown that they actually contribute in clearing of damaged tissues, apoptotic and necrotic cells, thereby participate in regeneration and repairing processes (Novak et al., 2011, Arnold et al., 2007). Moreover, a number of researchers have observed a clear retardation of skeletal muscle regeneration indicating by a delay in the formation of new myofibres due to a decrease in monocyte/macrophages entry into injured areas (Shireman et al., 2007).

Here we examined whether *Myostatin* deletion would affect the entry of macrophages into the injured sites of TA muscle, and sought to determine the consequences of *Erry* overexpression in the *Mtn*^{-/-} background on macrophages infiltration into the damaged areas. To do so, immunostaining for F4.80 (macrophage marker) was performed on injured TA muscles (n=5) from WT, *Mtn*^{-/-} and *Mtn*^{-/-}/*Erry*^{Tg/+} mice at day 3 post-injection.

We found that the density of macrophages in damaged TA muscles of *Mtn*^{-/-}/*Erry*^{Tg/+} mice was the highest (7127 ± 93.5) compared to either counterpart muscles from *Mtn*^{-/-} (5289.5 ± 64.3) or WT (3263.7 ± 44.6) mice. Of particular note, macrophage density was significantly higher in injured areas of TA muscles from *Mtn*^{-/-} compared to WT mice (Figure 5.6A and B).

These data suggest that overexpression of *Erry* in the *Mtn*^{-/-} background was sufficient to promote macrophage infiltration into the damaged areas of TA muscle.

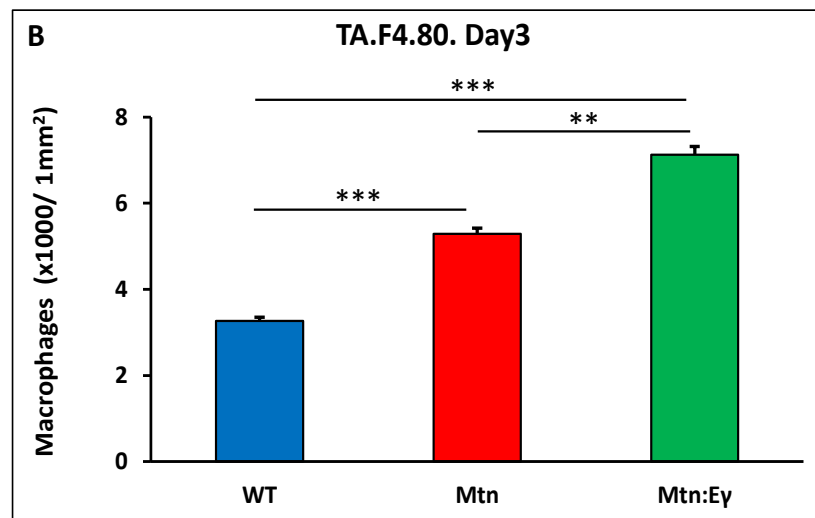
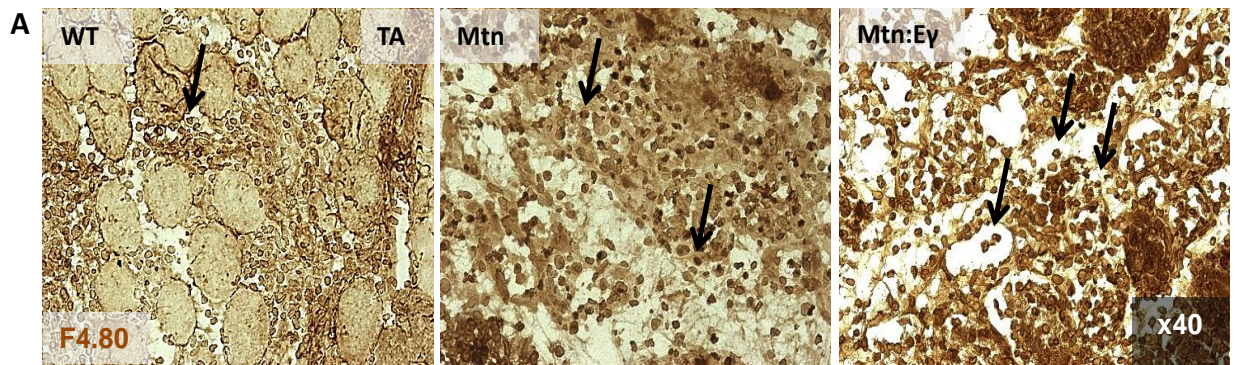


Figure 5.6. Skeletal muscle regeneration is accelerated by the expression of *Eryr* in *Myostatin* null mice through promoted macrophages activity in response to cardiotoxin injury

(A) Representative images of macrophage infiltration in the TA muscle sections of WT, *Mtn* and *Mtn:Ey* mice at day 3 post-injury using an F4.80 antibody (black arrows).

(B) Quantification of macrophage density per 1 mm² of damaged TA muscles.

(*n* = 5) male twelve-week old mice per group; One-way ANOVA followed by Bonferroni's multiple comparison tests, **=*p*<0.01 and ***=*p*<0.001.

5.6. High number of committed muscle cells in the damaged TA muscles from *Mtn*^{-/-}/*Erry*^{Tg/+} mice at day 3 post-injury

Following muscle injury, satellite cells activate and either downregulate *MyoD* and maintain a pool of quiescent *Pax7*⁺ satellite cells, or maintain *MyoD* expression but downregulate *Pax7* and activate *myogenin*, thereby committing to differentiate (Relaix and Zammit, 2012).

In this section, we examined whether genetic alteration of *Myostatin*, and overexpression of *Erry* in the *Myostatin* null muscles affected damaged TA muscle capacity to generate committing cells, hence affect muscle regeneration pace.

To that end, damaged TA muscles (n=5) from WT, *Mtn*^{-/-} and *Mtn*^{-/-}/*Erry*^{Tg/+} mice at day 3 post-injection were immunostained for Pax7 and MyoD antibodies. Satellite cells were categorised according to the expression of myogenic markers into uncommitted muscle cells (quiescent) (*Pax7*⁺/*MyoD*⁻), precursor muscle cells (*Pax7*⁺ and *MyoD*⁺), and committed cells (*Pax7*⁻/*MyoD*⁺).

We found that TA muscles from *Mtn*^{-/-}/*Erry*^{Tg/+} mice contain the highest percentage of committed muscle cells (18 ± 1.4) after three days of CTX injection, and *Mtn*^{-/-} muscles have the lowest percentage (4 ± 0.7), with TA muscles from WT mice in between (8.5 ± 0.8). Of particular note, there was no significant difference in a number of quiescent, and proliferated cells between the three muscle cohorts (Figure 5.7A and B).

Taken together, these observations suggest that muscle-specific expression of *Erry* in the *Mtn*^{-/-} background muscle promoted muscle stem cells proliferation and differentiation at day 3 post-injury indicated by high number of committed muscle cells.

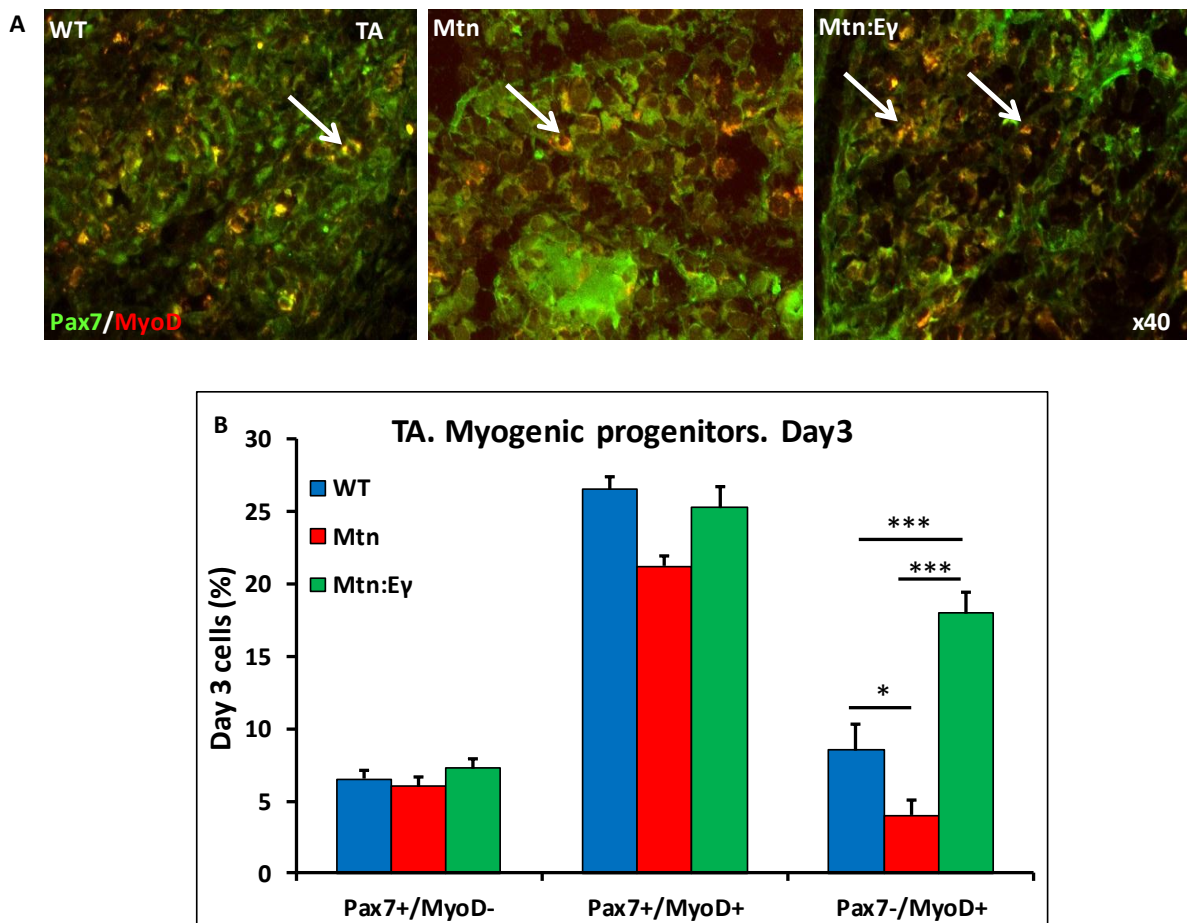


Figure 5.7. Skeletal muscle regeneration is accelerated by the expression of *Er* in *Myostatin* null mice through enhanced myoblast response to cardiotoxin injection

(A) Myogenic progenitors in TA muscles of WT, *Mtn* and *Mtn:Er* mice at day 3 post injection with CTX. Pax7 detection in green, MyoD expressing cells in red (white arrows).

(B) Quantification of uncommitted muscle cells (Pax7⁺/MyoD⁻), precursor muscle cells (Pax7⁺/MyoD⁺), and committed muscle cells (Pax7⁻/MyoD⁺) at day 3 post-injury.

(*n* = 5) male twelve-week old mice per group; One-way ANOVA followed by Bonferroni's multiple comparison tests, *=*p*<0.05 and ***=*p*<0.001.

5.7. Less severity of TA muscle damage at day 6 compared to day 3 post-injury

Six days after CTX injection, robust fibres regeneration should be evidenced. In order to determine the damage severity at day 6 post-injury, acid phosphatase stain was applied on the injured TA muscle sections (n=5) of the three animal cohorts of this study.

To quantify the level of staining, a scoring system was used as in Figure 5.2, with a score between 0 - 3 assigned. This grading showed a reduction in the staining intensity on the TA muscle sections from the three genotypic groups at day 6 compared to day 3 post-injection with CTX. Of particular note, the same pattern of acid phosphates intensity level at day 3 post-injury was identified at this time point (day 6). TA muscles from *Mtn*^{-/-} mice showed the highest intensity level (2.4 ± 0.12) compared to both WT and *Mtn*^{-/-}/*Erry*^{Tg/+} muscles (1.7 ± 0.08 and 1.8 ± 0.12) respectively, with no significant difference in stain intensity between WT and *Mtn*^{-/-}/*Erry*^{Tg/+} muscles (Figure 5.8A and B).

These data show that the damage level in TA muscles was reduced within 6 days post-injury. Importantly, muscles of *Mtn*^{-/-}/*Erry*^{Tg/+} mice show significant low level of muscle damage compared to *Mtn*^{-/-} muscles.

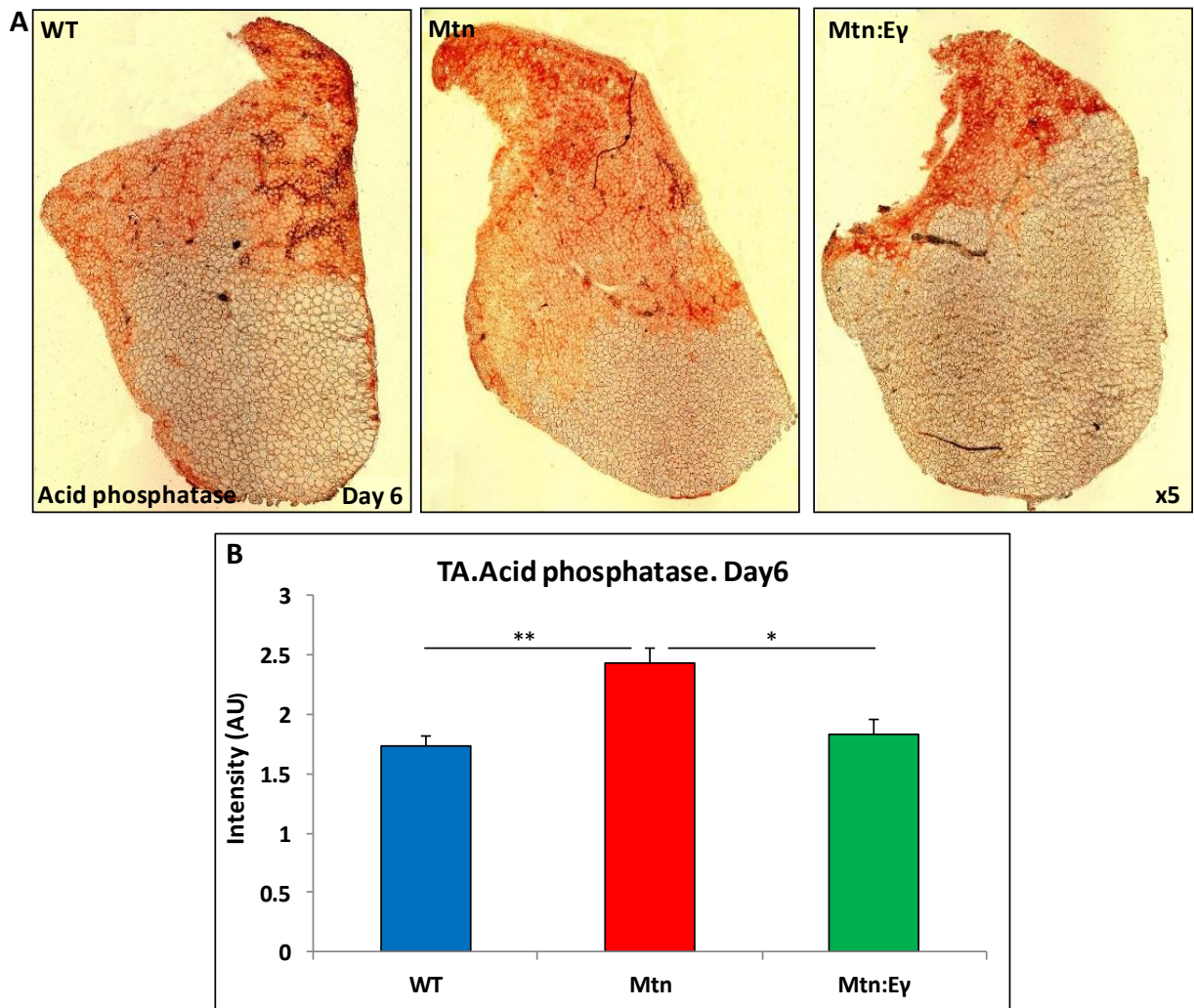


Figure 5.8. Intramuscular administration of cardiotoxin induces different levels of degeneration in TA muscles from WT, *Mtn* and *Mtn:Ey* mice at day 6

(A) Representative images for Acid phosphatase staining in the damaged TA muscles after 6 days of cardiotoxin injection.

(B) Quantification of acid phosphatase intensity in the injured areas of TA muscles at day 6 post-injury.

($n = 5$) male twelve-week old mice per group; One-way ANOVA followed by Bonferroni's multiple comparison tests, $*=p<0.05$ and $**=p<0.05$.

5.8. Advanced removal of necrotic and dying cells in $Mtn^{-/-}/Erry^{Tg/+}$ muscle at day 6 post-injury

After six days of CTX treatment, degenerated myofibres are usually removed and replaced with regeneration fibres (Pelosi et al., 2007). To evaluate muscle degeneration level at this time point (6 days), a measurement of necrotic myofibre number and size was carried out via immunohistochemistry.

We found that the number of necrotic fibres in whole TA muscle sections from the three genotypic groups (WT, $Mtn^{-/-}$ and $Mtn^{-/-}/Erry^{Tg/+}$) of the study was reduced compared to day 3 post-injury. However, while muscle sections from $Mtn^{-/-}$ mice still showed a considerable presence of necrotic fibres (33 ± 16.1) compared to WT muscles (2 ± 1.1), we observed a significantly lower number of necrotic fibres in TA muscles from $Mtn^{-/-}/Erry^{Tg/+}$ mice (13.3 ± 3.3) (Figure 5.9A and B). Nevertheless, necrotic fibre numbers were significantly higher in $Mtn^{-/-}/Erry^{Tg/+}$ compared to WT muscles (Figure 5.9A and B).

Similar to the degeneration fibres size in damaged TA muscles after 3 days of CTX injection, CSA of necrotic fibres from $Mtn^{-/-}$ muscles was the largest compared to those in muscles from both WT and $Mtn^{-/-}/Erry^{Tg/+}$ mice after 6 days of CTX injection (Figure 5.9A and C).

Next we examined the number of apoptotic cells in the damaged areas of TA muscles following 6 days of CTX treatment. We observed that muscle sections from $Mtn^{-/-}/Erry^{Tg/+}$ mice showed much lower number of apoptotic cells (7.6 ± 0.9) compared to either WT (19.25 ± 2) or $Mtn^{-/-}$ (31 ± 3.3) muscles (Figure 5.10A and B).

Taken together, these data suggest that damaged TA muscles from all animal cohorts displayed a reduction in numbers and size of necrotic myofibres at day 6 compared to day 3 post-injury. Importantly, overexpression of *Erry* in the $Mtn^{-/-}$ background muscles markedly promoted elimination of necrotic fibres, and reduced amount of cell death.

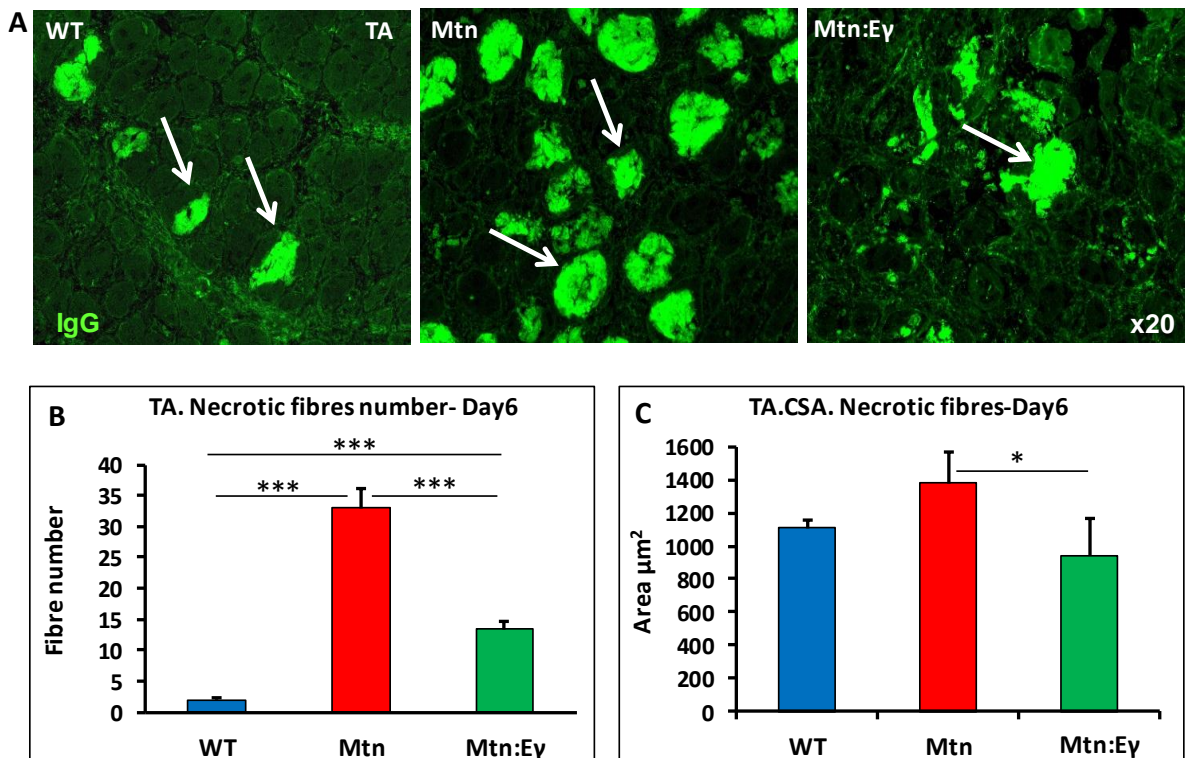


Figure 5.9. Skeletal muscle regeneration is accelerated by the expression of *Erry* in *Myostatin* null mice through enhanced clearing of necrotic fibres in response to cardiotoxin injury at day 6 post-injury

(A) Muscle necrotic fibres visualized by IgG staining on TA muscles of WT, *Mtn* and *Mtn:Erry* mice at Day 6 (white arrows).

(B) Quantification of dying fibre number at day 6 post-injury.

(C) Quantification of dying fibre size at day 6 post-injury.

($n = 5$) male twelve-week old mice per group; One-way ANOVA followed by Bonferroni's multiple comparison tests, *= $p < 0.05$ and ***= $p < 0.001$.

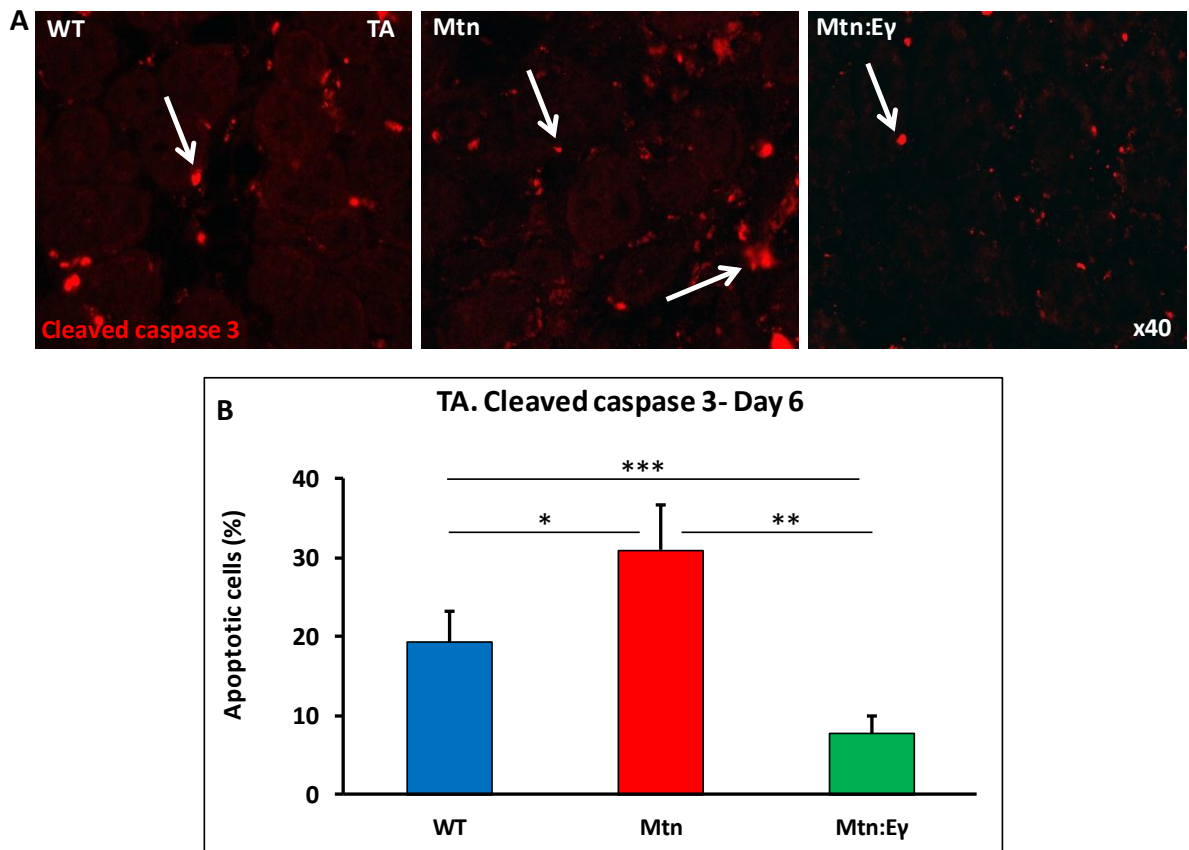


Figure 5.10. Skeletal muscle regeneration is accelerated by the expression of *Erty* in *Myostatin* null mice through reduce cell death

(A) Representative images of Cleaved caspase-3 immunostaining at day 6 post-injury as a marker of apoptosis (white arrows) in injured TA muscles of WT, *Mtn* and *Mtn:Erty* mice.

(B) Quantification of apoptotic cells density at day 6 post-injury.

($n = 5$) male twelve-week old mice per group; One-way ANOVA followed by Bonferroni's multiple comparison tests, $*=p<0.05$, $**= p<0.01$ and $***= p<0.001$.

5.9. High macrophages activity in $Mtn^{-/-}/Erry^{Tg/+}$ muscles at day 6 post-injury

We showed that damaged TA muscles from $Mtn^{-/-}/Erry^{Tg/+}$ mice displayed more advance removal of dying myofibres with a lower amount of cell death after 6 days of CTX injection. At this time point post-injury, damaged skeletal muscles would be expected to contain mostly M2 macrophages that are associated with deactivation of M1 macrophages, simultaneously induce tissue healing and repair (Chazaud et al., 2009, Serhan and Savill, 2005).

A macrophage marker (F4.80) was used to determine the rate of macrophages infiltration into the damaged TA muscles (n=5) from WT, $Mtn^{-/-}$ and $Mtn^{-/-}/Erry^{Tg/+}$ mice at day 6 post-injury.

Counting the number of macrophages in the damaged areas of TA muscles showed a reduction in these cells number in WT and $Mtn^{-/-}/Erry^{Tg/+}$ muscles, but not $Mtn^{-/-}$ compared to day 3. Interestingly, damaged areas of TA muscles from $Mtn^{-/-}/Erry^{Tg/+}$ displayed significantly high activity of macrophages (6991.5 ± 64.3) compared to either WT (2833.5 ± 53.9) or $Mtn^{-/-}$ (5872.5 ± 50.5) muscles following 6 days of CTX injection (Figure 5.11A and B). These observations imply that muscle-specific expression of *Erry* in the $Mtn^{-/-}$ background muscles promote macrophages activity at day 6 post-injury.

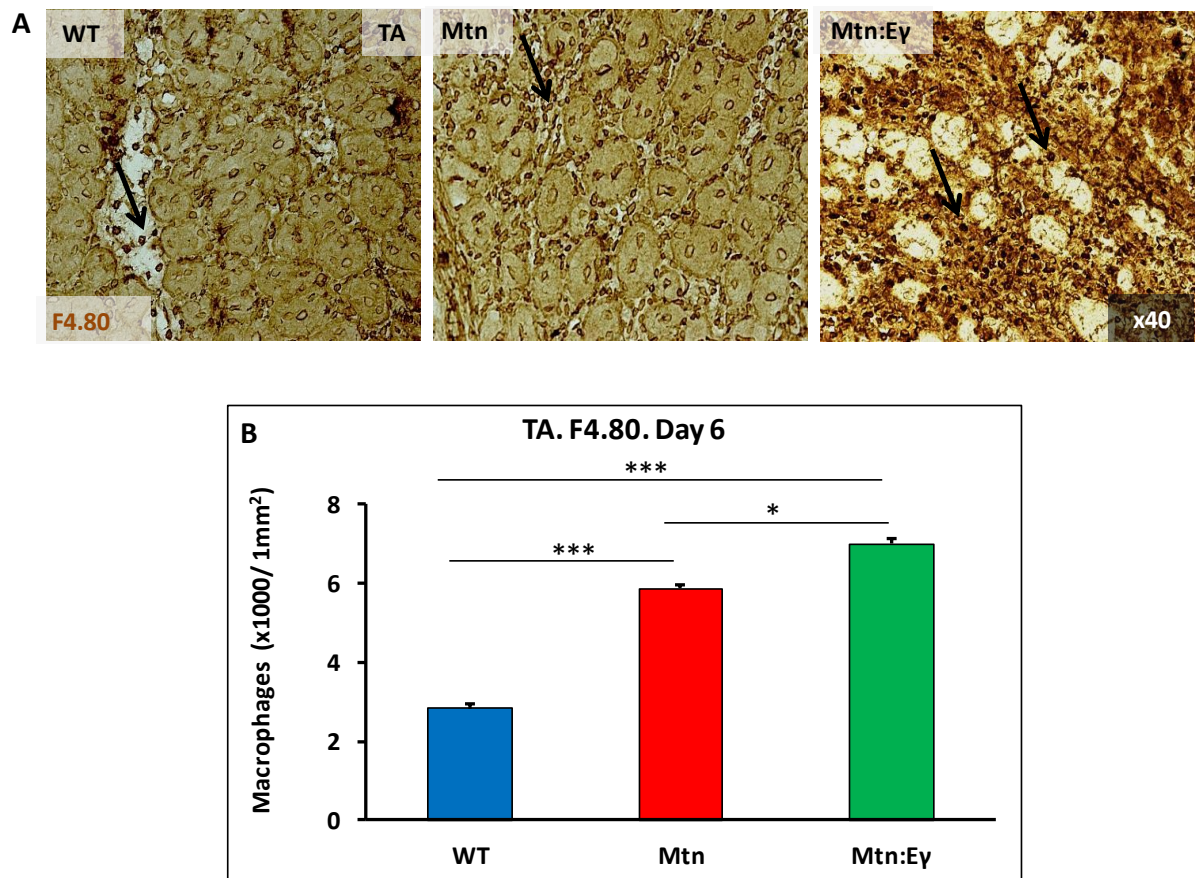


Figure 5.11. Skeletal muscle regeneration is accelerated by the expression of *Erty* in *Myostatin* null mice through promoted macrophages activity in response to cardiotoxin injury

(A) Representative images of macrophage infiltration in the TA muscles of WT, *Mtn* and *Mtn:Er* mice at day 6 using an F4.80 antibody (black arrows).

(B) Quantification of macrophage density in 1 mm² of damaged TA muscle.

(*n* = 5) male twelve-week old mice per group; One-way ANOVA followed by Bonferroni's multiple comparison tests, *=*p*<0.05 and ***= *p*<0.001.

5.10. *Erry* overexpression increases the number of committed cells at day 6 post-injury

We showed previously that muscle-specific overexpression of *Erry* in the *Mtn*^{-/-} background muscles induced the number of committed progenitor cells at day 3 post-injury of CTX.

Here we examined whether the population of the committed muscle cells would be affected by metabolic reprogramming imparted by muscle-specific *Erry* overexpression in the *Mtn*^{-/-} muscles after six days of CTX treatment.

Counting the number of uncommitted (quiescent) (Pax7⁺/MyoD⁻), precursor (Pax7⁺/MyoD⁺), and committed (Pax7⁻/MyoD⁺) muscle cells at day 6 showed a difference in the average of these cell cohorts between TA muscle sections from WT, *Mtn*^{-/-} and *Mtn*^{-/-}/*Erry*^{Tg/+} mice. Of particular note, the regenerated areas of TA muscles from *Mtn*^{-/-}/*Erry*^{Tg/+} mice showed a significantly high percentage of committed muscle cells (17.6 ± 2.1) compared to either WT (2.5 ± 1.03) or *Mtn*^{-/-} (1.1 ± 0.5) muscles (Figure 5.12A and B). Moreover, the highest percentage of precursor muscle cells was seen as well in TA muscle sections of *Mtn*^{-/-}/*Erry*^{Tg/+} mice, with no significant difference in a number of uncommitted muscle cells between any of the genotypic groups (Figure 5.12A and B).

These data show that muscle-specific expression of *Erry* in the *Mtn*^{-/-} muscles markedly elevates the number of committed progenitor cells after six days of CTX, thereby raising the possibility of enhancing regeneration rate in these muscles.

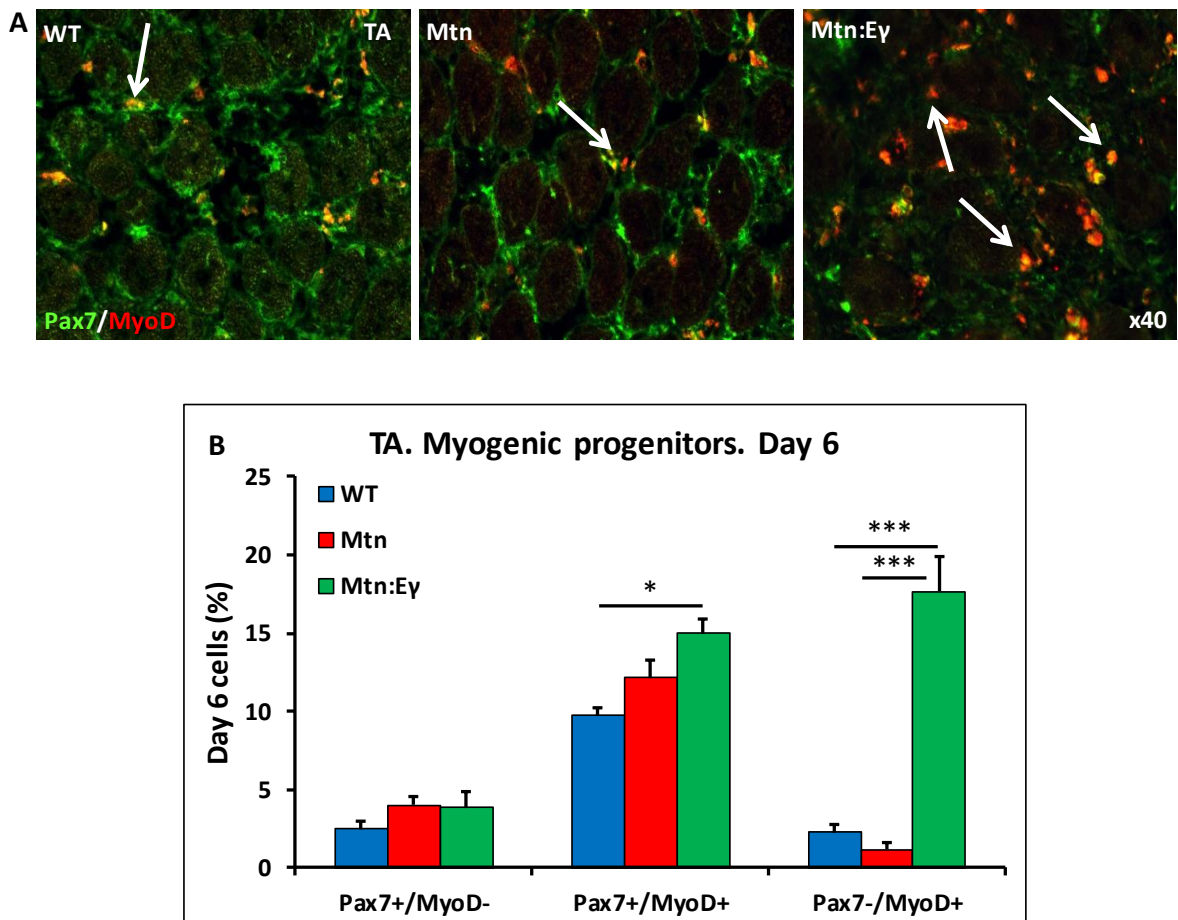


Figure 5.12. Skeletal muscle regeneration is accelerated by the expression of *Erry* in *Myostatin* null mice through enhanced myoblast population in response to cardiotoxin injection

(A) Myogenic progenitors in TA muscles of WT, *Mtn* and *Mtn:Er* mice at day 6. Pax7 detection in green, MyoD expressing cells in red (whit arrows).

(B) Quantification of uncommitted muscle cells (Pax7⁺/MyoD⁻), precursor muscle cells (Pax7⁺/MyoD⁺), and committed muscle cells (Pax7⁻/MyoD⁺) at day 6 post-injury.

(*n* = 5) male twelve-week old mice per group; One-way ANOVA followed by Bonferroni's multiple comparison tests, *=*p*<0.05 and ***=*p*<0.001.

5.11. Greater degree of regeneration in *Mtn*^{-/-}/*Erry*^{Tg/+} muscles at day 6 post-injury

Building on our observations, we examined whether besides the observed protective effect on muscle degeneration and promote oxidative metabolism, introducing of *Erry* in the *Mtn*^{-/-} background has also effect on the muscle regeneration efficiency following six days of CTX injection.

To that end, immunostaining for embryonic myosin heavy chain (MHC3) was undertaken on the damaged TA muscle sections (n=5) of WT, *Mtn*^{-/-} and *Mtn*^{-/-}/*Erry*^{Tg/+} mice at day 6 post-injury. Regenerating fibres can be identified by the presence of centrally located nuclei, not in peripheral as in mature myofibres.

Counting number and measuring the size of newly formed eMHC indicated a greater degree of regeneration in *Mtn*^{-/-}/*Erry*^{Tg/+} muscle compared to other two cohorts. More specifically, the density of eMHC fibres in regenerated areas of *Mtn*^{-/-}/*Erry*^{Tg/+} muscles was significantly higher (522 ± 35.3) than the fibre numbers in either WT (428 ± 21.90) or *Mtn*^{-/-} (455 ± 14.5) muscles at day 6 post-injury (Figure 5.13A-C).

The area of regenerated myofibres was bigger in TA muscles of *Mtn*^{-/-}/*Erry*^{Tg/+} mice than their counterpart myofibres in WT and *Mtn*^{-/-} muscles albeit, non-significant (Figure 5.13B and D).

Together, these observations highlight the beneficial role of overexpression of *Erry* on the *Mtn*^{-/-} background muscles to induce muscle regeneration capacity after six days of CTX treatment, which indicated by large number of newly formed eMHC. Thereby, challenge the notion that oxidative muscle fibres have to have a high number of satellite cells to regenerate normally.

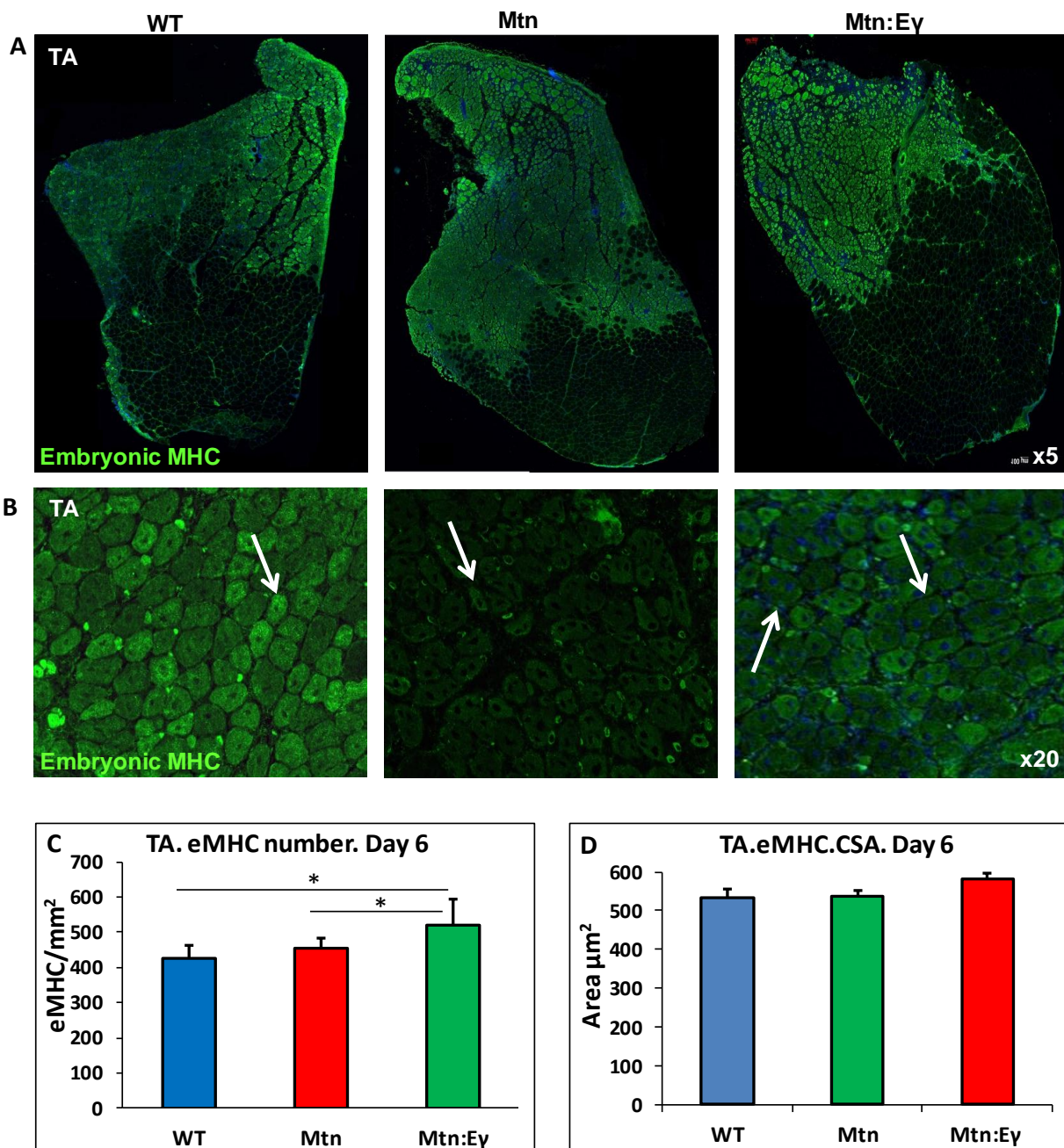


Figure 5.13. Skeletal muscle regeneration is accelerated by the expression of *Erry* in *Myostatin* null mice at day 6

(A) Expression of embryonic myosin heavy chain fibres visualized by MHC3 staining on whole TA muscles of WT, *Mtn* and *Mtn:Er* mice at Day 6 post-injury.

(B) Expression of embryonic myosin heavy chain fibres visualized by high magnification images of MHC3 staining on injured TA muscles of WT, *Mtn* and *Mtn:Er* mice at day 6 post treatment (white arrows).

(C) Quantification the number of regenerating muscle fibres at day 6 post-injury.

(D) Measurement area of regenerating muscle fibres at day 6 post-injury.

(*n* = 5) male twelve-week old mice per group; One-way ANOVA followed by Bonferroni's multiple comparison tests, *= $p < 0.05$.

5.12. Day 14 post-injury show high regeneration capacity of *Mtn*^{-/-}/*Erry*^{Tg/+} muscles

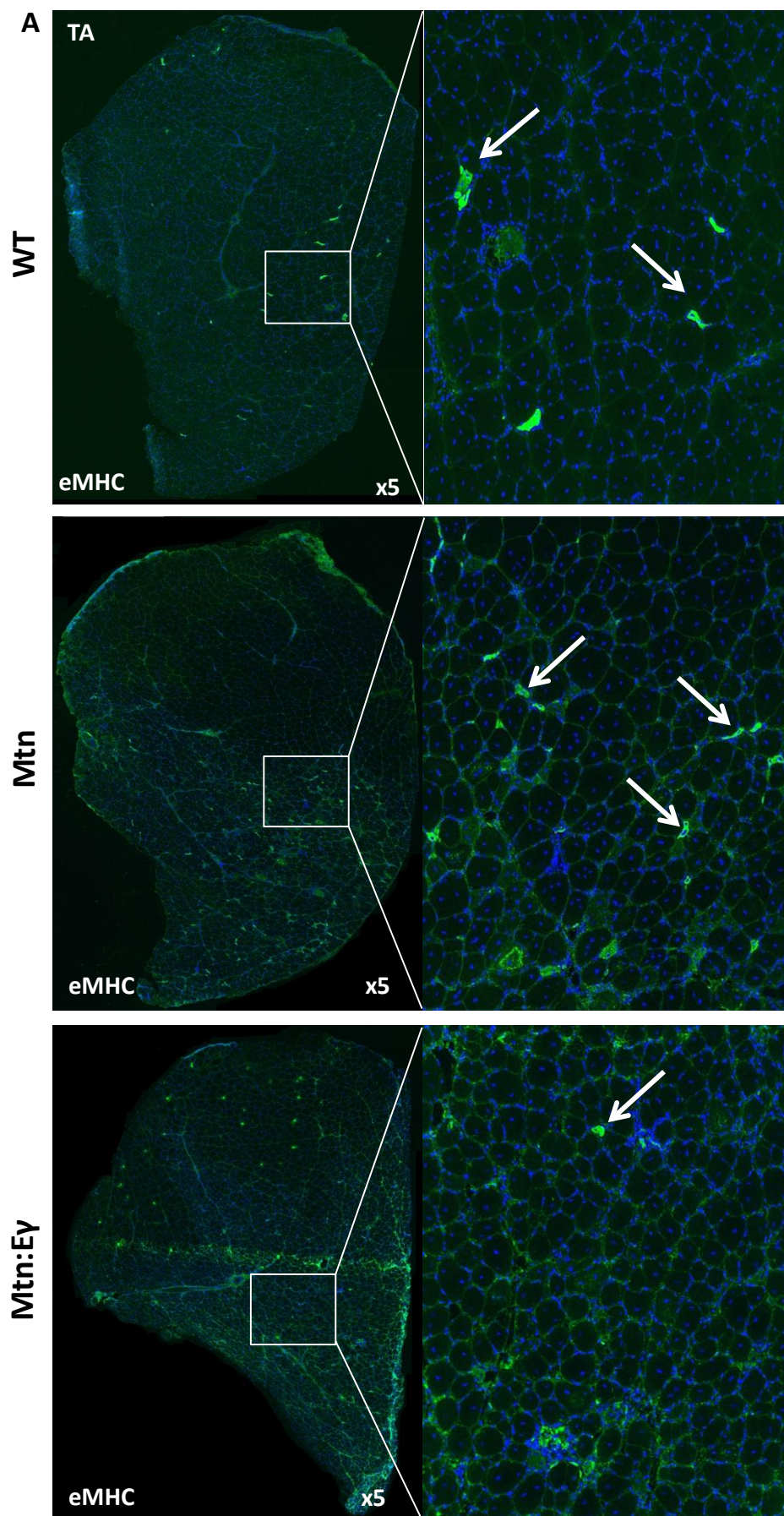
The muscles of *Mtn*^{-/-}/*Erry*^{Tg/+} have fewer satellite cells than other muscles of WT and *Mtn*^{-/-} mice, but their regeneration capacity exceeded that of both WT and *Mtn*^{-/-} muscles. Precocious muscle cells differentiation could lead to an exhaustion of cells which would ultimately attenuate myofibre size.

In order to test this notion, we examined damaged TA muscles of the three genotypic groups of present study (WT, *Mtn*^{-/-} and *Mtn*^{-/-}/*Erry*^{Tg/+}) at advanced stage of muscle regeneration process (day 14). Thus, immunostaining for embryonic myosin heavy chain (MHC3) was performed to determine density and size of the newly regenerated fibre.

Counting the number of newly formed fibres provided evidence for accelerated regeneration capacity in *Mtn*^{-/-}/*Erry*^{Tg/+} muscles indicated by significantly lower density of fibres still expressing eMHC (10.6 ± 4.09) compared to both *Mtn*^{-/-} (30.6 ± 1.3) and WT (23.6 ± 3.7) muscles (Figure 5.14 A and B).

Next we examined whether the size of newly generated fibres in *Mtn*^{-/-}/*Erry*^{Tg/+} muscles was reduced. Therefore, measurement of CSA for regenerating fibres was performed on TA muscle sections of the three cohorts. We found no difference in the size of newly regenerated fibres in the TA muscles of *Mtn*^{-/-}/*Erry*^{Tg/+} mice compared to either *Mtn*^{-/-} or WT at day 14 post-injury (Figure 5.14 A and C).

These data indicate the potential of *Erry* overexpression in the *Mtn*^{-/-} background muscles to promote regeneration capacity at day 14 post-injection with CTX.



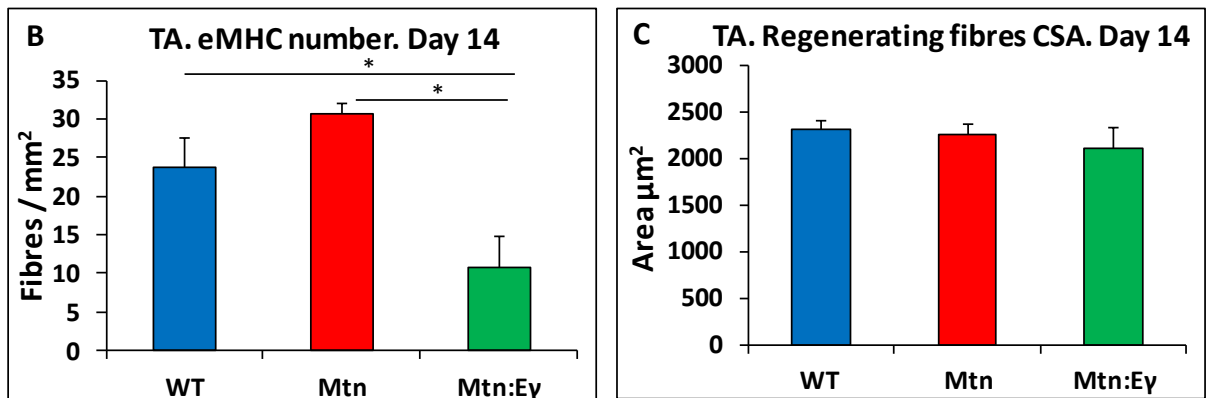


Figure 5.14. Skeletal muscle regeneration is accelerated by the expression of *Eryr* in *Myostatin* null mice through decrease density of the eMHC fibres, and generates new fibres with normal size

(A) Expression of embryonic myosin heavy chain fibres visualized by MHC3 staining on whole TA muscles and magnified areas from the same muscles of WT, *Mtn* and *Mtn:Ev* mice after 14 days of cardiotoxin injection (white arrows). DAPI stain (blue) was used to visualize myonuclei.

(B) Quantification of eMHC muscle fibres number at day 14 post-injury.

(C) Measurement of regenerating muscle fibres size at day 14 post-injury.

($n = 5$) male twelve-week old mice per group; One-way ANOVA followed by Bonferroni's multiple comparison tests, $*=p<0.05$.

5.13. Discussion

Following the observations in previous chapters, we can infer that muscle-specific superimposition of *Erry* on the *Mtn*^{-/-} background muscles was sufficient to normalize muscles histological, ultrastructural and molecular features, and clearly improved muscles oxidative capacity and vascularization, hence enhanced animals exercise capacity. However, the metabolic reprogramming imparted by this genetic manipulation was not able to restore satellite cells population that was markedly diminished due to genetic deletion of *Myostatin*. Skeletal muscle regeneration dependent on the resident muscle satellite cells SCs, that are capable of forming new fibres while simultaneously maintaining initial SCs pool through self-renew (Collins et al., 2005). Moreover, it has been implied that slow muscle fibres contain higher number of satellite cells than the fast phenotypes (Putman et al., 1999, Christov et al., 2007). We showed that overexpression of *Erry* on the *Mtn*^{-/-} muscles caused partial reversal transition of muscle fibres from fast-twitch to slow-twitch phenotypes within MHCII subsets. However, there was a significant decrease in number of satellite cells at least in EDL muscles. Numerous studies have revealed high regeneration capacity of skeletal muscles that show a high level of oxidative metabolism (Lowrie et al., 1982, Matsakas et al., 2012b). Previous work has revealed vital role of blood supply for tissue repair, as the microenvironment that is created by circulating factors is essential for proper muscle regeneration process (Conboy et al., 2005, Bencze et al., 2012).

We have demonstrated in previous chapters that genetic deletion of *Myostatin* led to compromise muscle capillary density and oxidative properties (Amthor et al., 2007, Lipina et al., 2010). However, we and others have shown that muscle-specific expression of *Erry* is sufficient to induce skeletal muscle neoangiogenesis, triggers revascularization, and promotes oxidative capacity (Rangwala et al., 2010, Matsakas et al., 2012b).

Building on these observations, we investigated the effects of muscle-specific overexpression of *Erry* on the *Mtn*^{-/-} background on skeletal muscles response to injury induced by CTX treatment. The hypothesis was that the metabolic reprogramming imparted by *Erry* introducing in a muscle lacking *Myostatin* would promote protection against muscle damage and enhance regeneration. In this *in vivo* experimental model, we showed that muscle-specific introducing of *Erry* in the *Mtn*^{-/-} muscles was efficacious to reduce damage level induced by CTX injection, enhanced removal rate of necrotic myofibres, decreased the

amount of cells death, increased the proportions of committed muscle cells at both day 3 and day 6 post-injury. Importantly, the metabolic reprogramming driven by *Erry* strongly promoted muscle capacity to generate new embryonic myosin heavy chain (eMHC) fibres in the regenerated areas at day 6 post-injury. We also provided evidence for accelerated regeneration process in the *Mtn*^{-/-}/*Erry*^{Tg/+} muscles at advance stage indicated by few number of eMHC, and normal size of newly regenerated fibres after 14 days of CTX injection. The *Mtn*^{-/-}/*Erry*^{Tg/+} muscles that were injected with CTX showed a significant reduction in their myofibre permeability compared to the counterpart damaged muscles from WT and *Mtn*^{-/-} animals indicated by a reduction in acid phosphatase intensity at day 3 and day 6 post-injury. At both time points, the same muscles showed a drop-in cells death events, decreased number of necrotic fibres, and these fibres were significantly smaller than their counterparts in WT and *Mtn*^{-/-} muscles.

A number of studies have reported that CTX injection induces skeletal muscle fibres necrosis and cells death, that are probably due to a high influx of Ca⁺ from the extracellular milieu into the muscle cytoplasm, which leads to rupture of the membrane within the myofibres (Zhao et al., 2009, Ramadasan-Nair et al., 2014). Accordingly, there is a release of acid phosphatase from the lysosome (Shu et al., 2007). Therefore, the increased acid phosphatase intensity of *Mtn*^{-/-} muscles evidences a high level of muscle degeneration that was significantly reduced by muscle-specific expression of *Erry*. Previous work has reported a disruption of muscle membrane integrity due to altered in calcium concentration that subsequently resulted in lipid peroxidation by elevating ROS production (Duncan and Jackson, 1987, Nethery et al., 2000).

Since we observed that introducing of *Erry* into *Mtn*^{-/-} muscles reduced membrane permeability induced by CTX injection, we wondered whether the protective effect of *Erry* overexpression could be attributed in some way to regulate calcium concentration.

By a way of explanation, it was documented that healthy mitochondria perform several functions and biochemical processes such as (OXPOS) pathway and calcium homeostasis (Scarpulla, 2008). Further study has revealed a vital role of *Erry* in regulating expression level of genes that encode pathways for muscle calcium handling and contractile proteins for slow muscles (Rangwala et al., 2010). Our previous data showed a number of mitochondrial

abnormalities that were accompanied with a high level of ROS production in *Mtn*^{-/-} muscles, were largely normalised by overexpression of *Erry*.

Thus, we suggest that one main mechanism by which *Erry* overexpression in the *Mtn*^{-/-} muscles limits the CTX damage, is by protecting against necrosis and apoptosis induced by calcium influx.

Following muscle fibres degeneration, the efficient inflammatory response is required for effective repair and regeneration processes. Conversely, delaying the inflammatory or pro-inflammatory response would negatively affect the rate of fibres clearance, thereby preventing generation of new tissue (Mann et al., 2011). Further, a critical role of microenvironment to promote stem cells commitment and differentiation has been reported (Carlson and Faulkner, 1989). Building on these observations, high inflammatory response, diminish tissue necrosis and fibrosis, possibly provides an environment that sustains efficient muscle regeneration.

We showed previously that hypertrophic myofibres that resulted from the genetic alteration of *Myostatin* displayed a marked decrease in a number of blood vessels that serve each muscle fibre. However, overexpression of *Erry* on the *Mtn*^{-/-} background muscles was sufficient to drive a robust angiogenesis program that restored capillary density to even more than in WT muscles (Figure 4.4). An interesting feature highlighted in this chapter was the high density of macrophages in the regenerated areas of *Mtn*^{-/-}/*Erry*^{Tg/+} muscles at both day 3 and day 6 post-injury (Figures 5.6 AND 5.11). Therefore, the central question to be addressed in this chapter is to what extent that the rich microcirculation environment established by *Erry* overexpression would promote muscle regeneration capacity following CTX treatment, even with a low population of satellite cells as we showed previously (Figures 4.12 and 4.13).

Prior to the regeneration, tissue necrotic debris needs to be cleaned, which can mainly be achieved by recruiting monocytes from the circulation that subsequently differentiate into pro-inflammatory macrophages (M1) within the tissue (Zhang et al., 2013). In support of this view, previous studies have revealed a marked reduction in muscle repair process due to depletion of monocyte from blood that gives an origin for both M1 and M2, or because of the impairment in monocyte/macrophage recruitment into the damaged areas (Arnold et al., 2007). While M1 macrophages promote phagocytosis to remove necrotic and apoptotic cells

in the damage areas, they are preventing myogenic differentiation too early in the repair process (Serhan and Savill, 2005, Rigamonti et al., 2014). Approximately 24 hours after injury, the pro-inflammatory macrophages M1 convert to macrophages M2. These anti-inflammatory macrophages derive the second phase of muscle repair by reducing environmental inflammatory signals, stimulate satellite cells, and directly support myogenesis process and myofibre growth (Prisk and Huard, 2003).

It seems that a regulated sequence of macrophage phenotypes is necessary for the effective regeneration process. Study by Bordon (Bordon, 2013) has revealed a critical role of AMPK (a master regulator of energy homeostasis) in particular AMPK α 1 subunit, in macrophages skewing from M1 to M2. Consistently, it has been reported that the ablation of AMPK α 1 causes accumulation of necrotic tissue and a deficit in the acquisition of the M2 macrophage phenotype, thereby impairing skeletal muscle regeneration (Mounier et al., 2013). Along the same line of thought, it has been shown that AMPK, which is essential for the exercise-mediated switch to aerobic myofibres, is activated by *Erry* in skeletal muscles (Jensen et al., 2007).

Thus, we believe that the high proportion of committed muscle cells in the regenerated areas of *Mtn*^{-/-}/*Erry*^{Tg/+} muscles (Figures 5.7 and 5.12), could be attributed to, firstly, high density of macrophages in these muscles that reflected high vascularization, and promoted clearing process of necrotic and apoptotic cells. And secondly, proper conversion of pro-inflammatory M1 to anti-inflammatory M2 macrophages that is in part regulated by AMPK which is upregulated following overexpression of *Erry* in these muscles.

Upon muscle injury, satellite cells activate, enter the cell cycle, and give rise of muscle precursor population that proliferate, differentiate and then fuse to form new myofibres, allowing muscle regeneration. At the same time, a subpopulation of SCs return to their quiescent state to replenish the initial pool (Charge and Rudnicki, 2004). The onset activation of satellite cells is due to a signal from infiltrating anti-inflammatory macrophages, that occurs following ordinary stages of muscle degeneration (Prisk and Huard, 2003). Consistent with this notion, it has been reported that pro-inflammatory M1 macrophages exert a negative effect on satellite cells differentiation and fusion. Conversely, anti-inflammatory macrophages M2 stimulates differentiation and increases myoblast fusion (Bondesen et al., 2007). Most satellite cells express the paired box transcriptional factor

Pax7, whereas activated SCs co-express *Pax7* and *MyoD*, upon differentiation SCs maintain *MyoD* expression and downregulate *Pax7* (Seale et al., 2000). It is worth noting that absence of *MyoD* negatively impacts on muscle regeneration, as it delays myoblast transition from proliferation to differentiation (Megency et al., 1996, Sabourin et al., 1999).

An interesting finding made with satellite cell populations induced by CTX treatment is that the *Mtn*^{-/-}/*Erry*^{Tg/+} muscles showed high proportion of committed muscle cells (*Pax7*⁻/*MyoD*⁺) at both time points (day 3 and day 6) post-injury compared to the other genotypic groups. This may be explained by the vast capacity of the satellite cells in these muscles (*Mtn*^{-/-}/*Erry*^{Tg/+}) to expand, proliferate and differentiate, which is probably induced by the surrounding environment (hyper-oxidative and hyper-vascularization) provided by *Erry* overexpression in the *Mtn*^{-/-} mice.

Our work examining the effect of muscle-specific overexpression of *Erry* in the *Mtn*^{-/-} muscles on the regenerating capacity even with a lower number in satellite cells as we showed in the previous chapter, offers interesting insights into the importance of surrounding environment on muscle regeneration process. The *Mtn*^{-/-}/*Erry*^{Tg/+} muscles showed high regeneration degree indicated by large size and high numbers of newly formed centrally located nuclei myofibres (eMHC⁺) at day 6 post-injury.

Previous work has reported that metabolism perturbation modulates stem cells function and fate, thereby affecting muscle recovery from injury (Cerletti et al., 2012). Consistently, a number of studies have demonstrated that muscle with oxidative metabolism have high rate of regeneration capacity (Lowrie et al., 1982). Moreover, genetic manipulation that increased muscle oxidative capacity accelerates regeneration pace (Li et al., 2007b). Conversely, it was well established that muscle metabolic deficit leads to elevate ROS production that markedly contributes to attenuate muscle differentiation, since it impairs myogenesis process (Langen et al., 2002, Ardite et al., 2004). Given these considerations, our work carried out in previous chapters showed that genetic deletion of *Myostatin* resulted in a reduction of muscle oxidative capacity, capillary density, and increased ROS level. However, muscle-specific expression of *Erry* in the *Mtn*^{-/-} background robustly restored muscle oxidative capacity, increased vascularization, and reduced ROS production.

Linking the mentioned observations with previous work that revealed an increase in ROS production, and impairment of myogenesis process in *Erry*^{-/-} monocytes (Murray et al., 2013), support a potential role of *Erry* in regulating muscle myogenesis.

By a way of explanation of our findings that *Erry* induces muscle regeneration even with the depletion of SCs to less than 50% of their normal population, that the oxidative environment established by introducing of *Erry* on a muscle lacking *Myostatin* is the key determinant in accelerating regeneration. Moreover, angiogenesis is an imperative factor for muscles regeneration process. Therefore, we suggest that the reduction in SCs did not impact regeneration capacity in *Mtn*^{-/-}/*Erry*^{Tg/+} muscles, because of *Erry* ability to promote muscle vascularization, thereby induce clearance of necrotic and damaged tissues, ultimately allowing the small number of satellite cells to expand greatly to achieve rapid repair of the damaged tissue. Such opinion is supported by our data showed high macrophages density, and generation of myoblast in *Mtn*^{-/-}/*Erry*^{Tg/+} muscles compared to either WT or *Mtn*^{-/-}.

Finally, we expanded our investigation in the present study by examining the impact of muscle-specific overexpression of *Erry* in the *Mtn*^{-/-} background on muscle regeneration at advance stage (day 14 post-injury). We provided further evidence for accelerated regeneration process in *Mtn*^{-/-}/*Erry*^{Tg/+} muscles compared to other genotypic groups, that evidenced by few number of fibres still express eMHC, with the normal size of newly formed myofibres in these muscles. Previous work has revealed that muscle repair programme is usually at expense of SCs population, which is presumed not to be available for future degeneration/regeneration cycles, thereby affecting the size of newly generated muscle fibres (Castets et al., 2011). Moreover, adult satellite cells are the primary source of muscle regenerating after repetitive injury (Kuang et al., 2008, Zammit, 2008), and more particular satellite cells that express *Pax7* are required for this capability (Seale et al., 2000). Importantly, we found that despite *Mtn*^{-/-}/*Erry*^{Tg/+} muscles displayed high populations of myogenic precursors (*Pax7*⁺/*MyoD*⁺), as well as committed muscle cells (*Pax7*⁻/*MyoD*⁺) at day 6 post-injury, this was not at expense of satellite cells character (*Pax7*⁺/*MyoD*⁻).

Although precocious differentiation might cause cells exhaustion, the myofibres regenerating at a quick cadence, it also indicates a fast degeneration steps. There is a wide body of evidence that a correct inflammatory response following muscle injury, which reflects a proper level of capillary density, is necessary for effective regeneration and repair

(Goetsch et al., 2003, Tidball, 2005). This hypothesis supported by our observations investigating capillary and macrophages density, as well as necrotic fibre numbers.

In summary we can conclude, the increased oxidative capacity and microvascular network that was imparted by superimposition of *Errγ* in a muscle lacking *Myostatin* played a vital role to reduce muscle damage, stimulate functioning inflammatory response, induce clearing of necrotic and died tissues, thereby accelerated muscle regeneration capacity following CTX treatment. Importantly, we demonstrate that even decreased number of satellite cells in the *Mtn*^{-/-}/*Errγ*^{Tg/+} muscles had a very little impact on regeneration. Indeed, their regeneration capacity exceeded not only *Mtn*^{-/-} but also WT muscles. We also provided evidence that the metabolic reprogramming driven by *Errγ* overexpression was efficacious to maintain high regeneration pace at advance stages following acute injury.

Chapter 6; Results

Impact of post-natal antagonism of *Myostatin* signalling on the skeletal muscles of the *Erry* mice

6.1. Introduction

Skeletal muscle is a composite structure that composed of muscle fibres, blood vessels, sensory cells and connective tissue (Gumerson and Michele, 2011, Gillies and Lieber, 2011). It is a highly adaptable tissue that changing its phenotype with regards to size and composition as a response to the physiological and environmental stimuli. Thus a series of alterations in the metabolic, molecular, and physiological profiles of the tissue habitually accompanied muscle mass changes (Matsakas and Patel, 2009a). Despite the profound impact of the animal breed and genetic background on muscle mass, it is mainly determined by muscle fibre numbers and size (Martyn et al., 2004). Myofibre numbers are fixed at prenatal stage (Sandri, 2008), whereas the balance between muscle protein synthesis and degradation rates fundamentally determines muscle mass by influencing fibre size (Nader, 2005). A huge amount of research has revealed a vital role of Insulin-like Growth Factor (IGF-I and IGFII) in promoting muscle fibres hypertrophy by activating signalling pathways that attenuate proteolysis and induce protein synthesis (Glass, 2005, Giannoulis et al., 2012). In contrast, we and others have focused on attenuating signalling mechanisms that usually inhibit muscle development, to promote muscle growth. One of the potent inhibitors of skeletal muscle development is *Myostatin*, an evolutionary conserved member of the Transforming Growth Factor beta (TGF- β) superfamily of secreted proteins (McPherron et al., 1997). We have previously shown that genetic alteration of *Myostatin* leads to the development of a hypermuscular phenotype through both myofibre hyperplasia and hypertrophy, these observations were conformed to the aforementioned studies (McPherron and Lee, 1997, Schuelke et al., 2004, Clop et al., 2006). In addition, it was well documented that Myostatin promotes muscle oxidative capacity and connective tissue development, since its deletion leads to the development of glycolytic phenotype, and reduce fibroblast proliferation (McPherron et al., 1997, Mendias et al., 2006, Zhu et al., 2000).

An adequate level of skeletal muscle size and functions is very important for health and quality of life (Pistilli et al., 2011, Cooper et al., 2010, Zhou et al., 2010). Skeletal muscle wasting occurs as a result of a variety of pathophysiological settings, including muscular dystrophies (Whittemore et al., 2003, Patel and Amthor, 2005), and progressive loss of skeletal muscle mass with age advance, a process called sarcopenia, that leads to lack

muscle strength and increased fatigability (Faulkner et al., 1990). Furthermore, prolonged bed rest and immobilization are inducing muscle atrophy (Han et al., 2013). Therefore, bearing in mind the inhibitory effects of Myostatin on skeletal muscle growth, a number of strategies have been developed in order to inhibit Myostatin signalling post-natally as promising therapeutic approaches against muscle wasting. For instance, it has been reported that Myostatin is synthesized as a precursor protein that gives rise to N-terminal propeptide and a C-terminal biologically active following proteolysis process (Lee et al., 2004). The N-terminal peptide is capable to maintain Myostatin in a latent state by direct binding, then inhibiting of the biologically active C-terminal peptide (Shelton and Engvall, 2007, Zimmers et al., 2002). Adeno-associated virus (AAV) mediated Myostatin pro-peptide systemic delivery has been applied to enhance muscle growth in adult and aged mice (Collins-Hooper et al., 2014, Matsakas et al., 2009). Moreover, muscle mass can be increased by follistatin administrating that neutralizing Myostatin (Hill et al., 2002, Lee and McPherron, 2001). Previous other work has revealed a robust increase in skeletal muscle mass following mice treatment with Myostatin neutralizing antibody (Whittemore et al., 2003). A significant number of studies have established that Myostatin initiates an intracellular signalling by binding its transmembrane activin receptor IIB (AcRIIB), thus suppressing of this pathway may greatly stimulate muscle growth (Lee and McPherron, 2001, Schuelke et al., 2004). Although the above mentioned methods that inhibits Myostatin signalling at post-natal stage offered a good increase in muscle growth, administration of soluble ActRIIB (sActRIIB) resulted in greater increase in muscle mass, suggesting that in addition to Myostatin, there are other ligands that limit muscle development (Lee et al., 2005, Zhou et al., 2010). Thus, we believe that weekly injection of sActRIIB that mediate inhibition of Myostatin and relative proteins would lead to greater level of muscle growth. Despite the variable levels of increase in muscle mass following Myostatin inhibition at post-natal stage using different strategies, there is evidence that muscles with Myostatin blocking have number of abnormalities besides fibre hypertrophy. Previous work has reported that the expression levels of a network of genes linked to mitochondrial function and oxidative phosphorylation pathways are reduced markedly in WT muscles after sActRIIB treatment (Rahimov et al., 2011). Further investigation has revealed a shift of aged muscle fibres toward anaerobic glycolysis phenotype as a result of Myostatin blocking through

AAV8MyoPPT injection (Collins-Hooper et al., 2014). In the line with these findings, it has been demonstrated that blocking of Myostatin signalling in muscles from *mdx* mice via sActRIIB treatment lead to compromise muscle angiogenic program, capillary density, and oxidative metabolism thereby a declines of muscle force generation capacity and increase fatigability (Relizani et al., 2014). In addition, both Wagner and Krivickas (Krivickas et al., 2009, Wagner et al., 2008) failed to find any evidence of improved muscle function in human dystrophy following the systemic administration of MYO-029, a neutralizing antibody to MYOSTATIN.

On the other hand, a number of elegant studies have shown the potential of *Erry* transgenic to promote muscle angiogenesis and enhance oxidative capacity, hence promote aerobic muscles properties (Narkar et al., 2011, Rangwala et al., 2010). It was established that ETC and TCA, mitochondrial pathways considered as an important source of ROS production, are controlling by a number of genes that are profoundly regulated by *Erry* to prevent the excessive generation of superoxide leads to oxidative stress (Harper et al., 2004, Eichner and Giguere, 2011). Additionally, we have shown previously that muscle-specific expression of *Erry* in *Mtn*^{-/-} background mice was sufficient to develop hyper-oxidative hypertrophic myofibres, thereby challenging the trade-off that thought to be existent between muscle fibre oxidative capacity and its size (Van der Laarse WJ, 1998).

The newly generated hyper-muscular, hyper-oxidative mouse line (*Mtn*^{-/-}/*Erry*^{Tg/+}) displays a number of characteristics that make them attractive both in terms of physiology and regeneration capacity. However, the muscle phenotype in these models is largely established during embryonic stage. Here we asked whether similar phenotypes could be obtained via non-genetic modifications. To do so, we inhibited Myostatin at post-natal stages in *Erry*^{Tg/+} (which displays an increased oxidative profile) and WT mice (n=5) by twice weekly injections for 8 weeks (start at week 5 and stop at week 12 of age) of soluble activin receptor IIB protein (sActRIIB) which has been shown to antagonize signalling mediated by Myostatin and related-proteins.

Representative muscles of fast and slow phenotypes (EDL and soleus respectively) were isolated, weighed and frozen. The sectioned slides were stained for (SDH), and (DHE) stains to identify muscle oxidative capacity, and Reactive Oxygen Species (ROS) level respectively. Then the cryo-sectioned slides of both muscles were immunostained using antibodies for

myosin heavy chains (MHCs) (type I, IIA and IIB) to identify total muscle fibre number, types and size (CSA), and CD31 antibody to identify capillary density. Finally, immunostaining for Collagen type IV, dystrophin and laminin antibodies accompanied with MHCIIIB was performed on muscle sections from all cohorts in order to examine the signal intensity and expression domain thickness of these proteins in intracellular and extracellular compartments, and basement membrane.

This study shows that weekly injection of sActRIIB, which has been shown to antagonize Myostatin signalling, firstly induce a significant increase in body and muscle mass due to myofibres hypertrophy. Secondly, administration of sActRIIB for 8 weeks do not cause any change in myofibres composition at MHC level, however, it compromises oxidative capacity of muscles from WT, but not *Errγ^{Tg/+}* mice. Subsequently, sActRIIB treatment promotes the capillary density in *Errγ^{Tg/+}*, but not WT muscles. Furthermore, treated WT muscles show high level of ROS, with no change in ROS generation in treated muscles from *Errγ^{Tg/+}* compared to the control. Finally, sActRIIB injection reduces connective tissue content in WT muscles, without notable change of this parameter in muscles from *Errγ^{Tg/+}* mice.

6.2. *Erry* expression following post-natal inhibition of Myostatin using sActRIIB

Here we examined whether post-natal inhibition of Myostatin using a systemic injection of sActRIIB would affect *Erry* level prompted through transgenic approach. Therefore, *Erry* expression was determined in soleus muscles (n=5) from (WT, *Erry*^{Tg/+}, WT.sActRIIB and *Erry*^{Tg/+}.sActRIIB). We found a significant increase in expression level of *Erry* in soleus muscles from the transgenic mice compared to its level in muscles from WT.PBS and WT injected with sActRIIB mice. Interestingly, the expression level of *Erry* was similar in soleus muscles from *Erry*^{Tg/+} and *Erry*^{Tg/+}.sActRIIB mice (Figure 6.1). These data indicate that sActRIIB treatment for 8 weeks to inhibit Myostatin signalling did not affect *Erry* expression.

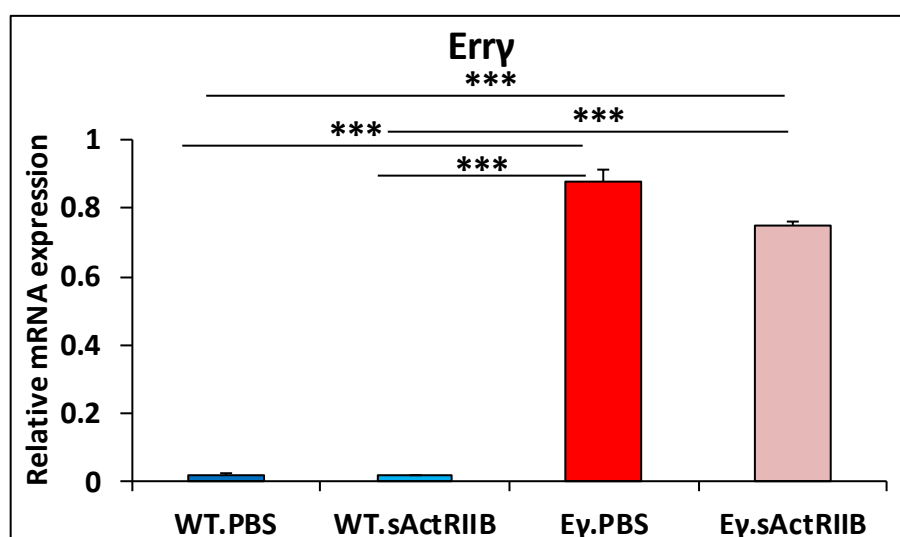


Figure 6.1. Post-natal inhibition of Myostatin in the WT and muscle-specific *Ey* mice doesn't affect *Ey* expression

Displaying *Erry* mRNA level in soleus muscles of wild type (WT), *Erry* transgenic (*Ey*), wild type injected with sActRIIB (WT.sActRIIB) and *Erry* transgenic injected with sActRIIB (*Ey*.sActRIIB) mice.

(n=5) three months old male WT and *Ey* injected with PBS, and WT and *Ey* injected with sActRIIB twice weekly for 8 weeks; One-way ANOVA followed by Bonferroni's multiple comparison tests, ***=p<0.001.

6.3. Treatment with Activin ligand trap increases body and muscle mass in WT and *Erry*^{Tg/+} mice

We showed previously that body mass of mice with *Myostatin* mutation was similar to those of WT, and muscle-specific expression of *Erry* into *Mtn*^{-/-} background muscles did not affect this parameter. Previous work has reported that type of effects of *Myostatin* absence on individual muscle and body mass depending on whether *Myostatin* loss of function occurs prenatally or post-natally (McPherron, 2010).

Here we examined the effect of 8 weeks intraperitoneally injection (IP) on a twice weekly basis with sActRIIB which antagonize signalling mediated by *Myostatin*, on body mass of WT and *Erry*^{Tg/+} mice. We found that the increase of body mass started from the first two weeks of injection (Figure 6.2A). At the day of animals culling (12 weeks old) WT and *Erry*^{Tg/+} mice injected with sActRIIB were significantly heavier than their counterpart injected with PBS (Figure 6.2B).

Unlike in the genetic deletion of *Myostatin*, these data show that post-natal inhibiting of *Myostatin* by systemic administration of sActRIIB induces a remarkable increase of animals' body mass.

Next we determined the change in hind limb muscles (EDL, gastrocnemius, soleus and TA) mass from WT and *Erry*^{Tg/+} mice following 8 weeks of treatment with sActRIIB. Previously we demonstrated a significant increase in mass of muscles from *Mtn*^{-/-} and *Mtn*^{-/-}/*Erry*^{Tg/+} compared to muscles of WT mice. In agreement with previous studies (Relizani et al., 2014, Collins-Hooper et al., 2014), our data showed a significant increase in weight of all muscles examined (n=10) following post-natal inhibition of *Myostatin* (Figure 6.3). Strikingly we found an apparent muscle-specific response to the sActRIIB treatment with TA muscles showing the largest gain in mass (~82% and 77%) in WT.sActRIIB and *Erry*^{Tg/+}.sActRIIB mice respectively, and the soleus muscles with the smallest increase (46%) in WT with no significant increase in *Erry*^{Tg/+} mice following 8 weeks of sActRIIB injection (Figure 6.3).

Together, these data show that while germline deletion of *Myostatin* induced muscle mass increase without change in body weight, the post-natal inhibition of *Myostatin* via sActRIIB injection resulted in a significant increase in both body and muscle mass with specific muscle response.

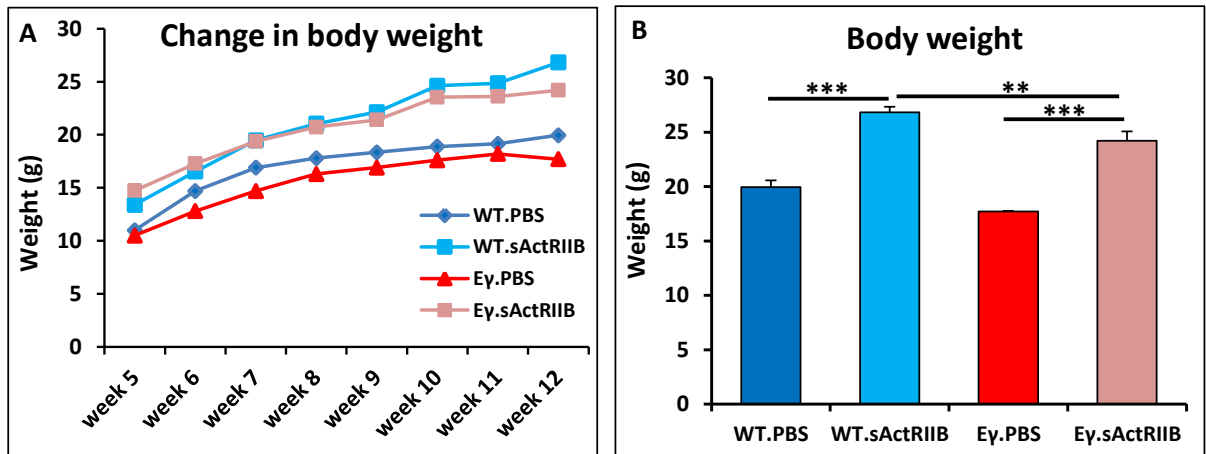


Figure 6.2. Post-natal inhibition of Myostatin in the WT and muscle-specific *Ey* mice induces body weight

Body weight of WT and *Ey* mice increased significantly following 8 weeks of intra peritoneal (IP) injection of sActRIIB.

(A) Relative changes in body mass over time. IP injection of WT and *Ey* mice with sActRIIB started at week 5 and tissues collected at the end of week 12.

(B) Body weight of WT, *Ey*, WT.sActRIIB and *Ey*.sActRIIB mice.

($n=5$) three months old male WT and *Ey* injected with PBS, and WT and *Ey* injected with sActRIIB twice weekly for 8 weeks; Two-way ANOVA followed by Bonferroni post-tests to compare replicate means by row, **= $p<0.01$ and ***= $p<0.001$

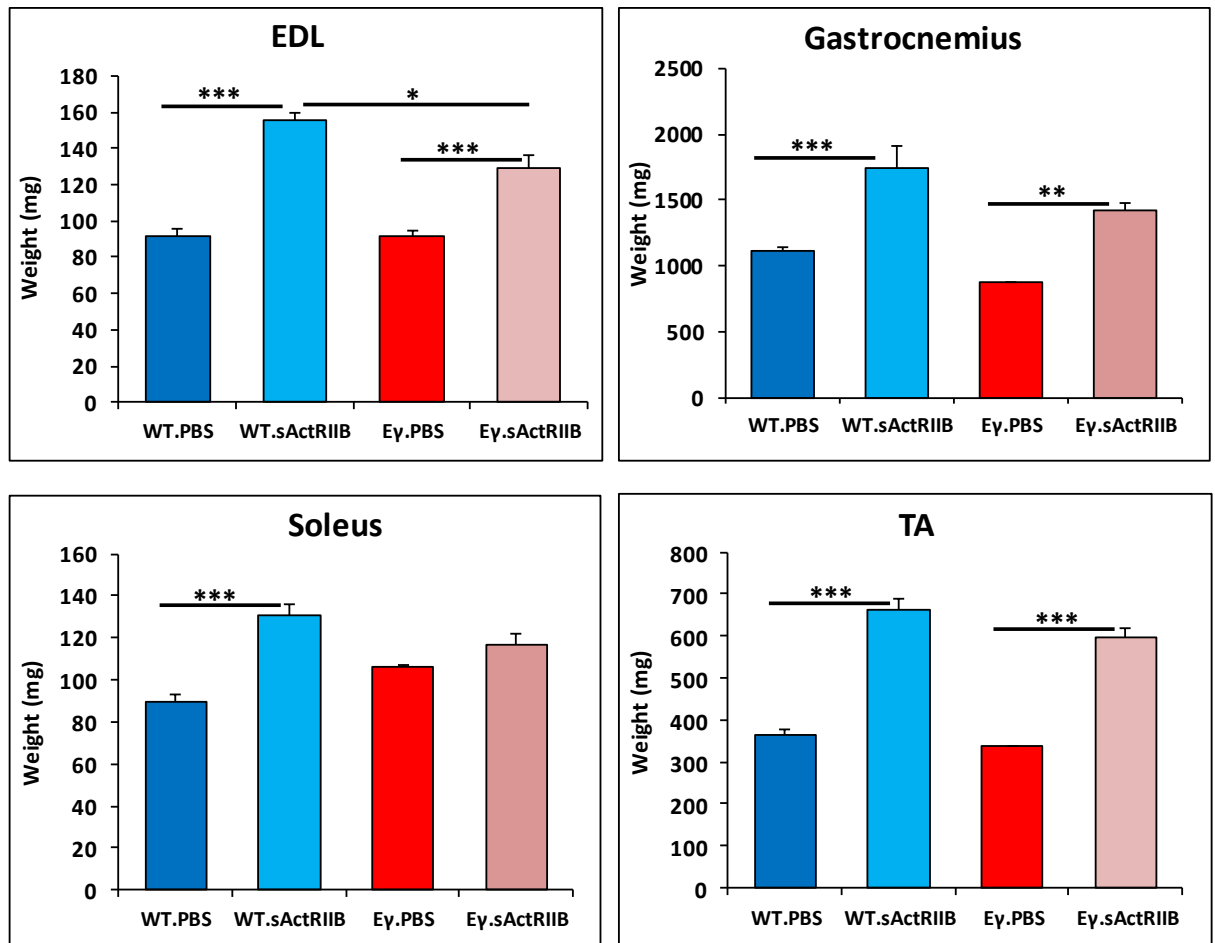


Figure 6.3. Post-natal inhibition of Myostatin in the WT and muscle-specific *Ey* mice increases muscle mass

Quantification of skeletal muscles (EDL, gastrocnemius, soleus and TA) mass of WT, *Ey* WT.sActRIIB and *Ey*.sActRIIB mice.

Display a significant increase in muscles mass due to post-natal blocking of *Myostatin* using sActRIIB.

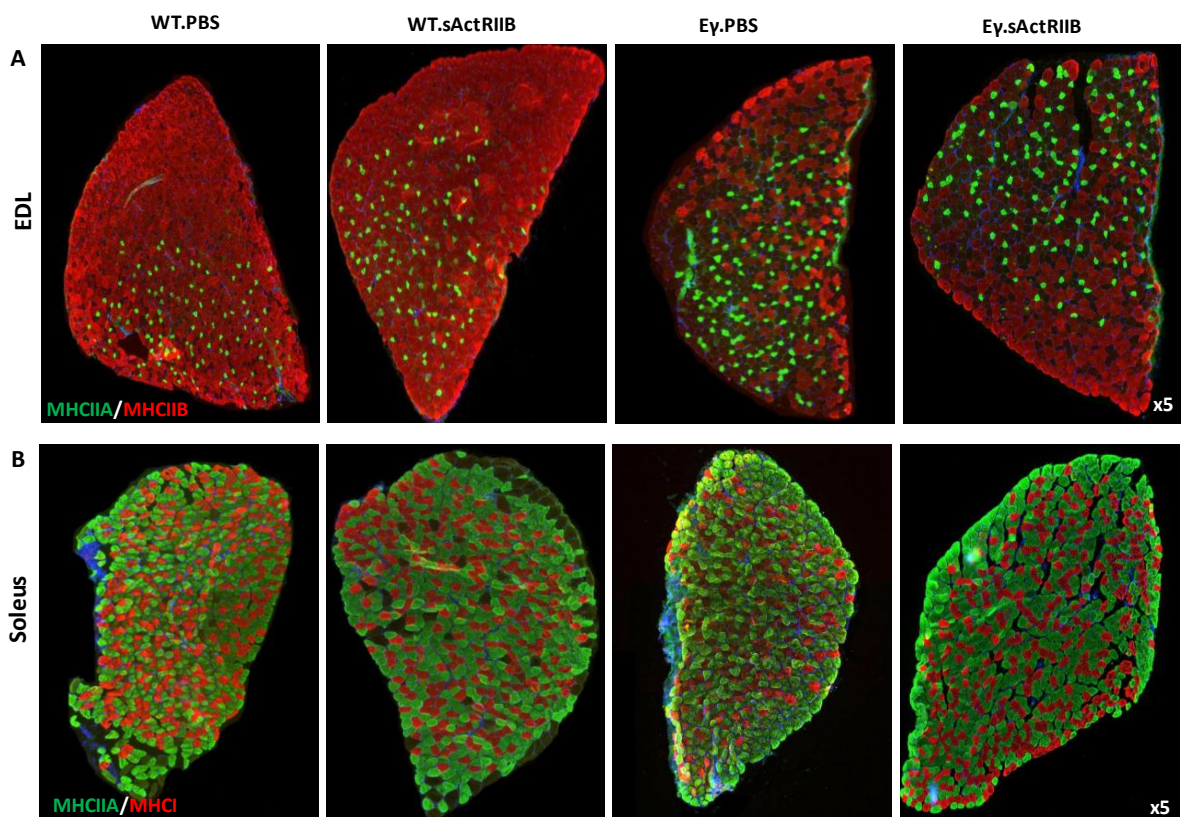
($n=10$) three months old male WT and *Ey* injected with PBS, and WT and *Ey* injected with sActRIIB twice weekly for 8 weeks; Two-way ANOVA followed by Bonferroni post-tests to compare replicate means by row, *= $p<0.05$ **= $p<0.01$ ***= $p<0.001$.

6.4. Skeletal muscle enlargement induced by sActRIIB treatment is not associated with muscle fibre hyperplasia

Next we examined whether the increase in muscle mass was due to muscle hyperplasia, muscle hypertrophy or a combination of both. Therefore, Immunohistochemistry protocol using antibodies against myosin heavy chain (MHC) isoforms (type I, IIA and IIB) was performed to determine the cellular changes elicited by administration of sActRIIB in a representative muscle of fast and slow phenotypes (EDL and soleus respectively) (n=5) of WT, and *Erry*^{Tg/+}, WT.sActRIIB and *Erry*^{Tg/+}.sActRIIB mice (Figure 6.4A and B).

Quantification of the total fibre number of EDL and soleus muscles at 12 weeks old age mice revealed no significant difference between the fibre numbers of muscles injected with PBS and muscles treated with sActRIIB from WT and *Erry*^{Tg/+} mice (Figure 6.4C and D).

These data indicate that the enlargement in muscle mass of WT and *Erry*^{Tg/+} following 8 weeks intraperitoneal injection of sActRIIB occurred in both muscles (EDL and soleus) without increase in myofibre numbers.



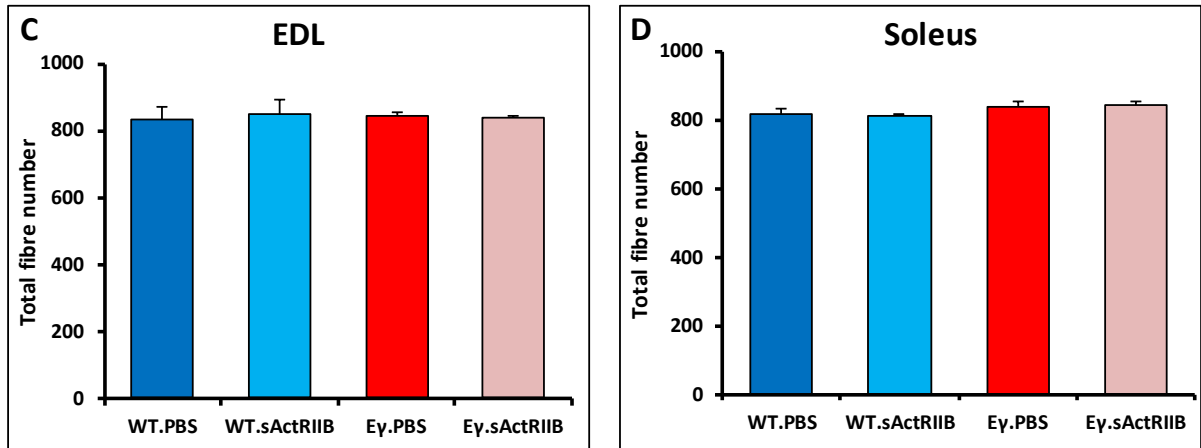


Figure 6.4. Myostatin blocking doesn't change fibre number of WT and muscle-specific *Ey* mice

Display total fibre number of EDL and soleus muscles.

(A) Immunohistochemical images of EDL muscles from WT, *Ey*, WT.sActRIIB and *Ey*.sActRIIB mice. Green fibres signify the expression of MHCIIA with MHCIIIB appearing as red.

(B) Immunohistochemical images of soleus muscles from WT, *Ey*, WT.sActRIIB and *Ey*.sActRIIB mice. Green fibres signify the expression of MHCIIA with MHCI appearing as red.

(C) Quantification of total fibre number in EDL muscles.

(D) Quantification of total fibre number in soleus muscles.

($n=5$) three months old male WT and *Ey* injected with PBS, and WT and *Ey* injected with sActRIIB twice weekly for 8 weeks; Two-way ANOVA followed by Bonferroni post-tests to compare replicate means by row.

6.5. Increase in muscle mass following sActRIIB administration is caused by myofibre hypertrophy

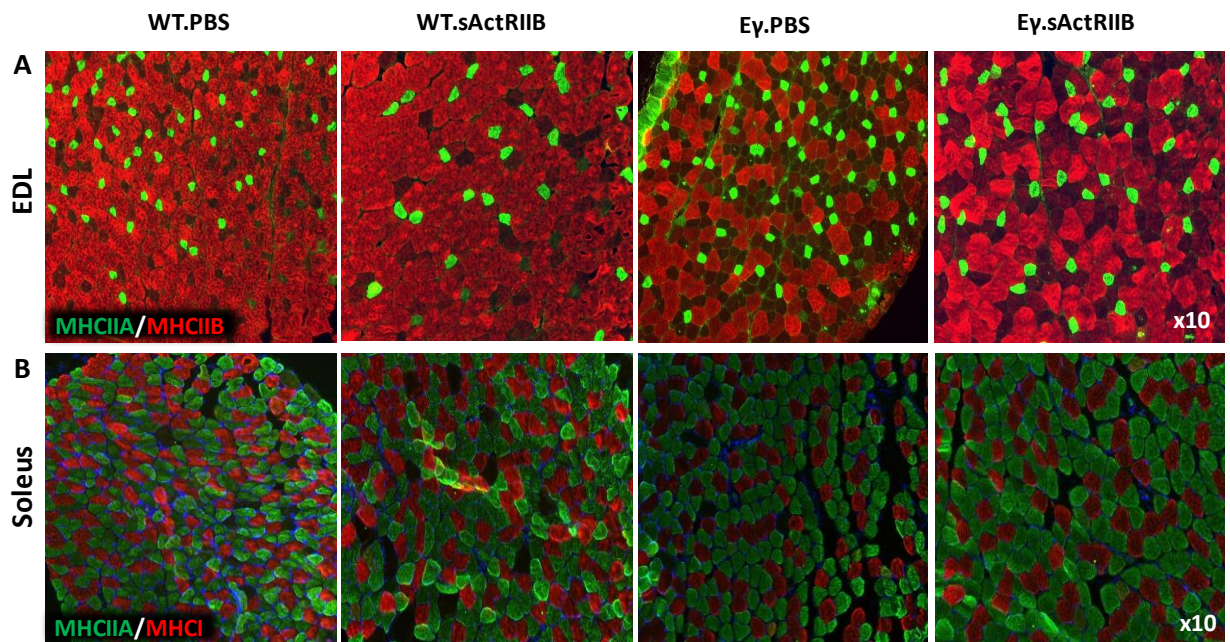
Having shown no evidence for an increase in fibre numbers of muscles from WT and *Erry^{Tg/+}* mice following 8 weeks of sActRIIB treatment in the present study, we next examined the reason underpinning the increase in muscle mass of WT.sActRIIB and *Erry^{Tg/+}*.sActRIIB mice. Thus, we determined the cross-sectional area of myofibres in representative muscles of fast and slow phenotypes (EDL and soleus respectively) from WT, *Erry^{Tg/+}*, WT.sActRIIB and *Erry^{Tg/+}*.sActRIIB mice (n=5). Muscle sections were immunostained using antibodies against MHC isoforms (type I, IIA and IIB). A minimum of 150-200 measurements per myofibre type was taken in each muscle section (Figure 6.5A and B).

We found that the CSA of all muscle fibre types of WT and *Erry^{Tg/+}* mice were increased significantly by sActRIIB treatment, except MHCI isoform which was absent in EDL muscle sections from WT.PBS and WT.sActRIIB mice (Figure 6.5C). Of particular note was that the MHCIIA in EDL muscles of WT.sActRIIB and *Erry^{Tg/+}*.sActRIIB were significantly larger than those from EDL muscles of WT.PBS and *Erry^{Tg/+}*.PBS mice respectively, with that of the MHCIIA from *Erry^{Tg/+}*.sActRIIB greater than the counterpart myofibre from WT.sActRIIB (Figure 6.5A and C). Same scenario of CSA increase was noticed in MHCIIX and MHCIIIB isoforms of EDL muscles. Notably, fast phenotypes (MHCIIX and MHCIIIB) from both genotypic groups were more prone to size increase than the slow phenotypes (MHCI and MHCIIA) (Figure 6.5C).

Next we examined muscle fibres CSA in the soleus muscles. We found that the size of myofibre type I in the soleus muscles of WT.sActRIIB and *Erry^{Tg/+}*.sActRIIB were significantly larger than their counterpart from soleus muscles of WT.PBS and *Erry^{Tg/+}*.PBS mice respectively. The size of muscle fibre type I was larger in soleus muscles from *Erry^{Tg/+}*.sActRIIB than the WT.sActRIIB mice (Figure 6.5B and D). Measurement of MHCIIA and MHCIIX size of soleus muscles showed same pattern of increase was observed in MHCI fibres, with no significant difference in size of myofibre type IIA in soleus muscles from WT.sActRIIB and *Erry^{Tg/+}*.sActRIIB (Figure 6.5D).

These findings show that the post-natal increase in muscle mass of WT and *Erry^{Tg/+}* mice following sActRIIB treatment results from muscle hypertrophy but not hyperplasia. Such

data in particular the increase in myofibre CSA of *Erry*^{Tg/+} muscles that showed hyper-oxidative properties raises the possibility of breaking the inverse relationship between muscle fibre size and oxidative capacity (Degens, 2012) during post-natal life.



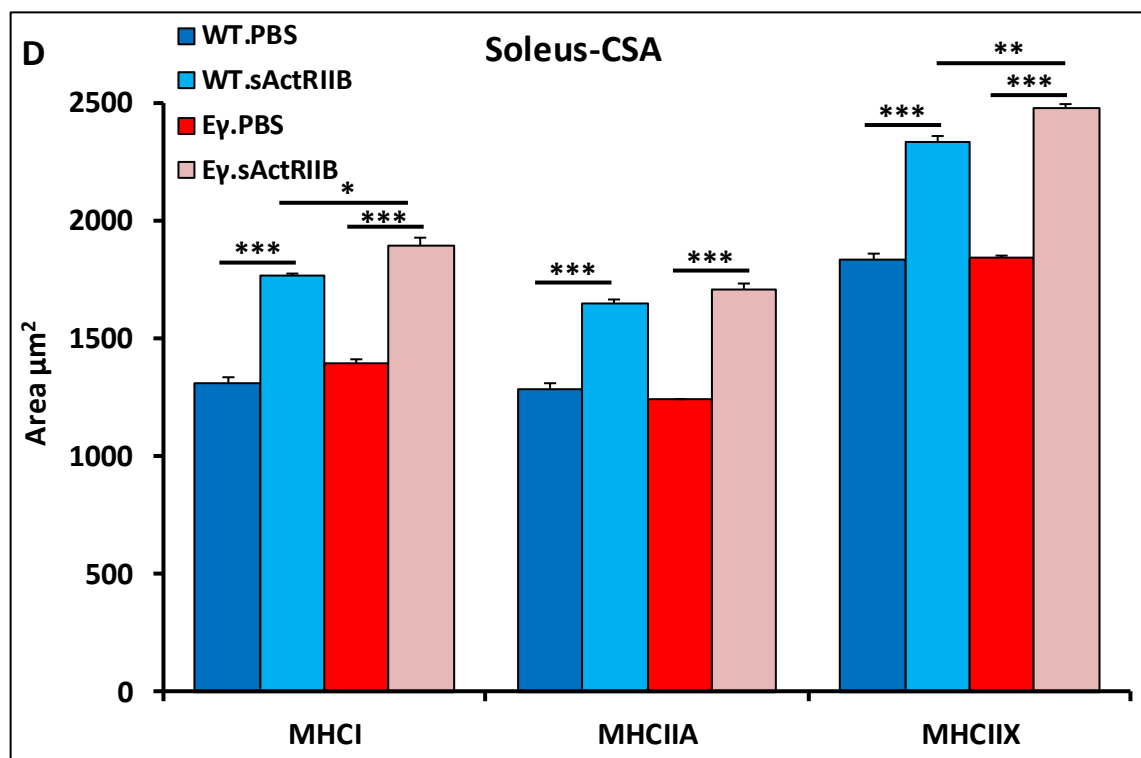
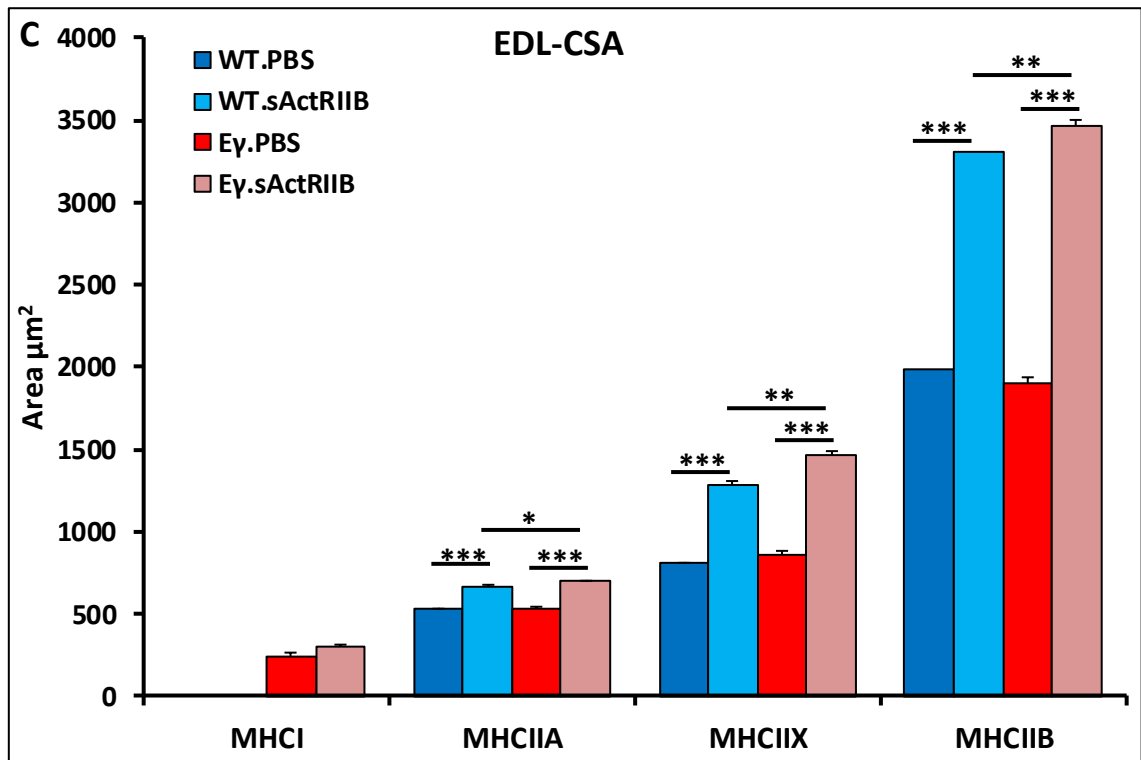


Figure 6.5. Treatment of WT and *Eγ* mice with sActRIIB increases muscle fibres cross-sectional area

Large muscle fibres from WT and *Eγ* mice following *Myostatin* inhibition using sActRIIB

(A) Immunohistochemical images of EDL muscles from WT, *Eγ*, WT.sActRIIB and *Eγ*.sActRIIB mice. Green fibres signify the expression of MHCIIA with MHCIIIB appearing as red. Non green and red fibres represent MHCIIIX.

(B) Immunohistochemical images of soleus muscles from WT, *Eγ*, WT.sActRIIB and *Eγ*.sActRIIB mice. Green fibres signify the expression of MHCIIA with MHCI appearing as red. Non green and red fibres represent MHCIIIX.

(C) Quantification of muscle fibres cross-sectional area in EDL muscles.

(D) Quantification of muscle fibres cross-sectional area in soleus muscles.

(*n*=5) three months old male WT and *Eγ* injected with PBS, and WT and *Eγ* injected with sActRIIB twice weekly for 8 weeks; Two-way ANOVA followed by Bonferroni post-tests to compare replicate means by row, *=*p*<0.05 **=*p*<0.01 ***=*p*<0.001.

6.6. Myosin heavy chain profile does not alter by sActRIIB treatment

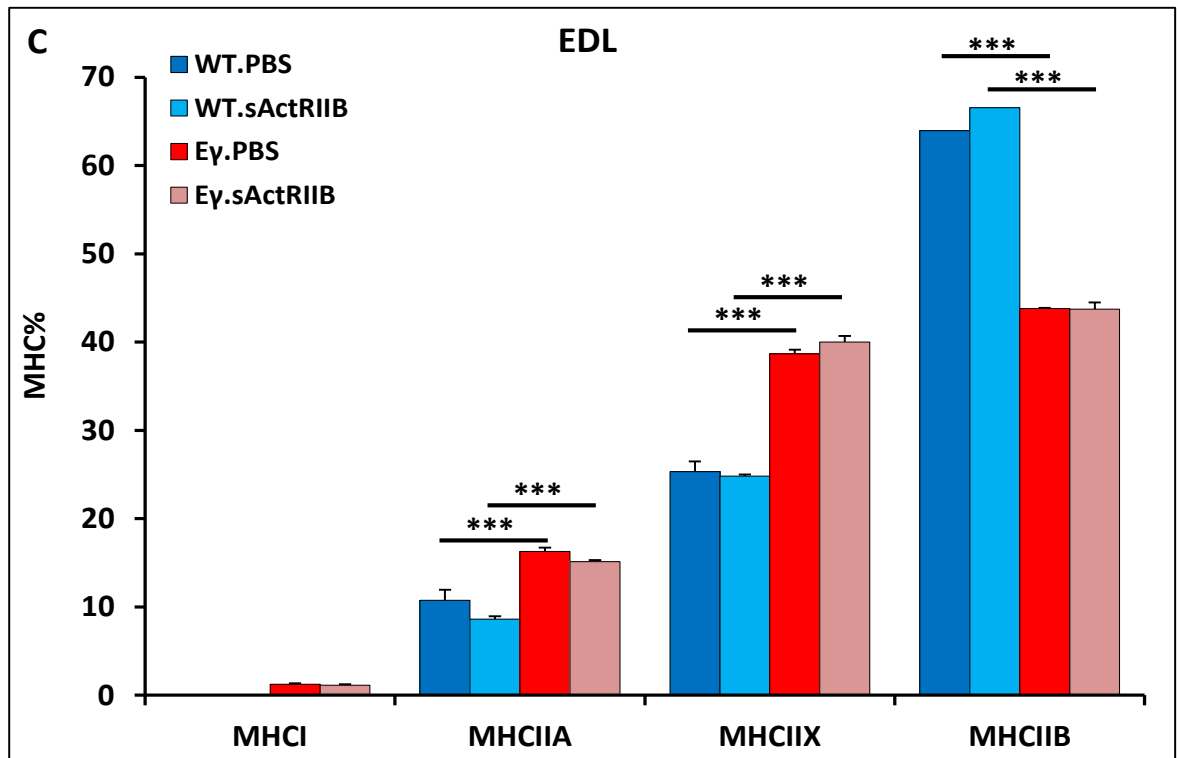
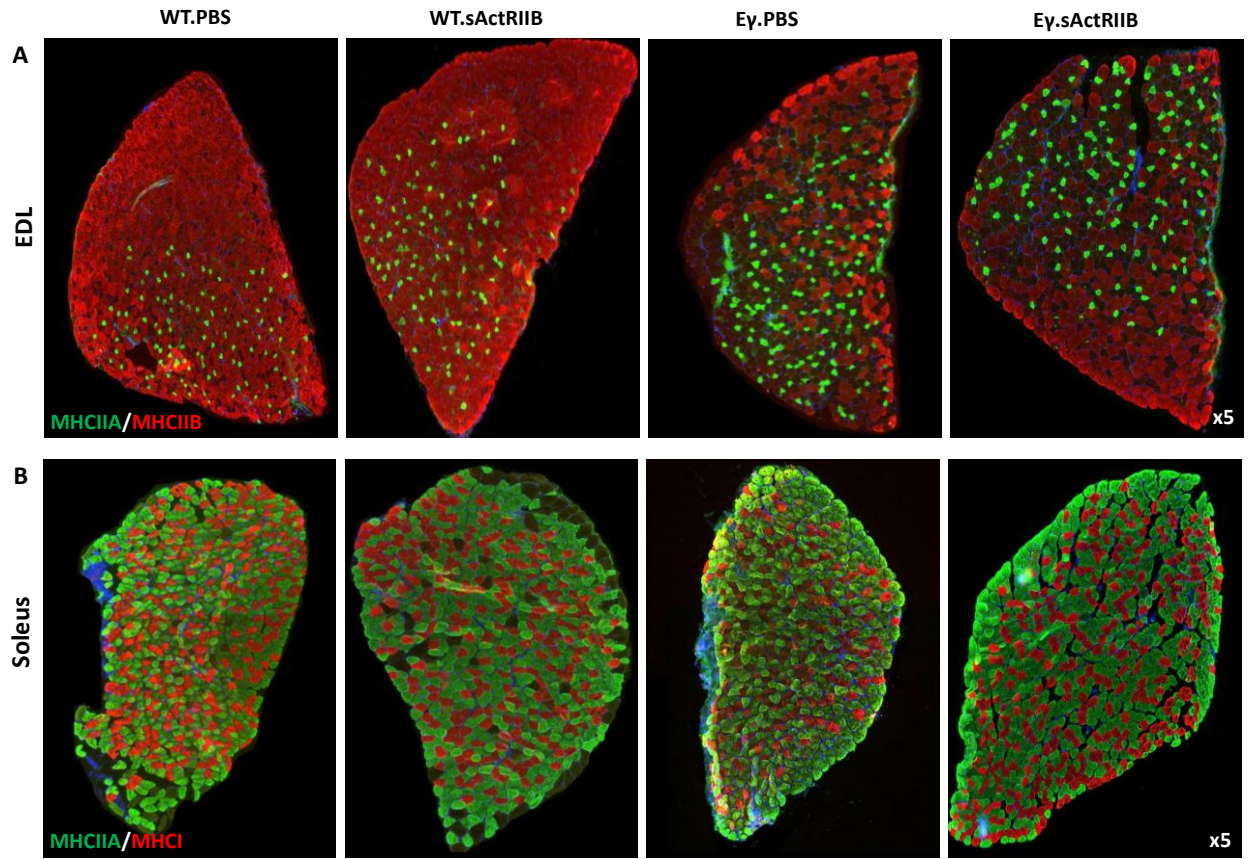
Given our data of this study showed muscle-specific enlargement of skeletal muscles from WT and *Erry*^{Tg/+} mice following 8 weeks of post-injection of sActRIIB was completely attributed to the increase of muscle fibres size with no change in muscle fibre numbers. On the contrary, we and others have demonstrated that the constitutive deficiency of *Myostatin* (*Mtn*^{-/-}) resulted in a dramatic increase in muscle mass due to both muscle fibre hyperplasia and hypertrophy (McPherron and Lee, 1997, Amthor et al., 2007). Interestingly, our observations showed that the metabolic reprogramming imparted by muscle-specific overexpression of *Erry* into *Mtn*^{-/-} background was efficacious to maintain the increase of muscle fibre size and number exhibited by *Myostatin* deletion. Meanwhile driven a partial reversal transition of myofibres profiling within MHCII isoforms toward WT condition, and promoted muscle oxidative capacity.

A number of studies have documented that skeletal muscle is a highly adaptable tissue that capable to change its phenotype with regard to the size and composition in response to various stimuli (Matsakas and Patel, 2009a, Hornberger et al., 2006). However, recent studies have reported that blocking of Myostatin/ActRIIB signalling through post-natal treatment with sActRIIB-Fc induces skeletal muscle mass of adult mice without altering muscle fibre type composition (Akpan et al., 2009, Cadena et al., 2010). Similarly, other studies in the *mdx* mice model of duchenne muscular dystrophy (DMD) have confirmed that post-natal inhibition of Myostatin has no impact on muscle fibre type distribution (Morine et al., 2010, Pistilli et al., 2011). On the other hand, previous work has reported that *Erry* overexpression into WT background mice leads to an increase in the proportions of slow-twitch myofibres (IIA and IIX), and decreases proportions of fast-twitch phenotypes (IIB) (Matsakas et al., 2012b). However, there are no studies regarding the *Erry* potential to maintain the high proportions of the slow muscle fibres following post-natal modification that induces glycolytic status. Therefore, we examined MHC profiling in representative muscles of fast and slow phenotypes (EDL and soleus respectively) (n=5) from four cohorts of mice (WT, *Erry*^{Tg/+} WT.sActRIIB and *Erry*^{Tg/+}.sActRIIB).

In agreement with previous studies (Rangwala et al., 2010, Matsakas et al., 2012b), our findings showed high proportions of MHCIIA and MHCIIX, with a concomitant reduction in the percentage of MHCIIIB phenotypes in EDL muscle sections from *Erry^{Tg/+}* compared to WT mice. Of particular note, EDL muscles from *Erry^{Tg/+}* displayed presence a number of MHC type I isoform which was absent in counterpart muscles from WT.PBS (Figure 6.6A and C). Most importantly, we found that 8 weeks of post-natal treatment with sActRIIB did not change myofibres distribution either in EDL from WT, nor in hyper-oxidative muscles from *Erry^{Tg/+}* mice (Figure 6.6C).

Next we examined soleus muscle fibre profiling. We found that muscles from *Erry^{Tg/+}* mice displayed greater proportion of MHCIIA, and lower proportion of MHCIIX isoforms compared to the WT. More specifically, soleus muscle from WT and transgenic *Erry* mice showed same percentages of MHC type I (Figure 6.6 B and D). Interesting, myofibres profiling in soleus muscles from both WT and transgenic *Erry* mice was conserved followed sActRIIB treatment (Figure 6.6D).

These data show that even hind limb muscles from *Erry^{Tg/+}* mice displayed high numbers of slow-twitch muscle fibres compared to WT, the post-natal treatment with sActRIIB did not affect these muscle fibres distribution. Moreover, the sActRIIB injection to antagonise Myostatin signalling post-natally did not affect MHC profiling of the WT muscles as well.



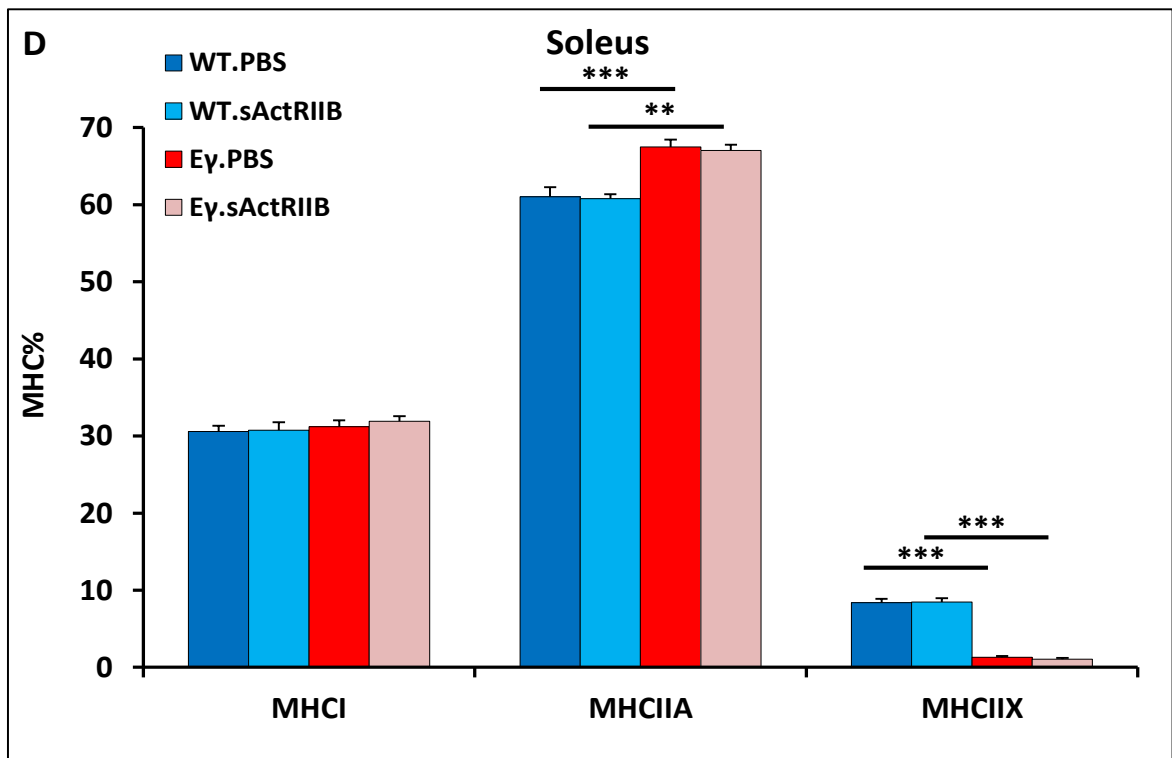


Figure 6.6. Post-natal inhibition of Myostatin do not impact myosin heavy chain profile of EDL and soleus muscles of WT and *E γ* mice

Same muscle fibre phenotype of WT and *E γ* mice following sActRIIB treatment.

(A) Immunohistochemical images of EDL muscles from WT, *E γ* , WT.sActRIIB and *E γ* .sActRIIB mice. Green fibres signify the expression of MHCIIA with MHCIIIB appearing as red. Non green and red fibres represent MHCIIIX.

(B) Immunohistochemical images of soleus muscles from WT, *E γ* , WT.sActRIIB and *E γ* .sActRIIB mice. Green fibres signify the expression of MHCIIA with MHC I appearing as red. Non green and red fibres represent MHCIIIX.

(C) Graph showing fibre type composition in EDL muscles from WT, *E γ* , WT.sActRIIB and *E γ* .sActRIIB mice.

(D) Graph showing fibre type composition in soleus muscles from WT, *E γ* , WT.sActRIIB and *E γ* .sActRIIB mice.

($n=5$) three months old male WT and *E γ* injected with PBS, and WT and *E γ* injected with sActRIIB twice weekly for 8 weeks; Two-way ANOVA followed by Bonferroni post-tests to compare replicate means by row, ***= $p<0.001$.

6.7. Treatment with sActRIIB attenuates oxidative capacity of muscles from WT, but not *Erry*^{Tg/+} mice

We demonstrated that post developmental inhibition of Myostatin by administering sActRIIB for a period of 8 weeks resulted in an enlargement of muscle fibres thereby increased muscle and body mass of both WT and *Erry*^{Tg/+} mice. However, the increase was not accompanied by any alteration in muscle fibre numbers and MHC distribution. Our previous findings showed that germline deletion of *Myostatin* leads to a significant reduction in muscle oxidative capacity, however, muscle-specific expression of *Erry*^{Tg/+} into *Mtn*^{-/-} background was sufficient to restore the proportion of oxidative myofibres to normal condition. We therefore investigated myofibres distribution at metabolic level following sActRIIB treatment.

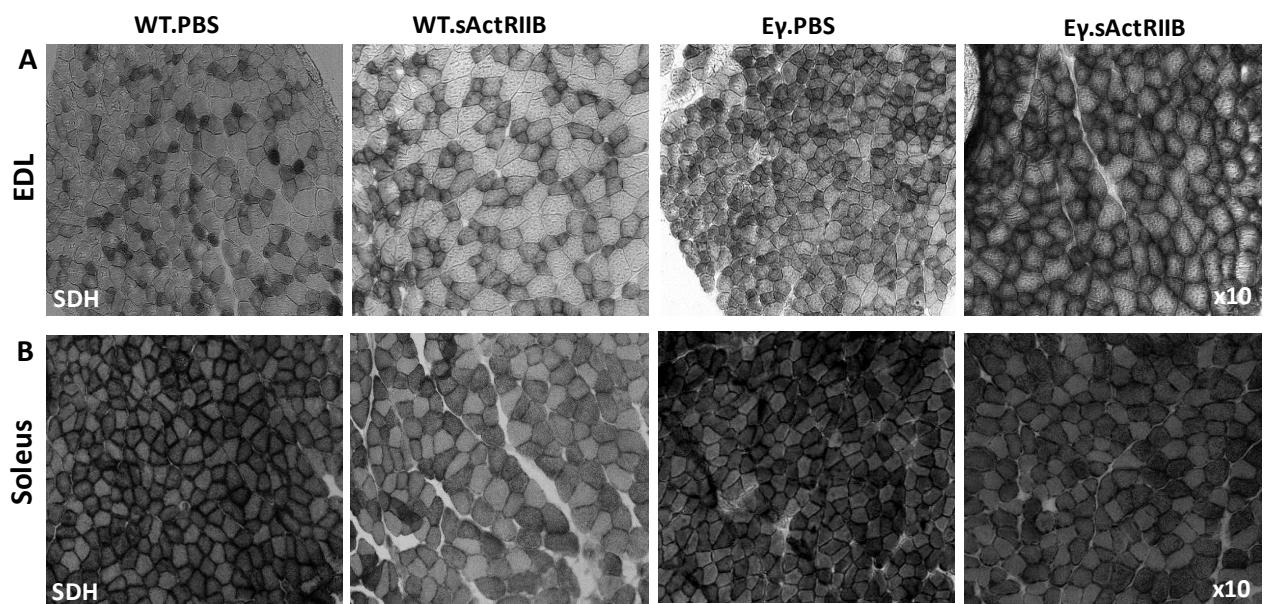
It has been illustrated that post-injection of sActRIIB-Fc resulted in a marked reduction in level of molecules that involved in regulation of skeletal muscle mitochondrial functions and oxidative phosphorylation (Rahimov et al., 2011).

However we have shown that *Erry* is a key regulator of skeletal muscle aerobic metabolism and mitochondrial functions and biogenesis. Thus we sought to investigate systemically how post-natal blocking of Myostatin signalling by sActRIIB injection might affect oxidative capacity in WT muscles and hyper-oxidative muscles from *Erry*^{Tg/+} mice. To do so, we performed staining for the mitochondrion-associate enzyme succinate dehydrogenase (SDH) in sections of EDL and soleus muscles ($n=5$) from four cohorts of mice (WT, *Erry*^{Tg/+} WT.sActRIIB and *Erry*^{Tg/+}.sActRIIB) (Figure 6.7A and B).

We found a few number of strongly stained oxidative muscle fibres (SDH⁺), with a concomitant increase in the proportion of pale non-oxidative fibres (SDH⁻) in muscles from WT.sActRIIB compared to WT.PBS muscles. However, the proportion of oxidative myofibres in muscles from *Erry*^{Tg/+} and *Erry*^{Tg/+}.sActRIIB was similar (Figure 6.7A-D). Of particular note, EDL muscles from WT mice injected with sActRIIB displayed lower percentage of oxidative myofibres (26.2%) compared to control (39.7%). Interestingly, post-natal treatment with sActRIIB didn't affect the percentage of oxidative myofibres in EDL muscles from the transgenic mice, hence no significant difference noticed in numbers of oxidative fibres between muscle sections from *Erry*^{Tg/+}.PBS and *Erry*^{Tg/+}.sActRIIB mice. It is also noteworthy

that we found EDL muscle fibres of *Erry*^{Tg/+}.PBS and *Erry*^{Tg/+}.sActRIIB mice showed significantly higher oxidative capacity compared to counterpart muscles from WT and WT.sActRIIB mice respectively (Figure 6.7A and C). Same scenario of myofibres distribution of EDL muscles at metabolic level was seen in soleus muscle sections from the four genotypic groups (WT, *Erry*^{Tg/+} WT.sActRIIB and *Erry*^{Tg/+}.sActRIIB) (Figure 6.7B and D).

These data suggest that muscle-specific expression of *Erry* was sufficient to avert the reduction in oxidative capacity of hypertrophic muscle fibres developed following post-natal treatment with sActRIIB, thereby challenging the tread-off between myofibre size and its oxidative capacity (van Wessel et al., 2010).



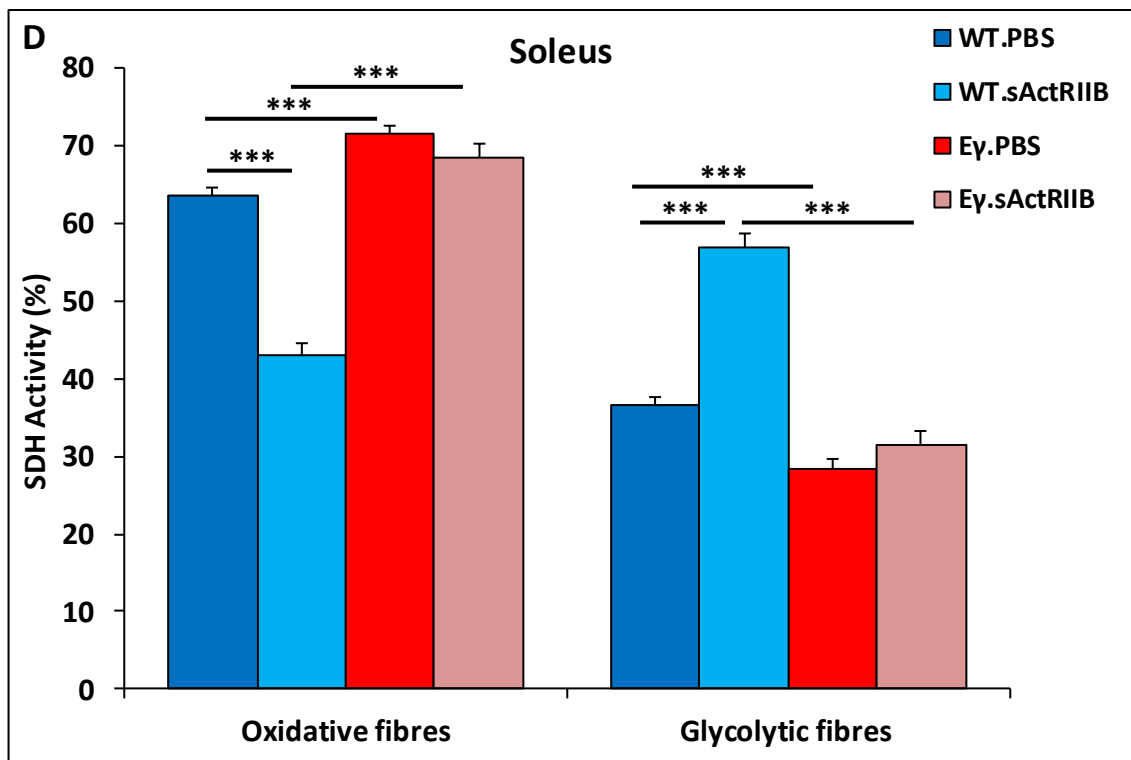
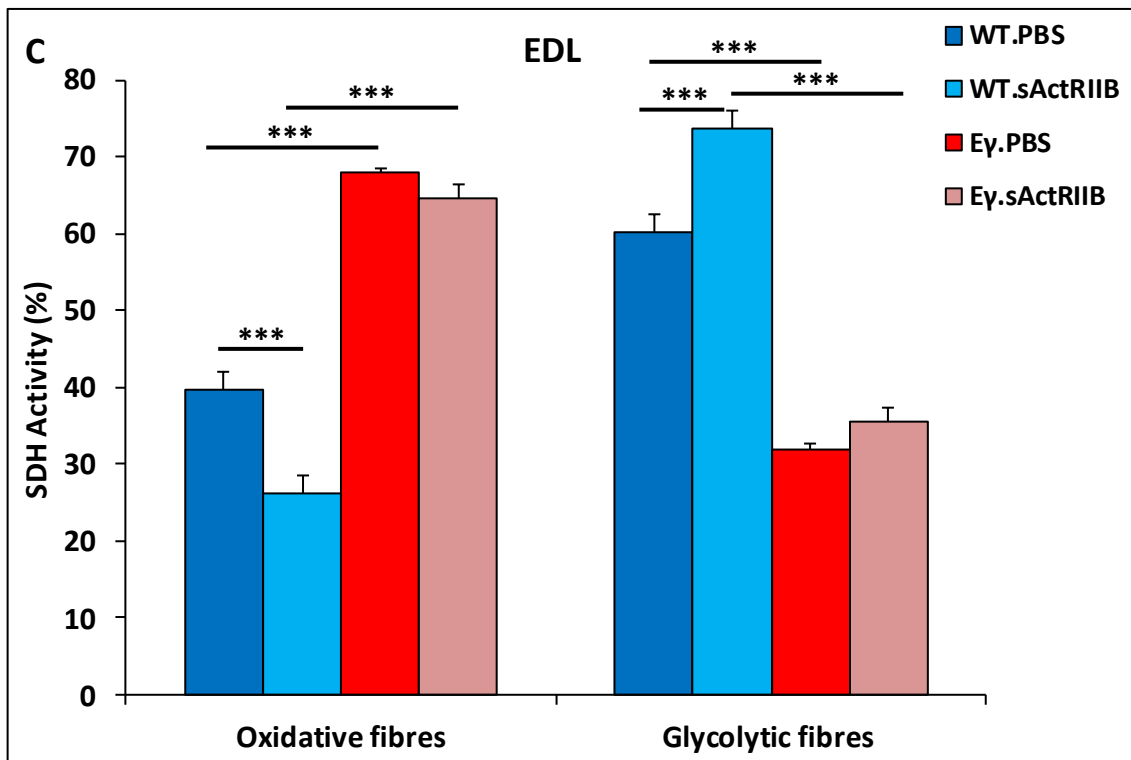


Figure 6.7. sActRIIB treatment induces glycolytic transformation of WT but not *Eγ* muscles

Post-natal inhibition of Myostatin doesn't affect muscle-specific *Eγ* myofibres profiling at metabolic level.

(A – B) Succinate dehydrogenase (SDH) staining Images of (EDL and soleus) muscles from WT, *Eγ*, WT.sActRIIB and *Eγ*.sActRIIB mice. Black fibres signify the SDH positive fibres (Oxidative fibres), and pale (white) fibres signify the SDH negative fibres (Glycolytic fibres).

(C) SDH-positive and negative fibre profile of EDL muscle from WT, *Eγ*, WT.sActRIIB and *Eγ*.sActRIIB mice.

(D) SDH-positive and -negative fibre profile of soleus muscle from WT, *Eγ*, WT.sActRIIB and *Eγ*.sActRIIB mice.

(*n*=5) three months old male WT and *Eγ* injected with PBS, and WT and *Eγ* injected with sActRIIB twice weekly for 8 weeks; Two-way ANOVA followed by Bonferroni post-tests to compare replicate means by row, ***=*p*<0.001.

6.8. Post-natal inhibition of Myostatin caused an increase in CSA of both SDH⁺ and SDH⁻ muscle fibres

We showed that 8 weeks of intraperitoneal injection of sActRIIB to inhibit Myostatin signalling didn't diminish the oxidative capacity of myofibres from hind limb muscles of *Erry^{Tg/+}* mice, while reduced proportion of oxidative fibres in WT muscles. However, whether the oxidative myofibre phenotypes developed in the *Erry^{Tg/+}* muscles would be able to get hypertrophied following sActRIIB treatment, remain to be elucidated. To that end we determined the cross-sectional area (CSA) of oxidative and glycolytic myofibres in EDL and soleus muscles from WT, *Erry^{Tg/+}* WT.sActRIIB and *Erry^{Tg/+}*.sActRIIB mice. A minimum of 150-200 measurements per myofibre types were taken in each muscle section (Figure 6.7A and B).

In both muscles examined, there was a significant increase in the CSA of both SDH⁺ and SDH⁻ muscle fibres of WT.sActRIIB and *Erry^{Tg/+}*.sActRIIB compared to WT.PBS and *Erry^{Tg/+}*.PBS mice (Figure 6.7A and B, and Figure 6.8A and B). More specifically, we found that both SDH⁺ and SDH⁻ myofibres of EDL muscles from *Erry^{Tg/+}*.sActRIIB displayed larger CSA than their counterpart from WT.sActRIIB animals (Figure 6.8A). Soleus muscles showed no significant difference neither between SDH⁺, nor SDH⁻ myofibres CSA from WT.sActRIIB and *Erry^{Tg/+}*.sActRIIB mice (Figure 6.8B).

Taken together, these data indicate that post-natal inhibition of Myostatin by systemic administration of sActRIIB that increased CSA of *Erry^{Tg/+}* muscle fibres which is associated with hyper-oxidative phenotype would challenge the trade-off that is thought to exist between oxidative capacity and fibre size (Van der Laarse WJ, 1998).

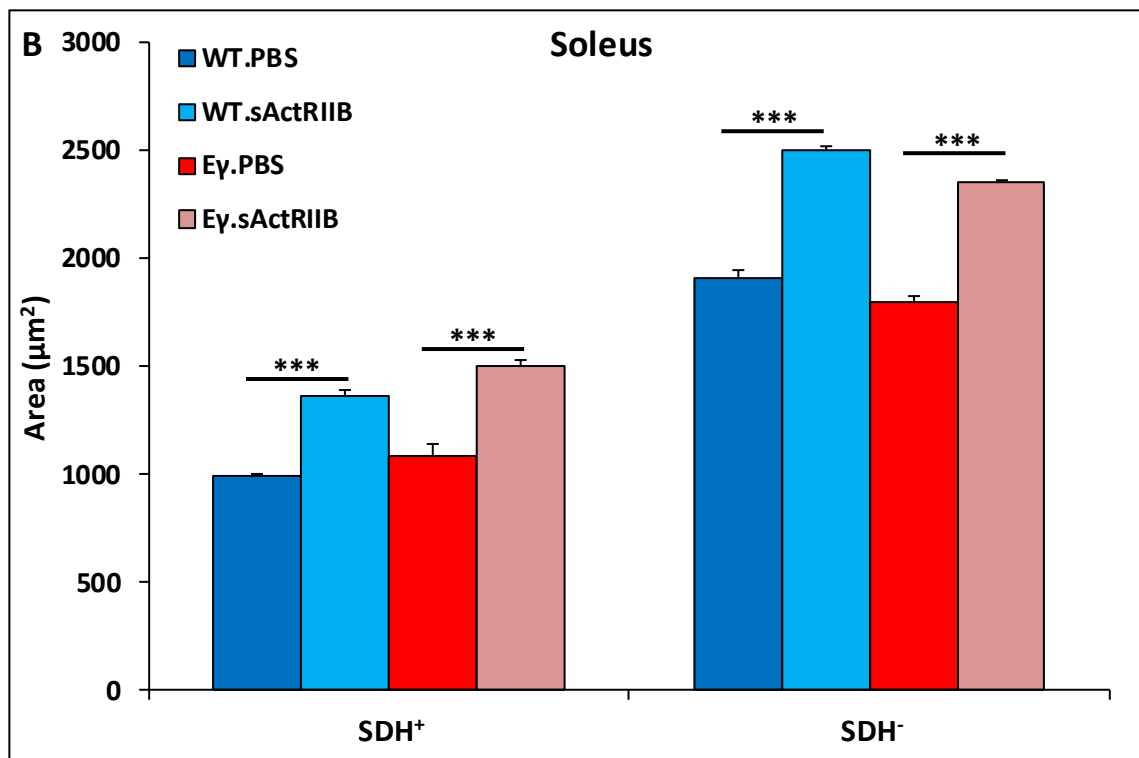
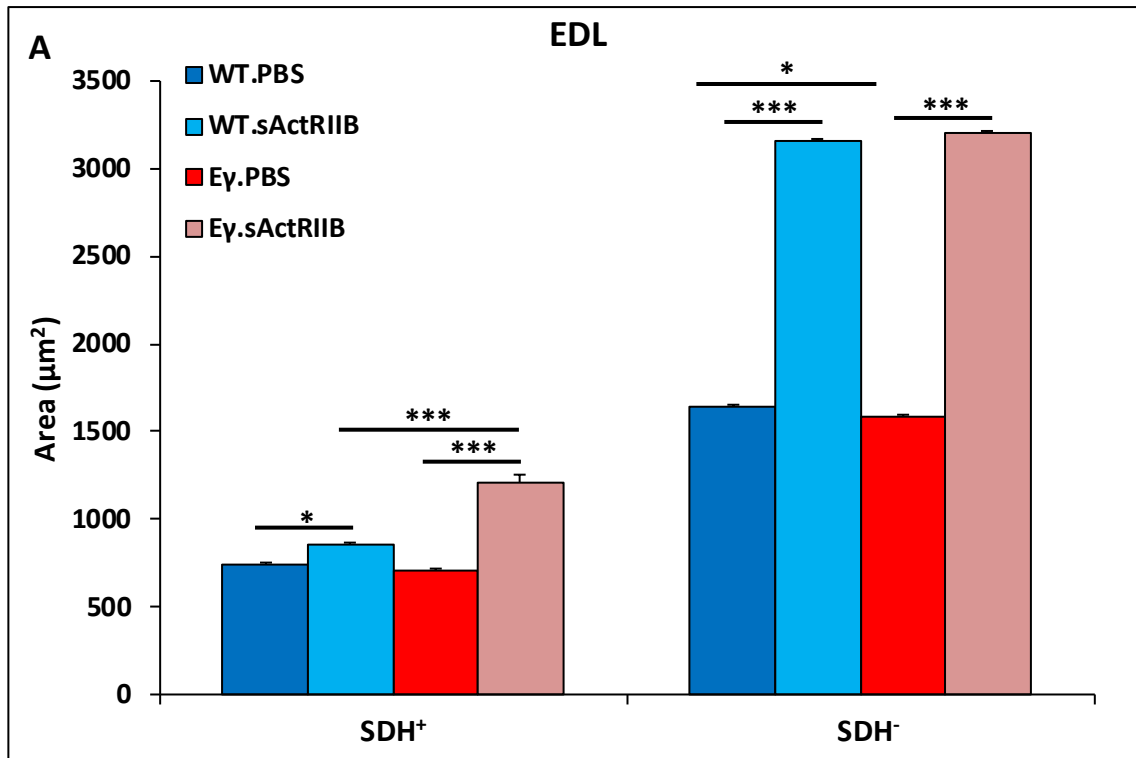


Figure 6.8. sActRIIB induces enlargement of both SDH⁺ and SDH⁻ myofibres

Post-natal inhibition of Myostatin in WT and *Eγ* leads to hypertrophy SDH⁺ and SDH⁻ muscle fibres.

(A) Quantification of SDH⁺ and SDH⁻ muscle fibres cross-sectional area in EDL muscles from WT, *Eγ*, WT.sActRIIB and *Eγ*.sActRIIB mice.

(B) Quantification of SDH⁺ and SDH⁻ muscle fibres cross-sectional area in soleus muscles from WT, *Eγ*, WT.sActRIIB and *Eγ*.sActRIIB mice.

(*n*=5) three months old male WT and *Eγ* injected with PBS, and WT and *Eγ* injected with sActRIIB twice weekly for 8 weeks; Two-way ANOVA followed by Bonferroni post-tests to compare replicate means by row, *=*p*<0.05 and ***=*p*<0.001

6.9. sActRIIB treatment increases blood vessels density of *Erry*^{Tg/+} muscles

We demonstrated fibres enlargement of muscles from *Erry*^{Tg/+} mice with no change in their oxidative capacity indicated by constant level of SDH expression.

It has been shown that the number of blood vessels per muscle fibre is correlated with myofibre cross-sectional area, thereby increases the average of oxygen diffusion to mitochondria (Plyley et al., 1998). Further studies have referred to a unique feature of skeletal muscle beds that the oxidative capacity of myofibres is tightly coupled to the tissue vascular supply (Fluck and Hoppeler, 2003, Pette and Staron, 2000). Moreover, investigation of the effect of sActRIIB treatment on mice as well as on C2C12 myotubes unveiled a drop in the expression of molecules that regulate muscle angiogenesis program and the capillary density (Relizani et al., 2014, Personius et al., 2010). In contrast, *Erry* has been described a key transcriptional regulator that induces skeletal muscles vascular features and oxidative phosphorylation properties (Narkar et al., 2011). Therefore, we here investigated the effect of administration of sActRIIB would have on the vascularization of muscles from *Erry*^{Tg/+} mice that displayed fibre hypertrophy while prevented the reduction of oxidative capacity might be prompted by Myostatin inhibition. To test this we examined the density of blood vessels in EDL muscle sections (n=5) from WT, *Erry*^{Tg/+}, WT.sActRIIB and *Erry*^{Tg/+}.sActRIIB mice using the endothelial cell marker (CD31) (Figure 6.9A).

We found that capillary to fibre ratio (C:F) was the highest in muscles of *Erry*^{Tg/+}.sActRIIB mice (Figure 6.9A and B). Of particular note, WT muscles were treated with sActRIIB did not show any significant difference in capillary density compared to muscles from WT.PBS. Interestingly, the 8 weeks injection of sActRIIB caused an increase in the number of capillaries serving each myofibre in muscles from *Erry*^{Tg/+} mice (Figure 6.9A and B). We also showed that the capillary density was higher in muscle from *Erry*^{Tg/+} than the control (Figure 6.9A and B).

These observations suggest that 8 weeks of treatment with sActRIIB was efficacious to induce capillary density, hence matched the increased size and oxidative capacity demands of hyper-oxidative hypertrophic myofibres from *Erry*^{Tg/+}.sActRIIB mice.

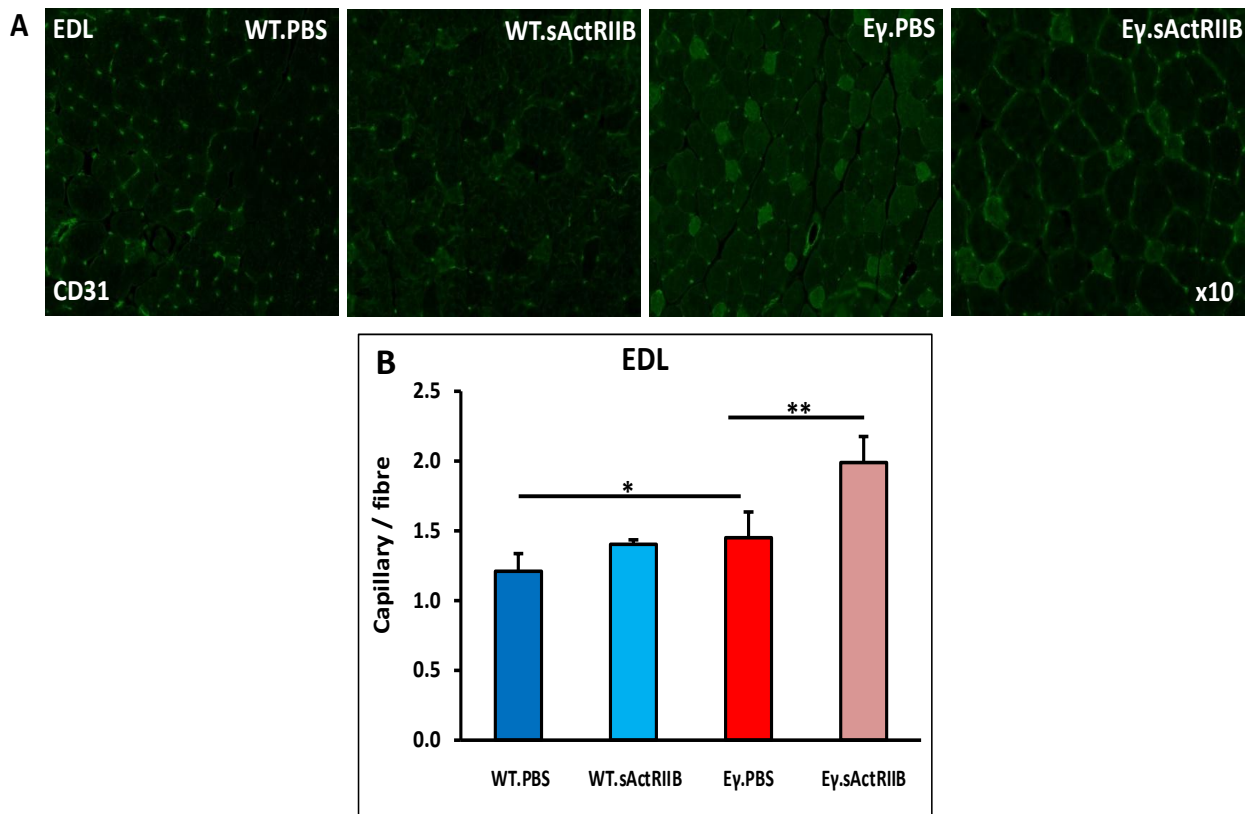


Figure 6.9. Post-natal inhibition of Myostatin induces blood vessels number in muscle-specific *Ey* mice

sActRIIB treatment increases capillary density of muscle-specific *Ey* muscles but not WT.

(A) Muscle capillary density determined by CD31 staining on EDL muscle sections from WT, *Ey*, WT.sActRIIB and *Ey*.sActRIIB mice.

(B) Quantification of blood vessels per myofibre in EDL muscles.

($n=5$) three months old male WT and *Ey* injected with PBS, and WT and *Ey* injected with sActRIIB twice weekly for 8 weeks; Two-way ANOVA followed by Bonferroni post-tests to compare replicate means by row, $*=p<0.05$ and $**=p<0.01$.

6.10. Inhibition of Myostatin causes elevation in level of superoxide in WT but not in *Erry*^{Tg/+} muscles

It has been documented that Reactive Oxygen Species (ROS) are produced through the mitochondrial electron transport chain (ETC) pathway of the dysfunctional mitochondria (Harper et al., 2004). Further investigation of transcriptome profiling of skeletal muscles were treated with sActRIIB-Fc has shown a remarkable reduction in expression level of genes that regulate mitochondrial functions (Rahimov et al., 2011). In contrast, previous work has revealed a vital role of *Erry* in regulating of mitochondrial biogenesis and functions in skeletal muscles (Rangwala et al., 2010), therefore its knockout severely impaired mitochondrial formation hence resulted in high level of ROS production (Murray et al., 2013). Here we investigated whether the deficit in mitochondrial enzyme activity that we showed in WT muscles followed post-natal inhibition of Myostatin would induce ROS level, as well as sought to determine the potential of *Erry* to mitigate ROS production. Therefore, we evaluated the level of superoxide using Dihydroethidium (DHE) dye (Bindokas et al., 1996, Li et al., 2003) in EDL muscle sections (n=5) from WT, *Erry*^{Tg/+} WT.sActRIIB and *Erry*^{Tg/+}.sActRIIB mice (Figure 6.10A). We found elevated levels of superoxide indicated by high DHE intensity in both small (slow oxidative) and large (fast glycolytic) myofibres in EDL muscles from WT.sActRIIB compared to counterpart muscles from WT.PBS mice (Figure 6.10A and B). Interestingly, introduction of sActRIIB into *Erry*^{Tg/+} muscles did not induce DHE intensity (Figure 6.10 A and B). We also showed that ROS levels was significantly lower in EDL muscles from *Erry*^{Tg/+} compared to WT (Figure 6.10 A and B). These data suggest that post-natal inhibition of Myostatin using systemic administration of sActRIIB leads to increase ROS level in WT muscles. However, same treatment did not affect superoxide level in muscles from *Erry*^{Tg/+} mice.

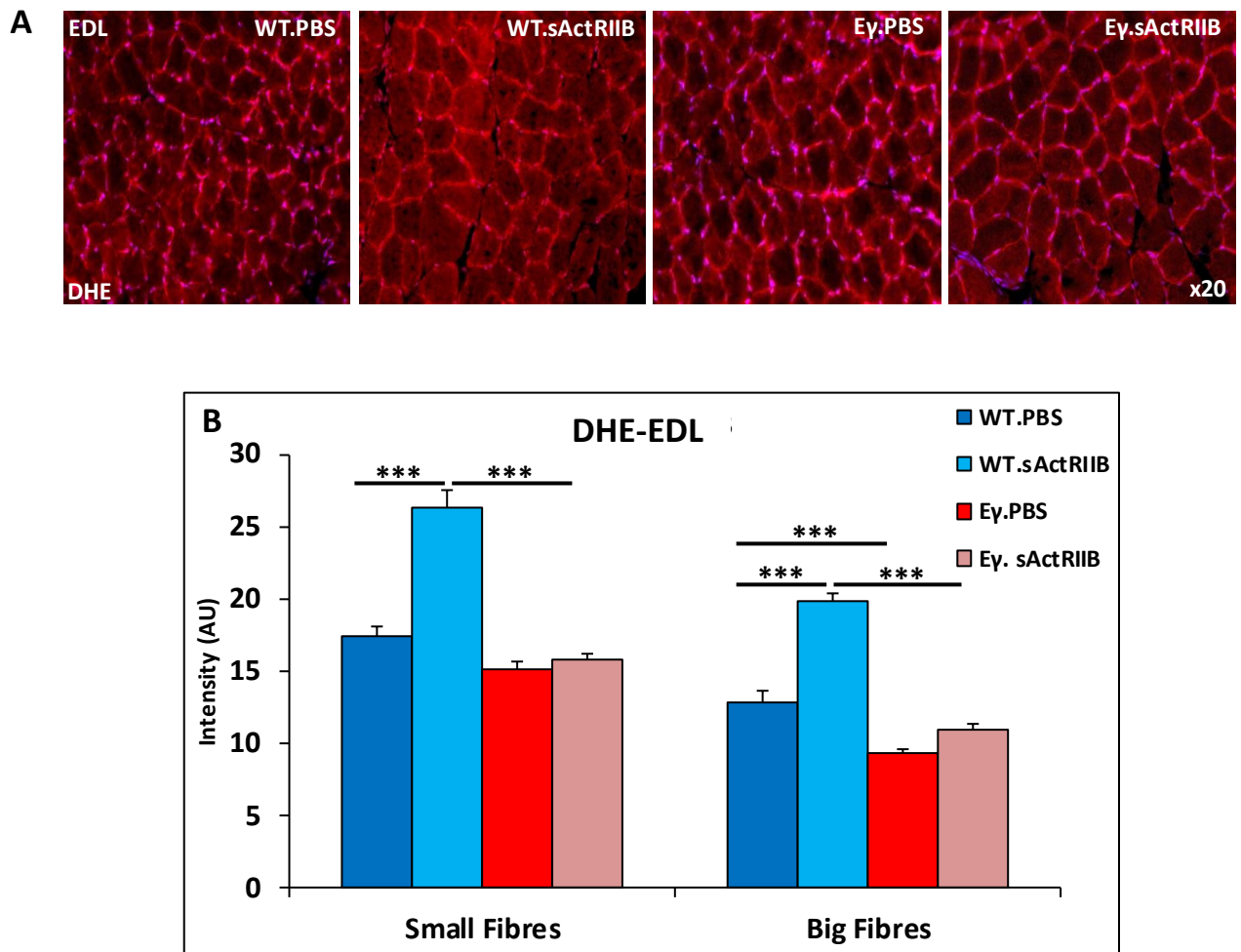


Figure 6.10. *Ey* overexpression is necessary to mitigate ROS emission

Muscle-specific expression of *Ey* prevents post-natal inhibition of Myostatin to promote excessive level of reactive oxygen species (ROS).

(A) DHE fluorescence in the body of EDL muscle fibres from WT, *Ey*, WT.sActRIIB and *Ey*.sActRIIB mice.

(B) Quantification of DHE intensity in small and large myofibres in EDL muscles.

($n=5$) three months old male WT and *Ey* injected with PBS, and WT and *Ey* injected with sActRIIB twice weekly for 8 weeks; Two-way ANOVA followed by Bonferroni post-tests to compare replicate means by row, ***= $p<0.001$.

6.11. Muscle-specific expression of *Erry* prevents the decrease in connective tissue level that induced by sActRIIB treatment in WT muscles.

It was well established that extracellular matrix (ECM) of skeletal muscle is a dynamic tissue that it is essential for myofibres force transmission and protection of these fibres against injury (Alameddine, 2012, Gustafsson, 2011). Further investigations have reported that the molecules which are constituting the ECM vary depending on the mechanical demands of the tissue that helps to optimize efficient force transmission (Koskinen et al., 2004, Mackey et al., 2004). The main structural and functional component of muscle ECM is collagen (Heinemeier et al., 2007). Moreover, it was well established that skeletal muscle fibres are protected from contraction induced damages by a number of proteins that collectively known as the dystrophin-glycoprotein complex (DGC) (Gumerson and Michele, 2011). Dystrophin is the largest identified member of the DGC that with the other members link the cytoskeleton to collagen in the ECM of perimysium and endomysium (Gumerson and Michele, 2011, Gillies and Lieber, 2011). In addition, it has been revealed that laminin links the ECM to the DGC through its ability to bind collagen with the members of DGC (Gao and McNally, 2015).

Previous work has shown that the endomysium of muscles from *Myostatin* null mice is thinner than the counterpart muscles from WT mice (Elashry et al., 2012). Moreover, a number of studies have reported that glycolytic/fast contraction muscle fibres which characterised by large cross-sectional area are invested with less amount of ECM than the oxidative/slow contraction fibres (Kovanen et al., 1980). As Myostatin might potentially contribute in regulating and promoting of muscle connective tissue, we here investigated whether post-natal inactivation of this negative regulator of skeletal muscle development by systemic administration of sActRIIB would affect the whole amount of ECM in muscles from WT and *Erry*^{Tg/+} mice. To that end, we examined the relationship between MHC fibres and expression of collagen type IV, dystrophin and laminin within muscle fibres of the same genotypes, and we also compared the amount of these proteins in muscles from each cohort using semi-quantitative immunofluorescence methods. The protocols that have been developed allowed us to determine expression levels of particular proteins at the sarcolemma based on the intensity of the signal (Schindler et al., 2016, Cirak et al., 2012),

and correlate this with fibres phenotypes. Furthermore, we measured the thickness of the expression domain size (de Bruin et al., 2014) for each of the three marker proteins.

Muscle sections of fast and slow phenotypes (EDL and soleus respectively) (n=5) from WT, *Erry*^{Tg/+}, WT.sActRIIB and *Erry*^{Tg/+}.sActRIIB mice were immunostained using antibodies for (MHCIIB, collagen type IV, dystrophin and laminin) (Figures 6.11A, 6.12A, 6.13A and 6.14A) to determine the intensity and the thickness of these proteins between MHCIIB⁺ and MHCIIB⁻ in EDL muscles. As we found that soleus muscles of WT did not contain MHCIIB⁺, and as we showed sActRIIB treatment did not change MHC profiling in any muscle of both genotypes (WT and *Erry*^{Tg/+}), we used soleus muscle sections that were immunostained previously for antibodies against (MHCIIA and MHCI) (Figure 6.4) as a guide to measure the intensity and thickness of collagen type IV, dystrophin and laminin between MHCI⁺ only in serial sections (Figures 6.11B, 6.12B, 6.13B and 6.14B). Connective tissue intensity and thickness between approximately 50 fibres of same MHC isoform (MHCIIB⁺-IIB⁺ and MHCIIB⁻-IIB⁻) in EDL muscles, and between (MHCI⁺-I⁺) in soleus muscles from the four cohorts were measured.

Using these techniques we first examined the expression level and domain size of collagen IV in the endomysium between MHCIIB⁻ and MHCIIB⁺ of EDL muscles within the individual cohort. Then we compared these parameters in the endomysium between MHCIIB⁻ and MHCIIB⁺ in EDL muscles, and between MHCI⁺ in soleus muscles from the four cohorts of this study (WT, *Erry*^{Tg/+}, WT.sActRIIB and *Erry*^{Tg/+}.sActRIIB). Our findings supported previous observations (Kovanen et al., 1980) that the collagen IV expression level and domain size were significantly greater in the endomysium between MHCIIB⁻ relative to MHCIIB⁺ in all EDL muscle samples examined from the four genotypic groups (Figure 6.12A, C and D). Quantification of signal intensity as well as thickness between MHCIIB⁻ and MHCIIB⁺ in EDL muscles, and between MHCI⁺ in soleus muscles of all cohorts demonstrated that 8 weeks of sActRIIB treatment caused an overall decrease in the collagen type IV in all myofibres of WT.sActRIIB muscles compared to the counterpart of WT.PBS. Importantly, we found that muscle-specific expression of *Erry* that induces oxidative metabolism was sufficient to prevent the reduction in intensity and thickness of collagen IV, between MHCIIB⁻ and

MHCIIB⁺ in EDL muscles (Figure 6.12C and D), and between MHCI⁺ in soleus muscles (Figure 6.12E and F), following post developmental inhibition of Myostatin using activin ligand trap.

Next we examined intracellular membrane associated protein (dystrophin), as well as extracellular component that link the myofibre cytoskeleton to the collagen (laminin).

We found that the expression of these proteins displayed marked changes in relation to MHCIIIB within muscles of individual genotypic group. Of particular note, the expression of dystrophin and laminin based on intensity and thickness measurements were significantly greater in the endomysium between MHCIIIB⁻ than MHCIIIB⁺ myofibre in EDL muscles examined from the four cohorts (Figure 6.13A, C and D) and (Figure 6.14A, C and D) respectively. We next examined the signal intensity and thickness in the endomysium between MHCIIIB⁻ and MHCIIIB⁺ in EDL muscles, and in the endomysium between MHCI⁺ in soleus muscles from mice treated with PBS versus mice treated with sActRIIB. We found that the intensity and thickness of dystrophin and laminin were significantly lower in between all MHC cohorts (MHCIIIB⁻, MHCIIIB⁺ and MHCI⁺) of EDL and soleus muscles from WT.sActRIIB compared to their counterpart from WT.PBS animals (Figure 6.13A-F) and (Figure 6.14A-F) respectively. Interestingly, we found that expression of *Erry* had profound impact on the intracellular and extracellular protein levels. More specifically, the hypertrophic MHCIIIB⁻ and MHCIIIB⁺ in EDL muscles, and hypertrophic MHCI⁺ in soleus muscles from *Erry*^{Tg/+}.sActRIIB mice showed similar intensity and thickness of dystrophin and laminin following 8 weeks of twice weekly injection of sActRIIB (Figure 6.13A-F) and (Figure 6.14A-F).

Together, these data firstly indicate that fibre type based on myosin Heavy Chain IIB influences the level of collagen IV, dystrophin and laminin within the same genotype muscles. Secondly, the levels of all three proteins examined were decreased in muscles from WT.sActRIIB compared to WT.PBS. Interestingly, we show that levels of the examined protein at sarcolemma does not change in muscles of *Erry*^{Tg/+} mice following sActRIIB treatment, which suggest a robust impact of the metabolic programme imparted by *Erry* overexpression in determinant of connective tissue level.

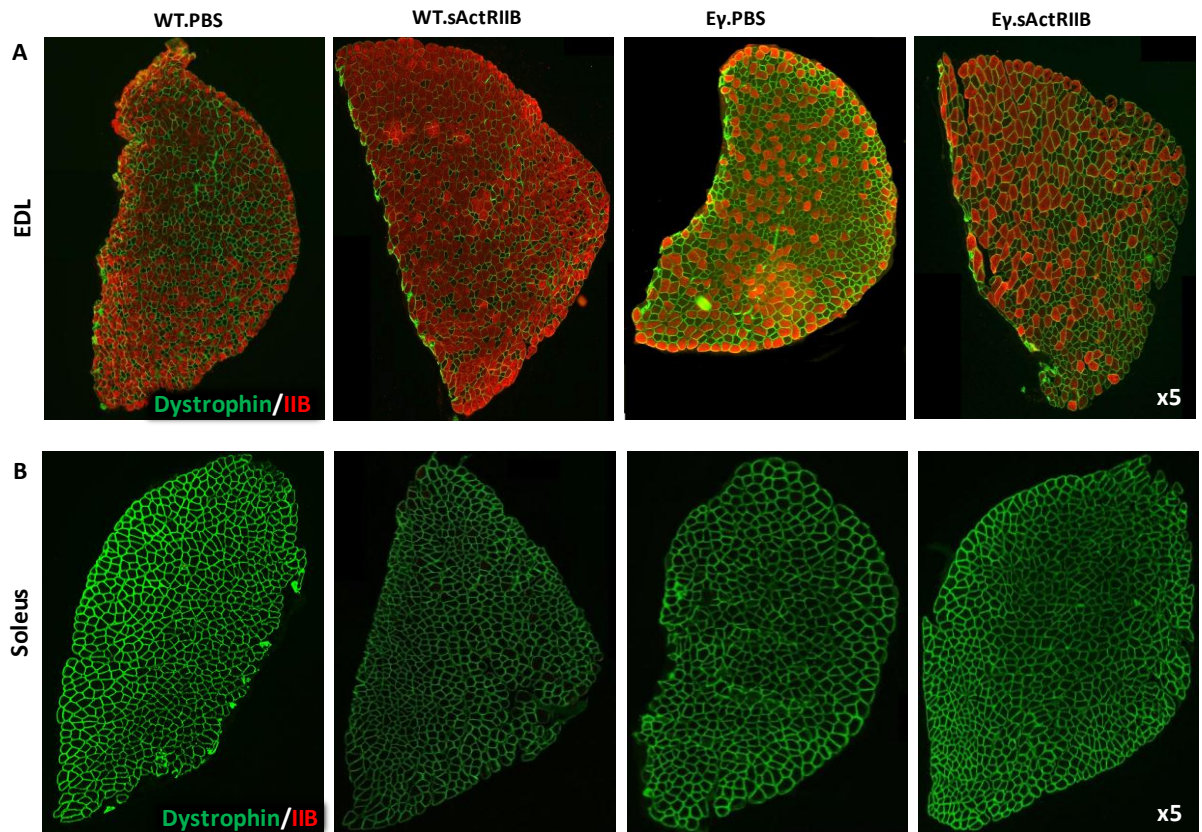


Figure 6.11. Expression of dystrophin in the entire EDL and soleus muscle sections

A) Immunohistochemical images of EDL muscles from WT, *E γ* , WT.sActRIIB and *E γ* .sActRIIB mice. Green colour signifies the expression of dystrophin, with MHCIIb appearing as red.

B) Immunohistochemical images of soleus muscles from WT, *E γ* , WT.sActRIIB and *E γ* .sActRIIB mice. Green colour signifies the expression of dystrophin, with no MHCIIb⁺ in these sections.

(*n*=5) three months old male WT and *E γ* injected with PBS, and WT and *E γ* injected with sActRIIB twice weekly for 8 weeks.

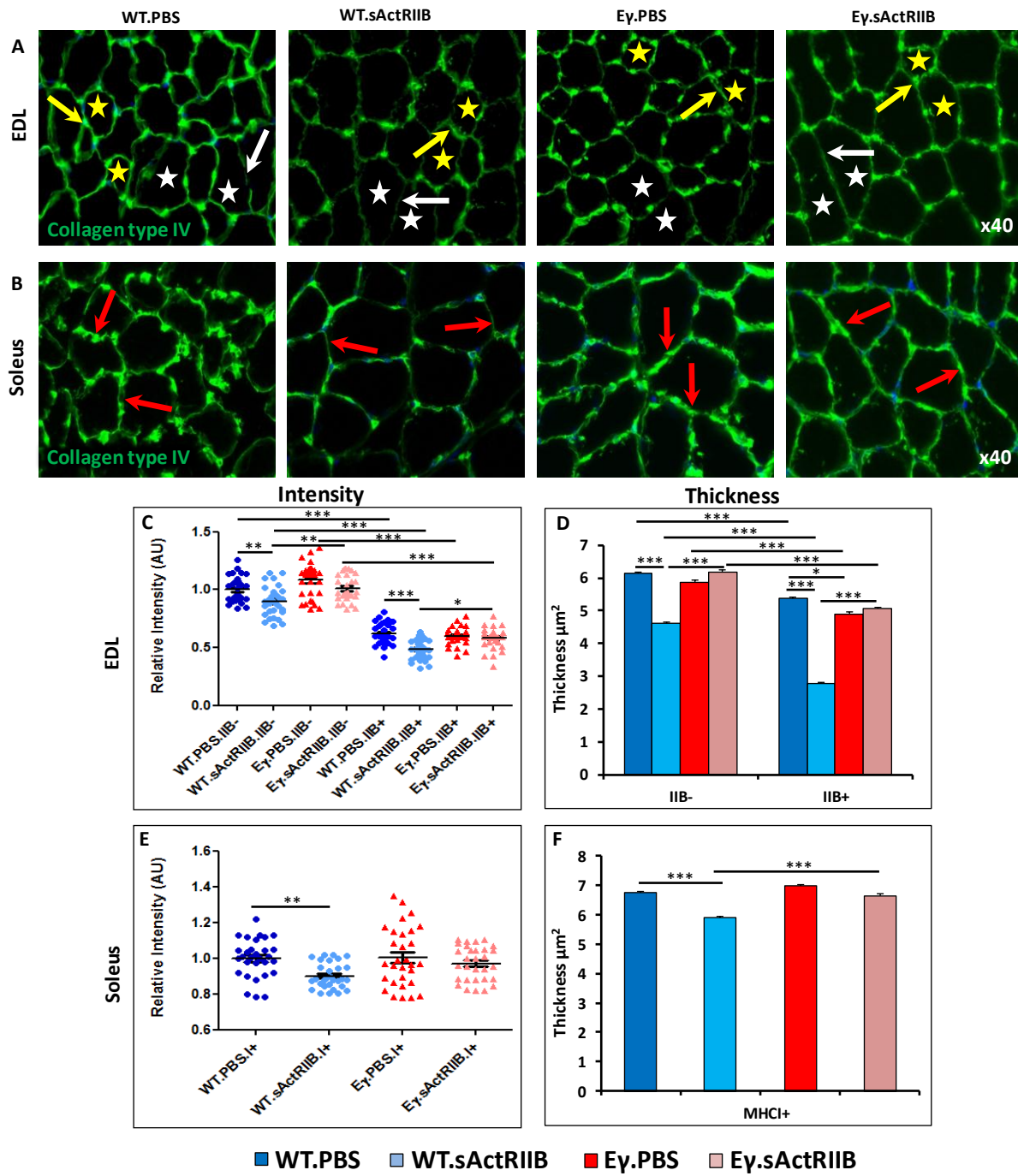


Figure 6.12. sActRIIB treatment caused a reduction in collagen IV intensity and thickness in muscles from WT but not *Eγ*

A) Serial sections of EDL muscles staining with MHCIIIB and collagen IV. MHCIIIB was used to identify MHCIIIB⁻ (yellow stars) and MHCIIIB⁺ fibres (white stars). Expression of collagen IV more robust in ECM between two MHCIIIB⁻ fibres (yellow arrow) compared to that between MHCIIIB⁺ fibres (white arrows) in wild type muscle. Same relationship with lower levels in WT.sActRIIB muscles. Similar expression domain in ECM between MHCIIIB⁻ (yellow arrows) as well as MHCIIIB⁺ (white arrows) of EDL muscles from *Eγ* and *Eγ*.sActRIIB mice.

B) Serial sections of soleus muscles staining with MHCIIIB and collagen IV. Lower level of collagen IV between MHCIIIB⁺ (red arrows) in WT.sActRIIB compared to WT.PBS muscles. Similar expression domain in ECM between MHCII⁺ (red arrows) soleus muscles from *Eγ* and *Eγ*.sActRIIB mice.

C) Expression of collagen IV quantifies by intensity by setting standard value of 1 for the level between MHCIIIB⁻ fibres from WT mice.

D) Collagen IV expression quantifies in terms of thick domain in EDL muscles.

E) Expression of collagen IV quantifies by intensity by setting standard value of 1 for the level between MHCII⁺ fibres from WT mice.

F) Collagen IV expression quantifies in terms of thick domain in soleus muscles.

(*n*=50) three months old male WT and *Eγ* injected with PBS, and WT and *Eγ* injected with sActRIIB twice weekly for 8 weeks; Two-way ANOVA followed by Bonferroni post-tests to compare replicate means by row, and Two-tailed Student's t-test for independent variables, *=*p*<0.05, **=*p*<0.01 and ***=*p*<0.001.

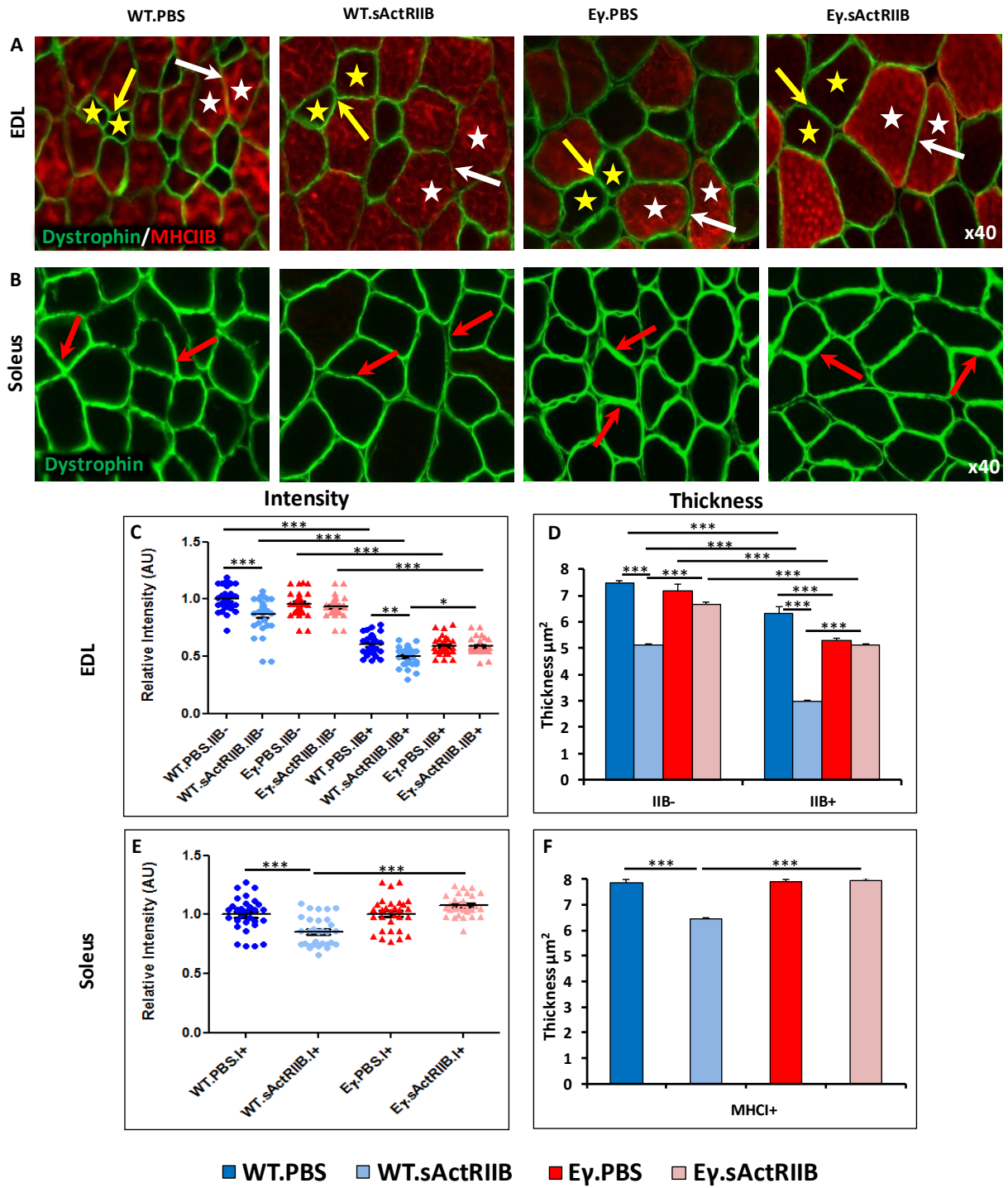


Figure 6.13. sActRIIB treatment caused a reduction in dystrophin intensity and thickness in muscles from WT but not *Eγ*

A) Serial sections of EDL muscles staining with MHCIIB and dystrophin. MHCIIB expression in red and dystrophin in green. MHCIIB was used to identify MHCIIB⁻ (yellow stars) and MHCIIB⁺ fibres (white stars). Expression of dystrophin more robust in ECM between two MHCIIB⁻ fibres (yellow arrow) compared to that between MHCIIB⁺ fibres (white arrows) in wild type muscle. Same relationship with lower levels in WT.sActRIIB muscles. Similar expression domain in ECM between MHCIIB⁻ (yellow arrows) as well as MHCIIB⁺ (white arrows) of EDL muscles from *Eγ* and *Eγ*.sActRIIB mice.

B) Serial sections of soleus muscles staining with MHCIIB and dystrophin. Lower level of dystrophin between MHCI⁺ (red arrows) in WT.sActRIIB compared to WT.PBS muscles. Similar expression domain in ECM between MHCI⁺ (red arrows) soleus muscles from *Eγ* and *Eγ*.sActRIIB mice.

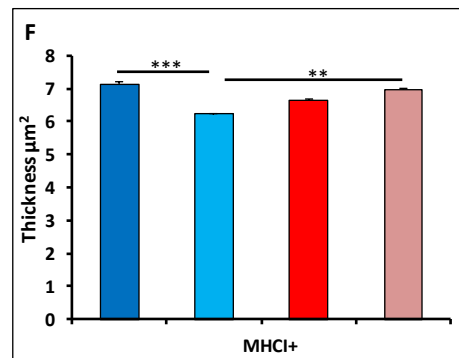
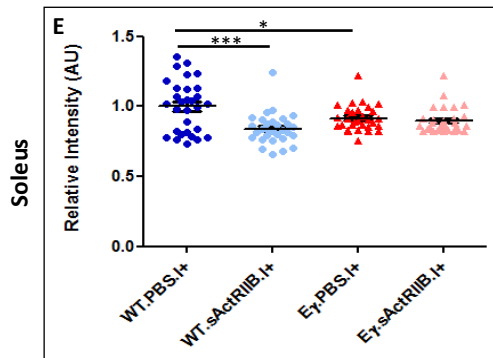
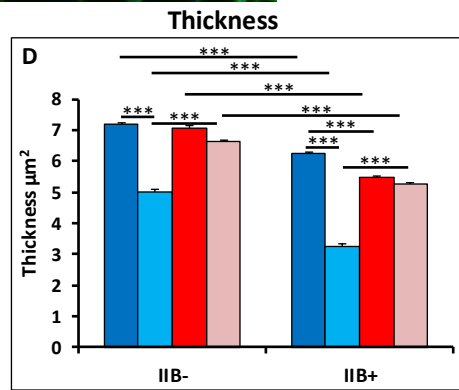
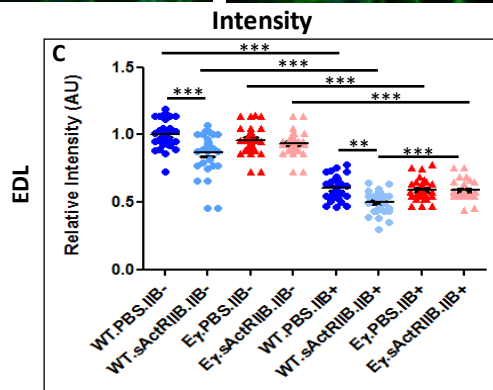
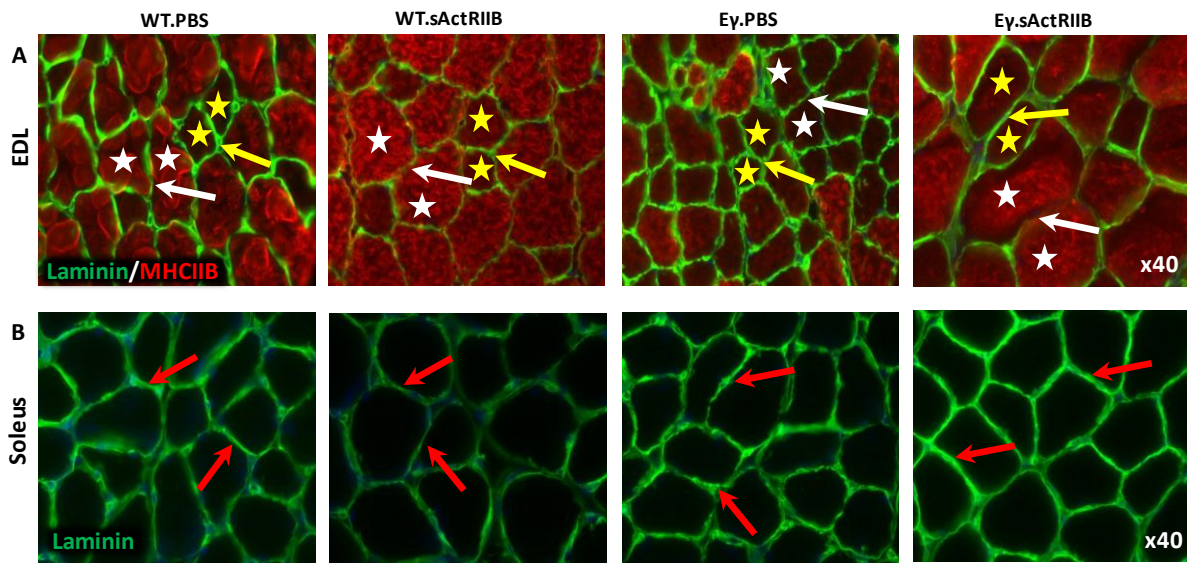
C) Expression of dystrophin quantifies by intensity by setting standard value of 1 for the level between MHCIIB⁻ fibres from WT mice.

D) Dystrophin expression quantifies in terms of thick domain in EDL muscles.

E) Expression of dystrophin quantifies by intensity by setting standard value of 1 for the level between MHCI⁺ fibres from WT mice.

F) Dystrophin expression quantifies in terms of thick domain in soleus muscles.

(*n*=50) three months old male WT and *Eγ* injected with PBS, and WT and *Eγ* injected with sActRIIB twice weekly for 8 weeks; Two-way ANOVA followed by Bonferroni post-tests to compare replicate means by row, and Two-tailed Student's t-test for independent variables, *=*p*<0.05, **=*p*<0.01 and ***=*p*<0.001.



■ WT.PBS ■ WT.sActRIIB ■ Ey.PBS ■ Ey.sActRIIB

Figure 6.14. sActRIIB treatment caused a reduction in laminin intensity and thickness in muscles from WT but not *Eγ*

A) Serial sections of EDL muscles staining with MHCIIB and laminin. MHCIIB expression in red and laminin in green. MHCIIB was used to identify MHCIIB⁻ (yellow stars) and MHCIIB⁺ fibres (white stars). Expression of laminin more robust in ECM between two MHCIIB⁻ fibres (yellow arrow) compared to that between MHCIIB⁺ fibres (white arrows) in wild type muscle. Same relationship with lower levels in WT.sActRIIB muscles. Similar expression domain in ECM between MHCIIB⁻ (yellow arrows) as well as MHCIIB⁺ (white arrows) of EDL muscles from *Eγ* and *Eγ*.sActRIIB mice.

B) Serial sections of soleus muscles staining with MHCIIB and laminin. Lower level of laminin between MHCI⁺ (red arrows) in WT.sActRIIB compared to WT.PBS muscles. Similar expression domain in ECM between MHCI⁺ (red arrows) soleus muscles from *Eγ* and *Eγ*.sActRIIB mice.

C) Expression of laminin quantifies by intensity by setting standard value of 1 for the level between MHCIIB⁻ fibres from WT mice.

D) Laminin expression quantifies in terms of thick domain in EDL muscles.

E) Expression of laminin quantifies by intensity by setting standard value of 1 for the level between MHCI⁺ fibres from WT mice.

F) Laminin expression quantifies in terms of thick domain in soleus muscles.

(*n*=50) three months old male WT and *Eγ* injected with PBS, and WT and *Eγ* injected with sActRIIB twice weekly for 8 weeks; Two-way ANOVA followed by Bonferroni post-tests to compare replicate means by row, and Two-tailed Student's t-test for independent variables, *=*p*<0.05, **=*p*<0.01 and ***=*p*<0.001.

6.12. Discussion

The important health implications of maintaining an adequate level of skeletal muscle size and functions, and its consequences on the life quality has been recognized during the past few years by a number of researchers (Anker et al., 1997, Wolfe, 2006, Pistilli et al., 2011). It has been established that the skeletal muscle has internal mechanisms to prevent overgrowth. This crucial function is performed at least in part by members of the Transforming Growth Factor- β (TGF- β) family, especially *Myostatin* (McPherron et al., 1997). *Myostatin* signals through its transmembrane activin receptor IIB (ActRIIB), and suppression of this pathway induces skeletal muscle growth (Lee and McPherron, 2001, Schuelke et al., 2004). Therefore, a number of studies have used different strategies that interfere with the ActRIIB receptor mediated *Myostatin* pathway in order to ameliorate muscle wasting through either injection of sActRIIB-Fc (Pistilli et al., 2011, George Carlson et al., 2011), AAV-mediated gene transfer (Morine et al., 2010), or antibodies direct against the ActRIIB receptor (Lach-Trifilieff et al., 2014). However, it remains a matter to determine whether the increase in muscle mass following post-natal blocking of *Myostatin* would have any functional benefits, because we and others have shown a reduction in mitochondrial quantity, oxidative capacity and capillary density thereby loss of specific force and increase fatigability of large muscles from *Myostatin* null mice (Amthor et al., 2007, Mendias et al., 2006). Previous studies have revealed a remarkable decrease in the markers of oxidative energy production capacity of skeletal muscle following *Myostatin* blocking (Rahimov et al., 2011, Relizani et al., 2014). Moreover, it has been documented that *Myostatin* inhibition leads to compromise muscle capillary density (Personius et al., 2010). In addition, a marked decline in the expression levels of biomarker genes that regulate mitochondrial functions has been found in muscles were treated with sActRIIB-Fc (Rahimov et al., 2011). On the contrary, estrogen-related receptor gamma (*Erry*) has been identified as a key molecule that capable to enhance muscle fibre oxidative properties in parallel with promoting a network of genes that regulate skeletal muscle energy production and vascularization (Alaynick et al., 2007, Narkar et al., 2011, Matsakas et al., 2012b). Furthermore, both Rangwala and Dufour's groups have revealed a vital role of *Erry* in regulating of mitochondrial biogenesis and biomarker genes that encoding slow muscle fibres contractile pathways (Rangwala et al., 2010, Dufour et al., 2007).

Therefore, we asked whether *Erry* and its metabolic and angiogenic targets are able to prevent muscle's metabolic and functional deficits that resulted from Myostatin inhibition. And we sought to identify to what extent that inhibition of Myostatin at a post-natal stage in *Erry*^{Tg/+} mice by weekly injection of sActRIIB would affect oxidative features that imparted by *Erry* overexpression.

Our analysis shows that 8 weeks of a weekly injection of sActRIIB caused a significant increase in the body mass of both WT and *Erry*^{Tg/+} mice. Further, examination of isolated muscles showed an increase in the mass of all examined muscles from WT and *Erry*^{Tg/+} mice following sActRIIB treatment compared to age-matched control animals. We provided evidence that the increase in muscle mass was not due to an increase in muscle fibre numbers, but resulted from an increase in CSA of all MHC fibre types. We showed that the injection of sActRIIB induced a decrease in the oxidative capacity of the muscle in WT mice as indicated by the low proportion of SDH⁺ fibres. Strikingly, sActRIIB did not cause a reduction in muscle oxidative capacity of *Erry*^{Tg/+} mice indicated by the same proportion of oxidative myofibres (SDH⁺) in both *Erry*^{Tg/+}.PBS and *Erry*^{Tg/+}.sActRIIB muscles. Furthermore, this study showed that the high level of oxidative capacity in muscles from *Erry*^{Tg/+}.PBS and *Erry*^{Tg/+}.sActRIIB was accompanied by an elevated number of blood vessels. However, sActRIIB treatment does not cause any change in capillary density of WT muscles. We also provided evidence that the diminish in the mitochondrial enzyme (SDH) activity in WT muscles following 8 weeks of sActRIIB injection accompanied with an increase in ROS level indicated by high intensity of DHE. However, muscles of *Erry*^{Tg/+}.PBS and *Erry*^{Tg/+}.sActRIIB mice display a similar level of DHE intensity. Additionally, our observations demonstrated lower levels of intensity and thickness of collagen IV, dystrophin and laminin in WT muscles injected with sActRIIB compared to the control. Importantly, muscles from *Erry*^{Tg/+}.PBS and *Erry*^{Tg/+}.sActRIIB mice show no significant differences in either intensity or thickness of all examined proteins.

Despite the enlargement of individual muscles mass from *Mtn*^{-/-} and *Mtn*^{-/-}/*Erry*^{Tg/+} compared to their counterparts from WT mice, we have previously shown that all three genotypic groups displayed same body weight, which might attribute to a decrease of fat deposition induced by germline deletion of *Myostatin* (Lebrasseur, 2012). However, data of

present study demonstrated that weekly IP injection of sActRIIB for 8 weeks which antagonize signalling mediated by Myostatin caused a significant increase in body and all examined muscles mass of both WT and *Erry^{Tg/+}* mice. Previous studies have reported that there is an age window for inducing body and muscle mass by antagonizing action of Myostatin might be limited to relatively early post-natal life (Qiao et al., 2009, Qiao et al., 2008). Subsequently, there was no change in body mass following Myostatin blocking at 16 weeks age (Qiao et al., 2008). Therefore, we performed Myostatin inhibition using sActRIIB injection for 8 weeks within this period (4-12 weeks), and we showed that the increase in body mass can be brought about when the animal at this age. A number of studies have reported a significant increase in body weight together with a robust growth of individual skeletal muscle following four months administration of sActRIIB to wild type mice (Relizani et al., 2014, Lee et al., 2005). Further investigations have demonstrated that treatment of healthy adult mice using a soluble form of activin receptor for four weeks resulted in clearly hypertrophied muscles without any effect on fat mass in mice fed a standard diet (Whittemore et al., 2003, Akpan et al., 2009). Moreover, a study by Benny Klimek et al found an increase in abdominal fat pad weight following injection of athymic *nude* mice with a chinese hamster ovary (CHO) cell line engendered to secrete the sActRIIB (Benny Klimek et al., 2010). By a way of explanation, the significant increase in body weight of both genotypic groups (WT and *Erry^{Tg/+}*) in present study following 8 weeks of weekly injection of sActRIIB might in addition to muscle hypertrophy, it attributes to the increase or at least no change in fat mass (Benny Klimek et al., 2010, Whittemore et al., 2003), which was decreased in mice with genetic alteration of *Myostatin* (Lebrasseur, 2012), thereby no difference in body weight of WT and *Mtn^{-/-}* mice as we showed previously (Figure 3.2). We believe that muscle response to post-natal blocking of Myostatin in term of secreting myokines that mediate the cross-talking between skeletal muscle and adipose tissue, was however very slow, hence did not affect fat mass.

Our data examining individual muscle weights showed that the changes were dependent on specific muscles. We found at 12 weeks old age, the EDL, gastrocnemius and TA muscles from sActRIIB treated WT and *Erry^{Tg/+}* animals were significantly heavier than muscles from the untreated mice, whereas soleus muscle was only significantly heavier in WT treated but not in *Erry^{Tg/+}* treated mice compared to the controls. Expanding on this finding, all muscles

from WT.sActRIIB showed high percentages of increase in their weights than those from *Erry^{Tg/+}*.sActRIIB mice compared to the untreated muscles from both cohorts respectively. These findings supported observations of Matsakas et al (Matsakas et al., 2009), that referred to a varying degree of muscles response to post-natal inhibition of Myostatin using AAV8ProMyo injection. Further investigation of Myostatin inhibition effects on muscles mass from aged mice (20 months) using same treatment above (AAV8ProMyo) displayed a disparate significant increase in muscle weights from treated animals compared to the aged-match controls (Collins-Hooper et al., 2014). Giving our interpretation, the differences in muscle weights response to the sActRIIB treatment could be attributed to infiltration rate of the treatment through connective tissue compartments, that is supposed to differ in relative to muscle fibre profile (Elashry et al., 2012). Alternatively, we believe that some muscle may have received more sActRIIB treatment than the others, however, even if that occurred, it would have only a minor impact on muscle weights.

To investigate this further, we examined whether the increase in muscles mass following sActRIIB injection was due to an increase in muscle fibre number, size, or both of them as we noticed previously in muscles from *Mtn^{-/-}* mice. In agreement with aforementioned reports (Whittemore et al., 2003, Lee et al., 2005, Zhu et al., 2000), we found a hypertrophy without hyperplasia in all muscle fibres following 8 weeks of a weekly injection of sActRIIB. Moreover, the hypertrophy seems to affect all muscle fibres from treated mice, particularly the most glycolytic types, entitled the MHCIIb fibres, such data supported by a number of studies (Foster et al., 2009, Matsakas et al., 2009). A number of investigators have established that Myostatin controls both skeletal muscle fibre numbers through inhibition of myoblast proliferation and differentiation, and muscle fibres size by inhibiting protein synthesis mediating by reducing of Akt level, while upregulating FoxO activity (Thomas et al., 2000, Yang et al., 2007). Therefore, we and others have shown that germline deletion of *Myostatin* led to a dramatic increase in muscle mass as a result of both hyperplasia and hypertrophy (McPherron et al., 1997, Hulmi et al., 2013b). However, in this experiment we found no evidence of an increase in the total fibre numbers within each examined muscle, confirming that the post-natal elevation of muscle mass due to Myostatin inhibition using sActRIIB injection was not relative to muscle hyperplasia. Previous work has revealed a constant number of resting satellite cells of injured EDL muscle fibres from mice were

injected with AAV8ProMyo compared to the controls, indicating no effect of post-natal inhibition of Myostatin on satellite cell numbers (Matsakas et al., 2009). In the line of investigation, an important finding of in vitro study by Amthor et al. (Amthor et al., 2009) has shown that there is no significant difference in the rate of myoblast proliferation following Myostatin blocking. Further investigation has revealed a normal rate of satellite cells differentiation following postnatal inhibition of Myostatin (Foster et al., 2009). The absence response of satellite cells to the post-natal blocking of Myostatin is might be explained by the downregulation of activin receptors of these cells (Amthor et al., 2009). It seems that there is no impact of post-natal inhibition of Myostatin using sActRIIB on neither proliferation, nor differentiation abilities of satellite cells, thereby myofibre numbers.

Observations of the present study revealed that a significant increase in the average of the cross-sectional area of all myofibre types of the EDL and soleus muscles from WT mice treated with sActRIIB for 8 weeks was statistically detectable compared to the control. As we stated above there was no change in total fibres number in examined muscles of both genotypes (WT and *Erry^{Tg/+}*), thus we infer that the main means of muscle enlargement in this study has been brought about through a cellular hypertrophic response. Although all muscle fibre types of EDL and soleus muscles from treated WT and *Erry^{Tg/+}* mice underwent enlargement, we found that the glycolytic fast myofibres IIB displayed the greatest response to sActRIIB treatment. Previous work has reported that myofibres IIB have the highest levels of ActRIIB and *Myostatin* expression (Mendias et al., 2006), therefore releasing these fibres from Myostatin inhibitory effect lead them to display the larges CSA. Further investigation has reported that there is an upper threshold for each muscle fibre type, and muscles with a high proportion of MHCIIB fibres can reach the greatest size (Thomas, 2007). In this line of thought, it has been documented that post-natal inhibition of Myostatin had no effect on the myonuclei numbers, thus the increase in CSA of all fibre types might indicating a reduction of the nuclear: cytoplasmic ratio following inactivation of Myostatin (Matsakas et al., 2009). We have previously shown that *Myostatin* absence resulted in a significant increase in muscle fibre size compared to WT, due to a marked elevation of protein synthesis process mediated by Akt, simultaneously suppressed FoxO3 expression that mediating protein degradation pathways. As stated above that myonuclear number was not been affected by Myostatin inhibition, therefore we suggest that 8 weeks treatment with

sActRIIB could induce muscle fibre hypertrophy through inhibiting Myostatin ability to repress protein synthesis, possibly by the Akt pathway (Yang et al., 2007). Importantly, several other studies, however, revealed no evidence of strength or function benefits in human with muscle dystrophy accompanied the enlargement muscle fibres following post-natal inactivation of MYOSTATIN (Krivickas et al., 2009, Wagner et al., 2008). Moreover, it has been demonstrated that post-natal treatment with sActRIIB-Fc resulted in downregulation of genes that involve in mitochondrial function and oxidative phosphorylation (Rahimov et al., 2011). Therefore, we induced muscle oxidative metabolism in advance through muscle-specific overexpression of *Erry* that described as a key regulator of a network of biomarker genes linked to mitochondrial biogenesis and function, oxidative metabolism, angiogenic programme and fatty acid oxidation (Narkar et al., 2011, Rangwala et al., 2010).

Our examining of myofibre proportions in the controls and sActRIIB treated EDL and soleus muscles from both genotypic groups of this study at the first time confirmed previous studies (Matsakas et al., 2012b, Narkar et al., 2011), that *Erry* transgenic muscles have a higher percentages of slow-twitch than the fast-twitch myofibres compared to WT control muscles. Secondly, there was no change in the fibre type distribution at myosin heavy chains (MHC) level following 8 weeks of sActRIIB treatment in any muscle of both genotypic groups. We and others have demonstrated previously that muscles with germline deletion of *Myostatin* displayed a predominant of MHCIIB myofibres concomitant with a marked reduction in numbers of MHCIIA and MHCIIIX (Girgenrath et al., 2005, Amthor et al., 2007). Unlike in the genetic mutant, previous work has unveiled that inactivation of Myostatin in aged mice using AAV8MyoPPT did not cause any change in the expression of myosin heavy chain (Collins-Hooper et al., 2014). Further studies have reported that blocking of ActRIIB signalling in adult WT mice do not have any impact on fibre types composition (Relizani et al., 2014, Cadena et al., 2010). We infer from these studies that the shift of muscle fibres of *Mtn*^{-/-} mice toward the fast phenotypes commonly attributed to the changes in muscle-specification during a developmental period (Baligand et al., 2010, Savage and McPherron, 2010). Moreover, these investigations imply that protocol of post-developmental blocking of Myostatin through 8 weeks of sActRIIB injection is unable to influence myofibre contractile properties shifting because it does not act at an embryonic stage of muscle

development as occurred in *Mtn*^{-/-} mice. Additionally, MHC proteins are stable to some extent, thus their turnover rates might require many weeks (Papageorgopoulos et al., 2002). The hypertrophied myofibres from WT.sActRIIB mice showed a marked decrease of muscle oxidative capacity indicated by low SDH activity. Such combination of large muscle fibres with low oxidative capacity fits nicely with the trade-off that thought to exist between muscle fibres size and oxidative capacity (Van der Laarse WJ, 1998). In contrast, an interesting feature highlighted by our work is the significant increase in myofibres size of *Erry*^{Tg/+} muscles following sActRIIB treatment, was not accompanied with reduction in muscle oxidative capacity as occurred in WT mice, thereby challenging the inverse relationship between muscle fibre oxidative capacity and its size (van Wessel et al., 2010, Degens, 2012). It was well established that ActRIIB/Myostatin signalling is essential to maintain the balance between muscle fibres size and strength via optimizing muscle energy metabolism (Relizani et al., 2014). Same study unveiled a direct effect of the mentioned signalling on muscle oxidative metabolism indicating by a significant reduction in the expression of genes that controlling muscle aerobic metabolism following 24hr of C2C12 treatment with sActRIIB (Relizani et al., 2014). In agreement with our findings in WT mice, previous work has reported that inactivation of Myostatin in aged mice leads to a significant diminishing of muscle oxidative capacity indicating by lower number of SDH⁺ fibres (Collins-Hooper et al., 2014). In addition, our results are in agreement with the phenotype of *Myostatin null* mice that we and others showed previously, which displayed an increase in glycolytic fibres, a meanwhile decrease of oxidative fibres compared to WT (Girgenrath et al., 2005). These findings can be interpreting that the metabolic profile of skeletal muscle which is mirrored in part by SDH concentration can be quickly manipulated (George Carlson et al., 2011), whereas MHC profiling seems more stable (Lach-Trifilieff et al., 2014). Strikingly, sActRIIB treatment did not change the oxidative capacity of *Erry*^{Tg/+} muscles. We showed previously that the reduction in oxidative capacity of muscles from *Mtn*^{-/-} mice was coupled with depletion in mitochondrial number, as reported by Amthor et al (Amthor et al., 2007). In contrast, we found that muscle-specific overexpression of *Erry* into *Mtn*^{-/-} background muscles was sufficient to induce mitochondrial density, thereby restored muscle oxidative capacity to the control conditions. Moreover, it has been documented that *Erry* is highly expressed in metabolically active and highly oxidative capacity tissues (Hong et al., 1999,

Giguere, 2008). This would infer that the robust oxidative metabolic reprogram imparted by muscle-specific *Erry* overexpression was efficacious to prevent metabolic shifting toward glycolytic profile that would be influenced by post-natal inhibition of Myostatin via sActRIIB treatment.

Previous studies have reported that skeletal muscle oxidative capacity and vascular supply are strongly relative to each other (Fluck and Hoppeler, 2003, Pette and Staron, 2000). Further investigation has unveiled that the blood supply per each muscle fibre is correlated to muscle fibre size (Degens et al., 1992), thus muscle fibres with high oxidative phosphorylation try to limit their size for better diffusion of oxygen from capillaries to mitochondria (van Wessel et al., 2010, Kinsey et al., 2007). To further solidify of our results, we quantified capillary density per each myofibre; we found that the elevated oxidative capacity was accompanied with an increase in the capillary to muscle fibres ratio (C:F) in muscles from *Erry*^{Tg/+}, but not WT mice following 8 weeks of sActRIIB treatment. Previous work has demonstrated a clear drop in capillary density in muscles from *mdx* mice following sActRIIB treatment (Relizani et al., 2014, Personius et al., 2010). Interestingly, it has been revealed a high expression of *Myostatin* is essential to improve metabolic functioning and to increase capillary density in the state of chronic hypoxia, indicating a direct effect of *Myostatin* on endothelial cells proliferation, at the same time explaining the muscle wasting of those patients (Hayot et al., 2011). In this line of thought, it has been established that muscle-specific transgenic expression of *Erry* is sufficient to induce mitochondrial biogenesis and muscle capillary supply, hence coordinates metabolic and vasculature demand in oxidative myofibres (Narkar et al., 2011, Matsakas et al., 2012b). Giving our explanation, post-natal inhibition of Myostatin altered the supposed correlation between muscle fibres size and its capillary numbers, however, *Erry* overexpression in advance was sufficient to increase the number of blood vessels that serve each muscle fibres, thereby matched the increased CSA, and oxidative capacity demands. Such coinciding of hypertrophic myofibres, high oxidative capacity and capillary density would challenge the dogma that large fibres have to be glycolytic (Van der Laarse WJ, 1998).

We and others showed previously that the reduction in oxidative capacity and capillary density in muscles from *Myostatin* deficient mice was coupled to disruption in mitochondrial

quantity and quality (Amthor et al., 2007, Rehfeldt et al., 2005). Furthermore, we demonstrated that the high fatigability of *Mtn*^{-/-} muscles might attribute to the mitochondrial perturbing that resulted from germline deletion of *Myostatin*, such data confirmed outcomes of previous work (Amthor et al., 2007). In addition, we found a high level of ROS synchronous with the mitochondrial depletion as consequent to *Myostatin* ablation. Previous work has reported an increase in muscle fatigue, and mice exhaustion during incremental running test following post-natal inhibition of Myostatin via sActRIIB treatment (Relizani et al., 2014). Further study has illustrated a drop in muscle autophagy level concurrently with running decrease following two weeks of sActRIIB administration (Mizushima et al., 2010). On the other hand, we showed previously that superimposition of *Erry* into *Mtn*^{-/-} muscles was sufficient to induce muscle oxidative capacity and blood supply, normalised mitochondrial abnormalities, numbers and location, and reduced ROS level, ultimately improved muscle physiology and enhanced exercise capacity. Moreover, Dufour's (Dufour et al., 2007) revealed a central role of *Erry* in regulating of mitochondrial biogenesis in skeletal muscles. Along the same lines of investigation, observations of the present study showed a high level of ROS indicated by high DHE activity (Diaz et al., 2003) following 8 weeks of a weekly injection of sActRIIB in WT muscles but not *Erry*^{Tg/+}. These data add to growing body of evidence that the reduction of muscle autophagy level, cellular route to remove unwanted long-live proteins and cytoplasmic organelles (Giannoulis et al., 2012, Cooper et al., 2010), as a consequence of Myostatin inhibition leads to accumulation of dysfunctional mitochondria, hence more ROS emission. However, muscle-specific expression of *Erry* maintains muscle mitochondrial biogenesis and function, controls the expression of genes that regulate ETC pathway in mitochondria (Alaynick et al., 2007), prevent excessive ROS production, ultimately promotes muscle functions.

Finally, we investigated the effect of Myostatin inhibition on the connective tissue development. Our observations highlighted a number of interesting features of connective tissue changes in relation to myofibres type and muscle metabolic status. We found higher levels of all examined proteins (collagen IV, dystrophin and Laminin) between MHCIIB⁻ than MHCIIB⁺ myofibres in all muscle cohorts. We also found that the intensity signal and domain size were lower in WT.sActRIIB muscles compared to controls. Most importantly, we found that the oxidative program imparted by *Erry* overexpression prevented the reduction in the

intensity and thickness of connective tissue following sActRIIB treatment. Previous study has demonstrated that Myostatin controls muscle development via myogenesis inhibition, whereas the same pathway induces fibroblast proliferation and development of connective tissue (Li et al., 2008, Zhang et al., 2012). Others have reported that the large glycolytic/fast contracting myofibres have thinner connective tissue compared to the small oxidative/slow muscle fibres (Kovanen et al., 1980). Moreover, it has been illustrated that the formation of muscle and connective tissue is *Myostatin* independent, however, Myostatin then mediates these two tissues modification via paracrine and autocrine- positive feedback mechanisms that have been demonstrated in myogenic and fibroblast cells (Zhu et al., 2000). We suggest that inhibition of Myostatin in WT mice via sActRIIB administration resulted in the development of thin connective tissue suited to the glycolytic myofibres induced by Myostatin blocking. However, the high oxidative phosphorylation induced in hypertrophic muscle fibres via *Erry* overexpression prevents the reduction in ECM protein levels. The possible explanations here, Myostatin inhibition in WT muscles resulted in increased CSA, while reduced fibroblast proliferation which resulted in less connective tissue production. Interestingly, muscle-specific expression of *Erry* either increase fibroblast numbers, or stimulate their activity, thereby attenuating connective tissue decrease. Additionally, the fast glycolytic fibres in all muscles examined have less ECM compared to the slow oxidative phenotypes to reduce the amount of energy stored in connective tissue and use it for force exertion on tendons.

In conclusion, post-natal inhibition of Myostatin via sActRIIB administration increased muscle mass, but decreased muscle oxidative capacity and connective tissue content, and induced superoxide level in WT muscles. These changes may negatively contribute to reduce physical activity and be potentially associated with various health risks (Zhou et al., 2010, Faulkner et al., 1990). However, we demonstrate that muscle-specific overexpression of *Erry* in combination with Myostatin blocking; muscle preserved its large size, displayed high oxidative capacity and capillary density, reduced ROS emission and avoided connective tissue reduction. These manifestations imply that it is possible to develop hyper-oxidative hypertrophic muscle fibres phenotypes during post-natal life via non-genetic methods.

Chapter 7; Results

Regulation of extracellular matrix and dystrophin-associated glycoprotein complex composition by the metabolic properties of muscle fibres

7.1. Introduction

Skeletal muscle consists of a number of compartments that are working co-ordinately in order to form a functional organ. In addition to muscle fibres, skeletal muscle contains additional entities that play a supportive role to maintain muscle structure and health (Gillies and Lieber, 2011). An important support compartment is dystrophin-glycoprotein complex (DGC), a complex of proteins that link the cytoskeleton to the extracellular matrix (ECM) (Gumerson and Michele, 2011, Gillies and Lieber, 2011). It is well established that dystrophin binds to β -Dystroglycan (β -DG) in transmembrane, which is bound to α -DG on the extracellular surface of the myofibre. Laminin, a component of the ECM binds to α -DG as well as to collagen IV in the basal lamina and indirectly to collagen I in the interstitial matrix (Allamand et al., 2011).

In fact, the elaborate network of proteins in DGC provide skeletal muscle with the ability to transmit force to tendons to produce locomotion, as well as protecting it from contraction induce damage (Kjaer, 2004). Moreover, It has been demonstrated that ECM, rather than the muscle fibres, actually bear the stress during skeletal muscle contraction (Meyer and Lieber, 2011). In support of this view, previous work revealed a number of pathological conditions that occurred due to mutations in genes of DGC or ECM, for example *Dystrophin* mutation leads to Duchenne Muscular Dystrophy (DMD) and Becker Muscular Dystrophy (BMD) (Kunkel et al., 1989). Limb-Girdle muscular dystrophies and other pathologies result from mutations in Dystroglycan (DG) and Sarcoglycans (SG) (Hara et al., 2011, Wicklund and Kissel, 2014).

Skeletal muscle is a highly compliant tissue that undergoes both qualitative and quantitative alterations as a part of its adaptation to the physiological and environmental stimuli (Matsakas and Patel, 2009b). As the ECM and DGC represent a dynamic environment that supports the cellular elements and maintains muscle integrity; this raises the possibility of their changes as a part of skeletal muscle adaptation in response to intrinsic or extrinsic stimuli. This is clearly demonstrated in the phenotype of mice lacking *Myostatin* (*Mtn*^{-/-}), a member of the TGF- β family of secreted proteins. Previous studies have shown that in addition to muscle fibre hypertrophy and MHC transition toward glycolytic fast phenotypes as a result of genetic alteration of *Myostatin* (Amthor et al., 2007, McPherron et al., 1997),

there is a remarkable reduction of ECM components compared to age and sex-matched wild type muscles (Elashry et al., 2012). These changes in ECM following *Myostatin* absence were either due to the increase in muscle fibre size which was not accompanied with a proportional increase in ECM production, or an adaptive change to complement ECM to muscle physiology. The later hypothesis is robustly supported by previous findings of Kovanen's study, who showed less ECM content surrounds the glycolytic/fast myofibres compared to the oxidative/slow ones (Kovanen et al., 1980).

Investigation of DGC and ECM in skeletal muscle is an important approach that can give insights of the communication and interaction between muscle fibres and the surrounding environment. Changes in skeletal muscle connective tissue in response to a diseases context have been intensely studied (Matsumura et al., 1993, Williams et al., 2015). However, little is known about the effect of non-disease scenarios on these components of skeletal muscle tissue. Therefore, we believe it is vital to investigate the relationship between myofibre phenotype (size and composition) and its force transduction apparatus that mainly formed from DGC and ECM.

To do so, the hind limb muscles (EDL, soleus and TA) from three months old WT, *Mtn*^{-/-} and *Mtn*^{-/-}/*Erry*^{Tg/+} were utilised in this study. Muscle sections were immunostained using antibodies for collagen IV, collagen I, dystrophin, α , β , γ , δ -sarcoglycan, α , β -dystroglycan, and laminin. In order to determine levels of specific proteins at the sarcolemma and correlate this with fibre phenotype, semi-quantitative immunofluorescence methods were applied (Arechavala-Gomez et al., 2010, Taylor et al., 2012). A number of soleus muscles were homogenized and RNA samples extracted to determine the expression of a number of genes that encoded ECM and DGC proteins using RT-PCR technique. Other soleus muscles were used to determine the expression of ECM and DGC molecules via western blotting.

Here we show that fibre type, based on myosin heavy chain IIB expression (MHCIIB), influences the levels of DGC and ECM components at the sarcolemma. Secondly, sarcolemmal levels of all DGC proteins examined were lower in hypertrophic muscle from *Mtn*^{-/-} mice compared to WT. Thirdly we show that levels of DGC at the sarcolemma were significantly increased in *Mtn*^{-/-} fibres following superimposition of an oxidative metabolic

programme established by *Erry*. These results demonstrate that the metabolic programme of muscle is a key determinant of the DGC and ECM.

7.2. Muscle-specific expression of *Erry* restores the reduction in basal lamina and interstitial components of ECM resulted from *Myostatin* absence

Previous work using cryo-scanning electron microscopy has reported that genetic deletion of *Myostatin* leads to develop a thinner endomysium layer compared to age and sex matched WT muscles (Elashry et al., 2012). Moreover, deposition level of collagen I and collagen IV was higher in between MHCII⁻ relative to between MHCII⁺, this relationship was constant in both WT and *Mtn*^{-/-} muscles (Elashry et al., 2012).

In this study, we used fluorescence microscopy based techniques in order to determine how they compared to electron microscopic approaches to quantify the ECM content of skeletal muscle. In fact, recently developed protocols enable the investigators to semi-quantitatively determine expression levels of a target protein based on intensity of signal (Arechavala-Gomez et al., 2010, Cirak et al., 2012, Taylor et al., 2012), as well as thickness of the connective tissue based on expression domain size (de Bruin et al., 2014).

We first assessed the expression levels and thickness of collagen IV in the endomysium between MHCII⁻ - IIB⁻, as well as between MHCII⁺ - IIB⁺ fibres. Measurements were taken from four non-overlapping regions from three WT muscles that represent differing MHC and metabolic profiles (EDL, soleus, deep and superficial portions of the TA muscles). Specifically, MHC profile, going from fast to slowest, adheres to the following order: superficial TA, EDL, deep TA, soleus. In agreement with aforementioned report's findings (Elashry et al., 2012), we found that collagen IV signal intensity and thickness was greater between MHCII⁻ fibres compared to MHCII⁺ fibres in all examined wild type muscles (Figure 7.1A-C) (note that there was no MHCII⁺ fibres in soleus muscles from WT mice). Knockout of *Myostatin* resulted in an overall decrease in collagen IV around all fibres compared to WT. Importantly, immunofluorescence quantifications confirmed that the difference in collagen IV levels between MHCII⁻ and MHCII⁺ fibres is not affected by the loss of *Myostatin* expression in any of the muscles examined, so MHCII⁺ contained less collagen IV than MHCII⁻ fibres (Figure 7.1A-C).

Next we examined the effect of over-activation of the oxidative programme on collagen IV deposition in mice over-expressing *Erry* on the *Myostatin* null background (*Mtn*^{-/-}/*Erry*^{Tg/+}) muscles. Using immunofluorescence, we showed that overexpression of *Erry* was sufficient

to normalise collagen IV levels in *Mtn*^{-/-} to that level of WT mice. This increase in both intensity and thickness of collagen IV staining in-between fibres occurred in all muscles examined and was irrespective of MHCII_B expression (Figure 7.1A-C).

Thereafter, we examined the expression of collagen type I, an interstitial component of the ECM. Our observations found that the signal intensity and thickness of this protein showed the same pattern as collagen IV with respect to MHCII_B expression and genotypes of the three cohorts (Figure 7.2.A-C).

These data suggest that loss of *Myostatin* expression causes a global decrease in collagen IV and I, and the decrease levels were similar on MHCII_B⁻ and MHCII_B⁺ fibres. Interestingly, introducing of *Erry* normalised levels of both proteins with respect to MHCII_B fibre.

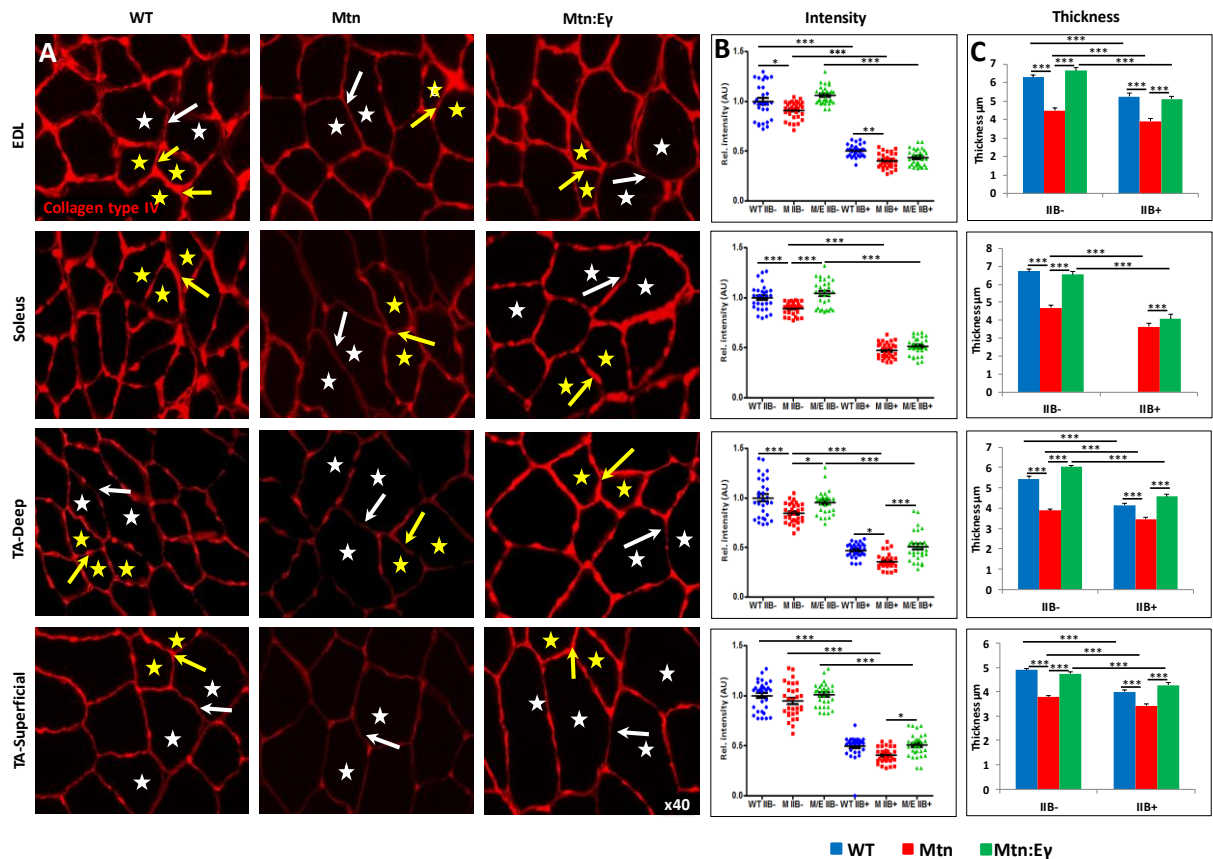


Figure 7.1. Collagen IV profiles in WT, *Mtn* and *Mtn:Er* mouse muscle

(A) Expression of collagen IV in relation to MHC fibre type. Serial sections processed with an anti-MHCCIIB antibody was used to identify MHCCIIB⁻ and MHCCIIB⁺ fibres. Representative MHCCIIB⁻ fibres indicated with yellow stars and MHCCIIB⁺ fibres by white stars. Expression of collagen IV more robust in ECM between two MHCCIIB⁻ fibres (yellow arrows) compared to that between MHCCIIB⁺ fibres (white arrows) in wild type muscles. The same relationship albeit at lower levels was noted in *Mtn* muscles. Expression levels were increased by *Er* in ECM between MHCCIIB⁻ (yellow arrows) as well as MHCCIIB⁺ (white arrows) compared to *Mtn* fibres.

(B) Intensity of collagen IV expression quantified by setting standard value of 1 for the level between MHCCIIB⁻ fibres from WT mice.

(C) Collagen IV expression also quantified in terms of thick domain.

($n = 30$) from each cohort. Statistical analysis performed by One-way ANOVA followed by Bonferroni's multiple comparison tests, $p < 0.05$, $p^{**} < 0.01$, and $p^{***} < 0.001$.

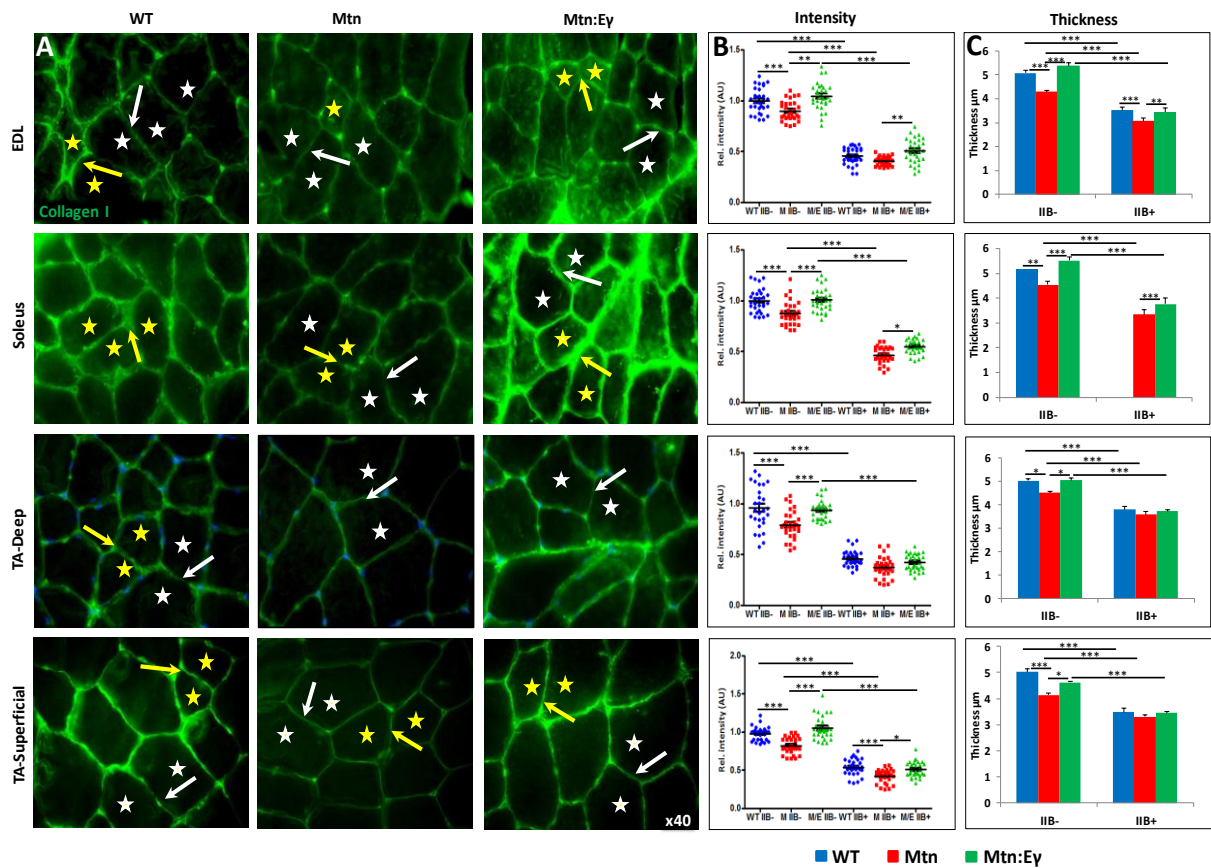


Figure 7.2. Collagen I profiles in WT, *Mtn* and *Mtn:Ey* mouse muscle

(A) Expression of collagen I in relation to MHC fibre type. Serial sections processed with an anti-MHCIIB antibody was used to identify MHCIIIB⁻ and MHCIIIB⁺ fibres. Representative MHCIIIB⁻ fibres indicated with yellow stars and MHCIIIB⁺ fibres indicated by white stars. Expression of collagen I more robust in ECM between two MHCIIIB⁻ fibres (yellow arrows) compared to that between MHCIIIB⁺ fibres (white arrows) in wild type muscles. Same relationship albeit at lower levels in *Mtn* muscles. Expression domain increased by *Ery* in ECM between MHCIIIB⁻ (yellow arrows) as well as MHCIIIB⁺ (white arrows) compared to *Mtn* fibres.

(B) Expression of collagen I quantified through intensity measurements by setting standard value of 1 for the level between MHCIIIB⁻ fibres from WT mice.

(C) Collagen I expression also quantified in terms of thick domain.

($n = 30$) from each cohort. Statistical analysis performed by One-way ANOVA followed by Bonferroni's multiple comparison tests, $p^* < 0.05$, $p^{**} < 0.01$, and $p^{***} < 0.001$.

7.3. Overexpression of *Erry* redresses the decrease of dystrophin level in *Mtn*^{-/-} muscles

In order to investigate whether the metabolic reprogramming established in this study induce changes in the expression of intercellular component of DGC, fluorescence microscopy based techniques were applied to identify the signal intensity and thickness of dystrophin, the first identified member of DGC that binds actin to β -DG in muscle membrane (Hoffman et al., 1987, Ervasti and Campbell, 1993). Based on intensity and thickness measures, we found that dystrophin expression was greater between MHCII⁻ than between MHCII⁺ fibres in EDL, soleus, and TA muscles from WT mice. *Myostatin* deletion induces a significant reduction in dystrophin expression in both MHCII⁻ and MHCII⁺ when compared to their counterparts from WT muscles. Importantly, expression of *Erry* on the *Mtn*^{-/-} background muscles revealed a profound impact of the oxidative programme on dystrophin level. *Mtn*^{-/-}/*Erry*^{Tg/+} MHCII⁻ and MHCII⁺ fibres showed significantly greater expression of dystrophin than their *Mtn*^{-/-} counterparts, with most instances in the four muscle regions examined reaching WT levels (Figure 7.3A-C). These data indicate that muscle fibre size and metabolic activity can induce changes in muscle dystrophin level.

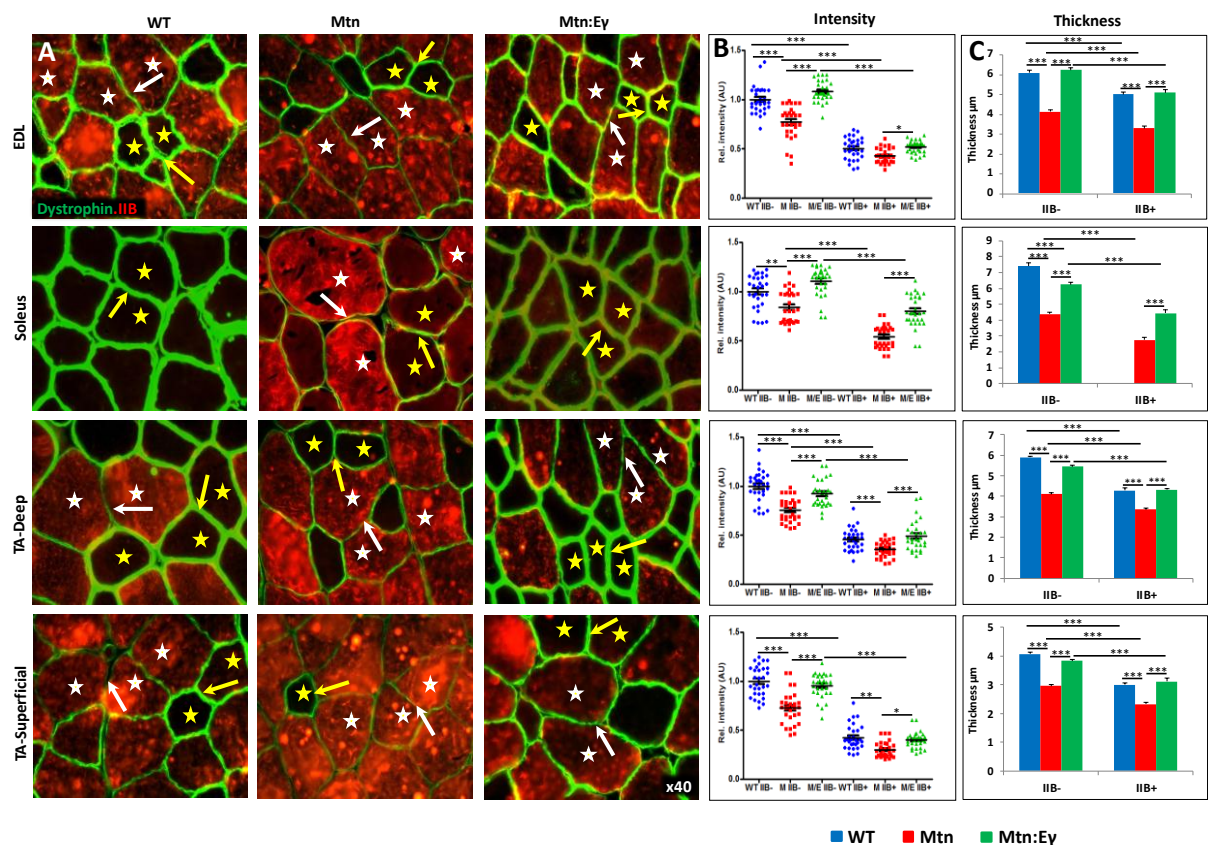


Figure 7.3. Dystrophin profiles in WT, *Mtn* and *Mtn:Ey* mouse muscle

(A) Immunofluorescence profile of dystrophin in relation to MHC fibre type. MHCIIIB expression in red. Representative MHCIIIB⁻ fibres indicated by yellow stars and MHCIIIB⁺ fibres by white stars. Expression of dystrophin was stronger in ECM between two MHCIIIB⁻ fibres (yellow arrow) compared to between MHCIIIB⁺ fibres (white arrows) in wild type muscles. Same relationship albeit at lower levels in *Mtn* muscles between MHCIIIB⁻ fibres and MHCIIIB⁺ fibres. Expression increased in by *Erry* in ECM between MHCIIIB⁻ (yellow arrows) as well as between MHCIIIB⁺ (white arrows) fibres compared to those from *Mtn* mice.

(B) Expression of dystrophin quantified by intensity by setting standard value of 1 for the level between MHCIIIB⁻ fibres from WT mice.

(C) Dystrophin expression quantification in terms of thickness.

(*n* = 30) for each cohort. Statistical analysis performed by One-way ANOVA followed by Bonferroni's multiple comparison tests, *p* < 0.05, *p* < 0.01, and *p* < 0.001.

7.4. *Myostatin* mutation has disparate impacts on expression levels of transmembrane proteins of DGC.

Measurements of signal intensity and thickness of membrane-associated proteins of DGC (β -dystroglycan (DG), α , β , γ and δ -sarcoglycan (SG)) revealed that expression of these proteins relative to MHCII B expression and genotype segregated into one of two groups. Group 1 consisted of β -DG, α and γ -SG, and group 2 consisted of β and δ -SG.

Group 1 proteins of DGC had expression profiles that changed with regards to MHCII B expression and genotype in a manner similar to that of collagens IV, I and dystrophin. All the proteins (β -DG, α and γ -SG) displayed high level between MHCII B $^-$ than MHCII B $^+$ fibres in all muscles examined from the three genotypic groups. Importantly, the significant reduction in these protein levels due to *Myostatin* ablation, were restored to normal conditions following introducing of *Erry* on the *Mtn* $^{-/-}$ muscles (Figure 7.4A-C, Figure 7.5A-C and Figure 7.6A-C).

Next we examined the expression levels of group 2 members. We discovered that expression of β and δ -SG failed to follow the trend of group 1 proteins and were thereafter designated to comprise a distinct group. Group 2 proteins like group 1 show higher expression in MHCII B $^-$ fibres compared to MHCII B $^+$ in all three cohorts. However, the expression of group 2 proteins was higher in the fibres from *Mtn* $^{-/-}$ compared to their MHCII B $^-$ /MHCII B $^+$ counterparts from WT animals. Lastly, our study revealed that the expression of group 2 proteins in *Mtn* $^{-/-}$ fibres was largely refractory to the expression of *Erry*; their higher levels of expression being maintained to those levels found in the *Mtn* $^{-/-}$ fibres (Figure 7.7A-C and Figure 7.8A-C).

Together, these observations demonstrate that membrane-associated molecules of DGC show different manners of influencing following metabolic programmes established in current study.

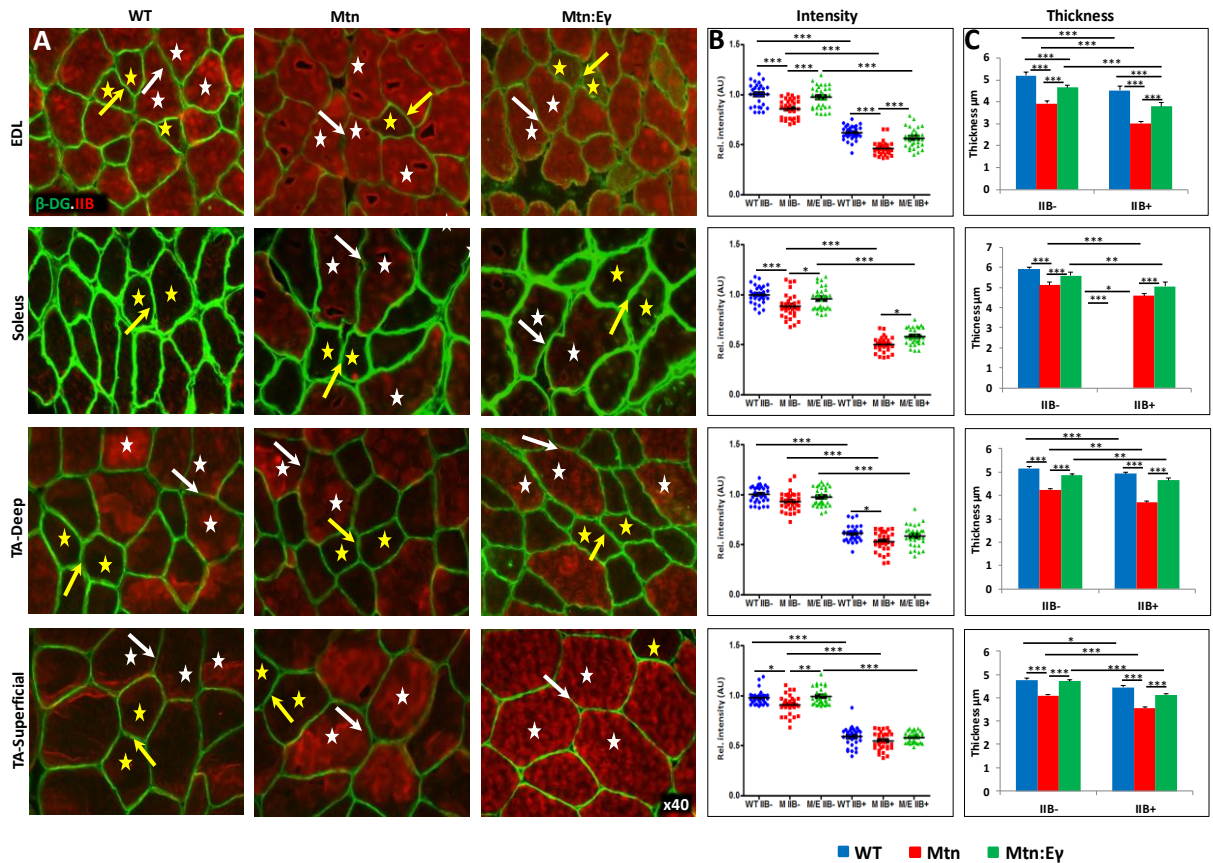


Figure 7.4. β -dystroglycan profiles in WT, *Mtn* and *Mtn:Ey* mouse muscle

(A) Immunofluorescence profile of β -dystroglycan in relation to MHC fibre type. MHCIIB expression in red. Representative MHCIIB⁻ fibres indicated by yellow stars and MHCIIB⁺ fibres by white stars. Expression of β -dystroglycan was stronger in ECM between two MHCIIB⁻ fibres (yellow arrow) compared to between MHCIIB⁺ fibres (white arrows) in wild type muscles. Same relationship albeit at lower levels in *Mtn* muscles between MHCIIB⁻ fibres and MHCIIB⁺ fibres. Expression increased in by *Erry* in ECM between MHCIIB⁻ (yellow arrows) as well as between MHCIIB⁺ (white arrows) fibres compared to those from *Mtn* mice.

(B) Expression of β -dystroglycan quantified by intensity by setting standard value of 1 for the level between MHCIIB⁻ fibres from WT mice.

(C) β -Dystroglycan expression quantification in terms of thickness domain.

($n = 30$) from each cohort. Statistical analysis performed by One-way ANOVA followed by Bonferroni's multiple comparison tests, $p^* < 0.05$, $p^{**} < 0.01$, and $p^{***} < 0.001$.

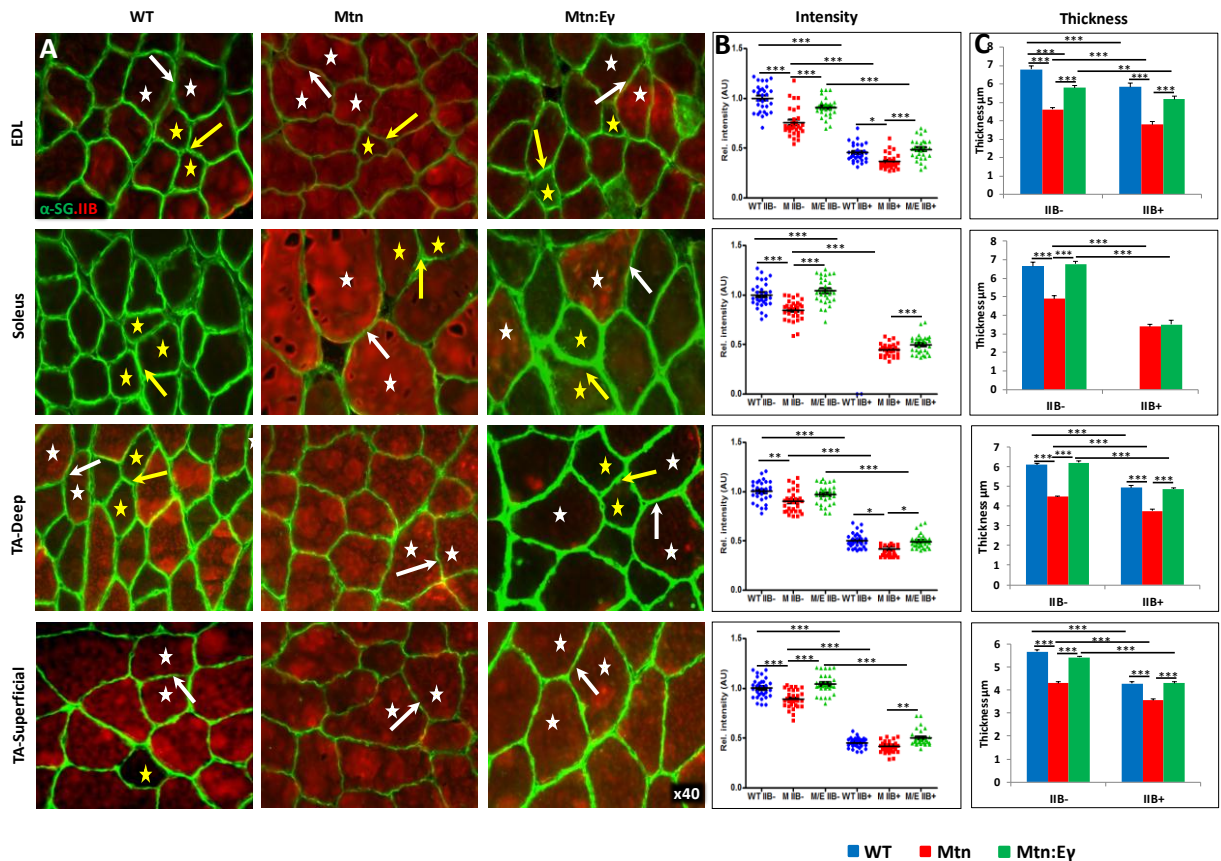


Figure 7.5. α -Sarcoglycan profiles in WT, *Mtn* and *Mtn:Ey* mouse muscle

(A) Immunofluorescence profile of α -sarcoglycan in relation to MHC fibre type. MHCIIb expression in red. Representative MHCIIb⁻ fibres indicated by yellow stars and MHCIIb⁺ fibres by white stars. Expression of α -sarcoglycan was greater in ECM between two MHCIIb⁻ fibres (yellow arrow) compared to between MHCIIb⁺ fibres (white arrows) in wild type muscles. Same relationship albeit at lower levels in *Mtn* muscles between MHCIIb⁻ fibres and MHCIIb⁺ fibres. Expression increased in by *Erry* in ECM between MHCIIb⁻ (yellow arrows) as well as between MHCIIb⁺ (white arrows) fibres compared to those from *Mtn* mice.

(B) Expression of α -sarcoglycan quantified by intensity by setting standard value of 1 for the level between MHCIIb⁻ fibres from WT mice.

(C) α -Sarcoglycan expression quantification in terms of thick domain.

($n=30$) from each cohort. Statistical analysis performed by One-way ANOVA followed by Bonferroni's multiple comparison tests, $p^* < 0.05$, $p^{**} < 0.01$, and $p^{***} < 0.001$.

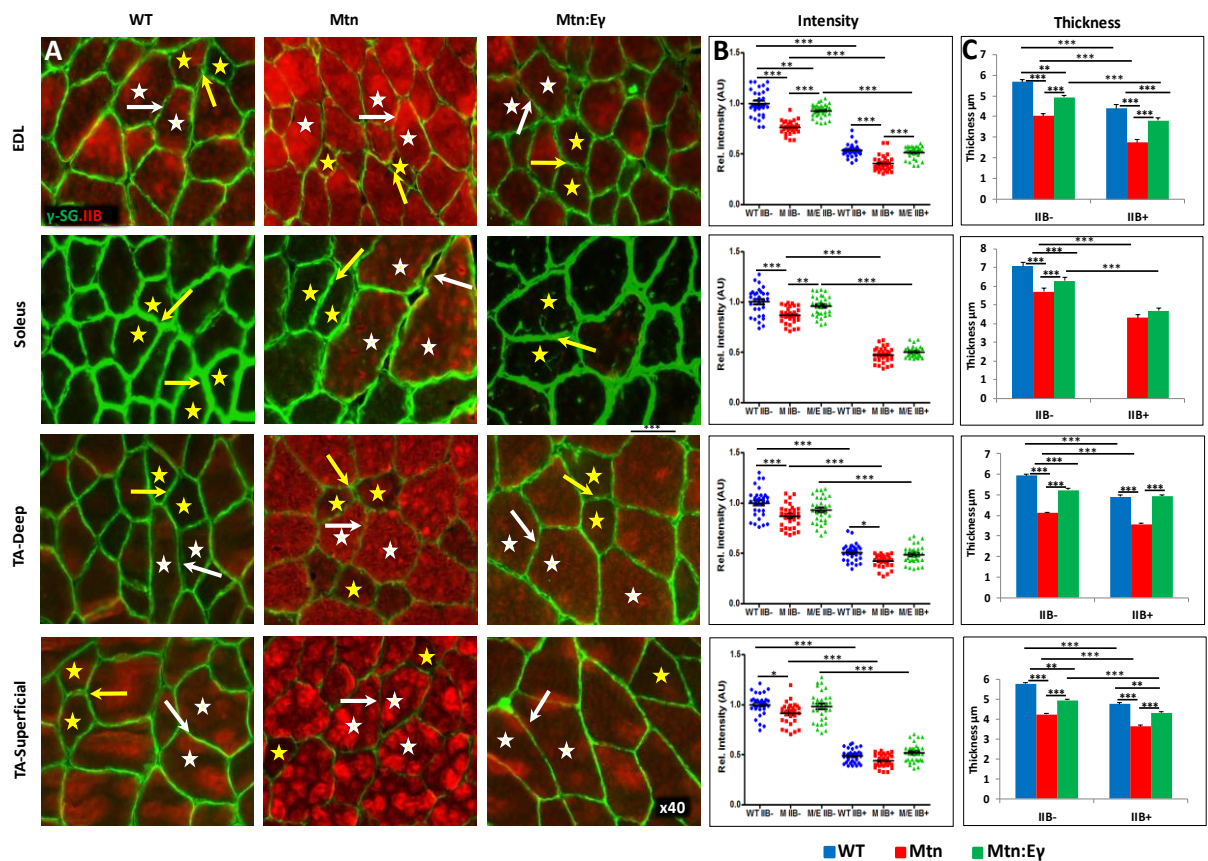


Figure 7.6. γ -Sarcoglycan profiles in WT, *Mtn* and *Mtn:Ey* mouse muscle

(A) Immunofluorescence profile of γ -Sarcoglycan in relation to MHC fibre type. MHC IIB expression in red. Representative MHC IIB⁻ fibres indicated by yellow stars and MHC IIB⁺ fibres by white stars. Expression of γ -sarcoglycan was greater in ECM between two MHC IIB⁻ fibres (yellow arrow) compared to between MHC IIB⁺ fibres (white arrows) in wild type muscles. Same relationship albeit at lower levels in *Mtn* muscles between MHC IIB⁻ fibres and MHC IIB⁺ fibres. Expression increased in by *Ery* in ECM between MHC IIB⁻ (yellow arrows) as well as between MHC IIB⁺ (white arrows) fibres compared to those from *Mtn* mice.

(B) Expression of γ -Sarcoglycan quantified by intensity by setting standard value of 1 for the level between MHC IIB⁻ fibres from WT mice.

(C) γ -Sarcoglycan expression quantification in terms of thick domain.

($n=30$) from each cohort. Statistical analysis performed by One-way ANOVA followed by Bonferroni's multiple comparison tests, $p^* < 0.05$, $p^{**} < 0.01$, and $p^{***} < 0.001$.

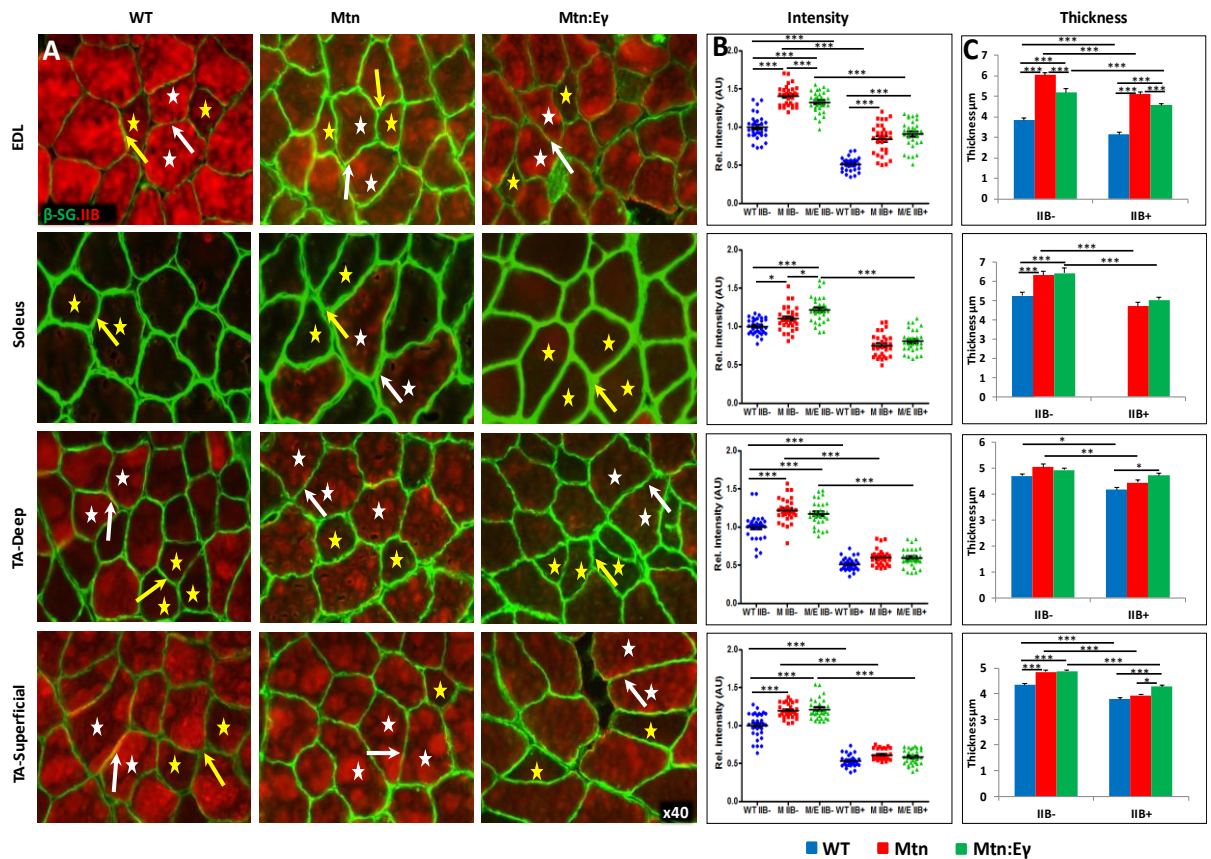


Figure 7.7. β -Sarcoglycan profiles in WT, *Mtn* and *Mtn:Ey* mouse muscle

(A) Immunofluorescence profile of β -sarcoglycan in relation to MHC fibre type. MHC IIB expression identified by bright red colouring. Representative MHC IIB⁻ fibres indicated by yellow stars and MHC IIB⁺ fibres by white stars. Note higher levels of β -sarcoglycan in all genotypes between MHC IIB⁻ (yellow arrows) compared to MHC IIB⁺ (white arrows).

(B) Expression of β -sarcoglycan quantified by intensity by setting standard value of 1 for the level between MHC IIB⁻ fibres from WT mice.

(C) β -Sarcoglycan expression quantification in terms of thick domain.

($n = 30$) from each cohort. Statistical analysis performed by One-way ANOVA followed by Bonferroni's multiple comparison tests, $p^* < 0.05$, $p^{**} < 0.01$, and $p^{***} < 0.001$.

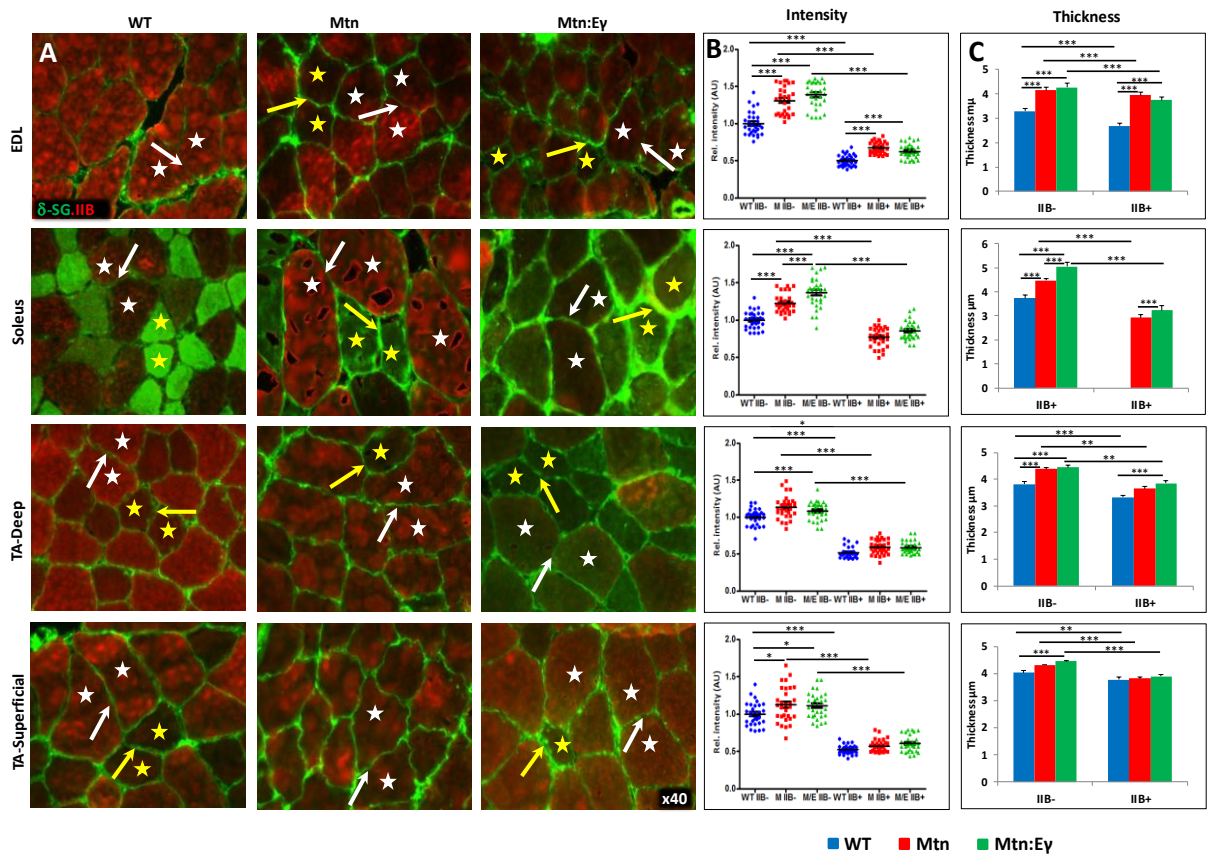


Figure 7.8. δ -Sarcoglycan profiles in WT, *Mtn* and *Mtn:Ey* mouse muscle

(A) Immunofluorescence profile of δ -sarcoglycan in relation to MHC fibre type. MHC IIB expression in red. Representative MHC IIB⁻ indicated by yellow stars and MHC IIB⁺ fibres by white stars. Note higher levels of δ -sarcoglycan in all genotypes between MHC IIB⁻ (yellow arrows) compared to MHC IIB⁺ (white arrows).

(B) Expression of δ -sarcoglycan quantified by intensity by setting standard value of 1 for the level between MHC IIB⁻ fibres from WT mice.

(C) δ -Sarcoglycan expression quantification in terms of thick domain.

($n = 30$) from each cohort. Statistical analysis performed by One-way ANOVA followed by Bonferroni's multiple comparison tests, * < 0.05 , ** < 0.01 , and *** < 0.001 .

7.5. Superimposition of an oxidative metabolic programme increases expression levels of extracellular components of DGC

Our results showed that collagen IV and I, intracellular and membrane associated components of DGC are influenced following metabolic reprograms in this study. Next, we performed details investigation to address the changes in extracellular molecules of DGC following *Myostatin* deletion or introducing of *Erry* in the *Mtn*^{-/-} muscles. To do so, we profiled the expression of α -DG in EDL, soleus, and TA muscles, and laminin in only EDL and TA muscles from WT, *Mtn*^{-/-} and *Mtn*^{-/-}/*Erry*^{Tg/+} mice, as an extracellular entities.

We firstly found that expression of these proteins was greater between MHCII⁻ fibres based on intensity and thickness measures compared to MHCII⁺ fibres in WT muscle. Secondly, expression of α -DG and laminin was lower in muscle fibres from *Mtn*^{-/-} mice when compared to their MHCII⁻/MHCII⁺ counterparts from WT animals. Finally, the oxidative metabolism programme imparted by introducing of *Erry* in the *Mtn*^{-/-} was efficacious to induce the expression levels of α -DG and laminin but not in all muscles in particular for α -DG protein (Figure 7.9A-C and Figure 7.10A-C). These indicate that muscle fibre metabolic status could influence the extracellular compositions of DGC.

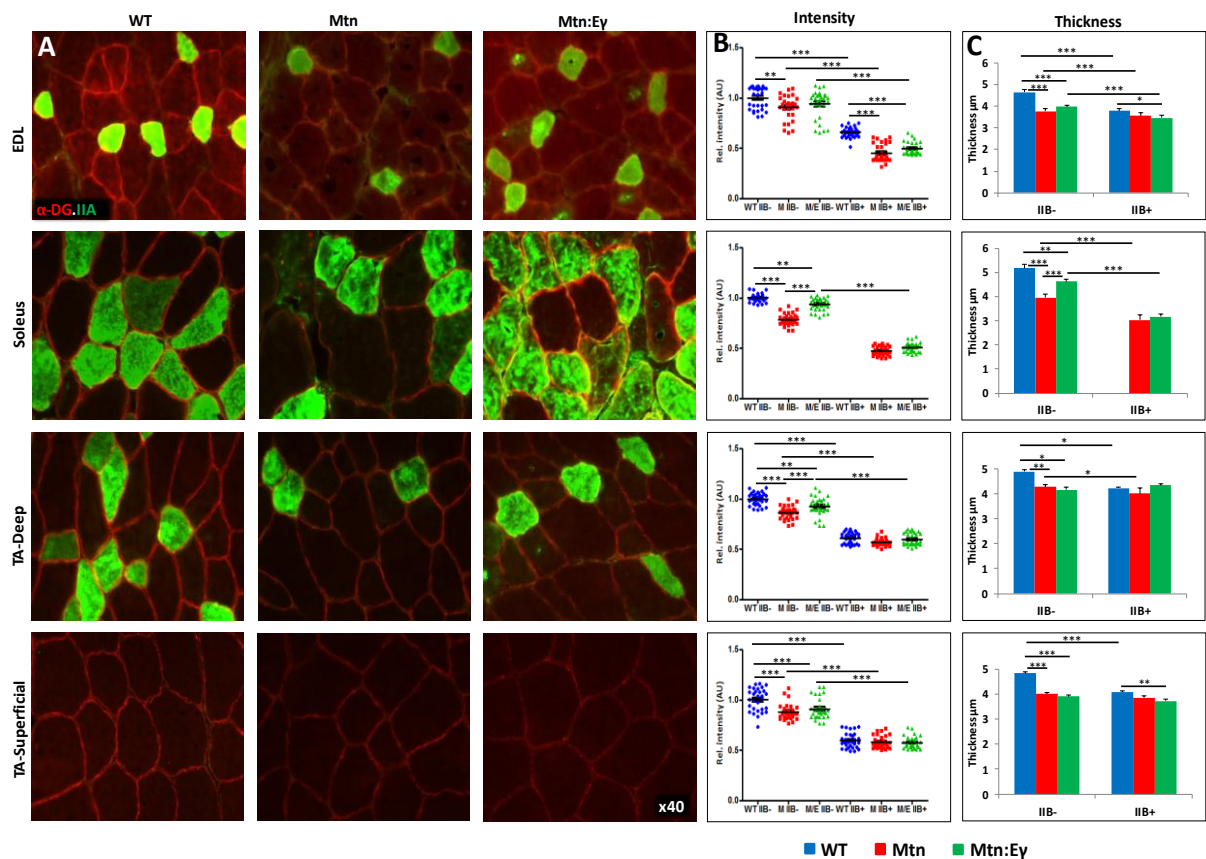


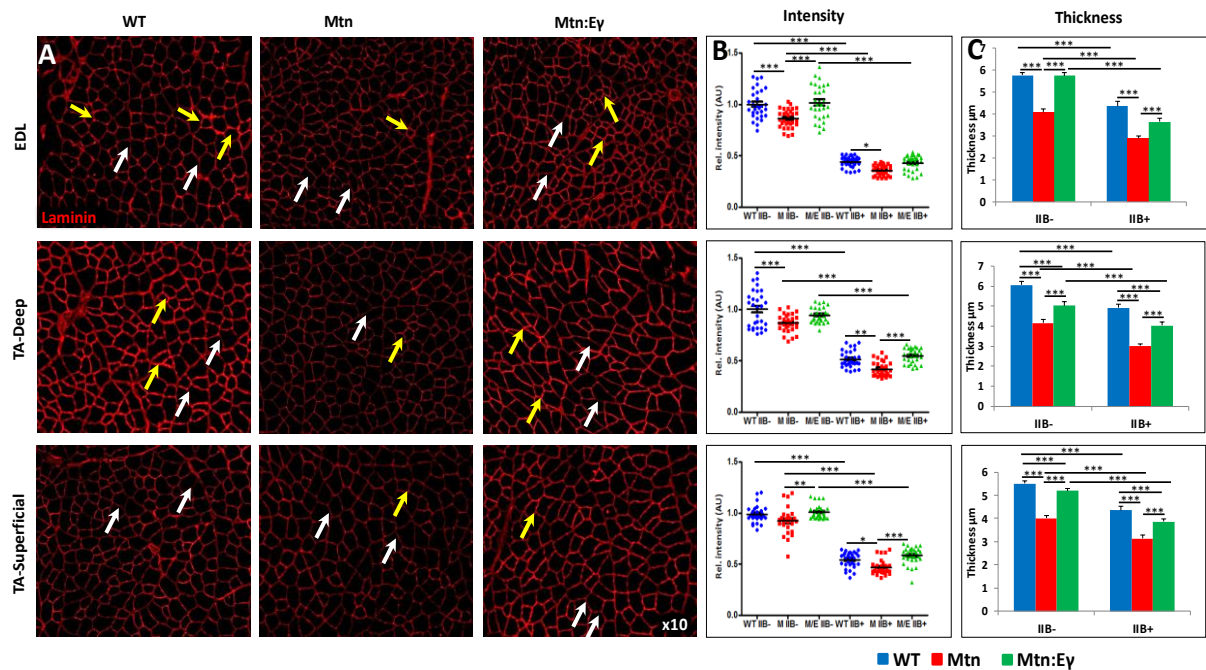
Figure 7.9. α-Dystroglycan profiles in WT, *Mtn* and *Mtn:Ey* mouse muscle

(A) Expression of α-dystroglycan in relation to MHC fibre type. MHCIIA in green. Note higher levels of α-dystroglycan expression in all genotypes between MHCIIB⁻ compared to MHCIIB⁺.

(B) Expression of α-dystroglycan quantified through intensity measurements by setting standard value of 1 for the level between MHCIIB⁻ fibres from WT mice.

(C) α-Dystroglycan expression also quantified in terms of thick domain.

($n = 30$) from each cohort. Statistical analysis performed by One-way ANOVA followed by Bonferroni's multiple comparison tests, $p < 0.05$, $p^{**} < 0.01$, and $p^{***} < 0.001$.



7.6. Muscle fibre properties influence DGC molecules at transcriptional level and total protein expression

The potential impact of muscle fibres size and metabolic nature on the levels of DGC proteins at the myofibre membrane, encouraged us to identify whether the effects of metabolic reprogramming would be mirrored at the transcriptional level, and total protein expression. Therefore, we examined how differences in the intensity of protein labelling among the three genotypes correlate with mRNA expression levels as well as protein amounts. To do so, soleus muscles (n=4) from WT, *Mtn*^{-/-} and *Mtn*^{-/-}/*Erry*^{Tg/+} mice were homogenised and total RNA was reverse-transcribed to cDNA and analysed using quantitative real-time RT-PCR. Profiling of transcript abundance revealed a number of interesting features. We found that the expression level of *Dystrophin*, α -DG and β -SG genes showed exactly the same relationship with regards to the three genetic cohorts as the immunofluorescence survey. Of particular note, expression levels of *Dystrophin* and α -DG genes reduced significantly due to *Myostatin* deletion, however, overexpression of *Erry* restored their expression to WT level, or even more for *Dystrophin* biomarker gene (Figure 7.11A). Moreover, introducing of *Erry* maintained the increased expression level of β -SG in *Mtn*^{-/-} muscles (Figure 7.11A).

Thereafter, western blot analysis was performed in order to compare the DGC protein levels between soleus muscles from the three animal cohorts of this study. Our analysis showed that even though differences in *Dystrophin* and β -SG levels did not reach significance, they displayed same profile in terms of level and the influence of the different genotypes as shown by immunofluorescence and RT-PCR. Interestingly, both α and β -DG appeared to be expressed at higher levels in *Mtn*^{-/-}/*Erry*^{Tg/+} muscle compared to either wild type or *Mtn*^{-/-} muscles. Moreover, densitometric analysis confirmed the elevated expression of α and β -DG in *Mtn*^{-/-}/*Erry*^{Tg/+} muscles analysed (Figure 7.11B).

These data confirm our histochemical results and suggest that muscle fibres metabolic status effects on DGC molecules can be extended to transcriptional and total protein expression levels.

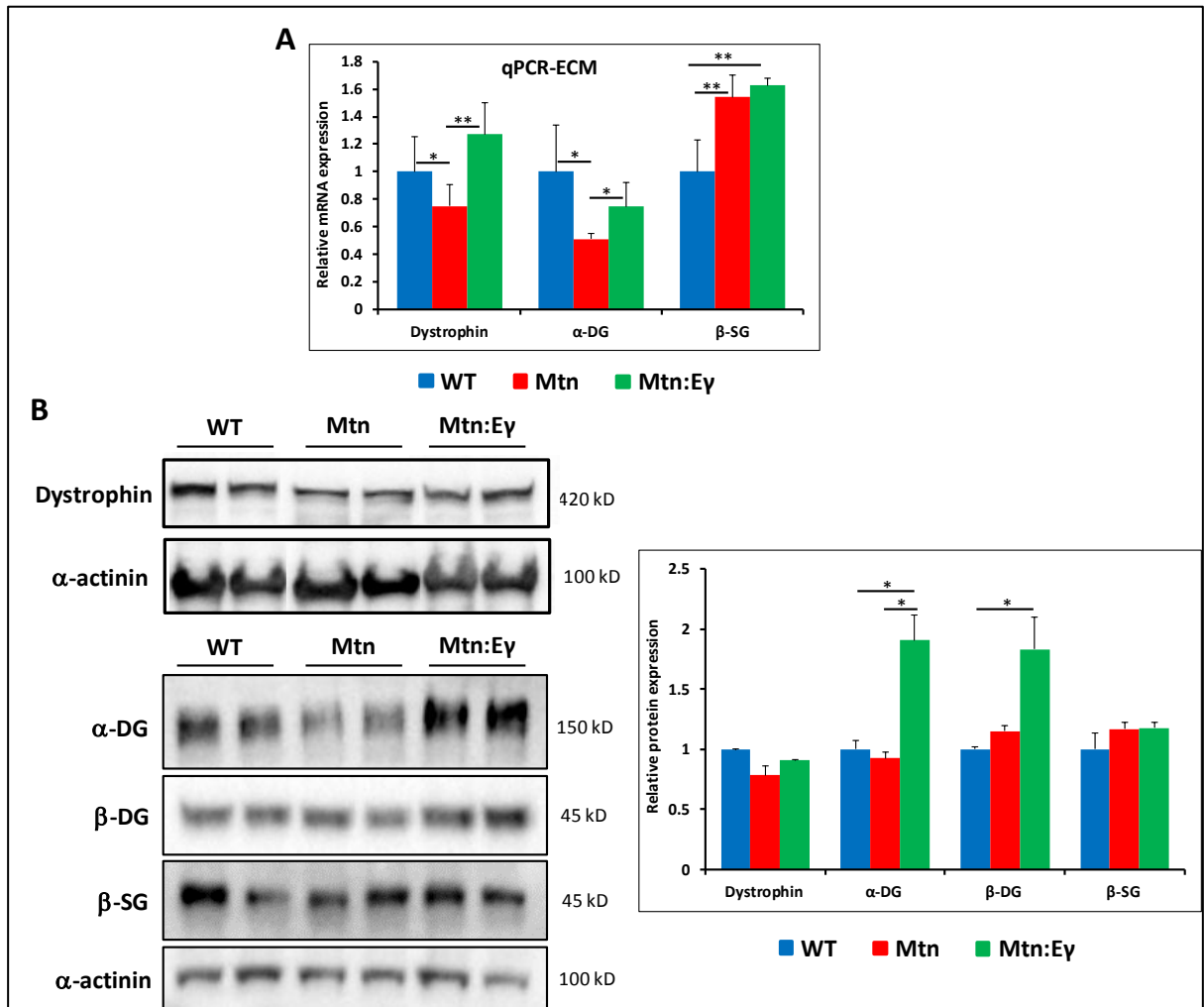


Figure 7.11. Molecular and Western blot profiling of soleus ECM associated molecules

(A) RT.PCR profile of DGC associated genes in soleus muscles ($n=4$) muscle.

(B) Western blot data and quantification of protein levels in soleus muscles ($n=2$) mice per genotype.

Statistical analysis performed by One-way ANOVA followed by Bonferroni's multiple comparison tests, $p^* < 0.05$, $p^{**} < 0.01$, and $p^{***} < 0.001$.

7.7. Discussion

In this section we exploited a technique that permits an accurate measurement of force transduction apparatus components relative to muscle fibre type. Skeletal muscle is a composite tissue that formed from muscle fibres, blood vessels, nerves and connective tissue. In spite of the essential role of the latter component in skeletal muscle function, it is the least studied portion of this tissue. In order to expand our understanding of skeletal muscle functionality, investigation of its components is required. Indeed, very few studies have examined the relationship between muscle ECM and metabolism at the single fibre level. This is mainly due to lack of techniques that afford the resolution and sensitivity required to quantify ECM components and their receptors at the membrane of single fibres. Thus, in this study we have taken advantage of the development of semi-quantitative immunofluorescence-based techniques that allow us to investigate levels of DGC and ECM entities in specific myofibre types (Arechavala-Gomez et al., 2010, Anthony et al., 2011).

Results of this study reveal new features regarding the molecules associated with physically coupling the force generating sarcomeres with the ECM via sarcolemma spanning proteins. Firstly, we showed that fibre type related to the expression of MHCIIB influences levels of DGC proteins at the sarcolemma. Secondly, results of the current study confirmed previous findings (Elashry et al., 2012) that demonstrated low levels of connective tissue components in hypertrophic myofibres developed in the absence of *Myostatin*. Importantly, our analysis showed that the oxidative programme imparted by introducing of *Errγ* in the *Mtn*^{-/-} background muscles was able to increase levels of many DGC and ECM components in *Mtn*^{-/-} muscles. We also found that membrane-associated proteins of DGC could be divided into two groups. First one that consists of β-DG and α, γ-SG proteins showed higher levels in WT fibres than those from *Mtn*^{-/-} mice for a specific MHCII isoform, and a second group which consists of β and δ-SG proteins displayed reversed relationship (higher levels in *Mtn*^{-/-} than WT muscle fibres).

Several studies have documented that Myostatin regulates muscle development and growth through Smad and AKT signalling pathways which in turn inhibit muscle myogenesis, same pathways known to induce fibroblast proliferation thereby connective tissue production (Langley et al., 2002, Li et al., 2008). Therefore, it would be expected that genetic alteration

of *Myostatin* results in the development of large muscle fibres with less connective tissue content. In support of this view, previous work showed that hypertrophic muscle fibres from *Mtn*^{-/-} have less collagen compared to counterparts muscles from WT mice (Elashry et al., 2012). This hypothesis confirmed by our observations in this study. By a way of an explanation of the reduction in DGC and ECM components in *Mtn*^{-/-} muscles, it is might be an adaptive change to the fast contracting glycolytic nature of the mutant muscle (Kovanen et al., 1984b). Moreover, the hypertrophic muscle fibre would have a limited amount of key proteins and therefore due to its size, there would be less of each component relative to the size of hypertrophic muscle fibre. In the latter, fast contracting muscle fibres are postulated to have lower levels of ECM in order to decrease the amount of energy stored in the connective tissue thereby making more available for force exertion on tendons (Kovanen et al., 1984a). In fact, a variety of studies have shown that slow muscle fibre has more abundant of ECM than the fast phenotypes (Kovanen et al., 1980, Kovanen et al., 1984b).

An interesting feature highlighted by our work in this chapter is that irrespective of genotype, MHCII⁻ fibres have higher levels of DGC than MHCII⁺ fibres. Most importantly, muscle-specific expression of *Erry* in the *Mtn*^{-/-} results in an increase of almost all DGC proteins at the sarcolemma. It is important to note that due to the nature of our experimental design we are detecting these effects independent of fibre type switching. We believe that these results highlight novel and unexpected findings. Kovanen and colleagues (Kovanen et al., 1980, Kovanen et al., 1984a) predicted that equivalent MHCII myofibres from differing genotypes should have the same levels of DGC proteins. Interestingly, our data contradict this prediction, meanwhile reveals that the metabolic feature of muscle is more important than the MHCII isoform being expressed.

Our work examining the intercellular and extracellular components of the DGC and the ECM offers interesting insights into the ability of muscle metabolic programme to influence not only the muscle fibre but also the cells that give origin of ECM compositions, named fibroblast (Kuhl et al., 1984, Fry et al., 2017). To our knowledge, there are no experimental data available on fibre metabolic specific expression of DGC and ECM proteins in healthy muscles. Therefore, a central question to be addressed here is whether metabolic programmes established in this study able to coordinate the production of DGC and ECM

from these two cellular sources to generate appropriate stoichiometric levels for a particular muscle (oxidative/glycolytic) phenotype. We believe that our work highlights an interesting relationship between muscle and fibroblasts in relation to ECM production. *Myostatin* null muscles show less intracellular, extracellular, and many membrane-associated components in all muscle examined compared to counterparts muscles from WT mice. However, our remodelling of *Mtn*^{-/-} muscles through the muscle-specific expression of *Erry* reveals that the oxidative metabolic programme of the muscle fibre is able to overcome whatever effects of the absence of *Myostatin* might have on not only muscle fibres but also associated fibroblasts. This could be on either the secretion of signalling molecules from muscle that increase fibroblast number or by augmenting fibroblast secretion of ECM components. These outcomes again suggest that features induced by a germline deletion of *Myostatin* are not genetically locked down, but can be modified by metabolic reprogram established by *Erry* overexpression.

A number of studies have demonstrated that sarcoglycan subcomplex within DGC is essential to provide support for the plasma membrane because it associates with dystrophin and dystroglycan complex, which they in turn interact with actin and laminin respectively, this molecular linkage directly connects the cytoskeleton and the ECM (Yoshida et al., 1994, Ervasti and Campbell, 1993). It has been shown by a number of investigators that β and δ -SG are forming a core of the sarcoglycan complex (Chan et al., 1998, Vainzof et al., 1999). Further work reported that mutation in δ -SG gene results in complete absence of other members of sarcoglycan subcomplex, in contrast, loss of γ -SG might reduce but did not eliminate expression of other components (Hack et al., 1998).

An important finding from our study relates to the impact of the *Mtn* mutation on the composition of the DGC, is the considerable variation in the fully formed DGC complex at the sarcolemma. In this case, we identified increased levels of β -SG and δ -SG in *Mtn*^{-/-} fibres compared to other DGC components (Figures 7.7 and 7.8). The biological significance of changes in the stoichiometry of the DGC complex in *Mtn*^{-/-} mutant remains to be established. This is certainly important since a body of work has demonstrated that a fully assembled sarcoglycan subcomplex increases stability and renders it less prone to degradation (Jung et al., 1996a). Additional study has illustrated that absence of one member of sarcoglycan subcomplex has an important effect, but variable consequences for

the stability of the other components that depending on the specific sarcoglycan subcomplex mutated (Bushby, 1999, Araishi et al., 1999, Liu and Engvall, 1999). Therefore, based on the essential role of β and δ -SG to support the plasma membrane against the force generated during muscle contraction (Hack et al., 1998), $Mtn^{-/-}$ muscles maintained these molecules in order to avoid the complete loosing of this complex function as it could be stable with fewer than four members (Straub et al., 1997). Interestingly, the high levels of these molecules preserved in $Mtn^{-/-}/Erry^{Tg/+}$ muscles to provide entities required for the functional unit.

In addition, we propose a functional significance for altered SG content of the DGC in hypertrophic fibres based on the fact that each SG seems to have a unique biological property. This hypothesis supported by a huge body of work that has shown that mutations in each SG manifest in a specific disease (mutations in α , β , γ , δ cause limb-girdle muscular dystrophy type (LGMD) 2D, 2E, 2C and 2F respectively (Wicklund and Kissel, 2014).

Finally, we provide additional evidence of the impact of muscle metabolic nature to influence DGC molecules at the transcriptional level. A number of biomarker genes that encoded DGC proteins (*Dystrophin*, α -DG and β -SG) display similar differences remarked by immunofluorescence survey, the expression of these genes detected by RT-PCR technique (Figure 7.11A). However, results from Western blot analysis of total protein lysates did not mirror our semi-quantitative immunofluorescence findings (Figure 7.11B). Possible explanations include differences in sensitivity or protein localization. Changes in immunofluorescence intensity between genotypes are relatively small and may be below the resolution of densitometry performed on Western blot. Furthermore, while immunofluorescence quantifications focused on proteins at the plasma membrane level, Western blot analyses were performed on total protein lysates without enrichment for membrane fractions. However, even with membrane fractionation, Western blot analysis would not be able to resolve differences in ECM and DGC proteins between different fibre types. Therefore, Western blot analysis and semi-quantitative immunofluorescence provide complementary information. Of note, Western blot analyses suggest a possible increase in α -DG and β -DG proteins in $Mtn^{-/-}/Erry^{Tg/+}$ compared to either WT or $Mtn^{-/-}$ muscles. This increase was not accompanied by a similar increase in dystrophin or β -SG, suggesting that *Erry* differentially might up-regulate or stabilize dystroglycan complexes that do not contain

dystrophin (Johnson et al., 2013). Further studies with larger numbers of animals and more targeted biochemical approaches will be needed to confirm and define the connection between oxidative metabolism and dystroglycan. Moreover, the multifunctional nature of the sarcoglycan complex, and the entire DGC, highlights the importance of understanding the full role of each component in both healthy muscle function and disease.

In summary, this study provided a detailed examination of DGC and ECM components alterations due to muscle fibres size and metabolic status change. It adds to the growing body of work that the muscle metabolic nature is not only affects muscle fibres but also influences the components of DGC and ECM. Glycolytic phenotypes develop in the absence of *Myostatin* have less level of many of these compartments. Importantly, oxidative metabolic programme imparted by overexpressing of *Erry* was efficacious to overcome the impacts of *Myostatin* deletion on these compartments. Furthermore, our work highlights the benefit of the semi-quantitative immunofluorescence protocol.

Chapter 8

General discussion and conclusion

General discussion

The principle endeavour behind this project was to determine whether it is possible to produce large muscle fibres, at the same time able to support prolonged period of work. For the last few decades, it was thought that large muscle fibres have to be fast and glycolytic, as there is a trade-off between muscle fibre size and its oxidative capacity (Van der Laarse WJ, 1998, Degens, 2012). The greater our knowledge of hypertrophic fibre functions, in particular exercise and regeneration capacity, the better we are able to develop clinical treatments and so improve the quality of life for people. Skeletal muscle possesses a remarkable plasticity and responds to environmental and physiological stimuli by changing its phenotype in terms of size, composition, and metabolic properties (Pette and Staron, 2001, Mounier et al., 2015, Matsakas and Patel, 2009b). Myostatin is a negative regulator of muscle development belongs to the Transforming Growth Factor- β (TGF- β) superfamily (McPherron and Lee, 1997). Genetic or pharmacological inhibition of its signalling has been utilised to induce muscle mass (McPherron et al., 1997, Pistilli et al., 2011). Despite the enlarged muscles appearing normal at the histological level, their ability to generate tension is markedly reduced (Mendias et al., 2006, Relizani et al., 2014). On the other hand, *Erry* is an orphan nuclear receptor with abundant expression in mitochondrial rich, and high energy demands tissues (Giguere, 2008, Narkar et al., 2011). It has emerged as a key transcriptional regulator of pathways crucial in the regulation of muscle energy metabolism, contractile function, and growth (Rangwala et al., 2010, Cho et al., 2013).

Over the last decade, the generation of tissue-specific *Erry* transgenic or knockout has rapidly advanced our understanding of its roles in regulating different aspects of muscle metabolism and energy production. Transgenic mice expressing *Erry* in the skeletal muscle showed an increase in mitochondrial size, improved oxidative capacity, and increased exercise tolerance, indicating that *Erry* may control the metabolic response of skeletal muscle during exercise (Narkar et al., 2011, Badin et al., 2016).

For this study, we introduced the expression of *Erry* into a muscle lacking *Myostatin* using specific promote named human α -skeletal actin (HSA). We hypothesis that superimposition of *Erry* that would induce oxidative metabolism in a *Mtn*^{-/-} muscles that are associated with

hypertrophy, challenges the suggested inverse relationship between muscle fibre oxidative capacity and its size.

Large muscle mass developed in the absence of *Myostatin* is conserved in *Mtn*^{-/-}/*Erry*^{Tg/+} muscles

Lack or inhibition of *Myostatin* function produces mice with a phenotype exhibiting a dramatic increase in muscle mass (McPherron and Lee, 1997, Hulmi et al., 2013a). The work carried out in chapter 3 showed that despite the increased muscle mass, body weight of *Mtn*^{-/-} and *Mtn*^{-/-}/*Erry*^{Tg/+} was similar to that of WT mice, indicating a reduction in other tissues mass. We and others have shown a remarkable reduction of connective tissue content in hypertrophic muscle of *Mtn*^{-/-} mice (Elashry et al., 2012). Moreover, a study by Lebrasseur has revealed that the large muscle in *Mtn*^{-/-} phenotypes develops concurrently with a decrease in fat deposition (Lebrasseur, 2012). In fact, the newly known myokine Irisin that is secreted from skeletal muscles in blood effectively promotes thermogenesis in adipose tissue (Bostrom et al., 2012). Importantly, it was reported that *Myostatin* deletion results in an increase of Irisin production from skeletal muscle, hence promotes tissue thermogenesis and reduces fat deposition (Shan et al., 2013). Although the *Mtn*^{-/-}/*Erry*^{Tg/+} muscles showed a restoration of most DGC and ECM proteins at the sarcolemma to normal levels as shown in chapter seven, the body weight of these animals still similar to WT and *Mtn*^{-/-} mice. It has been demonstrated that *Erry* can promote expression level of uncoupling protein 1 (*UCP1*) mediated by ERR response element (ERREs) that is present in the enhancer of the *UCP1* (Giguere, 2008, Dixen et al., 2013). Moreover, the elevated expression of *UCP1* gene that transduces brown adipocytes in *Erry* transgenic muscles was concomitant with an enhanced rate of fatty acid oxidation (Dixen et al., 2013). The later hypothesis robustly supported by our results at the transcriptional level, evidenced by upregulation of fatty acid oxidation and metabolism genes following *Erry* overexpression in *Mtn*^{-/-} muscles. We suggest that *Myostatin* deletion increases muscle mass, at the same time reduces connective tissue production, and promote browning of WAT, thereby preventing an excessive increase in body weight. Interestingly, introducing of *Erry* provides the requirements of browning process that include high expression of *UCP1*, and high mitochondrial number and activity

(Cannon and Nedergaard, 2004). Ultimately, it prevents WAT accumulation, and hence displays same body weight of other two genotypic groups.

The reasons behind an increase in muscle mass are related to the stage of *Myostatin* absence. Unlike in genetic alteration, post developmental blocking of Myostatin induces muscle mass due to the increase in muscle fibre size but not the number (McPherron et al., 1997, Whittmore et al., 2003). Previous studies have shown that Myostatin acts as a regulator of embryonic muscle progenitors proliferation and differentiation mediating by interfering with the cells cycle progression from G1 to S-phase through upregulation of P21 and a Cdk inhibitors (Manceau et al., 2008, McCroskery et al., 2003). Further work that supported the developmental origin of the hypermuscular phenotype, has shown a marked acceleration of the myogenic programs of primary and secondary myogenesis due to *Myostatin* absence (Matsakas et al., 2010). These data with our results clearly evidenced the embryonic origin of myofibre hyperplasia without a post-natal change in fibre number. Consequently, the only determinate factor that causes the increase in muscle mass following sActRIIB injection is the enlargement of muscle fibres.

In fact, this action directed our plans to investigate the relationship between the increase in muscle mass in *Mtn*^{-/-} and *Mtn*^{-/-}/*Erry*^{Tg/+}, as well as WT and *Erry*^{Tg/+} mice injected with sActRIIB, and protein synthesis that might profoundly contribute to this increase.

Our work examining muscle fibre size extends previous findings of Mendias et al. and Relizani et al. (Mendias et al., 2006, Relizani et al., 2014), who demonstrated a dramatic increase in muscle fibre size following *Myostatin* deletion or post-natal inhibition of its function. Myostatin was suggested to negatively regulate muscle growth by inhibiting myoblast differentiation, and Akt/mTOR pathway by promoting phosphorylation of Smad2 and Smad3, that in turn preventing Akt phosphorylation, ultimately induce muscle atrophy (Glass, 2005). In addition to Myostatin, (IGF1/ PI3K/ Akt/ mTOR) (Sakamoto et al., 2002), and FoxO3, mediated proteasomes and autophagy (Stitt et al., 2004) pathways are known for their roles in regulating of muscle fibre size. The interaction between these pathways determines the rates of protein synthesis and degradation. It has been shown that during conditions of disuse, *FoxO* transcription factors are strongly upregulated expression of *Atrogin1* and *MuRF*, which are associated with protein degradation (Sandri et al., 2004, Stitt

et al., 2004). In response to muscle fibre hypertrophy following *Myostatin* deletion or blocking, Akt is activated, and subsequently inhibits protein degradation by phosphorylating FoxO, that results in a decrease in transcription of FoxO target genes (Sandri et al., 2004). This hypothesis is supported by our data shown in chapter 3. Alternative reason beyond the large mass of *Mtn*^{-/-} muscles, is a high proportion of glycolytic phenotypes that associated with large CSA as shown in chapter three.

Additional evidence has been provided in chapter four that despite the increase in muscle fibres size of *Mtn*^{-/-} muscles, myonuclei number per each muscle fibre is not proportionally increased, resulted in a reduction of nuclear : cytoplasmic ratio. These data are supported by Amthor's findings (Amthor et al., 2009). Based on the idea that each nucleus can supply a limited volume of cytoplasm with gene transcripts, the addition of myonuclei is a prerequisite for muscle fibre hypertrophy (McCarthy et al., 2011). Further investigators have shown that the accretion of myonuclei number is correlated linearly to muscle cross-sectional area increase, thus cytoplasmic volume per nucleus is constant (Hall and Ralston, 1989, Roy et al., 1999). Here we show a significant increase in myonuclei number following *Erry* overexpression onto *Mtn*^{-/-} background muscles. In support of this view, it has been illustrated that high oxidative muscle fibres contain a high number of myonuclei compared to low oxidative ones (Allen et al., 1995). Interestingly, the oxidative fibres are characterised by large potential for transcription (i.e., myonuclei and mitochondria), as well as possessing high capacity for protein synthesis (van Wessel et al., 2010). Such higher myonuclear density in oxidative fibres that developed due to *Erry* overexpression may indicate that these fibres have relatively higher potential for transcription and protein synthesis, thereby maintain the increase in muscle fibres size.

Additionally, previous work has reported that the rate of protein degradation is mainly induced by oxidative stress (Powers et al., 1999). Thus, the low oxidative stress that indicated by low level of ROS production in *Mtn*^{-/-}/*Erry*^{Tg/+} and *Erry*^{Tg/+} muscles treated with sActRIIB, may provide additional evidence of the potential of *Erry* transgenic to support protein synthesis, sustain the increased muscle fibre size and hence muscle mass.

High oxidative metabolism, energy production and physiological activity in *Mtn*^{-/-}/*Erry*^{Tg/+} muscles

The balance between myofibrillar protein synthesis, mitochondrial biosynthesis and degradation is a major factor that determines muscle fibre size and oxidative capacity. Indeed, the relationship between muscle fibre CSA and mitochondrial number denotes that muscle fibres can get larger at the expense of endurance capacity (van Wessel et al., 2010). In order to prevent the decrease in maximum steady state power of hypertrophic fibre, oxygen supply to the mitochondria must be maintained. To accomplish this, high level of capillary density is required to increase oxygen transport to muscle fibres (Des Tombe et al., 2002), as well as an appropriate media needed to facilitate oxygen transport to mitochondria (van Beek-Harmsen et al., 2004). Moreover, the diffusion distance of oxygen from blood vessels to mitochondria should be reduced, which might be in a part mediated by increasing the number of mitochondria into the sub sarcolemma region (Deveci et al., 2001). Taken together, these studies might explain why muscle fibres with high oxidative capacity try to limit their size, so it can be considered an evolutionary design constraint. Therefore, the question to be addressed in this study is whether such adaptations can occur synchronously with an increase in muscle fibre size.

Myostatin regulates skeletal muscle metabolism, since its genetic ablation, or epigenetic interfering with its function, leads to a predominance of glycolytic fibres as a result of a marked depress in muscle oxidative capacity (Matsakas et al., 2010, Relizani et al., 2014). Similar bias toward the glycolytic myofibres phenotype has also been identified in cattle with muscle hypertrophy that is associated with mutation in *Myostatin* gene (Wegner et al., 2000). Further work has revealed the role of activin-receptor IIB that is activated by Myostatin to regulate SDH activity (Matsakas et al., 2012a). In addition to the low oxidative capacity, the hypertrophic-glycolytic phenotype that develops in the absence of *Myostatin* was associated with a decrease in force generation and exercise capacity. Previous work has reported that the exercise failure could be attributed to the reduction in mitochondrial density as a consequence of *Myostatin* deletion (Amthor et al., 2007). Therefore, an important point addressed here is whether inducing mitochondrial number will be efficacious to restore exercise capacity via promoting energy production, thereby enhancing

muscle physiological activity. A study by Desplanches et al. demonstrated that the ability of mitochondria to produce ATP depends on oxygen supply via tissue blood perfusion (Desplanches et al., 1996). As we mentioned above such process requires a high density of blood vessels to deliver oxygen to muscle fibre, as well as the proper distribution of mitochondria. In agreement with data shown in chapter four of this study, previous work has identified a decreased in capillary density of a muscle lacking *Myostatin* (Rehfeldt et al., 2005, Amthor et al., 2007), which might attribute to the direct effect of *Myostatin* on regulating of muscle capillary density via controlling endothelial cells proliferation (Hayot et al., 2011). Moreover, an aforementioned study has reported a decrease in *Vegf- α* expression following treatment of C2C12 myotubes with sActRIIB, providing additional evidence of the indirect negative impact of Myostatin inhibition on capillary formation (Relizani et al., 2014). In fact, the unfavourable combination of decreased muscle vascularization and metabolic changes after *Myostatin* ablation or inhibition would likely result in insufficient mitochondrial ATP synthesis during exhaustive exercise, which might explain rapid fatigability of these animals (Robergs et al., 2004).

The decreased oxidative capacity, mitochondrial number and capillary density of *Mtn*^{-/-} muscles, was associated with an increase in the proportion of the fast MHCIIB that is known to be related to the increase in muscle fatigability (Girgenrath et al., 2005). It was well established that muscle fibres have the ability to modify MHC type in response to changes in the internal or external environment (Pette and Staron, 2001). Myostatin plays a vital role in the determination of adult muscle fibre type. Notably, its absence inhibits proliferation or differentiation of primary myoblasts that results in a decline in slow muscle fibre number. Conversely, increases the proliferation or differentiation of secondary myoblasts leading to a high number of fast-twitch phenotypes. Accordingly, increased type IIB fibres would cause the muscle to be predominantly glycolytic (Girgenrath et al., 2005, Langley et al., 2002). Significantly, the predominance of fast glycolytic fibres may well explain the increase in contraction speed, and shortening in relaxation time in *Mtn*^{-/-} muscles. However, there is no benefit of these muscles in term of the high tetanic generation to be expected of glycolytic fibres (Wegner et al., 2000, McPherron et al., 1997).

Alternatively, low level of connective tissue in *Mtn*^{-/-} muscles (shown in chapter seven) may act as an additional contributor that promote further rapid twitch kinetics (Amthor et al., 2007).

Nevertheless the similarity in muscle fibre size and muscle mass of *Mtn*^{-/-} and *Mtn*^{-/-}/*Erry*^{Tg/+}, the later muscle fibres showed high oxidative capacity indicated by the high proportion of SDH⁺ fibres. Such combination could challenge the constraint between muscle fibre aerobic metabolism and its size. A number of studies have reported that *Erry* directly or indirectly regulates the expression of numerous target genes that are related to different metabolic pathways, specifically mitochondrial biogenesis and respiration in response to cellular stress (Narkar et al., 2011, Badin et al., 2016). Therefore, superimposition of *Erry* onto *Mtn*^{-/-} or WT muscles may be a powerful strategy to overcome the metabolic disorders following *Myostatin* deletion or inhibition of its function at the post-natal stage. Previous studies have revealed a robust increase in SDH activity following *Erry* overexpression, and the oxidative phenotype stimulated even with the absence of ligands (including PGC-1 α) (Rangwala et al., 2010, Greschik et al., 2002). Further work has demonstrated that the overexpression of *Erry* leads to an increase in oxidative metabolism and heat generation (Dixen et al., 2013). These outcomes which are in agreement with findings of the current study may well explain the high level of *Erry* during physical exercise as a part of an adaptive metabolic response (Narkar et al., 2011, Badin et al., 2016). By understanding the phenotype of *Myostatin* null mice, our work provides key mechanisms that need to be induced in order to promote fatigue resistance. Therefore, we suggest that the ability of *Mtn*^{-/-}/*Erry*^{Tg/+} mice to run longer than other genotypic groups, is possibly attributed to the increased mitochondrial density that associated with high ATP production, and improved oxidative capacity which evidences *Erry* potential to control the metabolic response of skeletal muscle during exercise.

The increased exercise capacity of *Mtn*^{-/-}/*Erry*^{Tg/+} mice raises interest in the understanding of *Erry* role in regulating other pathways that might contribute to the improvement muscle physiological function, that might need to be raised in order to meet the energy demands. We showed previously that the coupling between muscle fibre size and capillary density has been altered in *Mtn*^{-/-} muscle fibres that reflected negatively on muscle energy status and thereby reduced muscle physiological performance. On the other hand, numerous studies

have reported that transgenic expression of *Erry* in anaerobic fast muscle fibre promotes aerobic transformation, angiogenic programming and mitochondrial biogenesis in absence of exercise (Narkar et al., 2011, Matsakas et al., 2012b). In support of this view, previous work has revealed an essential role of *Erry* to transcribe all *Vegf- α* isoforms mediating by stimulating of this biomarker gene's promoter that contains *Erry* binding sites (Arany et al., 2008a). It is worth noting that *Erry* effect on angiogenesis may not only be due to *Vegf- α* induction, but in addition to its role in activation of *Fgf1*, *Erry* also regulates endothelial cell proliferation and migration (Zheng et al., 2007, Partridge et al., 2000). Most importantly, the angiogenesis programme established by introducing of *Erry* in the either *Mtn*^{-/-} or WT muscles is responsive to the increase in muscle fibres size resulted from *Myostatin* deletion or sActRIIB administration. Collectively, these findings indicate a direct transcriptional activation of angiogenesis genes by *Erry*, as well as evidence its positive impacts on endothelial cells proliferation, thereby increases muscle capillary density, to provide a suitable microenvironment that matches the increased muscle fibres size and oxidative capacity requirements.

Although *Erry* overexpression induces mitochondrial density and blood supply in hypertrophic myofibres, high rate of oxygen diffusion from capillary to mitochondria is required to sustain high energy level, and hence support a long time of exercise. Interestingly, important modifications take place in *Mtn*^{-/-}/*Erry*^{Tg/+} muscles are, firstly, the hyper-oxidative hypertrophic myofibres displayed a high mitochondria subpopulation at subsarcolemmal than the intrafibrillar ones. Secondly, introducing of *Erry* in the *Mtn*^{-/-} muscles significantly induced myoglobin transcription and this protein would facilitate oxygen diffusion and storage into mitochondria in the developed hypertrophic myofibres (Hoofd and Egginton, 1997). Indeed, mitochondria were brought to attention here due to its central role in producing ATP to meet cellular requirements, and sustain high metabolic rate and physical performance, which are characteristics of oxidative fibres. The mitochondrial density is dynamically regulated in response to oxygen availability, that supporting mitochondrial biogenesis (Levett et al., 2012). Although the precise mechanism through which *Erry* promote mitochondrial biogenesis is uncertain, there is ample evidence that it enhances oxygen diffusion. Previous work has shown that mitochondrial biogenesis is regulated by signalling given by nitric oxide (NO) and hydrogen peroxide H₂O₂ diffusion from

mitochondria to cytosol, the process that is controlled by membrane potential, and reliant on the mitochondrial metabolic state (Nisoli et al., 2004). Moreover, the mitochondrial nitric oxide synthase (mtNOS) activity is also regulated by membrane potential, and it works as a regulatory enzyme that is in turn regulates mitochondrial O₂ uptake, thereby promotes oxidative phosphorylation to repeat the biogenesis cycle (Navarro et al., 2005). It seems that the increased capillary density, mitochondrial number at the appropriate area of muscle fibre, accompanied with a high level of myoglobin are contributing to the preventing of a decline in maximum steady state power when oxidative fibre get larger (Heard et al., 2000). Taken together, these data would challenge the inverse relationship between muscle fibre size and oxidative capacity by taking into account the capability of hypertrophic hyper-oxidative myofibres from *Mtn*^{-/-}/*Erry*^{Tg/+} muscles to produce angiogenic factors, and promote mitochondrial biogenesis. Ultimately, it permits the formation of new blood vessels, and improves oxygen diffusion rate to mitochondria that is associated with high level of ATP production, which are positively affected animals' behavioural performance and physical exercise.

An interesting feature highlighted by our work is the high proportion of SDH⁺ fibres in *Mtn*^{-/-}/*Erry*^{Tg/+} muscles was accompanied with a partial normalisation of the MHC fibre profile; indicated by a decrease in the proportion of MHCIIb, and increase in MHCIIa and MHCIIx fibre numbers. However, the conversion does not lead to the formation of MHC type I. It was well established that *Erry* is highly expressed in oxidative (type I) slow-twitch muscle fibres, and it works coordinately with AMPK to initiate formation of this myofibre type possibly via activation of miRNA-208b and miRNA-499 (Gan et al., 2013). However, the protocol of overexpression of *Erry* in the *Mtn*^{-/-} muscles we established in this study was unable to influence this process. In fact, a number of studies have reported that MHC isoforms clearly correlate with the kinetics of stretch activation that induces delayed force increase (Galler et al., 1994, Hilber et al., 1999). Such correlation indicates that different MHC isoforms are generating different speeds of force. Further work reported that the kinetics of stretch activation is proportional to the ratio between MHC-IIx and MHC-IIb (Andruchov et al., 2004), which possibly explain the transition between these two types of muscle fibres. Alternatively, the post-translational modifications of MHC could be another crucial reason behind the protein variations with altered functions (Maggs et al., 2000,

Ramamurthy et al., 2001). Furthermore, presence of other myofibrillar proteins such as myosin light chain (MLC), and thin filament proteins also could influence muscle fibres kinetic, thereby induce the transition in muscle fibre phenotypes (Bottinelli et al., 1994a, D'Antona et al., 2002). These data provide ample evidence that MHCII fibres are more plastic and adaptable phenotypes, but it is not the case with MHC type I (Sutherland et al., 1998). Moreover, changes in MHC profiling following either *Myostatin* deletion or *Erry* overexpression anticipated as an adaptive step to preserve the contractile function.

A number of studies have shown that ECM in skeletal muscle is critical for force transmission from muscle fibres to tendons (Purslow, 2002, Kjaer, 2004), thus precise regulation of ECM is necessary to ensure optimal muscle functions. Interestingly, our findings show that the restored ECM and DGC proteins due to remodelling of *Mtn*^{-/-} muscles through muscle-specific expression of *Erry* distributed regularly on between muscle fibre types, slow fibres contain high ECM than the fast ones. Notably, restoration and distribution of ECM and DGC compartments in *Mtn*^{-/-}/*Erry*^{Tg/+} muscles were positively correlated to the increased capillary density, oxidative capacity, force generation and exercise tolerance of these mice. Collectively, these findings provide evidence that the oxidative metabolic program established by *Erry* expression is not only influence muscle fibres, but also their associated ECM and DGC components that positively affected muscle physiological performance.

An important aspect to be elucidated here is the potential involvement of metabolic genes in the improvement of physiological activity. Interestingly, the features of metabolic profile of *Mtn*^{-/-}/*Erry*^{Tg/+} muscles were mirrored at the transcriptional level. The increased oxidative capacity, energy production and capillary density accompanied by a marked upregulation of genes known to regulate oxidative and energy metabolism, glucose metabolism and transport, angiogenesis, and fatty acid metabolism, uptake and transport. These observations strongly supported by previous studies that revealed a central role of *Erry* in regulating multiple genes that linked to mitochondrial function and biogenesis, fatty acid oxidation and metabolism, and glucose metabolism (Zhang et al., 2006, Dufour et al., 2007).

In this study, the observed large myofibres CSA in *Mtn*^{-/-} muscles was attributed to the high level of protein synthesis that driven by upregulating of Akt that subsequently phosphorylates and inactivates of FoxO3, a key regulator of protein degradation pathways,

autophagy and proteasome. These results support data of others showing that autophagy is reduced in *Mtn*^{-/-} muscles (Amthor et al., 2007). Further work has unveiled a marked reduction in autophagy level and exercise tolerance due to post-natal inhibition of Myostatin by sActRIIB administration (Mizushima et al., 2010). Alternative factor that might contribute to the low autophagy flux in the *Mtn*^{-/-} muscles is the marked reduction of ECM content (Grumati et al., 2010). It has been demonstrated that autophagy is a conserved homeostatic process that is responsible for removing damaged organelles and other unwanted cytoplasmic components to support cell survival (Sandri, 2013, Mizushima et al., 2010). Thus, we believe that the reduced autophagy rate may well explain the unfavourable accumulation of damaged organelles, and hence the appearance of ultrastructural abnormalities (misaligned and disrupted Z-lines, large intra-sarcomeric space, and altered mitochondrial size and distribution) in *Mtn*^{-/-} muscles as shown in chapter three, which possibly hamper muscle contractile functions and reduced exercise capacity. Furthermore, the proteolytic enzymes that degrade the modified proteins (Grune et al., 2003), were lower in *Mtn*^{-/-} muscles which imply less efficient removal and thereby an accumulation of unwanted organelles. Moreover, the high level of ROS production was found in *Mtn*^{-/-} and WT.sActRIIB muscles may consider another important reason for the reduced force generation and exercise capacity, as it induces mitochondrial dysfunction, and because of mitochondria are sites of ROS production, so they become a potential target of damage. The observed loss of specific force in *Mtn*^{-/-} muscles in the current study might also attribute to the impairment in muscle excitation-contraction (EC) coupling, a Ca²⁺ dependent process. It has been documented that during muscle contraction, the Ca²⁺ channels in the transverse tubules are activated due to membrane depolarization, which in turn trigger activation of sarcoplasmic reticulum (SR) Ca²⁺ release channels named ryanodine receptor 1 (RyR1). Subsequently, increased cytoplasmic Ca²⁺ level, which is essential for actin-myosin cross-bridging, sarcomeric shortening, and muscle contraction (Allen et al., 2008, Andersson and Marks, 2010). There is an evidence that skeletal muscle RyR1 function and Ca²⁺ signalling are negatively affected by the oxidative stress resulted from high production of ROS in aged muscles (Aracena-Parks et al., 2006, Jang et al., 2010). In the same line of thought, Durham et al. reported that mice with a malignant hypothermia mutation (Y522S) in RyR1 displayed SR Ca²⁺ leakage and high ROS production, which induces mitochondrial dysfunction and

oxidative stress, ultimately mediated changes of the RyR1 (Durham et al., 2008). Moreover, the increased level of ROS production in the aged muscles is associated with alteration of cellular Ca^{2+} handling (Durham et al., 2008). Taken together these data suggest that RyR1 mediated SR Ca^{2+} leak may exacerbate mitochondrial dysfunction by causing mitochondrial Ca^{2+} overload, which in turn leads to increase ROS production, that further induces RyR1 SR Ca^{2+} leak via oxidising the channels. Given our observations show that muscles developed in the absence of *Myostatin* were associated with high level of ROS and ultrastructural abnormalities, we suggest that *Myostatin* null phenotypes likely share a common mechanism that contributes to impaired force generation and exercise capacity.

Interestingly, the ultrastructural abnormalities were largely eliminated following *Erry* overexpression possibly by inducing and normalising FoxO3 level. Additionally, ROS production was significantly reduced in *Mtn^{-/-}/Erry^{Tg/+}* and *Erry^{Tg/+}. sActRIIB* muscles. A key aspect of our work is that unwanted organelles clearance programmes are being mediated by FoxO3, are not anabolic, but are essential for maintaining muscle homeostasis. Therefore, removal of dysfunctional sarcomeres and mitochondria in *Erry* transgenic muscles robustly attributed to the efficient autophagy and proteasome systems. Alternatively, energy sensor AMPK that known to be induced by *Erry*, has been shown to have a critical role in regulating autophagy (Hoyer-Hansen and Jaattela, 2007). The additional modification that takes place in *Mtn^{-/-}/Erry^{Tg/+}* muscles is the high level of antioxidants (anserine and catalase), that play a positive role as scavenger agents for byproducts arising from elevated oxidative activity in these muscles. Consistently, it was well established that aged mice received antioxidants exhibited better performance in behavioural tests, as these compounds induced mitochondrial oxygen uptake and oxidative phosphorylation, thereby less ROS emission, and more ATP production that robustly supporting physiological functions (Navarro et al., 2005). Furthermore, *Erry* regulates expression level of genes that control ETC pathway in mitochondria, which is the main sources of ROS production (Alaynick et al., 2007). In the same line of thought, numerous studies have unveiled the *Erry* potential to regulate expression of genes that control calcium handling pathways (Stein and McDonnell, 2006, Rangwala et al., 2010). Together, *Erry* transgenic potentially promotes autophagy and proteasome pathways, increases antioxidants level and hence reduces ROS production, and prevent Ca^{2+} overload on mitochondria by regulating its signalling pathway. Importantly,

these modifications positively correlate with improvement in physiological performance, force generation capacity and exercise tolerance.

Experiments looking at myonuclei distribution within individual muscle fibres show that myonuclei are not scattered randomly. This view is confirmed by Bruusgaard et al. who revealed evenly and orderly distribution of myonuclei throughout cytosol (Bruusgaard et al., 2003). Moreover, it has been shown that proper nuclei spacing is a prerequisite for normal muscle function (Metzger et al., 2012). Substantially, nuclear disorganization is a hallmark of aged skeletal muscle, and is detected in models of muscular dystrophy (Bruusgaard et al., 2006, Meinke et al., 2014). Further work has reported that myonuclear domain size is mainly defined by mitochondrial protein systems (Liu et al., 2009). Although the number of myonuclei increased significantly following *Erry* overexpression in the *Mtn*^{-/-} muscles, they were disorganised. We mentioned above that in addition to the high number of myonuclei, *Mtn*^{-/-}/*Erry*^{Tg/+} muscles showed a high density of functional mitochondria. Possible explanation that the increased myonuclei and mitochondrial numbers are beneficial to compensate the alteration in myonuclei distribution, hence offers appropriate transcriptional level for protein synthesis in order to meet the increased cytoplasmic volume demand, ultimately restores muscle physical activity.

Although the muscle's active contractile properties take a major focusing of skeletal muscle research, it is evident that muscle ECM is structurally and functionally important. More specifically, skeletal muscle ECM is essential for providing mechanical stability to muscle fibres and blood vessels (Kjaer, 2004). Skeletal muscle is a composite structure that consists of muscle fibres, blood vessels, and connective tissue. Therefore, in order to generate an optimally functional organ, it is important that all these components develop and work in a coordinated manner. We demonstrated notable changes in oxidative properties, myofibre phenotypes and blood capillary density following the metabolic reprograms underwent in this study. Previous work has reported that the contractile properties of muscle fibres are a key factor that can modulate surrounding ECM quality and quantity (Kovanen et al., 1980). Despite that the majority of functional ECM proteins are produced by fibroblast cells, other cell types such as skeletal myoblast have also been shown to contribute to the production of this tissue content like collagen (Kuhl et al., 1982, Gatchalian et al., 1989). Thus, we believe

it is feasible to understand the relationship between muscle metabolism, myofibre types, and extracellular matrix (ECM) components, thereby identify the importance of this supporting tissue. In fact, the dearth of knowledge regarding the relationship between muscle metabolism and ECM, might be attributed to the absence of techniques that allow an accurate measurement required for significant outcomes. Therefore, we have taken advantage of the development of semi-quantitative immunofluorescence-based techniques that can expand our knowledge regarding these components role in the force transduction apparatus in specific muscle fibre types (Ho-Kim and Rogers, 1992, Anthony et al., 2011). Our work examining the intensity and thickness of ECM components offers interesting insights into the interaction between muscle metabolic status and connective tissue content. A number of studies have revealed an inhibition effect of Smad and AKT pathways that are driven by Myostatin signalling on myogenesis, while the same pathways induce fibroblast proliferation, and promote connective tissue development (Li et al., 2008, Langley et al., 2002). Therefore, it would be expected that either genetic deletion or post-natal blocking of Myostatin, the muscle would develop hypertrophic myofibres that are invested with less ECM, which is what we observed in *Mtn*^{-/-} and WT muscles treated with sActRIIB in the current study. Alternatively, *Myostatin* absence leads to the development a thin connective tissue that is suited to the contractile profile of the developed muscle (fast/glycolytic). These findings indicate the critical role of muscle fibres type in the determination of ECM content. Interestingly, this possible thought was confirmed at the individual muscle fibre level, we found that slow-twitch oxidative myofibres content more ECM than the fast-twitch glycolytic phenotypes. Indeed, there is an interaction between muscle fibre and connective tissue has been recognised during embryonic and adult life. It was well established that fibroblast plays a vital role in regulating of muscle fibre type through Tcf-4 signalling pathway, suggesting an indirect control on MHC via connective tissue (Mathew et al., 2011). Moreover, it has been illustrated that TGF- β , which plays a similar role as Myostatin, as it induces fibroblast differentiation and promotes ECM production (Cui et al., 2011). Thus, *Myostatin* deletion or blockage might negatively affect TGF- β receptor sensitivity in ECM compartment, which in turn leads to a reduction in fibroblast proliferation thereby less connective tissue formation. Interestingly, muscle-specific overexpression of *Erry*^{Tg/+} in the *Mtn*^{-/-} background, or in the WT muscles before being treated with sActRIIB overcomes the

negative impacts of *Myostatin* absence or inhibition on ECM and DGC contents. It was efficacious to restore almost all proteins constituting ECM and DGC to their normal levels. Importantly, the restoration of these compartments was correlated to the improvement of animals' behavioural performance, muscles tension production, and regeneration capacity. We suggest that metabolic program of muscle is profoundly affect ECM and DGC components. Additionally, *Erry* overexpression might stimulate the muscles to secrete molecules that either increase fibroblast number, or promote their capacity to proliferate and produce more connective tissue.

Using an acute skeletal muscle in vivo model to investigate effect of *Erry* overexpression on muscle regeneration with low population of satellite cells

Study of muscle regeneration has been used extensively to understand satellite cells functional (Czerwinska et al., 2012). Thus, in this study we offer a new perspective regarding the relationship between muscle metabolism, connective tissue content, and satellite cells number and their activity during regeneration. In agreement with aforementioned reports, work covered in chapter seven showed that the oxidative muscle fibres were invested with more ECM compared to the glycolytic phenotypes (Kovanen et al., 1980, Elashry et al., 2012). In the line of thought, a number of investigators have revealed a high population of satellite cells in slow myofibres than the fast ones (Putman et al., 1999, Christov et al., 2007). Furthermore, satellite cells maintained their ability to proliferate and differentiate in response to the need of myofibre hypertrophy (Schmalbruch and Lewis, 2000). Indeed, skeletal muscle metabolism effectively modulates satellite cells function, fate and capability to induce recovery from injury (Cerletti et al., 2012). In addition to the effects of muscle metabolism on satellite cells activity, previous work has demonstrated regulatory impacts of ECM composition changes on satellite cells, thus influencing their quiescent, activation, differentiation, and maintaining SCs pool via self-renewal (Calve et al., 2010). Other studies have revealed a crucial role of ECM components on mechanical properties of tissue microenvironment, accordingly induce the activity of satellite cells (Gilbert et al., 2010, Guilak et al., 2009). Moreover, Murphy et al. reported that fibroblast cells are required for proper regeneration of skeletal muscle, a process drives by satellite cells (Murphy et al., 2011). Subsequently, fibroblast depletion resulted in a marked alteration in satellite cells

dynamics, that led to the premature differentiation of these cells with poorly regeneration capacity indicated by relatively small size regenerated myofibres (Murphy et al., 2011).

In spite data in chapter three showed a partial transition of myofibres toward the slow-twitch phenotypes within MHCII subsets following *Erry* overexpression on *Mtn*^{-/-} muscles, the number of SCs in these muscles (*Mtn*^{-/-}/*Erry*^{Tg/+}) was lower than those in other genotypic groups. Taking into account the high number of myonuclei per each muscle fibres of *Mtn*^{-/-}/*Erry*^{Tg/+}, it is possible that *Myostatin* deletion induces myoblast fusion at the expense of satellite cells, and overexpression of *Erry* profoundly exacerbates this relationship. Further studies have reported that glycolysis negatively regulates Notch pathway, which in turn makes myoblast competent to fuse (Saj et al., 2010, Gildor et al., 2012). In fact, satellite cells population and activity underpin skeletal muscle regeneration. Therefore, a reduction in their number has been reported to be severely hinder muscle regeneration process (Schuster-Gossler et al., 2007, Vasyutina et al., 2007). Strikingly, a decrease to less than 50% of satellite cells population did not affect the regeneration capacity of *Mtn*^{-/-}/*Erry*^{Tg/+} muscles, possibly because they have a vast capacity to generate precursors which in most situation is never realized fully (Collins et al., 2005). A study by Carlson and Faulkner has unveiled an effective role of the microenvironment on satellite cells activation, proliferation and differentiation, thereby whole regeneration process (Carlson and Faulkner, 1989). Related to this, a number of studies referred to a positive correlation between oxidative metabolism and muscle regeneration capacity (Lowrie et al., 1982, Matsakas et al., 2013). Consistently, genetic manipulation that induces oxidative capacity profoundly accelerates muscle regeneration (Li et al., 2007b).

On the other hand, it was well identified that glycolysis genes are essential in embryogenesis for muscle precursors to increase their size via fusing with surrounding fusion-competent myoblast (Johnson et al., 2003). It seems that glycolysis effectively contributes to cell proliferation and growth during muscle regeneration and development. We suggest that oxidative metabolism resulted from remodelling of *Mtn*^{-/-} muscle through overexpression of *Erry*^{Tg/+} did not overcome entire glycolysis pathway, thus imparts more efficient growth and development approach.

As mentioned earlier, $Mtn^{-/-}/Erry^{Tg/+}$ muscle fibres show high capillary density. Work by Bencze et al. showed that efficient skeletal muscle angiogenesis is necessary for proper regeneration process (Bencze et al., 2012). Data shown in chapter five revealed a high rate of clearing process indicated by the low number and small size necrotic fibres, high macrophages density, and elevated proportion of committed muscle cells in regenerated areas of $Mtn^{-/-}/Erry^{Tg/+}$ muscles at both time points (day 3 and day 6) after CTX injection. By a way of explanation, the high capillary density that robustly enabling an efficient clearing of debris and necrotic tissue in the $Mtn^{-/-}/Erry^{Tg/+}$ muscles, allows the small number of satellite cells to expand greatly, thereby leads to rapid muscle regenerate and repair.

Alternatively, other non-muscle stem cell population named endothelial-associated cells may also contribute in the regeneration process. They reside either within the muscles or can be recruited via the circulation in response to signals producing from the injured muscles (De Angelis et al., 1999). Previous work has reported a vital role of Myostatin in regulating of endothelial cells proliferation (Hayot et al., 2011), since its deletion negatively affects the activity of these cells, and reduces muscle capillarization. In contrast, *Erry* is able to induce endothelial cells proliferation and migration (Zheng et al., 2007, Partridge et al., 2000). Together, these studies provide additional evidence of the importance of surrounding environment that induced by introducing of *Erry* on the $Mtn^{-/-}$ to accelerate muscle regeneration and repair even with a low number of satellite cells.

During muscle regeneration, an interaction between satellite cells and ECM of skeletal muscle is essential for muscle repair and adaptation (MAURO, 1961). A number of studies have shown that the interstitial muscle niche is vital for satellite cells activation in response to external stimuli associated with muscle repair (Barberi et al., 2013, Urciuolo et al., 2013). Consistently, it was established that satellite cells contribute to their own environment through inducing ECM synthesis (Brohl et al., 2012), as its components are required for proper SCs activity during muscle regeneration (Calve et al., 2010). Satellite cells are able to regulate their surrounding ECM composition via exosome-mediated regulation of fibrogenic cell ECM (Fry et al., 2014). Furthermore, work by Engler et al. demonstrated that satellite cells differentiation into myoblast requires optimal connective tissue level that can offer an ideal tissue elasticity (Engler et al., 2006). It seems that correct regulation of satellite cells

activity is crucial for maintaining tissue homeostasis after CTX injury. Given our observations in chapter seven showed a restoration of almost all examined ECM and DGC components to their normal levels and distribution following *Erry* overexpression in the *Mtn*^{-/-} background muscles could have dual function : on one hand it is critical for the regulation of skeletal muscle mechanical properties that were related to high exercise and force generation capacity, and on the other hand it induces interaction between CT components and SCs, that simultaneously enhances satellite cells activity, thereby the regeneration rate. Another important molecule within ECM that can induce muscle regeneration after injury is Fibromodulin, an extracellular matrix component that was found to be upregulated during muscle regeneration (Svensson et al., 1999). As *Mtn*^{-/-}/*Erry*^{Tg/+} muscles show high levels of ECM and DGC proteins, so there is more Fibromodulin production that is associated with the recruitment of satellite cells into the site of injury (Lee et al., 2016), thereby promotes regeneration pace.

Expanding on this finding, the increased in numbers of myogenic precursor and committed cells in regenerated areas of *Mtn*^{-/-}/*Erry*^{Tg/+} muscles did not affect the population of satellite cells (*Pax7*⁺ / *MyoD*⁻), which are essential for future degeneration/regeneration cycle. Previous work has demonstrated that ECM components are required for maintaining SCs self-renewal and muscle regeneration (Calve et al., 2010). Our findings provide novel insights into the relevance of ECM molecules in the regulation of SCs homeostasis. In fact, this is again clearly evident the prominence of microenvironment to promote muscle regeneration following repetitive injury. This hypothesis supported by our data investigating a number of (eMHC) fibres, and size of newly generated myofibres after 14 days of muscle injury.

Introducing of *Erry* in the *Mtn*^{-/-} background muscles failed to eliminate all abnormalities

Although the attractive impacts of oxidative programme imparted by introducing of *Erry* in the *Mtn*^{-/-} background muscles, a number of abnormalities were not normalised in *Mtn*^{-/-}/*Erry*^{Tg/+} muscles.

The transgenic protocol utilised in this study caused partial conversion of MHC profiling toward the slow phenotypes, however it was unable to induce the proportion of MHC type I.

This data extends findings of previous work by Matsakas et al. who revealed an absence of complete transition from MHCIIA to MHCI following *Erry* transgenic (Matsakas et al., 2012b). Previous work has demonstrated that there is a large gap between the kinetics of type IIA and type I myofibres that possibly disrupt the continuum transition between the two phenotypes (Andruchov et al., 2004). A number of investigators have examined whether it is possible to get the final step of conversion from MHCIIA to MHCI. Indeed, Chronic low-frequency stimulation (CLFS) is a profound example to describe MHCI development in a number of conditions (Kwong and Vrbova, 1981). However, further investigation to determine whether MHCI fibres formed as a consequence of the remodelling of type II muscle fibres or through the formation of new fibres, is required. It was well identified that the development of muscle fibre type I following extended CLFS can only be induced to significant levels when accompanied by robust myofibre regeneration (Maier et al., 1988). We deduced from this, Myostatin signalling plays a critical role at the embryonic stage of muscle development to form myofibres type I mediating by patterning a subpopulation of satellite cells/muscle precursor. In opposition, the protocol applied in this study (*Erry* introducing onto *Mtn*^{-/-} muscles) was unable to influence the final step of myofibres transition.

Our work examining the impacts of genetic deletion of *Myostatin* and muscle-specific overexpression of *Erry* onto *Mtn*^{-/-} muscles offers important findings in related to DGC composition. Although almost all decreased ECM and DGC proteins in *Mtn*^{-/-} muscles were restored to their normal level following *Erry* expression, β and δ -SG show high expression levels in *Mtn*^{-/-} and *Mtn*^{-/-}/*Erry*^{Tg/+} than the WT muscles. It has been reported that DGC components have identical roles in this complex (Jung et al., 1996a). Further work has demonstrated the importance of a fully assembled of sarcoglycan complex in order to support sarcolemma stability and to reduce possible degradation during physiological activity (Jung et al., 1996b), which might explain the maintaining of increased β and δ -SG in *Mtn*^{-/-}/*Erry*^{Tg/+} muscle that correlated to the increased level of other ECM and DGC proteins, as well as muscle physiological activity. On the other hand, we believe that the alteration of relative SGs in hypertrophic muscle fibres developed in absence of *Myostatin* may attribute to the unique functional property of each component. In support of this view, previous work

demonstrated that different diseases could result from a mutation in each SG complex member (Wicklund and Kissel, 2014).

Investigation at the cellular level in the current study revealed some abnormalities that metabolic reprogramming driven by muscle-specific overexpression of *Erry* onto *Mtn*^{-/-} muscles was unable to eliminate. Firstly, single myofibres from *Mtn*^{-/-}/*Erry*^{Tg/+} muscles show few satellite cells number compared to either WT or *Mtn*^{-/-} myofibres. Secondly, unlike in WT, myonuclei distribution was randomly and irregularly in *Mtn*^{-/-} and *Mtn*^{-/-}/*Erry*^{Tg/+} muscles.

The predominance glycolysis in muscles due to the absence of *Myostatin* may promote myoblast fusion mediating by downregulating of Notch pathway (Gildor et al., 2012). An interpretative view that genetic alteration of *Myostatin* induces myoblast to fuse to each other at the expense of satellite cells population, and notably introducing of *Erry* in the *Mtn*^{-/-} muscles intensify this phenomenon.

The results from this work show that the accretion in myonuclei number in *Mtn*^{-/-}/*Erry*^{Tg/+} muscle, was coupled with an increase in mitochondrial biogenesis and activity, which were positively correlated to the improvement of the animal's physiological performance. Previous work by Liu et al. reported a critical role of mitochondrial protein systems to define myonuclear domain size in hypertrophic muscle fibres (Liu et al., 2009). We suggest that the high density of myonuclei and mitochondria in *Mtn*^{-/-}/*Erry*^{Tg/+} muscle was efficacious to compensate the far disorganization in myonuclei positioning, thereby overcoming the possible reduction in muscle functions.

It seems that the oxidative programme established by remodelling of *Mtn*^{-/-} muscles through muscle-specific expression of *Erry* was impotent to overcome all the defects of *Myostatin* absence.

Conclusion

A number of key conclusions can be drawn from this body of work. Firstly, the lack of *Myostatin* has been utilised as treatment of various muscle wasting disorders. However, we and others have demonstrated that, despite the larger muscle mass of *Mtn*^{-/-} compared to age-matched wild type, *Myostatin* deletion compromises strength production in association with a reduction of muscle oxidative properties and connective tissue contents (Amthor et al., 2007, Elashry et al., 2012). Consequently, these changes profoundly contribute to the decreased level of physical activity and exercise tolerance. Importantly, superimposition of *Erry* in the *Mtn*^{-/-} background muscles maintains the increase in muscle mass exhibited by *Mtn*^{-/-} muscles, while promotes muscle force generation capacity and in fact even resulted in improvement in animal exercise capacity, ultimately challenges the dogma of an inverse relationship between muscle fibre size and oxidative capacity. Such deviation might result from the significantly increased capillarization, muscle myoglobin content, ECM components, and normalised mitochondrial quality and quantity. Furthermore, although we show that *Mtn*^{-/-}/*Erry*^{Tg/+} muscles content few number of satellite cells, their regeneration capacity exceeded that of other genotypic groups (WT and *Mtn*^{-/-}). Most likely the surrounding environment, in particular the high oxidative capacity, angiogenesis program and high connective tissue abundant that are imparted by *Erry* overexpression play a crucial role in accelerating muscle regeneration.

Secondly, Myostatin/ActRIIB signalling is essential for optimizing skeletal muscle oxidative metabolism leading to lower muscle fatigability. Despite blocking of this pathway increases muscle mass, it results in a reduction of oxidative capacity which can negatively affect muscle physiological performance (Hulmi et al., 2013a, Relizani et al., 2014). Consequently, the fundamental functions of this signalling should be taken into account in order to develop therapies based on its inhibition. Alternatively, a genetic modification that might complement this approach should be performed. We showed that muscle-specific expression of *Erry* in the *Mtn*^{-/-} background restored the markers of oxidative metabolism and autophagy to that level of healthy mice. Indeed, an adequate level of muscle size and function has beneficial effects on overall health and life quality (Safdar et al., 2011), since a low aerobic fitness and low level of muscle function are associated with various health risks (Kujala et al., 1998). We show that combined approaches (blocking of Myostatin signalling in

Errγ^{Tg/+} mice) result in an increase in muscle size, and oxidative capacity appear to offer more. Such combination might be appropriate for both genetic and acquired muscle diseases where treatment options are limited.

Future direction priorities

This body of work has utilised the transgenic method in order to optimize a therapeutic approach that can offer a synchronized development of a large and functional muscle, hence improve quality of life. This was attained by taking advantage of the high power of *Myostatin* to negatively regulate skeletal muscle development and growth (McPherron et al., 1997), and most importantly the potential of *Erry* in regulating metabolic and energy profiles mainly in mitochondrial rich and energy-dependent tissues including brain, heart, skeletal muscles, and brown adipose tissue (BAT) (Hong et al., 1999).

Further investigations following on from this study should focus on special areas that were uncovered by this work. Thereafter, advancement of this therapeutic agent into a clinical investigation, which may provide a new conduit for the treatment of an adult with metabolic disorders, and physical limitation of elderly people is required.

Previous work reported that *Myostatin* null muscles had elevated levels of both proteolytic and autophagy programmes, as well as shutting down protein synthesis extensively during acute starvation compared to age-matched wild type mice (Collins-Hooper et al., 2015). Therefore, future investigation of consequences of overexpression of *Erry* in the starved muscle lacking *Myostatin* would be feasible in order to verify results shown in chapter 3 of this study that provided evidence of *Erry* potential to normalise autophagy and proteolytic systems activity. Moreover, it would expand our understanding of *Erry* roles to attenuate hypertrophic myofibres functional lack during starvation.

It was well established that obesity is mainly caused by excessive accumulation of white adipose tissue (WAT), that can eventually lead to type 2 diabetes, and other metabolic deteriorations (Gesta et al., 2007). Thus, the transition of WAT to BAT is necessary to burn body fat, induce heat production and avoid obesity risk (Cannon and Nedergaard, 2004). It has been reported that *Erry* markedly induces expression of uncoupling protein 1 (*UCP1*), brown-fat specific gene, and improve fatty acid oxidation in differentiated white pre-adipocytes and BAT (Dixen et al., 2013). This hypothesis is supported in a part by our observations shown in chapter 4 at least at the transcriptional level. Therefore, developing a therapeutic intervention that enables efficacious delivery of *Erry* actions into human

muscles, and hence enhance muscle functions would halt risks of fat deposition; ultimately contribute to offer healthy life.

The world population is ageing, and as society ages, physical performance limitation incident will be increased, which in turn raise the possibility of predisposition to a number of diseases and premature death as well (Louie and Ward, 2010). Although numerous factors contribute to physical disability with age advance, a reduction in muscle performance is the major contributor (Janssen et al., 2002). Old age is associated with progressive loss of skeletal muscle mass, a process is known sarcopenia, which leads to diminish of muscle strength, induce fatigability, and ultimately decrease the quality of life (Cruz-Jentoft et al., 2010, Faulkner et al., 1990). A number of studies on the effects of ageing on skeletal muscles have revealed a considerable reduction in muscle fibres size in the elderly people (Larsson, 1978, Verdijk et al., 2007). Notably, muscle fibres type II are more prone to size decrease observed in the elderly, however type I muscle fibre appears largely sustained with ageing (Larsson, 1978). With regard to muscle energetic, previous work has reported that aged muscles show an elevated level of mitochondrial abnormalities (Berger and Doherty, 2010). Consistently, it was well established that muscle aerobic metabolism is profoundly affected by ageing (Fleg et al., 2005), which might be attributed to the impairment of ATP synthesis pathways in aged muscle (Russ and Lanza, 2011). We and others have identified *Erry* potential to promote muscle energy production, and mitochondrial biogenesis and activity (Alaynick et al., 2007, Rangwala et al., 2010). Moreover, it has been documented that *Erry* is exclusively and abundantly expressed in oxidative (type I) slow-twitch fibre (Narkar et al., 2011) which may impart capability of this muscle fibre type to resistant the age-related ailments.

Therefore, in order to convert the *Erry* biological versatility into the effective therapeutic target, identification of synthesized ligands for *Erry* that displaying better specificity and are able to positively regulate the transcriptional activity of this nuclear receptor is required. Work by Wang et al. showed that it is a challenge to identify a small molecule that can improve *Erry* transcriptional functions, because of the small volume of its ligand binding pocket (Wang et al., 2006). In fact, a number of synthetic ligands have been developed, DY131 and GSK4716, a phenolic acyl hydrazine compounds, have been described to

selectively upregulate the transcriptional functions of *Erry* and potentially stimulate the browning process of white adipose tissue (Zuercher et al., 2005, Kim et al., 2009). Furthermore, Bisphenol A is another ligand that can positively regulate the transcriptional activity of a human isoform of *Erry* (Tohme et al., 2014), however, recent data has linked Bisphenol A levels with type 2 diabetes and metabolic dysfunction in human (Lang et al., 2008).

The fundamental strategy for delivering *Erry* synthesized ligands could potentially accomplish by utilising gene therapy vectors that provide a continuous source of exogenous ligand. In fact, the main obstacle to the successful application of gene therapy is not a paucity of the therapeutic gene, but the deficit of an efficient non-toxic gene delivery system. Adeno-associated virus (AAV), a single-stranded of DNA viruses, has attracted considerable interest in gene therapy approach due to its lack of pathogenicity, and the ability to integrate into host cell genome (Surosky et al., 1997, Miller et al., 2004). Moreover, AAVs characterized by low immunogenicity, with low possibility to induce a cytotoxic response (Chirmule et al., 1999). Indeed, using different AAV serotypes has been discovered in order to improve transduction of specific cell type. AAV-5 able to transduce airway epithelial cells in the murine and human model (Rabinowitz et al., 2002), AAV-6 shows very efficient uptake into skeletal muscles (Zabner et al., 2000), and AAV-8 has been successfully used for post-natal inhibition of Myostatin by delivering Myostatin propeptide (MyoPPT) into adult mice via tail vein injection (Yue and Dongsheng, 2002), and same serotype was utilised to induce human Survival of Motor Neuron (hSMN) into the CNS of Spinal muscular atrophy (SMA) mouse model (McCarty, 2008). Moreover, AAV9 has been utilised to infect different tissues due to its wide tropism, which make it a strong candidate for gene therapy in multisystem disorders (Gadalla et al., 2013). Therefore, further investigation of the most efficient vector to be used should be carried out in order to ascertain the best way to attain the greatest value of *Erry* transcriptional activity.

Discoveries of efficient methods of gene transducing with exciting observations of our work may provide valuable knowledge and opportunity to expand the search of more potent and selective compounds that may represent unique chemical tools that able to elucidate *Erry* functions and could be new potential therapeutic value for the treatment of human energy

and metabolic disorders during the life, and prevent or attenuate physical performance limitation in the elderly.

Appendices

Appendix 1 - Antibodies used

Antibodies used for Immunostaining

Primary antibodies

Antigen	Type	Immuno-globulin	Species	Dilution factor	Supplier
MYHCI	Monoclonal	IgM	Mouse	1:1	DSHB A4.840
MYHCIIA	Monoclonal	IgG	Mouse	1:1	DSHB A4.74
MYHCIIIB	Monoclonal	IgM	Mouse	1:1	DSHB BF.F3
CD31	Polyclonal	IgG	Rat	1:40	AbD serotec MCA2388
Pax7	Monoclonal	IgG	Mouse	1:1	DSHB
MyoD	Polyclonal	IgG	Rabbit	1:200	Santa Cruz Biot, # sc-760
F4/80	Monoclonal	IgG	Rat	1:100	Bio-RAD, MCA4978
MYH3	Monoclonal	IgG	Mouse	1:200	Santa Cruz Biot, sc-53091
Cleaved Caspase-3	Monoclonal	IgG	Rabbit	1:200	Cell signalling Technology, #9664S
Collagen type I	Monoclonal	IgG	Mouse	1:500	Abcam, 6308
Collagen type IV	Polyclonal	IgG	Rabbit	1:500	Abcam, 6586
Dystrophin	Polyclonal	IgG	Rabbit	1:200	Abcam, 15277
α-DG	Monoclonal	IgM	Mouse	1:50	Millipore, 05-593
β-DG	Monoclonal	IgG	Mouse	1:10	Leica Biosystems, B-DG-CE
α-SG	Monoclonal	IgG	Mouse	1:40	Leica Biosystems, A-SARC-L-CE
β-SG	Monoclonal	IgG	Mouse	1:50	Leica Biosystems, B-SARC-L-CE
γ-SG	Monoclonal	IgG	Mouse	1:30	Leica Biosystems, G-SARC-CE
δ-SG	Monoclonal	IgG	Mouse	1:25	Leica Biosystems, D-SARC-CE
Laminin 1	Polyclonal	IgG	Rabbit	1:200	Sigma L9393

Secondary antibodies

Antibody	Species	Dilution factor	Supplier
Alexa fluor 633 anti-mouse	Goat	1:200	Life Technologies # A20146
Alexa fluor 488 anti-mouse	Goat	1:200	Life Technologies # A11029
Alexa fluor 488 anti-rabbit	Goat	1:200	Life Technologies # A11034

Alexa fluor 594 anti-rabbit	Goat	1:200	Life Technologies # A11037
Alexa fluor 594 anti-rat	Goat	1:200	Life Technologies # A11007

Antibodies used for western blotting

Primary antibodies

Antigen	Type	Immuno-globulin	Molecular Weight	Species	Dilution factor	Supplier
AKT	Polyclonal	IgG	60 kDa	Rabbit	1:200	Cell signalling Technology #9272
pAkt (Ser473)	Monoclonal	IgG	60 kDa	Rabbit	1:200	Cell signalling Technology #4060
4E-BP1 (53H11)	Polyclonal	IgG	15-20 kDa	Rabbit	1:200	Cell signalling Technology #9644
p4EBP1 (T37/46)	Polyclonal	IgG	15-20 kDa	Rabbit	1:200	Cell signalling Technology #9459
FoxO3a (H-144)	Polyclonal	IgG	97 kDa	Rabbit	1:200	Santa Cruz Biot, sc-11351
pFoxO3a (Ser253)	Polyclonal	IgG	97 kDa	Rabbit	1:200	Cell signalling Technology #9466
Dystrophin	Polyclonal	IgG	420 kDa	Rabbit	1:200	Abcam ab15277
α-DG	Monoclonal	IgM	156 kDa	Mouse	1:2000	Millipore 05-593
β-DG	Monoclonal	IgG	45 kDa	Mouse	1:1000	DSHB 7D11
β-SG	Polyclonal	IgG	45 kDa	Rabbit	1:200	Abcam ab203392
α-Actinin	Monoclonal	IgG1	100 kDa	Mouse	1:10000	Sigma A7811

Secondary antibodies for western blot

Antibody	Species	Dilution factor	Supplier
HRP-anti rabbit	Goat	1:50,000	Jackson ImmunoResearch 111-035-045
HRP-anti mouse	Goat	1:50,000	Jackson ImmunoResearch 115-035-166
IgM-HRP- anti mouse	Goat	1:10,000	MilliporeAP128

Appendix 2 - Materials

Reagents:

Reagent	Supplier
100bp DNA Ladder	Promega G2101
4, 6-diamidino-2-phenylindole (DAPI) (2.5µg/ml)	DakoCytomation DAKO Corp, Carpinteria, Calif
Acid phosphatase	Sigma Aldrich N2250
Agarose Powder	BIOLINE BIO-41025
CaCl ₂	Fisher Scientific 10161800
Cardiotoxin	Sigma- Aldrich C9759
Chloroform	ACROS ORGANIC
DMEM	Gibco 31966-021
DPX	Fisher Scientific D/5319/05
DHE	Sigma-Aldrich 7008
Eosin	Sigma-Aldrich 318906-500ML
Epoxy resin	Durcopan, Roth, Germany
FBS	Gibco 10270-106
Gluteraldehyde Solution 25%	Merck, Germany 1042390250
Glycerol	Sigma-Aldrich G6279-1L
Haematoxylin	Sigma-Aldrich MHS16-500ML
HEPES	Fisher Scientific BP410-500
Horse serum	Gibco 16050-122
Hydro mounting media	Agar scientific R1356
Isopropanol	Fisher Scientific P/7490/17
KCl	BDH 101984L
KCN	Fisher Scientific 1059938
KH ₂ PO ₄	BDH 10203
Methanol	Fisher Scientific M/4056/17
MgCl ₂	Sigma-Aldrich M2670-500
MgSO ₄	BDH 101514Y
NaCl	Sigma-Aldrich 71382
NaHCO ₃	Sigma S-8875
NaOH	Sigma S-5881
NBT	Sigma Aldrich 74032
Na Citrate	BDH # 30128
OsO ₄	Roth, Germany
PBS Tablets	Oxoid BR0014G
Penicillin-streptomycin	Invitrogen 15240-062
Periodic acid solution	Thermo Scientific 88016
PFA	Fisher Scientific P/0840/53
Phenazin methosulphate	Sigma P9625-1G
Protease Inhibitor Cocktail Set I	CALBIOCHEM #539131

RevertAid H Minus First Strand cDNA Synthesis Kit	Life Technologies k1631
RNase-Free DNase Set (50)	QIAGEN 79254
RNeasy Mini Kit (50)	QIAGEN 74104
Schif reagent	Thermo Scientific 88017
SDS	Fisher Scientific S/200/53
Sodium azide	Fluka
Sodium succinate	Fisher Scientific 11418852
Sodium-Cacodylate	TAAB S007
Sucrose	Fisher chemical S/8560/53
SYBER Safe DNA gel	Invitrogen S33102
SYBR® Green PCR Master Mix	Applied Biosystems 4309155
Taq 2X Master Mix	New England Biolabs M0270L
Triton X-100	Fisher Scientific T/3751/08
TRIzol	Sigma-Aldrich T9424-100ml
Type 1 collagenase	Sigma C0130
Uranyl acetate	Polysciences, Germany
Urea	BDH, 102908D

Solutions:

Taq 2X Master Mix

10 mM Tris-HCl, 50 mM KCl, 1.5 mM MgCl₂, 0.2 mM dNTPs, 5% Glycerol, 0.08% IGEPAL® CA-630, 0.05% Tween® 20, 25 units/ml Taq DNA Polymerase pH 8.6 at 25°C. The solution was stored at -20°C.

TAE buffer

40 mM Tris base, 5 mM Na Acetate, and 1 mM EDTA, adjusted to pH 7.8. The solution was stored at room temperature.

Krebs solution

124 mM NaCl, 3 mM KCl, 1.25 mM KH₂PO₄, 36 mM NaHCO₃, 1 mM MgSO₄, 2 mM CaCl₂, , and Glucose. The solution was stored at 4°C.

1 x Phosphate Buffer Saline (PBS)

5 PBS tablets was dissolved in 500 ml distilled water and then autoclaved.

4% Paraformaldehyde (PFA)

20 g of paraformaldehyde powder dissolved in 480 ml 1 x PBS by heating to 65°C. Volume was then made to 500 ml with 1 x PBS and stored at room temperature.

Permeabilisation buffer

0.952 g HEPES, 0.260 g MgCl₂, 0.584 g NaCl, 0.1 g Sodium azide, 20.54 g Sucrose and 1 ml Triton X-100 were made up to 200 ml distilled water. The buffer was stored at 4°C.

Wash buffer

25 ml Foetal bovine serum (FBS), 200 mg Sodium azide and 250 µl Triton X-100 were dissolved in 500 ml 1 x PBS and stored at 4°C.

Preparation of type 1 collagenase

To digest two EDL muscles, 2 mg type 1 collagenase was dissolved in 1 ml serum free DMEM GlutamaxTM (0.2% w/v) under septic conditions.

Single Fibre Culture Medium (SFCM)

45 ml of DMEM GlutamaxTM was supplemented with 250 µl of chick embryo extract, 5 ml of 10% horse serum and 500 µl penicillin-streptomycin. The medium was stored at 4°C.

Chick embryo extract

Fertilised white leghorn chicken (*Gallus gallus*) eggs were incubated for a period of 10 days at 39°C, 80% humidity. Following incubation the chick embryos were harvested and the eyes from the embryos were removed using a pair of sterile forceps. The chick embryos were then transferred to 50 ml Falcon tube. An equal volume of sterile 1 x PBS was added. The embryos were then finely triturated and the resultant mixture was allowed to stand for 30 minutes at room temperature. The mixture was then centrifuged at 2000 g for 15 minutes. The supernatant was then aspirated and aliquoted into 250 µl aliquots. The aliquots were stored at -20°C.

Antigen retrieval solution

2.14 g of Sodium Citrate was dissolved in 50 ml of deionised H₂O. Then 50 µl of tween was added to the mix, the solution's pH was adjusted to 6 before being made up to 100 ml with distilled water and stored at RT.

Nitro blue tetrazolium (NBT) stock

Phosphate buffer (100 mM, pH 7.6) was prepared by mixing two solutions; Solution A (1.36 g KH₂PO₄ /100 ml) 12 ml, and Solution B (1.42 g Na₂HPO₄/100 ml) 88 ml. Then 6.5 mg KCN, 185 mg EDTA, and 100 mg Nitroblue tetrazolium (NBT) were dissolved in 100 ml Phosphate buffer. The mixture was stored as aliquots of 2 ml at -20°C.

Sodium succinate stock

2.7 g Sodium succinate was dissolved in 20 ml distilled water. Then aliquots of 2 ml were stored at -20°C.

Formal calcium

10 g of Sodium chloride was dissolved in 900 ml distilled water, and 100 ml 40% Formaldehyde was added to the mixture. The solution was stored at room temperature.

Acid phosphatase incubation medium

2 ml HPR reagent, 0.1 M acetate buffer pH 5.0, 50 mg/ml naphthol AS-BI phosphate, solution was adjusted to pH 5.0 and stored at -20°C.

Preparation of fixative solution for TEM samples

10 ml Glutaraldehyde 25% was added to 50 ml 0.2 M Na- cacodylate buffer pH 7.4, volume was then made to 100 ml with distilled water. The fixative solution was prepared freshly and kept in ice during work.

Appendix 3 – RT-PCR Primer sequences

R_mERRg.F	ACT TGG CTG ACC GAG AGT TG
R_mERRg.R	GCC AGG GAC AGT GTG GAG AA
R.MHCIIA F	AGTCCCAGGTCAACAAGCTG
R.MHCIIA R	GCATGACCAAAGGTTTCACA
R.MHCIIIX F	AGTCCCAGGTCAACAAGCTG
R.MHCIIIX R	CACATTTTGCTCATCTCTTTG
R.MHCIIIB F	AGTCCCAGGTCAACAAGCTG
R.MHCIIIB R	TTTCTCCTGTACCTCTCAACA
R_mCYCLO.F	TGG AGA GCA CCA AGA CAG ACA
R_mCYCLO.R	TGC CGG AGT CGA CAA TGA T
R_mGAPDH.F	TGAAGCAGGCATCTGAGCG
R_mGAPDH.R	CGAAGGTGGAAGAGTGGG
R_mHPRT.F	GCTCGAGATGTCATGAAGGAGAT
R_mHPRT.R	AAAGAACTTATAGCCCCCTTGA
R.mPGC1A.F	AAC CAC ACC CAC AGG ATC AGA
R.mPGC1A.R	TCT TCG CTT TAT TGC TCC ATG A
R_mPERM1.F	CCTGGTTCGTAAGAAGAGGCG
R_mPERM1.R	CTTGGGCCTGGTAAGCTGT
R_mGlut1.F	CTCTGTGCGCCTCTTTGTTAAT
R_mGlut1.R	CCAGTTTGGAGAAGCCCATAAG
R_mGlut4.F	ACACTGGTCCTAGCTGTATTCT
R_mGlut4.R	CCAGCCACGTTGCATTGTA
R_mPDK4.F	AAG CAA AAC ACA AAC ACG AGT A
R_mPDK4.R	CCC GGG TCA TCC AAC CA
R_mHAD.F	GCTGGGCCTAACTTTGAGTATG
R_mHAD.R	CAAATCAGCGTCATCAGGAGAA
R_mLPL.F	GCTGGGCCTAACTTTGAGTATG
R_mLPL.R	CAAATCAGCGTCATCAGGAGAA
R_mcycs.F	CCA AAT CTC CAC GGT CTG TTC
R_mcycs.R	ATC AGG GTA TCC TCT CCC CAG
R_mCat.F	GGATTATGGCCTCCGAGATCTT
R_mCat.R	TAAAACGTCCAGGACGGGTAA
R_mMYOG.F	CTG TTT AAG ACT CAC CCT GAG AC
R_mMYOG.R	GGT GCA ACC ATG CTT CTT CA
R_mCD36.F	AGATGACGTGGCAAAGAACAG
R_mCD36.R	CCTTGGCTAGATAACGAACTCTG
R_mSlc25a20.F	CAACCACCAAGTTTGTCTGGA
R_mSlc25a20.R	CCCTCTCTCATAAGAGTCTTCCG
R_mFATP1.F	AGGTCAATGAGGACACGATGGAG
R_mFATP1.R	CTGGTACATTGAGTTAGGGTCCAAC

R_mFabp3.F	ACCTGGAAGCTAGTGGACAG
R_mFabp3.R	TGATGGTAGTAGGCTTGGTCAT
R_mACADL.F	TGCCCTATATTGCGAATTACGG
R_mACADL.R	CTATGGCACCGATACACTTGC
R_mACADM.F	CCAGAGAGGAGATTATCCCCG
R_mACADM.R	TACACCCATACGCCAACTCTT
R_mVEGFA165.F	TGC AGG CTG CTG TAA CGA TG
R_mVEGFA165.R	GAA CAA GGC TCA CAG TGA TTT TCT
R_mVEGFA189.F	TGC AGG CTG CTG TAA CGA TG
R_mVEGFA189.R	CTC CAG GAT TTA AAC CGG GAT T
R_mFGF1.F	GAAGCATGCGGAGAAGAAGTCTG
R_mFGF1.R	CGAGGACCGCGCTTACAG
mDmdF	ACTCAGCCACCCAAAGACTG
mDmdR	TGTCTGGATAAGTGGTAGCAACA
mDag1F	CAGTGTGTTCTCTATCGAGGTCT
mDag1R	CACAGGCAGATGGCACTACC
mSgcbF	GGACCGGCTCCATAAGACTG
mSgcbR	GATGACGGCCAGGATAAACAG

References

- AHMED, S. K., EGGINTON, S., JAKEMAN, P. M., MANNION, A. F. & ROSS, H. F. 1997. Is human skeletal muscle capillary supply modelled according to fibre size or fibre type? *Exp Physiol*, 82, 231-4.
- AIDLEY, D. J. 1998. The physiology of excitable cells. Cambridge, Cambridge University press.
- AKPAN, I., GONCALVES, M. D., DHIR, R., YIN, X., PISTILLI, E. E., BOGDANOVICH, S., KHURANA, T. S., UCRAN, J., LACHEY, J. & AHIMA, R. S. 2009. The effects of a soluble activin type IIB receptor on obesity and insulin sensitivity. *Int J Obes (Lond)*, 33, 1265-73.
- ALAMEDDINE, H. S. 2012. Matrix metalloproteinases in skeletal muscles: friends or foes? *Neurobiol Dis*, 48, 508-18.
- ALAYNICK, W. A. 2008. Nuclear receptors, mitochondria and lipid metabolism. *Mitochondrion*, 8, 329-37.
- ALAYNICK, W. A., KONDO, R. P., XIE, W., HE, W., DUFOUR, C. R., DOWNES, M., JONKER, J. W., GILES, W., NAVIAUX, R. K., GIGUERE, V. & EVANS, R. M. 2007. ERRgamma directs and maintains the transition to oxidative metabolism in the postnatal heart. *Cell Metab*, 6, 13-24.
- ALLAMAND, V., BRINAS, L., RICHARD, P., STOJKOVIC, T., QUIJANO-ROY, S. & BONNE, G. 2011. CoVI myopathies: where do we stand, where do we go? *Skelet Muscle*, 1, 30.
- ALLEN, D. G., LAMB, G. D. & WESTERBLAD, H. 2008. Skeletal muscle fatigue: cellular mechanisms. *Physiol Rev*, 88, 287-332.
- ALLEN, D. L., MONKE, S. R., TALMADGE, R. J., ROY, R. R. & EDGERTON, V. R. 1995. Plasticity of myonuclear number in hypertrophied and atrophied mammalian skeletal muscle fibers. *J Appl Physiol (1985)*, 78, 1969-76.
- ALLEN, D. L., ROY, R. R. & EDGERTON, V. R. 1999. Myonuclear domains in muscle adaptation and disease. *Muscle Nerve*, 22, 1350-60.
- ALLEN, D. L. & UNTERMAN, T. G. 2007. Regulation of myostatin expression and myoblast differentiation by FoxO and SMAD transcription factors. *Am J Physiol Cell Physiol*, 292, C188-99.
- ALLEN, R. E. & BOXHORN, L. K. 1987. Inhibition of skeletal muscle satellite cell differentiation by transforming growth factor-beta. *J Cell Physiol*, 133, 567-72.
- AMTHOR, H., HUANG, R., MCKINNELL, I., CHRIST, B., KAMBADUR, R., SHARMA, M. & PATEL, K. 2002. The regulation and action of myostatin as a negative regulator of muscle development during avian embryogenesis. *Dev Biol*, 251, 241-57.
- AMTHOR, H., MACHARIA, R., NAVARRETE, R., SCHUELKE, M., BROWN, S. C., OTTO, A., VOIT, T., MUNTONI, F., VRBOVA, G., PARTRIDGE, T., ZAMMIT, P., BUNGER, L. & PATEL, K. 2007. Lack of myostatin results in excessive muscle growth but impaired force generation. *Proc Natl Acad Sci U S A*, 104, 1835-40.
- AMTHOR, H., OTTO, A., VULIN, A., ROCHAT, A., DUMONCEAUX, J., GARCIA, L., MOUISEL, E., HOURDE, C., MACHARIA, R., FRIEDRICH, M., RELAX, F., ZAMMIT, P. S., MATSAKAS, A., PATEL, K. & PARTRIDGE, T. 2009. Muscle hypertrophy driven by myostatin blockade does not require stem/precursor-cell activity. *Proc Natl Acad Sci U S A*, 106, 7479-84.
- ANDERSEN, P. & HENRIKSSON, J. 1977. Training induced changes in the subgroups of human type II skeletal muscle fibres. *Acta Physiol Scand*, 99, 123-5.
- ANDERSSON, D. C. & MARKS, A. R. 2010. Fixing ryanodine receptor Ca leak - a novel therapeutic strategy for contractile failure in heart and skeletal muscle. *Drug Discov Today Dis Mech*, 7, e151-e157.
- ANDRUCHOV, O., ANDRUCHOVA, O., WANG, Y. & GALLER, S. 2004. Kinetic properties of myosin heavy chain isoforms in mouse skeletal muscle: comparison with rat, rabbit, and human and correlation with amino acid sequence. *Am J Physiol Cell Physiol*, 287, C1725-32.

- ANKER, S. D., PONIKOWSKI, P., VARNEY, S., CHUA, T. P., CLARK, A. L., WEBB-PEPLOE, K. M., HARRINGTON, D., KOX, W. J., POOLE-WILSON, P. A. & COATS, A. J. 1997. Wasting as independent risk factor for mortality in chronic heart failure. *Lancet*, 349, 1050-3.
- ANNEX, B. H., TORGAN, C. E., LIN, P., TAYLOR, D. A., THOMPSON, M. A., PETERS, K. G. & KRAUS, W. E. 1998. Induction and maintenance of increased VEGF protein by chronic motor nerve stimulation in skeletal muscle. *Am J Physiol*, 274, H860-7.
- ANTHONY, K., CIRAK, S., TORELLI, S., TASCIA, G., FENG, L., ARECHAVALA-GOMEZA, V., ARMAROLI, A., GUGLIERI, M., STRAATHOF, C. S., VERSCHUUREN, J. J., AARTSMA-RUS, A., HELDERMAN-VAN DEN ENDEN, P., BUSHBY, K., STRAUB, V., SEWRY, C., FERLINI, A., RICCI, E., MORGAN, J. E. & MUNTONI, F. 2011. Dystrophin quantification and clinical correlations in Becker muscular dystrophy: implications for clinical trials. *Brain*, 134, 3547-59.
- ARACENA-PARKS, P., GOONASEKERA, S. A., GILMAN, C. P., DIRKSEN, R. T., HIDALGO, C. & HAMILTON, S. L. 2006. Identification of cysteines involved in S-nitrosylation, S-glutathionylation, and oxidation to disulfides in ryanodine receptor type 1. *J Biol Chem*, 281, 40354-68.
- ARAIISHI, K., SASAOKA, T., IMAMURA, M., NOGUCHI, S., HAMA, H., WAKABAYASHI, E., YOSHIDA, M., HORI, T. & OZAWA, E. 1999. Loss of the sarcoglycan complex and sarcospan leads to muscular dystrophy in beta-sarcoglycan-deficient mice. *Hum Mol Genet*, 8, 1589-98.
- ARANY, Z., FOO, S. Y., MA, Y., RUAS, J. L., BOMMI-REDDY, A., GIRNUN, G., COOPER, M., LAZNIK, D., CHINSOMBOON, J., RANGWALA, S. M., BAEK, K. H., ROSENZWEIG, A. & SPIEGELMAN, B. M. 2008a. HIF-independent regulation of VEGF and angiogenesis by the transcriptional coactivator PGC-1alpha. *Nature*, 451, 1008-12.
- ARANY, Z., LEBRASSEUR, N., MORRIS, C., SMITH, E., YANG, W., MA, Y., CHIN, S. & SPIEGELMAN, B. M. 2007. The transcriptional coactivator PGC-1beta drives the formation of oxidative type IIX fibers in skeletal muscle. *Cell Metab*, 5, 35-46.
- ARANY, Z., WAGNER, B. K., MA, Y., CHINSOMBOON, J., LAZNIK, D. & SPIEGELMAN, B. M. 2008b. Gene expression-based screening identifies microtubule inhibitors as inducers of PGC-1alpha and oxidative phosphorylation. *Proc Natl Acad Sci U S A*, 105, 4721-6.
- ARAVAMUDAN, B., MANTILLA, C. B., ZHAN, W. Z. & SIECK, G. C. 2006. Denervation effects on myonuclear domain size of rat diaphragm fibers. *J Appl Physiol (1985)*, 100, 1617-22.
- ARDITE, E., BARBERA, J. A., ROCA, J. & FERNANDEZ-CHECA, J. C. 2004. Glutathione depletion impairs myogenic differentiation of murine skeletal muscle C2C12 cells through sustained NF-kappaB activation. *Am J Pathol*, 165, 719-28.
- ARECHAVALA-GOMEZA, V., KINALI, M., FENG, L., BROWN, S. C., SEWRY, C., MORGAN, J. E. & MUNTONI, F. 2010. Immunohistological intensity measurements as a tool to assess sarcolemma-associated protein expression. *Neuropathol Appl Neurobiol*, 36, 265-74.
- ARMSTRONG, R. B., IANUZZO, C. D. & LAUGHLIN, M. H. 1986. Blood flow and glycogen use in hypertrophied rat muscles during exercise. *J Appl Physiol (1985)*, 61, 683-7.
- ARMSTRONG, R. B. & PHELPS, R. O. 1984. Muscle fiber type composition of the rat hindlimb. *Am J Anat*, 171, 259-72.
- ARNOLD, L., HENRY, A., PORON, F., BABA-AMER, Y., VAN ROOIJEN, N., PLONQUET, A., GHERARDI, R. K. & CHAZAUD, B. 2007. Inflammatory monocytes recruited after skeletal muscle injury switch into antiinflammatory macrophages to support myogenesis. *J Exp Med*, 204, 1057-69.
- ATTISANO, L. & WRANA, J. L. 2000. Smads as transcriptional co-modulators. *Curr Opin Cell Biol*, 12, 235-43.
- AUGEREAU, P., BADIA, E., CARASCOSSA, S., CASTET, A., FRITSCH, S., HARMAND, P. O., JALAGUIER, S. & CAVAILLES, V. 2006. The nuclear receptor transcriptional coregulator RIP140. *Nucl Recept Signal*, 4, e024.
- BADIN, P. M., VILA, I. K., SOPARIWALA, D. H., YADAV, V., LORCA, S., LOUCHE, K., KIM, E. R., TONG, Q., SONG, M. S., MORO, C. & NARKAR, V. A. 2016. Exercise-like effects by Estrogen-related receptor-gamma in muscle do not prevent insulin resistance in db/db mice. *Sci Rep*, 6, 26442.

- BAINS, W., PONTE, P., BLAU, H. & KEDES, L. 1984. Cardiac actin is the major actin gene product in skeletal muscle cell differentiation in vitro. *Mol Cell Biol*, 4, 1449-53.
- BAJANCA, F., LUZ, M., RAYMOND, K., MARTINS, G. G., SONNENBERG, A., TAJBAKSH, S., BUCKINGHAM, M. & THORSTEINSDOTTIR, S. 2006. Integrin alpha6beta1-laminin interactions regulate early myotome formation in the mouse embryo. *Development*, 133, 1635-44.
- BAJARD, L., RELAIX, F., LAGHA, M., ROCANCOURT, D., DAUBAS, P. & BUCKINGHAM, M. E. 2006. A novel genetic hierarchy functions during hypaxial myogenesis: Pax3 directly activates Myf5 in muscle progenitor cells in the limb. *Genes Dev*, 20, 2450-64.
- BALDWIN, K. M., MARTINEZ, O. M. & CHEADLE, W. G. 1976. Enzymatic changes in hypertrophied fast-twitch skeletal muscle. *Pflugers Arch*, 364, 229-34.
- BALIGAND, C., GILSON, H., MENARD, J. C., SCHAKMAN, O., WARY, C., THISSEN, J. P. & CARLIER, P. G. 2010. Functional assessment of skeletal muscle in intact mice lacking myostatin by concurrent NMR imaging and spectroscopy. *Gene Ther*, 17, 328-37.
- BANNISTER, L. H. B., M. M. COLLINS, P. DYSON, M. DUSSEK, J. E. FERGUSON, M. W. J. 1995. Gray's Anatomy 38th edition, Churchill Livingstone. 737-763.
- BARBERI, L., SCICCHITANO, B. M., DE ROSSI, M., BIGOT, A., DUGUEZ, S., WIELGOSIK, A., STEWART, C., MCPHEE, J., CONTE, M., NARICI, M., FRANCESCHI, C., MOULY, V., BUTLER-BROWNE, G. & MUSARO, A. 2013. Age-dependent alteration in muscle regeneration: the critical role of tissue niche. *Biogerontology*, 14, 273-92.
- BASSEL-DUBY, R. & OLSON, E. N. 2006. Signaling pathways in skeletal muscle remodeling. *Annu Rev Biochem*, 75, 19-37.
- BEAUCHAMP, J. R., HESLOP, L., YU, D. S., TAJBAKSH, S., KELLY, R. G., WERNIG, A., BUCKINGHAM, M. E., PARTRIDGE, T. A. & ZAMMIT, P. S. 2000. Expression of CD34 and Myf5 defines the majority of quiescent adult skeletal muscle satellite cells. *J Cell Biol*, 151, 1221-34.
- BENCZE, M., NEGRONI, E., VALLESE, D., YACOUB-YOUSSEF, H., CHAOUCH, S., WOLFF, A., AAMIRI, A., DI SANTO, J. P., CHAZAUD, B., BUTLER-BROWNE, G., SAVINO, W., MOULY, V. & RIEDERER, I. 2012. Proinflammatory macrophages enhance the regenerative capacity of human myoblasts by modifying their kinetics of proliferation and differentiation. *Mol Ther*, 20, 2168-79.
- BENNY KLIMEK, M. E., AYDOGDU, T., LINK, M. J., PONS, M., KONIARIS, L. G. & ZIMMERS, T. A. 2010. Acute inhibition of myostatin-family proteins preserves skeletal muscle in mouse models of cancer cachexia. *Biochem Biophys Res Commun*, 391, 1548-54.
- BERGER, M. J. & DOHERTY, T. J. 2010. Sarcopenia: prevalence, mechanisms, and functional consequences. *Interdiscip Top Gerontol*, 37, 94-114.
- BERGSMAN, D. J., GRICHNIK, J. M., GOSSETT, L. M. & SCHWARTZ, R. J. 1986. Delimitation and characterization of cis-acting DNA sequences required for the regulated expression and transcriptional control of the chicken skeletal alpha-actin gene. *Mol Cell Biol*, 6, 2462-75.
- BINDOKAS, V. P., JORDAN, J., LEE, C. C. & MILLER, R. J. 1996. Superoxide production in rat hippocampal neurons: selective imaging with hydroethidine. *J Neurosci*, 16, 1324-36.
- BIRESSI, S., MOLINARO, M. & COSSU, G. 2007. Cellular heterogeneity during vertebrate skeletal muscle development. *Dev Biol*, 308, 281-93.
- BISCHOFF, R. 1986. A satellite cell mitogen from crushed adult muscle. *Dev Biol*, 115, 140-7.
- BISCHOFF, R. 1990. Interaction between satellite cells and skeletal muscle fibers. *Development*, 109, 943-52.
- BISCHOFF, R. & HEINTZ, C. 1994. Enhancement of skeletal muscle regeneration. *Dev Dyn*, 201, 41-54.
- BJORNSON, C. R., CHEUNG, T. H., LIU, L., TRIPATHI, P. V., STEEPER, K. M. & RANDO, T. A. 2012. Notch signaling is necessary to maintain quiescence in adult muscle stem cells. *Stem Cells*, 30, 232-42.
- BLOOR, C. M. 2005. Angiogenesis during exercise and training. *Angiogenesis*, 8, 263-71.

- BODINE, S. C., STITT, T. N., GONZALEZ, M., KLINE, W. O., STOVER, G. L., BAUERLEIN, R., ZLOTCHENKO, E., SCRIMGEOUR, A., LAWRENCE, J. C., GLASS, D. J. & YANCOPOULOS, G. D. 2001. Akt/mTOR pathway is a crucial regulator of skeletal muscle hypertrophy and can prevent muscle atrophy in vivo. *Nat Cell Biol*, 3, 1014-9.
- BOGDANOVICH, S., KRAG, T. O., BARTON, E. R., MORRIS, L. D., WHITTEMORE, L. A., AHIMA, R. S. & KHURANA, T. S. 2002. Functional improvement of dystrophic muscle by myostatin blockade. *Nature*, 420, 418-21.
- BOGDANOVICH, S., PERKINS, K. J., KRAG, T. O., WHITTEMORE, L. A. & KHURANA, T. S. 2005. Myostatin propeptide-mediated amelioration of dystrophic pathophysiology. *Faseb j*, 19, 543-9.
- BONALDO, P. & SANDRI, M. 2013. Cellular and molecular mechanisms of muscle atrophy. *Dis Model Mech*, 6, 25-39.
- BONDESEN, B. A., JONES, K. A., GLASGOW, W. C. & PAVLATH, G. K. 2007. Inhibition of myoblast migration by prostacyclin is associated with enhanced cell fusion. *Faseb j*, 21, 3338-45.
- BOPP, D., BURRI, M., BAUMGARTNER, S., FRIGERIO, G. & NOLL, M. 1986. Conservation of a large protein domain in the segmentation gene paired and in functionally related genes of *Drosophila*. *Cell*, 47, 1033-40.
- BORDON, Y. 2013. Macrophages: metabolic master prompts a change of tack. *Nat Rev Immunol*, 13, 706.
- BORYCKI, A. G. & EMERSON, C. P., JR. 2000. Multiple tissue interactions and signal transduction pathways control somite myogenesis. *Curr Top Dev Biol*, 48, 165-224.
- BOSTROM, P., WU, J., JEDRYCHOWSKI, M. P., KORDE, A., YE, L., LO, J. C., RASBACH, K. A., BOSTROM, E. A., CHOI, J. H., LONG, J. Z., KAJIMURA, S., ZINGARETTI, M. C., VIND, B. F., TU, H., CINTI, S., HOJLUND, K., GYGI, S. P. & SPIEGELMAN, B. M. 2012. A PGC1-alpha-dependent myokine that drives brown-fat-like development of white fat and thermogenesis. *Nature*, 481, 463-8.
- BOTTINELLI, R., BETTO, R., SCHIAFFINO, S. & REGGIANI, C. 1994a. Unloaded shortening velocity and myosin heavy chain and alkali light chain isoform composition in rat skeletal muscle fibres. *J Physiol*, 478 (Pt 2), 341-9.
- BOTTINELLI, R., CANEPARI, M., REGGIANI, C. & STIENEN, G. J. 1994b. Myofibrillar ATPase activity during isometric contraction and isomyosin composition in rat single skinned muscle fibres. *J Physiol*, 481 (Pt 3), 663-75.
- BOTTINELLI, R., SCHIAFFINO, S. & REGGIANI, C. 1991. Force-velocity relations and myosin heavy chain isoform compositions of skinned fibres from rat skeletal muscle. *J Physiol*, 437, 655-72.
- BRAND-SABERI, B. & CHRIST, B. 2000. Evolution and development of distinct cell lineages derived from somites. *Curr Top Dev Biol*, 48, 1-42.
- BREITBART, A., AUGER-MESSIER, M., MOKKENTIN, J. D. & HEINEKE, J. 2011. Myostatin from the heart: local and systemic actions in cardiac failure and muscle wasting. *Am J Physiol Heart Circ Physiol*, 300, H1973-82.
- BROHL, D., VASYUTINA, E., CZAJKOWSKI, M. T., GRIGER, J., RASSEK, C., RAHN, H. P., PURFURST, B., WENDE, H. & BIRCHMEIER, C. 2012. Colonization of the satellite cell niche by skeletal muscle progenitor cells depends on Notch signals. *Dev Cell*, 23, 469-81.
- BRUNET, A., BONNI, A., ZIGMOND, M. J., LIN, M. Z., JUO, P., HU, L. S., ANDERSON, M. J., ARDEN, K. C., BLENIS, J. & GREENBERG, M. E. 1999. Akt promotes cell survival by phosphorylating and inhibiting a Forkhead transcription factor. *Cell*, 96, 857-68.
- BRUUSGAARD, J. C., LIESTOL, K., EKMARK, M., KOLLSTAD, K. & GUNDERSEN, K. 2003. Number and spatial distribution of nuclei in the muscle fibres of normal mice studied in vivo. *J Physiol*, 551, 467-78.
- BRUUSGAARD, J. C., LIESTØL, K. & GUNDERSEN, K. 2006. Distribution of myonuclei and microtubules in live muscle fibers of young, middle-aged, and old mice. *J Appl Physiol (1985)*, 100, 2024-30.

- BULLER, A. J., ECCLES, J. C. & ECCLES, R. M. 1960. Differentiation of fast and slow muscles in the cat hind limb. *J Physiol*, 150, 399-416.
- BURKITT, H. G., YUONG, B., HEATH, J. W. 1993. Wheater's Functional Histology, A Text and colour Atlas. New York, Churchill livingstone.
- BUSHBY, K. M. 1999. The limb-girdle muscular dystrophies-multiple genes, multiple mechanisms. *Hum Mol Genet*, 8, 1875-82.
- CADENA, S. M., TOMKINSON, K. N., MONNELL, T. E., SPAITS, M. S., KUMAR, R., UNDERWOOD, K. W., PEARSALL, R. S. & LACHEY, J. L. 2010. Administration of a soluble activin type IIB receptor promotes skeletal muscle growth independent of fiber type. *J Appl Physiol (1985)*, 109, 635-42.
- CALVE, S., ODELBERG, S. J. & SIMON, H. G. 2010. A transitional extracellular matrix instructs cell behavior during muscle regeneration. *Dev Biol*, 344, 259-71.
- CAMPBELL, K. P. & STULL, J. T. 2003. Skeletal muscle basement membrane-sarcolemma-cytoskeleton interaction minireview series. *J Biol Chem*, 278, 12599-600.
- CANNON, B. & NEDERGAARD, J. 2004. Brown adipose tissue: function and physiological significance. *Physiol Rev*, 84, 277-359.
- CANTO, C., JIANG, L. Q., DESHMUKH, A. S., MATAKI, C., COSTE, A., LAGOUGE, M., ZIERATH, J. R. & AUWERX, J. 2010. Interdependence of AMPK and SIRT1 for metabolic adaptation to fasting and exercise in skeletal muscle. *Cell Metab*, 11, 213-9.
- CARLSON, B. M. & FAULKNER, J. A. 1989. Muscle transplantation between young and old rats: age of host determines recovery. *Am J Physiol*, 256, C1262-6.
- CASTET, A., HERLEDAN, A., BONNET, S., JALAGUIER, S., VANACKER, J. M. & CAVAILLES, V. 2006. Receptor-interacting protein 140 differentially regulates estrogen receptor-related receptor transactivation depending on target genes. *Mol Endocrinol*, 20, 1035-47.
- CASTETS, P., BERTRAND, A. T., BEUVIN, M., FERRY, A., LE GRAND, F., CASTETS, M., CHAZOT, G., REDERSTORFF, M., KROL, A., LESCURE, A., ROMERO, N. B., GUICHENEY, P. & ALLAMAND, V. 2011. Satellite cell loss and impaired muscle regeneration in selenoprotein N deficiency. *Hum Mol Genet*, 20, 694-704.
- CERLETTI, M., JANG, Y. C., FINLEY, L. W., HAIGIS, M. C. & WAGERS, A. J. 2012. Short-term calorie restriction enhances skeletal muscle stem cell function. *Cell Stem Cell*, 10, 515-9.
- CHAN, Y. M., BONNEMANN, C. G., LIDOV, H. G. & KUNKEL, L. M. 1998. Molecular organization of sarcoglycan complex in mouse myotubes in culture. *J Cell Biol*, 143, 2033-44.
- CHAO, E. Y., COLLINS, J. L., GAILLARD, S., MILLER, A. B., WANG, L., ORBAND-MILLER, L. A., NOLTE, R. T., MCDONNELL, D. P., WILLSON, T. M. & ZUERCHER, W. J. 2006. Structure-guided synthesis of tamoxifen analogs with improved selectivity for the orphan ERRgamma. *Bioorg Med Chem Lett*, 16, 821-4.
- CHARGE, S. B. & RUDNICKI, M. A. 2004. Cellular and molecular regulation of muscle regeneration. *Physiol Rev*, 84, 209-38.
- CHATTERJEE, S., YIN, H., NAM, D., LI, Y. & MA, K. 2015. Brain and muscle Arnt-like 1 promotes skeletal muscle regeneration through satellite cell expansion. *Exp Cell Res*, 331, 200-10.
- CHAZAUD, B., BRIGITTE, M., YACOUB-YOUSSEF, H., ARNOLD, L., GHERARDI, R., SONNET, C., LAFUSTE, P. & CHRETIEN, F. 2009. Dual and beneficial roles of macrophages during skeletal muscle regeneration. *Exerc Sport Sci Rev*, 37, 18-22.
- CHELH, I., MEUNIER, B., PICARD, B., REECY, M. J., CHEVALIER, C., HOCQUETTE, J.-F. & CASSAR-MALEK, I. 2009. Molecular profiles of Quadriceps muscle in myostatin-null mice reveal PI3K and apoptotic pathways as myostatin targets. *BMC Genomics*, 10, 196.
- CHELH, I., PICARD, B., HOCQUETTE, J. F. & CASSAR-MALEK, I. 2011. Myostatin inactivation induces a similar muscle molecular signature in double-musled cattle as in mice. *Animal*, 5, 278-86.

- CHERWEK, D. H., HOPKINS, M. B., THOMPSON, M. J., ANNEX, B. H. & TAYLOR, D. A. 2000. Fiber type-specific differential expression of angiogenic factors in response to chronic hindlimb ischemia. *Am J Physiol Heart Circ Physiol*, 279, H932-8.
- CHIRMULE, N., PROPERT, K., MAGOSIN, S., QIAN, Y., QIAN, R. & WILSON, J. 1999. Immune responses to adenovirus and adeno-associated virus in humans. *Gene Ther*, 6, 1574-83.
- CHO, Y., HAZEN, B. C., RUSSELL, A. P. & KRALLI, A. 2013. Peroxisome proliferator-activated receptor gamma coactivator 1 (PGC-1)- and estrogen-related receptor (ERR)-induced regulator in muscle 1 (Perm1) is a tissue-specific regulator of oxidative capacity in skeletal muscle cells. *J Biol Chem*, 288, 25207-18.
- CHRISTOV, C., CHRETIEN, F., ABOU-KHALIL, R., BASSEZ, G., VALLET, G., AUTHIER, F. J., BASSAGLIA, Y., SHININ, V., TAJBAKSH, S., CHAZAUD, B. & GHERARDI, R. K. 2007. Muscle satellite cells and endothelial cells: close neighbors and privileged partners. *Mol Biol Cell*, 18, 1397-409.
- CICILIOT, S., ROSSI, A. C., DYAR, K. A., BLAAUW, B. & SCHIAFFINO, S. 2013. Muscle type and fiber type specificity in muscle wasting. *Int J Biochem Cell Biol*, 45, 2191-9.
- CIRAK, S., FENG, L., ANTHONY, K., ARECHAVALA-GOMEZA, V., TORELLI, S., SEWRY, C., MORGAN, J. E. & MUNTONI, F. 2012. Restoration of the dystrophin-associated glycoprotein complex after exon skipping therapy in Duchenne muscular dystrophy. *Mol Ther*, 20, 462-7.
- CLOP, A., MARCQ, F., TAKEDA, H., PIROTTIN, D., TORDOIR, X., BIBE, B., BOUIX, J., CAIMENT, F., ELSÉN, J. M., EYCHENNE, F., LARZUL, C., LAVILLE, E., MEISH, F., MILENKOVIC, D., TOBIN, J., CHARLIER, C. & GEORGES, M. 2006. A mutation creating a potential illegitimate microRNA target site in the myostatin gene affects muscularity in sheep. *Nat Genet*, 38, 813-8.
- COLEMAN, M. E., DEMAYO, F., YIN, K. C., LEE, H. M., GESKE, R., MONTGOMERY, C. & SCHWARTZ, R. J. 1995. Myogenic vector expression of insulin-like growth factor I stimulates muscle cell differentiation and myofiber hypertrophy in transgenic mice. *J Biol Chem*, 270, 12109-16.
- COLLINS-HOOPER, H., SARTORI, R., GIALLOUROU, N., MATSAKAS, A., MITCHELL, R., MAKARENKOVA, H. P., FLASSKAMP, H., MACHARIA, R., RAY, S., SWANN, J. R., SANDRI, M. & PATEL, K. 2015. Correction: Symmorphosis through Dietary Regulation: A Combinatorial Role for Proteolysis, Autophagy and Protein Synthesis in Normalising Muscle Metabolism and Function of Hypertrophic Mice after Acute Starvation. *PLoS One*, 10, e0128731.
- COLLINS-HOOPER, H., SARTORI, R., MACHARIA, R., VISANUVIMOL, K., FOSTER, K., MATSAKAS, A., FLASSKAMP, H., RAY, S., DASH, P. R., SANDRI, M. & PATEL, K. 2014. Propeptide-mediated inhibition of myostatin increases muscle mass through inhibiting proteolytic pathways in aged mice. *J Gerontol A Biol Sci Med Sci*, 69, 1049-59.
- COLLINS, C. A., OLSEN, I., ZAMMIT, P. S., HESLOP, L., PETRIE, A., PARTRIDGE, T. A. & MORGAN, J. E. 2005. Stem cell function, self-renewal, and behavioral heterogeneity of cells from the adult muscle satellite cell niche. *Cell*, 122, 289-301.
- CONBOY, I. M., CONBOY, M. J., WAGERS, A. J., GIRMA, E. R., WEISSMAN, I. L. & RANDO, T. A. 2005. Rejuvenation of aged progenitor cells by exposure to a young systemic environment. *Nature*, 433, 760-4.
- CONERY, A. R., CAO, Y., THOMPSON, E. A., TOWNSEND, C. M., KO, T. C. & LUO, K. 2004. Akt interacts directly with Smad3 to regulate the sensitivity to TGF-beta induced apoptosis. *Nat Cell Biol*, 6, 366-72.
- CONJARD, A., PEUKER, H. & PETTE, D. 1998. Energy state and myosin heavy chain isoforms in single fibres of normal and transforming rabbit muscles. *Pflugers Arch*, 436, 962-9.
- CONLON, I. & RAFF, M. 1999. Size control in animal development. *Cell*, 96, 235-44.
- COOPER, R., KUH, D. & HARDY, R. 2010. Objectively measured physical capability levels and mortality: systematic review and meta-analysis. *Bmj*, 341, c4467.
- CORNELISON, D. D., WILCOX-ADELMAN, S. A., GOETINCK, P. F., RAUVALA, H., RAPRAEGER, A. C. & OLWIN, B. B. 2004. Essential and separable roles for Syndecan-3 and Syndecan-4 in skeletal muscle development and regeneration. *Genes Dev*, 18, 2231-6.

- CORNELISON, D. D. & WOLD, B. J. 1997. Single-cell analysis of regulatory gene expression in quiescent and activated mouse skeletal muscle satellite cells. *Dev Biol*, 191, 270-83.
- CRUZ-JENTOFT, A. J., BAEYENS, J. P., BAUER, J. M., BOIRIE, Y., CEDERHOLM, T., LANDI, F., MARTIN, F. C., MICHEL, J. P., ROLLAND, Y., SCHNEIDER, S. M., TOPINKOVA, E., VANDEWOUDE, M. & ZAMBONI, M. 2010. Sarcopenia: European consensus on definition and diagnosis: Report of the European Working Group on Sarcopenia in Older People. *Age Ageing*, 39, 412-23.
- CUI, Q., WANG, Z., JIANG, D., QU, L., GUO, J. & LI, Z. 2011. HGF inhibits TGF-beta1-induced myofibroblast differentiation and ECM deposition via MMP-2 in Achilles tendon in rat. *Eur J Appl Physiol*, 111, 1457-63.
- CZERWINSKA, A. M., STREMIŃSKA, W., CIEMERYCH, M. A. & GRABOWSKA, I. 2012. Mouse gastrocnemius muscle regeneration after mechanical or cardiotoxin injury. *Folia Histochem Cytobiol*, 50, 144-53.
- D'ALBIS, A., COUTEAUX, R., JANMOT, C., ROULET, A. & MIRA, J. C. 1988. Regeneration after cardiotoxin injury of innervated and denervated slow and fast muscles of mammals. Myosin isoform analysis. *Eur J Biochem*, 174, 103-10.
- D'ANTONA, G., MEGIGHIAN, A., BORTOLOTTI, S., PELLEGRINO, M. A., MARCHESE-RAGONA, R., STAFFIERI, A., BOTTINELLI, R. & REGGIANI, C. 2002. Contractile properties and myosin heavy chain isoform composition in single fibre of human laryngeal muscles. *J Muscle Res Cell Motil*, 23, 187-95.
- DE ANGELIS, L., BERGHELLA, L., COLETTA, M., LATTANZI, L., ZANCHI, M., CUSELLA-DE ANGELIS, M. G., PONZETTO, C. & COSSU, G. 1999. Skeletal myogenic progenitors originating from embryonic dorsal aorta coexpress endothelial and myogenic markers and contribute to postnatal muscle growth and regeneration. *J Cell Biol*, 147, 869-78.
- DE BRUIN, M., SMEULDERS, M. J., KREULEN, M., HUIJING, P. A. & JASPERS, R. T. 2014. Intramuscular connective tissue differences in spastic and control muscle: a mechanical and histological study. *PLoS One*, 9, e101038.
- DE KONING, J., HOOFD, L. J. & KREUZER, F. 1981. Oxygen transport and the function of myoglobin. Theoretical model and experiments in chicken gizzard smooth muscle. *Pflugers Arch*, 389, 211-7.
- DEBLOIS, G., HALL, J. A., PERRY, M. C., LAGANIERE, J., GHAHREMANI, M., PARK, M., HALLETT, M. & GIGUERE, V. 2009. Genome-wide identification of direct target genes implicates estrogen-related receptor alpha as a determinant of breast cancer heterogeneity. *Cancer Res*, 69, 6149-57.
- DEGENS, H. 2012. Determinants of Skeletal Muscle Hypertrophy and the Attenuated Hypertrophic Response at Old Age. *J Sports Medicine & Dopng Studies*, S1:003.
- DEGENS, H., TUREK, Z., HOOFD, L. J., VAN'T HOF, M. A. & BINKHORST, R. A. 1992. The relationship between capillarisation and fibre types during compensatory hypertrophy of the plantaris muscle in the rat. *J Anat*, 180 (Pt 3), 455-63.
- DELFINI, M. C., DE LA CELLE, M., GROS, J., SERRALBO, O., MARICS, I., SEUX, M., SCAAL, M. & MARCELLE, C. 2009. The timing of emergence of muscle progenitors is controlled by an FGF/ERK/SNAIL1 pathway. *Dev Biol*, 333, 229-37.
- DEMONTIS, F., PICCIRILLO, R., GOLDBERG, A. L. & PERRIMON, N. 2013. The influence of skeletal muscle on systemic aging and lifespan. *Aging Cell*, 12, 943-9.
- DES TOMBE, A. L., VAN BEEK-HARMSSEN, B. J., LEE-DE GROOT, M. B. & VAN DER LAARSE, W. J. 2002. Calibrated histochemistry applied to oxygen supply and demand in hypertrophied rat myocardium. *Microsc Res Tech*, 58, 412-20.
- DESPLANCHES, D., HOPPELER, H., TUSCHER, L., MAYET, M. H., SPIELVOGEL, H., FERRETTI, G., KAYSER, B., LEUENBERGER, M., GRUNENFELDER, A. & FAVIER, R. 1996. Muscle tissue adaptations of high-altitude natives to training in chronic hypoxia or acute normoxia. *J Appl Physiol (1985)*, 81, 1946-51.

- DESERGNE, B., MICHALIK, L. & WAHLI, W. 2006. Transcriptional regulation of metabolism. *Physiol Rev*, 86, 465-514.
- DEVARAKONDA, S., GUPTA, K., CHALMERS, M. J., HUNT, J. F., GRIFFIN, P. R., VAN DUYN, G. D. & SPIEGELMAN, B. M. 2011. Disorder-to-order transition underlies the structural basis for the assembly of a transcriptionally active PGC-1 α /ERR γ complex. *Proc Natl Acad Sci U S A*, 108, 18678-83.
- DEVECI, D., MARSHALL, J. M. & EGGINTON, S. 2001. Relationship between capillary angiogenesis, fiber type, and fiber size in chronic systemic hypoxia. *Am J Physiol Heart Circ Physiol*, 281, H241-52.
- DHOOT, G. K., HALES, M. C., GRAIL, B. M. & PERRY, S. V. 1985. The isoforms of C protein and their distribution in mammalian skeletal muscle. *J Muscle Res Cell Motil*, 6, 487-505.
- DIAZ, G., LIU, S., ISOLA, R., DIANA, A. & FALCHI, A. M. 2003. Mitochondrial localization of reactive oxygen species by dihydrofluorescein probes. *Histochem Cell Biol*, 120, 319-25.
- DIXEN, K., BASSE, A. L., MURHOLM, M., ISIDOR, M. S., HANSEN, L. H., PETERSEN, M. C., MADSEN, L., PETROVIC, N., NEDERGAARD, J., QUISTORFF, B. & HANSEN, J. B. 2013. ERR γ enhances UCP1 expression and fatty acid oxidation in brown adipocytes. *Obesity (Silver Spring)*, 21, 516-24.
- DUFOUR, C. R., WILSON, B. J., HUSS, J. M., KELLY, D. P., ALAYNICK, W. A., DOWNES, M., EVANS, R. M., BLANCHETTE, M. & GIGUÈRE, V. 2007. Genome-wide orchestration of cardiac functions by the orphan nuclear receptors ERR α and γ . *Cell Metab*, 5, 345-56.
- DUNCAN, C. J. & JACKSON, M. J. 1987. Different mechanisms mediate structural changes and intracellular enzyme efflux following damage to skeletal muscle. *J Cell Sci*, 87 (Pt 1), 183-8.
- DUNNETT, M., HARRIS, R. C., SOLIMAN, M. Z. & SUWAR, A. A. 1997. Carnosine, anserine and taurine contents in individual fibres from the middle gluteal muscle of the camel. *Res Vet Sci*, 62, 213-6.
- DURHAM, W. J., ARACENA-PARKS, P., LONG, C., ROSSI, A. E., GOONASEKERA, S. A., BONCOMPAGNI, S., GALVAN, D. L., GILMAN, C. P., BAKER, M. R., SHIROKOVA, N., PROTASI, F., DIRKSEN, R. & HAMILTON, S. L. 2008. RyR1 S-nitrosylation underlies environmental heat stroke and sudden death in Y522S RyR1 knockin mice. *Cell*, 133, 53-65.
- DURIEUX, A. C., AMIROUCHE, A., BANZET, S., KOULMANN, N., BONNEFOY, R., PASDELOUP, M., MOURET, C., BIGARD, X., PEINNEQUIN, A. & FREYSSENET, D. 2007. Ectopic expression of myostatin induces atrophy of adult skeletal muscle by decreasing muscle gene expression. *Endocrinology*, 148, 3140-7.
- EDGERTON, V. R. & ROY, R. R. 1991. Regulation of skeletal muscle fiber size, shape and function. *J Biomech*, 24 Suppl 1, 123-33.
- EGGINTON, S., HUDLICKA, O., BROWN, M. D., WALTER, H., WEISS, J. B. & BATE, A. 1998. Capillary growth in relation to blood flow and performance in overloaded rat skeletal muscle. *J Appl Physiol (1985)*, 85, 2025-32.
- EICHNER, L. J. & GIGUÈRE, V. 2011. Estrogen related receptors (ERRs): a new dawn in transcriptional control of mitochondrial gene networks. *Mitochondrion*, 11, 544-52.
- EICHNER, L. J., PERRY, M.-C., DUFOUR, C. R., BERTOS, N., PARK, M., ST-PIERRE, J. & GIGUÈRE, V. 2010. miR-378(*) mediates metabolic shift in breast cancer cells via the PGC-1 β /ERR γ transcriptional pathway. *Cell Metab*, 12, 352-61.
- EISENBERG-LERNER, A., BIALIK, S., SIMON, H. U. & KIMCHI, A. 2009. Life and death partners: apoptosis, autophagy and the cross-talk between them. *Cell Death Differ*, 16, 966-75.
- ELASHRY, M. I., COLLINS-HOOPER, H., VAIYAPURI, S. & PATEL, K. 2012. Characterisation of connective tissue from the hypertrophic skeletal muscle of myostatin null mice. *J Anat*, 220, 603-11.
- ELASHRY, M. I., OTTO, A., MATSAKAS, A., EL-MORSY, S. E. & PATEL, K. 2009. Morphology and myofiber composition of skeletal musculature of the forelimb in young and aged wild type and myostatin null mice. *Rejuvenation Res*, 12, 269-81.

- ELLIOTT, B., RENSHAW, D., GETTING, S. & MACKENZIE, R. 2012. The central role of myostatin in skeletal muscle and whole body homeostasis. *Acta Physiol (Oxf)*, 205, 324-40.
- ENGLER, A. J., SEN, S., SWEENEY, H. L. & DISCHER, D. E. 2006. Matrix elasticity directs stem cell lineage specification. *Cell*, 126, 677-89.
- EPSTEIN, J. A., SHAPIRO, D. N., CHENG, J., LAM, P. Y. & MAAS, R. L. 1996. Pax3 modulates expression of the c-Met receptor during limb muscle development. *Proc Natl Acad Sci U S A*, 93, 4213-8.
- ERSKINE, R. M., JONES, D. A., WILLIAMS, A. G., STEWART, C. E. & DEGENS, H. 2010. Resistance training increases in vivo quadriceps femoris muscle specific tension in young men. *Acta Physiol (Oxf)*, 199, 83-9.
- ERVASTI, J. M. & CAMPBELL, K. P. 1993. A role for the dystrophin-glycoprotein complex as a transmembrane linker between laminin and actin. *J Cell Biol*, 122, 809-23.
- EUDY, J. D., YAO, S., WESTON, M. D., MA-EDMONDS, M., TALMADGE, C. B., CHENG, J. J., KIMBERLING, W. J. & SUMEGI, J. 1998. Isolation of a gene encoding a novel member of the nuclear receptor superfamily from the critical region of Usher syndrome type IIa at 1q41. *Genomics*, 50, 382-4.
- FAULKNER, J. A., BROOKS, S. V. & ZERBA, E. 1990. Skeletal muscle weakness and fatigue in old age: underlying mechanisms. *Annu Rev Gerontol Geriatr*, 10, 147-66.
- FEIGE, J. N. & AUWERX, J. 2007. Transcriptional coregulators in the control of energy homeostasis. *Trends Cell Biol*, 17, 292-301.
- FELDMAN, B. J., STREPPER, R. S., FARESE, R. V., JR. & YAMAMOTO, K. R. 2006. Myostatin modulates adipogenesis to generate adipocytes with favorable metabolic effects. *Proc Natl Acad Sci U S A*, 103, 15675-80.
- FELDMAN, J. L. & STOCKDALE, F. E. 1992. Temporal appearance of satellite cells during myogenesis. *Dev Biol*, 153, 217-26.
- FLEG, J. L., MORRELL, C. H., BOS, A. G., BRANT, L. J., TALBOT, L. A., WRIGHT, J. G. & LAKATTA, E. G. 2005. Accelerated longitudinal decline of aerobic capacity in healthy older adults. *Circulation*, 112, 674-82.
- FLUCK, M. & HOPPELER, H. 2003. Molecular basis of skeletal muscle plasticity--from gene to form and function. *Rev Physiol Biochem Pharmacol*, 146, 159-216.
- FOSTER, K., GRAHAM, I. R., OTTO, A., FOSTER, H., TROLLET, C., YAWORSKY, P. J., WALSH, F. S., BICKHAM, D., CURTIN, N. A., KAWAR, S. L., PATEL, K. & DICKSON, G. 2009. Adeno-associated virus-8-mediated intravenous transfer of myostatin propeptide leads to systemic functional improvements of slow but not fast muscle. *Rejuvenation Res*, 12, 85-94.
- FRANK, S., GAUME, B., BERGMANN-LEITNER, E. S., LEITNER, W. W., ROBERT, E. G., CATEZ, F., SMITH, C. L. & YOULE, R. J. 2001. The role of dynamin-related protein 1, a mediator of mitochondrial fission, in apoptosis. *Dev Cell*, 1, 515-25.
- FRY, C. S., KIRBY, T. J., KOSMAC, K., MCCARTHY, J. J. & PETERSON, C. A. 2017. Myogenic Progenitor Cells Control Extracellular Matrix Production by Fibroblasts during Skeletal Muscle Hypertrophy. *Cell Stem Cell*, 20, 56-69.
- FRY, C. S., LEE, J. D., JACKSON, J. R., KIRBY, T. J., STASKO, S. A., LIU, H., DUPONT-VERSTEEGDEN, E. E., MCCARTHY, J. J. & PETERSON, C. A. 2014. Regulation of the muscle fiber microenvironment by activated satellite cells during hypertrophy. *Faseb j*, 28, 1654-65.
- FUJII, N., HAYASHI, T., HIRSHMAN, M. F., SMITH, J. T., HABINOWSKI, S. A., KAIJSER, L., MU, J., LJUNGQVIST, O., BIRNBAUM, M. J., WITTERS, L. A., THORELL, A. & GOODYEAR, L. J. 2000. Exercise induces isoform-specific increase in 5'AMP-activated protein kinase activity in human skeletal muscle. *Biochem Biophys Res Commun*, 273, 1150-5.
- FUJII, N., SEIFERT, M. M., KANE, E. M., PETER, L. E., HO, R. C., WINSTEAD, S., HIRSHMAN, M. F. & GOODYEAR, L. J. 2007. Role of AMP-activated protein kinase in exercise capacity, whole body glucose homeostasis, and glucose transport in skeletal muscle -insight from analysis of a transgenic mouse model. *Diabetes Res Clin Pract*, 77 Suppl 1, S92-8.

- GADALLA, K. K., BAILEY, M. E., SPIKE, R. C., ROSS, P. D., WOODARD, K. T., KALBURGI, S. N., BACHABOINA, L., DENG, J. V., WEST, A. E., SAMULSKI, R. J., GRAY, S. J. & COBB, S. R. 2013. Improved survival and reduced phenotypic severity following AAV9/MECP2 gene transfer to neonatal and juvenile male Mecp2 knockout mice. *Mol Ther*, 21, 18-30.
- GADEAU, A. P. & ARNAL, J. F. 2012. Estrogen-related receptor-gamma: conductor of muscle angiogenesis through conversion of fast- to slow-twitch fibers? *Circ Res*, 110, 1042-4.
- GALLER, S., SCHMITT, T. L. & PETTE, D. 1994. Stretch activation, unloaded shortening velocity, and myosin heavy chain isoforms of rat skeletal muscle fibres. *J Physiol*, 478 Pt 3, 513-21.
- GAN, Z., RUMSEY, J., HAZEN, B. C., LAI, L., LEONE, T. C., VEGA, R. B., XIE, H., CONLEY, K. E., AUWERX, J., SMITH, S. R., OLSON, E. N., KRALLI, A. & KELLY, D. P. 2013. Nuclear receptor/microRNA circuitry links muscle fiber type to energy metabolism. *J Clin Invest*, 123, 2564-75.
- GANONG, W. F. 2005. Review of medical physiology, McGraw-Hill Medical.
- GAO, Q. Q. & MCNALLY, E. M. 2015. The Dystrophin Complex: Structure, Function, and Implications for Therapy. *Compr Physiol*, 5, 1223-39.
- GATCHALIAN, C. L., SCHACHNER, M. & SANES, J. R. 1989. Fibroblasts that proliferate near denervated synaptic sites in skeletal muscle synthesize the adhesive molecules tenascin(J1), N-CAM, fibronectin, and a heparan sulfate proteoglycan. *J Cell Biol*, 108, 1873-90.
- GAUDEL, C., SCHWARTZ, C., GIORDANO, C., ABUMRAD, N. A. & GRIMALDI, P. A. 2008. Pharmacological activation of PPARbeta promotes rapid and calcineurin-dependent fiber remodeling and angiogenesis in mouse skeletal muscle. *Am J Physiol Endocrinol Metab*, 295, E297-304.
- GAVIN, T. P., RUSTER, R. S., CARRITHERS, J. A., ZWETSLOOT, K. A., KRAUS, R. M., EVANS, C. A., KNAPP, D. J., DREW, J. L., MCCARTNEY, J. S., GARRY, J. P. & HICKNER, R. C. 2007. No difference in the skeletal muscle angiogenic response to aerobic exercise training between young and aged men. *J Physiol*, 585, 231-9.
- GAYRAUD-MOREL, B., CHRETIEN, F. & TAJBAKHS, S. 2009. Skeletal muscle as a paradigm for regenerative biology and medicine. *Regen Med*, 4, 293-319.
- GENG, J. & KLIONSKY, D. J. 2008. The Atg8 and Atg12 ubiquitin-like conjugation systems in macroautophagy. 'Protein modifications: beyond the usual suspects' review series. *EMBO Rep*, 9, 859-64.
- GEORGE CARLSON, C., BRUEMMER, K., SESTI, J., STEFANSKI, C., CURTIS, H., UCRAN, J., LACHEY, J. & SEEHRA, J. S. 2011. Soluble activin receptor type IIB increases forward pulling tension in the mdx mouse. *Muscle Nerve*, 43, 694-9.
- GERHART-HINES, Z., RODGERS, J. T., BARE, O., LERIN, C., KIM, S. H., MOSTOSLAVSKY, R., ALT, F. W., WU, Z. & PUIGSERVER, P. 2007. Metabolic control of muscle mitochondrial function and fatty acid oxidation through SIRT1/PGC-1alpha. *Embo j*, 26, 1913-23.
- GESTA, S., TSENG, Y. H. & KAHN, C. R. 2007. Developmental origin of fat: tracking obesity to its source. *Cell*, 131, 242-56.
- GIANNOULIS, M. G., MARTIN, F. C., NAIR, K. S., UMPLEBY, A. M. & SONKSEN, P. 2012. Hormone replacement therapy and physical function in healthy older men. Time to talk hormones? *Endocr Rev*, 33, 314-77.
- GIBSON, M. C. & SCHULTZ, E. 1983. Age-related differences in absolute numbers of skeletal muscle satellite cells. *Muscle Nerve*, 6, 574-80.
- GIGUERE, V. 2008. Transcriptional control of energy homeostasis by the estrogen-related receptors. *Endocr Rev*, 29, 677-96.
- GILBERT, P. M., HAVENSTRITE, K. L., MAGNUSSON, K. E., SACCO, A., LEONARDI, N. A., KRAFT, P., NGUYEN, N. K., THRUN, S., LUTOLF, M. P. & BLAU, H. M. 2010. Substrate elasticity regulates skeletal muscle stem cell self-renewal in culture. *Science*, 329, 1078-81.
- GILDOR, B., SCHEJTER, E. D. & SHILO, B. Z. 2012. Bidirectional Notch activation represses fusion competence in swarming adult *Drosophila* myoblasts. *Development*, 139, 4040-50.

- GILLIES, A. R., BUSHONG, E. A., DEERINCK, T. J., ELLISMAN, M. H. & LIEBER, R. L. 2014. Three-dimensional reconstruction of skeletal muscle extracellular matrix ultrastructure. *Microsc Microanal*, 20, 1835-40.
- GILLIES, A. R. & LIEBER, R. L. 2011. Structure and function of the skeletal muscle extracellular matrix. *Muscle Nerve*, 44, 318-31.
- GIRGENRATH, S., SONG, K. & WHITTEMORE, L. A. 2005. Loss of myostatin expression alters fiber-type distribution and expression of myosin heavy chain isoforms in slow- and fast-type skeletal muscle. *Muscle Nerve*, 31, 34-40.
- GLASS, D. J. 2005. Skeletal muscle hypertrophy and atrophy signaling pathways. *Int J Biochem Cell Biol*, 37, 1974-84.
- GLASS, D. J. 2010. PI3 kinase regulation of skeletal muscle hypertrophy and atrophy. *Curr Top Microbiol Immunol*, 346, 267-78.
- GOETSCH, S. C., HAWKE, T. J., GALLARDO, T. D., RICHARDSON, J. A. & GARRY, D. J. 2003. Transcriptional profiling and regulation of the extracellular matrix during muscle regeneration. *Physiol Genomics*, 14, 261-71.
- GONZALEZ-CADAVID, N. F., TAYLOR, W. E., YARASHESKI, K., SINHA-HIKIM, I., MA, K., EZZAT, S., SHEN, R., LALANI, R., ASA, S., MAMITA, M., NAIR, G., ARVER, S. & BHASIN, S. 1998. Organization of the human myostatin gene and expression in healthy men and HIV-infected men with muscle wasting. *Proc Natl Acad Sci U S A*, 95, 14938-43.
- GOULDING, M., LUMSDEN, A. & PAQUETTE, A. J. 1994. Regulation of Pax-3 expression in the dermomyotome and its role in muscle development. *Development*, 120, 957-71.
- GOULDING, M. D., CHALEPAKIS, G., DEUTSCH, U., ERSELIUS, J. R. & GRUSS, P. 1991. Pax-3, a novel murine DNA binding protein expressed during early neurogenesis. *Embo j*, 10, 1135-47.
- GREER, E. L., OSKOU, P. R., BANKO, M. R., MANIAR, J. M., GYGI, M. P., GYGI, S. P. & BRUNET, A. 2007. The energy sensor AMP-activated protein kinase directly regulates the mammalian FOXO3 transcription factor. *J Biol Chem*, 282, 30107-19.
- GRESCHIK, H., WURTZ, J. M., SANGLIER, S., BOURGUET, W., VAN DORSSELAER, A., MORAS, D. & RENAUD, J. P. 2002. Structural and functional evidence for ligand-independent transcriptional activation by the estrogen-related receptor 3. *Mol Cell*, 9, 303-13.
- GRICHNIK, J. M., BERGSMA, D. J. & SCHWARTZ, R. J. 1986. Tissue restricted and stage specific transcription is maintained within 411 nucleotides flanking the 5' end of the chicken alpha-skeletal actin gene. *Nucleic Acids Res*, 14, 1683-701.
- GRONEMEYER, H. & LAUDET, V. 1995. Transcription factors 3: nuclear receptors. *Protein Profile*, 2, 1173-308.
- GROS, J., MANCEAU, M., THOME, V. & MARCELLE, C. 2005. A common somitic origin for embryonic muscle progenitors and satellite cells. *Nature*, 435, 954-8.
- GROUNDS, M. D. 1987. Phagocytosis of necrotic muscle in muscle isografts is influenced by the strain, age, and sex of host mice. *J Pathol*, 153, 71-82.
- GROUNDS, M. D. & YABLONKA-REUVENI, Z. 1993. Molecular and cell biology of skeletal muscle regeneration. *Mol Cell Biol Hum Dis Ser*, 3, 210-56.
- GRUMATI, P., COLETTI, L., SABATELLI, P., CESCONE, M., ANGELIN, A., BERTAGGIA, E., BLAAUW, B., URCIUOLO, A., TIEPOLO, T., MERLINI, L., MARALDI, N. M., BERNARDI, P., SANDRI, M. & BONALDO, P. 2010. Autophagy is defective in collagen VI muscular dystrophies, and its reactivation rescues myofiber degeneration. *Nat Med*, 16, 1313-20.
- GRUNE, T., MERKER, K., SANDIG, G. & DAVIES, K. J. 2003. Selective degradation of oxidatively modified protein substrates by the proteasome. *Biochem Biophys Res Commun*, 305, 709-18.
- GUDBJORNSDOTTIR, S., SJOSTRAND, M., STRINDBERG, L., WAHREN, J. & LONNROTH, P. 2003. Direct measurements of the permeability surface area for insulin and glucose in human skeletal muscle. *J Clin Endocrinol Metab*, 88, 4559-64.

- GUERTIN, D. A., STEVENS, D. M., THOREEN, C. C., BURDS, A. A., KALAANY, N. Y., MOFFAT, J., BROWN, M., FITZGERALD, K. J. & SABATINI, D. M. 2006. Ablation in mice of the mTORC components raptor, rictor, or mLST8 reveals that mTORC2 is required for signaling to Akt-FOXO and PKCalpha, but not S6K1. *Dev Cell*, 11, 859-71.
- GUILAK, F., COHEN, D. M., ESTES, B. T., GIMBLE, J. M., LIEDTKE, W. & CHEN, C. S. 2009. Control of stem cell fate by physical interactions with the extracellular matrix. *Cell Stem Cell*, 5, 17-26.
- GULICK, T., CRESCI, S., CAIRA, T., MOORE, D. D. & KELLY, D. P. 1994. The peroxisome proliferator-activated receptor regulates mitochondrial fatty acid oxidative enzyme gene expression. *Proc Natl Acad Sci U S A*, 91, 11012-6.
- GUMERSON, J. D. & MICHELE, D. E. 2011. The dystrophin-glycoprotein complex in the prevention of muscle damage. *J Biomed Biotechnol*, 2011, 210797.
- GUNDERSEN, K. 2011. Excitation-transcription coupling in skeletal muscle: the molecular pathways of exercise. *Biol Rev Camb Philos Soc*, 86, 564-600.
- GUNN, H. M. 1978. Differences in the histochemical properties of skeletal muscles of different breeds of horses and dogs. *J Anat*, 127, 615-34.
- GUO, T., JOU, W., CHANTURIYA, T., PORTAS, J., GAVRILOVA, O. & MCPHERRON, A. C. 2009. Myostatin inhibition in muscle, but not adipose tissue, decreases fat mass and improves insulin sensitivity. *PLoS One*, 4, e4937.
- GUO, W., MILLER, A. D., PENCINA, K., WONG, S., LEE, A., YEE, M., TORALDO, G., JASUJA, R. & BHASIN, S. 2016. Joint dysfunction and functional decline in middle age myostatin null mice. *Bone*, 83, 141-8.
- GUSTAFSSON, T. 2011. Vascular remodelling in human skeletal muscle. *Biochem Soc Trans*, 39, 1628-32.
- GUTMANN, E. & HANZLIKOVA, V. 1966. Motor unit in old age. *Nature*, 209, 921-2.
- HACK, A. A., LY, C. T., JIANG, F., CLENDENIN, C. J., SIGRIST, K. S., WOLLMANN, R. L. & MCNALLY, E. M. 1998. Gamma-sarcoglycan deficiency leads to muscle membrane defects and apoptosis independent of dystrophin. *J Cell Biol*, 142, 1279-87.
- HAIDET, A. M., RIZO, L., HANDY, C., UMAPATHI, P., EAGLE, A., SHILLING, C., BOUE, D., MARTIN, P. T., SAHENK, Z., MENDELL, J. R. & KASPAR, B. K. 2008. Long-term enhancement of skeletal muscle mass and strength by single gene administration of myostatin inhibitors. *Proc Natl Acad Sci U S A*, 105, 4318-22.
- HALL, Z. W. & RALSTON, E. 1989. Nuclear domains in muscle cells. *Cell*, 59, 771-2.
- HAMAI, N., NAKAMURA, M. & ASANO, A. 1997. Inhibition of mitochondrial protein synthesis impaired C2C12 myoblast differentiation. *Cell Struct Funct*, 22, 421-31.
- HAN, H. Q., ZHOU, X., MITCH, W. E. & GOLDBERG, A. L. 2013. Myostatin/activin pathway antagonism: molecular basis and therapeutic potential. *Int J Biochem Cell Biol*, 45, 2333-47.
- HANSEN, J. M., KLASS, M., HARRIS, C. & CSETE, M. 2007. A reducing redox environment promotes C2C12 myogenesis: implications for regeneration in aged muscle. *Cell Biol Int*, 31, 546-53.
- HARA, Y., BALCI-HAYTA, B., YOSHIDA-MORIGUCHI, T., KANAGAWA, M., BELTRAN-VALERO DE BERNABE, D., GUNDESLI, H., WILLER, T., SATZ, J. S., CRAWFORD, R. W., BURDEN, S. J., KUNZ, S., OLDSTONE, M. B., ACCARDI, A., TALIM, B., MUNTONI, F., TOPALOGLU, H., DINCER, P. & CAMPBELL, K. P. 2011. A dystroglycan mutation associated with limb-girdle muscular dystrophy. *N Engl J Med*, 364, 939-46.
- HARPER, M. E., BEVILACQUA, L., HAGOPIAN, K., WEINDRUCH, R. & RAMSEY, J. J. 2004. Ageing, oxidative stress, and mitochondrial uncoupling. *Acta Physiol Scand*, 182, 321-31.
- HARRINGTON, L. S., FINDLAY, G. M., GRAY, A., TOLKACHEVA, T., WIGFIELD, S., REBHOLZ, H., BARNETT, J., LESLIE, N. R., CHENG, S., SHEPHERD, P. R., GOUT, I., DOWNES, C. P. & LAMB, R. F. 2004. The TSC1-2 tumor suppressor controls insulin-PI3K signaling via regulation of IRS proteins. *J Cell Biol*, 166, 213-23.

- HASTINGS, K. E. & EMERSON, C. P., JR. 1982. cDNA clone analysis of six co-regulated mRNAs encoding skeletal muscle contractile proteins. *Proc Natl Acad Sci U S A*, 79, 1553-7.
- HASTY, P., BRADLEY, A., MORRIS, J. H., EDMONDSON, D. G., VENUTI, J. M., OLSON, E. N. & KLEIN, W. H. 1993. Muscle deficiency and neonatal death in mice with a targeted mutation in the myogenin gene. *Nature*, 364, 501-6.
- HATHER, B. M., TESCH, P. A., BUCHANAN, P. & DUDLEY, G. A. 1991. Influence of eccentric actions on skeletal muscle adaptations to resistance training. *Acta Physiol Scand*, 143, 177-85.
- HAWKE, T. J. & GARRY, D. J. 2001. Myogenic satellite cells: physiology to molecular biology. *J Appl Physiol (1985)*, 91, 534-51.
- HAYOT, M., RODRIGUEZ, J., VERNUS, B., CARNAC, G., JEAN, E., ALLEN, D., GORET, L., OBERT, P., CANDAU, R. & BONNIEU, A. 2011. Myostatin up-regulation is associated with the skeletal muscle response to hypoxic stimuli. *Mol Cell Endocrinol*, 332, 38-47.
- HEARD, D. J., NORBY, P. L., HOLLOWAY, J. & VISSING, H. 2000. Human ERRgamma, a third member of the estrogen receptor-related receptor (ERR) subfamily of orphan nuclear receptors: tissue-specific isoforms are expressed during development and in the adult. *Mol Endocrinol*, 14, 382-92.
- HEESCH, M. W., SHUTE, R. J., KREILING, J. L. & SLIVKA, D. R. 2016. Transcriptional control, but not subcellular location, of PGC-1 α is altered following exercise in a hot environment. *J Appl Physiol (1985)*, 121, 741-9.
- HEINEMEIER, K. M., OLESEN, J. L., HADDAD, F., LANGBERG, H., KJAER, M., BALDWIN, K. M. & SCHJERLING, P. 2007. Expression of collagen and related growth factors in rat tendon and skeletal muscle in response to specific contraction types. *J Physiol*, 582, 1303-16.
- HERBISON, G. J., JAWEED, M. M. & DITUNNO, J. F. 1979. Muscle atrophy in rats following denervation, casting, inflammation, and tenotomy. *Arch Phys Med Rehabil*, 60, 401-4.
- HICKSON, R. C. 1980. Interference of strength development by simultaneously training for strength and endurance. *Eur J Appl Physiol Occup Physiol*, 45, 255-63.
- HILBER, K., GALLER, S., GOHLSCH, B. & PETTE, D. 1999. Kinetic properties of myosin heavy chain isoforms in single fibers from human skeletal muscle. *FEBS Lett*, 455, 267-70.
- HILL, J. J., DAVIES, M. V., PEARSON, A. A., WANG, J. H., HEWICK, R. M., WOLFMAN, N. M. & QIU, Y. 2002. The myostatin propeptide and the follistatin-related gene are inhibitory binding proteins of myostatin in normal serum. *J Biol Chem*, 277, 40735-41.
- HO-KIM, M. A. & ROGERS, P. A. 1992. Quantitative analysis of dystrophin in fast- and slow-twitch mammalian skeletal muscle. *FEBS Lett*, 304, 187-91.
- HOFFMAN, E. P., BROWN, R. H., JR. & KUNKEL, L. M. 1987. Dystrophin: the protein product of the Duchenne muscular dystrophy locus. *Cell*, 51, 919-28.
- HOLMES, J. H., ASHMORE, C. R. & ROBINSON, D. W. 1973. Effects of stress on cattle with hereditary muscular hypertrophy. *J Anim Sci*, 36, 684-94.
- HONG, H., KOHLI, K., TRIVEDI, A., JOHNSON, D. L. & STALLCUP, M. R. 1996. GRIP1, a novel mouse protein that serves as a transcriptional coactivator in yeast for the hormone binding domains of steroid receptors. *Proc Natl Acad Sci U S A*, 93, 4948-52.
- HONG, H., YANG, L. & STALLCUP, M. R. 1999. Hormone-independent transcriptional activation and coactivator binding by novel orphan nuclear receptor ERR3. *J Biol Chem*, 274, 22618-26.
- HOOFD, L. & EGGINTON, S. 1997. The possible role of intracellular lipid in determining oxygen delivery to fish skeletal muscle. *Respir Physiol*, 107, 191-202.
- HORNBERGER, T. A., SUKHIJA, K. B. & CHIEN, S. 2006. Regulation of mTOR by mechanically induced signaling events in skeletal muscle. *Cell Cycle*, 5, 1391-6.
- HOYER-HANSEN, M. & JAATTELA, M. 2007. AMP-activated protein kinase: a universal regulator of autophagy? *Autophagy*, 3, 381-3.
- HUANG, Z., CHEN, D., ZHANG, K., YU, B., CHEN, X. & MENG, J. 2007. Regulation of myostatin signaling by c-Jun N-terminal kinase in C2C12 cells. *Cell Signal*, 19, 2286-95.

- HUDLICKA, O., BROWN, M. & EGGINTON, S. 1992. Angiogenesis in skeletal and cardiac muscle. *Physiol Rev*, 72, 369-417.
- HULMI, J. J., OLIVEIRA, B. M., SILVENNOINEN, M., HOOGAARS, W. M., MA, H., PIERRE, P., PASTERNAK, A., KAINULAINEN, H. & RITVOS, O. 2013a. Muscle protein synthesis, mTORC1/MAPK/Hippo signaling, and capillary density are altered by blocking of myostatin and activins. *Am J Physiol Endocrinol Metab*, 304, E41-50.
- HULMI, J. J., OLIVEIRA, B. M., SILVENNOINEN, M., HOOGAARS, W. M., PASTERNAK, A., KAINULAINEN, H. & RITVOS, O. 2013b. Exercise restores decreased physical activity levels and increases markers of autophagy and oxidative capacity in myostatin/activin-blocked mdx mice. *Am J Physiol Endocrinol Metab*, 305, E171-82.
- HUSS, J. M., GARBACZ, W. G. & XIE, W. 2015. Constitutive activities of estrogen-related receptors: Transcriptional regulation of metabolism by the ERR pathways in health and disease. *Biochim Biophys Acta*, 1852, 1912-27.
- HUSS, J. M., KOPP, R. P. & KELLY, D. P. 2002. Peroxisome proliferator-activated receptor coactivator-1alpha (PGC-1alpha) coactivates the cardiac-enriched nuclear receptors estrogen-related receptor-alpha and -gamma. Identification of novel leucine-rich interaction motif within PGC-1alpha. *J Biol Chem*, 277, 40265-74.
- INOKI, K., ZHU, T. & GUAN, K. L. 2003. TSC2 mediates cellular energy response to control cell growth and survival. *Cell*, 115, 577-90.
- JACKSON, M. J. 2011. Control of reactive oxygen species production in contracting skeletal muscle. *Antioxid Redox Signal*, 15, 2477-86.
- JAGER, S. B., RONCHI, G., VAEGTER, C. B. & GEUNA, S. 2014. The mouse median nerve experimental model in regenerative research. *Biomed Res Int*, 2014, 701682.
- JANG, Y. C., LUSTGARTEN, M. S., LIU, Y., MULLER, F. L., BHATTACHARYA, A., LIANG, H., SALMON, A. B., BROOKS, S. V., LARKIN, L., HAYWORTH, C. R., RICHARDSON, A. & VAN REMMEN, H. 2010. Increased superoxide in vivo accelerates age-associated muscle atrophy through mitochondrial dysfunction and neuromuscular junction degeneration. *Faseb j*, 24, 1376-90.
- JANSSEN, I., HEYMSFIELD, S. B. & ROSS, R. 2002. Low relative skeletal muscle mass (sarcopenia) in older persons is associated with functional impairment and physical disability. *J Am Geriatr Soc*, 50, 889-96.
- JANSSON, E. & KAIJSER, L. 1977. Muscle adaptation to extreme endurance training in man. *Acta Physiol Scand*, 100, 315-24.
- JAYNES, J. B., JOHNSON, J. E., BUSKIN, J. N., GARTSIDE, C. L. & HAUSCHKA, S. D. 1988. The muscle creatine kinase gene is regulated by multiple upstream elements, including a muscle-specific enhancer. *Mol Cell Biol*, 8, 62-70.
- JENSEN, T. E., ROSE, A. J., JORGENSEN, S. B., BRANDT, N., SCHJERLING, P., WOJTASZEWSKI, J. F. & RICHTER, E. A. 2007. Possible CaMKK-dependent regulation of AMPK phosphorylation and glucose uptake at the onset of mild tetanic skeletal muscle contraction. *Am J Physiol Endocrinol Metab*, 292, E1308-17.
- JEONG, J. W., KWAK, I., LEE, K. Y., WHITE, L. D., WANG, X. P., BRUNICARDI, F. C., O'MALLEY, B. W. & DEMAYO, F. J. 2006. The genomic analysis of the impact of steroid receptor coactivators ablation on hepatic metabolism. *Mol Endocrinol*, 20, 1138-52.
- JOHNSON, E. K., LI, B., YOON, J. H., FLANIGAN, K. M., MARTIN, P. T., ERVASTI, J. & MONTANARO, F. 2013. Identification of new dystroglycan complexes in skeletal muscle. *PLoS One*, 8, e73224.
- JOHNSON, M. T., MAHMOOD, S. & PATEL, M. S. 2003. Intermediary metabolism and energetics during murine early embryogenesis. *J Biol Chem*, 278, 31457-60.
- JONES, E. J., BISHOP, P. A., WOODS, A. K. & GREEN, J. M. 2008. Cross-sectional area and muscular strength: a brief review. *Sports Med*, 38, 987-94.

- JOSTES, B., WALTHER, C. & GRUSS, P. 1990. The murine paired box gene, Pax7, is expressed specifically during the development of the nervous and muscular system. *Mech Dev*, 33, 27-37.
- JOULIA, D., BERNARDI, H., GARANDEL, V., RABENOELINA, F., VERNUS, B. & CABELLO, G. 2003. Mechanisms involved in the inhibition of myoblast proliferation and differentiation by myostatin. *Exp Cell Res*, 286, 263-75.
- JUNG, D., DUCLOS, F., APOSTOL, B., STRAUB, V., LEE, J. C., ALLAMAND, V., VENZKE, D. P., SUNADA, Y., MOOMAW, C. R., LEVEILLE, C. J., SLAUGHTER, C. A., CRAWFORD, T. O., MCPHERSON, J. D. & CAMPBELL, K. P. 1996a. Characterization of delta-sarcoglycan, a novel component of the oligomeric sarcoglycan complex involved in limb-girdle muscular dystrophy. *J Biol Chem*, 271, 32321-9.
- JUNG, D., LETURCQ, F., SUNADA, Y., DUCLOS, F., TOME, F. M., MOOMAW, C., MERLINI, L., AZIBI, K., CHAOUCH, M., SLAUGHTER, C., FARDEAU, M., KAPLAN, J. C. & CAMPBELL, K. P. 1996b. Absence of gamma-sarcoglycan (35 DAG) in autosomal recessive muscular dystrophy linked to chromosome 13q12. *FEBS Lett*, 381, 15-20.
- KAMBADUR, R., SHARMA, M., SMITH, T. P. & BASS, J. J. 1997. Mutations in myostatin (GDF8) in double-musled Belgian Blue and Piedmontese cattle. *Genome Res*, 7, 910-6.
- KAMMOUN, M., CASSAR-MALEK, I., MEUNIER, B. & PICARD, B. 2014. A simplified immunohistochemical classification of skeletal muscle fibres in mouse. *Eur J Histochem*, 58, 2254.
- KANG, J. S. & KRAUSS, R. S. 2010. Muscle stem cells in developmental and regenerative myogenesis. *Curr Opin Clin Nutr Metab Care*, 13, 243-8.
- KASSAR-DUCHOSSOY, L., GIACONE, E., GAYRAUD-MOREL, B., JORY, A., GOMES, D. & TAJBAKSHI, S. 2005. Pax3/Pax7 mark a novel population of primitive myogenic cells during development. *Genes Dev*, 19, 1426-31.
- KIDA, Y. S., KAWAMURA, T., WEI, Z., SOGO, T., JACINTO, S., SHIGENO, A., KUSHIGE, H., YOSHIHARA, E., LIDDLE, C., ECKER, J. R., YU, R. T., ATKINS, A. R., DOWNES, M. & EVANS, R. M. 2015. ERRs Mediate a Metabolic Switch Required for Somatic Cell Reprogramming to Pluripotency. *Cell Stem Cell*, 16, 547-55.
- KIENS, B. 2006. Skeletal muscle lipid metabolism in exercise and insulin resistance. *Physiol Rev*, 86, 205-43.
- KIM, D. K., JEONG, J. H., LEE, J. M., KIM, K. S., PARK, S. H., KIM, Y. D., KOH, M., SHIN, M., JUNG, Y. S., KIM, H. S., LEE, T. H., OH, B. C., KIM, J. I., PARK, H. T., JEONG, W. I., LEE, C. H., PARK, S. B., MIN, J. J., JUNG, S. I., CHOI, S. Y., CHOY, H. E. & CHOI, H. S. 2014. Inverse agonist of estrogen-related receptor gamma controls Salmonella typhimurium infection by modulating host iron homeostasis. *Nat Med*, 20, 419-24.
- KIM, D. K., KIM, J. R., KOH, M., KIM, Y. D., LEE, J. M., CHANDA, D., PARK, S. B., MIN, J. J., LEE, C. H., PARK, T. S. & CHOI, H. S. 2011. Estrogen-related receptor gamma (ERRgamma) is a novel transcriptional regulator of phosphatidic acid phosphatase, LIPIN1, and inhibits hepatic insulin signaling. *J Biol Chem*, 286, 38035-42.
- KIM, D. K., RYU, D., KOH, M., LEE, M. W., LIM, D., KIM, M. J., KIM, Y. H., CHO, W. J., LEE, C. H., PARK, S. B., KOO, S. H. & CHOI, H. S. 2012a. Orphan nuclear receptor estrogen-related receptor gamma (ERRgamma) is key regulator of hepatic gluconeogenesis. *J Biol Chem*, 287, 21628-39.
- KIM, W. K., CHOI, H. R., PARK, S. G., KO, Y., BAE, K. H. & LEE, S. C. 2012b. Myostatin inhibits brown adipocyte differentiation via regulation of Smad3-mediated beta-catenin stabilization. *Int J Biochem Cell Biol*, 44, 327-34.
- KIM, Y., KOH, M., KIM, D. K., CHOI, H. S. & PARK, S. B. 2009. Efficient discovery of selective small molecule agonists of estrogen-related receptor gamma using combinatorial approach. *J Comb Chem*, 11, 928-37.

- KINSEY, S. T., HARDY, K. M. & LOCKE, B. R. 2007. The long and winding road: influences of intracellular metabolite diffusion on cellular organization and metabolism in skeletal muscle. *J Exp Biol*, 210, 3505-12.
- KJAER, M. 2004. Role of extracellular matrix in adaptation of tendon and skeletal muscle to mechanical loading. *Physiol Rev*, 84, 649-98.
- KLIONSKY, D. J. 2010. The autophagy connection. *Dev Cell*, 19, 11-2.
- KOHEN, R., YAMAMOTO, Y., CUNDY, K. C. & AMES, B. N. 1988. Antioxidant activity of carnosine, homocarnosine, and anserine present in muscle and brain. *Proc Natl Acad Sci U S A*, 85, 3175-9.
- KOSKINEN, S. O., HEINEMEIER, K. M., OLESEN, J. L., LANGBERG, H. & KJAER, M. 2004. Physical exercise can influence local levels of matrix metalloproteinases and their inhibitors in tendon-related connective tissue. *J Appl Physiol (1985)*, 96, 861-4.
- KOVANEN, V., SUOMINEN, H. & HEIKKINEN, E. 1980. Connective tissue of "fast" and "slow" skeletal muscle in rats--effects of endurance training. *Acta Physiol Scand*, 108, 173-80.
- KOVANEN, V., SUOMINEN, H. & HEIKKINEN, E. 1984a. Collagen of slow twitch and fast twitch muscle fibres in different types of rat skeletal muscle. *Eur J Appl Physiol Occup Physiol*, 52, 235-42.
- KOVANEN, V., SUOMINEN, H. & HEIKKINEN, E. 1984b. Mechanical properties of fast and slow skeletal muscle with special reference to collagen and endurance training. *J Biomech*, 17, 725-35.
- KRIVICKAS, L. S., DORER, D. J., OCHALA, J. & FRONTERA, W. R. 2011. Relationship between force and size in human single muscle fibres. *Exp Physiol*, 96, 539-47.
- KRIVICKAS, L. S., WALSH, R. & AMATO, A. A. 2009. Single muscle fiber contractile properties in adults with muscular dystrophy treated with MYO-029. *Muscle Nerve*, 39, 3-9.
- KUANG, S., GILLESPIE, M. A. & RUDNICKI, M. A. 2008. Niche regulation of muscle satellite cell self-renewal and differentiation. *Cell Stem Cell*, 2, 22-31.
- KUANG, S., KURODA, K., LE GRAND, F. & RUDNICKI, M. A. 2007. Asymmetric self-renewal and commitment of satellite stem cells in muscle. *Cell*, 129, 999-1010.
- KUBO, M., IJICHI, N., IKEDA, K., HORIE-INOUE, K., TAKEDA, S. & INOUE, S. 2009. Modulation of adipogenesis-related gene expression by estrogen-related receptor gamma during adipocytic differentiation. *Biochim Biophys Acta*, 1789, 71-7.
- KUHL, U., OCALAN, M., TIMPL, R., MAYNE, R., HAY, E. & VON DER MARK, K. 1984. Role of muscle fibroblasts in the deposition of type-IV collagen in the basal lamina of myotubes. *Differentiation*, 28, 164-72.
- KUHL, U., TIMPL, R. & VON DER MARK, K. 1982. Synthesis of type IV collagen and laminin in cultures of skeletal muscle cells and their assembly on the surface of myotubes. *Dev Biol*, 93, 344-54.
- KUJALA, U. M., KAPRIO, J., SARNA, S. & KOSKENVUO, M. 1998. Relationship of leisure-time physical activity and mortality: the Finnish twin cohort. *Jama*, 279, 440-4.
- KUMAR, P. & MENDELSON, C. R. 2011. Estrogen-related receptor gamma (ERRgamma) mediates oxygen-dependent induction of aromatase (CYP19) gene expression during human trophoblast differentiation. *Mol Endocrinol*, 25, 1513-26.
- KUNKEL, L. M., BEGGS, A. H. & HOFFMAN, E. P. 1989. Molecular genetics of Duchenne and Becker muscular dystrophy: emphasis on improved diagnosis. *Clin Chem*, 35, B21-4.
- KWONG, W. H. & VRBOVA, G. 1981. Effects of low-frequency electrical stimulation on fast and slow muscles of the rat. *Pflugers Arch*, 391, 200-7.
- LACH-TRIFILIEFF, E., MINETTI, G. C., SHEPPARD, K., IBEBUNJO, C., FEIGE, J. N., HARTMANN, S., BRACHAT, S., RIVET, H., KOELBING, C., MORVAN, F., HATAKEYAMA, S. & GLASS, D. J. 2014. An antibody blocking activin type II receptors induces strong skeletal muscle hypertrophy and protects from atrophy. *Mol Cell Biol*, 34, 606-18.
- LAGOUGE, M., ARGMANN, C., GERHART-HINES, Z., MEZIANE, H., LERIN, C., DAUSSIN, F., MESSADEQ, N., MILNE, J., LAMBERT, P., ELLIOTT, P., GENY, B., LAAKSO, M., PUIGSERVER, P. & AUWERX, J.

2006. Resveratrol improves mitochondrial function and protects against metabolic disease by activating SIRT1 and PGC-1 α . *Cell*, 127, 1109-22.
- LANG, I. A., GALLOWAY, T. S., SCARLETT, A., HENLEY, W. E., DEPLEDGE, M., WALLACE, R. B. & MELZER, D. 2008. Association of urinary bisphenol A concentration with medical disorders and laboratory abnormalities in adults. *Jama*, 300, 1303-10.
- LANGEN, R. C., SCHOLS, A. M., KELDERS, M. C., VAN DER VELDEN, J. L., WOUTERS, E. F. & JANSSEN-HEININGER, Y. M. 2002. Tumor necrosis factor- α inhibits myogenesis through redox-dependent and -independent pathways. *Am J Physiol Cell Physiol*, 283, C714-21.
- LANGLEY, B., THOMAS, M., BISHOP, A., SHARMA, M., GILMOUR, S. & KAMBADUR, R. 2002. Myostatin inhibits myoblast differentiation by down-regulating MyoD expression. *J Biol Chem*, 277, 49831-40.
- LANGONE, F., CANNATA, S., FUOCO, C., LETTIERI BARBATO, D., TESTA, S., NARDOZZA, A. P., CIRIOLO, M. R., CASTAGNOLI, L., GARGIOLI, C. & CESARENI, G. 2014. Metformin protects skeletal muscle from cardiotoxin induced degeneration. *PLoS One*, 9, e114018.
- LARSSON, L. 1978. Morphological and functional characteristics of the ageing skeletal muscle in man. A cross-sectional study. *Acta Physiol Scand Suppl*, 457, 1-36.
- LEBRASSEUR, N. K. 2012. Building muscle, browning fat and preventing obesity by inhibiting myostatin. *Diabetologia*, 55, 13-7.
- LEE, E. J., JAN, A. T., BAIG, M. H., ASHRAF, J. M., NAHM, S. S., KIM, Y. W., PARK, S. Y. & CHOI, I. 2016. Fibromodulin: a master regulator of myostatin controlling progression of satellite cells through a myogenic program. *Faseb j*, 30, 2708-19.
- LEE, J. H., KIM, E. J., KIM, D. K., LEE, J. M., PARK, S. B., LEE, I. K., HARRIS, R. A., LEE, M. O. & CHOI, H. S. 2012a. Hypoxia induces PDK4 gene expression through induction of the orphan nuclear receptor ERR γ . *PLoS One*, 7, e46324.
- LEE, K. Y., SINGH, M. K., USSAR, S., WETZEL, P., HIRSHMAN, M. F., GOODYEAR, L. J., KISPERS, A. & KAHN, C. R. 2015. Tbx15 controls skeletal muscle fibre-type determination and muscle metabolism. *Nat Commun*, 6, 8054.
- LEE, S.-J., HUYNH, T. V., LEE, Y.-S., SEBALD, S. M., WILCOX-ADELMAN, S. A., IWAMORI, N., LEPPER, C., MATZUK, M. M. & FAN, C.-M. 2012b. Role of satellite cells versus myofibers in muscle hypertrophy induced by inhibition of the myostatin/activin signaling pathway. *Proc Natl Acad Sci U S A*, 109, E2353-60.
- LEE, S. J. 2004. Regulation of muscle mass by myostatin. *Annu Rev Cell Dev Biol*, 20, 61-86.
- LEE, S. J. & MCPHERRON, A. C. 2001. Regulation of myostatin activity and muscle growth. *Proc Natl Acad Sci U S A*, 98, 9306-11.
- LEE, S. J., REED, L. A., DAVIES, M. V., GIRGENRATH, S., GOAD, M. E., TOMKINSON, K. N., WRIGHT, J. F., BARKER, C., EHRMANTRAUT, G., HOLMSTROM, J., TROWELL, B., GERTZ, B., JIANG, M. S., SEBALD, S. M., MATZUK, M., LI, E., LIANG, L. F., QUATTLEBAUM, E., STOTISH, R. L. & WOLFMAN, N. M. 2005. Regulation of muscle growth by multiple ligands signaling through activin type II receptors. *Proc Natl Acad Sci U S A*, 102, 18117-22.
- LEE, S. N., PRODHOMME, E. & LINDBERG, I. 2004. Prohormone convertase 1 (PC1) processing and sorting: effect of PC1 propeptide and proSAAS. *J Endocrinol*, 182, 353-64.
- LEVETT, D. Z., RADFORD, E. J., MENASSA, D. A., GRABER, E. F., MORASH, A. J., HOPPELER, H., CLARKE, K., MARTIN, D. S., FERGUSON-SMITH, A. C., MONTGOMERY, H. E., GROCOTT, M. P. & MURRAY, A. J. 2012. Acclimatization of skeletal muscle mitochondria to high-altitude hypoxia during an ascent of Everest. *Faseb j*, 26, 1431-41.
- LI, H. H., WILLIS, M. S., LOCKYER, P., MILLER, N., MCDONOUGH, H., GLASS, D. J. & PATTERSON, C. 2007a. Atrogin-1 inhibits Akt-dependent cardiac hypertrophy in mice via ubiquitin-dependent coactivation of Forkhead proteins. *J Clin Invest*, 117, 3211-23.

- LI, N., RAGHEB, K., LAWLER, G., STURGIS, J., RAJWA, B., MELENDEZ, J. A. & ROBINSON, J. P. 2003a. Mitochondrial complex I inhibitor rotenone induces apoptosis through enhancing mitochondrial reactive oxygen species production. *J Biol Chem*, 278, 8516-25.
- LI, Y., FOSTER, W., DEASY, B. M., CHAN, Y., PRISK, V., TANG, Y., CUMMINS, J. & HUARD, J. 2004. Transforming growth factor-beta1 induces the differentiation of myogenic cells into fibrotic cells in injured skeletal muscle: a key event in muscle fibrogenesis. *Am J Pathol*, 164, 1007-19.
- LI, Y., LI, J., ZHU, J., SUN, B., BRANCA, M., TANG, Y., FOSTER, W., XIAO, X. & HUARD, J. 2007b. Decorin gene transfer promotes muscle cell differentiation and muscle regeneration. *Mol Ther*, 15, 1616-22.
- LI, Y. P., CHEN, Y., LI, A. S. & REID, M. B. 2003b. Hydrogen peroxide stimulates ubiquitin-conjugating activity and expression of genes for specific E2 and E3 proteins in skeletal muscle myotubes. *Am J Physiol Cell Physiol*, 285, C806-12.
- LI, Z. B., KOLLIAS, H. D. & WAGNER, K. R. 2008. Myostatin directly regulates skeletal muscle fibrosis. *J Biol Chem*, 283, 19371-8.
- LIN, J., WU, H., TARR, P. T., ZHANG, C. Y., WU, Z., BOSS, O., MICHAEL, L. F., PUIGSERVER, P., ISOTANI, E., OLSON, E. N., LOWELL, B. B., BASSEL-DUBY, R. & SPIEGELMAN, B. M. 2002. Transcriptional co-activator PGC-1 alpha drives the formation of slow-twitch muscle fibres. *Nature*, 418, 797-801.
- LIPINA, C., KENDALL, H., MCPHERRON, A. C., TAYLOR, P. M. & HUNDAL, H. S. 2010. Mechanisms involved in the enhancement of mammalian target of rapamycin signalling and hypertrophy in skeletal muscle of myostatin-deficient mice. *FEBS Lett*, 584, 2403-8.
- LIPTON, B. H. 1977. Collagen synthesis by normal and bromodeoxyuridine-modulated cells in myogenic culture. *Dev Biol*, 61, 153-65.
- LIU, J. X., HOGLUND, A. S., KARLSSON, P., LINDBLAD, J., QAISAR, R., AARE, S., BENGTSSON, E. & LARSSON, L. 2009. Myonuclear domain size and myosin isoform expression in muscle fibres from mammals representing a 100,000-fold difference in body size. *Exp Physiol*, 94, 117-29.
- LIU, L. A. & ENGVALL, E. 1999. Sarcoglycan isoforms in skeletal muscle. *J Biol Chem*, 274, 38171-6.
- LONARD, D. M. & O'MALLEY B, W. 2007. Nuclear receptor coregulators: judges, juries, and executioners of cellular regulation. *Mol Cell*, 27, 691-700.
- LOUET, J. F., COSTE, A., AMAZIT, L., TANNOUR-LOUET, M., WU, R. C., TSAI, S. Y., TSAI, M. J., AUWERX, J. & O'MALLEY, B. W. 2006. Oncogenic steroid receptor coactivator-3 is a key regulator of the white adipogenic program. *Proc Natl Acad Sci U S A*, 103, 17868-73.
- LOUIE, G. H. & WARD, M. M. 2010. Sex disparities in self-reported physical functioning: true differences, reporting bias, or incomplete adjustment for confounding? *J Am Geriatr Soc*, 58, 1117-22.
- LOWRIE, M. B., KRISHNAN, S. & VRBOVA, G. 1982. Recovery of slow and fast muscles following nerve injury during early post-natal development in the rat. *J Physiol*, 331, 51-66.
- LUND, N., DAMON, D. H., DAMON, D. N. & DULING, B. R. 1987. Capillary grouping in hamster tibialis anterior muscles: flow patterns, and physiological significance. *Int J Microcirc Clin Exp*, 5, 359-72.
- LUO, Y., KUMAR, P. & MENDELSON, C. R. 2013. Estrogen-related receptor gamma (ERRgamma) regulates oxygen-dependent expression of voltage-gated potassium (K+) channels and tissue kallikrein during human trophoblast differentiation. *Mol Endocrinol*, 27, 940-52.
- MACKEY, A. L., DONNELLY, A. E., TURPEENIEMI-HUJANEN, T. & ROPER, H. P. 2004. Skeletal muscle collagen content in humans after high-force eccentric contractions. *J Appl Physiol (1985)*, 97, 197-203.
- MAGEE, T. R., ARTAZA, J. N., FERRINI, M. G., VERNET, D., ZUNIGA, F. I., CANTINI, L., REISZ-PORSZASZ, S., RAJFER, J. & GONZALEZ-CADAVID, N. F. 2006. Myostatin short interfering hairpin RNA gene transfer increases skeletal muscle mass. *J Gene Med*, 8, 1171-81.

- MAGGS, A. M., TAYLOR-HARRIS, P., PECKHAM, M. & HUGHES, S. M. 2000. Evidence for differential post-translational modifications of slow myosin heavy chain during murine skeletal muscle development. *J Muscle Res Cell Motil*, 21, 101-13.
- MAIER, A., LEBERER, E. & PETTE, D. 1988. Distribution of sarcoplasmic reticulum Ca-ATPase and of calsequestrin at the polar regions of rat, rabbit and cat intrafusal fibers. *Histochemistry*, 88, 273-6.
- MANCEAU, M., GROS, J., SAVAGE, K., THOME, V., MCPHERRON, A., PATERSON, B. & MARCELLE, C. 2008. Myostatin promotes the terminal differentiation of embryonic muscle progenitors. *Genes Dev*, 22, 668-81.
- MANCEAU, M., MARCELLE, C. & GROS, J. 2005. [A common somitic origin for embryonic muscle progenitors]. *Med Sci (Paris)*, 21, 915-7.
- MANGELSDORF, D. J., THUMMEL, C., BEATO, M., HERRLICH, P., SCHUTZ, G., UMESONO, K., BLUMBERG, B., KASTNER, P., MARK, M., CHAMBON, P. & EVANS, R. M. 1995. The nuclear receptor superfamily: the second decade. *Cell*, 83, 835-9.
- MANN, C. J., PERDIGUERO, E., KHARRAZ, Y., AGUILAR, S., PESSINA, P., SERRANO, A. L. & MUNOZ-CANOVES, P. 2011. Aberrant repair and fibrosis development in skeletal muscle. *Skelet Muscle*, 1, 21.
- MANNING, B. D. & CANTLEY, L. C. 2007. AKT/PKB signaling: navigating downstream. *Cell*, 129, 1261-74.
- MANTOVANI, A., SICA, A., SOZZANI, S., ALLAVENA, P., VECCHI, A. & LOCATI, M. 2004. The chemokine system in diverse forms of macrophage activation and polarization. *Trends Immunol*, 25, 677-86.
- MARCHITELLI, C., SAVARESE, M. C., CRISA, A., NARDONE, A., MARSAN, P. A. & VALENTINI, A. 2003. Double muscling in Marchigiana beef breed is caused by a stop codon in the third exon of myostatin gene. *Mamm Genome*, 14, 392-5.
- MARIEB, E. N., HOEHN, K. 2008. Human Anatomy and Physiology. Benjamin Cummings Pub Co.
- MARTINI, H. F., OBER, C. W., GARRISON, W. C., WELCH, K. AND HUTCHINGS, T. R. 2006. *Fundamentals of Anatomy and Physiology - Muscle Tissue. 7th edition. 284 - 325 Benjamin Cummings: USA.*
- MARTYN, J. K., BASS, J. J. & OLDHAM, J. M. 2004. Skeletal muscle development in normal and double-muscling cattle. *Anat Rec A Discov Mol Cell Evol Biol*, 281, 1363-71.
- MASUDA, K., KANO, Y. & KATSUTA, S. 1997. Adaptation of myoglobin in compensatory hypertrophied rat muscle. *Acta Physiol Scand*, 160, 327-31.
- MATHEW, S. J., HANSEN, J. M., MERRELL, A. J., MURPHY, M. M., LAWSON, J. A., HUTCHESON, D. A., HANSEN, M. S., ANGUS-HILL, M. & KARDON, G. 2011. Connective tissue fibroblasts and Tcf4 regulate myogenesis. *Development*, 138, 371-84.
- MATSAKAS, A., FOSTER, K., OTTO, A., MACHARIA, R., ELASHRY, M. I., FEIST, S., GRAHAM, I., FOSTER, H., YAWORSKY, P., WALSH, F., DICKSON, G. & PATEL, K. 2009. Molecular, cellular and physiological investigation of myostatin propeptide-mediated muscle growth in adult mice. *Neuromuscul Disord*, 19, 489-99.
- MATSAKAS, A., MACHARIA, R., OTTO, A., ELASHRY, M. I., MOUISEL, E., ROMANELLO, V., SARTORI, R., AMTHOR, H., SANDRI, M., NARKAR, V. & PATEL, K. 2012a. Exercise training attenuates the hypermuscular phenotype and restores skeletal muscle function in the myostatin null mouse. *Exp Physiol*, 97, 125-40.
- MATSAKAS, A., OTTO, A., ELASHRY, M. I., BROWN, S. C. & PATEL, K. 2010. Altered primary and secondary myogenesis in the myostatin-null mouse. *Rejuvenation Res*, 13, 717-27.
- MATSAKAS, A. & PATEL, K. 2009a. Intracellular signalling pathways regulating the adaptation of skeletal muscle to exercise and nutritional changes. *Histol Histopathol*, 24, 209-22.
- MATSAKAS, A. & PATEL, K. 2009b. Skeletal muscle fibre plasticity in response to selected environmental and physiological stimuli. *Histol Histopathol*, 24, 611-29.

- MATSAKAS, A., YADAV, V., LORCA, S., EVANS, R. M. & NARKAR, V. A. 2012b. Revascularization of ischemic skeletal muscle by estrogen-related receptor- γ . *Circ Res*, 110, 1087-96.
- MATSAKAS, A., YADAV, V., LORCA, S. & NARKAR, V. 2013. Muscle ERRgamma mitigates Duchenne muscular dystrophy via metabolic and angiogenic reprogramming. *FASEB J*, 27, 4004-16.
- MATSUDA, R., NISHIKAWA, A. & TANAKA, H. 1995. Visualization of dystrophic muscle fibers in mdx mouse by vital staining with Evans blue: evidence of apoptosis in dystrophin-deficient muscle. *J Biochem*, 118, 959-64.
- MATSUMURA, K., TOME, F. M., IONASESCU, V., ERVASTI, J. M., ANDERSON, R. D., ROMERO, N. B., SIMON, D., RECAN, D., KAPLAN, J. C., FARDEAU, M. & ET AL. 1993. Deficiency of dystrophin-associated proteins in Duchenne muscular dystrophy patients lacking COOH-terminal domains of dystrophin. *J Clin Invest*, 92, 866-71.
- MAURO, A. 1961. Satellite cell of skeletal muscle fibers. *J Biophys Biochem Cytol*, 9, 493-5.
- MCCARTHY, J. J., MULA, J., MIYAZAKI, M., ERFANI, R., GARRISON, K., FAROOQUI, A. B., SRIKUEA, R., LAWSON, B. A., GRIMES, B., KELLER, C., VAN ZANT, G., CAMPBELL, K. S., ESSER, K. A., DUPONT-VERSTEEGDEN, E. E. & PETERSON, C. A. 2011. Effective fiber hypertrophy in satellite cell-depleted skeletal muscle. *Development*, 138, 3657-66.
- MCCARTY, D. M. 2008. Self-complementary AAV vectors; advances and applications. *Mol Ther*, 16, 1648-56.
- MCCOMAS, A. J. 1991. Invited review: motor unit estimation: methods, results, and present status. *Muscle Nerve*, 14, 585-97.
- MCCROSKERY, S., THOMAS, M., MAXWELL, L., SHARMA, M. & KAMBADUR, R. 2003. Myostatin negatively regulates satellite cell activation and self-renewal. *J Cell Biol*, 162, 1135-47.
- MCLENNAN, I. S. 1996. Degenerating and regenerating skeletal muscles contain several subpopulations of macrophages with distinct spatial and temporal distributions. *J Anat*, 188 (Pt 1), 17-28.
- MCPHERRON, A. C. 2010. METABOLIC FUNCTIONS OF MYOSTATIN AND GDF11. *Immunol Endocr Metab Agents Med Chem*, 10, 217-231.
- MCPHERRON, A. C., HUYNH, T. V. & LEE, S. J. 2009. Redundancy of myostatin and growth/differentiation factor 11 function. *BMC Dev Biol*, 9, 24.
- MCPHERRON, A. C., LAWLER, A. M. & LEE, S. J. 1997. Regulation of skeletal muscle mass in mice by a new TGF-beta superfamily member. *Nature*, 387, 83-90.
- MCPHERRON, A. C. & LEE, S. J. 1997. Double muscling in cattle due to mutations in the myostatin gene. *Proc Natl Acad Sci U S A*, 94, 12457-61.
- MEGENEY, L. A., KABLAR, B., GARRETT, K., ANDERSON, J. E. & RUDNICKI, M. A. 1996. MyoD is required for myogenic stem cell function in adult skeletal muscle. *Genes Dev*, 10, 1173-83.
- MEINKE, P., MATTIOLI, E., HAQUE, F., ANTOKU, S., COLUMBARO, M., STRAATMAN, K. R., WORMAN, H. J., GUNDERSEN, G. G., LATTANZI, G., WEHNERT, M. & SHACKLETON, S. 2014. Muscular dystrophy-associated SUN1 and SUN2 variants disrupt nuclear-cytoskeletal connections and myonuclear organization. *PLoS Genet*, 10, e1004605.
- MELEY, D., BAUVY, C., HOUBEN-WEERTS, J. H., DUBBELHUIS, P. F., HELMOND, M. T., CODOGNO, P. & MEIJER, A. J. 2006. AMP-activated protein kinase and the regulation of autophagic proteolysis. *J Biol Chem*, 281, 34870-9.
- MELLOUL, D., ALONI, B., CALVO, J., YAFFE, D. & NUDEL, U. 1984. Developmentally regulated expression of chimeric genes containing muscle actin DNA sequences in transfected myogenic cells. *EMBO J*, 3, 983-90.
- MENDIAS, C. L., MARCIN, J. E., CALERDON, D. R. & FAULKNER, J. A. 2006. Contractile properties of EDL and soleus muscles of myostatin-deficient mice. *J Appl Physiol (1985)*, 101, 898-905.
- MENG, Z. X., WANG, L., XIAO, Y. & LIN, J. D. 2014. The Baf60c/Deptor pathway links skeletal muscle inflammation to glucose homeostasis in obesity. *Diabetes*, 63, 1533-45.
- MESHER, A. 2010. *Basic Histology*, New York, McGraw Hill.

- METZGER, T., GACHE, V., XU, M., CADOT, B., FOLKER, E. S., RICHARDSON, B. E., GOMES, E. R. & BAYLIES, M. K. 2012. MAP and kinesin-dependent nuclear positioning is required for skeletal muscle function. *Nature*, 484, 120-4.
- MEYER, C., DOSTOU, J. M., WELLE, S. L. & GERICH, J. E. 2002. Role of human liver, kidney, and skeletal muscle in postprandial glucose homeostasis. *Am J Physiol Endocrinol Metab*, 282, E419-27.
- MEYER, G. A. & LIEBER, R. L. 2011. Elucidation of extracellular matrix mechanics from muscle fibers and fiber bundles. *J Biomech*, 44, 771-3.
- MILLER, D. G., PETEK, L. M. & RUSSELL, D. W. 2004. Adeno-associated virus vectors integrate at chromosome breakage sites. *Nat Genet*, 36, 767-73.
- MISRA, J., KIM, D. K. & CHOI, H. S. 2017. ERRgamma: a Junior Orphan with a Senior Role in Metabolism. *Trends Endocrinol Metab*, 28, 261-272.
- MISRA, J., KIM, D. K., JUNG, Y. S., KIM, H. B., KIM, Y. H., YOO, E. K., KIM, B. G., KIM, S., LEE, I. K., HARRIS, R. A., KIM, J. S., LEE, C. H., CHO, J. W. & CHOI, H. S. 2016. O-GlcNAcylation of Orphan Nuclear Receptor Estrogen-Related Receptor gamma Promotes Hepatic Gluconeogenesis. *Diabetes*, 65, 2835-48.
- MIWA, T. & KEDES, L. 1987. Duplicated CARG box domains have positive and mutually dependent regulatory roles in expression of the human alpha-cardiac actin gene. *Mol Cell Biol*, 7, 2803-13.
- MIYAKE, M., HAYASHI, S., SATO, T., TAKETA, Y., WATANABE, K., HAYASHI, S., TANAKA, S., OHWADA, S., ASO, H. & YAMAGUCHI, T. 2007. Myostatin and MyoD family expression in skeletal muscle of IGF-1 knockout mice. *Cell Biol Int*, 31, 1274-9.
- MIZUSHIMA, N., YOSHIMORI, T. & LEVINE, B. 2010. Methods in mammalian autophagy research. *Cell*, 140, 313-26.
- MORIMOTO, R. I. & CUERVO, A. M. 2014. Proteostasis and the aging proteome in health and disease. *J Gerontol A Biol Sci Med Sci*, 69 Suppl 1, S33-8.
- MORINE, K. J., BISH, L. T., SELSBY, J. T., GAZZARA, J. A., PENDRAK, K., SLEEPER, M. M., BARTON, E. R., LEE, S.-J. & SWEENEY, H. L. 2010. Activin IIB receptor blockade attenuates dystrophic pathology in a mouse model of Duchenne muscular dystrophy. *Muscle Nerve*, 42, 722-30.
- MORISSETTE, M. R., COOK, S. A., BURANASOMBATI, C., ROSENBERG, M. A. & ROSENZWEIG, A. 2009. Myostatin inhibits IGF-I-induced myotube hypertrophy through Akt. *Am J Physiol Cell Physiol*, 297, C1124-32.
- MORTENSEN, S. P. & SALTIN, B. 2014. Regulation of the skeletal muscle blood flow in humans. *Exp Physiol*, 99, 1552-8.
- MOSHER, D. S., QUIGNON, P., BUSTAMANTE, C. D., SUTTER, N. B., MELLERSH, C. S., PARKER, H. G. & OSTRANDER, E. A. 2007. A mutation in the myostatin gene increases muscle mass and enhances racing performance in heterozygote dogs. *PLoS Genet*, 3, e79.
- MOSS, F. P. & LEBLOND, C. P. 1971. Satellite cells as the source of nuclei in muscles of growing rats. *Anat Rec*, 170, 421-35.
- MOUNIER, R., THERET, M., ARNOLD, L., CUVELLIER, S., BULTOT, L., GORANSSON, O., SANZ, N., FERRY, A., SAKAMOTO, K., FORETZ, M., VIOLLET, B. & CHAZAUD, B. 2013. AMPKalpha1 regulates macrophage skewing at the time of resolution of inflammation during skeletal muscle regeneration. *Cell Metab*, 18, 251-64.
- MOUNIER, R., THERET, M., LANTIER, L., FORETZ, M. & VIOLLET, B. 2015. Expanding roles for AMPK in skeletal muscle plasticity. *Trends Endocrinol Metab*, 26, 275-86.
- MOZDZIAK, P. E., PULVERMACHER, P. M. & SCHULTZ, E. 2001. Muscle regeneration during hindlimb unloading results in a reduction in muscle size after reloading. *J Appl Physiol (1985)*, 91, 183-90.

- MUNSTERBERG, A. E., KITAJEWSKI, J., BUMCROT, D. A., MCMAHON, A. P. & LASSAR, A. B. 1995. Combinatorial signaling by Sonic hedgehog and Wnt family members induces myogenic bHLH gene expression in the somite. *Genes Dev*, 9, 2911-22.
- MURPHY, M. M., LAWSON, J. A., MATHEW, S. J., HUTCHESON, D. A. & KARDON, G. 2011. Satellite cells, connective tissue fibroblasts and their interactions are crucial for muscle regeneration. *Development*, 138, 3625-37.
- MURRAY, J., AUWERX, J. & HUSS, J. M. 2013. Impaired myogenesis in estrogen-related receptor gamma (ERRgamma)-deficient skeletal myocytes due to oxidative stress. *FASEB J*, 27, 135-50.
- MURRAY, J. & HUSS, J. M. 2011. Estrogen-related receptor α regulates skeletal myocyte differentiation via modulation of the ERK MAP kinase pathway. *Am J Physiol Cell Physiol*, 301, C630-45.
- MUSARO, A. 2014. The Basis of Muscle Regeneration *Hindawi*, 2014
- MUSCAT, G. E. & KEDES, L. 1987. Multiple 5'-flanking regions of the human alpha-skeletal actin gene synergistically modulate muscle-specific expression. *Mol Cell Biol*, 7, 4089-99.
- NADER, G. A. 2005. Molecular determinants of skeletal muscle mass: getting the "AKT" together. *Int J Biochem Cell Biol*, 37, 1985-96.
- NAGAO, M., PARIMOO, B. & TANAKA, K. 1993. Developmental, nutritional, and hormonal regulation of tissue-specific expression of the genes encoding various acyl-CoA dehydrogenases and alpha-subunit of electron transfer flavoprotein in rat. *J Biol Chem*, 268, 24114-24.
- NAKATANI, M., TAKEHARA, Y., SUGINO, H., MATSUMOTO, M., HASHIMOTO, O., HASEGAWA, Y., MURAKAMI, T., UEZUMI, A., TAKEDA, S., NOJI, S., SUNADA, Y. & TSUCHIDA, K. 2008. Transgenic expression of a myostatin inhibitor derived from follistatin increases skeletal muscle mass and ameliorates dystrophic pathology in mdx mice. *FASEB J*, 22, 477-87.
- NARKAR, V. A., DOWNES, M., YU, R. T., EMBLER, E., WANG, Y. X., BANAYO, E., MIHAYLOVA, M. M., NELSON, M. C., ZOU, Y., JUGUILON, H., KANG, H., SHAW, R. J. & EVANS, R. M. 2008. AMPK and PPARdelta agonists are exercise mimetics. *Cell*, 134, 405-15.
- NARKAR, V. A., FAN, W., DOWNES, M., YU, R. T., JONKER, J. W., ALAYNICK, W. A., BANAYO, E., KARUNASIRI, M. S., LORCA, S. & EVANS, R. M. 2011. Exercise and PGC1 α -independent Synchronization of Type I Muscle Metabolism and Vasculature by ERR γ . *Cell Metab*, 13, 283-93.
- NAVARRO, A., GOMEZ, C., SANCHEZ-PINO, M. J., GONZALEZ, H., BANDEZ, M. J., BOVERIS, A. D. & BOVERIS, A. 2005. Vitamin E at high doses improves survival, neurological performance, and brain mitochondrial function in aging male mice. *Am J Physiol Regul Integr Comp Physiol*, 289, R1392-9.
- NETHERY, D., CALLAHAN, L. A., STOFAN, D., MATTERA, R., DIMARCO, A. & SUPINSKI, G. 2000. PLA(2) dependence of diaphragm mitochondrial formation of reactive oxygen species. *J Appl Physiol* (1985), 89, 72-80.
- NGUYEN, M. H., CHENG, M. & KOH, T. J. 2011. Impaired muscle regeneration in ob/ob and db/db mice. *ScientificWorldJournal*, 11, 1525-35.
- NIR, U., WALKER, M. D. & RUTTER, W. J. 1986. Regulation of rat insulin 1 gene expression: evidence for negative regulation in nonpancreatic cells. *Proc Natl Acad Sci U S A*, 83, 3180-4.
- NISOLI, E., FALCONE, S., TONELLO, C., COZZI, V., PALOMBA, L., FIORANI, M., PISCONTI, A., BRUNELLI, S., CARDILE, A., FRANCOLINI, M., CANTONI, O., CARRUBA, M. O., MONCADA, S. & CLEMENTI, E. 2004. Mitochondrial biogenesis by NO yields functionally active mitochondria in mammals. *Proc Natl Acad Sci U S A*, 101, 16507-12.
- NOVAK, M. L., BRYER, S. C., CHENG, M., NGUYEN, M. H., CONLEY, K. L., CUNNINGHAM, A. K., XUE, B., SISSON, T. H., YOU, J. S., HORNBERGER, T. A. & KOH, T. J. 2011. Macrophage-specific expression of urokinase-type plasminogen activator promotes skeletal muscle regeneration. *J Immunol*, 187, 1448-57.

- OHIRA, Y., YOSHINAGA, T., OHARA, M., KAWANO, F., WANG, X. D., HIGO, Y., TERADA, M., MATSUOKA, Y., ROY, R. R. & EDGERTON, V. R. 2006. The role of neural and mechanical influences in maintaining normal fast and slow muscle properties. *Cells Tissues Organs*, 182, 129-42.
- OHLENDIECK, K., ERVASTI, J. M., SNOOK, J. B. & CAMPBELL, K. P. 1991. Dystrophin-glycoprotein complex is highly enriched in isolated skeletal muscle sarcolemma. *J Cell Biol*, 112, 135-48.
- OLGUIN, H. C. & OLWIN, B. B. 2004. Pax-7 up-regulation inhibits myogenesis and cell cycle progression in satellite cells: a potential mechanism for self-renewal. *Dev Biol*, 275, 375-88.
- OLGUIN, H. C., YANG, Z., TAPSCOTT, S. J. & OLWIN, B. B. 2007. Reciprocal inhibition between Pax7 and muscle regulatory factors modulates myogenic cell fate determination. *J Cell Biol*, 177, 769-79.
- OLSON, E. N. & WILLIAMS, R. S. 2000. Calcineurin signaling and muscle remodeling. *Cell*, 101, 689-92.
- ONO, T., ISOBE, K., NAKADA, K. & HAYASHI, J. I. 2001. Human cells are protected from mitochondrial dysfunction by complementation of DNA products in fused mitochondria. *Nat Genet*, 28, 272-5.
- ORDHAL, C. P. 2000. Somatogenesis. Current topics of Developmental Biology.
- OTTO, A., SCHMIDT, C., LUKE, G., ALLEN, S., VALASEK, P., MUNTONI, F., LAWRENCE-WATT, D. & PATEL, K. 2008. Canonical Wnt signalling induces satellite-cell proliferation during adult skeletal muscle regeneration. *J Cell Sci*, 121, 2939-50.
- OUSTANINA, S., HAUSE, G. & BRAUN, T. 2004. Pax7 directs postnatal renewal and propagation of myogenic satellite cells but not their specification. *Embo j*, 23, 3430-9.
- PAPAGEORGOPOULOS, C., CALDWELL, K., SCHWEINGRUBBER, H., NEESE, R. A., SHACKLETON, C. H. & HELLERSTEIN, M. 2002. Measuring synthesis rates of muscle creatine kinase and myosin with stable isotopes and mass spectrometry. *Anal Biochem*, 309, 1-10.
- PARTRIDGE, C. R., HAWKER, J. R., JR. & FROUGH, R. 2000. Overexpression of a secretory form of FGF-1 promotes MMP-1-mediated endothelial cell migration. *J Cell Biochem*, 78, 487-99.
- PASSERIEUX, E., ROSSIGNOL, R., LETELLIER, T. & DELAGE, J. P. 2007. Physical continuity of the perimysium from myofibers to tendons: involvement in lateral force transmission in skeletal muscle. *J Struct Biol*, 159, 19-28.
- PATEL, K. & AMTHOR, H. 2005. The function of Myostatin and strategies of Myostatin blockade-new hope for therapies aimed at promoting growth of skeletal muscle. *Neuromuscul Disord*, 15, 117-26.
- PATTERSON, M. F., STEPHENSON, G. M. & STEPHENSON, D. G. 2006. Denervation produces different single fiber phenotypes in fast- and slow-twitch hindlimb muscles of the rat. *Am J Physiol Cell Physiol*, 291, C518-28.
- PELOSI, L., GIACINTI, C., NARDIS, C., BORSELLINO, G., RIZZUTO, E., NICOLETTI, C., WANNENES, F., BATTISTINI, L., ROSENTHAL, N., MOLINARO, M. & MUSARO, A. 2007. Local expression of IGF-1 accelerates muscle regeneration by rapidly modulating inflammatory cytokines and chemokines. *Faseb j*, 21, 1393-402.
- PERRIELLO, G., NURJHAN, N., STUMVOLL, M., BUCCI, A., WELLE, S., DAILEY, G., BIER, D. M., TOFT, I., JENSSEN, T. G. & GERICH, J. E. 1997. Regulation of gluconeogenesis by glutamine in normal postabsorptive humans. *Am J Physiol*, 272, E437-45.
- PERSONIUS, K. E., JAYARAM, A., KRULL, D., BROWN, R., XU, T., HAN, B., BURGESS, K., STOREY, C., SHAH, B., TAWIL, R. & WELLE, S. 2010. Grip force, EDL contractile properties, and voluntary wheel running after postdevelopmental myostatin depletion in mice. *J Appl Physiol (1985)*, 109, 886-94.
- PETTE, D., PEUKER, H. & STARON, R. S. 1999. The impact of biochemical methods for single muscle fibre analysis. *Acta Physiol Scand*, 166, 261-77.
- PETTE, D. & STARON, R. S. 1990. Cellular and molecular diversities of mammalian skeletal muscle fibers. *Rev Physiol Biochem Pharmacol*, 116, 1-76.

- PETTE, D. & STARON, R. S. 1997. Mammalian skeletal muscle fiber type transitions. *Int Rev Cytol*, 170, 143-223.
- PETTE, D. & STARON, R. S. 2000. Myosin isoforms, muscle fiber types, and transitions. *Microsc Res Tech*, 50, 500-9.
- PETTE, D. & STARON, R. S. 2001. Transitions of muscle fiber phenotypic profiles. *Histochem Cell Biol*, 115, 359-72.
- PETTE, D. & VRBOVA, G. 1992. Adaptation of mammalian skeletal muscle fibers to chronic electrical stimulation. *Rev Physiol Biochem Pharmacol*, 120, 115-202.
- PEUKER, H., CONJARD, A., PUTMAN, C. T. & PETTE, D. 1999. Transient expression of myosin heavy chain MHCI alpha in rabbit muscle during fast-to-slow transition. *J Muscle Res Cell Motil*, 20, 147-54.
- PISTILLI, E. E., BOGDANOVICH, S., GONCALVES, M. D., AHIMA, R. S., LACHEY, J., SEEHRA, J. & KHURANA, T. 2011. Targeting the activin type IIB receptor to improve muscle mass and function in the mdx mouse model of Duchenne muscular dystrophy. *Am J Pathol*, 178, 1287-97.
- PLOQUIN, C., CHABI, B., FOURET, G., VERNUS, B., FEILLET-COUDRAY, C., COUDRAY, C., BONNIEU, A. & RAMONATXO, C. 2012. Lack of myostatin alters intermyofibrillar mitochondria activity, unbalances redox status, and impairs tolerance to chronic repetitive contractions in muscle. *Am J Physiol Endocrinol Metab*, 302, E1000-8.
- PLYLEY, M. J., OLMSTEAD, B. J. & NOBLE, E. G. 1998. Time course of changes in capillarization in hypertrophied rat plantaris muscle. *J Appl Physiol (1985)*, 84, 902-7.
- POWERS, S. K., JI, L. L. & LEEUWENBURGH, C. 1999. Exercise training-induced alterations in skeletal muscle antioxidant capacity: a brief review. *Med Sci Sports Exerc*, 31, 987-97.
- POWERS, S. K., WIGGS, M. P., DUARTE, J. A., ZERGEROGLU, A. M. & DEMIREL, H. A. 2012. Mitochondrial signaling contributes to disuse muscle atrophy. *Am J Physiol Endocrinol Metab*, 303, E31-9.
- PRISK, V. & HUARD, J. 2003. Muscle injuries and repair: the role of prostaglandins and inflammation. *Histol Histopathol*, 18, 1243-56.
- PULLEN, A. H. 1977. The distribution and relative sizes of three histochemical fibre types in the rat tibialis anterior muscle. *J Anat*, 123, 1-19.
- PURSLOW, P. P. 2002. The structure and functional significance of variations in the connective tissue within muscle. *Comp Biochem Physiol A Mol Integr Physiol*, 133, 947-66.
- PUTMAN, C. T., DUSTERHOFT, S. & PETTE, D. 1999. Changes in satellite cell content and myosin isoforms in low-frequency-stimulated fast muscle of hypothyroid rat. *J Appl Physiol (1985)*, 86, 40-51.
- QIAO, C., LI, J., JIANG, J., ZHU, X., WANG, B., LI, J. & XIAO, X. 2008. Myostatin propeptide gene delivery by adeno-associated virus serotype 8 vectors enhances muscle growth and ameliorates dystrophic phenotypes in mdx mice. *Hum Gene Ther*, 19, 241-54.
- QIAO, C., LI, J., ZHENG, H., BOGAN, J., LI, J., YUAN, Z., ZHANG, C., BOGAN, D., KORNEGAY, J. & XIAO, X. 2009. Hydrodynamic limb vein injection of adeno-associated virus serotype 8 vector carrying canine myostatin propeptide gene into normal dogs enhances muscle growth. *Hum Gene Ther*, 20, 1-10.
- RABINOWITZ, J. E., ROLLING, F., LI, C., CONRATH, H., XIAO, W., XIAO, X. & SAMULSKI, R. J. 2002. Cross-packaging of a single adeno-associated virus (AAV) type 2 vector genome into multiple AAV serotypes enables transduction with broad specificity. *J Virol*, 76, 791-801.
- RAHIMOV, F., KING, O. D., WARSING, L. C., POWELL, R. E., EMERSON, C. P., JR., KUNKEL, L. M. & WAGNER, K. R. 2011. Gene expression profiling of skeletal muscles treated with a soluble activin type IIB receptor. *Physiol Genomics*, 43, 398-407.
- RAMADASAN-NAIR, R., GAYATHRI, N., MISHRA, S., SUNITHA, B., MYTHRI, R. B., NALINI, A., SUBBANNAYYA, Y., HARSHA, H. C., KOLTHUR-SEETHARAM, U. & SRINIVAS BHARATH, M. M.

2014. Mitochondrial alterations and oxidative stress in an acute transient mouse model of muscle degeneration: implications for muscular dystrophy and related muscle pathologies. *J Biol Chem*, 289, 485-509.
- RAMAMURTHY, B., HOOK, P., JONES, A. D. & LARSSON, L. 2001. Changes in myosin structure and function in response to glycation. *Faseb j*, 15, 2415-22.
- RANGWALA, S. M., WANG, X., CALVO, J. A., LINDSLEY, L., ZHANG, Y., DEYNEKO, G., BEAULIEU, V., GAO, J., TURNER, G. & MARKOVITS, J. 2010. Estrogen-related receptor gamma is a key regulator of muscle mitochondrial activity and oxidative capacity. *J Biol Chem*, 285, 22619-29.
- RAYNOR, R. L., ZHENG, B. & KUO, J. F. 1991. Membrane interactions of amphiphilic polypeptides mastoparan, melittin, polymyxin B, and cardiotoxin. Differential inhibition of protein kinase C, Ca²⁺/calmodulin-dependent protein kinase II and synaptosomal membrane Na,K-ATPase, and Na⁺ pump and differentiation of HL60 cells. *J Biol Chem*, 266, 2753-8.
- REARDON, K. A., DAVIS, J., KAPSA, R. M., CHOONG, P. & BYRNE, E. 2001. Myostatin, insulin-like growth factor-1, and leukemia inhibitory factor mRNAs are upregulated in chronic human disuse muscle atrophy. *Muscle Nerve*, 24, 893-9.
- REHFELDT, C., OTT, G., GERRARD, D. E., VARGA, L., SCHLOTE, W., WILLIAMS, J. L., RENNE, U. & BUNGER, L. 2005. Effects of the compact mutant myostatin allele Mstn (Cmpt-dl1Abc) introgressed into a high growth mouse line on skeletal muscle cellularity. *J Muscle Res Cell Motil*, 26, 103-12.
- RELAIX, F., ROCANCOURT, D., MANSOURI, A. & BUCKINGHAM, M. 2005. A Pax3/Pax7-dependent population of skeletal muscle progenitor cells. *Nature*, 435, 948-53.
- RELAIX, F. & ZAMMIT, P. S. 2012. Satellite cells are essential for skeletal muscle regeneration: the cell on the edge returns centre stage. *Development*, 139, 2845-56.
- RELIZANI, K., MOUISEL, E., GIANNESINI, B., HOURDE, C., PATEL, K., MORALES GONZALEZ, S., JULICH, K., VIGNAUD, A., PIETRI-ROUXEL, F., FORTIN, D., GARCIA, L., BLOT, S., RITVOS, O., BENDAHAN, D., FERRY, A., VENTURA-CLAPIER, R., SCHUELKE, M. & AMTHOR, H. 2014. Blockade of ActRIIB signaling triggers muscle fatigability and metabolic myopathy. *Mol Ther*, 22, 1423-33.
- REZNIK, M. 1969. Thymidine-3H uptake by satellite cells of regenerating skeletal muscle. *J Cell Biol*, 40, 568-71.
- RICHTER, E. A., DERAIVE, W. & WOJTASZEWSKI, J. F. 2001. Glucose, exercise and insulin: emerging concepts. *J Physiol*, 535, 313-22.
- RIGAMONTI, E., ZORDAN, P., SCIORATI, C., ROVERE-QUERINI, P. & BRUNELLI, S. 2014. Macrophage plasticity in skeletal muscle repair. *Biomed Res Int*, 2014, 560629.
- RIOS, R., CARNEIRO, I., ARCE, V. M. & DEVESA, J. 2002. Myostatin is an inhibitor of myogenic differentiation. *Am J Physiol Cell Physiol*, 282, C993-9.
- ROBERGS, R. A., GHIASVAND, F. & PARKER, D. 2004. Biochemistry of exercise-induced metabolic acidosis. *Am J Physiol Regul Integr Comp Physiol*, 287, R502-16.
- ROCHARD, P., RODIER, A., CASAS, F., CASSAR-MALEK, I., MARCHAL-VICTORION, S., DAURY, L., WRUTNIAK, C. & CABELLO, G. 2000. Mitochondrial activity is involved in the regulation of myoblast differentiation through myogenin expression and activity of myogenic factors. *J Biol Chem*, 275, 2733-44.
- RODRIGUES, M., ECHIGOYA, Y., FUKADA, S. I. & YOKOTA, T. 2016. Current Translational Research and Murine Models For Duchenne Muscular Dystrophy. *J Neuromuscul Dis*, 3, 29-48.
- RODRIGUEZ, J., VERNUS, B., CHELH, I., CASSAR-MALEK, I., GABILLARD, J. C., HADJ SASSI, A., SEILIEZ, I., PICARD, B. & BONNIEU, A. 2014. Myostatin and the skeletal muscle atrophy and hypertrophy signaling pathways. *Cell Mol Life Sci*.
- ROMMEL, C., BODINE, S. C., CLARKE, B. A., ROSSMAN, R., NUNEZ, L., STITT, T. N., YANCOPOULOS, G. D. & GLASS, D. J. 2001. Mediation of IGF-1-induced skeletal myotube hypertrophy by PI(3)K/Akt/mTOR and PI(3)K/Akt/GSK3 pathways. *Nat Cell Biol*, 3, 1009-13.

- ROSSI, A. E. & DIRKSEN, R. T. 2006. Sarcoplasmic reticulum: the dynamic calcium governor of muscle. *Muscle Nerve*, 33, 715-31.
- ROY, R. R., HODGSON, J. A., LAURETZ, S. D., PIEROTTI, D. J., GAYEK, R. J. & EDGERTON, V. R. 1992. Chronic spinal cord-injured cats: surgical procedures and management. *Lab Anim Sci*, 42, 335-43.
- ROY, R. R., MONKE, S. R., ALLEN, D. L. & EDGERTON, V. R. 1999. Modulation of myonuclear number in functionally overloaded and exercised rat plantaris fibers. *J Appl Physiol (1985)*, 87, 634-42.
- RUDNICKI, M. A., SCHNEGELSBERG, P. N., STEAD, R. H., BRAUN, T., ARNOLD, H. H. & JAENISCH, R. 1993. MyoD or Myf-5 is required for the formation of skeletal muscle. *Cell*, 75, 1351-9.
- RUEGG, M. A. & GLASS, D. J. 2011. Molecular mechanisms and treatment options for muscle wasting diseases. *Annu Rev Pharmacol Toxicol*, 51, 373-95.
- RUSS, D. W. & LANZA, I. R. 2011. The impact of old age on skeletal muscle energetics: supply and demand. *Curr Aging Sci*, 4, 234-47.
- RUSSELL-JONES, D. L., UMPLEBY, A. M., HENNESSY, T. R., BOWES, S. B., SHOJAEI-MORADIE, F., HOPKINS, K. D., JACKSON, N. C., KELLY, J. M., JONES, R. H. & SONKSEN, P. H. 1994. Use of a leucine clamp to demonstrate that IGF-I actively stimulates protein synthesis in normal humans. *Am J Physiol*, 267, E591-8.
- SABOURIN, L. A., GIRGIS-GABARDO, A., SEALE, P., ASAKURA, A. & RUDNICKI, M. A. 1999. Reduced differentiation potential of primary MyoD^{-/-} myogenic cells derived from adult skeletal muscle. *J Cell Biol*, 144, 631-43.
- SADLER, T. W. 2012. Medical Embryology, 12th EDITION. Wolters Kluwer - Lippincott Williams and Wilkins.
- SAFDAR, A., BOURGEOIS, J. M., OGBORN, D. I., LITTLE, J. P., HETTINGA, B. P., AKHTAR, M., THOMPSON, J. E., MELOV, S., MOCELLIN, N. J., KUJOTH, G. C., PROLLA, T. A. & TARNOPOLSKY, M. A. 2011. Endurance exercise rescues progeroid aging and induces systemic mitochondrial rejuvenation in mtDNA mutator mice. *Proc Natl Acad Sci U S A*, 108, 4135-40.
- SAJ, A., ARZIMAN, Z., STEMPFLE, D., VAN BELLE, W., SAUDER, U., HORN, T., DURRENBERGER, M., PARO, R., BOUTROS, M. & MERDES, G. 2010. A combined ex vivo and in vivo RNAi screen for notch regulators in Drosophila reveals an extensive notch interaction network. *Dev Cell*, 18, 862-76.
- SAKAMOTO, K., HIRSHMAN, M. F., ASCHENBACH, W. G. & GOODYEAR, L. J. 2002. Contraction regulation of Akt in rat skeletal muscle. *J Biol Chem*, 277, 11910-7.
- SANDRI, M. 2008. Signaling in muscle atrophy and hypertrophy. *Physiology (Bethesda)*, 23, 160-70.
- SANDRI, M. 2013. Protein breakdown in muscle wasting: role of autophagy-lysosome and ubiquitin-proteasome. *Int J Biochem Cell Biol*, 45, 2121-9.
- SANDRI, M., SANDRI, C., GILBERT, A., SKURK, C., CALABRIA, E., PICARD, A., WALSH, K., SCHIAFFINO, S., LECKER, S. H. & GOLDBERG, A. L. 2004. Foxo transcription factors induce the atrophy-related ubiquitin ligase atrogin-1 and cause skeletal muscle atrophy. *Cell*, 117, 399-412.
- SANES, J. R. 2003. The basement membrane/basal lamina of skeletal muscle. *J Biol Chem*, 278, 12601-4.
- SARTORI, R., MILAN, G., PATRON, M., MAMMUCARI, C., BLAAUW, B., ABRAHAM, R. & SANDRI, M. 2009. Smad2 and 3 transcription factors control muscle mass in adulthood. *Am J Physiol Cell Physiol*, 296, C1248-57.
- SAVAGE, K. J. & MCPHERRON, A. C. 2010. Endurance exercise training in myostatin null mice. *Muscle Nerve*, 42, 355-62.
- SCARPULLA, R. C. 2008. Transcriptional paradigms in mammalian mitochondrial biogenesis and function. *Physiol Rev*, 88, 611-38.
- SCHARNER, J. & ZAMMIT, P. S. 2011. The muscle satellite cell at 50: the formative years. *Skelet Muscle*, 1, 28.

- SCHIAFFINO, S. & MAMMUCARI, C. 2011. Regulation of skeletal muscle growth by the IGF1-Akt/PKB pathway: insights from genetic models. *Skelet Muscle*, 1, 4.
- SCHIAFFINO, S. & REGGIANI, C. 1996. Molecular diversity of myofibrillar proteins: gene regulation and functional significance. *Physiol Rev*, 76, 371-423.
- SCHINDLER, R. F., SCOTTON, C., ZHANG, J., PASSARELLI, C., ORTIZ-BONNIN, B., SIMRICK, S., SCHWERTE, T., POON, K. L., FANG, M., RINNE, S., FROESE, A., NIKOLAEV, V. O., GRUNERT, C., MULLER, T., TASCA, G., SARATHCHANDRA, P., DRAGO, F., DALLAPICCOLA, B., RAPEZZI, C., ARBUSTINI, E., DI RAIMO, F. R., NERI, M., SELVATICI, R., GUALANDI, F., FATTORI, F., PIETRANGELO, A., LI, W., JIANG, H., XU, X., BERTINI, E., DECHER, N., WANG, J., BRAND, T. & FERLINI, A. 2016. POPDC1(S201F) causes muscular dystrophy and arrhythmia by affecting protein trafficking. *J Clin Invest*, 126, 239-53.
- SCHMALBRUCH, H. & LEWIS, D. M. 2000. Dynamics of nuclei of muscle fibers and connective tissue cells in normal and denervated rat muscles. *Muscle Nerve*, 23, 617-26.
- SCHUELKE, M., WAGNER, K. R., STOLZ, L. E., HUBNER, C., RIEBEL, T., KOMEN, W., BRAUN, T., TOBIN, J. F. & LEE, S. J. 2004. Myostatin mutation associated with gross muscle hypertrophy in a child. *N Engl J Med*, 350, 2682-8.
- SCHULTZ, E. & MCCORMICK, K. M. 1994. Skeletal muscle satellite cells. *Rev Physiol Biochem Pharmacol*, 123, 213-57.
- SCHULZ, H. 1991. Beta oxidation of fatty acids. *Biochim Biophys Acta*, 1081, 109-20.
- SCHUSTER-GOSSLER, K., CORDES, R. & GOSSLER, A. 2007. Premature myogenic differentiation and depletion of progenitor cells cause severe muscle hypotrophy in Delta1 mutants. *Proc Natl Acad Sci U S A*, 104, 537-42.
- SCIOTE, J. J. & MORRIS, T. J. 2000. Skeletal muscle function and fibre types: the relationship between occlusal function and the phenotype of jaw-closing muscles in human. *J Orthod*, 27, 15-30.
- SCOTT, W., STEVENS, J. & BINDER-MACLEOD, S. A. 2001. Human skeletal muscle fiber type classifications. *Phys Ther*, 81, 1810-6.
- SEALE, P. & RUDNICKI, M. A. 2000. A new look at the origin, function, and "stem-cell" status of muscle satellite cells. *Dev Biol*, 218, 115-24.
- SEALE, P., SABOURIN, L. A., GIRGIS-GABARDO, A., MANSOURI, A., GRUSS, P. & RUDNICKI, M. A. 2000. Pax7 is required for the specification of myogenic satellite cells. *Cell*, 102, 777-86.
- SEGAL, S. S. 2005. Regulation of blood flow in the microcirculation. *Microcirculation*, 12, 33-45.
- SERHAN, C. N. & SAVILL, J. 2005. Resolution of inflammation: the beginning programs the end. *Nat Immunol*, 6, 1191-7.
- SETH, A., STEEL, J. H., NICHOL, D., POCOCK, V., KUMARAN, M. K., FRITAH, A., MOBBERLEY, M., RYDER, T. A., ROWLERSON, A., SCOTT, J., POUTANEN, M., WHITE, R. & PARKER, M. 2007. The transcriptional corepressor RIP140 regulates oxidative metabolism in skeletal muscle. *Cell Metab*, 6, 236-45.
- SHAN, T., LIANG, X., BI, P. & KUANG, S. 2013. Myostatin knockout drives browning of white adipose tissue through activating the AMPK-PGC1 α -Fndc5 pathway in muscle. *FASEB J*, 27, 1981-9.
- SHELTON, G. D. & ENGVALL, E. 2007. Gross muscle hypertrophy in whippet dogs is caused by a mutation in the myostatin gene. *Neuromuscul Disord*, 17, 721-2.
- SHI, X. & GARRY, D. J. 2006. Muscle stem cells in development, regeneration, and disease. *Genes Dev*, 20, 1692-708.
- SHI, Y. & MASSAGUE, J. 2003. Mechanisms of TGF-beta signaling from cell membrane to the nucleus. *Cell*, 113, 685-700.
- SHININ, V., GAYRAUD-MOREL, B., GOMES, D. & TAJBAKHSI, S. 2006. Asymmetric division and cosegregation of template DNA strands in adult muscle satellite cells. *Nat Cell Biol*, 8, 677-87.
- SHIREMAN, P. K., CONTRERAS-SHANNON, V., OCHOA, O., KARIA, B. P., MICHALEK, J. E. & MCMANUS, L. M. 2007. MCP-1 deficiency causes altered inflammation with impaired skeletal muscle regeneration. *J Leukoc Biol*, 81, 775-85.

- SHU, B., SHEN, Y., WANG, A. M., FANG, X. Q., LI, X., DENG, H. Y. & YU, Z. Q. 2007. Histological, enzymohistochemical and biomechanical observation of skeletal muscle injury in rabbits. *Chin J Traumatol*, 10, 150-3.
- SMERDU, V., KARSCH-MIZRACHI, I., CAMPIONE, M., LEINWAND, L. & SCHIAFFINO, S. 1994. Type IIx myosin heavy chain transcripts are expressed in type IIb fibers of human skeletal muscle. *Am J Physiol*, 267, C1723-8.
- SNOW, M. H. 1977. Myogenic cell formation in regenerating rat skeletal muscle injured by mincing. II. An autoradiographic study. *Anat Rec*, 188, 201-17.
- ST PIERRE, B. A. & TIDBALL, J. G. 1994. Differential response of macrophage subpopulations to soleus muscle reloading after rat hindlimb suspension. *J Appl Physiol (1985)*, 77, 290-7.
- STEIN, R. A. & MCDONNELL, D. P. 2006. Estrogen-related receptor alpha as a therapeutic target in cancer. *Endocr Relat Cancer*, 13 Suppl 1, S25-32.
- STITT, T. N., DRUJAN, D., CLARKE, B. A., PANARO, F., TIMOFEYVA, Y., KLINE, W. O., GONZALEZ, M., YANCOPOULOS, G. D. & GLASS, D. J. 2004. The IGF-1/PI3K/Akt pathway prevents expression of muscle atrophy-induced ubiquitin ligases by inhibiting FOXO transcription factors. *Mol Cell*, 14, 395-403.
- STOUT, R. D., JIANG, C., MATTA, B., TIETZEL, I., WATKINS, S. K. & SUTTLES, J. 2005. Macrophages sequentially change their functional phenotype in response to changes in microenvironmental influences. *J Immunol*, 175, 342-9.
- STOUT, R. D. & SUTTLES, J. 2004. Functional plasticity of macrophages: reversible adaptation to changing microenvironments. *J Leukoc Biol*, 76, 509-13.
- STRAUB, V., RAFAEL, J. A., CHAMBERLAIN, J. S. & CAMPBELL, K. P. 1997. Animal models for muscular dystrophy show different patterns of sarcolemmal disruption. *J Cell Biol*, 139, 375-85.
- SUN, D. F., CHEN, Y. & RABKIN, R. 2006. Work-induced changes in skeletal muscle IGF-1 and myostatin gene expression in uremia. *Kidney Int*, 70, 453-9.
- SUROSKY, R. T., URABE, M., GODWIN, S. G., MCQUISTON, S. A., KURTZMAN, G. J., OZAWA, K. & NATSOULIS, G. 1997. Adeno-associated virus Rep proteins target DNA sequences to a unique locus in the human genome. *J Virol*, 71, 7951-9.
- SUTHERLAND, H., JARVIS, J. C., KWENDE, M. M., GILROY, S. J. & SALMONS, S. 1998. The dose-related response of rabbit fast muscle to long-term low-frequency stimulation. *Muscle Nerve*, 21, 1632-46.
- SVENSSON, L., ASZODI, A., REINHOLT, F. P., FASSLER, R., HEINEGARD, D. & OLDBERG, A. 1999. Fibromodulin-null mice have abnormal collagen fibrils, tissue organization, and altered lumican deposition in tendon. *J Biol Chem*, 274, 9636-47.
- TAJBAKSH, S. & BUCKINGHAM, M. 2000. The birth of muscle progenitor cells in the mouse: spatiotemporal considerations. *Curr Top Dev Biol*, 48, 225-68.
- TAJBAKSH, S. & COSSU, G. 1997. Establishing myogenic identity during somitogenesis. *Curr Opin Genet Dev*, 7, 634-41.
- TAJBAKSH, S., ROCAN COURT, D., COSSU, G. & BUCKINGHAM, M. 1997. Redefining the genetic hierarchies controlling skeletal myogenesis: Pax-3 and Myf-5 act upstream of MyoD. *Cell*, 89, 127-38.
- TAYLOR, L. E., KAMINOH, Y. J., RODESCH, C. K. & FLANIGAN, K. M. 2012. Quantification of dystrophin immunofluorescence in dystrophinopathy muscle specimens. *Neuropathol Appl Neurobiol*, 38, 591-601.
- TAYLOR, W. E., BHASIN, S., ARTAZA, J., BYHOWER, F., AZAM, M., WILLARD, D. H., JR., KULL, F. C., JR. & GONZALEZ-CADAVID, N. 2001. Myostatin inhibits cell proliferation and protein synthesis in C2C12 muscle cells. *Am J Physiol Endocrinol Metab*, 280, E221-8.
- TEE, A. R. & BLENIS, J. 2005. mTOR, translational control and human disease. *Semin Cell Dev Biol*, 16, 29-37.

- TEIXEIRA, C. F., ZAMUNER, S. R., ZULIANI, J. P., FERNANDES, C. M., CRUZ-HOFLING, M. A., FERNANDES, I., CHAVES, F. & GUTIERREZ, J. M. 2003. Neutrophils do not contribute to local tissue damage, but play a key role in skeletal muscle regeneration, in mice injected with *Bothrops asper* snake venom. *Muscle Nerve*, 28, 449-59.
- TESCH, P. A., THORSSON, A. & COLLIANDER, E. B. 1990. Effects of eccentric and concentric resistance training on skeletal muscle substrates, enzyme activities and capillary supply. *Acta Physiol Scand*, 140, 575-80.
- THOMAS, D. R. 2007. Loss of skeletal muscle mass in aging: examining the relationship of starvation, sarcopenia and cachexia. *Clin Nutr*, 26, 389-99.
- THOMAS, M., LANGLEY, B., BERRY, C., SHARMA, M., KIRK, S., BASS, J. & KAMBADUR, R. 2000. Myostatin, a negative regulator of muscle growth, functions by inhibiting myoblast proliferation. *J Biol Chem*, 275, 40235-43.
- THOMAS, P. K. 1963. The connective tissue of peripheral nerve: an electron microscope study. *J Anat*, 97, 35-44.
- TIDBALL, J. G. 2005. Inflammatory processes in muscle injury and repair. *Am J Physiol Regul Integr Comp Physiol*, 288, R345-53.
- TOHME, M., PRUD'HOMME, S. M., BOULAHTOUF, A., SAMARUT, E., BRUNET, F., BERNARD, L., BOURGUET, W., GIBERT, Y., BALAGUER, P. & LAUDET, V. 2014. Estrogen-related receptor gamma is an in vivo receptor of bisphenol A. *Faseb j*, 28, 3124-33.
- TRENDELENBURG, A. U., MEYER, A., ROHNER, D., BOYLE, J., HATAKEYAMA, S. & GLASS, D. J. 2009. Myostatin reduces Akt/TORC1/p70S6K signaling, inhibiting myoblast differentiation and myotube size. *Am J Physiol Cell Physiol*, 296, C1258-70.
- TROTTER, J. A. & PURSLOW, P. P. 1992. Functional morphology of the endomysium in series fibered muscles. *J Morphol*, 212, 109-22.
- URCIUOLO, A., QUARTA, M., MORBIDONI, V., GATTAZZO, F., MOLON, S., GRUMATI, P., MONTEMURRO, F., TEDESCO, F. S., BLAAUW, B., COSSU, G., VOZZI, G., RANDO, T. A. & BONALDO, P. 2013. Collagen VI regulates satellite cell self-renewal and muscle regeneration. *Nat Commun*, 4, 1964.
- VAINZOF, M., MOREIRA, E. S., FERRAZ, G., PASSOS-BUENO, M. R., MARIE, S. K. & ZATZ, M. 1999. Further evidence for the organisation of the four sarcoglycans proteins within the dystrophin-glycoprotein complex. *Eur J Hum Genet*, 7, 251-4.
- VAN BEEK-HARMSSEN, B. J., BEKEDAM, M. A., FEENSTRA, H. M., VISSER, F. C. & VAN DER LAARSE, W. J. 2004. Determination of myoglobin concentration and oxidative capacity in cryostat sections of human and rat skeletal muscle fibres and rat cardiomyocytes. *Histochem Cell Biol*, 121, 335-42.
- VAN DER LAARSE WJ, D. T. A., LEE-DE GROOT MBE, DIEGENBACH PC 1998. Size principle of striated muscle cells. *Neth J Zool* 48: 213-223.
- VAN DER MEER, S. F., JASPERS, R. T., JONES, D. A. & DEGENS, H. 2011. The time course of myonuclear accretion during hypertrophy in young adult and older rat plantaris muscle. *Ann Anat*, 193, 56-63.
- VAN WESSEL, T., DE HAAN, A., VAN DER LAARSE, W. J. & JASPERS, R. T. 2010. The muscle fiber type-fiber size paradox: hypertrophy or oxidative metabolism? *Eur J Appl Physiol*, 110, 665-94.
- VASYUTINA, E., LENHARD, D. C., WENDE, H., ERDMANN, B., EPSTEIN, J. A. & BIRCHMEIER, C. 2007. RBP-J (Rbpsi) is essential to maintain muscle progenitor cells and to generate satellite cells. *Proc Natl Acad Sci U S A*, 104, 4443-8.
- VERDIJK, L. B., KOOPMAN, R., SCHAART, G., MEIJER, K., SAVELBERG, H. H. & VAN LOON, L. J. 2007. Satellite cell content is specifically reduced in type II skeletal muscle fibers in the elderly. *Am J Physiol Endocrinol Metab*, 292, E151-7.

- VILLALTA, S. A., RINALDI, C., DENG, B., LIU, G., FEDOR, B. & TIDBALL, J. G. 2011. Interleukin-10 reduces the pathology of mdx muscular dystrophy by deactivating M1 macrophages and modulating macrophage phenotype. *Hum Mol Genet*, 20, 790-805.
- VON HOFSTEN, J., ELWORTHY, S., GILCHRIST, M. J., SMITH, J. C., WARDLE, F. C. & INGHAM, P. W. 2008. Prdm1- and Sox6-mediated transcriptional repression specifies muscle fibre type in the zebrafish embryo. *EMBO Rep*, 9, 683-9.
- WAGNER, K. R., FLECKENSTEIN, J. L., AMATO, A. A., BAROHN, R. J., BUSHBY, K., ESCOLAR, D. M., FLANIGAN, K. M., PESTRONK, A., TAWIL, R., WOLFE, G. I., EAGLE, M., FLORENCE, J. M., KING, W. M., PANDYA, S., STRAUB, V., JUNEAU, P., MEYERS, K., CSIMMA, C., ARAUJO, T., ALLEN, R., PARSONS, S. A., WOZNEY, J. M., LAVALLIE, E. R. & MENDELL, J. R. 2008. A phase I/II trial of MYO-029 in adult subjects with muscular dystrophy. *Ann Neurol*, 63, 561-71.
- WAGNER, K. R., MCPHERRON, A. C., WINIK, N. & LEE, S. J. 2002. Loss of myostatin attenuates severity of muscular dystrophy in mdx mice. *Ann Neurol*, 52, 832-6.
- WALSH, F. S. & CELESTE, A. J. 2005. Myostatin: a modulator of skeletal-muscle stem cells. *Biochem Soc Trans*, 33, 1513-7.
- WANG, H. X., LAU, S. Y., HUANG, S. J., KWAN, C. Y. & WONG, T. M. 1997. Cobra venom cardiotoxin induces perturbations of cytosolic calcium homeostasis and hypercontracture in adult rat ventricular myocytes. *J Mol Cell Cardiol*, 29, 2759-70.
- WANG, L., LIU, J., SAHA, P., HUANG, J., CHAN, L., SPIEGELMAN, B. & MOORE, D. D. 2005. The orphan nuclear receptor SHP regulates PGC-1alpha expression and energy production in brown adipocytes. *Cell Metab*, 2, 227-38.
- WANG, L., ZUERCHER, W. J., CONSLER, T. G., LAMBERT, M. H., MILLER, A. B., ORBAND-MILLER, L. A., MCKEE, D. D., WILLSON, T. M. & NOLTE, R. T. 2006. X-ray crystal structures of the estrogen-related receptor-gamma ligand binding domain in three functional states reveal the molecular basis of small molecule regulation. *J Biol Chem*, 281, 37773-81.
- WANG, Q. & MCPHERRON, A. C. 2012. Myostatin inhibition induces muscle fibre hypertrophy prior to satellite cell activation. *J Physiol*, 590, 2151-65.
- WANG, T., MCDONALD, C., PETRENKO, N. B., LEBLANC, M., WANG, T., GIGUERE, V., EVANS, R. M., PATEL, V. V. & PEI, L. 2015. Estrogen-related receptor alpha (ERRalpha) and ERRgamma are essential coordinators of cardiac metabolism and function. *Mol Cell Biol*, 35, 1281-98.
- WANG, Y. X., ZHANG, C. L., YU, R. T., CHO, H. K., NELSON, M. C., BAYUGA-OCAMPO, C. R., HAM, J., KANG, H. & EVANS, R. M. 2004. Regulation of muscle fiber type and running endurance by PPARdelta. *PLoS Biol*, 2, e294.
- WARBURG, O. 1956. On respiratory impairment in cancer cells. *Science*, 124, 269-70.
- WEGNER, J., ALBRECHT, E., FIEDLER, I., TEUSCHER, F., PAPSTEIN, H. J. & ENDER, K. 2000. Growth- and breed-related changes of muscle fiber characteristics in cattle. *J Anim Sci*, 78, 1485-96.
- WEI, Q. & PATERSON, B. M. 2001. Regulation of MyoD function in the dividing myoblast. *FEBS Lett*, 490, 171-8.
- WEISS, A. & LEINWAND, L. A. 1996. The mammalian myosin heavy chain gene family. *Annu Rev Cell Dev Biol*, 12, 417-39.
- WELLE, S., BHATT, K., PINKERT, C. A., TAWIL, R. & THORNTON, C. A. 2007. Muscle growth after postdevelopmental myostatin gene knockout. *Am J Physiol Endocrinol Metab*, 292, E985-91.
- WELLE, S., MEHTA, S. & BURGESS, K. 2011. Effect of postdevelopmental myostatin depletion on myofibrillar protein metabolism. *Am J Physiol Endocrinol Metab*, 300, E993-E1001.
- WENDE, A. R., HUSS, J. M., SCHAEFFER, P. J., GIGUERE, V. & KELLY, D. P. 2005. PGC-1alpha coactivates PDK4 gene expression via the orphan nuclear receptor ERRalpha: a mechanism for transcriptional control of muscle glucose metabolism. *Mol Cell Biol*, 25, 10684-94.
- WHITTEMORE, L. A., SONG, K., LI, X., AGHAJANIAN, J., DAVIES, M., GIRGENRATH, S., HILL, J. J., JALENAK, M., KELLEY, P., KNIGHT, A., MAYLOR, R., O'HARA, D., PEARSON, A., QUAZI, A., RYERSON, S., TAN, X. Y., TOMKINSON, K. N., VELDMAN, G. M., WIDOM, A., WRIGHT, J. F.,

- WUDYKA, S., ZHAO, L. & WOLFMAN, N. M. 2003. Inhibition of myostatin in adult mice increases skeletal muscle mass and strength. *Biochem Biophys Res Commun*, 300, 965-71.
- WICKLUND, M. P. & KISSEL, J. T. 2014. The limb-girdle muscular dystrophies. *Neurol Clin*, 32, 729-49, ix.
- WILKES, J. J., LLOYD, D. J. & GEKAKIS, N. 2009. Loss-of-function mutation in myostatin reduces tumor necrosis factor alpha production and protects liver against obesity-induced insulin resistance. *Diabetes*, 58, 1133-43.
- WILLIAMS 1999. *Gray's Anatomy, The Anatomical basis of medicine and surgery*, Churchill Livingstone.
- WILLIAMS, A. S., KANG, L. & WASSERMAN, D. H. 2015. The extracellular matrix and insulin resistance. *Trends Endocrinol Metab*, 26, 357-66.
- WINEGRAD, S. 1999. Cardiac myosin binding protein C. *Circ Res*, 84, 1117-26.
- WOLFE, R. R. 2006. The underappreciated role of muscle in health and disease. *Am J Clin Nutr*, 84, 475-82.
- WULLSCHLEGER, S., LOEWITH, R. & HALL, M. N. 2006. TOR signaling in growth and metabolism. *Cell*, 124, 471-84.
- XIE, W., HONG, H., YANG, N. N., LIN, R. J., SIMON, C. M., STALLCUP, M. R. & EVANS, R. M. 1999. Constitutive activation of transcription and binding of coactivator by estrogen-related receptors 1 and 2. *Mol Endocrinol*, 13, 2151-62.
- XIE, Z. & KLIONSKY, D. J. 2007. Autophagosome formation: core machinery and adaptations. *Nat Cell Biol*, 9, 1102-9.
- YAN, Z., OKUTSU, M., AKHTAR, Y. N. & LIRA, V. A. 2011. Regulation of exercise-induced fiber type transformation, mitochondrial biogenesis, and angiogenesis in skeletal muscle. *J Appl Physiol (1985)*, 110, 264-74.
- YANG, H. T., PRIOR, B. M., LLOYD, P. G., TAYLOR, J. C., LI, Z., LAUGHLIN, M. H. & TERJUNG, R. L. 2008. Training-induced vascular adaptations to ischemic muscle. *J Physiol Pharmacol*, 59 Suppl 7, 57-70.
- YANG, W., ZHANG, Y., LI, Y., WU, Z. & ZHU, D. 2007. Myostatin induces cyclin D1 degradation to cause cell cycle arrest through a phosphatidylinositol 3-kinase/AKT/GSK-3 beta pathway and is antagonized by insulin-like growth factor 1. *J Biol Chem*, 282, 3799-808.
- YARASHESKI, K. E., BHASIN, S., SINHA-HIKIM, I., PAK-LODUCA, J. & GONZALEZ-CADAVID, N. F. 2002. Serum myostatin-immunoreactive protein is increased in 60-92 year old women and men with muscle wasting. *J Nutr Health Aging*, 6, 343-8.
- YOSHIDA, M., SUZUKI, A., YAMAMOTO, H., NOGUCHI, S., MIZUNO, Y. & OZAWA, E. 1994. Dissociation of the complex of dystrophin and its associated proteins into several unique groups by n-octyl beta-D-glucoside. *Eur J Biochem*, 222, 1055-61.
- YU, D. D. & FORMAN, B. M. 2005. Identification of an agonist ligand for estrogen-related receptors ERRbeta/gamma. *Bioorg Med Chem Lett*, 15, 1311-3.
- YUE, Y. & DONGSHENG, D. 2002. Development of multiple cloning site cis-vectors for recombinant adeno-associated virus production. *Biotechniques*, 33, 672, 674, 676-8.
- ZABNER, J., SEILER, M., WALTERS, R., KOTIN, R. M., FULGERAS, W., DAVIDSON, B. L. & CHIORINI, J. A. 2000. Adeno-associated virus type 5 (AAV5) but not AAV2 binds to the apical surfaces of airway epithelia and facilitates gene transfer. *J Virol*, 74, 3852-8.
- ZACHWIEJA, J. J., SMITH, S. R., SINHA-HIKIM, I., GONZALEZ-CADAVID, N. & BHASIN, S. 1999. Plasma myostatin-immunoreactive protein is increased after prolonged bed rest with low-dose T3 administration. *J Gravit Physiol*, 6, 11-5.
- ZAMMIT, P. & BEAUCHAMP, J. 2001. The skeletal muscle satellite cell: stem cell or son of stem cell? *Differentiation*, 68, 193-204.
- ZAMMIT, P. S. 2008. All muscle satellite cells are equal, but are some more equal than others? *J Cell Sci*, 121, 2975-82.

- ZAMMIT, P. S., GOLDING, J. P., NAGATA, Y., HUDON, V., PARTRIDGE, T. A. & BEAUCHAMP, J. R. 2004. Muscle satellite cells adopt divergent fates: a mechanism for self-renewal? *J Cell Biol*, 166, 347-57.
- ZAMMIT, P. S., RELAIX, F., NAGATA, Y., RUIZ, A. P., COLLINS, C. A., PARTRIDGE, T. A. & BEAUCHAMP, J. R. 2006. Pax7 and myogenic progression in skeletal muscle satellite cells. *J Cell Sci*, 119, 1824-32.
- ZECHNER, C., LAI, L., ZECHNER, J. F., GENG, T., YAN, Z., RUMSEY, J. W., COLLIA, D., CHEN, Z., WOZNIAK, D. F., LEONE, T. C. & KELLY, D. P. 2010. Total skeletal muscle PGC-1 deficiency uncouples mitochondrial derangements from fiber type determination and insulin sensitivity. *Cell Metab*, 12, 633-42.
- ZHANG, C., LI, Y., WU, Y., WANG, L., WANG, X. & DU, J. 2013. Interleukin-6/signal transducer and activator of transcription 3 (STAT3) pathway is essential for macrophage infiltration and myoblast proliferation during muscle regeneration. *J Biol Chem*, 288, 1489-99.
- ZHANG, C., MCFARLANE, C., LOKIREDDY, S., MASUDA, S., GE, X., GLUCKMAN, P. D., SHARMA, M. & KAMBADUR, R. 2012. Inhibition of myostatin protects against diet-induced obesity by enhancing fatty acid oxidation and promoting a brown adipose phenotype in mice. *Diabetologia*, 55, 183-93.
- ZHANG, Y., KIM, D. K., LEE, J. M., PARK, S. B., JEONG, W. I., KIM, S. H., LEE, I. K., LEE, C. H., CHIANG, J. Y. & CHOI, H. S. 2015. Orphan nuclear receptor oestrogen-related receptor gamma (ERRgamma) plays a key role in hepatic cannabinoid receptor type 1-mediated induction of CYP7A1 gene expression. *Biochem J*, 470, 181-93.
- ZHANG, Y., MA, K., SADANA, P., CHOWDHURY, F., GAILLARD, S., WANG, F., MCDONNELL, D. P., UNTERMAN, T. G., ELAM, M. B. & PARK, E. A. 2006. Estrogen-related receptors stimulate pyruvate dehydrogenase kinase isoform 4 gene expression. *J Biol Chem*, 281, 39897-906.
- ZHAO, Y., URGANUS, A. L., SPEVAK, L., SHRESTHA, S., DOTY, S. B., BOSKEY, A. L. & PACHMAN, L. M. 2009. Characterization of dystrophic calcification induced in mice by cardiotoxin. *Calcif Tissue Int*, 85, 267-75.
- ZHENG, H., FU, G., DAI, T. & HUANG, H. 2007. Migration of endothelial progenitor cells mediated by stromal cell-derived factor-1alpha/CXCR4 via PI3K/Akt/eNOS signal transduction pathway. *J Cardiovasc Pharmacol*, 50, 274-80.
- ZHOU, X., WANG, J. L., LU, J., SONG, Y., KWAK, K. S., JIAO, Q., ROSENFELD, R., CHEN, Q., BOONE, T., SIMONET, W. S., LACEY, D. L., GOLDBERG, A. L. & HAN, H. Q. 2010. Reversal of cancer cachexia and muscle wasting by ActRIIB antagonism leads to prolonged survival. *Cell*, 142, 531-43.
- ZHU, X., HADHAZY, M., WEHLING, M., TIDBALL, J. G. & MCNALLY, E. M. 2000. Dominant negative myostatin produces hypertrophy without hyperplasia in muscle. *FEBS Lett*, 474, 71-5.
- ZHU, X., TOPOUZIS, S., LIANG, L. F. & STOTISH, R. L. 2004. Myostatin signaling through Smad2, Smad3 and Smad4 is regulated by the inhibitory Smad7 by a negative feedback mechanism. *Cytokine*, 26, 262-72.
- ZIMMERS, T. A., DAVIES, M. V., KONIARIS, L. G., HAYNES, P., ESQUELA, A. F., TOMKINSON, K. N., MCPHERRON, A. C., WOLFMAN, N. M. & LEE, S. J. 2002. Induction of cachexia in mice by systemically administered myostatin. *Science*, 296, 1486-8.
- ZONCU, R., EFEYAN, A. & SABATINI, D. M. 2011. mTOR: from growth signal integration to cancer, diabetes and ageing. *Nat Rev Mol Cell Biol*, 12, 21-35.
- ZUERCHER, W. J., GAILLARD, S., ORBAND-MILLER, L. A., CHAO, E. Y., SHEARER, B. G., JONES, D. G., MILLER, A. B., COLLINS, J. L., MCDONNELL, D. P. & WILLSON, T. M. 2005. Identification and structure-activity relationship of phenolic acyl hydrazones as selective agonists for the estrogen-related orphan nuclear receptors ERRbeta and ERRgamma. *J Med Chem*, 48, 3107-9.

Publications

Enhanced exercise and regenerative capacity in a mouse model that violates size constraints of oxidative muscle fibres

Saleh Omairi^{1†}, Antonios Matsakas^{2†}, Hans Degens^{3,4}, Oliver Kretz^{5,6}, Kenth-Arne Hansson⁷, Andreas Våvang Solbrå^{7,8}, Jo C Bruusgaard^{7,9}, Barbara Joch^{10,11}, Roberta Sartori¹², Natasa Giallourou¹³, Robert Mitchell¹, Henry Collins-Hooper¹, Keith Foster¹, Arja Pasternack¹⁴, Olli Ritvos¹⁴, Marco Sandri¹², Vihang Narkar¹⁵, Jonathan R Swann¹³, Tobias Huber^{5,6,16,17}, Ketan Patel^{1,17*}

¹School of Biological Sciences, University of Reading, Reading, United Kingdom; ²Hull York Medical School, Hull, United Kingdom; ³School of Healthcare Science, Manchester Metropolitan University, Manchester, United Kingdom; ⁴Lithuanian Sports University, Kaunas, Lithuania; ⁵Renal Division, University Medical Center Freiburg, Freiburg, Germany; ⁶Faculty of Medicine, University of Freiburg, Freiburg, Germany; ⁷Centre for Integrative Neuroplasticity, Department of Biosciences, University of Oslo, Oslo, Norway; ⁸Department of Physics, University of Oslo, Oslo, Norway; ⁹Department of Health Sciences, Kristiania University College, Oslo, Norway; ¹⁰Department of Neuroanatomy, University of Freiburg, Freiburg, Germany; ¹¹Faculty of Medicine, University of Freiburg, Freiburg, Germany; ¹²Venetian Institute of Molecular Medicine, University of Padua, Padua, Italy; ¹³Department of Food and Nutritional Sciences, University of Reading, Reading, United Kingdom; ¹⁴Department of Bacteriology and Immunology, Haartman Institute, University of Helsinki, Helsinki, Finland; ¹⁵Institute of Molecular Medicine, University of Health Science Center, Houston, Texas; ¹⁶BIOSS Center for Biological Signalling Studies, Albert-Ludwigs-University Freiburg, Houston, Texas; ¹⁷FRIAS, Freiburg Institute for Advanced Studies and Center for Biological System Analysis ZBSA, Freiburg, Germany

*For correspondence: ketan.patel@reading.ac.uk

†These authors contributed equally to this work

Competing interests: The authors declare that no competing interests exist.

Funding: See page 21

Received: 14 April 2016

Accepted: 19 July 2016

Published: 05 August 2016

Reviewing editor: Giulio Cossu, University of Manchester, United Kingdom

© Copyright Omairi et al. This article is distributed under the terms of the [Creative Commons Attribution License](#), which permits unrestricted use and redistribution provided that the original author and source are credited.

Abstract A central tenet of skeletal muscle biology is the existence of an inverse relationship between the oxidative fibre capacity and its size. However, robustness of this relationship is unknown. We show that superimposition of Estrogen-related receptor gamma (*Errγ*) on the myostatin (*Mtn*) mouse null background (*Mtn*^{-/-}/*Errγ*^{Tg/+}) results in hypertrophic muscle with a high oxidative capacity thus violating the inverse relationship between fibre size and oxidative capacity. We also examined the canonical view that oxidative muscle phenotype positively correlate with Satellite cell number, the resident stem cells of skeletal muscle. Surprisingly, hypertrophic fibres from *Mtn*^{-/-}/*Errγ*^{Tg/+} mouse showed satellite cell deficit which unexpectedly did not affect muscle regeneration. These observations 1) challenge the concept of a constraint between fibre size and oxidative capacity and 2) indicate the important role of the microcirculation in the regenerative capacity of a muscle even when satellite cell numbers are reduced.

DOI: [10.7554/eLife.16940.001](https://doi.org/10.7554/eLife.16940.001)

Introduction

John Eccles and colleagues first applied the concept of 'plasticity' to skeletal muscle to describe the effect of cross-innervation experiments in cats on the size and fibre characteristics of skeletal muscle (Buller *et al.*, 1960). Many factors have since been shown to profoundly effect on skeletal muscle structure and function, including chronic electrical stimulation, exercise, diet and ageing (Salmons and Vrbová, 1969; Hickson, 1980; Wade *et al.*, 1990; Mitchell *et al.*, 2012).

In mammalian skeletal muscle, fibres are broadly characterized as slow or fast fibres, where slow fibres express the myosin heavy chain (MHC) isoform I, whereas fast fibres express MHC IIA, IIX and/or IIB. Slow fibres generally have a smaller cross sectional area (CSA), contain more mitochondria which sustain a high oxidative capacity, and a denser microvascular network than fast fibres that rely predominantly on glycolysis for ATP production. Muscle fibres can change their phenotype, such as the expression of MHC, mitochondrial content and capillary supply in response to external stimuli (Pette and Staron, 1997, 2001).

We are beginning to understand some of the cellular, biochemical and molecular processes that act to concord muscle structure and morphology to the functional demands placed on the muscle. For instance, it has been shown that the development of the slow muscle fibre phenotype is largely controlled by Protein Kinase C, Calcineurin/NFAT, AMP Activated Protein kinase (AMPK), peroxisome proliferator-activated receptor gamma co-activator 1-alpha (PGC-1 α) and Sex determining region Y-box 6 (Sox6) (Gundersen, 2011; von Hofsten *et al.*, 2008). Recently, we have shown that the Estrogenrelated receptor gamma (Err γ) is robustly expressed in slow muscle and can promote the formation of oxidative fibres in a PGC-1 α independent manner (Narkar *et al.*, 2011). Fast, glycolytic muscle development on the other hand seems to involve the activation of the Akt signalling pathway through the transcriptional regulation by molecules including Baf60c (also called Smarcd3) and T-box 15 (Tbx15) (Meng *et al.*, 2013, 2014; Lee *et al.*, 2015). Lifting the inhibition of Akt signalling mediated by Myostatin is also a potent means of inducing the formation of glycolytic muscle fibres (Trendelenburg *et al.*, 2009). Additionally, a recent study has shown that the DNA binding protein Nuclear Factor I X (Nfix) acts to inhibit the slow muscle phenotype (Rossi *et al.*, 2016).

Myostatin (Mtn), a member of the Transforming Growth Factor Beta (TGF- β) family of secreted proteins, is highly expressed in skeletal muscle (McPherron *et al.*, 1997). It is a potent inhibitor of skeletal muscle growth and its deletion results in a hypermuscular phenotype called 'Muscle Doubling' seen in mice, cattle and even humans (McPherron *et al.*, 1997; McPherron and Lee, 1997; Schuelke *et al.*, 2004). We and others have shown that the glycolytic muscles that develop in the absence of Mtn have a mitochondrial deficit and a low specific force (Amthor *et al.*, 2007; Mendias *et al.*, 2006).

A fundamental concept of skeletal muscle biology is the existence of the inverse relationship between the oxidative capacity of a fibre and its cross-sectional area (CSA) that applies to muscles as diverse as the limb, diaphragm and masseter muscle within an animal and even across species boundaries (van Wessel *et al.*, 2010; Degens, 2012; Van Der Laarse *et al.*, 1997). This relationship, in theory, ultimately imparts a constraint on the size that mitochondria-rich and therefore high O₂ - dependent oxidative fibres can attain before they become anoxic or adapt to a glycolytic phenotype less reliant on O₂ (Desplanches *et al.*, 1996; Deveci *et al.*, 2001). The metabolic properties of muscle are believed not only to control fibre size but also the number of satellite cells. A number of correlative studies have described the number of SC increases as a muscle becomes progressively oxidative (Putman *et al.*, 1999; Christov *et al.*, 2007).

Here we investigated whether this suggested constraint between fibre size and oxidative capacity can be broken and sought to develop large oxidative fibres without compromising function, such as fatigue resistance. To that end, we developed a novel mouse line by introducing an Err γ over-expression allele driven by a skeletal muscle fibre promoter (Human α -Skeletal Muscle Actin) (Muscat and Kedes, 1987) that enhances the oxidative capacity (Narkar *et al.*, 2011) into a hypertrophic Mtn^{-/-} background. Based on the concept of a constraint between the CSA and oxidative capacity of a fibre we postulated three possible outcomes of the cross: (1) the Akt pathway that is de-repressed due to the absence of Mtn would prevail and lead to hypertrophic, but glycolytic fibres; (2) oxidative features would be imparted by the Err γ programme that would follow the inverse size relationship and lead to mitochondria-rich fibres which could be smaller than wild-type

(Rangwala et al., 2010); (3) the constraint is broken in this strain and results in the development of hypertrophic yet oxidative fibres.

The main observations of the study are firstly that the muscles of $Mtn^{-/-}/Err\gamma^{Tg/+}$ mice have large fibres with a larger than expected oxidative capacity, breaking the constraint of the inverse size-oxidative capacity relationship. This was attained through the activation of the Akt pathway, increased myoglobin gene expression, relocation of mitochondria to the sub sarcolemma and hyper-capillarisation of the muscle. We show that these modifications not only bring about normalization of many ultrastructural abnormalities in the hypertrophic muscles of $Mtn^{-/-}$ mice, but the $Mtn^{-/-}/Err\gamma^{Tg/+}$ mice even outperform wild type mice during an incremental exercise test. Secondly that the hypertrophic oxidative muscles from the $Mtn^{-/-}/Err\gamma^{Tg/+}$ mice do not follow the dogma regarding metabolism and satellite cells number. We actually show that the metabolic reprogramming in this study led to a decrease in satellite cell number. However, this deficit did not impact at all in terms of the muscle's ability to regenerate. We believe this highlights the importance of the microcirculation during regeneration and has major clinical implications.

Results

Body and skeletal muscle mass

Introduction of *Err* γ in a skeletal muscle-specific manner into the $Mtn^{-/-}$ background to generate double transgenic $Mtn^{-/-}/Err\gamma^{Tg/+}$ resulted in viable, fertile offspring that were born at the expected Mendelian ratios. Firstly, we found that the HSA promoter used induced robust over-expression of *Err* γ in the $Mtn^{-/-}$ background (Figure 1A). The body mass of WT, $Mtn^{-/-}$ and $Mtn^{-/-}/Err\gamma^{Tg/+}$ animals was similar at 12 weeks of age (Figure 1B). However, the EDL, gastrocnemius, soleus and TA muscles were in both $Mtn^{-/-}$ and $Mtn^{-/-}/Err\gamma^{Tg/+}$ approximately 43%, 44%, 47% and 70% larger than their WT counterpart, respectively (Figure 1C–F). Importantly, there was no significant difference in mass for any of the muscles from $Mtn^{-/-}$ and $Mtn^{-/-}/Err\gamma^{Tg/+}$ mice (Figure 1C–F).

Exercise capacity

Using the running to exhaustion protocol on a treadmill, we found that $Mtn^{-/-}$ mice performed worse than WT. However the $Mtn^{-/-}/Err\gamma^{Tg/+}$ ran for approximately 80% longer than the $Mtn^{-/-}$ and 25% longer than the WT mice (Figure 1G).

Force generating capacity

We found that the maximal isometric tetanic force generated by the EDL of $Mtn^{-/-}$ was not significantly different from that of the WT mice, despite the larger muscle mass (Figure 1H). The tetanic force generated by $Mtn^{-/-}/Err\gamma^{Tg/+}$ EDL was, however, greater than that of the EDL from both WT and $Mtn^{-/-}$ mice. We next calculated the Specific Force (sP_o), the tetanic force per muscle mass. The sP_o of the EDL of $Mtn^{-/-}$ mice was lower than that of the other groups, with that of the $Mtn^{-/-}/Err\gamma^{Tg/+}$ mice being significantly greater than $Mtn^{-/-}$ mice, but not normalized to WT levels (Figure 1I). We also examined the force generating capacity of the soleus. The tetanic force of $Mtn^{-/-}$ soleus muscle was significantly lower than those of WT. There was no difference in this parameter between the soleus muscles of WT and $Mtn^{-/-}/Err\gamma^{Tg/+}$ (Figure 1—figure supplement 1A). The specific force of the soleus showed the same overall profile as that of the EDL but did not reach statistical significance, possibly due to low sample size (Figure 1—figure supplement 1A).

Muscle fibre number, area and MHC profile

The increased muscle mass in $Mtn^{-/-}$ mice are due to both hypertrophy and hyperplasia. We found that the introduction of *Err* γ into $Mtn^{-/-}$ did not significantly change the number of fibres normally seen in $Mtn^{-/-}$ EDL (Figure 2A–B) or soleus muscles (Figure 2—figure supplement 1A–B) both of which were greater than in WT. The fibre sizes were equivalent in the EDL of $Mtn^{-/-}$ and $Mtn^{-/-}/Err\gamma^{Tg/+}$ mice. Of particular note was that the MHCIIb fibres in the EDL were approximately 270% larger in both $Mtn^{-/-}$ and $Mtn^{-/-}/Err\gamma^{Tg/+}$ compared to WT (Figure 2B). The other notable result was the smaller size of MHCIIa fibres in $Mtn^{-/-}/Err\gamma^{Tg/+}$ than $Mtn^{-/-}$, but they were still larger than those in the WT (Figure 2B).

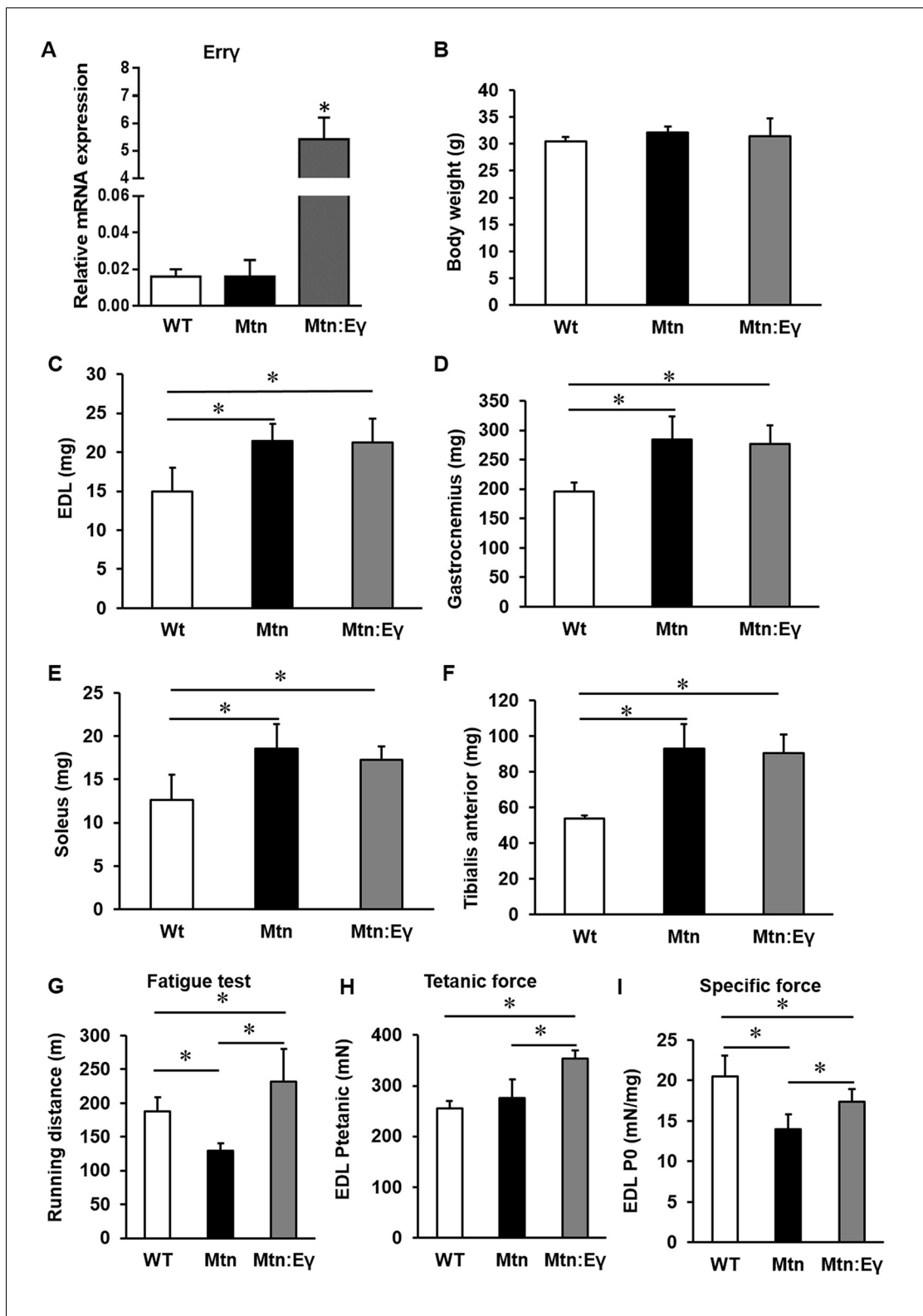


Figure 1. Concomitant skeletal muscle hypertrophy and tissue specific expression of ERRγ and resultant fatigue resistant characteristics. (A) ERRγ mRNA levels. (B) Body and (C–F) skeletal muscle mass in wild type (Wt), myostatin null (Mtn) and ERRγ transgenic mice on the myostatin null background (Mtn:Ey). (G) Exercise tolerance test on a mouse treadmill. (H–I) Contractile properties of the EDL muscle. Specific force denotes tetanic force normalized to wet muscle mass. N = 5 male twelve-week old mice per group; One-way ANOVA followed by Bonferroni’s multiple comparison tests, *p<0.05.

Figure 1 continued on next page

Figure 1 continued

DOI: 10.7554/eLife.16940.002

The following figure supplement is available for figure 1:

Figure supplement 1. Contractile properties of the soleus.

DOI: 10.7554/eLife.16940.003

Introduction of Erry into *Mtn*^{-/-} caused a partial reversal of MHC profile of *Mtn*^{-/-} towards the WT condition in all muscles examined (**Figure 2C** and **Figure 2—figure supplement 1A and C**). This conversion was only detected within the MHCII subtypes but did not extend to normalization of the proportion of MHC I fibres; in the soleus of *Mtn*^{-/-}/*Erry*^{Tg/+}, the proportion of MHC IIB fibres was lower than that in *Mtn*^{-/-} while that of MHC IIA fibres was higher. Nevertheless, both *Mtn*^{-/-} and *Mtn*^{-/-}/*Erry*^{Tg/+} display a lower proportion of MHC I fibres in the soleus muscle than WT (**Figure 2C**).

Next, we examined the mechanism underpinning fibre enlargement. We found that the levels of phosphorylated Akt (an inducer of anabolism) were higher in the muscle of *Mtn*^{-/-} and *Mtn*^{-/-}/*Erry*^{Tg/+} compared to WT (**Figure 2D**). A similar relationship was discovered for its downstream target 4EBP1 (**Figure 2D**). Akt not only promotes protein synthesis but also suppresses catabolism partly by phosphorylating and thereby inactivating FoxO3. We found that deletion of *Mtn* resulted in an increased ratio of the inactive:active (phosphorylated:non-phosphorylated) form of FoxO3. However, in muscles of *Mtn*^{-/-}/*Erry*^{Tg/+} mice the levels of inactive FoxO3 were lower than in that of the *Mtn*^{-/-} (**Figure 2D**).

Oxidative fibre profiling and vascular organisation

In all muscles examined, the intensity of the SDH staining (measure of oxidative activity) of fibres was lower in muscle from *Mtn*^{-/-} compared to WT (**Figure 3A** and **Figure 3—figure supplement 1A–B**). However, upon over-expression of Erry, the intensity of SDH staining in fibres of *Mtn*^{-/-} muscle was restored to that of WT. Indeed, also the number of SDH positive fibres was higher than that seen in even the WT muscles albeit not significantly so (**Figure 3A** and **Figure 3—figure supplement 1C**). Introduction of Erry into *Mtn*^{-/-} also caused normalization of the number PAS positive fibres (**Figure 3A** and **Figure 3—figure supplement 1D**). The capillary to fibre ratio (C:F); was lowest in the muscles of *Mtn*^{-/-} mice and highest in those of the *Mtn*^{-/-}/*Erry*^{Tg/+} mice (**Figure 3B**).

Metabonomics

The muscle metabolite profile was characterized by ¹H NMR spectroscopy. To identify any metabolic variation driven by the genotypic differences, principal components analysis (PCA) was applied to these profiles. A clear clustering was observed in the scores plot comparing all three genotypic groups demonstrating that they had distinctive metabolite profiles (**Figure 3C**). Comparing the metabolic signature of the *Mtn*^{-/-} muscle to the *Mtn*^{-/-}/*Erry*^{Tg/+} showed clear differences between the two groups (**Figure 3C**) characterised by significantly greater levels of muscle lactate in *Mtn*^{-/-} muscle compared to that of the *Mtn*^{-/-}/*Erry*^{Tg/+} consistent with a greater glycolytic phenotype. Furthermore the levels of creatine/phosphocreatine were also more pronounced in the muscle from *Mtn*^{-/-} compared to *Mtn*^{-/-}/*Erry*^{Tg/+}. Erry modification led to higher taurine and anserine content in the muscle of these animals.

Therefore, histochemical and NMR muscle profiles of the three genotypic groups provide further evidence that Erry modification of *Mtn*^{-/-} results in a remodeling of phenotype to a state that differentiates it not only from *Mtn*^{-/-} but also WT.

Metabolic gene profile

Key molecular and cellular features that would explain the metabolic profile of *Mtn*^{-/-}/*Erry*^{Tg/+} muscle were defined. In the first instance, we examined key regulators of energy metabolism. We found that Erry over-expression induced changes in levels of two key transcriptional regulators of metabolism; *Per1* and *Pgc1a* in *Mtn*^{-/-} muscle (**Figure 4A**).

Next, we examined the expression of key regulators of glucose and fatty acid oxidation (*Glut1*, *Glut4*, *Pdk4* and *Had*, *Lpl* and *Cyts* respectively). We found that *Glut4* and *Pdk4* were lower in *Mtn*^{-/-}/*Erry*^{Tg/+} compared to *Mtn*^{-/-}. Moreover, *Had* and *Lpl*, was higher in *Mtn*^{-/-}/*Erry*^{Tg/+} than in

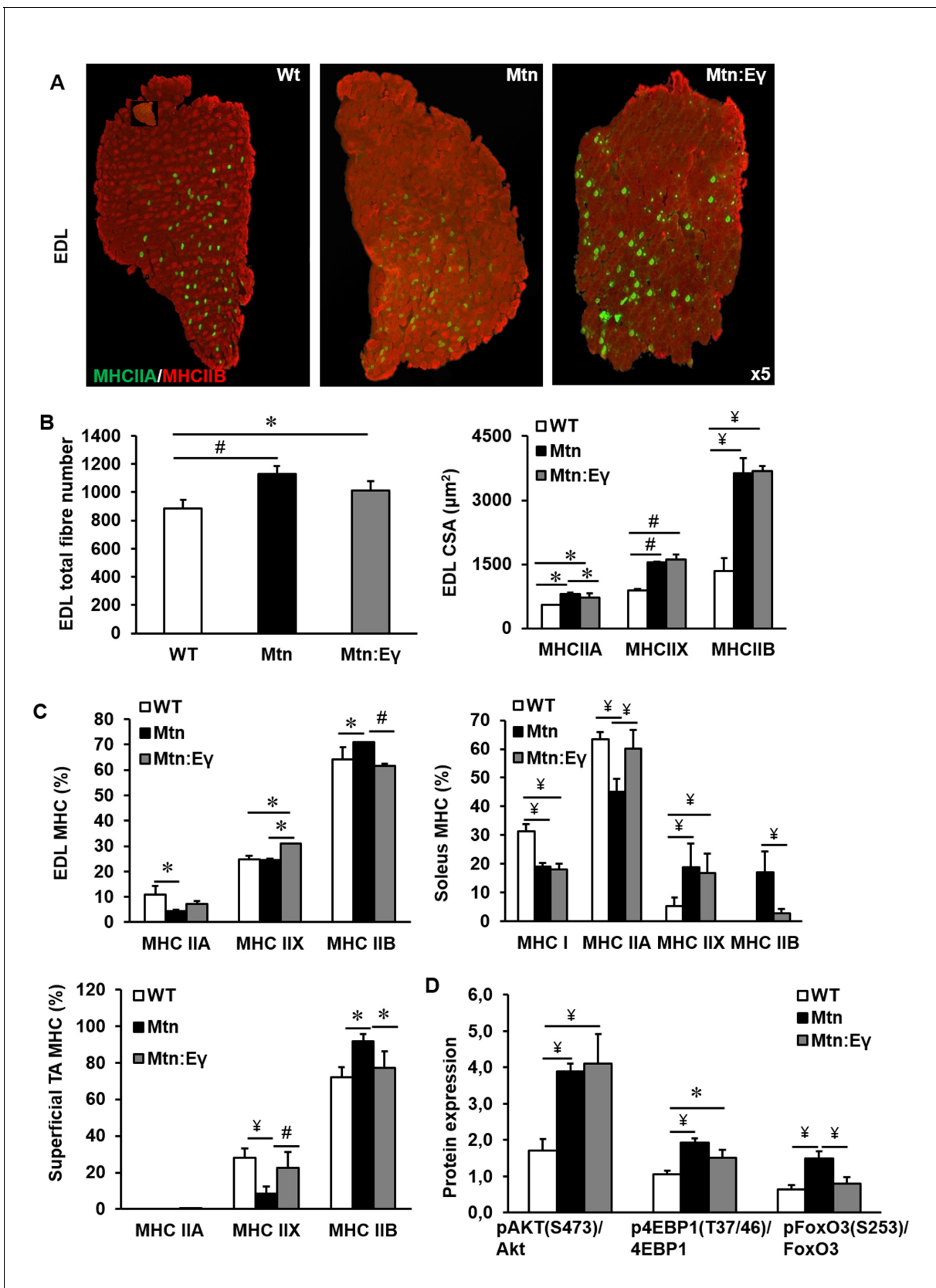


Figure 2. Musclespecific expression of ERR γ maintain the hyperplasia in the myostatin null background and normalizes myosin type II phenotype. (A) Representative immunohistochemical images for MHC IIA and IIB staining in the EDL muscle. (B) EDL total fibre number and myofibre cross sectional area. (C) EDL and Soleus MHC (%) and Superficial TA MHC (%). (D) Protein expression of pAKT(S473)/Akt, p4EBP1(T37/46)/4EBP1, and pFoxO3(S253)/FoxO3. Figure 2 continued on next page

Figure 2 continued

area (CSA, μm^2). (C) EDL, soleus and superficial TA muscle fibre type composition (D) Protein expression of key regulators that control anabolism (pAKT, p4EBP1) and catabolism (pFoxO3) in the gastrocnemius muscle. N = 5 male twelve-week old mice per group; One-way ANOVA followed by Bonferroni's multiple comparison tests, * $p < 0.05$, # $p < 0.01$, ¥ $p < 0.001$.

DOI: 10.7554/eLife.16940.004

The following figure supplement is available for figure 2:

Figure supplement 1. Reprogramming of the soleus myostatin null muscle by ERR γ .

DOI: 10.7554/eLife.16940.005

Mtn^{-/-}. Of particular note was the finding that the expression of markers of fatty acid metabolism, *Had* and *Lpl*, were not only higher in *Mtn*^{-/-}/*Erry*^{Tg/+} than in *Mtn*^{-/-} but also than in the WT condition (Figure 4A).

Oxidative metabolism relies on oxygen that can be stored in muscle by myoglobin. Secondly, oxidative metabolism generates destructive radicals which can be broken down by enzymes including catalase. We found that expression of *myoglobin*, which facilitates the diffusion of oxygen, and *catalase*, an anti-oxidant enzyme, were higher in the muscle of *Mtn*^{-/-}/*Erry*^{Tg/+} than in WT and *Mtn*^{-/-} mice (Figure 4A).

Then we investigated genes that control oxidative energetics and examined the expression of molecules controlling fat metabolism (fatty acid transport and uptake molecules: *Cd36*, *Slc25a20*, *Fatp1*, *Fabp3* and regulators of fatty acid oxidation: *Acadl*, *Acadm*). We found that all six genes were expressed to a higher degree in *Mtn*^{-/-}/*Erry*^{Tg/+} than in *Mtn*^{-/-} and WT mice (Figure 4A).

We established if the differences in oxidative metabolism between *Mtn*^{-/-} and *Mtn*^{-/-}/*Erry*^{Tg/+} in muscle were mirrored by factors related to the microvascular supply to the muscle. We found that the expression of endothelial mitogenic factors (*Vegfa165*, *Vegf189* and *Ffg1*) was lower in the muscles of *Mtn*^{-/-} than WT mice, but similar in those of *Mtn*^{-/-}/*Erry*^{Tg/+} and WT mice (Figure 4B).

Therefore, the musclespecific expression of *Erry* in *Mtn*^{-/-} mice not only normalizes its metabolic molecular profile but also results in a better microvascular supply of the muscle.

Ultra-structure

The ultra-structure of muscle in the three cohorts were examined. Using transmission electron microscopy, we found a number of abnormalities in the structure of muscle from *Mtn*^{-/-} mice heterogeneously sized sarcomeres, misaligned and disrupted Z-Lines, large inter-sarcomeric spaces and altered mitochondrial distribution and size (Figure 5A). In contrast, the muscle from *Mtn*^{-/-}/*Erry*^{Tg/+} largely lacked these abnormalities (Figure 5A). We found that the density of mitochondria in both sub-membrane and intrafusal locations was decreased significantly following the deletion of *Mtn*. However, the expression of *Erry* significantly increased the mitochondrial density at both locations compared to *Mtn*^{-/-} and at the major site, the sub-membrane region, increased it even compared to WT. Mitochondrial hypertrophy has been postulated to compensate for decreased mitochondrial number or function. Hypertrophy is thought to either protect against apoptosis or for functional mitochondria to fuse with aberrant ones resulting in the maintenance of cell function (Frank et al., 2001; Ono et al., 2001). Mitochondrial hypertrophy was evident in both compartments in muscle from *Mtn*^{-/-} (Figure 5B–E) and was normalized by *Erry* in the sub-membrane region (Figure 5D).

These results show that the deletion of *Mtn* leads to numerous ultra-structural abnormalities. Over-expression of *Erry* in the *Mtn*^{-/-} prevents almost all the ultra-structural abnormalities.

Myonuclear organization and satellite cell

We next examined the features of individual muscle fibres to determine the effect of *Erry* in *Mtn*^{-/-} mice. We found, that deletion of *Mtn* resulted in fewer satellite cells compared to WT and that the number of satellite cells was even lower in the muscles of the *Mtn*^{-/-}/*Erry*^{Tg/+} mice (Figure 6A,C and D). Next, we determined proliferation and differentiation characteristics of satellite cells in the three cohorts. We found that following 48 hr of culture, the number of progeny had increased in all the genotypes but the proportional relationship found in uncultured fibres persisted (Figure 6E–F). During the 48 hr period of culture, satellite cells not only divide but also form clusters (Figure 6G–H). We found that the number of clusters were similar in fibres from WT and *Mtn*^{-/-} (Figure 6G), but

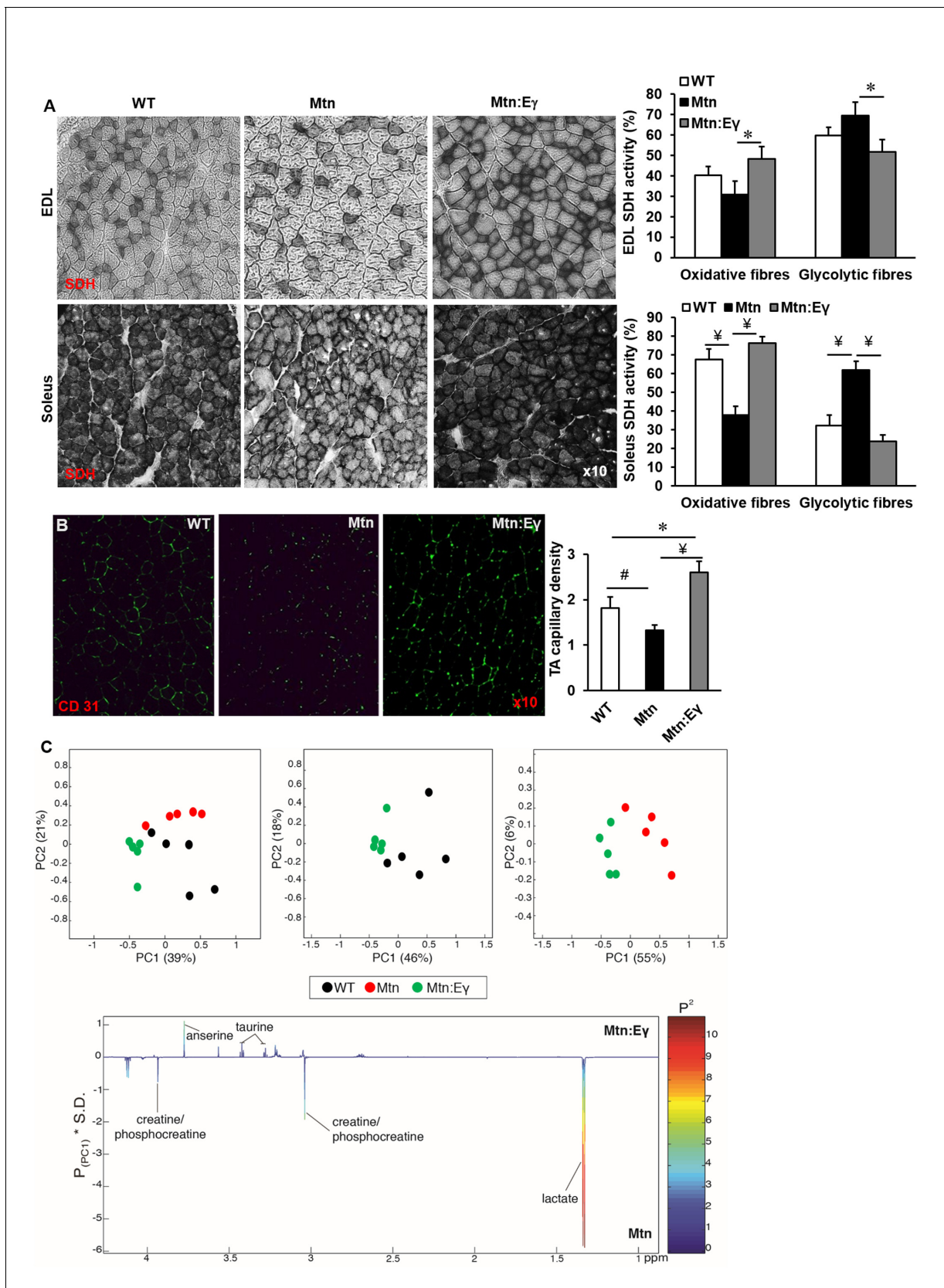


Figure 3. Musclespecific expression of ERR γ normalizes the metabolic and capillary profile of myostatin null mice. (A) SDH staining and quantification of EDL and soleus muscles of Wt, Mtn and Mtn:Ey mice. N = 5 male twelve-week old mice per group; One-way ANOVA followed by Bonferroni's

Figure 3 continued on next page

Figure 3 continued

multiple comparison tests, * $p < 0.05$, # $p < 0.01$, ¥ $p < 0.001$. (B) Muscle capillary density as determined by CD31 staining. (C) Pair-wise comparisons of the metabolic profiles obtained from the gastrocnemius muscle from WT, *Mtn* and *Mtn:Erry* mice. Principal components analysis (PCA) scores plots comparing WT, *Mtn* and *Mtn:Erry*; WT and *Mtn:Erry*; as well as *Mtn* and *Mtn:Erry*; (% variance in the parenthesis). Colour loadings plots shown for PC1 of the model comparing *Mtn* and *Mtn:Erry*. Product of PC loadings with standard deviation of the entire data set coloured by the square of the PC loading. DOI: 10.7554/eLife.16940.006

The following figure supplement is available for figure 3:

Figure supplement 1. Reprogramming of the tibialis anterior muscle of myostatin null mice by ERR γ .

DOI: 10.7554/eLife.16940.007

there were fewer clusters in the *Mtn*^{-/-}/*Erry*^{Tg/+}-derived cultures. The number of cells per cluster was highest in WT and lowest in the *Mtn*^{-/-} with that of the *Mtn*^{-/-}/*Erry*^{Tg/+} in between the two (Figure 6H). Finally, we found deletion of *Mtn* and the introduction of *Erry* did not impact on the process of differentiation (Figure 6I).

Myonuclear number and organization were then determined. First, there were significantly more myonuclei in the fibres of *Mtn*^{-/-}/*Erry*^{Tg/+} compared to WT (Figure 6A–B). Secondly, we examined the distribution of myonuclei within a fibre. This is thought to be a regulated process since myonuclei position is important to minimize issues related to macromolecule movement in larger cells. Therefore the degree of regulation is inversely proportional to random positioning of the nuclei (Bruusgaard et al., 2003). In order to quantify this, we calculated the distance to the nearest

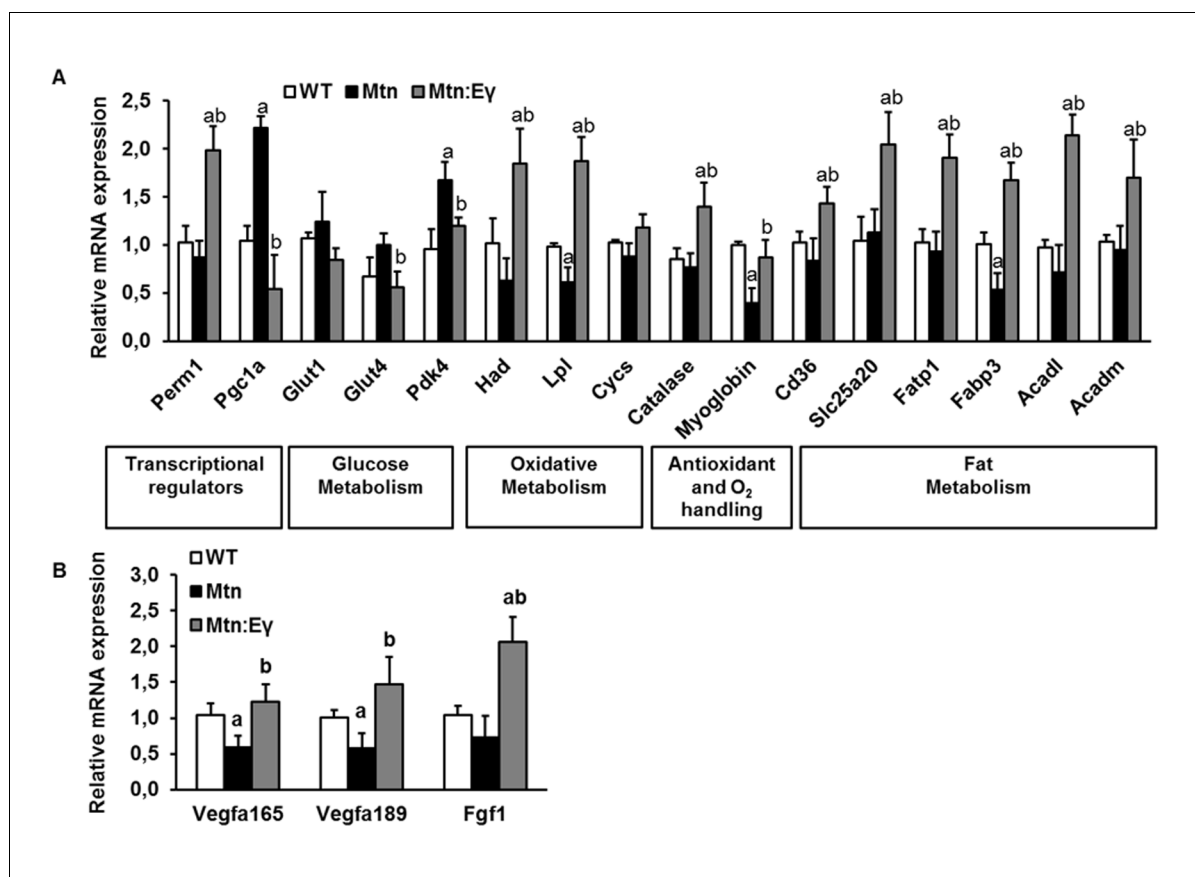


Figure 4. Molecular reprogramming of myostatin null muscle by ERR γ and its ability to promote capillary formation by the expression of angiogenic factors. (A) Gene expression levels of transcriptional regulators, glucose metabolism regulators, oxidative metabolism genes, antioxidant and oxygen handling genes and fat metabolism genes. (B) Angiogenic gene expression. ‘a’ denotes changed significantly from WT and ‘b’ denotes changes significantly from *Mtn*. N = 5 male twelve-week old mice per group; One-way ANOVA followed by Bonferroni’s multiple comparison tests, $p < 0.05$. DOI: 10.7554/eLife.16940.008

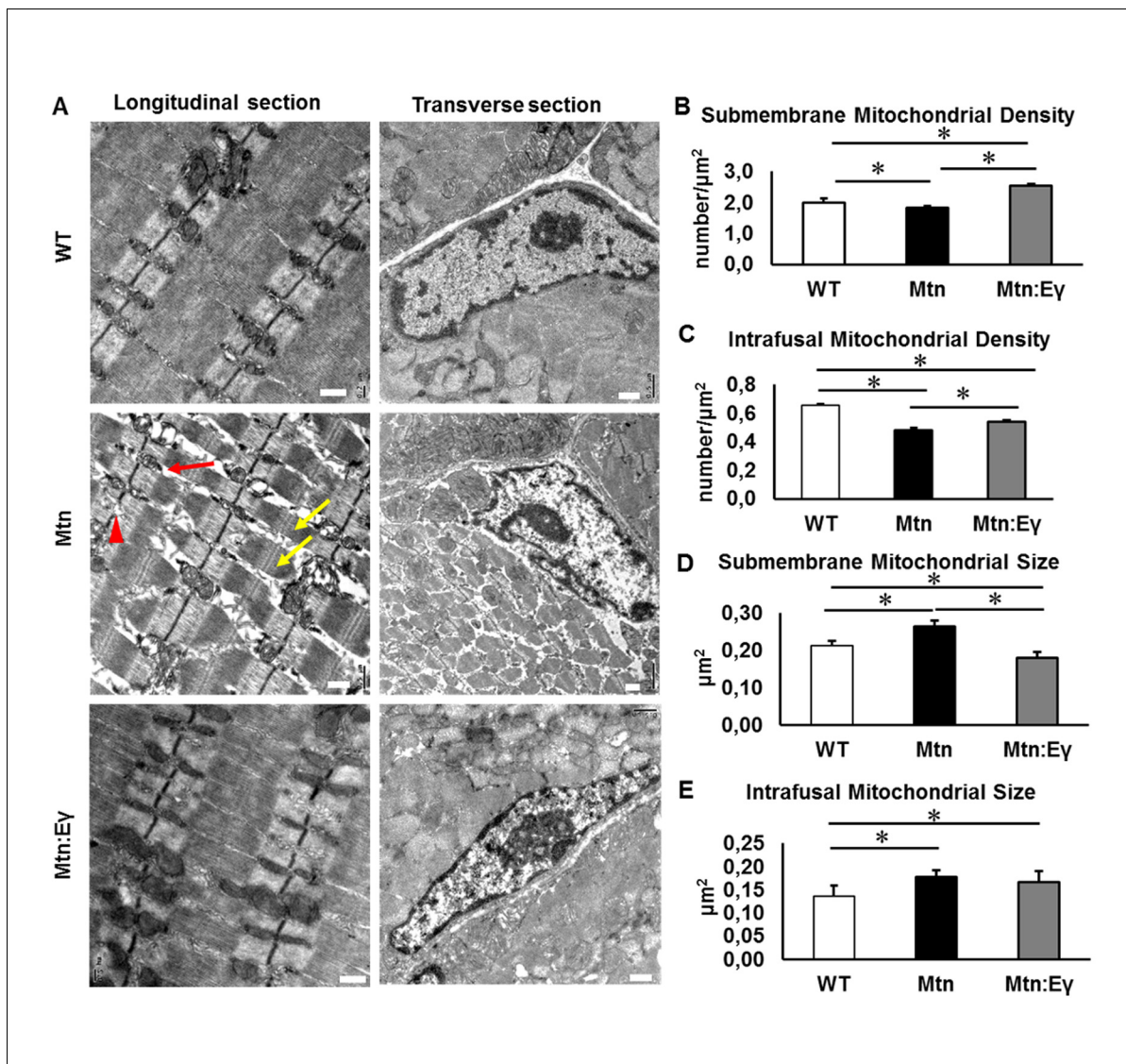


Figure 5. Musclespecific expression of ERR γ normalizes ultra-structural abnormalities myostatin null mice. (A) Transmission electron microscopy images in longitudinal and transverse sections of WT, *Mtn* and *Mtn:E γ* muscle, scale 0.5 μm . Note the large spaces (red arrow) disrupted Z-lines (red arrowhead) and non-uniform sarcomere width (yellow arrows). (B) Quantification of submembrane mitochondrial density. (C) Quantification of Intrafusal mitochondrial density. (D) Quantification of submembrane mitochondrial size. (E) Quantification of intrafusal mitochondrial size. N = 3 male twelve-week old mice per group; One-way ANOVA followed by Bonferroni's multiple comparison tests, * $p < 0.05$.

DOI: [10.7554/eLife.16940.009](https://doi.org/10.7554/eLife.16940.009)

neighbour for the nuclei located at the periphery of single fibres from WT, *Mtn*^{-/-} and *Mtn*^{-/-}/*Err γ* ^{Tg/+} mice. Confocal stacks of single fibres labelled with DAPI (Figure 6J) were used to generate the 3D coordinates of each nucleus in a fibre (Figure 6K) using Imaris software. Using custom made software, a simulation of randomly and optimally distributed nuclei was compared to the actual distribution (see Materials and methods). The WT fibres displayed an improvement from a random distribution of 20%. However *Mtn*^{-/-} and *Mtn*^{-/-}/*Err γ* ^{Tg/+} fibres had distributions that were more random, with significantly lower improvements of 10% and 4%, respectively (Figure 6L). These results show that the expression of *Err γ* in the *Mtn*^{-/-} does not normalize key features related to either the satellite cells, myonuclei number or their positioning.

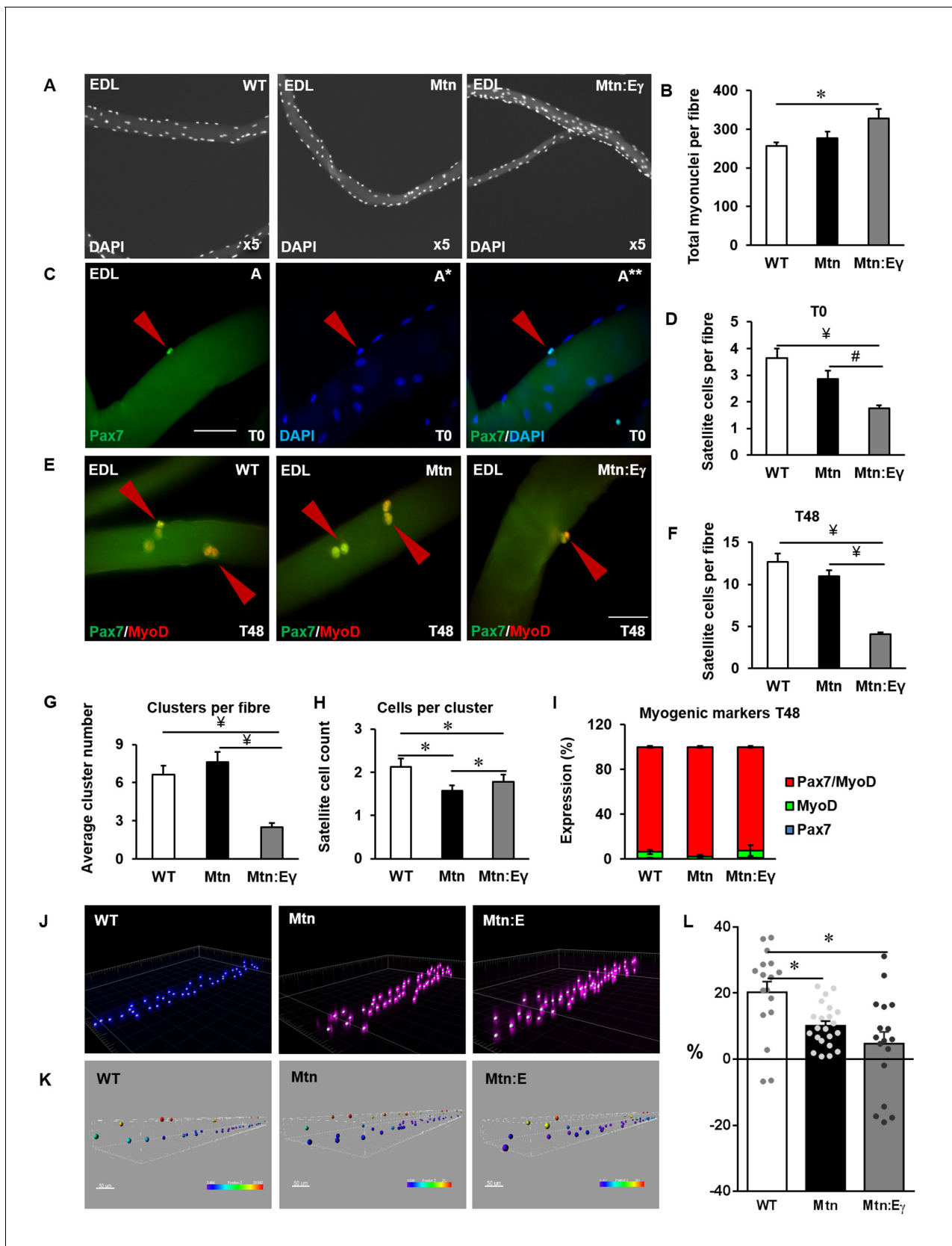


Figure 6. Oxidative muscle developed through $ERR\gamma$ in the muscle of myostatin null mice shows depletion of satellite cells and increased myonuclear content. (A) Single EDL muscle fibres stained with DAPI to visualize myonuclei. (B) Quantification of myonuclear number in EDL fibres. (C) Quiescent Figure 6 continued on next page

Figure 6 continued

satellite cells stained for Pax7 on freshly isolated ($T = 0$ hr) muscle fibres from the EDL (arrowhead). (D) Quantification of satellite cell number on freshly isolated EDL fibres. (E) Single muscle fibres after 48 hr in cell culture stained for DAPI, Pax7 and MyoD (arrowhead). (F) Quantification of total number of cells on muscle fibre at 48 hr. (G) Quantification of satellite cell clusters at 48 hr. (H) Cluster size at 48 hr on muscle fibres. (I) Profiling of differentiation at 48 hr. (J) Confocal stacks of single fibres labelled with DAPI to study myonuclear organization. (K) Virtual reconstruction of single muscle fibres, colour encodes distance in the z-plane. (L) Improvement in myonuclear organization, where 0% denote a random distribution. Fibres were from 4 male twelve-week old mice per group; One-way ANOVA followed by Bonferroni's multiple comparison tests, * $p < 0.05$, # $p < 0.01$, ¥ $p < 0.001$.

DOI: 10.7554/eLife.16940.010

Skeletal muscle regeneration

Thus, far all the changes in muscle resulting from the over-expression of Erry in the $Mtn^{-/-}$ were beneficial except for a lower number of satellite cells. In this section we determined the consequence of this deficit on the ability of skeletal muscle to regenerate, a process reliant on satellite cells. To that end, we induced injury of the TA using cardiotoxin and the progression of regeneration assessed at three crucial time points; day three (D3) as the process of debris clearance is ongoing and regeneration of fibres begins, day six (D6) when robust fibre regeneration can be quantified and day fourteen (D14) when debris clearance has been completed.

At D3 the muscle clearance of dying fibres was slowest in $Mtn^{-/-}$ compared to the other two genotypes (Figure 7A–B). Clearance is mediated in part by macrophages and we found that the density of macrophages was highest in the muscle of $Mtn^{-/-}/Erry^{Tg/+}$ compared to either $Mtn^{-/-}$ or WT (Figure 7C–D). Furthermore, we found that the TA from $Mtn^{-/-}/Erry^{Tg/+}$ at the early stages of generation contained the highest number of committed muscle cells (Figure 7E–F).

By D6, there was a greater degree of regeneration (size of newly formed eMHC⁺ fibres) in $Mtn^{-/-}/Erry^{Tg/+}$ compared to either $Mtn^{-/-}$ or WT (Figure 7G–H) and a more advanced removal of dying fibres in $Mtn^{-/-}/Erry^{Tg/+}$ than in $Mtn^{-/-}$ (Figure 7I–J). We also found evidence for a lower amount of cell death in the regenerating areas of $Mtn^{-/-}/Erry^{Tg/+}$ than $Mtn^{-/-}$ or WT mice (Figure 7K–L). At D6 macrophage activity was still high in the muscle of $Mtn^{-/-}/Erry^{Tg/+}$ compared to either $Mtn^{-/-}$ or wild type (Figure 7M–N) as were the number of committed (Myo⁺/Pax7⁺) muscle progenitor cells (Figure 7O–P). Precocious differentiation could lead to an exhaustion of cells which would ultimately attenuate fibre size. To examine this line of thought we examined damaged muscles at an advanced stage of regeneration (D14). We found further evidence for accelerated regeneration in the $Mtn^{-/-}/Erry^{Tg/+}$ compared to either $Mtn^{-/-}$ or WT gauged by a decrease in the density of fibres still expressing eMHC (Figure 7—figure supplement 1A). Importantly, there was no deficit in the size of newly regenerated fibre in the muscle of $Mtn^{-/-}/Erry^{Tg/+}$ mice (Figure 7—figure supplement 1B). These results show that even though the muscles of $Mtn^{-/-}/Erry^{Tg/+}$ have fewer satellite cells than the muscles of the WT and $Mtn^{-/-}$ mice, their muscle regenerating capacity exceeds that of both $Mtn^{-/-}$ and WT mice.

Non-genetic post-natal induction of oxidative skeletal muscle growth

Our newly generated hypermuscular, hyper-oxidative mouse line ($Mtn^{-/-}/Erry^{Tg/+}$) displays a number of characteristics that make them attractive both in terms of physiology and regeneration. However, the muscle phenotype in these models is largely established during embryonic and post-natal development. Therefore, we next established if similar phenotypes could be obtained via non-genetic modifications. To do so, we inhibited Mtn at post-natal stages in $Erry^{Tg/+}$ mice (which displays an increased oxidative profile) by weekly injections of soluble activin receptor IIB protein (sActRIIB), which has been shown to antagonize signalling mediated by myostatin and related-proteins.

Following 8 weeks of weekly injections we found that sActRIIB caused an increase in the body mass of both WT and $Erry^{Tg/+}$ mice (Figure 8A). Examination of isolated muscles showed an increase in muscle mass of approximately 70% in the EDL of WT and 44% in $Erry^{Tg/+}$ above age-matched control animals (Figure 8B). Other muscles examined showed a similar increase in muscle mass (Figure 8—figure supplement 1A). The increase in muscle mass was not due to an increase in fibre number (data not shown) but due to hypertrophy of all MHC fibre types (Figure 8—figure supplement 1B). There was no change in the MHC fibre type composition following the injection of sActRIIB in either genotype (Figure 8C and F). However, we found that injection of sActRIIB induced a decrease in the oxidative capacity of the muscle in WT mice as indicated by a decreased proportion

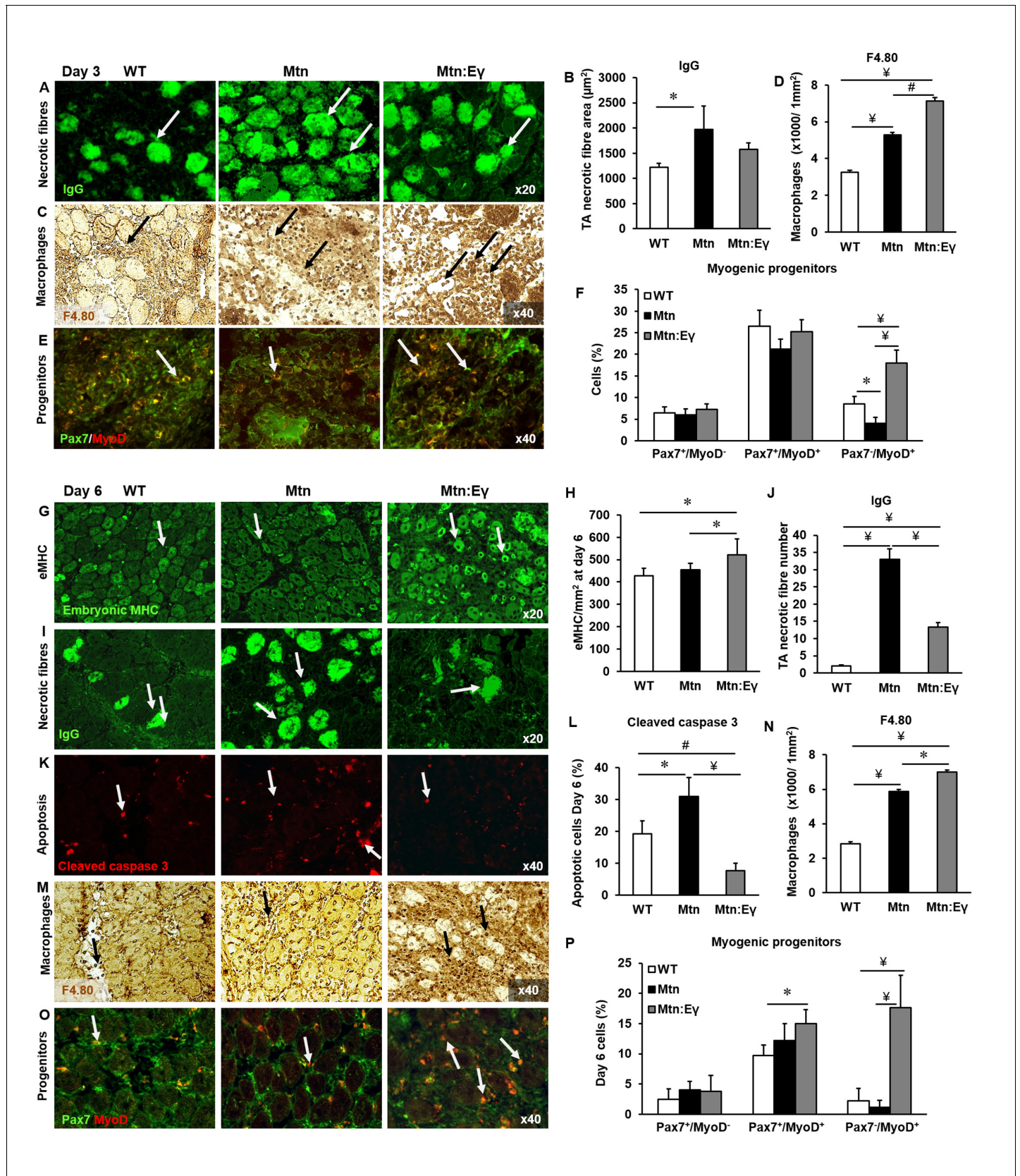


Figure 7. Skeletal muscle regeneration is accelerated by the expression of Erry in myostatin null mice through enhanced macrophage and satellite cell activity. Skeletal muscle regeneration in response to cardiotoxin injury. (A) Muscle necrotic fibres visualized by IgG staining at Day 3 (arrows). (B) Figure 7 continued on next page

Figure 7 continued

Quantification of dying fibre size at Day 3. (C) Macrophage infiltration in the TA muscle using an F4.80 antibody at Day 3 (arrows). (D) Quantification of macrophage density in damaged muscle. (E) Myogenic progenitors at Day 3. Pax-7 detection in green, MyoD expressing cells in red (arrows). (F) Quantification of uncommitted muscle cells (Pax-7⁺/MyoD⁻), precursor (Pax-7⁺/MyoD⁺) and committed (Pax-7⁻/MyoD⁺) muscle cells at Day 3. (G) Expression of embryonic myosin heavy chain on Day 6 (arrows). (H) Quantification of regenerating muscle fibres at Day 6. (I) Necrotic fibres at Day 6 detected via infiltrated fibre IgG profiling (arrows). (J) Quantification of dying muscle fibres at Day 6. (K) Cleaved caspase 3 staining at Day 6 as a marker of apoptosis (arrows). (L) Quantification of apoptotic density at Day 6. (M) Macrophage infiltration in the TA on Day 6 (arrows). (N) Quantification of macrophage infiltration at Day 6. (O) Myogenic progenitors on Day 6. Pax-7 detection in green, MyoD expressing cells in red (arrows). (P) Quantification of uncommitted muscle cells (Pax-7⁺/MyoD⁻), precursor (Pax-7⁺/MyoD⁺) and committed (Pax-7⁻/MyoD⁺) muscle cells at Day 6. N = 4/5 male twelve-week old mice per group; One-way ANOVA followed by Bonferroni's multiple comparison tests, *p<0.05, #p<0.01, ¥p<0.001.

DOI: [10.7554/eLife.16940.011](https://doi.org/10.7554/eLife.16940.011)

The following figure supplement is available for figure 7:

Figure supplement 1. Characterisation of regenerating tibialis anterior muscle at day 14.

DOI: [10.7554/eLife.16940.012](https://doi.org/10.7554/eLife.16940.012)

of SDH⁺ fibres (**Figure 8D and G**). Strikingly, sActRIIB did not cause a reduction in the proportion of SDH⁺ fibres in *Erry*^{Tg/+} (**Figure 8D and G**). The increased oxidative capacity of the muscle was accompanied with a rise in the number of capillaries serving each fibre in the muscle from *Erry*^{Tg/+} but not WT mice (**Figure 8E and H** and **Figure 8—figure supplement 1D**). These results show that it is possible to induce substantial muscle enlargement while maintaining oxidative capacity, challenging the generally accepted dogma that the size and oxidative capacity of a fibre are, because of diffusion constraints, inversely related.

Discussion

The main observations of this study are firstly that substantial hypertrophy can occur without a concomitant reduction in fibre oxidative capacity. This observation challenges the dogma that there is a trade-off between muscle fibre size and oxidative capacity. Secondly, our results challenge the notion that slow oxidative muscle has a higher number of satellite cells than those that are fast glycolytic.

A number of studies have shown that deletion of myostatin leads to the development of hypertrophic muscle. Although such enlarged muscles appear essentially normal at the histological level, their ability to generate tension is impaired, particularly during prolonged periods of work (**Amthor et al., 2007; Mendias et al., 2006; Relizani et al., 2014**). The higher than normal fatigability of the muscle could be attributable to the lower number of mitochondria consequent to deletion of myostatin in the germline (**Amthor et al., 2007**).

To alleviate this mitochondrial deficit in *Mtn*^{-/-} mice, we introduced the expression of *Erry* into skeletal muscle. This gene is highly expressed in tissues with a high oxidative capacity, such as the heart, kidneys, brain and slow oxidative skeletal muscle where it has been demonstrated to trigger mitochondrial biogenesis (**Hong et al., 1996; Heard et al., 2000; Giguère, 2008; Narkar et al., 2011**). Introduction of *Erry* overexpression that would increase oxidative capacity on a *Mtn*^{-/-} background that is associated with hypertrophy would challenge the trade-off that is thought to exist between oxidative capacity and fibre size (**Van Der Laarse et al., 1997; Degens, 2012**).

One of the key features of *Mtn*^{-/-} muscle is the lower SDH activity, indicative of a low oxidative status. This combination of a low oxidative capacity and a large fibre size fits nicely with the concept of the trade-off between fibre size and oxidative capacity. It also is associated with a larger proportion of type IIB fibres than seen in muscles from WT mice. Here we show that even though the muscle mass and fibre sizes did not differ between *Mtn*^{-/-} and *Mtn*^{-/-}/*Erry*^{Tg/+} mice, the latter had a higher SDH activity.

The higher SDH activity in *Mtn*^{-/-}/*Erry*^{Tg/+} than *Mtn*^{-/-} mice was associated with a partial normalisation of the MHC fibre profile; a decrease in the proportion of IIB fibres in all muscles examined. What was conspicuous, however, was the absence of normalization of the proportion of MHC I fibres. We believe that this is significant and reveals a key feature of the influence of a metabolic programme on muscle physiology. We suggest that the oxidative programme, here driven by *Erry*, readily converts IIB to IIA fibres but is that it is unable to induce the transition to type I MHC

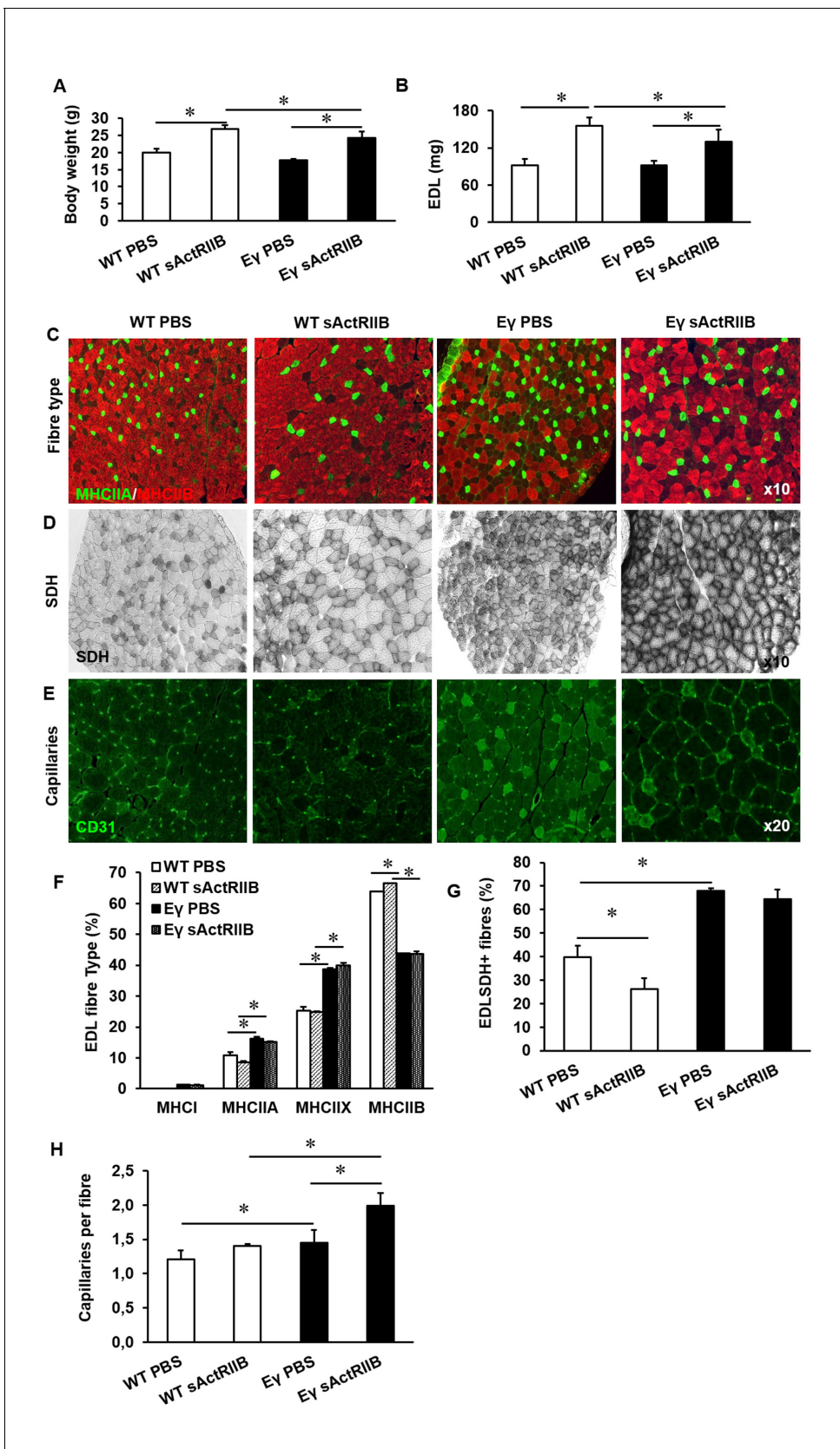


Figure 8. Post-natal inhibition of myostatin in the muscle-specific *ERRγ* mice leads to hypertrophic muscle with enhanced oxidative and vascular features. (A) Body mass in 12-week-old mice after an 8 week treatment regime. (B) EDL muscle mass after sActRIIB treatment. (C) Muscle fiber type Figure 8 continued on next page

Figure 8 continued

profiling with MHCIIA (green) and MHCIIIB (red) antibodies. (D) Oxidative enzyme profiling using SDH histochemistry. (E) Muscle capillary density profiling with CD31 antibody. Quantification of (F) MHC EDL fibre type, (G) SDH positive fibres, (H) capillary density. Intrafibre staining in the *Erry* muscle in (D) is artefact and was ignored in all quantification procedures; One-way ANOVA followed by Bonferroni's multiple comparison tests, * $p < 0.05$.

DOI: [10.7554/eLife.16940.013](https://doi.org/10.7554/eLife.16940.013)

The following figure supplement is available for figure 8:

Figure supplement 1. Muscle characterisation after post-natal inhibition of myostatin in the muscle specific *Erry* mice.

DOI: [10.7554/eLife.16940.014](https://doi.org/10.7554/eLife.16940.014)

isoforms. Energy status (ATP/ADP or phosphocreatine) has been implicated as a determinant of the MHC fibre type with high levels inducing ever more fast forms in keeping with their myofibrillar ATPase activity (Conjard et al., 1998; Bottinelli et al., 1994). We show here from our NMR profiling that indeed the muscle of *Mtn*^{-/-} has high levels of phosphocreatine, which would be in keeping with the high ATPase activity of Type IIB fibres found in its muscle. Furthermore, we show *Erry* over-expression in the muscle of *Mtn*^{-/-} normalizes this feature yet does not lead to the formation of I fibres. This observation adds to a growing body of evidence that the type II programme is plastic and adaptable whereas the Type I fibres are more resistant to change (Sutherland et al., 1998) and may not be part of the IIB ↔ IIX ↔ IIA continuum. Indeed a number of studies have questioned whether the 'final step' (conversion of Type IIA to I) is even possible. Development of type I fibres has been described in a number of conditions, for example following Chronic low-frequency stimulation (CLFS) (Peucker et al., 1999; Kwong and Vrbová, 1981). However, these studies never examined whether Type I were formed as a consequence of the remodeling of Type II fibres or through the formation of new fibres, a process that would require satellite cells. Indeed the development of Type I fibres following extended CLFS can only be induced to significant levels when accompanied by robust myofibre regeneration (Pette et al., 2002; Maier et al., 1988). Taken together, these studies imply that myostatin signalling acts at an embryonic/foetal stage of muscle development to pattern a subpopulation of satellite cells/muscle precursors in a muscle specific manner to form Type I fibres. The protocol of over-expressing *Erry* used in this study is unable to influence this process.

One of the intriguing aspects of the *Mtn*^{-/-} phenotype is the concurrence of a larger muscle mass and a low oxidative capacity, as also reflected by a low mitochondrial content (Amthor et al., 2007). As mentioned above, this association corresponds with the prediction of the concept of a trade-off between muscle fibre size and oxidative capacity. There could, however, also be another function for the high glycolytic capacity. For instance, the Warburg Effect is the observation that most cancer cells rely on glycolysis even in the presence of oxygen (Warburg et al., 1927) for the production of intermediates essential for the building blocks of any cell including nucleic acids, lipids and proteins (Deberardinis et al., 2008). In a similar way, glycolysis in the muscles of *Mtn*^{-/-} mice may support the high levels of protein synthesis required for the initial muscle hypertrophy and maintenance of the large muscle mass. An interesting point is that such cells are not only dependent on glycolysis but also often have decreased oxidative phosphorylation capacity (Petros et al., 2005). Where the similarities between the Warburg Effect in cancer cells and findings from this study differ is the outcome following an intervention that promotes oxidative metabolism. In cancer cells such an intervention reduces cell growth (Wang and Moraes, 2011) while we have shown with *Erry* overexpression on a *Mtn*^{-/-} background not only re-establishes the oxidative capacity but also maintains the hypertrophic state. Consistent with the oxidative metabolic phenotype of the *Mtn*^{-/-}/*Erry*^{Tg/+} mice are the higher levels of taurine and anserine observed in the NMR metabolomic analysis, since taurine is positively correlated with the oxidative capacity of muscle tissues (Dunnett et al., 1997). Anserine is β-alanine and histidine related dipeptide with antioxidant properties commonly found in skeletal muscle of many animals (Kohen et al., 1988). Thus, it may act as a scavenging agent of the byproducts arising from elevated oxidative activity in the muscle of *Mtn*^{-/-}/*Erry*^{Tg/+} mice.

A number of studies have suggested that fibres that rely on oxidative phosphorylation limit their size in order that oxygen from the capillaries diffuses efficiently into the cells and to the mitochondria for ATP production (Kinsey et al., 2007; Van Der Laarse et al., 1997; van Wessel et al., 2010). The large fibres with a low oxidative capacity in *Mtn*^{-/-} mice conform to this concept and have a low capillary supply per fibre. During compensatory hypertrophy the time course of angiogenesis

and fibre hypertrophy are similar (Egginton et al., 1998; Pyley et al., 1998) and the capillary supply to a fibre is related to the size of the fibre (Ahmed et al., 1997; Degens et al., 1994). Such a coupling between the fibre size and capillary supply seems to be altered in the *Mtn*^{-/-} mice in such a way that they have fewer capillaries than expected for the size of the fibre. However, over-expression of Erry in either WT or *Mtn*^{-/-} drives a robust angiogenic gene programme, increases the number of capillaries per fibre and ultimately muscle blood flow as shown previously (See Figure 3B and (Narkar et al., 2011; Matsakas et al., 2012b)). An important finding here is that the angiogenesis programme promoted by muscle expression of Erry is responsive to change in fibre size so that when a fibre grows, it stimulates the formation of blood vessels presumably to ensure optimal perfusion (Figure 8H). Two additional modifications take place, an increase in myoglobin transcription and increasing the density of mitochondria at the sarcolemma that would sustain large oxidative fibres developed as a consequence of Erry in the *Mtn*^{-/-} background. These outcomes have been postulated to prevent a decline in maximum steady state power as an oxidative fibre increases size (Hickson, 1980; Heard et al., 2000).

In this study, we show that the muscle hypertrophy that develops following germline deletion of *Mtn* has many ultrastructural abnormalities including splitting of sarcomeres, misaligned Z-lines and alteration in mitochondrial distribution and morphology. The maintenance of muscle structure is largely mediated by mechanisms that remove unwanted proteins and organelles through either the proteasome or autophagic pathways (Sandri, 2013; Bonaldo and Sandri, 2013). Furthermore, deregulated proteasome activity or autophagy leads to muscle wasting in a number of diseased conditions (Sandri et al., 2004; Carmignac et al., 2011). As these pathways are involved in anabolic processes, it seems intuitive that they should be tuned down in order to support muscle growth. Indeed, we show that the activity of a key regulator of these processes, FoxO3 is suppressed in the absence of *Mtn*. However, we show that Erry expression in muscle leads to a substantial normalization of the ultrastructure *Mtn*^{-/-} skeletal muscle as well an improvement in the specific force. Most importantly, we show that a more physiological measure of muscle function- fatigability, is not only normalized but exceeds the value of WT mice. Our data demonstrate that the suppression of FoxO3 activity is alleviated by Erry. We suggest that the molecular and organelle clearance programmes being mediated by FoxO3 are generally not anabolic but are rather there to maintain cellular homeostasis. However, when its activity is attenuated, it leads to an accumulation of structural abnormalities that compromises muscle function. Nevertheless, not all features of the *Mtn*^{-/-} muscle were normalised by Erry expression; Myonuclei in *Mtn*^{-/-} and *Mtn*^{-/-}/*Erry*^{Tg/+} were more disorganized than those in WT fibres. Proper nuclear positioning is probably required for normal muscle function, possibly due to irregular size and spacing of myonuclear domains (Metzger et al., 2012) and myonuclear disorganization is observed both in ageing skeletal muscle and in models of muscular dystrophies (Bruusgaard et al., 2006; Meinke et al., 2014). Additionally, accretion of myonuclei is a prerequisite for maintaining specific force during hypertrophy and mitochondrial protein systems have been suggested to play a role in defining myonuclear domain size in rodents (Liu et al., 2009). The increased number of myonuclei and increased synthesis of mitochondria in the *Mtn*^{-/-}/*Erry*^{Tg/+} mice might compensate for the observed disorganized myonuclei, restoring specific force and ultrastructure.

Finally, our study gives a new perspective on the relationship between metabolism, satellite cell numbers and their activity during regeneration. A number of studies have implied that slow muscles contain more satellite cells than fast (Putman et al., 1999; Christov et al., 2007). In this study, we show that at least in the EDL as the fibres transitioned from Type IIB to Type IIA, the number of associated satellite cells was significantly reduced. One possible explanation for this finding is by taking into account the concomitant increase in the number of nuclei in the myofibre. Here, the relationship is opposite to satellite cell fibre number. We postulate that the absence of myostatin promotes myoblast fusion at the expense of satellite cell. Furthermore, that over-expression of Erry exacerbates this relationship. Severe depletion of satellite cell numbers has been reported to severely retard the process of muscle regeneration (Schuster-Gossler et al., 2007; Vasyutina et al., 2007). Here, we show that the depletion of satellite cells to less than 50% of their normal levels does not impact on skeletal muscle regeneration since they have a vast capacity to generate precursors which in most situations are never realized fully (Collins et al., 2005). Instead, we suggest that oxidative environment established by Erry is the key determinant in accelerating regeneration. Our work supports previous work showing that oxidative metabolism supports muscle regeneration (Lowrie et al.,

1982; Matsakas et al., 2012b, 2013) and are in agreement with a number of studies showing that genetic manipulations leading to a greater oxidative capacity accelerate muscle regeneration (Li et al., 2007; Hussain et al., 2013). One possible explanation for our results is our finding that Erry promotes hyper-vascularization. Angiogenesis is a key determinant in the muscle regeneration process. We suggest that the reduction of satellite cell is off-set by the ability to promote vascularization and clearance of the necrotic tissues, allowing the small number of satellite cells to expand greatly to enact rapid repair. This hypothesis is supported by our data investigating both macrophage density and the generation of myoblast in the *Mtn*^{-/-}/*Erry*^{Tg/+} mice. Many studies have found that programmes of muscle repair are often at the expense of satellite cells which are not available for future cycles of degeneration/regeneration (Castets et al., 2011). We will investigate this avenue of research in the future by conducting a second round tissue damage in the three genetic lines described here. Encouragingly, our data show that although there was an increase in the number of myogenic precursors (Pax7⁺/MyoD⁺) as well as committed cells (Pax7⁺/MyoD⁺) in the *Mtn*^{-/-}/*Erry*^{Tg/+} compared to WT at D6, this was not at the expense of cells with satellite cell character (Pax7⁺/MyoD⁻).

In summary, our work challenges the dogma of an inverse relationship between muscle fibre size and oxidative capacity. The deviation from this relationship may be realized by the increased capillarisation and myoglobin content of the muscle and redistribution of mitochondria to a subsarcolemmal location. These adaptations were not associated with the loss of muscle force generating capacity and in fact even resulted in improved exercise capacity. It is likely that the increased microvascular network plays a crucial role in muscle regeneration as the *Mtn*^{-/-}/*Erry*^{Tg/+} mice had even lower satellite cell numbers than *Mtn*^{-/-} mice, yet a regenerative capacity that even exceeded that of WT mice. In future we will determine whether it confers other advantages in particular the ability to confer resistance to obesity and sarcopenia.

Materials and methods

Ethical approval

The experiments were performed under a project license from the United Kingdom Home Office in agreement with the Animals (Scientific Procedures) Act 1986. The University of Reading Animal Care and Ethical Review Committee approved all procedures. Animals were humanely sacrificed via Schedule 1 killing between 8:00–13:00.

Animal maintenance

Healthy C57Bl/6 (WT), *Mtn*^{-/-}, *Mtn*^{-/-}/*Erry*^{Tg/+} and *Erry*^{Tg/+} mice were bred and maintained in accordance to the Animals (Scientific Procedures) Act 1986 (UK) and approved by the University of Reading in the Biological Resource Unit of Reading University. Mice were housed under standard environmental conditions (20–22°C, 12–12 hr light–dark cycle) and provided food and water *ad libitum*. We used male mice that were 4–5 months old at the start of the study. Each experimental group consisted of 3–12 mice. *Mtn*^{-/-} and *Erry*^{Tg/+} mice were a gift of Se-Jin Lee (John's Hopkins USA) and Ronald Evans respectively (Salk Institute for Biological Studies, La Jolla, USA). Post-natal muscle growth was induced in one month-old males WT and *Erry*^{Tg/+} mice that were injected twice weekly intraperitoneally with 10 mg/kg of the soluble activin receptor IIB (sActRIIB-Fc) for a period of two months. Each experimental group consisted of 5–6 mice.

Exercise fatigue test

Mice were acclimatized to running on a treadmill in three sessions (10 m·min⁻¹ for 15 min followed by a 1 m·min⁻¹ increase per minute to a maximum of 12 m·min⁻¹) (Columbus Instruments Model Exer 3/6 Treadmill, Serial S/N 120416). Exhaustion was determined by exercising the mice at 12 m·min⁻¹ for 5 min, followed by 1 m·min⁻¹ increases to a maximum of 20 m·min⁻¹ until the mouse was unable to run.

Muscle tension measurements

Dissection of the hind limb was carried out under oxygenated Krebs solution (95% O₂ and 5% CO₂). Under circulating oxygenated Krebs solution one end of a silk suture was attached to the distal

tendon of the extensor digitorum longus (EDL) and the other to a Grass Telefactor force transducer (FT03). The proximal tendon remained attached to the tibial bone. The leg was pinned to a Sylgard-coated experimental chamber. Two silver electrodes were positioned longitudinally on either side of the EDL. A constant voltage stimulator (S48, Grass Telefactor) was used to directly stimulate the EDL which was stretched to attain the optimal muscle length to produce maximum twitch tension (P_t). Tetanic contractions were provoked by stimulus trains of 500 ms duration at, 10, 20, 50, 100 and 200 Hz. The maximum tetanic tension (P_o) was determined from the plateau of the frequency-tension curve. Specific force was estimated by normalising tetanic force to EDL muscle mass (g).

Histological analysis and immunohistochemistry

Following dissection, the muscle was immediately frozen in liquid nitrogen-cooled isopentane and mounted in Tissue Tech freezing medium (Jung) cooled by dry ice/ethanol. Immunohistochemistry was performed on 10 μ m cryosections that were dried for 30 min before the application of block wash buffer (PBS with 5% foetal calf serum (v/v), 0.05% Triton X-100). Antibodies were diluted in wash buffer 30 min before use. Details of primary and secondary antibodies are given in **Supplementary file 1**. F4/80 was detected using the Vector Laboratories ImmPRESS Excel Staining Kit. Morphometric analysis of fibre size was performed as previously described (**Matsakas et al., 2012a**).

Succinate dehydrogenase (SDH) staining

Transverse EDL muscle sections were incubated for 3 min at room temperature in a sodium phosphate buffer containing 75 mM sodium succinate (Sigma), 1.1 mM Nitroblue Tetrazolium (Sigma) and 1.03 mM Phenazine Methosulphate (Sigma). Samples were then fixed in 10% formal-calcium and cleared in xylene prior to mounting with DPX mounting medium (Fisher). Densitometry of the samples was performed on a Zeiss Axioskop2 microscope mounted with an AxioCam HRc camera. Axio-vision Rel. 4.8 software was used to capture the images.

Transmission electron microscopy

To identify the distribution of the mitochondria in the muscle fibres, biceps and extensor carpi radialis muscle were removed cut in pieces of 1 mm³ and immerse fixed in 4% PFA and 2.5% glutaraldehyde in 0.1 M cacodylate buffer pH 7.4 (4°C, 48 hr). Tissue blocks were contrasted using 0.5% OsO₄ (Roth, Germany; RT, 1.5 hr) and 1% uranyl acetate (Polysciences, Germany) in 70% ethanol (RT, 1 hr). After dehydration tissue blocks were embedded in epoxy resin (Durcupan, Roth, Germany) and ultrathin sections of 40 nm thickness were cut using a Leica UC6 ultramicrotome (Leica, Wetzlar, Germany). Sections were imaged using a Zeiss 906 TEM (Zeiss, Oberkochen, Germany) and analysed using ITEM software (Olympus, Germany).

¹H NMR spectroscopy-based metabonomic analysis

Polar metabolites were extracted from the gastrocnemius muscle using previously described protocols (**Beckonert et al., 2007**). Briefly, 40–50 mg of muscle tissue was snap frozen in liquid nitrogen and finely ground in 300 μ L of chloroform: methanol (2:1) using a tissue lyzer. The homogenate was combined with 300 μ L of water, vortexed and spun (13,000 g for 10 min) to separate the aqueous (upper) and organic (lower) phases. A vacuum concentrator (SpeedVac) was used to remove the water and methanol from the aqueous phase before reconstitution in 550 μ L of phosphate buffer (pH 7.4) in 100% D₂O containing 1 mM of the internal standard, 3-(trimethylsilyl)-[2,2,3,3-²H₄]-propionic acid (TSP). For each sample, a standard one-dimensional NMR spectrum was acquired with water peak suppression using a standard pulse sequence (recycle delay (RD)-90°-t₁-90°-t_m-90°-acquire free induction decay (FID)). RD was set as 2 s, the 90° pulse length was 16.98 μ s, and the mixing time (t_m) was 10 ms. For each spectrum, 8 dummy scans were followed by 128 scans with an acquisition time per scan of 3.8 s and collected in 64 K data points with a spectral width of 12.001 ppm. ¹H nuclear magnetic resonance (NMR) spectra were manually corrected for phase and baseline distortions and referenced to the TSP singlet at δ 0.0. Spectra were digitized using an in-house MATLAB (version R2009b, The Mathworks, Inc.; Natick, MA) script. To minimize baseline distortions arising from imperfect water saturation, the region containing the water resonance was excised from

the spectra. Principal components analysis (PCA) was performed with Pareto scaling in MATLAB using scripts provided by Korrigan Sciences Ltd, UK.

Protein expression by western blotting

Frozen muscles were powdered and lysed in a buffer containing 50 mM Tris, pH7.5, 150 mM NaCl, 5 mM MgCl₂, 1 mM DTT, 10% glycerol, 1%SDS, 1%Triton X-100, 1XRoche Complete Protease Inhibitor Cocktail, 1X Sigma-Aldrich Phosphatase Inhibitor Cocktail 1 and 3. Then, the samples were immunoblotted and visualized with SuperSignal West Pico Chemiluminescent substrate (Pierce). Blots were stripped using Restore Western Blotting Stripping Buffer (Pierce) according to the manufacturer's instructions and were reprobbed if necessary. Details of antibodies are given in [Supplementary file 1](#).

Quantitative PCR

Tissue samples were solubilised in TRIzol (Fisher) using a tissue homogeniser. Total RNA was prepared from skeletal muscles using the RNeasy Mini Kit (Qiagen, Manchester, UK). Total RNA (5 µg) was reverse-transcribed to cDNA with SuperScript II Reverse Transcriptase (Invitrogen) and analyzed by quantitative real-time RT-PCR on a StepOne Plus cycler, using the Applied Biosystems SYBR-Green PCR Master Mix. Primers were designed using the software Primer Express 3.0 (Applied Biosystems). Relative expression was calculated using the $\Delta\Delta C_t$ method with normalization to the housekeeping genes cyclophilin-B, hypoxanthine-guanine phosphoribosyltransferase (hpert) and glyceraldehyde-3-phosphate dehydrogenase (GAPDH). Specific primer sequences are given in [Supplementary file 1](#).

Myonuclear organisation

For visualizing myonuclei, fibres were mounted with ProLong Diamons Antifade Mountant with DAPI (Molecular Probes, P36962), and a confocal microscope (Olympus Fluoview 1000, BX61W1, Olympus, Japan) was used to observe single muscle fibres. Pictures were taken in confocal planes, separated by z-axis steps varying between 0.4 and 2 µm according to the optical thickness and the desired Nyquist sampling frequency. Confocal microscope images used for mapping of Euclidean positions of myonuclei were processed and analysed using Imaris (Bitplane) and ImageJ (NIH, Bethesda, MD, USA).

For each muscle fibre, an idealized circular cylinder segment with constant radius was constructed, and the distance from each nucleus to its nearest neighbour was calculated.

In order to measure how ordered the nuclei distribution for a particular fibre is, the mean nearest neighbour distance was calculated for the experimental data, as well as for the random and optimal distribution using parameters from the experiment. We denote the experimental, random and optimal means by M_E , M_R and M_O . An 'orderness-score', $g(M_E)$, was then calculated as:

$$g(M_E, M_R, M_O) = \frac{M_E - M_R}{M_O - M_R}$$

Further details and availability of custom made software, please contact j.c.bruusgaard@ibv.uio.no.

Satellite cell culture

Single fibres from EDL were isolated using 0.2% collagenase I in DMEM medium and either fixed or cultured for 48 and 72 hr as previously described ([Otto et al., 2008](#)).

Skeletal muscle regeneration

Skeletal muscle damage was induced by injecting 30 µl of 50 µM cardiotoxin in the tibialis anterior (TA) muscle of one limb while the contralateral TA of the other limb was injected with 30 µL PBS to serve as an internal control. The degree of muscle regeneration was assessed on day 3 and day 6 post-injury.

Statistical analysis

Data are presented as mean ± SE. Significant differences between two groups were performed by Student's t-test for independent variables. The normality of the data for two samples was checked

with a Kolmogorov–Smirnov test ($\alpha = 10\%$). Differences among groups were analysed by one-way or two-way analysis of variance (ANOVA) followed by Bonferroni's multiple comparison tests as appropriate. In the case of non-homogeneous variances (Lavene's test; $p < 0.05$) for a variable, ANOVA was performed using the square root of the observations. Statistical analysis was performed on SPSS 18.0 (Chicago, IL). Differences were considered statistically significant at $p < 0.05$.

Acknowledgements

The financial support from the Biotechnology and Biological Sciences Research Council is gratefully acknowledged (Grants BB/J016454/1 to HCH and BB/I015787/1 to RM). The study was also supported by the European Union and The Royal Society (Grants: FP7-PEOPLE-PCIG14-GA-2013-631440 and RG140470 Research Grant to AM).

Additional information

Funding

Funder	Grant reference number	Author
European Commission	FP7-PEOPLE-676	Antonios Matsakas
European Commission	PCIG14-GA-2013-631440	Antonios Matsakas
Royal Society	Research Grant, RG140470	Antonios Matsakas
Biotechnology and Biological Sciences Research Council	BB/I015787/1	Robert Mitchell
Biotechnology and Biological Sciences Research Council	BB/J016454/1	Henry Collins-Hooper

The funders had no role in study design, data collection and interpretation, or the decision to submit the work for publication.

Author contributions

SO, Acquisition of data, Analysis and interpretation of data; AM, NG, Acquisition of data, Analysis and interpretation of data, Drafting or revising the article; HD, Experimental design, Experimentation, data analysis, Manuscript preparation; OK, JCB, Experimentation, data analysis, Manuscript preparation; K-AH, AVS, Experimentation, data analysis; BJ, Experimentation; RS, RM, HC-H, Acquisition of data; KF, Analysis and interpretation of data, Drafting or revising the article; AP, OR, JRS, Conception and design; MS, Drafting or revising the article; VN, Conception and design, Drafting or revising the article; TH, Conception and design, Analysis and interpretation of data, Drafting or revising the article; KP, Conception and design, Acquisition of data, Analysis and interpretation of data, Drafting or revising the article

Author ORCIDs

Ketan Patel,  <http://orcid.org/0000-0002-7131-749X>

Ethics

Animal experimentation: The experiments were performed under a project license (PPL70/7516) from the United Kingdom Home Office in agreement with the Animals (Scientific Procedures) Act 1986. The University of Reading Animal Care and Ethical Review Committee approved all procedures. All of the animals were handled according to approved institutional animal care and guidelines set out by the Home Office of the UK. The protocol was approved by the Committee on the Ethics of Animal Experiments of the University of Reading. All surgery was performed under recommended anesthesia, and every effort was made to minimize suffering.

Additional files

Supplementary files

- Supplementary file 1. List of primary and secondary antibodies and qPCR primer sequences.

DOI: [10.7554/eLife.16940.015](https://doi.org/10.7554/eLife.16940.015)

References

- Ahmed SK, Egginton S, Jakeman PM, Mannion AF, Ross HF. 1997. Is human skeletal muscle capillary supply modelled according to fibre size or fibre type? *Experimental Physiology* **82**:231–234. doi: [10.1113/expphysiol.1997.sp004012](https://doi.org/10.1113/expphysiol.1997.sp004012)
- Amthor H, Macharia R, Navarrete R, Schuelke M, Brown SC, Otto A, Voit T, Muntoni F, Vrbova G, Partridge T, Zammit P, Bunker L, Patel K. 2007. Lack of myostatin results in excessive muscle growth but impaired force generation. *PNAS* **104**:1835–1840. doi: [10.1073/pnas.0604893104](https://doi.org/10.1073/pnas.0604893104)
- Beckonert O, Keun HC, Ebbels TM, Bundy J, Holmes E, Lindon JC, Nicholson JK. 2007. Metabolic profiling, metabolomic and metabonomic procedures for NMR spectroscopy of urine, plasma, serum and tissue extracts. *Nature Protocols* **2**:2692–2703. doi: [10.1038/nprot.2007.376](https://doi.org/10.1038/nprot.2007.376)
- Bonaldo P, Sandri M. 2013. Cellular and molecular mechanisms of muscle atrophy. *Disease Models & Mechanisms* **6**:25–39. doi: [10.1242/dmm.010389](https://doi.org/10.1242/dmm.010389)
- Bottinelli R, Canepari M, Reggiani C, Stienen GJ. 1994. Myofibrillar ATPase activity during isometric contraction and isomyosin composition in rat single skinned muscle fibres. *The Journal of Physiology* **481**:663–675. doi: [10.1113/jphysiol.1994.sp020472](https://doi.org/10.1113/jphysiol.1994.sp020472)
- Bruusgaard JC, Liestøl K, Gundersen K. 2006. Distribution of myonuclei and microtubules in live muscle fibers of young, middle-aged, and old mice. *Journal of Applied Physiology* **100**:2024–2030. doi: [10.1152/jappphysiol.00913.2005](https://doi.org/10.1152/jappphysiol.00913.2005)
- Bruusgaard JC, Liestøl K, Ekmark M, Kollstad K, Gundersen K. 2003. Number and spatial distribution of nuclei in the muscle fibres of normal mice studied in vivo. *Journal of Physiology* **551**:467–478. doi: [10.1113/jphysiol.2003.045328](https://doi.org/10.1113/jphysiol.2003.045328)
- Buller AJ, Eccles JC, Eccles RM. 1960. Interactions between motoneurons and muscles in respect of the characteristic speeds of their responses. *Journal of Physiology* **150**:417–439. doi: [10.1113/jphysiol.1960.sp006395](https://doi.org/10.1113/jphysiol.1960.sp006395)
- Carmignac V, Svensson M, Körner Z, Elowsson L, Matsumura C, Gawlik KI, Allamand V, Durbeek M. 2011. Autophagy is increased in laminin $\alpha 2$ chain-deficient muscle and its inhibition improves muscle morphology in a mouse model of MDC1A. *Human Molecular Genetics* **20**:4891–4902. doi: [10.1093/hmg/ddr427](https://doi.org/10.1093/hmg/ddr427)
- Castets P, Bertrand AT, Beuvin M, Ferry A, Le Grand F, Castets M, Chazot G, Rederstorff M, Krol A, Lescure A, Romero NB, Guicheney P, Allamand V. 2011. Satellite cell loss and impaired muscle regeneration in selenoprotein N deficiency. *Human Molecular Genetics* **20**:694–704. doi: [10.1093/hmg/ddq515](https://doi.org/10.1093/hmg/ddq515)
- Christov C, Chrétien F, Abou-Khalil R, Bassez G, Vallet G, Authier FJ, Bassaglia Y, Shinin V, Tajbakhsh S, Chazaud B, Gherardi RK. 2007. Muscle satellite cells and endothelial cells: close neighbors and privileged partners. *Molecular Biology of the Cell* **18**:1397–1409. doi: [10.1091/mbc.E06-08-0693](https://doi.org/10.1091/mbc.E06-08-0693)
- Collins CA, Olsen I, Zammit PS, Heslop L, Petrie A, Partridge TA, Morgan JE. 2005. Stem cell function, self-renewal, and behavioral heterogeneity of cells from the adult muscle satellite cell niche. *Cell* **122**:289–301. doi: [10.1016/j.cell.2005.05.010](https://doi.org/10.1016/j.cell.2005.05.010)
- Conjard A, Peuker H, Pette D. 1998. Energy state and myosin heavy chain isoforms in single fibres of normal and transforming rabbit muscles. *Pflügers Archiv European Journal of Physiology* **436**:962–969. doi: [10.1007/s004240050730](https://doi.org/10.1007/s004240050730)
- Deberardinis RJ, Sayed N, Ditsworth D, Thompson CB. 2008. Brick by brick: metabolism and tumor cell growth. *Current Opinion in Genetics & Development* **18**:54–61. doi: [10.1016/j.gde.2008.02.003](https://doi.org/10.1016/j.gde.2008.02.003)
- Degens H, Turek Z, Hoofd LJ, Binkhorst RA. 1994. Capillary proliferation related to fibre types in hypertrophied aging rat M. plantaris. *Advances in Experimental Medicine and Biology* **345**:669–676. doi: [10.1007/978-1-4615-2468-7_88](https://doi.org/10.1007/978-1-4615-2468-7_88)
- Degens H. 2012. Determinants of skeletal muscle hypertrophy and the attenuated hypertrophic response at old age. *Journal of Sports Medicine & Doping Studies* **s1**:2161–2173. doi: [10.4172/2161-0673.S1-003](https://doi.org/10.4172/2161-0673.S1-003)
- Desplanches D, Hoppeler H, Tüscher L, Mayet MH, Spielvogel H, Ferretti G, Kayser B, Leuenberger M, Grünenfelder A, Favier R. 1996. Muscle tissue adaptations of high-altitude natives to training in chronic hypoxia or acute normoxia. *Journal of Applied Physiology* **81**:1946–1951.
- Deveci D, Marshall JM, Egginton S. 2001. Relationship between capillary angiogenesis, fiber type, and fiber size in chronic systemic hypoxia. *American Journal of Physiology* **281**:H241–252.
- Dunnnett M, Harris RC, Soliman MZ, Suwar AA. 1997. Carnosine, anserine and taurine contents in individual fibres from the middle gluteal muscle of the camel. *Research in Veterinary Science* **62**:213–216. doi: [10.1016/S0034-5288\(97\)90192-2](https://doi.org/10.1016/S0034-5288(97)90192-2)
- Egginton S, Hudlická O, Brown MD, Walter H, Weiss JB, Bate A. 1998. Capillary growth in relation to blood flow and performance in overloaded rat skeletal muscle. *Journal of Applied Physiology* **85**:2025–2032.

- Frank S, Gaume B, Bergmann-Leitner ES, Leitner WW, Robert EG, Catez F, Smith CL, Youle RJ. 2001. The role of dynamin-related protein 1, a mediator of mitochondrial fission, in apoptosis. *Developmental Cell* **1**:515–525. doi: [10.1016/S1534-5807\(01\)00055-7](https://doi.org/10.1016/S1534-5807(01)00055-7)
- Giguère V. 2008. Transcriptional control of energy homeostasis by the estrogen-related receptors. *Endocrine Reviews* **29**:677–696. doi: [10.1210/er.2008-0017](https://doi.org/10.1210/er.2008-0017)
- Gundersen K. 2011. Excitation-transcription coupling in skeletal muscle: the molecular pathways of exercise. *Biological Reviews* **86**:564–600. doi: [10.1111/j.1469-185X.2010.00161.x](https://doi.org/10.1111/j.1469-185X.2010.00161.x)
- Heard DJ, Norby PL, Holloway J, Vissing H. 2000. Human ERRgamma, a third member of the estrogen receptor-related receptor (ERR) subfamily of orphan nuclear receptors: tissue-specific isoforms are expressed during development and in the adult. *Molecular Endocrinology* **14**:382–392. doi: [10.1210/mend.14.3.0431](https://doi.org/10.1210/mend.14.3.0431)
- Hickson RC. 1980. Interference of strength development by simultaneously training for strength and endurance. *European Journal of Applied Physiology and Occupational Physiology* **45**:255–263. doi: [10.1007/BF00421333](https://doi.org/10.1007/BF00421333)
- Hong H, Kohli K, Trivedi A, Johnson DL, Stallcup MR. 1996. GRIP1, a novel mouse protein that serves as a transcriptional coactivator in yeast for the hormone binding domains of steroid receptors. *PNAS* **93**:4948–4952. doi: [10.1073/pnas.93.10.4948](https://doi.org/10.1073/pnas.93.10.4948)
- Hussain G, Schmitt F, Henriques A, Lequeu T, Rene F, Bindler F, Dirrig-Grosch S, Oudart H, Palamiuc L, Metz-Boutigue M-H, Dupuis L, Marchioni E, Gonzalez De Aguilar J-L, Loeffler J-P. 2013. Systemic down-regulation of Delta-9 desaturase promotes muscle oxidative metabolism and accelerates muscle function recovery following nerve injury. *PLoS One* **8**:e64525. doi: [10.1371/journal.pone.0064525](https://doi.org/10.1371/journal.pone.0064525)
- Kinsey ST, Hardy KM, Locke BR. 2007. The long and winding road: influences of intracellular metabolite diffusion on cellular organization and metabolism in skeletal muscle. *Journal of Experimental Biology* **210**:3505–3512. doi: [10.1242/jeb.000331](https://doi.org/10.1242/jeb.000331)
- Kohen R, Yamamoto Y, Cundy KC, Ames BN. 1988. Antioxidant activity of carnosine, homocarnosine, and anserine present in muscle and brain. *PNAS* **85**:3175–3179. doi: [10.1073/pnas.85.9.3175](https://doi.org/10.1073/pnas.85.9.3175)
- Kwong WH, Vrbová G. 1981. Effects of low-frequency electrical stimulation on fast and slow muscles of the rat. *Pflügers Archiv - European Journal of Physiology* **391**:200–207. doi: [10.1007/BF00596171](https://doi.org/10.1007/BF00596171)
- Lee KY, Singh MK, Ussar S, Wetzel P, Hirshman MF, Goodyear LJ, Kispert A, Kahn CR. 2015. Tbx15 controls skeletal muscle fibre-type determination and muscle metabolism. *Nature Communications* **6**:8054. doi: [10.1038/ncomms9054](https://doi.org/10.1038/ncomms9054)
- Li Y, Li J, Zhu J, Sun B, Branca M, Tang Y, Foster W, Xiao X, Huard J. 2007. Decorin gene transfer promotes muscle cell differentiation and muscle regeneration. *Molecular Therapy* **15**:1616–1622. doi: [10.1038/sj.mt.6300250](https://doi.org/10.1038/sj.mt.6300250)
- Liu JX, Höglund AS, Karlsson P, Lindblad J, Qaisar R, Aare S, Bengtsson E, Larsson L. 2009. Myonuclear domain size and myosin isoform expression in muscle fibres from mammals representing a 100,000-fold difference in body size. *Experimental Physiology* **94**:117–129. doi: [10.1113/expphysiol.2008.043877](https://doi.org/10.1113/expphysiol.2008.043877)
- Lowrie MB, Krishnan S, Vrbová G. 1982. Recovery of slow and fast muscles following nerve injury during early post-natal development in the rat. *Journal of Physiology* **331**:51–66. doi: [10.1113/jphysiol.1982.sp014364](https://doi.org/10.1113/jphysiol.1982.sp014364)
- Maier A, Leberer E, Pette D. 1988. Distribution of sarcoplasmic reticulum Ca-ATPase and of calsequestrin at the polar regions of rat, rabbit and cat intrafusal fibers. *Histochemistry* **88**:273–276.
- Matsakas A, Macharia R, Otto A, Elashry MI, Mouisel E, Romanello V, Sartori R, Amthor H, Sandri M, Narkar V, Patel K. 2012a. Exercise training attenuates the hypermuscular phenotype and restores skeletal muscle function in the myostatin null mouse. *Experimental Physiology* **97**:125–140. doi: [10.1113/expphysiol.2011.063008](https://doi.org/10.1113/expphysiol.2011.063008)
- Matsakas A, Yadav V, Lorca S, Evans RM, Narkar VA. 2012. Revascularization of ischemic skeletal muscle by estrogen-related receptor-γ. *Circulation Research* **110**:1087–1096. doi: [10.1161/CIRCRESAHA.112.266478](https://doi.org/10.1161/CIRCRESAHA.112.266478)
- Matsakas A, Yadav V, Lorca S, Narkar V. 2013. Muscle ERRγ mitigates Duchenne muscular dystrophy via metabolic and angiogenic reprogramming. *The FASEB Journal* **27**:4004–4016. doi: [10.1096/fj.13-228296](https://doi.org/10.1096/fj.13-228296)
- McPherron AC, Lawler AM, Lee S-J. 1997a. Regulation of skeletal muscle mass in mice by a new TGF- β superfamily member. *Nature* **387**:83–90. doi: [10.1038/387083a0](https://doi.org/10.1038/387083a0)
- McPherron AC, Lee SJ. 1997. Double muscling in cattle due to mutations in the myostatin gene. *PNAS* **94**:12457–12461. doi: [10.1073/pnas.94.23.12457](https://doi.org/10.1073/pnas.94.23.12457)
- Meinke P, Mattioli E, Haque F, Antoku S, Columbaro M, Straatman KR, Worman HJ, Gundersen GG, Lattanzi G, Wehnert M, Shackleton S. 2014. Muscular dystrophy-associated SUN1 and SUN2 variants disrupt nuclear-cytoskeletal connections and myonuclear organization. *PLoS Genetics* **10**:e1004605. doi: [10.1371/journal.pgen.1004605](https://doi.org/10.1371/journal.pgen.1004605)
- Mendias CL, Marcin JE, Calerdon DR, Faulkner JA. 2006. Contractile properties of EDL and soleus muscles of myostatin-deficient mice. *Journal of Applied Physiology* **101**:898–905. doi: [10.1152/jappphysiol.00126.2006](https://doi.org/10.1152/jappphysiol.00126.2006)
- Meng Z-X, Li S, Wang L, Ko HJ, Lee Y, Jung DY, Okutsu M, Yan Z, Kim JK, Lin JD. 2013. Baf60c drives glycolytic metabolism in the muscle and improves systemic glucose homeostasis through Deptor-mediated Akt activation. *Nature Medicine* **19**:640–645. doi: [10.1038/nm.3144](https://doi.org/10.1038/nm.3144)
- Meng ZX, Wang L, Xiao Y, Lin JD. 2014. The Baf60c/Deptor pathway links skeletal muscle inflammation to glucose homeostasis in obesity. *Diabetes* **63**:1533–1545. doi: [10.2337/db13-1061](https://doi.org/10.2337/db13-1061)
- Metzger T, Gache V, Xu M, Cadot B, Folker ES, Richardson BE, Gomes ER, Baylies MK. 2012. MAP and kinesin-dependent nuclear positioning is required for skeletal muscle function. *Nature* **484**:120–124. doi: [10.1038/nature10914](https://doi.org/10.1038/nature10914)
- Mitchell WK, Williams J, Atherton P, Larvin M, Lund J, Narici M. 2012. Sarcopenia, dynapenia, and the impact of advancing age on human skeletal muscle size and strength; a quantitative review. *Frontiers in Physiology* **3**:260. doi: [10.3389/fphys.2012.00260](https://doi.org/10.3389/fphys.2012.00260)

- Muscat GE**, Kedes L. 1987. Multiple 5'-flanking regions of the human alpha-skeletal actin gene synergistically modulate muscle-specific expression. *Molecular and Cellular Biology* **7**:4089–4099. doi: [10.1128/MCB.7.11.4089](https://doi.org/10.1128/MCB.7.11.4089)
- Narkar VA**, Fan W, Downes M, Yu RT, Jonker JW, Alaynick WA, Banayo E, Karunasiri MS, Lorca S, Evans RM. 2011. Exercise and PGC-1 α -independent synchronization of type I muscle metabolism and vasculature by ERR γ . *Cell Metabolism* **13**:283–293. doi: [10.1016/j.cmet.2011.01.019](https://doi.org/10.1016/j.cmet.2011.01.019)
- Ono T**, Isobe K, Nakada K, Hayashi JI. 2001. Human cells are protected from mitochondrial dysfunction by complementation of DNA products in fused mitochondria. *Nature Genetics* **28**:272–275. doi: [10.1038/90116](https://doi.org/10.1038/90116)
- Otto A**, Schmidt C, Luke G, Allen S, Valasek P, Muntoni F, Lawrence-Watt D, Patel K. 2008. Canonical Wnt signalling induces satellite-cell proliferation during adult skeletal muscle regeneration. *Journal of Cell Science* **121**:2939–2950. doi: [10.1242/jcs.026534](https://doi.org/10.1242/jcs.026534)
- Petros JA**, Baumann AK, Ruiz-Pesini E, Amin MB, Sun CQ, Hall J, Lim S, Issa MM, Flanders WD, Hosseini SH, Marshall FF, Wallace DC. 2005. mtDNA mutations increase tumorigenicity in prostate cancer. *PNAS* **102**:719–724. doi: [10.1073/pnas.0408894102](https://doi.org/10.1073/pnas.0408894102)
- Pette D**, Sketelj J, Skorjanc D, Leisner E, Traub I, Bajrović F. 2002. Partial fast-to-slow conversion of regenerating rat fast-twitch muscle by chronic low-frequency stimulation. *Journal of Muscle Research and Cell Motility* **23**: 215–221.
- Pette D**, Staron RS. 1997. Mammalian skeletal muscle fiber type transitions. *International Review of Cytology* **170**:143–223. doi: [10.1016/s0074-7696\(08\)61622-8](https://doi.org/10.1016/s0074-7696(08)61622-8)
- Pette D**, Staron RS. 2001. Transitions of muscle fiber phenotypic profiles. *Histochemistry and Cell Biology* **115**: 359–372.
- Peuker H**, Conjard A, Putman CT, Pette D. 1999. Transient expression of myosin heavy chain MHCI alpha in rabbit muscle during fast-to-slow transition. *Journal of Muscle Research and Cell Motility* **20**:147–154.
- Plyley MJ**, Olmstead BJ, Noble EG. 1998. Time course of changes in capillarization in hypertrophied rat plantaris muscle. *Journal of Applied Physiology* **84**:902–907.
- Putman CT**, Düsterhöft S, Pette D. 1999. Changes in satellite cell content and myosin isoforms in low-frequency-stimulated fast muscle of hypothyroid rat. *Journal of Applied Physiology* **86**:40–51.
- Rangwala SM**, Wang X, Calvo JA, Lindsley L, Zhang Y, Deyneko G, Beaulieu V, Gao J, Turner G, Markovits J. 2010. Estrogen-related receptor gamma is a key regulator of muscle mitochondrial activity and oxidative capacity. *Journal of Biological Chemistry* **285**:22619–22629. doi: [10.1074/jbc.M110.125401](https://doi.org/10.1074/jbc.M110.125401)
- Relizani K**, Mouisel E, Giannesini B, Hourdé C, Patel K, Morales Gonzalez S, Jülich K, Vignaud A, Piétri-Rouxel F, Fortin D, Garcia L, Blot S, Ritvos O, Bendahan D, Ferry A, Ventura-Clapier R, Schuelke M, Amthor H. 2014. Blockade of ActR1B signaling triggers muscle fatigability and metabolic myopathy. *Molecular Therapy* **22**: 1423–1433. doi: [10.1038/mt.2014.90](https://doi.org/10.1038/mt.2014.90)
- Rossi G**, Antonini S, Bonfanti C, Monteverde S, Vezzali C, Tajbakhsh S, Cossu G, Messina G. 2016. Nfix regulates temporal progression of muscle regeneration through modulation of myostatin expression. *Cell Reports* **14**: 2238–2249. doi: [10.1016/j.celrep.2016.02.014](https://doi.org/10.1016/j.celrep.2016.02.014)
- Salmons S**, Vrbová G. 1969. The influence of activity on some contractile characteristics of mammalian fast and slow muscles. *Journal of Physiology* **201**:535–549. doi: [10.1113/jphysiol.1969.sp008771](https://doi.org/10.1113/jphysiol.1969.sp008771)
- Sandri M**, Sandri C, Gilbert A, Skurk C, Calabria E, Picard A, Walsh K, Schiaffino S, Lecker SH, Goldberg AL. 2004. Foxo transcription factors induce the atrophy-related ubiquitin ligase atrogin-1 and cause skeletal muscle atrophy. *Cell* **117**:399–412. doi: [10.1016/S0092-8674\(04\)00400-3](https://doi.org/10.1016/S0092-8674(04)00400-3)
- Sandri M**. 2013. Protein breakdown in muscle wasting: role of autophagy-lysosome and ubiquitin-proteasome. *The International Journal of Biochemistry & Cell Biology* **45**:2121–2129. doi: [10.1016/j.biocel.2013.04.023](https://doi.org/10.1016/j.biocel.2013.04.023)
- Schuelke M**, Wagner KR, Stolz LE, Hübner C, Riebel T, Kömen W, Braun T, Tobin JF, Lee SJ. 2004. Myostatin mutation associated with gross muscle hypertrophy in a child. *New England Journal of Medicine* **350**:2682–2688. doi: [10.1056/NEJMoa040933](https://doi.org/10.1056/NEJMoa040933)
- Schuster-Gossler K**, Cordes R, Gossler A. 2007. Premature myogenic differentiation and depletion of progenitor cells cause severe muscle hypotrophy in Delta1 mutants. *PNAS* **104**:537–542. doi: [10.1073/pnas.0608281104](https://doi.org/10.1073/pnas.0608281104)
- Sutherland H**, Jarvis JC, Kwende MM, Gilroy SJ, Salmons S. 1998. The dose-related response of rabbit fast muscle to long-term low-frequency stimulation. *Muscle & Nerve* **21**:1632–1646. doi: [10.1002/\(SICI\)1097-4598\(199812\)21:12<1632::AID-MUS3>3.0.CO;2-W](https://doi.org/10.1002/(SICI)1097-4598(199812)21:12<1632::AID-MUS3>3.0.CO;2-W)
- Trendelenburg AU**, Meyer A, Rohner D, Boyle J, Hatakeyama S, Glass DJ. 2009. Myostatin reduces Akt/TORC1/p70S6K signaling, inhibiting myoblast differentiation and myotube size. *AJP: Cell Physiology* **296**:C1258–C1270. doi: [10.1152/ajpcell.00105.2009](https://doi.org/10.1152/ajpcell.00105.2009)
- Van Der Laarse WJ**, Diegenbach PC, Lee-De Groot MBE, Des Tombe AL. 1997. Size principle of striated muscle cells. *Netherlands Journal of Zoology* **48**:213–223. doi: [10.1163/156854298X00075](https://doi.org/10.1163/156854298X00075)
- van Wessel T**, de Haan A, van der Laarse WJ, Jaspers RT. 2010. The muscle fiber type–fiber size paradox: hypertrophy or oxidative metabolism? *European Journal of Applied Physiology* **110**:665–694. doi: [10.1007/s00421-010-1545-0](https://doi.org/10.1007/s00421-010-1545-0)
- Vasyutina E**, Lenhard DC, Wende H, Erdmann B, Epstein JA, Birchmeier C. 2007. RBP-J (Rbpsi) is essential to maintain muscle progenitor cells and to generate satellite cells. *PNAS* **104**:4443–4448. doi: [10.1073/pnas.0610647104](https://doi.org/10.1073/pnas.0610647104)
- von Hofsten J**, Elworthy S, Gilchrist MJ, Smith JC, Wardle FC, Ingham PW. 2008. Prdm1- and Sox6-mediated transcriptional repression specifies muscle fibre type in the zebrafish embryo. *EMBO Reports* **9**:683–689. doi: [10.1038/embor.2008.73](https://doi.org/10.1038/embor.2008.73)

- Wade AJ**, Marbut MM, Round JM. 1990. Muscle fibre type and aetiology of obesity. *The Lancet* **335**:805–808. doi: [10.1016/0140-6736\(90\)90933-V](https://doi.org/10.1016/0140-6736(90)90933-V)
- Wang X**, Moraes CT. 2011. Increases in mitochondrial biogenesis impair carcinogenesis at multiple levels. *Molecular Oncology* **5**:399–409. doi: [10.1016/j.molonc.2011.07.008](https://doi.org/10.1016/j.molonc.2011.07.008)
- Warburg O**, Wind F, Negelein E. 1927. The metabolism of tumors in the body. *Journal of General Physiology* **8**: 519–530. doi: [10.1085/jgp.8.6.519](https://doi.org/10.1085/jgp.8.6.519)

Link between MHC Fiber Type and Restoration of Dystrophin Expression and Key Components of the DAPC by Tricyclo-DNA-Mediated Exon Skipping

Saleh Omairi,¹ Kwan-Leong Hau,² Henry Collin-Hooper,¹ Federica Montanaro,² Aurelie Goyenville,³ Luis Garcia,³ and Ketan Patel¹

¹School of Biological Sciences, University of Reading, Reading, UK; ²UCL Great Ormond Street Institute of Child Health, Developmental Neurosciences Programme, London, UK; ³Universite de Versailles St. Quentin, INSERM U1179, Montigny-le-Bretonneux, France

Exon skipping mediated by tricyclo-DNA (tc-DNA) antisense oligonucleotides has been shown to induce significant levels of dystrophin restoration in *mdx*, a mouse model of Duchenne muscular dystrophy. This translates into significant improvement in key disease indicators in muscle, cardio-respiratory function, heart, and the CNS. Here we examine the relationship between muscle fiber type, based on myosin heavy chain (MHC) profile, and the ability of tc-DNA to restore not only dystrophin but also other members of the dystrophin-associated glycoprotein complex (DAPC). We first profiled this relationship in untreated *mdx* muscle, and we found that all fiber types support reversion events to a dystrophin-positive state, in an unbiased manner. Importantly, we show that only a small fraction of revertant fibers expressed other members of the DAPC. Immunoblot analysis of protein levels, however, revealed robust expression of these components, which failed to correctly localize to the sarcolemma. We then show that tc-DNA treatment leads to nearly all fibers expressing not only dystrophin but also other key components of the DAPC. Of significance, our work shows that MHC fiber type does not bias the expression of any of these important proteins. This work also highlights that the improved muscle physiology following tc-DNA treatment reported previously results from the complete restoration of the dystrophin complex in all MHCII fibers with equal efficiencies.

INTRODUCTION

Duchenne muscular dystrophy (DMD) affects 1:5,000 male births, and it is the most common fatal childhood muscular disease.^{1,2} Mutations in the *DMD* gene affect expression of dystrophin, a protein normally localized to the inner surface of the sarcolemma in muscle fibers.^{3,4} Dystrophin together with a number of other proteins that constitute the dystrophin-associated glycoprotein complex (DAPC) acts to link the muscle fiber cytoskeleton, the sarcolemma, and the extracellular matrix (ECM) into a functional unit that maintains muscle integrity.^{5,6} The DAPC is composed of three sub-complexes: (1) the sarcoglycans (α , β , γ , and δ); (2) syntrophin, nNOS, and dystrobrevin; and (3) α and β dystroglycan. The absence of dystrophin results in a drastic reduction of all components of the DAPC at the

sarcolemma, and it renders muscle cells prone to stretch-induced muscle damage.⁷

A number of drug-based or surgical procedures have been developed, including the use of corticosteroids or addressing scoliosis, that greatly improve the quality of life for DMD patients or delay disease onset.^{8,9} However, none has completely halted progression of the disease. Gene-based approaches that aim to restore dystrophin in muscle hold great promise. One attractive approach is to take advantage of the molecular structure of the dystrophin gene and to use antisense oligonucleotides (AONs) to promote exon skipping to bypass mutated stretches of DNA and restore the open reading frame.¹⁰ The aim of the current study is to establish expression of a functional, albeit internally deleted, dystrophin protein. Restoration of dystrophin expression by exon skipping has been proven to be efficacious *in vitro*, in animal models and in DMD patients.^{11–13} Several classes of chemical modifications have been developed for AON-mediated exon skipping, among which are 2'-O-methylribooligonucleoside-phosphorothioate (2'OMe), phosphorodiamidate morpholino oligomers (PMOs), and tricyclo-DNA (tc-DNA). The latter has a number of properties that make it an attractive chemistry to exploit for therapeutic uses, including high RNA affinity, resistance to nuclease activity, and the ability to form nanoparticles that may facilitate uptake into cells.^{14–16} We have recently shown, using *mdx* mice as a rodent model for DMD, that tc-DNA mediates unprecedented levels of exon skipping after systemic delivery not only in skeletal muscle but also in the heart and brain.¹⁶ This translated into normalization of specific force in the tibialis anterior muscle as well as improved cardiovascular function and the correction of behavioral characteristics.¹⁶

A number of studies using AONs in both *mdx* mice and DMD patients have shown restoration of dystrophin in a subset of muscle fibers.^{13,17,18} Most skeletal muscles are composed of a heterogeneous

Received 20 July 2017; accepted 21 October 2017;
<https://doi.org/10.1016/j.omtn.2017.10.014>

Correspondence: Ketan Patel, School of Biological Sciences, University of Reading, Whiteknights, Reading RG6 6UB, UK.

E-mail: ketan.patel@reading.ac.uk

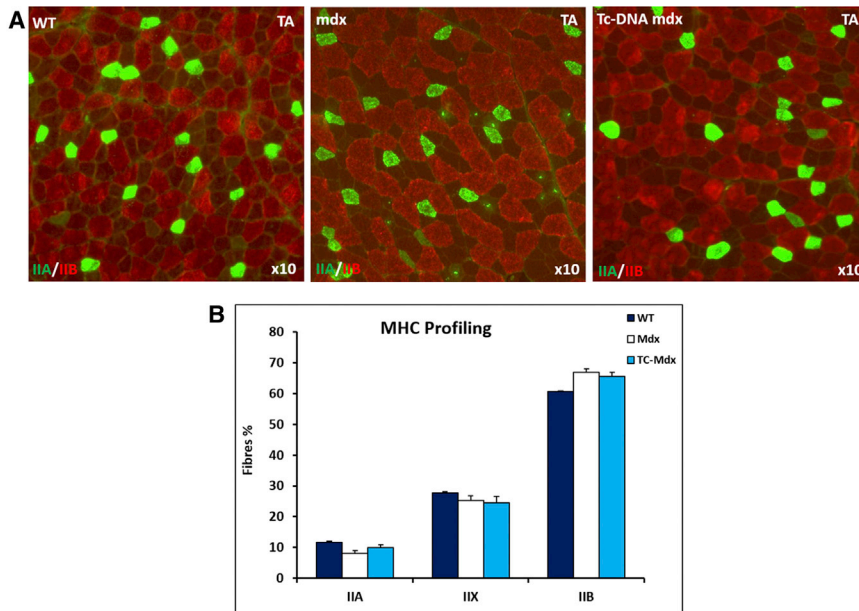


Figure 1. Myosin Heavy Chain Profile of the Tibialis Anterior Muscle

(A) Immunohistochemical images of TA muscle from 20- to 22-week-old male wild-type, *mdx*, and tc-DNA-treated *mdx* mice. Green fibers signify the expression of MHCIIA with MHCIIB appearing as red. Non-green and red fibers represent MHCIIIX. (B) MHC profile in the three cohorts. Results show that WT, *mdx*, and tc-DNA-treated *mdx* mice have the same proportion of each MHC subtype ($n = 4$ for each cohort). Statistical analysis was performed by one-way ANOVA followed by Bonferroni correction for multiple comparison.

population of muscle fibers that differ in their metabolic properties as well as contractile speeds, a feature impacted by the type of myosin heavy chain (MHC) being expressed. Muscle of adult mice is composed of MHCI, MHCIIA, MHCIIIX, and MHCIIIB fibers. MHCI has the slowest contraction rate and is highly reliant on oxidative phosphorylation for energy production. MHCIIIB is at the other end of the spectrum, displaying the fastest contraction rates and highly dependent on glycolytic metabolism. Slow fibers are invested with a higher capillary density as well as thicker ECM compared to fast fibers.^{19,20} Fast-contracting fiber with its decreased ability to store energy in the ECM is hypothesized to facilitate a greater proportion of force transfer to the skeletal elements.²¹ A number of studies have shown that slow muscle, based on MHC expression profiling as well as physical measures, expresses more dystrophin than fast muscle²² and that fast muscle fibers are preferentially affected in DMD.²³

Here we examined whether the efficacy of dystrophin exon skipping is influenced by MHC fiber type, possibly due to fiber type differences in ECM thickness impacting on the rate of AON diffusion into the muscle fiber. We first profiled revertant fibers in *mdx* mice with a view of establishing whether their appearance was related to MHC fiber type. We then investigated the relationship between the restoration of dystrophin and of members of the three DAPC sub-complexes by treatment with tc-DNA and by MHC fiber type. Our results demonstrate that revertant fibers caused by splicing events in untreated *mdx* mice develop in a manner independent of MHC fiber type. Importantly, we show that only a fraction of revertant fibers also express DAPC members. Treatment with tc-DNA results in over 90% of all fibers expressing all proteins examined, with no observed bias toward any one MHC fiber type. These data demonstrate that tc-DNA treatment is able to induce exon skipping in all MHCII fibers.

RESULTS

We first established the MHC landscape of the tibialis anterior (TA) muscle and the effect wrought upon it first by the *mdx* mutation and second after treatment with AONs consisting of tc-DNA. Previous work has reported that the *mdx* mutation affects the MHC fiber profile in a muscle-specific manner, with the extensor digitorum longus (EDL) and soleus unchanged by the mutation²⁴ whereas the diaphragm contains slower isoforms compared to control.²⁵ Analysis of the TA muscle of wild-type (WT) mice at its maximum circumference revealed an approximate ratio of 1:3:6 with respect to MHCIIA, MHCIIIX, and MHCIIIB fibers (Figures 1A and 1B). The same ratios were found in the TA muscles of *mdx* mice and tc-DNA-treated *mdx* mice (Figures 1A and 1B). Statistical analysis failed to reveal significant differences in the proportions of a particular MHC isoform among the three cohorts. Therefore, the MHCII profile of TA muscle was not affected by the absence of dystrophin or by treatment with tc-DNA.

We next examined the relationship between revertant fibers (dystrophin⁺), co-expression of one member of each of the three DAPC sub-complexes, and MHCII class in untreated *mdx* mice. There were approximately 60 dystrophin⁺ fibers in the TA muscle of 20- to 22-week-old mice. The ratio of dystrophin⁺ in relation to MHC fiber type (IIA:IIX:IIB) was approximately 1:3:6, respectively. Therefore, the segregation of dystrophin⁺ fibers within MHC subtypes followed the distribution of each isoform. Hence, there was no bias toward any one MHC isoform with regard to reversion to a dystrophin-positive state (Figure 2A). Profiling the expression of β -sarcoglycan, nNOS, and α -dystroglycan revealed a number of interesting features. First, they were found in all three MHC fiber isoforms, and, similar to dystrophin, there was no bias toward any one MHCII type (Figure 2A). β -sarcoglycan-, nNOS-, and α -dystroglycan-expressing fibers were a subset of those that expressed dystrophin. However, the number of fibers that expressed these three molecules was always lower than the number expressing dystrophin (Figure 2B). Indeed, nNOS-positive fibers, although being the most frequent of the three, only represented about half of dystrophin-positive fibers.

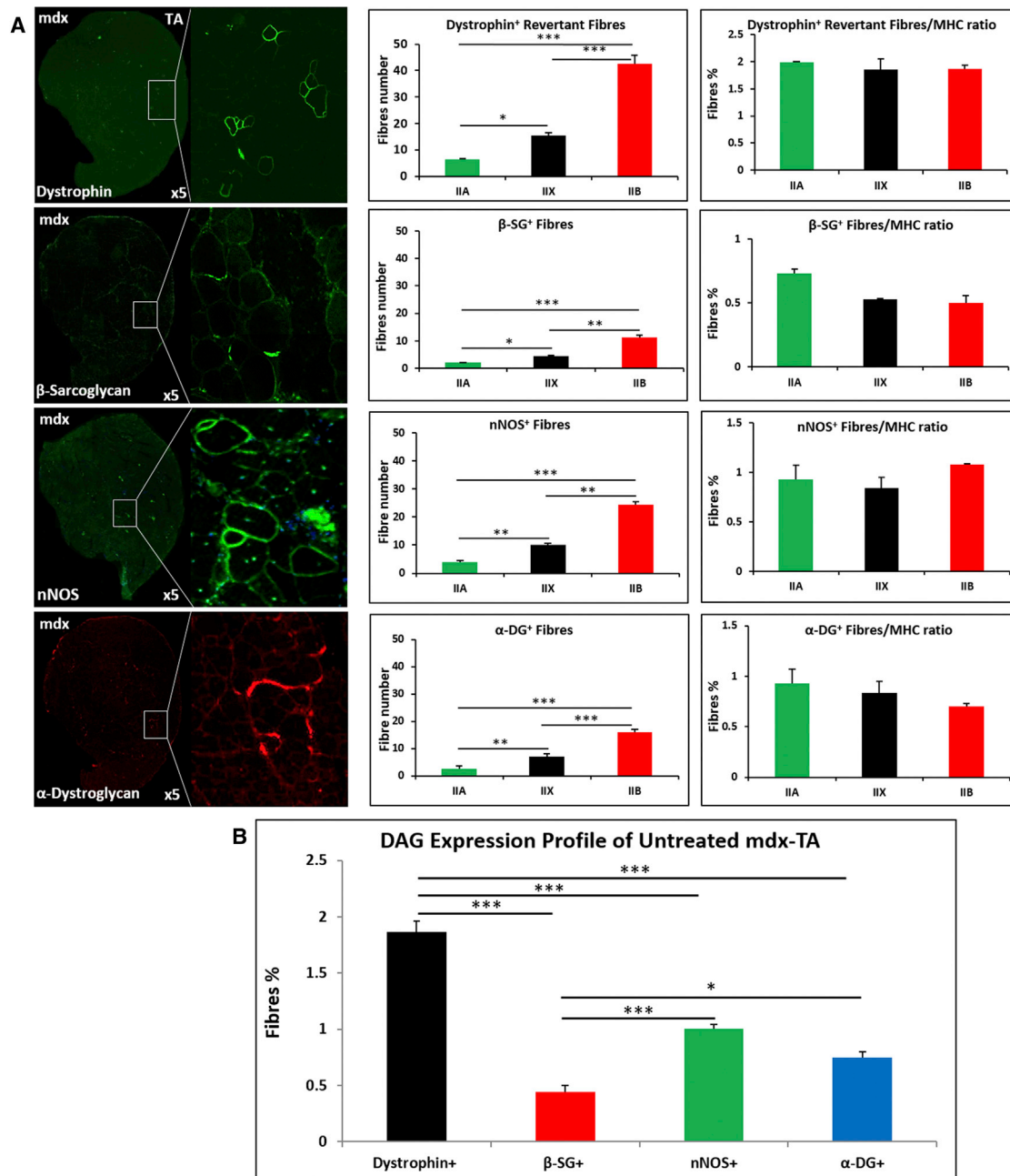


Figure 2. Expression of Dystrophin, β-Sarcoglycan, nNOS, and α-Dystroglycan in the TA Muscle of 20- to 22-Week-Old Male *mdx* Mice

(A) Each row shows the entire TA muscle stained for one of the four molecules together with a magnified detailed image. All positive fibers were correlated to the expression of an MHC isoform, and their distribution is given as the total number as well as proportion to the frequency of the MHC isoform. (B) Graph showing the proportion of TA fibers expressing the four investigated molecules (n = 4 for each cohort). *p < 0.05, **p < 0.01, and ***p < 0.001. Statistical analysis was performed by one-way ANOVA followed by Bonferroni correction for multiple comparison.

These results show that revertant fibers do not express the full complement of DAPC components.

Thereafter, we examined the expression of dystrophin, β-sarcoglycan, nNOS, and α-dystroglycan in relation to MHC fiber type in

the TA muscle of tc-DNA-treated *mdx* mice. Immunostaining revealed that the majority of fibers were positive for dystrophin after tc-DNA treatment, which is in agreement with previous findings of Goyenvallé and colleagues¹⁶ (Figure 3A). Robust expression of dystrophin was found in all MHC fiber types, and analysis of

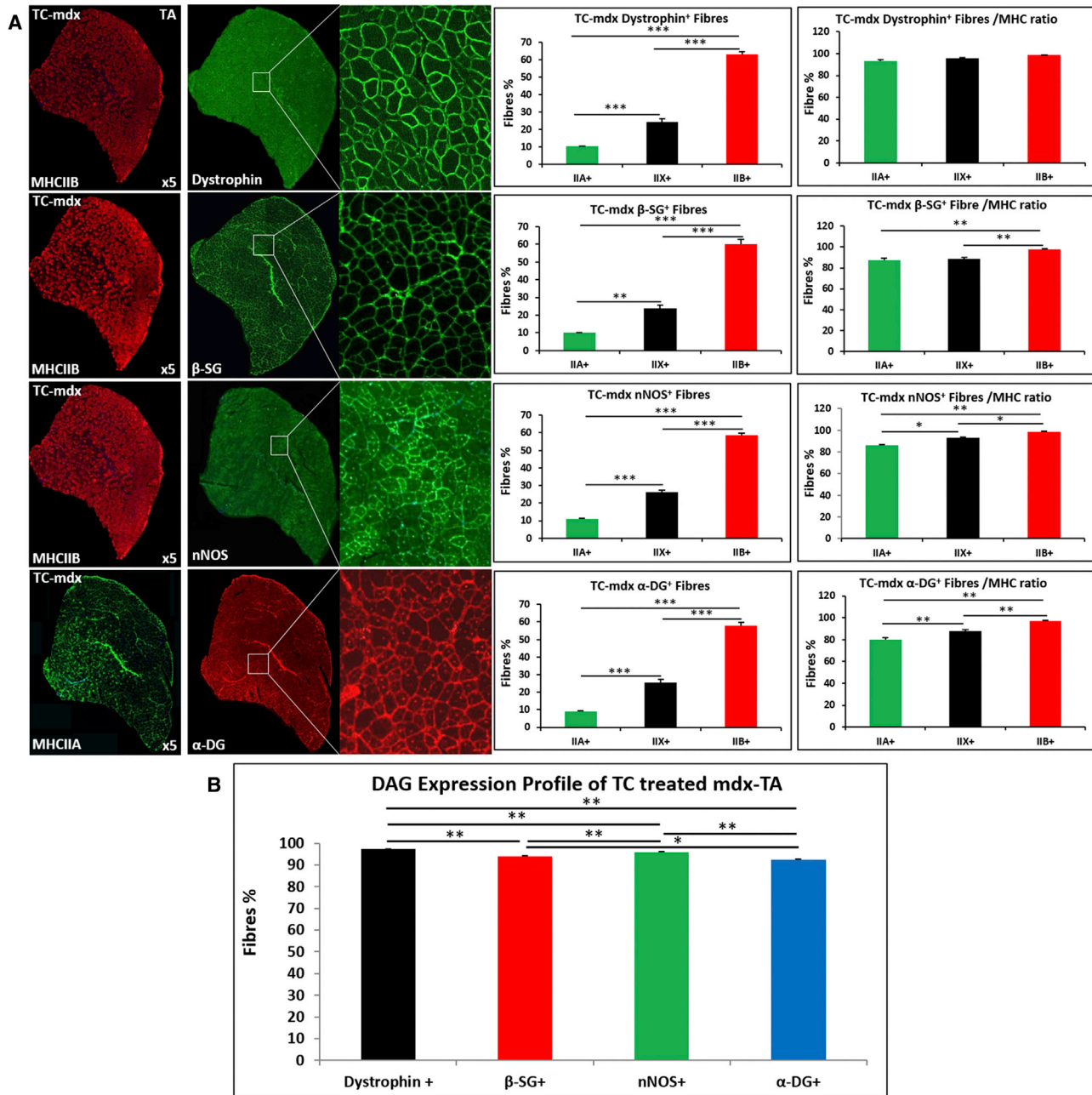


Figure 3. Expression of Dystrophin, β -Sarcoglycan, nNOS, and α -Dystroglycan in the TA Muscle of 20- to 22-Week-Old Male tc-DNA-Treated *mdx* Mice
 (A) Each row shows the entire TA muscle immunostained for dystrophin, β -sarcoglycan, nNOS, and α -dystroglycan together with a magnified detailed image. All positive fibers were correlated to the expression of an MHC isoform, and their distribution is given as the total number as well as proportion to the frequency of the MHC isoform.
 (B) Graph showing the proportion of TA fibers from tc-DNA-treated *mdx* mice expressing the four investigated molecules ($n = 4$ for each cohort). * $p < 0.05$, ** $p < 0.01$, and *** $p < 0.001$. Statistical analysis was performed by one-way ANOVA followed by Bonferroni correction for multiple comparison.

frequency with respect to fiber proportion revealed that there was no bias to any one fiber type. Immunostaining for β -sarcoglycan, nNOS, and α -dystroglycan revealed the same features as dystrophin; the vast majority of fibers expressed the three proteins, and their presence in a particular MHC fiber type was proportional

to the frequency of that form (Figure 3A). We then compared the relative frequency of fibers expressing each of the four proteins. We found there were significantly more fibers that expressed dystrophin than the other three components of the DAPC assessed (Figure 3B).

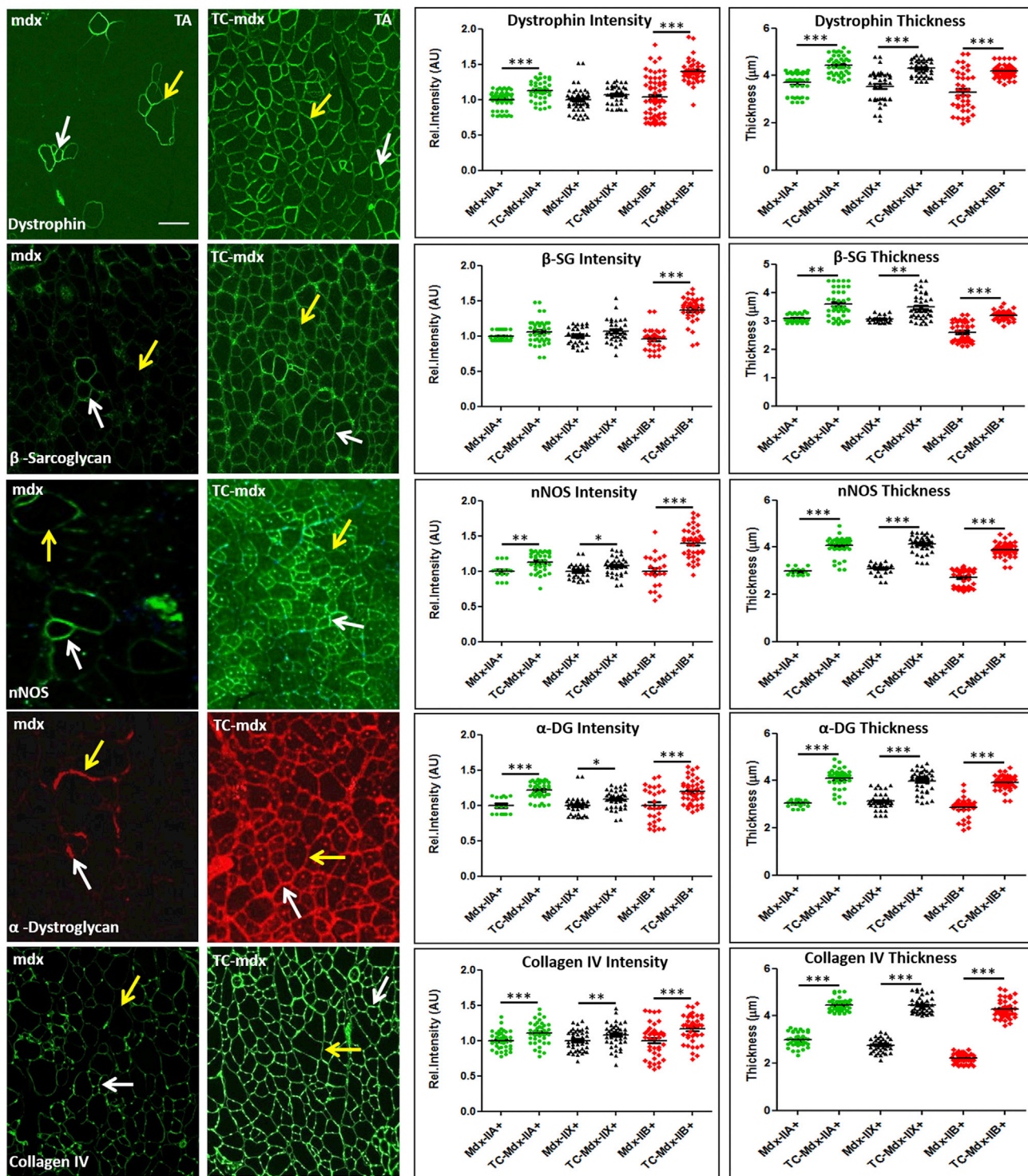


Figure 4. Semiquantitative Analysis of DAPC Restoration following tc-DNA Treatment of 20- to 22-Week-Old Male *mdx* Mice

Untreated and tc-DNA-treated muscle shows high levels of individual proteins in MHCIIA fibers (white arrows) compared to MHCIIIB fibers (yellow arrows). Intensities from over 30 regions for each fiber type were taken from revertant untreated *mdx* and set to a reference value of one. Similar numbers of intensity readings were plotted for each fiber (legend continued on next page)

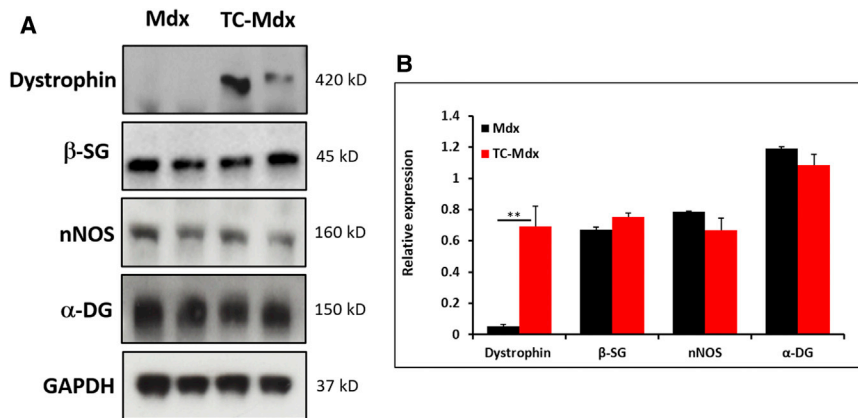


Figure 5. Western Blot Analysis of DAPC Proteins in 20- to 22-Week-Old Male Mice

(A) Western blot image of DAPC proteins in the TA muscle. (B) Quantification of DAPC proteins relative to GAPDH. Note the robust expression of β -sarcoglycan, nNOS, and α -dystroglycan in untreated *mdx* muscle ($n = 3$ for each cohort). ** $p < 0.01$. Statistical analysis was performed using two-tailed t test.

These results show that tc-DNA treatment of *mdx* mice results in the restoration of dystrophin in the majority of muscle fibers. This is also the case for α -dystroglycan, β -sarcoglycan, and nNOS. However, the number of fibers expressing β -sarcoglycan, nNOS, and α -dystroglycan was significantly lower compared to dystrophin.

Previous work has shown that contractile properties of a muscle fiber impact both qualitatively and quantitatively on its surrounding ECM.^{19,20} Here we examined the relationship between MHC fiber type and expression of components of the DAPC as well as an ECM component, collagen IV, using semiquantitative techniques. Fluorescence intensity was used as previously described to gain an indication of the amount of protein at the sarcolemma.¹⁸ We first determined the signal intensity for the five proteins in question in relation to MHC fiber type in the revertant fibers from the *mdx* mouse. For each fiber type, the signal intensity was set to a reference value of 1. Thereafter the same procedure was repeated for the tc-DNA-treated muscle, and intensity was compared to that of the untreated TA muscle. The outcome of the process showed that tc-DNA treatment resulted in an increase in the amount of each protein of interest in all fiber types compared to untreated revertant *mdx* fibers (Figure 4). We also measured the thickness of the expression domain for each of the five marker proteins, revealing that each expression domain was thicker in MHCIIA fibers compared to MHCIIB fibers (Figure 4). This relationship persisted following tc-DNA treatment. Second, we found that there was an increase in the expression domain following tc-DNA treatment for all fiber types (Figure 4).

These results show that the amount of each component of the DAPC and collagen IV at the sarcolemma were elevated above those found in revertant fibers.

Last, we examined the effect of tc-DNA treatment on the total level of expression of the DAPC components under investigation here. To

that end we carried out quantitation of western blots. Our results showed that there was a 14-fold increase in the amount of dystrophin following tc-DNA treatment (Figures 5A and 5B). Interestingly, we found robust expression of β -sarcoglycan, nNOS, and α -dystroglycan in untreated *mdx* muscle and that their levels were not changed significantly by tc-DNA treatment. In summary, components of the DAPC are translated in the absence of dystrophin, but they fail to localize to the sarcolemma.

DISCUSSION

Tc-DNA chemistry is an exciting development in the area of molecular medicine. We have previously shown that, in the context of a mouse model of DMD, tc-DNA treatment was more efficacious in restoring muscle function than many other approaches.¹⁶ Of particular note was the finding that tc-DNA AONs spontaneously form nanoparticles, which are believed to promote entry into the cell and may be the reason why these were able to penetrate the heart and the brain.¹⁶ In this study, we investigated the relationship between muscle compositions in terms of MHC fiber type and dystrophin restoration by tc-DNA AON with a view to developing an understanding of its specificity of action.

We commenced the study by comparing the MHC profile of the TA muscle in the three cohorts under investigation: WT, *mdx*, and tc-DNA-treated *mdx* mice. We found that all three shared the same MHC profile. Previous studies have shown that the MHC profile of the diaphragm underwent a significant change in its MHC compositions, with a decrease in the proportion of MHCIIA⁺ fibers and a concomitant increase in the number of MHCI⁺ fibers.²⁵ The change in MHC profile was proposed to be an adaptive step to preserve contractile function and fiber integrity by lowering energy requirements. In contrast, the EDL and soleus muscles of the *mdx* were shown to be identical to those from WT in terms of MHC profile.²⁴ Our results here now add the TA muscle to the list of muscles that show normal MHC profile in the *mdx* mouse. Nevertheless, all *mdx* muscles have reduced specific force. We propose that, if a change toward a slower MHC profile is an adaptive change to the absence of dystrophin, it must be a secondary step that is dependent on other upstream factors,

type from tc-DNA-treated *mdx* muscle. In all cases there was a significant increase in intensity compared to untreated revertant fibers of the same MHC type. Thickness of expression domain was measured and plotted for each MHC isoform originating from revertant untreated *mdx* and tc-DNA-treated *mdx* muscle. MHCIIA fibers had thicker expression domains compared to MHCIIB. Thickness for expression domains irrespective of MHC fiber type was increased by tc-DNA treatment ($n = 4$ for each cohort). Scale bar applicable to all images represents 50 μm . * $p < 0.05$, ** $p < 0.01$, and *** $p < 0.001$. Statistical analysis was performed using two-tailed t test.

one of which could be contractile activity, which would explain the change in constantly used muscles like the diaphragm and not in limb muscles. A number of studies have proposed mechanisms to explain the reduced specific force in *mdx*, including nitrosylation of the contractile machinery, which, if it occurred, would lead to long-term damage due to low turnover rate of MHC.^{26,27} However, recent work has shown that the MHC from *mdx* functions normally in terms of cross-bridging, which argues against long-term effect of altered muscle function.²⁸ This suggestion is indirectly corroborated by the efficacy of tc-DNA treatment being able to normalize specific force in the TA muscle of *mdx* mice.¹⁶

Our work examining the distribution of the DAPC protein in untreated *mdx* muscle offers interesting insights into the formation of the functional unit. First, we show that there was no bias in terms to MHC fiber type and the appearance of dystrophin. Therefore, if metabolic activity were to generate differential cellular stress based on fiber contraction rate, then this metric does not impact on the splicing events that restore dystrophin expression in *mdx* muscle. Furthermore, when serendipitous events lead to the restoration of dystrophin, they bring back the protein in a relatively normal manner with respect to MHC fiber type, with higher expression in slow fibers compared to faster ones.²² Additionally, there was no bias in terms of MHC fiber type and any of the other components of the DAPC examined here.

An interesting feature highlighted by our work in this section was the finding that revertant fibers (dystrophin⁺) are heterogeneous in terms of their DAPC composition as follows: dystrophin⁺ > nNOS⁺ > α -dystroglycan (α DG)⁺ > β -sarcoglycan (β SG)⁺. Our quantifications of DAPC expression in revertant fibers extends previous findings of Lu et al.²⁹ who showed co-expression of DAPC proteins in clusters of revertant fibers. Interestingly, our western blotting data agree with prior reports showing an abundance of nNOS, α DG, and β SG total protein in *mdx* muscle.³⁰ It follows, therefore, that a mechanism must be active that prevents the translocation of DAPC proteins to the sarcolemma of some revertant fibers. One possibility is that they may not have had sufficient time to correctly translocate. This is, however, unlikely since revertant fibers form from events that occur in muscle precursors.³¹ Another possibility is linked to the poor diffusion of dystrophin within the myofiber sarcolemma, limiting membrane expression to spatially confined nuclear domains. Moving out of this dystrophin domain during serial sectioning would affect detection of other components of the DAPC. While this phenomenon can contribute to a decreased co-detection of dystrophin and DAPC proteins, it should be noted that dystrophin expression in revertant fibers has been reported to span membrane segments of $654 \pm 409 \mu\text{m}$.³² It is unlikely that exiting a nuclear domain during collection of serial sections over a length of muscle not exceeding $160 \mu\text{m}$ (16 serial sections) could on its own account for over half of the revertant fibers lacking expression of other DAPC proteins (Figure 3B). It is therefore possible that a significant proportion of internally deleted dystrophins generated by revertant fibers is not able to assemble a functional DAPC but can be correctly localized

to the membrane. This hypothesis would be consistent with reports of truncated or internally deleted dystrophins that lack the cysteine-rich domain required for interaction with the DAPC but can still be correctly localized to the sarcolemma.³³ Overall our results highlight two interesting findings: first, the majority of revertant fibers produce internally deleted forms of dystrophin that cannot functionally contribute to force transduction, since they are uncoupled from the dystroglycan and sarcoglycan complexes; and, second, *mdx* muscle has a rich pool of DAPC proteins available for recruitment to the sarcolemma upon expression of a functional dystrophin protein.

Restoration of dystrophin expression following tc-DNA treatment resulted in near total coverage of TA fibers, consistent with our previous work.¹⁶ We do not believe that the variation in the affinities of antibodies for their epitopes is a decisive factor in showing a variation in DAPC profile between *mdx* and tc-*mdx* mice. We base this conclusion on the fact that we have compared the same strain (indeed littermates) with or without tc-DNA treatment. Therefore, the differing affinities between antibodies for their particular epitope would remain a constant factor. Hence, the appearance of a molecule at the sarcolemma in tc-*mdx* mice compared to *mdx* must be due to changes in the expression levels of the protein. The results of this study demonstrate that there is no bias with regard to dystrophin expression induction following tc-DNA treatment and fiber type. This is, we believe, highly relevant and important for prospective translation into therapies.

Previous work carried out in humans revealed restoration of dystrophin in a subset of muscle fibers, a differential restoration that may have been influenced by the structural properties of the muscle.^{13,17} Indeed, it is well established that slow muscle fibers have a thicker ECM in comparison to fast fibers.^{19,20} It would, therefore, be reasonable to postulate that slow fibers are more resistant to infiltration by tc-DNA AON. However, our work shows that, at least in terms of type II fiber sub-types, there is no preference to exon skipping. This bodes well for the use of this chemistry in a spectrum of muscles with differing fiber composition, as it seems they are all in principle able to take up the tc-DNA AON. In addition, we show that MHC fiber type does not influence the restoration of the other components examined here. Also, tc-DNA treatment leads to more of each component at the sarcolemma compared to revertant *mdx* fibers. Nevertheless, it is worth noting that not all the fibers that expressed dystrophin contained the other three components of the DAPC examined here (dystrophin⁺ > nNOS⁺ > β SG⁺ > α DG⁺). This again highlights the point that the presence of the DAPC proteins does not necessarily translate into them being assembled into a functional complex.

There is a dearth of knowledge regarding mechanisms that regulate the formation of the DAPC, a gap in our understanding that requires urgent attention. One potential consequence of this gap in our understanding is that it is possible that we will develop the means of inducing protein dystrophin expression but that it may not

translocate to the correct sub-cellular region and, therefore, reduce therapeutic benefit. Insights into this process could be gained by examining revertant fibers. Nevertheless, tc-DNA treatment resulted in over 90% of the fibers having all four of the DAPC components at the sarcoplasm. We believe that this high level of DAPC restoration explains the normalization of specific force following tc-DNA treatment, and, again, it bodes well for translation into the clinic since previous studies have demonstrated that restoration of dystrophin protein levels to 10%–20% of WT results in improved health.³⁴

In summary, we show that reversion of fibers to a dystrophin-positive state in *mdx* mice is a stochastic process with regard to MHC fiber type. However, expression of dystrophin in *mdx* revertant fibers only translates into a minority (>25%) of fibers expressing members of the three sub-complexes. Tc-DNA treatment results in over 90% of fibers' expression of dystrophin as well as members of the three sub-complexes in the TA muscle. Importantly, there is no bias in terms of expression of any component with regard to MHC fiber type. This work shows that, in principle, tc-DNA treatment is equally efficacious across all type II fibers.

MATERIALS AND METHODS

Animals

Animal procedures were performed in accordance with national and European legislation, approved by the French government (Ministère de l'enseignement supérieur et de la recherche, Autorisation APAFiS 6518). *Mdx* (C57BL/10ScSc-Dmdmdx/J) and C57BL/10 mice were bred in our specific opportunistic pathogen-free (SOPF) animal facility at the Plateform 2Care, UFR des Sciences de la santé, Université de Versailles Saint Quentin, and they were maintained in a standard 12-hour light/dark cycle with free access to deionized water and standard laboratory chow (M20, Dietex) *ad libitum*. Mice were weaned at postnatal weeks 4–5 and 2–5 individuals were housed per cage. Mice were randomly allocated to treatment and control groups, ensuring equal numbers of control and treated mice within the same litters.

The tc-DNA-AON PS M23D (5'-AACCTCGGCTTACCT-3') targeting the donor splice site of exon 23 of the mouse dystrophin pre-mRNA used in this study was synthesized by SYNTHENA (Bern, Switzerland). The 6- to 8-week-old male *mdx* mice were injected intravenously in the retro-orbital sinus, under general anesthesia using 1.5%–2% isoflurane, once a week with 200 mg/kg/week of the M23D-tc-DNA for a period of 12 weeks. Treated mice were sacrificed 2 weeks after the last injection, and muscles and tissues were harvested and snap-frozen in liquid nitrogen-cooled isopentane and stored at –80°C before further analysis.

Immunohistochemistry

Dissected and frozen muscles were mounted in Tissue Tech freezing medium (Jung) cooled by dry ice/ethanol. Immunohistochemistry staining was performed on 10- μ m cryosections that were dried for 30 min at room temperature (RT) prior to three washes in 1 \times PBS. Muscle sections were incubated in permeabilization buffer solution (0.952 g HEPES, 0.260 g MgCl₂, 0.584 g NaCl, 0.1 g Sodium azide,

20.54 g Sucrose, and 1 mL Triton X-100) for 15 min at room temperature, before the application of block wash buffer (PBS with 5% fetal calf serum [v/v] and 0.05% Triton X-100) for 30 min at room temperature.

Primary antibodies were pre-blocked in wash buffer for 30 min prior to incubation onto muscle sections overnight at 4°C. Pre-blocked-in wash buffer was performed for all secondary antibodies (in dark) for a minimum of 30 min prior to their addition onto the slides. Sections were then incubated for 1 hr in the dark at room temperature. Finally, slides were mounted in fluorescent mounting medium, and myonuclei were visualized using 2.5 μ g/mL DAPI. Details of primary and secondary antibodies are given in [Supplemental Materials and Methods](#).

Western Blotting

TA proteins from 20- to 22-week-old male mice (20 μ g/lane) were separated on 4%–12% gradient SDS-PAGE gels (Invitrogen), transferred to nitrocellulose membranes (Whatman), and blocked with 5% skim milk in 0.1% Tween 20/Tris-buffered saline. Membranes were cut at appropriate molecular weights in order to allow for simultaneous probing of the exact same samples for dystrophin and multiple DAPC proteins. Membrane strips were then incubated with appropriate primary antibodies overnight at 4°C, followed by a 1-hr incubation at room temperature with the appropriate horseradish peroxidase-conjugated secondary antibodies (Jackson ImmunoResearch Laboratories). Protein bands were visualized using enhanced chemiluminescence reagents (Pierce). Signal was detected on X-ray film (RPI) at multiple exposures. For densitometric analysis, protein band intensities from multiple non-saturated film exposures were quantified using ImageJ (NIH). Values in the linear range of pixel intensities were selected for quantifications. Signal intensities were normalized to GAPDH, used as an internal loading control, and probed on the same membrane. Details of primary and secondary antibodies are given in [Supplemental Materials and Methods](#).

Semiquantitative Measures of Sarcolemma Protein Expression

Intensity of signals of protein of interest was measured as previously described.¹⁸ Briefly, membrane signal intensities of approximately 30 muscle fibers of each MHC phenotype (IIA, IIX, and IIB) in each TA muscle section from *mdx* mice and *mdx* mice treated with tc-DNA were measured. Fiji software was used to measure signal from area of interest after images had been corrected for background to avoid regions of signal saturation. To calculate relative signal intensity levels, individual measurements from treated and control fibers were taken as a percentage of mean of control samples.

Sarcolemma Thickness Measurement

Connective tissue thickness between approximately 30 fibers of the same MHC phenotypes (IIA-IIA, IIX-IIX, and IIB-IIB) of TA muscle sections was measured using Fiji software. One measurement on the constant connective tissue thickness and multiple measurements on the fluctuating connective tissue thickness areas between each two myofibers that expressed the same MHC isoform were taken on all muscle sections of *mdx* mice and *mdx* mice treated with tc-DNA.

Imaging and Analysis

A fluorescence microscope (Zeiss AxioImegar A1) was used to examine immunofluorescently stained sections, and images were captured using an Axiocam digital camera with Zeiss Axiovision computer software version 4.8.

Statistical Analysis

Data are presented as mean \pm SE. Significant differences between two groups were performed by two-tailed Student's t test for independent variables. Differences among groups were analyzed by one-way ANOVA followed by Bonferroni multiple comparison tests as appropriate. Statistical analysis was performed on GraphPad Prism software. Differences were considered statistically significant at * $p < 0.05$, ** $p < 0.01$, or *** $p < 0.001$.

SUPPLEMENTAL INFORMATION

Supplemental Information includes Supplemental Materials and Methods and can be found with this article online at <https://doi.org/10.1016/j.omtn.2017.10.014>.

AUTHOR CONTRIBUTIONS

Conceptualization, K.P.; Methodology, A.G. and L.G.; Investigation, S.O., K.-L.H., H.C.-H., and F.M.; Writing, S.O., F.M., A.G., L.G., and K.P.; Supervision, K.P.

ACKNOWLEDGMENTS

This work was supported by the Ministry of Higher Education of Iraq, the Agence Nationale de la Recherche (France), the Association Monégasque Contre les Myopathies (Monaco), and the Biotechnology and Biological Sciences Research Council (BBSRC-UK) (J016454/1 to H.C.-H.). F.M. is supported by a European Horizon 2020 re-integration Marie-Sklodowska Curie Senior Fellowship. We are also grateful to two anonymous reviewers for comments that have greatly improved the manuscript. Finally, we are indebted to Dr. Patrick Lewis for proofreading the revised version.

REFERENCES

- Hoffman, E.P., and Connor, E.M. (2013). Orphan drug development in muscular dystrophy: update on two large clinical trials of dystrophin rescue therapies. *Discov. Med.* 16, 233–239.
- Chung, J., Smith, A.L., Hughes, S.C., Niizawa, G., Abdel-Hamid, H.Z., Naylor, E.W., Hughes, T., and Clemens, P.R. (2016). Twenty-year follow-up of newborn screening for patients with muscular dystrophy. *Muscle Nerve* 53, 570–578.
- Zubrzycka-Gaarn, E.E., Bulman, D.E., Karpati, G., Burghes, A.H., Belfall, B., Klamut, H.J., Talbot, J., Hodges, R.S., Ray, P.N., and Worton, R.G. (1988). The Duchenne muscular dystrophy gene product is localized in sarcolemma of human skeletal muscle. *Nature* 333, 466–469.
- Hoffman, E.P., Brown, R.H., Jr., and Kunkel, L.M. (1987). Dystrophin: the protein product of the Duchenne muscular dystrophy locus. *Cell* 51, 919–928.
- Ohlendieck, K., Ervasti, J.M., Snook, J.B., and Campbell, K.P. (1991). Dystrophin-glycoprotein complex is highly enriched in isolated skeletal muscle sarcolemma. *J. Cell Biol.* 112, 135–148.
- Dickson, G., Azad, A., Morris, G.E., Simon, H., Noursadeghi, M., and Walsh, F.S. (1992). Co-localization and molecular association of dystrophin with laminin at the surface of mouse and human myotubes. *J. Cell Sci.* 103, 1223–1233.

- Matsumura, K., Tomé, F.M., Ionasescu, V., Ervasti, J.M., Anderson, R.D., Romero, N.B., Simon, D., Récan, D., Kaplan, J.C., Fardeau, M., et al. (1993). Deficiency of dystrophin-associated proteins in Duchenne muscular dystrophy patients lacking COOH-terminal domains of dystrophin. *J. Clin. Invest.* 92, 866–871.
- Kim, S., Campbell, K.A., Fox, D.J., Matthews, D.J., and Valdez, R.; MD STARnet (2015). Corticosteroid Treatments in Males With Duchenne Muscular Dystrophy: Treatment Duration and Time to Loss of Ambulation. *J. Child Neurol.* 30, 1275–1280.
- Lee, J.W., Won, Y.H., Choi, W.A., Lee, S.K., and Kang, S.W. (2013). Successful surgery for scoliosis supported by pulmonary rehabilitation in a duchenne muscular dystrophy patient with forced vital capacity below 10%. *Ann. Rehabil. Med.* 37, 875–878.
- Wilton, S.D., and Fletcher, S. (2008). Exon skipping and Duchenne muscular dystrophy: hope, hype and how feasible? *Neurol. India* 56, 254–262.
- Alter, J., Lou, F., Rabinowitz, A., Yin, H., Rosenfeld, J., Wilton, S.D., Partridge, T.A., and Lu, Q.L. (2006). Systemic delivery of morpholino oligonucleotide restores dystrophin expression bodywide and improves dystrophic pathology. *Nat. Med.* 12, 175–177.
- Arechavala-Gomez, V., Graham, I.R., Popplewell, L.J., Adams, A.M., Aartsma-Rus, A., Kinali, M., Morgan, J.E., van Deutekom, J.C., Wilton, S.D., Dickson, G., and Muntoni, F. (2007). Comparative analysis of antisense oligonucleotide sequences for targeted skipping of exon 51 during dystrophin pre-mRNA splicing in human muscle. *Hum. Gene Ther.* 18, 798–810.
- Kinali, M., Arechavala-Gomez, V., Feng, L., Cirak, S., Hunt, D., Adkin, C., Guglieri, M., Ashton, E., Abbs, S., Nihoyannopoulos, P., et al. (2009). Local restoration of dystrophin expression with the morpholino oligomer AVI-4658 in Duchenne muscular dystrophy: a single-blind, placebo-controlled, dose-escalation, proof-of-concept study. *Lancet Neurol.* 8, 918–928.
- Renneberg, D., Bouliong, E., Reber, U., Schümperli, D., and Leumann, C.J. (2002). Antisense properties of tricyclo-DNA. *Nucleic Acids Res.* 30, 2751–2757.
- Murray, S., Ittig, D., Koller, E., Berdeja, A., Chappell, A., Prakash, T.P., Norrbom, M., Swayze, E.E., Leumann, C.J., and Seth, P.P. (2012). TricycloDNA-modified oligo-2'-deoxyribonucleotides reduce scavenger receptor B1 mRNA in hepatic and extra-hepatic tissues—a comparative study of oligonucleotide length, design and chemistry. *Nucleic Acids Res.* 40, 6135–6143.
- Goyenvalle, A., Griffith, G., Babbs, A., El Andaloussi, S., Ezzat, K., Avril, A., Dugovic, B., Chaussonot, R., Ferry, A., Voit, T., et al. (2015). Functional correction in mouse models of muscular dystrophy using exon-skipping tricyclo-DNA oligomers. *Nat. Med.* 21, 270–275.
- van Deutekom, J.C., Janson, A.A., Ginjaar, I.B., Frankhuizen, W.S., Aartsma-Rus, A., Bremmer-Bout, M., den Dunnen, J.T., Koop, K., van der Kooij, A.J., Goemans, N.M., et al. (2007). Local dystrophin restoration with antisense oligonucleotide PRO051. *N. Engl. J. Med.* 357, 2677–2686.
- Cirak, S., Feng, L., Anthony, K., Arechavala-Gomez, V., Torelli, S., Sewry, C., Morgan, J.E., and Muntoni, F. (2012). Restoration of the dystrophin-associated glycoprotein complex after exon skipping therapy in Duchenne muscular dystrophy. *Mol. Ther.* 20, 462–467.
- Elashry, M.I., Collins-Hooper, H., Vaiyapuri, S., and Patel, K. (2012). Characterisation of connective tissue from the hypertrophic skeletal muscle of myostatin null mice. *J. Anat.* 220, 603–611.
- Kovanen, V., Suominen, H., and Heikkinen, E. (1980). Connective tissue of “fast” and “slow” skeletal muscle in rats—effects of endurance training. *Acta Physiol. Scand.* 108, 173–180.
- Kovanen, V., Suominen, H., and Heikkinen, E. (1984). Mechanical properties of fast and slow skeletal muscle with special reference to collagen and endurance training. *J. Biomech.* 17, 725–735.
- Ho-Kim, M.A., and Rogers, P.A. (1992). Quantitative analysis of dystrophin in fast- and slow-twitch mammalian skeletal muscle. *FEBS Lett.* 304, 187–191.
- Webster, C., Silberstein, L., Hays, A.P., and Blau, H.M. (1988). Fast muscle fibers are preferentially affected in Duchenne muscular dystrophy. *Cell* 52, 503–513.
- Anderson, J.E., Bressler, B.H., and Ovalle, W.K. (1988). Functional regeneration in the hindlimb skeletal muscle of the mdx mouse. *J. Muscle Res. Cell Motil.* 9, 499–515.

25. Petrof, B.J., Stedman, H.H., Shrager, J.B., Eby, J., Sweeney, H.L., and Kelly, A.M. (1993). Adaptations in myosin heavy chain expression and contractile function in dystrophic mouse diaphragm. *Am. J. Physiol.* 265, C834–C841.
26. Li, D., Yue, Y., Lai, Y., Hakim, C.H., and Duan, D. (2011). Nitrosative stress elicited by nNOS μ delocalization inhibits muscle force in dystrophin-null mice. *J. Pathol.* 223, 88–98.
27. Guellich, A., Negroni, E., Decostre, V., Demoule, A., and Coirault, C. (2014). Altered cross-bridge properties in skeletal muscle dystrophies. *Front. Physiol.* 5, 393.
28. Bates, G., Sigurdardottir, S., Kachmar, L., Zitouni, N.B., Benedetti, A., Petrof, B.J., Rassier, D., and Lauzon, A.M. (2013). Molecular, cellular, and muscle strip mechanics of the mdx mouse diaphragm. *Am. J. Physiol. Cell Physiol.* 304, C873–880.
29. Lu, Q.L., Morris, G.E., Wilton, S.D., Ly, T., Artem'yeva, O.V., Strong, P., and Partridge, T.A. (2000). Massive idiosyncratic exon skipping corrects the nonsense mutation in dystrophic mouse muscle and produces functional revertant fibers by clonal expansion. *J. Cell Biol.* 148, 985–996.
30. Rezniczek, G.A., Konieczny, P., Nikolic, B., Reipert, S., Schneller, D., Abrahamsberg, C., Davies, K.E., Winder, S.J., and Wiche, G. (2007). Plectin 1f scaffolding at the sarcolemma of dystrophic (*mdx*) muscle fibers through multiple interactions with β -dystroglycan. *J. Cell Biol.* 176, 965–977.
31. Yokota, T., Lu, Q.L., Morgan, J.E., Davies, K.E., Fisher, R., Takeda, S., and Partridge, T.A. (2006). Expansion of revertant fibers in dystrophic mdx muscles reflects activity of muscle precursor cells and serves as an index of muscle regeneration. *J. Cell Sci.* 119, 2679–2687.
32. Chretien, F., Dreyfus, P.A., Christov, C., Caramelle, P., Lagrange, J.L., Chazaud, B., and Gherardi, R.K. (2005). In vivo fusion of circulating fluorescent cells with dystrophin-deficient myofibers results in extensive sarcoplasmic fluorescence expression but limited dystrophin sarcolemmal expression. *Am. J. Pathol.* 166, 1741–1748.
33. Rafael, J.A., Cox, G.A., Corrado, K., Jung, D., Campbell, K.P., and Chamberlain, J.S. (1996). Forced expression of dystrophin deletion constructs reveals structure-function correlations. *J. Cell Biol.* 134, 93–102.
34. Hoffman, E.P., Bronson, A., Levin, A.A., Takeda, S., Yokota, T., Baudy, A.R., and Connor, E.M. (2011). Restoring dystrophin expression in duchenne muscular dystrophy muscle progress in exon skipping and stop codon read through. *Am. J. Pathol.* 179, 12–22.

mouse models that allow for testing of such therapies in the context of the human *DMD* sequence *in vivo*. Therefore, we have created a novel mouse model whereby we have used the hDMD mouse (containing the full human *DMD* gene integrated into chromosome 5) and mutated it to be out-of-frame by deleting exon 45 using CRISPR/Cas9 in hDMD zygotes. We have crossed these hDMD del45 mice to mdx and mdx D2 backgrounds, both of which lack mouse dystrophin, to create a fully dystrophic model containing the human *DMD* gene. We have utilized this model to demonstrate proof of principle that our CRISPR/Cas9 platform, which targets deletion of human *DMD* exons 45–55, can be directly applied *in vivo* to restore dystrophin expression. These studies demonstrate that the hDMD del45 mdxD2 mouse is a useful model for pre-clinical testing of genetic therapies that act on the *DMD* gene and provide proof of principle that our CRISPR based gene editing strategy is functional *in vivo*.

<http://dx.doi.org/10.1016/j.nmd.2017.06.337>

P.298

Development of a CRISPR-based gene therapy approach targeting the large exon 45-exon 55 mutation hotspot in DMD gene

J. Bellec-Dyèvre, W. Lostal, E. Bernard, J. Cosette, I. Richard
Généthon, Inserm U951, INTEGRARE, Evry, France

Gene replacement and exon skipping therapies for Duchenne muscular dystrophy (DMD) showed successful improvements in preclinical studies. However, results obtained in recent clinical trials called for the development of new therapeutic strategies that would restore a full-length or nearly full-length dystrophin expression, provide long-term correction and answer challenges regarding body-wide targeting. *Dmd* gene editing approaches hold great promise and indeed have been shown to successfully excise exon 23 and exons 52–53 *in vivo*, leading to histopathological improvement. Targeting the larger exon 45-exon 55 (Ex45-Ex55) mutation hotspot would account for about 60% of the DMD patients. A proof-of-concept study validated this approach in iPSC cells. We are developing a CRISPR-based gene therapy approach targeting the *Dmd* Ex45-Ex55 region to restore reading-frame and protein expression *in vivo*. Both *Streptococcus pyogenes* (sp) and *Staphylococcus aureus* (sa) Cas9 endonucleases are used to edit *Dmd* gene following AAV transfer. First, gRNAs were designed and validated *in vitro*. Selected gRNAs have been injected either in mouse models with muscle-specific Cas9 expression or in wild-type mice with spCas9 or saCas9 as single or dual AAV vectors. Cas9 expression was confirmed at the RNA and protein levels. Nuclear localization and transduction efficiency was checked by immuno-histo-fluorescence (IHF). Endonuclease activity at the targeted loci and Ex45-Ex55 inversion or deletion events are being investigated at the DNA and RNA levels by PCR, qPCR and ddPCR.

<http://dx.doi.org/10.1016/j.nmd.2017.06.338>

P.299

A single neonatal injection of an AAV9.U7snRNA virus mediating skipping of dmd exon 2 allows dystrophin expression preventing apparition of pathologic features in the Dup2 mouse one year post injection

N. Wein¹, T. Simmons¹, F. Gumienny¹, N. Huang¹, K. Heller¹, J. Yurkoski¹, L. Rodino-Klapac¹, F. Muntoni², K. Flanigan³

¹Nationwide Childrens Hospital, Columbus, USA; ²UCL Institute of Child Health, London, UK; ³The Research Institute at Nationwide Children's Hospital, Columbus, USA

Mutations that truncate the reading frame 5' of exon 5 of the *DMD* gene result in use of an internal ribosome entry site (IRES). This element allows alternate translational initiation beginning within exon 6 that results in expression of an N-truncated isoform. Despite lacking half of the actin binding domain 1, this isoform is highly functional. We developed an AAV9.U7snRNA vector directed against exon 2 which induces skipping of this exon, thus

resulting in a truncation of the reading frame therefore forcing expression of the highly functional N-truncated protein. Injection of this vector have shown that in a Duchenne muscular dystrophy (DMD) mouse model carrying a duplication of exon 2 (the Dup2 mouse), postnatal intramuscular (IM) or late or early intravascular (IV) treatment results in functional and pathologic improvement in skeletal muscle. Importantly, early delivery of the vector results in almost complete protection of the muscle 6months post injection which is highly relevant to efforts to identify and treat DMD patients at an earlier age. Here we are presenting a follow up study one year post injection. In the Dup2 mouse, efficient skipping and abundant dystrophin expression were still present at one year following the single AAV injection. Dystrophic pathology was absent at all-time points; at one year, less than 1 % of fibers showed central nucleation, in comparison to ~70% in untreated Dup2 mice. Assessment of strength, and evaluation of sarcolemma stability were also performed. Both tests demonstrated a significant protection of the treated animals. Finally, to model the applicability of this approach beyond exon 2 duplication patients, the same vector was used to treat 6 human patient fibroblast-derived transdifferentiated myoblasts harboring various mutations within exons 1 to 4. In all FibroMyoD cultures, abundant exon 2 skipping and dystrophin expression were detected after treatment. These results suggest that this exon-skipping vector offers a therapeutic approach not only to patients with exon 2 duplications but with all mutations within the first four *DMD* exons (~6% of patients), an area of the gene largely ignored by the current therapeutic approaches. This work strongly supports the idea that early treatment of these patients will have longstanding and significant benefit resulting in a better outcome.

<http://dx.doi.org/10.1016/j.nmd.2017.06.339>

P.300

Correction of the exon 2 duplication in DMD myoblasts by a single CRISPR/Cas9 system

A. Lattanzi¹, S. Duguez², A. Moiani³, A. Izmiryan³, E. Barbon⁴, S. Martin¹, K. Mamchaoui², V. Mouly², F. Bernardi⁴, F. Mavilio¹, M. Bovolenta⁴

¹Généthon, Evry, France; ²Institut de Myologie, UMRS 974, Paris, France; ³Généthon, Paris, France; ⁴University of Ferrara, Ferrara, Italy

Exonic duplications account for 10–15% of all mutations in Duchenne muscular dystrophy (DMD), a severe hereditary neuromuscular disorder. We report a novel CRISPR (Clustered Regularly Interspaced Short Palindromic Repeat)/Cas9-based strategy to correct the most frequent (exon 2) duplication in the *DMD* gene by targeted deletion, and tested the efficacy of such an approach in patient-derived myogenic cells. We demonstrate restoration of wild-type dystrophin expression at transcriptional and protein level in myotubes derived from genome-edited myoblasts in the absence of selection. Removal of the duplicated exon was achieved by the use of only one gRNA directed against an intronic region, thereby increasing editing efficiency and reducing the risk of off-target effects. This study opens a novel therapeutic perspective for patients carrying disease-causing duplications independently from the duplication extension.

<http://dx.doi.org/10.1016/j.nmd.2017.06.340>

P.301

The relationship between dystrophin restoration through tricyclo DNA-AON treatment to myosin fast fibre phenotype and other members of the DAG complex

S. Omairi¹, A. Goyenvallé², H. Amthor², L. Garcia², K. Patel¹

¹University of Reading, Reading, UK; ²University de Versailles St-Quentin, Paris, France

Restoration of Dystrophin expression is a potential means of treating Duchenne muscular dystrophy. One exciting approach to achieve this endpoint through antisense oligonucleotide (AON) mediate exon skipping. Recently we described a novel class of AON made of tricyclo-DNA (tc) which due to their

unprecedented tissue uptake promoted a high degree of dystrophin expression. Here we examined whether muscle fibre characteristics influenced the efficacy of tcDNA-AON to restore dystrophin expression. We first examined untreated mdx muscle for dystrophin expression in revertant fibres and its relation to the expression of myosin heavy chain isoforms. We show that revertant fibres (less than 2% of all fibres) showed no bias for MHCII expression. Interestingly only about a quarter of revertant fibres expressed other components of the Dystrophin-Associated Glycoprotein (DAG) complex. As expected treatment with tcDNA-AON resulted in a dystrophin restoration, with 10% of fibres in the tibialis anterior muscle showing positivity. Importantly this restoration was equal between MHCIIB and non-IIB fibres. However two key components of the DAG only featured in 2–4% of all fibres again without any MHCII fibre type bias. Finally we show that amount of not only dystrophin but also of b-SG, a DG and collagen IV were increased in muscle fibres following TC-AON. These results show that dystrophin restoration does not necessitate the restoration of other members of the DAG. However the levels of each component when reinstated were higher than in revertant fibres. The importance of our work is that it demonstrates that a relatively small proportion of fibres with a full repertoire of DAG complex proteins are able to bring about major physiological improvement.

<http://dx.doi.org/10.1016/j.nmd.2017.06.341>

P.302

***In vivo* analysis of dystrophin (re-) expression in DmdEGFP and DmdEGFP-mdx reporter mice**

M. Petkova¹, C. Laplace-Builhé², A. Goyenvalle¹, L. Garcia¹, M. Schuelke³, H. Amthor¹

¹ University of Versailles St-Quentin, Montigny-le-Bretonneux, France;

² Institut Gustave Roussy, Villejuif, France; ³ Charité – Universitätsmedizin Berlin, Berlin, Germany

Duchenne muscular dystrophy (DMD), the most frequently inherited muscle disease in childhood, is caused by mutations in the gene encoding dystrophin. The modification of dystrophin mRNA splicing, called exon-skipping, is a promising therapeutic strategy. This approach uses small molecules, anti-sense oligonucleotides, that “repair” the open reading frame of the *Dmd* gene through skipping of exons, which flank the original mutation and lead to the production of truncated dystrophin. Animal models play an indispensable role in the development and optimization of therapeutic approaches for DMD as well as in understanding the role dystrophin in the muscle. Our group recently generated the first dystrophin reporter mice on the wildtype (*Dmd*^{EGFP}) and *mdx* (*Dmd*^{EGFP-mdx}) genetic background. These models express an endogenous dystrophin-EGFP fusion protein permitting the visualization of dystrophin expression using native fluorescence. We currently study the expression of dystrophin *in vivo* using intravital two photon microscopy in skeletal muscle from *Dmd*^{EGFP} mice. We analyze the dynamics of dystrophin during the course of an acute injury and reconstitute the regenerating muscle in 3D using the dystrophin-EGFP re-expression in myofibers. We use *Dmd*^{EGFP-mdx} and study *in vivo* the restoration of dystrophin following of exon skipping for direct visualization, quantification and precisising the dynamics of dystrophin restoration. Data of these ongoing experiments will improve our understanding of the pharmacodynamics of exon skipping strategies.

<http://dx.doi.org/10.1016/j.nmd.2017.06.342>

P.303

SGT-001 Micro-dystrophin gene therapy for Duchenne muscular dystrophy

J. Schneider, J. Gonzalez, K. Brown, D. Golebiowski, V. Ricotti, J. Quiroz, C. Morris

Solid Biosciences, Cambridge, USA

Duchenne muscular dystrophy (DMD) is a severe muscle disorder caused by loss-of-function mutations in the *DMD* gene, which lead to the absence of the dystrophin protein. Without dystrophin, the structural link between the actin cytoskeleton and extracellular matrix is broken, and muscles are highly susceptible to contraction-induced damage. Direct dystrophin replacement has thus far been unsuccessful due to large size of the *DMD* gene. As a wide variety of mutations can be responsible for the disease, therapeutic strategies aimed at specific mutations only have the potential to benefit subsets of patients. SGT-001 is an AAV micro-dystrophin gene therapy being developed to enter clinical trials for DMD. This represents a unique strategy to benefit DMD patients regardless of dystrophin mutation. The program is based on extensive research on the dystrophin protein, to develop shorter yet functional micro-dystrophin variants, and to deliver genes to muscle. Significant preclinical work has been conducted to fully characterize SGT-001. Solid has performed studies in dystrophic mouse and dog models to evaluate biodistribution and micro-dystrophin protein expression following systemic administration of SGT-001. Preclinical data show that a single dose of SGT-001 leads to widespread biodistribution and long-term micro-dystrophin expression in skeletal and cardiac muscle. Quantification of protein expression using immunofluorescence, Western blotting and mass spectrometry identified a dose-response increase in percent positive muscle and overall protein levels. Further, *in vivo* and *in vitro* functional assessments have demonstrated improved muscle function in a similar dose-dependent manner. The goal of the SGT-001 program is to develop a clinical candidate that will generate tolerated and efficacious levels of micro-dystrophin protein in all affected muscles in DMD. Solid is planning to develop SGT-001 to become a viable therapeutic option for DMD patients, regardless of mutation.

<http://dx.doi.org/10.1016/j.nmd.2017.06.343>

P.304

Dose finding study in the DMDmdx rat model to determine the efficacious dose of a rAAV9 vector encoding a human mini-dystrophin after IV administration

C. Le Guiner¹, M. McIntyre², T. Larcher¹, O. Adjali¹, A. Lafoux¹, G. Toumaniantz¹, L. Wood³, X. Xiao⁴, P. Moullier¹, R. Samulski²

¹ University of Nantes, Nantes, France; ² Bamboo Therapeutics, Pfizer, Chapel Hill, USA; ³ Pfizer, Cambridge, USA; ⁴ University of North Carolina, Chapel Hill, USA

We determined the pharmacologically effective dose range of rAAV9-dys3978, a recombinant AAV serotype 9 vector expressing a human mini-dystrophin gene under the control of a muscle-specific promoter, administered intravenously in 2-month old DMDmdx rat. Animals were followed for 3 and 6 months after vector administration. Primary measures of efficacy included the percentage of dystrophin-expressing myofibers in skeletal, cardiac and diaphragm muscle, dystrophic muscle pathology, strength and fatigue as measured by grip force test, and cardiac function as measured by 2D echocardiography. In-life clinical observations, clinical biochemistry measures and immuno-monitoring were included in the study design to provide dose-related information about the safety of the test article in an animal model of disease. The complete data will be presented.

<http://dx.doi.org/10.1016/j.nmd.2017.06.344>

P.305

Molecular therapy in a novel translational large animal model for Duchenne muscular dystrophy

S. Krause¹, S. Reichert¹, T. Donandt¹, C. Kalbe², M. Schmuck¹, N. Klymiuk³, B. Kessler³, A. Blütke⁴, E. Wolf³, B. Schoser¹, M. Walter¹

¹ Friedrich Baur Institute, Munich, Germany; ² Leibniz Institute for Farm Animal Biology, Dummerstorf, Germany; ³ Molecular Animal Breeding and Biotechnology and Laboratory for Functional Genome Analysis (LAFUGA),

Muscular dystrophies are characterized by weakness and wasting of skeletal muscle tissues and treating wasting muscle is one of the biggest issues in the neuromuscular field. Several drugs targeting the myostatin pathway have been used in clinical trials to increase muscle mass and function but so far, most drugs had no or limited effects in improving function in neuromuscular patients. In our study, the expression levels of different actors of the myostatin network were analysed at mRNA and protein levels in neuromuscular patients' sera and skeletal muscle specimens. In muscle wasting or atrophying diseases, a strong down-regulation of the whole myostatin pathway was observed with a decrease of myostatin and activin receptor, and an increase of the myostatin antagonist, follistatin. We also provide *in vivo* evidence in the congenital myopathy *mtm1* mouse model that a down-regulated myostatin pathway can be reactivated by correcting the underlying gene defect using AAV-mediated gene therapy. Importantly, we show that the MTM1 restoration effect on muscle mass can be further enhanced by anti-myostatin therapy. Our data may explain the poor clinical efficacy of anti-myostatin approaches in clinical studies and the apparent contradictory results in mice regarding the efficacy of anti-myostatin approaches and may profoundly affect patient selection and stratification for future trials.

<http://dx.doi.org/10.1016/j.nmd.2017.06.026>

EC.O.5

The multi-systemic protection against age-related tissue function decline in progeric mice through the attenuation of myostatin/activin signalling

K. Patel¹, K. Alyodawi¹, S. Omairi¹, W. Vermeij², O. Kretz³, F. Salagna³, T. Huber³

¹University of Reading, Reading, UK; ²Erasmus, Rotterdam, Netherlands;

³University of Freiburg, Freiburg, Germany

A dominant principle underpinning our understanding of the ageing process is that DNA damage induces a stress response that shifts cellular resources from growth towards maintenance. A contrasting and seemingly irreconcilable view is that prompting growth of, for example skeletal muscle, results in systemic benefit. To investigate the robustness of these axioms, we induced muscle growth in a murine progeric model. Here we show that the muscle of *Ercc1Δ/progeric* mice undergoes an extremely severe form of wasting which can be protected through an intervention that attenuates myostatin/activin signalling. Significantly we found that treated progeric mice not only maintained muscle activity but also kidney function, protected against the development of liver abnormalities and osteoporosis. This study fundamentally challenges the notion that tissue growth and the maintaining tissue function during ageing are incompatible mechanisms. As importantly, it highlights the potential of therapies based on myostatin/activin blockade to promote healthy ageing.

<http://dx.doi.org/10.1016/j.nmd.2017.06.027>

EC.O.6

Abolition of the NLRP3 inflammasome improves the dystrophic phenotype in a murine model of Duchenne muscular dystrophy

R. Boursereau, M. Abou-Samra, S. Lecompte, L. Noel, S. Brichard
Catholic University of Louvain (UCL), Brussels, Belgium

Assembly of the NLRP3 inflammasome leads to caspase-1 activation and mediates the cleaving and release of several inflammatory cytokines. The NLRP3 inflammasome can amplify inflammatory responses and thus worsen several diseases. Duchenne muscular dystrophy (DMD) is one of the most devastating muscle disease and it is known to harbour a severe inflammation. We have recently shown that NLRP3 was more expressed in skeletal muscle fibers of mdx mice (a murine model of DMD) than in Wild-Type (WT) mice. Adiponectine (ApN) is a hormone known to possess powerful anti-inflammatory effects on skeletal muscle. Interestingly, transgenic mdx mice that overexpress ApN exhibited lower muscle inflammation/damage as well as higher globular muscle force/endurance when compared to regular mdx mice. These beneficial effects of ApN were associated with a reduction in NLRP3 expression in skeletal muscle. In this study, we

investigated the effects of the absence of NLRP3 on the dystrophic phenotype by crossing mdx mice with NLRP3-knockout (NLRP3-KO) mice. First, functional *in vivo* studies (grip test, wire test and treadmill exercise) were performed on 4 groups of mice: WT, NLRP3-KO, mdx and NLRP3-KO-mdx. Compared to WT, mdx mice presented a strong decrease of global force and endurance that was partially restored in NLRP3-KO-mdx mice. In addition, NLRP3-KO-mdx mice also exhibited a significant decrease in muscle damage, oxidative stress and inflammation as well as a reduction in caspase-1 activation, when compared to regular mdx mice. Furthermore, satellite cells obtained from control and DMD subjects were cultured and differentiated into myotubes. We found that NLRP3 basal expression was 3.5-fold higher in DMD myotubes than in control myotubes. This expression was then reduced after ApN treatment. These novel data show that NLRP3 is implicated in DMD where it plays a key pathogenic role, thus opening new therapeutic perspectives to control muscle inflammation and damage.

<http://dx.doi.org/10.1016/j.nmd.2017.06.028>

EC.O.7

Necroptosis, a programmed form of necrosis, participates in muscle degeneration in Duchenne muscular dystrophy

M. Bencze, J. Meng, V. Pini, F. Conti, F. Muntoni, J. Morgan
UCL, London, UK

Efforts to treat Duchenne muscular dystrophy (DMD) mainly focus on strategies aimed at increasing dystrophin expression, or enhancing muscle regeneration/growth. However, the process of cell death in muscle wasting disorders has been largely overlooked. In DMD, fibres die with a necrotic morphology, making myonecrosis a central process in its pathogenesis. Inflammation and oxidative stress play a significant part in muscle loss, but how inflammation induces myonecrosis is still unknown. Lately, there has been a conceptual revolution in the cell death field, with the discovery of regulated forms of necrosis. In particular, necroptosis, a RIPK3-dependent programmed cell death, plays a major role in cell death following inflammation-induced injuries in several tissues and is commonly initiated by ligands to the TNF Receptor superfamily members. As a programmed cell death mode, necroptosis can be pharmacologically prevented. Its involvement in skeletal muscle degeneration has not yet been reported. We are currently investigating the involvement of necroptosis in inflammatory-induced myonecrosis, and more specifically in the pathogenesis of DMD. *In vitro*, we found that TNF α can trigger necroptosis in C2C12 cell line, suggesting that muscle cells can undergo necroptosis upon inflammatory challenge. *In vivo*, we found evidence of necroptosis in human and mouse dystrophin-deficient muscles. By depleting RIPK3 in mdx mice, we significantly decreased myonecrosis. Together, our data demonstrate that the necroptotic machinery is involved in DMD pathogenesis and that its prevention could represent a new therapeutic target.

<http://dx.doi.org/10.1016/j.nmd.2017.06.029>

EC.O.8

Epigenetic regulation of a mitochondrial apoptosis mediator, harakiri in maintaining muscle membrane stability in autoimmune myositis

K. Nagaraju¹, J. Boehler², A. Horn², J. Novak², S. Ghimbovski², I. Lundberg³, J. Jaiswal²

¹Binghamton University-SUNY, Binghamton, USA; ²Children's national medical center, Washington, DC, USA; ³Karolinska Institute, Stockholm, Sweden

Currently, the cause of myositis is unknown, but disease onset sometime has been associated with exposure to environmental agents such as viral infections. Although attempts to identify viruses in myositis skeletal muscle have failed, several studies have shown that a viral signature (e.g., Type 1 interferon) is present in myositis muscle. To investigate this, we hypothesized that certain virus alters DNA methylation in the promoter regions of genes, leading to their aberrant expression in target tissues and disease phenotype in susceptible